UNIVERSITY OF SOUTHAMPTON

Financial and Environmental Life Cycle Assessment of Domestic PV-Battery Systems

by

Susan Isaya Sun

Submitted for the degree of Doctor of Philosophy

Faculty of Engineering and the Environment
Energy Technology

March 2020

UNIVERSITY OF SOUTHAMPTON

ABSTRACT

FACULTY OF ENGINEERING AND THE ENVIRONMENT
ENERGY TECHNOLOGY

Doctor of Philosophy

FINANCIAL AND ENVIRONMENTAL LIFE CYCLE ASSESSMENT OF DOMESTIC PV-BATTERY SYSTEMS

by Susan Isaya Sun

How green is a home battery? With the rapid development of lithium-ion batteries in portable electronics and electric vehicles, they quickly found a use in the home, storing excess electricity generated by solar PV panels. Some literature estimates suggest that this is not beneficial to the environment, considering the energy lost in charging and discharging, and the embodied emissions of battery manufacture. But when the time-varying nature of grid CO_2 emissions intensity is accounted for, possibilities are opened up for scheduling battery operation more intelligently. Furthermore, second-life electric vehicle batteries are being researched as a potentially inexpensive, low-CO_2 source of batteries compared to manufacturing anew.

This project comprises the development of a model that takes real measured PV and load data as input, and calculates the time-series operation of the battery, accounting for the impacts of degradation on both its lifetime and short-term performance. A novel Emissions Arbitrage Algorithm was developed for scheduling the battery operation. Additionally, a novel method of predicting the evolution of second-life battery price decades into the future was developed to account for second-life battery replacement costs over the system lifetime.

It was found that for a grid-connected urban home, a PV-only system strikes the best balance between financial and environmental sustainability. While adding a new battery running the standard Greedy algorithm becomes more profitable by 2030, this option tends to reduce the environmental benefit. And while a second-life battery is significantly better for the environment than a new one in terms of metals depletion, freshwater ecotoxicity, freshwater eutrophication, human toxicity, water depletion and ozone depletion, it cannot beat a PV-only system except in terms of CO_2 emissions and fossil fuel depletion, and requires the Emissions Arbitrage Algorithm to do so.

Contrary to much of the literature on second-life battery usage, the financial net costs are similar to or greater than using new batteries. No configuration could be found that simultaneously maximised both financial and environmental sustainability. This does not preclude its existence, especially in other contexts and applications, and with more work on designing market structures that incentivise environmental sustainability. This work also highlights the need for improvements in material selection and recycling of PV, batteries and power electronics, especially to mitigate the impacts of metals depletion.

Contents

List of Figures

List of Tables

List of Publications

Peer-Reviewed Papers

Sun, S. I., Kiaee, M., Chipperfield, A. J., and Wills, R. G. A. (2018). Effects of market dynamics on the time-evolving price of second-life electric vehicle batteries. *Journal of Energy Storage*, 19:41 - 51.

This paper presents work which led to some content within Chapter 4.

Sun, S. I., Crossland, A. F., Chipperfield, A. J., and Wills, R. G. A. (2019). An emissions arbitrage algorithm to improve the environmental performance of domestic PV-battery systems. *Energies*, 12(3).

This paper presents work which led to Chapter 3, and some content within Chapter 2.

Conference Presentations

Sun, S. I., Kiaee, M., and Cruden, A. J. (2017). Achieving both economic and environmental objectives for a solar farm with co-located battery. In *1st International Conference on Large-Scale Grid Integration of Renewable Energy in India*, New Delhi, India.

Sun, S., Kiaee, M., Norman, S., and Wills, R. (2018). Self-sufficiency ratio: an insufficient metric for domestic PV-battery systems? *Energy Procedia*, 151:150 - 157. 3rd Annual Conference in Energy Storage and Its Applications, 3rd CDT-ESA-AC, 11-12 September 2018, The University of Sheffield, UK.

Sun, S. I., Kiaee, M., Chipperfield, A. J., and Wills, R. G. A. (2018). Techno-economic and environmental analysis of second-life batteries compared to new in a revenue-stacking network-constrained solar PV farm. In *Energy Systems Conference 2018*, London, UK.

Sun, S. I., Smith, B. D., Wills, R. G. A., and Crossland, A. F. (2020). Effects of time resolution on finances and self-consumption when modeling domestic PV-battery systems. *Under review.* 4th Annual Conference in Energy Storage and Its Applications, 4th CDT-ESA-AC, 9-10 July 2019, The University of Southampton, UK.

Acronyms

AC	Alternating Current
AEF	Average Emissions Factor
ALO	Agricultural Land Occupation
AUD	Australian Dollars
BEIS	(Department for) Business, Energy and Industrial Strategy, formerly DECC
BEV	Battery Electric Vehicle
BM	Balancing Mechanism
BMS	Battery Management System
BoS	Balance of System
CAES	Compressed Air Energy Storage
CAPEX	Capital Expenditure
CC	Climate Change
CCC	Committee on Climate Change
CCCV	Constant-Current Constant-Voltage
CCGT	Combined Cycle Gas Turbine
CCS	Carbon Capture and Storage
CED	Cumulative Energy Demand
CH_4	Methane, natural gas
CML	Centrum voor Milieuwetenschappen ('Institute of Environmental Sciences' in Dutch)
CNY	Chinese Yuan
CO_2	Carbon Dioxide
CPF	Carbon Price Floor
CPI, CPIH	Consumer Prices Index (including owner-occupiers' housing costs)
CR, CR30, CR50	Community Renewables (FES scenario), in 2030, 2050
DALY	Disability-Adjusted Life Year
DC	Direct Current
DECC	Department of Energy and Climate Change, now BEIS
DoD	Depth of Discharge
DPBT, DPP	Discounted Payback Time, Discounted Payback Period
EAA	Emissions Arbitrage Algorithm
EIS	Electro-Impedance Spectroscopy
EoL	End of Life
EPBT	Energy Payback Time
EROEI, EROI	Energy Return On (Energy) Invested
ESOI	Energy Stored On Investment

ESS	Energy Storage System
ETS	Emissions Trading Scheme
EUR	Euro
EV	Electric Vehicle
FB	Flow Battery
FD	Fossil Depletion
FE	Freshwater Eutrophication
FES	Flywheel Energy Storage OR Future Energy Scenarios
FiT	Feed-in Tariff
GB	Great Britain
GBP	Great British Pound
GDM	Generator Dispatch Model
GHG	Greenhouse Gas
GW, GWh	Gigawatt, Gigawatt-hour
HT	Human Toxicity
ICE	Internal Combustion Engine
IEA	International Energy Agency
IGBT	Integrated Gate Bipolar Transistor
ILCD	International Reference Life Cycle Data
IPCC	Intergovernmental Panel on Climate Change
IPBES	Intergovernmental Panel on Biodiversity and Ecosystem Services
IR	Ionising Radiation
IRENA	International Renewable Energy Agency
IRR	Internal Rate of Return
kV	Kilovolt
kW, kW_p, kWh	Kilowatt, Kilowatt-peak, Kilowatt-hour
LAES	Liquid Air Energy Storage
LCA	Life Cycle Assessment
LCC	Life Cycle Cost
LCI	Life Cycle Inventory
LCIA	Life Cycle Impact Assessment
LCO, $LiCoO_2$	Lithium Cobalt Oxide
LCoE, LCoES	Levelised Cost of Electricity, Levelised Cost of Energy Storage
LFP, $LiFePO_4$	Lithium Iron Phosphate
LNT	Linear No Threshold, assumption for radiation damage
MD	Metal Depletion
ME	Marine Eutrophication
MEF	Marginal Emissions Factor
MET	Marine Ecotoxicity
MCoE	Mean Cost of Electricity
MILP	Mixed Integer Linear Program
MJ	Megajoule
MOSFET	Metal Oxide Semiconductor Field Effect Transistor
MPPT	Maximum Power Point Tracking
MW, MWh	Megawatt, Megawatt-hour

NCA, Li-NCA	Lithium Nickel Cobalt Aluminium Oxide
NGCC	Natural Gas Combined Cycle (see CCGT)
NLT	Natural Land Transformation
(Li-)NMC, NCM	Lithium Nickel Manganese Cobalt Oxide
NMVOC	Non-Methane Volatile Organic Compound
NPV	Net Present Value
OCV	Open-Circuit Voltage
OD	Ozone Depletion
Ofgem	Office for Gas and Electricity Markets
O & M	Operations and Maintenance
P2P	Peer-to-Peer (trading)
PAA	Price Arbitrage Algorithm
PbA	Lead-Acid
PDF	Potential Disappeared Fraction (of species)
PHEV	Plug-in Hybrid Electric Vehicle
PHS	Pumped Hydroelectric Storage
PI	Profitability Index
PM2.5, PM10	Particulate Matter of scale 2.5 μm, 10 μm
PMF	Particulate Matter Formation
POF	Photochemical Oxidant Formation
PP	Payback Period
PV	Photovoltaic
PVDF	Polyvinylidene Difluoride
RoI	Return on Investment
SEI	Solid-Electrolyte Interface
SMES	Superconducting Magnetic Energy Storage
SoC	State of Charge
SSR	Self-Sufficiency Ratio
TA	Terrestrial Acidification
TD, TD30, TD50	Two Degrees (FES scenario), in 2030, 2050
T & D	Transmission and Distribution
TES	Thermal Energy Storage
TET	Terrestrial Ecotoxicity
ToU	Time of Use
TSO, TNO	Transmission System Operator, Transmission Network Operator
ULO	Urban Land Occupation
UK	United Kingdom
USA	United States of America
USD	United States Dollar
UV	Ultraviolet
V2G	Vehicle to Grid
VAT	Value Added Tax
WD	Water Depletion
WEEE	Waste Electronic and Electrical Equipment

Nomenclature

Symbols	Units	Description
a_x, b_x	GW, -	Shifting and scaling parameters to adjust $D(t)$ from 2017 to scenario x
C_B	GBP	Total battery cost (excluding balance of system)
$c_{B,0}$	GBP	Fixed portion of battery cost
$c_{B,1}$, $c_{B,1,y}$	GBP/kWh	Size-dependent portion of battery cost (in year y)
$c_{B,i}$	[unit$_i$]/kWh	Embodied impact i (= CC, OD, etc.) of battery
$C_{B,i}$, $C_{B,i,y}$	[unit$_i$]	manufacture (in year y)
C_{BoS}	GBP	Total balance of system (BoS) cost
$c_{BoS,0}$	GBP	Fixed portion of BoS cost
$c_{BoS,1}$	GBP/kW	Size-dependent portion of BoS cost
$c_{BoS,i}$	[unit$_i$]/kW	Embodied impact i (= CC, OD, etc.) of balance of system
$C_{BoS,i}$	[unit$_i$]	manufacture and installation
$C_{g,i,y}$	[unit$_i$]	Net impact in category i, year y, of interacting with the grid (import minus export)
c_i	[unit$_i$]/kWh	Total environmental impact in category i, per kWh consumed
$c_{j,i}$	[unit$_i$]/kWh	Intensity in impact category i for generator type j
$c_{j',i}$		or from extended set j', also includes components manufacture impacts
C_{PV}	GBP	Total PV cost
$c_{PV,0}$	GBP	Fixed portion of PV cost
$c_{PV,1}$	GBP/kW$_p$	Size-dependent portion of PV cost
$c_{PV,i}$	[unit$_i$]/kW$_p$	Embodied impact i (= CC, OD, etc.) of PV
$C_{PV,i}$	[unit$_i$]	manufacture and installation
c_{recyc}(y)	GBP/kWh	Cost of recycling EV batteries in year y
c_{repur}(y)	GBP/kWh	Cost of recpurposing EV batteries in year y
D, $D(t)$, $D_x(t)$	MW	National electricity demand (in year/scenario x)
D_1, D_2, D_3	-	Parameters describing battery degradation function
E	kWh	Quantity of second-life batteries (of which price-supply/demand curves are a function)
$E^*(y)$	kWh	Second-life battery quantity at joint between niche and mass markets
E_B	kWh	Battery capacity
$E_{B,1}$, $E_{B,2}$	kWh	Heuristically optimised capacity of new/ second-life battery
$E_{eqm}(y)$	kWh	Equilibrium quantity of second-life battery sales in year y

$E_{max}(y)$	kWh	Maximum global demand for stationary batteries in year y
$f_{EV}(y)$	kWh	Supply of used EV batteries in year y
$I(t)$	A	Current entering battery (negative for discharge)
k_1, k_2	-	Parameters for converter efficiency function
m_1, m_2	-, MW^{-2}	Parameters for T & D loss variable $\lambda(t)$
MEF^+, MEF^-	kg/kWh	Upper, lower thresholds for marginal emissions factor in EAA
$MEF(t)$, $MEF_{CC}(t)$	kg/kWh	Instantaneous marginal (CO_2) emissions factor
$MGR_j(t)$	MW/MW	Instantaneous marginal generator response for generator type j
N	years	Temporal boundary for financial and environmental calculations
N_d	-	Number of divisions to account for the country's total storage
n	cycles	Number of battery cycles, as energy throughput compared to E_B
$n_\perp$	-	Number of cells in series
$n_\parallel$	-	Number of cell strings in parallel
$P_c^+(t)$, $P_c^-(t)$	kW	Battery charge, discharge power
P_{conv}	kW	Rated capacity of battery DC-DC converter
$P_d(t)$	kW	Household load power
$p_{dem}(E, y)$	GBP/kWh	Second-life battery price-demand curve in year y
$p^*_{dem}(y)$	GBP/kWh	Second-life battery price at joint between niche and mass markets
P_{drain}	kW	Auxiliary drain on the battery, both self-discharge and powering the BoS
$p_{eqm}(y)$	GBP/kWh	Equilibrium second-life battery price in year y
$P_g^+(t)$, $P_g^-(t)$	kW	Grid export, import power
$P_{gen}(t)$	kW	PV generation power
P_{inv}	kW	Rated capacity of DC-AC inverter
$P_j(t)$	MW	Power generated by plant of type j
P_{PV}	kW_p	PV rated capacity
P_{set}	kW	Charge setpoint of battery (negative means discharge setpoint)
$p_{sup}(E, y)$	GBP/kWh	Second-life battery price-supply curve in year y
$P_{thru}(t)$	kW	Power flowing through DC-AC inverter (negative for backflow)
q	Ah	Nominal charge of a single cell
Q^+, Q^-	Ah	Battery upper, lower state-of-charge limits
$Q(t)$	Ah	Charge on battery
Q_{knee}	-	Charge degradation knee point
$Q_t(n)$	-	Charge degradation with cycling n
R	ohm	Battery internal resistance
R'	ohm	Single cell internal resistance
$r_j(y)$	kWh	Quantity of EV batteries from j^{th} generation that must be replaced in year y
$R_t(n)$	-	Resistance increase with cycling n
t	h	Time (restarts from 0 each year)
$u_{B,y}$	-	Battery replacement binary variable
$u_{BoS,y}$	-	BoS replacement binary variable
$V(t)$	kV	Terminal voltage of battery
V_0	kV	Nominal voltage of battery constant voltage source
v_0	kV	Single cell nominal voltage

Δt	h	Timestep
η_1	%	Battery DC-DC converter efficiency
η_2	%	Bi-directional inverter efficiency
$\lambda(t)$, $\lambda_x(t)$	%	Multiplicative factor to account for T & D loss (in scenario x)

Declaration of Authorship

I, Susan Isaya Sun, declare that this thesis entitled Financial and Environmental Life Cycle Assessment of Domestic PV-Battery Systems and the work presented in it are my own and has been generated by me as the result of my own original research.

I confirm that:

1. This work was done wholly or mainly while in candidature for a research degree at this University;
2. Where any part of this thesis has previously been submitted for a degree or any other qualification at this University or any other institution, this has been clearly stated;
3. Where I have consulted the published work of others, this is always clearly attributed;
4. Where I have quoted from the work of others, the source is always given. With the exception of such quotations, this thesis is entirely my own work;
5. I have acknowledged all main sources of help;
6. Where the thesis is based on work done by myself jointly with others, I have made clear exactly what was done by others and what I have contributed myself;
7. Either none of this work has been published before submission, or parts of this work have been published as: Sun et al. (2020).

Signed:

Date:

Copyright © and Moral Rights for this thesis and, where applicable, any accompanying data are retained by the author and/or other copyright owners. A copy can be downloaded for personal non-commercial research or study, without prior permission or charge. This thesis and the accompanying data cannot be reproduced or quoted extensively without first obtaining permission in writing from the copyright holder/s. The content of the thesis and accompanying research data (where applicable) must not be changed in any way or sold commercially in any format or medium without the formal permission of the copyright holder/s.

When referring to this thesis and any accompanying data, full bibliographic details must be given, e.g.

Thesis: S. I. Sun (2020) "Financial and Environmental Life Cycle Assessment of Domestic PV-Battery Systems", University of Southampton, Faculty of Engineering and the Environment, PhD Thesis.

Data: S. I. Sun (2020) "Code and Input Data for: Financial and Environmental Life Cycle Assessment of Domestic PV-Battery Systems in Great Britain, including Second-life Batteries".
URI `https://doi.org/10.5258/SOTON/D1269`.

Acknowledgements

With thanks to:

My supervisors, Dr. Richard G. A. Wills and Dr. Andrew J. Chipperfield, for their tireless patience,

My mentor, Dr. Mahdi Kiaee, for the same,

Dr. Andrew F. Crossland, serial collaborator extraordinaire,

My colleagues at JUICE, the Joint UK India Clean Energy Centre[1],

And those on the CDT ESA, the Centre for Doctoral Training in Energy Storage and its Applications[2],

All my friends, and other hippies of Campus Collective and Southampton University Conservation Volunteers, for keeping me grounded,

My parents, without whom literally none of this suffering would have occurred,

And Jules. May we have many more adventures together.

[1]Grant ref: EP/P003605/1
[2]Grant ref: EP/L016818/1

Chapter 1

Introduction

"What you don't know is what the knife does on its own. Your intentions may be good. The knife has intentions too."
- Iorek Byrnison in *The Amber Spyglass* by Philip Pullman

From around the time of the Industrial Revolution in the 18th century, humankind has enjoyed an unprecedented acceleration in standard of living. Automated production, motorised transport, mechanised farming, international trade, electrical appliances - all of these depend on the plentiful supply of energy. The source of most of this energy today is still the combustion of fossil fuels: coal, oil and natural gas (together 85 % of global primary energy supply in 2015, according to IRENA (2018)).

It is an unfortunate fact that the carbon dioxide (CO_2) emitted by their combustion is accumulating in the atmosphere and oceans faster than natural processes can remove them. The warming of the planet resulting from absorption of outgoing infrared radiation by CO_2 and other greenhouse gases (GHG) has been known since the work of Callendar (1938), who calculated the theoretical magnitude of this Greenhouse Effect to be 0.003 °C of planetary warming per year at the time, and confirmed it through measurements from weather stations around the world to be 0.005 °C per year.

It was only in recent decades that the Greenhouse Effect was realised to be detrimental to human development. Research into the effects of the rising global mean temperature on regional weather patterns, known collectively as climate change, or increasingly as 'climate breakdown', are well documented by the Intergovernmental Panel on Climate Change (IPCC, 2018). Their report comparing the potential consequences of a 2 °C and a 1.5 °C increase in global mean temperature since pre-Industrial times describes how the frequency of heat waves, droughts, storms, and other natural disasters in different parts of the world are likely to increase (IPCC, 2018). The impacts on agricultural productivity, disease risk, and simply whether or not a region is habitable, are likely to fall disproportionately on the world's poorest.

All the gains of modern civilisation described above are threatened by climate change, the result of the very fossil fuel combustion that makes modern life possible. At the same time, other human activity such as deforestation, intensive farming, unsustainable fishing, and pollution from industrial processes, are also threatening the planet's ecosystems. A report by the Intergovernmental Panel on Biodiversity and Ecosystem Services (IPBES, 2018) finds that a million animal and plant species are now threatened

with extinction, more than ever before in human history. As well as direct ecosystem services such as crop pollination and absorption of atmospheric CO_2, increased biodiversity has been shown to make habitats more resilient to change (IPBES, 2018). In other words, climate change, as well as other human activity, threatens the very biodiversity we rely on to help us adapt to the effects of climate change itself.

Knowing these facts, it is easy for an ordinary person to become dispirited. By merely living and consuming - food and other products - we all participate in the energy use and human activity that accelerate environmental degradation. Meanwhile, international agreements are made and targets set, with little scope for individual participation. For example, the Paris Agreement of 2015, where 195 countries pledged to reduce their GHG emissions by individual nationally defined contributions, aims to limit global temperature rise to 2 °C above pre-Industrial levels, with a view to limiting it to 1.5 °C (UNFCCC, 2018). Even if all anthropogenic GHG emissions stopped tomorrow, the world is already locked into at least this much warming by the end of the century (Frölicher et al., 2014). Any realistic attempts to meet the 2 °C target require negative-emissions technologies such as bio-energy with carbon capture and storage. And yet all the nationally defined contributions taken together would only be able to limit warming to 3 °C (Climate Action Tracker, 2018).

In this context, the enthusiasm for rooftop solar photovoltaic (PV) panels and home energy storage is very understandable. While still out of the price range of many individuals, at thousands of GBP, PV-battery installations are already a realistic option at least for some moderately well-off homeowners in developed countries. The Tesla Powerwall, for instance, has become a household name in recent years (Merchant, 2019). Home batteries, also known as domestic batteries, are often marketed as a way to increase a household's usage of their own low-carbon PV energy, by storing that energy when there is excess above the household electricity consumption and discharging the battery when consumption is high again. As well as the Tesla (2018) Powerwall, commercially available products include the Moixa (2016) Maslow, SolarWatt (2018) MyReserve, SimpliPhi (2018) PHI, and batteries by SolaX Power (2018) and LG Chem (2018a). Although they are all functionally similar, being a box that is connected to a house's electrical system and PV panels, they differ in details of the battery chemistry. This impacts on the battery's efficiency, cost, energy density, and lifetime. The algorithms programmed into the control unit and battery management system (BMS) are further ways that home battery products differentiate themselves.

What the marketing often neglects to mention is that excess PV electricity that goes unused in one home is rarely wasted, but flows to the next nearest point in the network where it is needed. More holistic analyses find repeatedly that a home battery slightly reduces the environmental benefit compared to having PV only (Babacan et al., 2018; Kabakian et al., 2015; Kurland and Benson, 2019; McKenna et al., 2013). This is because of energy losses in charging and discharging the battery, and negative environmental impacts caused by battery manufacture.

Rather than dismissing the concept of domestic batteries completely, this thesis explores the circumstances in which they can render an environmental benefit, and what can be done to bring these circumstances about. To this end, it is necessary to examine the financial as well as environmental aspects of domestic battery usage. After all, saving money is still the most highly cited reason for considering purchase of a home battery (Agnew and Dargusch, 2017; Which?, 2018). The same surveys find a desire to help the environment is usually the next most important consideration.

Before reviewing the existing literature and identifying gaps in the research, it is necessary to define what is meant by financial benefit and environmental benefit. The next two sections define terms that

are commonly used in those subject areas, and which are used throughout the thesis. Those familiar with business economics and environmental life cycle analysis may skip to Section 1.3.

1.1 Metrics of Financial Benefit

Although a home is not a business, it is instructive to study how a business evaluates the potential profitability of an investment option. Similar analyses are also conducted by governments, charities and international organisations such as the World Bank and International Monetary Fund. It is important for the accountability of such institutions to transparently show the cost-effectiveness of their activities.

While the details of any business model may differ in many ways, all can be generalised as follows (Harvey, 1994):

1. Initial investment, also known as capital expenditure (Capex), is made in buildings, land and/or machinery.
2. Running costs, also known as overheads, are incurred for process inputs such as fuel and raw materials, and if applicable, rent and labour.
3. Revenue, or income, is received from selling a product or service.

In the context of domestic PV-battery installations, the Capex is on the PV array, battery and peripheral equipment, also known as balance of systems (BoS). Capex may be reduced by government subsidies in some contexts: a 30 % discount on the purchase of solar panels is available in Germany, provided grid feed-in is limited to 50 % of the PV array's rated power (Truong et al., 2016). The household electricity bills, and if applicable, taxes, maintenance and equipment replacement costs constitute the overheads. Revenue is from sale of PV-generated electricity back to the supplier: these are called export payments, or net billing, in contrast to net metering where for billing purposes, PV-generated electricity fed back to the grid is subtracted from the household's electricity consumption from the grid. Net metering can be thought of as a special case of net billing where the export payment is equal to the retail electricity price (export payments are nearly always lower than the retail price in net billing). Net metering schemes have been operational in Belgium, Brazil, Finland, Israel, Mexico, Netherlands, Ontario (Canada) and 41 states in the USA (Prol and Steininger, 2017). Where applicable, revenue can also come from government subsidies such as a feed-in tariff (FiT). This is a payment per kWh of electricity generated, fixed at the rate locked on to when the system is installed. FiT payments were guaranteed for 25 years in the UK, at over 0.47 GBP/kWh for rooftop PV arrays below 4 kW_p in size when the scheme began in 2010, decreasing to 0.0379 GBP/kWh for arrays below 10 kW_p when the scheme ended in 2019 (Ofgem, 2019). Similar schemes have been operational in Germany, Austria, Italy, Spain, Portugal, Denmark, Sweden, Switzerland, Chile and Australia (Mulder et al., 2013; Prol and Steininger, 2017). The UK has pivoted from a FiT scheme towards a so-called Smart Export Guarantee, where export payments are to be paid by electricity suppliers, without government subsidy, at a level determined by an open market (BEIS, 2019b).

There follows an explanation of how some common metrics are calculated and used to make investment decisions:

- Net present value (NPV)

- Internal rate of return (IRR)
- Mean cost of electricity (MCoE)
- Return on investment (RoI)
- Payback period (PP)
- Self-sufficiency ratio (SSR).

It is rare to rely on only one of these metrics, as each may give a different assessment of the relative profitability of a given business model.

Net Present Value: Each year's profit is the revenue minus the overheads. The net present value (NPV) is a measure of the lifetime profit of the system, and is calculated by discounted cash flow analysis:

$$NPV = -CAPEX + \sum_{y=1}^{N} \left(\frac{1}{1+r}\right)^{(y-1)} (REV_y - COST_y) \tag{1.1}$$

where for years $y = 1$ to N, REV_y and $COST_y$ are respectively the revenue and running costs in year y, and r is the discount rate. The term $\left(\frac{1}{1+r}\right)^{(y-1)}$ de-values each future year's cash flows by another factor of $\left(\frac{1}{1+r}\right)$. If an option is considered risky, a higher discount rate r is chosen; hence the returns from a riskier option are valued at less than the returns from a more secure option, and even less the further into the future one goes. When $NPV > 0$, the option is considered profitable, and vice versa when $NPV < 0$. Given a choice of options, the one with greatest NPV would be the most profitable by this measure.

The choice of discount rate is partly subjective, but there is a typical range for a given context. For example, Camilo et al. (2017); Hoppmann et al. (2014); Kirmas and Madlener (2017); Truong et al. (2016) take 4 % to be the discount rate in their financial calculations of domestic PV-battery systems, while Mulder et al. (2013) take 4.5 %, Yu (2018) 5 %, Muthuvel et al. (2016) 6 %, and O'Shaughnessy et al. (2018) 6.2 %. In fact Hoppmann et al. (2014) calculated the sensitivity of the results to the discount rate being higher or lower, finding it to be the strongest factor in determining the NPV per EUR (euro) invested, where higher discount rate decreases NPV. This follows from the definition: higher discount rate de-values future cash flows more, thus a front-loaded investment such as PV and battery is disfavoured by higher discount rates. 4 % is a low discount rate compared to what is typical in a business context. However, homeowners have comparatively few other options for high returns on investment.

Heymans et al. (2014) and Bertsch et al. (2017) use an even lower discount rate of 1 %, although Heymans et al. (2014) appear to have confused the concept of discount rate with maintenance costs, and Bertsch et al. (2017) do not make it clear whether their discount rate accounts for inflation[1]. Farah et al. (2016) do make it clear that they use a nominal discount rate of 5 %, which with inflation 2.5 % results in real discount rate 2.5 %. The nominal discount rate, which does not take account of inflation, is higher than the real discount rate (Mulder et al., 2013):

$$\text{Real discount rate} = \frac{1 + \text{nominal discount rate}}{1 + \text{inflation}} - 1. \tag{1.2}$$

[1]Inflation, that is, the increase in the numerical prices of goods, arises as a result of the increasing supply (and hence de-valuing) of money from governments issuing bonds and private banks issuing loans. It is what causes 1 GBP today, for example, to be worth less than 1 GBP in the past, and more than 1 GBP in the future.

NPV calculated using the real discount rate is reported in units of currency at the investment start date.

The temporal boundary N represents the lifetime of the system. Hoppmann et al. (2014) and Camilo et al. (2017) take $N = 25$ years, this being the typical guarantee period of a PV array, the longest-lived component of a domestic PV-battery system (CAT Information Service, 2018). Some, such as Yu (2018) take a more conservative value of $N = 20$ years. Truong et al. (2016) use $N = 20$ years and Kirmas and Madlener (2017) take $N = 10$ years, focusing on the lifetime of the battery instead.

It is worth noting the related concept of life cycle cost (LCC), which Muthuvel et al. (2016) define as negative the NPV in equation (1.1).

In most of the literature, NPV is given relative to a baseline case, such as a house with no PV and no battery. This is done by including a term $+COST_{0,y}$ to equation (1.1), representing the expenditure on electricity bills in year y in the absence of PV and battery:

$$NPV' = -CAPEX + \sum_{y=1}^{N} \left(\frac{1}{1+r} \right)^{(y-1)} (REV_y - COST_y + COST_{0,y}). \tag{1.3}$$

This adjustment means NPV' represents lifetime savings rather than profits, as NPV does. This is an important distinction because it is possible to make a loss ($NPV < 0$) technically while still making savings ($NPV' > 0$), which most homeowners would still consider worthwhile because they would be spending money on electricity anyway.

It should be noted that NPV does not take into account how the business model is financed, whether by debt (taking out a loan) or equity (issuing shares) or a combination of both. A debt must be repaid in instalments with interest, while yearly dividends must be paid to shareholders. These are not included as running costs, as that would double-count the Capex. However, they can be accounted for by the annuity method, explained below under Mean Cost of Electricity.

Internal Rate of Return: IRR is the value of the discount rate r which makes $NPV = 0$ in Equation (1.1), or more commonly, which makes $NPV' = 0$ in (1.3). The IRR is a measure of the equivalent interest rate yielded by the business model, treating it as a series of loan repayments on $CAPEX$. Unlike NPV, calculating IRR requires no a priori assumptions about the discount rate. This is why Bertsch et al. (2017) used it in their work. It is also calculated by Prol and Steininger (2017), and by Camilo et al. (2017) in conjunction with NPV, PI, LCoE, and DPP (see below for the latter three).

It is customary for an investor to set a hurdle rate which if exceeded by IRR, a decision is made to invest in the option. The value of the hurdle rate depends on the investor: one who views the option as riskier would set a higher hurdle rate. As Mulder et al. (2013) discuss, this hurdle rate may be the nominal interest rate (not accounting for inflation), or zero if inflation is included in the calculation. This is a very low bar compared to most business contexts, where investors would wish to beat inflation by a greater margin. For example, Green and Staffell (2014) consider hurdle rates of 7-13 % when modelling decisions to invest in new nuclear plant.

Like NPV, IRR (and indeed all financial metrics) are affected by the temporal boundary of the system and projections of how costs and revenues may change over that time. It is common for studies to analyse the sensitivity of the metrics to the various assumptions used, as discussed in Section 1.3.2.

Return on Investment: RoI is the percentage return on Capex given by:

$$RoI = \left(\frac{\sum_{y=1}^{N} \left(\frac{1}{1+r}\right)^{(y-1)} (REV_y - COST_y)}{CAPEX} - 1 \right) \times 100\% \tag{1.4}$$

$$= \frac{NPV}{CAPEX} \times 100\%. \tag{1.5}$$

where all terms are as in equation (1.1). RoI may include a term $+COST_{0,y}$ like for NPV' in equation (1.3), where savings compared to a baseline case are counted rather than profits.

Naumann et al. (2015) and Truong et al. (2016) calculated RoI for domestic PV-battery systems, taking discount rate $r = 4$ % and system lifetime $N = 20$ years. Care must be taken interpreting RoI as sometimes equipment replacement costs are included in $CAPEX$ rather than $COST_y$, as Naumann et al. (2015) have done.

As RoI and IRR are both given as percentage values, care must be taken not to confuse the two. As a hypothetical example, suppose an investment of 5000 GBP yields a net return of 400 GBP every year for 25 years (not correcting for inflation, for simplicity). The IRR in this case is 7.0 %, as $-5000 + \sum_{y=1}^{25} \left(\frac{1}{1+r}\right)^{(y-1)} \times 400 = 0$ when $r = 0.07$. The RoI in this case is 30.0 % (for a discount rate of 4 %) as found by inserting $CAPEX = 5000$, $REV_y - COST_y = 400$ for $y = 1$ to 25, and $r = 0.04$ into equation (1.5). Incidentally, this would give an NPV of 1500 GBP (30 % of 5000 GBP).

There is a similar concept called profitability index (PI), which Yu (2018) defines identically to RoI in equation (1.5) but Camilo et al. (2017) take to include operations and maintenance (O & M) costs in the denominator, as Naumann et al. (2015) have done but called RoI.

Mean Cost of Electricity: MCoE is the cost per kWh of electricity consumed over the system lifetime, including investment costs in PV and battery. It allows comparison between cases with and without battery or PV, and has some similarity to the concept of reporting environmental impacts per functional unit (see Section 1.2). Where the functional unit is kWh of electricity consumed, then one can calculate kg CO_2 emitted per kWh consumed, for example, and compare how the carbon cost and monetary cost are affected by different interventions, on the same basis: per kWh consumed.

By this definition,

$$MCoE = \frac{-NPV}{\sum_{y=1}^{N} ELEC_y} \tag{1.6}$$

where $ELEC_y$ is the total electricity consumed in year y and other symbols are as in equation (1.1).

MCoE is similar conceptually to levelised cost of electricity (LCoE). The main differences are that LCoE counts the costs of generation but not the revenue, and the denominator is the total electricity generated in year y, not the electricity consumed. LCoE is used to compare the costs of different generation technologies (coal, nuclear, biomass, etc.), and is useful because it accounts for the fact that wind and solar power generate on average roughly 25 % and 12 % of the time at rated power respectively (Carbajales-Dale et al., 2014), while nuclear power, for example, generates at rated power for typically over 90 % of the time. Other measures of costs, such as per MW installed, would mask this effect and make intermittent renewable generators seem vastly more cost-effective than nuclear power.

There is a further related concept, levelised cost of energy storage (LCoES), defined as for MCoE in equation (1.6) but the denominator is total energy discharged, rather than consumed or generated (Parra et al., 2016).

MCoE is calculated by Weniger et al. (2013) for a PV-battery system, taking account of revenue from a FiT and costs of an increasing electricity tariff. They use the annuity method to amortise the Capex over the system lifetime of 20 years, that is, instead of taking Capex as a lump sum paid at the beginning, it is paid off in yearly instalments. The instalments are larger than simply 1/20 of Capex because of discounting of future cash flows, at 4 % in their case. While it is common to pay off large purchases such as cars and televisions in instalments in this way, the literature on PV-battery system economics rarely amortises the Capex. It is not clear whether this reflects the reality of PV-battery purchasing (if most customers do in fact pay up front in full rather than in instalments), or is a simplification due to the smallness of the effect of amortisation on results.

Note that by some definitions of LCoE, such as that of the World Bank, electricity generation in future years is discounted at the same rate r as the cash flows (Deichmann and Zhang, 2013). That is, a factor $\left(\frac{1}{1+r}\right)^{(y-1)}$ is included in the denominator of equation (1.6). This convention is not always followed when calculating MCoE: Weniger et al. (2013), for example, did not. Parra et al. (2016) did include the discount factor in calculating LCoES, and Camilo et al. (2017) and Yu (2018) too in calculating LCoE. The usefulness of calculating LCoE or LCoES rather than MCoE for domestic PV-battery systems is questionable: since the denominator of LCoE is the total electricity generated, LCoE is undefined for a system with no PV, which generates nothing. Similarly, LCoES is undefined for a system with no storage, which discharges nothing. LCoE and LCoES cannot then be compared to a baseline scenario without PV and battery.

Payback Period: PP is the time it takes to reach breakeven, in other words, to accumulate enough profit ($REV_y - COST_y$) to pay off $CAPEX$ in full. Future cash flows are not discounted (Mulder et al., 2013), although there is the related concept of discounted payback period (DPP, or discounted payback time DPBT), where future cash flows are discounted (Camilo et al., 2017). For the hypothetical example given above to illustrate RoI calculations, PP (without discounting) is 13 years: 13×400 GBP $= 5200$ GBP, which is the first year in which the investment of 5000 GBP is fully paid off.

When considering a homeowner rather than a business investor, payback period is more commonly the time to accumulate enough savings ($REV_y - COST_y + COST_{0,y}$) relative to a baseline case with costs $COST_{0,y}$ in year y, rather than profits. An investor may stipulate a maximum payback period, for example if they are unsure of their plans beyond that date. A company may be unsure whether they will still be in business beyond a few years, while a homeowner may plan to sell their house after a certain date, after which they will no longer own the PV-battery system they are considering investing in.

Self-Sufficiency Ratio: While not strictly a metric of financial return, SSR is nonetheless commonly calculated and reported in the literature (Bertsch et al., 2017; Hoppmann et al., 2014; Weniger et al., 2013). It is defined as the percentage of household electrical demand that is met by sources other than the grid, namely by PV generation and battery discharge:

$$SSR = \left(1 - \sum_t \frac{P_g^-(t)}{P_d(t)}\right) \times 100\% \tag{1.7}$$

where $P_g^-(t)$ is the time series of power imported from the grid, and $P_d(t)$ that of power consumed by the house. The sum is typically calculated over a year.

For a given capacity of PV and battery, and assuming a flat-rate electricity tariff, maximising SSR is equivalent to minimising costs, through reducing grid import and therefore exposure to the electricity import price (Mulder et al., 2013). SSR is increased by increasing either PV and/or battery capacity; Bertsch et al. (2017) showed that this is not equivalent to increasing IRR. The author confirmed (Sun et al., 2018a) that the link between SSR and financial return (as represented by NPV) only exists up to an optimal PV/battery size combination which depends on the particular household in question, after which higher-capacity components keep increasing SSR but not NPV. And further, that increasing the battery capacity reduces CO_2 savings despite increasing the SSR.

The related concept of self-consumption ratio (SCR) is defined:

$$SCR = \left(1 - \sum_t \frac{P_g^+(t)}{P_{gen}(t)}\right) \times 100\% \tag{1.8}$$

where $P_g^+(t)$ is the time series of power exported to the grid, and $P_{gen}(t)$ is the time series of power generated by onsite PV. In other words, SCR is the percentage of PV-generated electricity that goes into supplying the household load and charging the battery, rather than being exported to the grid.

A trivial way to maximise SCR follows from Equation (1.8): by eliminating the PV array. Given that financial returns of the kinds described above tend to be improved by non-zero PV capacity (see Section 1.3.2 below), the implication is that SCR is not a useful metric of financial benefit either. However, high SCR is beneficial to distribution network operators who then do not have to spend so much on upgrades to enable the network to accept more injection of exported PV energy. On the other hand, high SCR and high SSR are considered by some electricity suppliers to be detrimental to their revenues, as customers buy less from them and supply more of their own needs. This has led to both subsidies and taxes on PV self-consumption in different jurisdictions, as described further in Section 1.3.2.

1.2 Metrics of Environmental Benefit

Quantifying environmental benefits and burdens necessarily includes a degree of subjectivity. 'What do we value?' is a moral question rather than a scientific one. It is possible to use some seemingly objective measures such as energy payback time (EPBT), defined in analogy with financial payback time (see previous section), as the time taken for a device such as a solar panel to generate as much energy as it took to manufacture and install it. Energy return on investment (EROI, also known as energy return on energy invested, EROEI) can similarly be defined in analogy with financial RoI. EROI is the total energy generated over the lifetime of an energy-generating device divided by the energy required to manufacture, install, operate and maintain it.

The related concept of energy stored on investment (ESOI) is sometimes used for energy storage, where the numerator is the energy throughput of the storage device over its lifetime (Kurland and Benson, 2019). Complications arise when a combined generator-storage system such as PV-battery is considered. One resolution is to consider the total energy required to manufacture, install and operate the PV-battery system over its lifetime, and divide this by the total energy consumed in the home, in analogy with MCoE. This metric is often called cumulative energy demand (CED). It was calculated by Kabakian

et al. (2015) for a PV-battery system in the Lebanon, and is a commonly reported metric in life cycle analyses (LCA) of many other products (Klöpffer and Grahl, 2014).

The problem with EPBT, EROI, ESOI, CED and such metrics involving energy generation and consumption, is that there is not a perfect correlation between energy usage and environmental harm. For example, a battery factory running on hydroelectric power may incur a CED equal to one running on coal power, but the former would contribute significantly less GHG emissions to climate change. Recognising this, many researchers including McKenna et al. (2013) and Babacan et al. (2018) additionally calculate the equivalent CO_2 emissions of PV-battery systems (units kg CO_2-eq/kWh).

However, as discussed above, climate change is not the only problem degrading the environment. Climate change exacerbates biodiversity loss, which itself reduces ecosystems' resilience to climate change, but many other mechanisms threaten the habitats of plant and animal species and indeed human health too: air pollution, acid rain, ozone depletion, to name a few. A fixation on climate change to the exclusion of other considerations has repeatedly been shown to be detrimental to human welfare. One example is the expansion of biomass plantations into agricultural land and even rainforests. This has been recognised as undesirable, and it is now common for analyses of biomass production and usage to include constraints on land and water use, while maximising life-cycle GHG emissions savings or minimising costs (Fajardy and Mac Dowell, 2017). Another example is the UK's vehicle scrappage scheme which ran from May 2009 to February 2010: cars older than 10 years could be traded in for a 2000 GBP discount on a new, more efficient car, funded half-and-half by government and the manufacturer of the new car (Harari, 2009). Many of the new cars bought through the scheme were diesel vehicles, whose superior fuel efficiency led to reduced per-mile CO_2 emissions compared to petrol vehicles. However, the greater NO_x emissions of diesel vehicles contribute to urban air pollution. The extent of the problem has been deemed bad enough for the UK government to reverse their support for diesel vehicles, announcing that sales of petrol and diesel vehicles will be banned by 2040 (Petroff, 2017).

The techniques of Life Cycle Analysis (LCA) were developed to produce a more holistic picture of different environmental impacts of a given process. LCA involves calculating the impacts across the lifetime of a product, including its manufacture (cradle-to-gate), usage and disposal (cradle-to-grave) or recycling (cradle-to-cradle). An LCA proceeds first by presenting the goal and scope: identifying the unit processes that constitute the system under study, defining boundaries for what is and isn't included in the analysis, choosing the scenarios to be compared, and defining the functional unit (Klöpffer and Grahl, 2014). A life cycle inventory is then conducted: inputs (materials and energy) to each unit process are quantified (Klöpffer and Grahl, 2014). The next stage is life cycle impact assessment, where impacts are calculated and totalled using the results of the life cycle inventory and the conversion factors of whichever framework is being used (Klöpffer and Grahl, 2014), on which more below. Impacts are reported per functional unit - in this work, per kWh consumed, in keeping with MCoE. An interpretation stage discusses these results, comparing scenarios, putting them in context. This may involve normalising by a baseline scenario to find relative percentage changes, or by the total impacts in a country or globally, to find the relative significance of the process under study. The interpretation also involves analysing the results' sensitivity to relevant parameters and which unit processes are dominant, and if within scope, recommending further actions (Klöpffer and Grahl, 2014).

ISO 14040 (ISO, 2006a) and 14044 (ISO, 2006b) govern the conduct of LCAs. They require the inclusion of the sections described above, and set out the correct procedure to follow, where an organisation commissions an assessor to conduct the LCA, and a committee reviews the results in order to judge

compliance with the ISO standards. The standards aim to ensure transparency, reliability and comparability of results. That said, the LCA analyst has freedom to choose which framework to use in order to best achieve the aims set out in the LCA goal and scope. The CML2001 framework was commonly used until recently: it defines conversion factors between a comprehensive range of chemical emissions and environmental impact categories: global warming, acidification, eutrophication, ozone depletion, human toxicity, ecotoxicity and metals depletion (Dreyer et al., 2003).

CML2001 has been superseded in many areas by ReCiPe, which aimed to cover a wider range of so-called midpoint impacts, and relate them to three endpoint impact categories: human health, natural ecosystems, and natural resources. The 18 midpoint indicators (Table 1.2) cause impacts in one or more of the endpoint categories. Through reviewing physical models and ecological and medical studies, conversion factors have been calculated for the contribution of any chemical waste product emitted to each of the midpoint impacts, and for each of the midpoint impacts to each endpoint impact (Goedkoop et al., 2008a). Work has been published relating the conversion factors in a number of different LCA frameworks: for example, Owsianiak et al. (2014) relate IMPACT, ReCiPe and ILCD to each other, and Dreyer et al. (2003) compared EDIP97, CML2001 and Eco-indicator 99.

The development of LCA frameworks is an active area of research. The models and data used to quantify the conversion factors are continually improving. Surveys of public opinion build an increasingly comprehensive picture of what is valued in the environment, and what impacts are important to consider. Goedkoop et al. (2008a) themselves state of ReCiPe that due to lack of reliable data, it neglects to fully account for impacts on the man-made environment: "Corrosive pollutants affect buildings, roads, cars and other structures. Climate change may flood cities or agricultural areas, and may also cause hurricanes to destroy our built environment. Plagues of insects may eat our crops. And increased UV levels may deteriorate many man-made facilities."

Furthermore, scientific consensus and public opinion themselves change over time. While this active research is a good thing, it makes it difficult to find up-to-date environmental impact data for different system components reported under the same framework, which is necessary to conduct an LCA. The ReCiPe framework was chosen for this work, as most of the required data are reported either under this framework, or ones where conversion to ReCiPe is possible, such as through the work of Owsianiak et al. (2014).

A summary is given here of the ReCiPe midpoint impacts listed in Table 1.2, their main sources, and the mechanisms by which they contribute to the endpoint impacts of human health, natural ecosystems, and natural resources.

Acronym	**Midpoint Impact**	**Unit**
CC	Climate Change	kg CO_2-eq
OD	Ozone Depletion	kg CFC11-eq
HT	Human Toxicity	kg DCB-eq
POF	Photochemical Oxidant Formation	kg NMVOC-eq
PMF	Particulate Matter Formation	kg PM10-eq
IR	Ionising Radiation	kg U235-eq
TA	Terrestrial Acidification	kg SO_2-eq
FE	Freshwater Eutrophication	kg P-eq
ME	Marine Eutrophication	kg N-eq
TET	Terrestrial Ecotoxicity	kg DCB-eq

FET	Freshwater Ecotoxicity	kg DCB-eq
MET	Marine Ecotoxicity	kg DCB-eq
ULO	Urban Land Occupation	m^2·a
ALO	Agricultural Land Occupation	m^2·a
NLT	Natural Land Transformation	m^2
WD	Water Depletion	m^3
MD	Metal Depletion	kg Fe-eq
FD	Fossil Depletion	kg oil-eq

TABLE 1.2: ReCiPe midpoint impacts (Goedkoop et al., 2008a). '-eq', meaning -equivalent, is omitted for conciseness in the rest of the thesis.

Climate Change: GHGs mainly from fossil fuel combustion are emitted into the atmosphere and cause radiative forcing. Laboratory studies determined the infra-red radiative absorption strength of each GHG (methane, etc.) relative to the reference substance, CO_2. The resultant temperature rise leads to increased flooding, malaria, malnutrition, cardiovascular disease, diarrhoea, and loss of natural habitats, i.e. impacts on both human health and natural ecosystems (Goedkoop et al., 2008a, ch.3). Human health is measured in Disability-Adjusted Life Years (DALY), where 1 is a year of good health, 0 is a year dead, and different diseases are assigned a value between 0 and 1 for each year suffering with the disease (Goedkoop et al., 2008a, ch.2, p.7). Suffering is subjective and individual, but must be quantified in the aggregate for the whole affected population. Damage to natural ecosystems is measured in Potential Disappeared Fraction (PDF) of species. The value of each species relative to any other is a subjective matter, but it is generally accepted that a more biodiverse ecosystem (more different species co-existing) is more valuable, especially as it is more resilient to change. Uncertainties exist around the ability of species to disperse and occupy other regions in response to damage to their original habitat, rather than becoming extinct (Goedkoop et al., 2008a, ch.2, p.8).

Ozone Depletion: Ozone depletion catalysts (whose strength is reported relative to the reference chlorofluorocarbon CFC11) mainly from aerosols and refrigerants, catalyse breakdown of atmospheric ozone by free radicals. The absorption of solar ultraviolet radiation by ozone is thus reduced, leading to increased incidence of skin cancer and cataracts (Goedkoop et al., 2008a, ch.4).

Toxicities (Human, Terrestrial, Freshwater, Marine): Various substances (whose toxicity is reported relative to the poison dichlorobenzene, DCB) enter the air, water or soil. These enter humans through inhalation, or ingestion of crops, animal products, or drinking water, where they cause diseases, or accumulate in the soil, bodies of freshwater, and oceans, where they cause death of plant and animal species. The DCB-equivalent toxicity of each substance takes account of its solubility and degradation half-life when broken down by light, water or biological processes. For human toxicity, the passage of substances is modelled at continental scale with urban/rural distinction, accounting for population and diet. Data on resultant human disease incidence comes mainly from animal testing (Goedkoop et al., 2008a, ch.7).

Air Pollution (Photochemical Oxidant and Particulate Matter Formation): Both categories lead to respiratory diseases through inhalation. In the case of POF: Non-Methane Volatile Organic Compounds (NMVOC) emitted by various chemical processes, including outgassing of paints and varnishes inside buildings, form low-atmospheric ozone through photochemical reactions. In the case of PMF: SO_2, NO_x, NH_3, and PM10 (particulate matter on the scale of 10 μm) from fossil fuel burning, and car tyre wear,

brake dust, etc. react to form particulate matter including SO_4^{2-}, NH_4^+, NO_3^-, PM2.5s and PM10s (Goedkoop et al., 2008a, ch.8). Air pollution is estimated to cause over 4 million deaths worldwide annually (World Health Organisation, 2019).

Ionising Radiation: Radionuclides, mainly from mining and processing of nuclear fuels, are transported and dispersed (accounting for decay half-life). Radiation exposure through inhalation or ingestion of radionuclides, or external irradiation, leads to cancers and some hereditary effects (Goedkoop et al., 2008a, ch.9). Data come from animal testing and ongoing from survivors of the 1945 Hiroshima bombing and the 1986 Chernobyl accident. Note that the Linear No Threshold (LNT) assumption, where incidences of disease rise linearly with radiation dose, is widely believed to be inaccurate. Consensus is growing for a sigmoidal model, where radiation causes insignificant harm below a threshold, and the steepest rise in harm occurs around the threshold level. A 'dose and dose-rate effectiveness' approximation to this is made in ReCiPe, taking the disease incidence as linear with dose, but reducing by a factor of 2 for very low doses. There is uncertainty as to the value of this factor, and the threshold level (Goedkoop et al., 2008a, ch.9, p.85).

Terrestrial Acidification: SO_2, NO_x, NH_3, from fossil fuel burning and various chemical processes, flow into the atmosphere. They cause acid rain, leading to a reduction in soil pH. Excessive soil acidity is detrimental especially to plant growth, causing loss of plant species, and other species of organisms dependent on them (Goedkoop et al., 2008a, ch.5).

Eutrophication (Freshwater and Marine): Phosphorus and nitrogen, from manure, fertiliser, and wastewater treatment, run off soil into waterways. They encourage growth of phytoplankton, restricting light and oxygen available in freshwater and marine environments. This change to the habitats causes loss of species (Goedkoop et al., 2008a, ch.6).

Land Occupation (Agricultural and Urban) and Natural Land Transformation: An area of land used for agriculture, or for industrial, commercial or residential uses, for a length of time, reduces the species diversity compared to a natural reference state. What is the natural state of a piece of land, is a contentious question. The definition used by ReCiPe is "the potential land use types [...], which would appear when no human influence takes place" (Goedkoop et al., 2008a, ch.10, pp.91-92). Number of species has been observed to vary sub-linearly with land area, and depends on border length, as biodiversity is concentrated in the hedges bordering farms, and connectivity of remaining natural areas. Land occupation often occurs after transformation from a previous use, but as land can be occupied without first transforming it, ALO and ULO is separated from NLT within ReCiPe. Depending on the transformation type (agricultural to urban, natural to agricultural, etc.), different restoration times are assumed. The longer it takes to restore occupied land to a natural state, the greater the damage to biodiversity (Goedkoop et al., 2008a, ch.10).

Water Depletion: Consumption of freshwater without re-release (i.e. it evaporates, is incorporated into products, or is discharged into the sea) means less water available for irrigation, reduced volume of rivers and lakes, and less water entering the soil. This leads to human malnutrition, and reduced diversity of plant and freshwater fish species. This category was added in ReCiPe 2016, having lacked the necessary data to quantify relevant conversion factors previously (Huijbregts et al., 2016, ch.10).

Metals Depletion: Each kg of material extracted from a mineral deposit lowers the deposit's grade, that is, it is harder to extract more. This increases mining costs, which when summed over all deposits

worldwide for that material, marginally increases the commodity price. This is a cost to society, from increasing the price of non-renewable resources (Goedkoop et al., 2008a, ch.12).

Fossil Depletion: Like other minerals, fossil fuels are a non-renewable resource (or as good as, since they take millions of years to form under anaerobic compression of dead organic matter). Unlike MD, the increase in coal, oil and gas prices that results from depletion of existing reserves, is due to the higher costs of extracting from unconventional sources such as shale oil and hydraulic fracturing (fracking), more than from lowering the grade of existing reserves (Goedkoop et al., 2008a, ch.13). Note that FD is distinct from CC: significant damage can occur from burning a fraction of the fossil reserves in the ground, while reserves can be depleted with minimal CO_2 emissions if those emissions are captured and stored, or if they are used in non-emitting applications, such as oil for manufacturing plastics.

It is important to understand the limits of LCA. An LCA is not a risk assessment, which assigns probabilities to hazardous outcomes and stipulates preventive and corrective measures for avoiding and dealing with such outcomes. LCA seeks to answer the question 'How sustainable is this product or process?' by analysing a wide range of impacts across the product lifetime. However, true sustainability places requirements on the social aspects (job creation, use of child labour, visual or aesthetic 'pollution', etc.) and financial aspects (whether the system pays for itself), not just the environmental (Klöpffer and Grahl, 2014).

Note also that the judgements of an LCA are not fixed for all time. As an example, Stamford and Azapagic (2018) analysed the life-cycle impacts of PV installations in 2005 and 2015, finding an almost 50 % reduction in per-kWh impacts for most of the 11 CML categories they analysed, and ozone depletion in 2015 around a quarter of what it was in 2005. This is due to a combination of factors: the roughly 50 % improvement in PV cell efficiency over this time period, gaining more kWh from almost the same materials over the panels' lifetime; the reduction in thickness and weight of both glass and silicon used; reduction of waste in processes such as sawing the silicon wafers and metallising the back contacts with silver paste; swapping out materials such as the highly ozone-depleting tetrafluoroethylene for the less ozone-depleting NF_3 which is used primarily in cleaning chemical vapour deposition chambers. Industrial processes change, and the power of an LCA is to direct those changes.

In the case of this thesis, the findings of an LCA should be of interest to many different parties: environmentally-conscious homeowners who would take the information into account when deciding to purchase a PV-battery installation; the manufacturers and suppliers of PV panels, home batteries and associated equipment, to better appeal to the environmentally-conscious segment of the market. Government policy-makers are a particularly important audience: in assessing what part PV and domestic batteries may play in meeting national and international environmental targets, they may decide on policies to encourage such a market, or implement regulatory measures to mitigate any harm that may result as an unintended consequence, for example if CO_2 is saved but at the cost of greater metals depletion.

1.3 Domestic PV-Battery Systems

This section presents a survey of the existing literature on domestic PV-battery systems. First, the topic is put into context: other types of energy storage and other applications for them, from different parts of the world, are discussed. Existing techno-economic and environmental analyses of domestic PV-battery systems are then reviewed. There follows a discussion of the concept of second-life electric vehicle (EV)

batteries and the advantages they might offer above new batteries. The section closes with a summary of the current state of the research and what gaps exist in it. All this informs the research question and thesis structure, presented in the next section.

1.3.1 The wider world of energy storage

In the face of climate change, many countries are developing plans to reduce or even eliminate their GHG emissions. The majority of emissions originate from fossil fuel combustion to generate energy for heat, transport and electrical power. Consequently most plans center around shifting heat and transport to alternative fuels such as hydrogen, biomass, and electricity, while decarbonising electrical power generation. The fastest-growing low-carbon power sources are solar PV and wind, whose installed capacities have historically been increasing at 60 % and 20 % per year respectively (Carbajales-Dale et al., 2014), though this has slowed to 24 % and 10 % in recent years (IRENA, 2019). 486 GW of PV and 564 GW of wind capacity had been installed globally by the end of 2018 (IRENA, 2019), compared to a global electrical consumption of 26 700 TWh in that year, or on average 3048 GW throughout, itself less than a fifth of total energy consumption (IEA, 2019).

Unlike other low-carbon sources such as biomass, hydroelectric, geothermal and nuclear power, wind and solar power generation are intermittent and cannot be dispatched by a controller. This means some means of shifting supply to match demand is needed. Transmission networks shift supply spatially, and have been used for nearly a century to transport electrical energy from generation plants to load centres. Energy storage offers another option, by shifting supply temporally.

99 % of the bulk energy storage that exists in the world today is pumped hydroelectric storage (PHS), at a total of 129 GW (Luo et al., 2015). It is used primarily for energy arbitrage, that is, buying electricity when it is cheap in order to pump water from a lower reservoir to a higher one, and releasing water through a turbine to generate electricity when it is expensive. An electricity market ensures that electricity is cheap when supply is plentiful, and vice versa (Elexon, 2015). Thus the PHS station is rewarded for smoothing the supply-demand imbalance, as long as its earnings cover the roughly 25 % round-trip energy conversion losses (Luo et al., 2015).

In Great Britain (GB) and other countries where such market arrangements exist, energy storage also offers ancillary services such as reserve power and frequency response (National Grid, 2016b). In the case of reserve, the storage device operator would ensure a sufficient state of charge throughout the hours for which reserve is contracted. The transmission system operator (TSO - in GB, this is National Grid) can then call on the reserve in an emergency: when electrical demand is higher or increases faster than expected, or supply drops through an unexpected fault (National Grid, 2018c). Frequency response, also known as 'area regulation' in the USA, is the injection of power to the grid when its frequency drops below nominal (50.0 Hz in Europe, 60.0 Hz in the USA), and the absorption of power from the grid when frequency rises above nominal. Grid frequency deviates from nominal when there is an imbalance between electrical supply and demand; frequency response helps to correct the imbalance, which if left uncorrected, can affect the functioning of electrical appliances and in extreme cases, destabilise the grid (Klimstra, 2014). How these services are rewarded varies from country to country.

Ancillary services have so far been provided mostly by fossil-fuelled generators operating at a few percent below their maximum power so they have head-room to increase generation when needed. This means sub-optimal efficiency and therefore more GHG emissions. Furthermore, ancillary services must be

sourced from elsewhere if climate change targets render fossil-fuelled plants uneconomical or force them to shut down (Klimstra, 2014).

As well as PHS, other technologies exist with various capabilities and in various stages of development. These are summarised in Table 1.3 based on the review by Luo et al. (2015).

Acronym	**Storage Technology**	**Description**
PHS	Pumped Hydroelectric Storage	Gravitational potential energy is stored by pumping water from a lower reservoir to a higher one, and released by allowing water to flow back down through a turbine-generator, usually the pump operating in reverse. Requires appropriate geography such as mountain lakes, and/or significant construction work.
CAES	Compressed Air Energy Storage	Potential energy is stored by compressing air to high pressure; when it is needed again, the air is released through turbine-generators. Research has been conducted into different options for storing the high-pressure air: salt caverns, high-pressure gas storage tanks, under-sea balloons. The process is made more thermodynamically efficient by cooling the air before storing it, and warming before releasing it. The energy requirement for this can be minimised by effective use of heat exchangers.
FES	Flywheel Energy Storage	Kinetic energy is stored by spinning up the flywheel (a mass, most practically a cylinder made of steel or carbon fibre) via an electric motor; and released by running the motor in reverse as a generator, driven by the spinning mass which slows down as it loses kinetic energy.
PbA	Lead-acid battery	Electrochemical energy is stored via redox reactions converting lead sulphate in the electrodes and water in the sulphuric acid electrolyte, into lead and lead oxide. The redox reactions are reversed when the battery is discharged, releasing electrons into the external circuit. A polymer separator between the electrodes is designed to prevent short-circuit and self-discharge. PbA batteries are very common, being used as starter batteries in all motor vehicles except the most modern EVs.
Li-ion	Lithium-ion battery	Electrochemical energy is stored by the intercalation of lithium ions into the positive electrode, and released by their de-intercalation (the reverse happens at the negative electrode). Like PbA batteries, the electrolyte allows ion flow while the separator insulates against electron flow. Li-ion batteries are the most common energy store in EVs, being more energy-dense and longer-lasting than PbA.

Acronym	**Storage Technology**	**Description**
FB	Flow Battery	Rather than storing energy in the electrodes as PbA and Li-ion do, flow batteries store energy in the electrolyte. A typical setup consists of tanks for the electrolyte and pumps to regulate its flow across the electrodes, which connect to the external circuit like in other battery types. But unlike other types, the tank size and electrodes surface area, and hence the energy capacity and power capacity respectively, can be varied independently.
Supercap	Supercapacitor	Electrical potential energy is stored in a capacitor by charging up the electric field in the dielectric (insulator) separating two conducting surfaces, and released into the external circuit by discharging them, reducing the potential difference between them. What distinguishes a supercapacitor is the formation of a microscopic double layer at each electrode: the field across such a small thickness can be much greater than that across the roughly 0.1 mm thickness of the dielectric in a normal capacitor, meaning a much greater energy density for a supercapacitor.
SMES	Superconducting Magnetic Energy Storage	Energy is stored in the magnetic field formed by charging up a coil made of superconducting cable. The current that gives rise to the magnetic field persists indefinitely without resistance as long as the superconducting state is maintained. This requires cooling to below -200 °C, which consumes energy. Research is ongoing into creating materials that remain superconducting at higher temperatures.
H_2	Hydrogen	Chemical energy is stored by electrolysing H_2 from water; H_2 can be stored as a compressed gas or liquefied and stored in a cooled tank; heat energy can be released by combusting H_2 in air, or electrical energy by inputting H_2 to a fuel cell.
TES	Thermal Energy Storage	This can be as simple as heating up water in an insulated tank, but can refer to the heating (or cooling), storage and energy release of any material. Certain types of wax that melt at moderately low temperature are particularly effective because they remain at the same temperature throughout the phase change. A similar principle applies to liquid air energy storage (LAES), but cooling to 'charge' the system. Also of note are TES systems where heating drives a chemical reaction, whose products are stored separately, and only brought back into contact when the stored energy needs to be released. All the other storage types mentioned convert the stored energy into electricity upon release, except H_2 when combusted. However, the release of heat energy directly can be useful for heating and cooling applications.

TABLE 1.3: Characteristics of different types of energy storage (Luo et al., 2015).

Apart from PHS, PbA and Li-ion, most of these energy storage technologies are not widespread. In some cases there are technical reasons for this, but in many, the economics of the systems and the markets in which they could operate are such that they tend to fulfil only niche applications, or provide short-term frequency response services, if any at all. For example, the two flywheels at Culham Centre for Fusion Energy are slowly spun up using electricity from the grid and very quickly discharged to power equipment used in their experiments; otherwise powering the equipment directly from the grid would put unacceptable strain on the local network. As another example, National Grid put out a call for tenders in 2016 for an Enhanced Frequency Response service: the contracted party must be able to inject or absorb power from the grid in proportion to the frequency deviation from nominal, responding in under 1 s during all contracted hours, and when needed, maintaining the contracted maximum power for at least 15 minutes (National Grid, 2016a). All eight winning tenders were battery systems.

After PHS, batteries are arguably the next most mature energy storage technology. Li-ion batteries in particular have fallen in price by 85 % from 2010-2018 (Goldie-Scot, 2019). This is most likely due to their adoption as the energy source for EVs, and subsequent continuing development by car manufacturers, with technology transfers into other applications such as grid-level and domestic storage. For some years, much research and development was conducted into H_2 with fuel cells as an alternative to petrol and diesel. Even for domestic storage to accompany rooftop PV, not just batteries but some TES options can be suitable at this small scale, even if most of the technologies listed in Table 1.3 are not. There is some evidence that hot water tanks are more economical than batteries (Parra et al., 2016). Indeed, domestic TES systems are commercially available, including the Sunamp (2019) 'heat battery' which electrically heats up an "innovative material" with excess PV electricity, discharging the heat for domestic hot water when needed. Wilson et al. (2013) showed that daily demand for natural gas in the whole of GB (for space heating, water heating and cooking) is highly variable throughout the year, from just over 1 TWh/day in summer to over 4 TWh/day in winter, compared to a daily electrical demand that varies between roughly 0.75-1.2 TWh/day.

The reasons for batteries becoming the dominant technology include socio-economic as well as technical ones. The work of Tesla Motors in the EV sector has attracted much press coverage, as have their other ventures into home battery products (Merchant, 2019) and the 100 MW, 129 MWh Big Battery which was commissioned by the South Australia government to provide 70 MW of reserve power, fearing another blackout like the one in September 2016 which cut power to the region for 50 hours. The Tesla Big Battery's success in responding to the fault on 14 December 2017 at the Loy Yang generator 1000 km away has been much touted: the battery injected 7.3 MW power into the grid 140 ms after the frequency fell to 49.8 Hz, preventing further instability for a crucial 4 s until other power stations managed to react and restore the frequency to 50.0 Hz, 6 minutes later (Zeng et al., 2018).

Such is the confidence in battery technology that the World Bank Group has committed one billion USD to an "Accelerating Battery Storage for Development" programme, to "finance and de-risk investments such as utility-scale solar parks with battery storage, off-grid systems - including mini-grids - and stand-alone batteries that can help stabilize and strengthen grids", with a view to mobilising up to 4 billion USD altogether (World Bank, 2018). IRENA (2017) predicts battery storage in stationary (non-transport) applications to grow from 2 GW in 2017 to 235 GW in 2030. It is within this context of mature but continuing development that batteries in domestic contexts are discussed next.

1.3.2 Existing techno-economic analyses of domestic batteries

There have been many studies published on the economics of domestic PV-battery systems based on computer modelling. One by Mulder et al. (2013) is described in detail first, being a relatively early exemplar, and then compared to others based on aspects on which they differ. Refer back to Section 1.1 for explanations of any unfamiliar terms.

Mulder et al. (2013) conducted a modelling study, using a full year's electricity consumption (load) data measured at 15-minute resolution from 65 Belgian houses and 4 measured PV generation time series as input. The battery operating algorithm they modelled is thus:
- When PV generated power exceeds load, charge the battery with the excess,
- If the battery is full or its charging power limit is exceeded, export the excess to the grid,
- When load exceeds PV power, discharge the battery to meet the load,
- If the battery is empty or its discharging power limit is exceeded, import the remainder from the grid.

It is called the Greedy Algorithm by Truong et al. (2016) but is used so commonly in other papers without being named (Bertsch et al., 2017; Hoppmann et al., 2014; Kirmas and Madlener, 2017; Muthuvel et al., 2016; Naumann et al., 2015; Weniger et al., 2013), that for convenience it will be referred to as the Greedy Algorithm from hereon in. The popularity of the Greedy Algorithm, even in commercial battery products at least until recently, can be explained by its simplicity (not requiring any forecasting of load or PV generation, nor tuning of threshold parameters to determine charge/discharge modes) and the fact that it minimises import of electricity from the grid. This is equivalent to minimising costs under a flat-rate tariff, but is not the case for tariffs that vary throughout the day (time-of-use tariffs, ToU) (Mulder et al., 2013).

Mulder et al. (2013) calculated IRR, NPV (with 4.5 % nominal discount rate, 2 % inflation rate, 20-year temporal boundary) and PP, using grid import/export and battery charge/discharge time series that result from applying the Greedy Algorithm to the input data, timestep by timestep. They calculated these metrics under many different scenarios:

- Varying PV capacity (0-8 kW_p),
- Varying battery capacity (0-15 kWh),
- Different rates of electricity retail price increase (0, 4, 6 %),
- Different initial investment year (2012, 2017, 2021),
- Varying export payment and subsidies awarded for self-consumption (0.24-0.00 EUR/kWh).

The PV and battery costs were scaled according to their capacities, and battery cost was assumed to decline over time. Additionally, PbA and Li-ion batteries were compared by modelling them with different parameters: cost per kWh capacity, depth of discharge (DoD), efficiency, calendar life, cycle life (the latter two determining when the battery must be replaced).

They found the strongest driver of financial value was the rate at which electricity retail price would increase: the faster it increases, the greater the optimal PV and battery sizes (in terms of maximising IRR), with no battery being optimal if the retail price remains the same over 20 years. This is because the Greedy Algorithm reduces exposure to the retail price, which when it is higher, makes it more worthwhile to invest more in PV and battery to further avoid exposure to it.

The longer the homeowner delayed investment, the greater the optimal battery size, as the cost per kWh declines over time. In fact, the optimal size of Li-ion battery was zero for investment in 2012, regardless of electricity price increase in future, but waiting to 2017 or 2021 could achieve IRR (including inflation) between 1.5-5 times the postulated discount rate.

The removal of subsidies for self-consumption and the reduction of export payments reduced the optimal PV size, from 8 kW to 1-6 kW (greater for later investments and faster electricity retail price increases). At the time, PV installed costs were 1.51-1.72 EUR/W_p, similar to costs today. The effect of subsidies and benefits on optimal battery size was small, but reducing them tended to favour slightly larger batteries.

The first aspect for comparison is geographic location. This has an impact on PV generation, which is greater per kW_p installed for locations closer to the equator and with less cloud cover. The load profiles (time series) used for input may also differ: in Australia (Farah et al., 2016) and Las Vegas (USA) (O'Shaughnessy et al., 2018), for example, air conditioning is commonly used in the day/afternoon but is not installed in most houses in Northern/Western Europe; electric space heating and hot water are common in France, where they are encouraged to make use of copious off-peak nuclear-generated electricity during the night (Yu, 2018); electricity consumption in India tends to be lower overall and varies more between households compared to in developed countries, where social norms tend to affect electricity use patterns more strongly (Muthuvel et al., 2016). Electricity tariffs also differ between countries and regions, in terms of both price levels and structures. Electricity unit (per kWh) prices in Germany tend to be high compared to the rest of Europe, while those in France tend to be low (Yu, 2018). Flat-rate tariffs are common in most countries surveyed, but ToU tariffs, where different prices are charged at peak/off-peak periods in order to smooth out consumption across the day, are more common in countries where peak load is considered more problematic, due to both the size of coincident load and the large areas spanned by transmission lines, making them costly to upgrade if they prove inadequate to transmit power during peak periods. Australia (Farah et al., 2016; Muenzel et al., 2015) and the USA (O'Shaughnessy et al., 2018) are two such examples. For the same reasons, demand charges are almost unheard of in Europe, at least for residential consumers, but many electricity suppliers in the USA and Australia charge customers a fee per kW per month (O'Shaughnessy et al., 2018) or per day (Farah et al., 2016) for their maximum power consumption during that time period. This has stimulated research into battery operating strategies that can reduce peak consumption and therefore exposure to demand charges. O'Shaughnessy et al. (2018) and Farah et al. (2016) both found the economics at the time to be mostly unfavourable to using batteries for this application, despite finding them technically capable of doing so.

Germany appears to have been the most popular location for techno-economic studies of domestic PV-battery systems (Bertsch et al., 2017; Hoppmann et al., 2014; Naumann et al., 2015; Truong et al., 2016; Weniger et al., 2013). This is unsurprising considering the high retail price of electricity, which tends to encourage self-consumption of onsite PV electricity (immediately or after storage) in order to reduce exposure to the high cost of grid import, and the generous FiT and self-consumption subsidies that were available. (Hoppmann et al. (2014) did explicitly consider scenarios where subsidies were no longer available.) Even so, financial savings were not guaranteed, for the most part dependent on how electricity prices will evolve in future, and the annualised cost of the battery (improved by lower up-front cost and longer lifetime). At the other extreme, no FiT nor export payments could be earned in Spain, and self-consumption was taxed rather than subsidised (Prol and Steininger, 2017). The result of this was IRR < 0 for domestic PV-battery in all scenarios considered, though IRR > 0 could be achieved if export payments were as little as 0.05 EUR/kWh. Studies have also been conducted for Irish (Bertsch

et al., 2017) and English (Hassan et al., 2017; Uddin et al., 2017) contexts. They all found investment in a battery not financially worthwhile at the time, compared to PV only, though it could be if battery costs fall or electricity prices rise sufficiently in future. An appropriately sized PV array on its own was already profitable in England, as was the case in all the German studies, but not in Ireland, where the subsidy regime was less favourable.

Secondly, techno-economic analyses of domestic PV-battery systems differ in terms of input data used. Some use real measured PV (Naumann et al., 2015) and load time series (Bertsch et al., 2017), or both (Farah et al., 2016; Muenzel et al., 2015; Mulder et al., 2013; Truong et al., 2016), while others simulate PV generation from weather data (solar irradiance and temperature) (Bertsch et al., 2017; Hoppmann et al., 2014; Weniger et al., 2013). Some use standard load profiles (Hassan et al., 2017; Hoppmann et al., 2014; Weniger et al., 2013), or load profiles synthesised by adding the consumption of different appliances in a bottom-up fashion (Muthuvel et al., 2016; Naumann et al., 2015; O'Shaughnessy et al., 2018). Real measured data are preferable to artificial synthesised data, but the former may not be available for the region in question, and can be time- and resource-intensive to collect.

There are issues with using data of too low a time-resolution, as is often the case when PV generation is synthesised from weather data that is only available at half-hourly (Bertsch et al., 2017) or hourly resolution (Hoppmann et al., 2014); and if data have been averaged from many time series, as Hassan et al. (2017) effectively did in using Sheffield PV Live data, which are half-hourly PV generation in the whole of GB, synthesised from measured data from many sources. Both low resolution and averaging across datasets have the effect of smoothing out peaks in the data, over-stating the overlap between load and PV generation. The impacts of this on financial calculations are discussed in detail in Chapter 5. Additionally, GB solar PV capacity is increasing all the time as new installations are brought on line: a single household would not increase their PV capacity in the same way, calling into question the validity of using scaled-down PV Live data as input to modelling such a context.

Thirdly, the metrics used to evaluate financial value differ between studies. This has been discussed already in Section 1.1, but to recap:

- NPV: taking discount rates r of 1 % (Bertsch et al., 2017); 4 % (Camilo et al., 2017; Hoppmann et al., 2014; Truong et al., 2016); 4.5 % nominal (Mulder et al., 2013); 5 % nominal (Farah et al., 2016); 6 % (Muthuvel et al., 2016); 6.2 % (O'Shaughnessy et al., 2018). (Unclear if nominal or real discount rates if not stated.) Inflation rates 2 % (Bertsch et al., 2017; Mulder et al., 2013; Truong et al., 2016), 2.1 % (Hoppmann et al., 2014), 2.5 % (Farah et al., 2016). (Not given in the papers if not stated here.) Temporal boundary N of 20 years (Bertsch et al., 2017; Farah et al., 2016; Truong et al., 2016), or 25 years (Camilo et al., 2017; Hoppmann et al., 2014; Mulder et al., 2013; Muthuvel et al., 2016). Note that Hoppmann et al. (2014) calculated the NPV per EUR invested in the battery, rather than just NPV, and Muthuvel et al. (2016) and Farah et al. (2016) calculated LCC, which is -NPV. O'Shaughnessy et al. (2018) did not state the temporal boundary for their calculation.

- IRR: calculated by Bertsch et al. (2017); Mulder et al. (2013) taking $N = 20$ years, and by Camilo et al. (2017); Prol and Steininger (2017) with $N = 25$ years.

- RoI: calculated by Camilo et al. (2017); Naumann et al. (2015); Truong et al. (2016) taking discount rate 4 %, and by Yu (2018) with 5 %. Naumann et al. (2015); Truong et al. (2016); Yu (2018) took $N = 20$ years while Camilo et al. (2017) took $N = 25$ years. Yu (2018) called this metric PI rather

than RoI but defined it the same as equation (1.5). Camilo et al. (2017); Naumann et al. (2015) included costs over the lifetime in the denominator, not just Capex; Naumann et al. (2015) still called this RoI, while Camilo et al. (2017) called this PI.

- MCoE: calculated by Weniger et al. (2013) taking discount rate 4 % and temporal boundary 20 years. Yu (2018) calculated LCoE with 5 % over 20 years, and Camilo et al. (2017) with 4 % over 25 years.
- PP: Mulder et al. (2013) and Muenzel et al. (2015) calculated this without discounting, while Camilo et al. (2017) calculated DPP with discount rate 4 %.

The sensitivity of these metrics to various parameters was analysed: like Mulder et al. (2013), the sizing of both PV and battery capacities was explored by Weniger et al. (2013) and Hoppmann et al. (2014); Truong et al. (2016) varied PV capacity while keeping battery capacity at 6.4 kWh, emulating a Tesla Powerwall, while Naumann et al. (2015) varied battery size given a fixed PV capacity of 4.4 kW_p. Sensitivity to electricity retail price increase was also commonly studied (Hoppmann et al., 2014; Muenzel et al., 2015; Mulder et al., 2013; Naumann et al., 2015; Truong et al., 2016), as were variations in FiT subsidy (Mulder et al., 2013; Truong et al., 2016; Weniger et al., 2013) and export payment rate (Hoppmann et al., 2014; Mulder et al., 2013), and cost of storage (Naumann et al., 2015; Weniger et al., 2013). Weniger et al. (2013) also varied the azimuth angle (how far east or west the PV array points), finding it has minimal effect on MCoE. Bertsch et al. (2017); Truong et al. (2016) compared households of different annual consumption totals, finding the economics of PV-battery more favourable for higher-consuming ones.

Fourthly, it should be noted that there is variation in the modelling details used in the studies reviewed: Farah et al. (2016); Mulder et al. (2013); O'Shaughnessy et al. (2018) neglect degradation in PV and battery, while Hoppmann et al. (2014) and Muenzel et al. (2015) model the PV generation capacity degrading at 0.5 % per year, Camilo et al. (2017) at 0.75 %, Bertsch et al. (2017) at 1 %, and Weniger et al. (2013) at the remarkably optimistic value of 2 % over 20 years. Muenzel et al. (2015) used a cycle-counting method to account for battery degradation, but only in terms of the capacity reducing with cycling. Naumann et al. (2015); Truong et al. (2016) did similarly but combined with calendar aging too. Uddin et al. (2017) conducted detailed experiments into battery degradation of a PV-battery (Li-ion) system installed at a house in Loughborough (UK), finding that after only 5 years the battery's internal resistance had doubled and its capacity had reduced by 20 %. This would already be considered end-of-life (EoL) for an EV battery, although domestic batteries may be used for longer as energy density and power density are not such crucial considerations as in transport applications (Uddin et al., 2017). Even so, this calls into question the validity of neglecting the effect of battery degradation on both internal resistance (and therefore charge/discharge efficiency) and capacity, and the long lifetimes assumed by others: 20 (Muenzel et al., 2015; Weniger et al., 2013) or 25 (Mulder et al., 2013) years for Li-ion batteries, although Bertsch et al. (2017); Farah et al. (2016) account for one replacement within the 20-year temporal boundary they consider. As for O & M costs, Farah et al. (2016); Muenzel et al. (2015); Mulder et al. (2013); Truong et al. (2016) neglect them, while Camilo et al. (2017) include them at 1 % of Capex per year, Hoppmann et al. (2014); Naumann et al. (2015); Weniger et al. (2013) at 1.5 %, Muthuvel et al. (2016) at 2 %. Bertsch et al. (2017); O'Shaughnessy et al. (2018) include O & M costs relative to the PV capacity at respectively 10 EUR/kW_p/year and 20 USD/kW_p/year.

The studies mentioned above consider primarily the costs and benefits to the homeowner, who invests in and owns the PV-battery system under consideration. The existence of such systems has effects on

the wider network too. Each country or region has a nominal mains voltage, which the actual voltage should not deviate from by more than a given percentage (230 V -5/+10 % in the EU (Klimstra, 2014)), otherwise the functioning of consumer appliances is affected. Resistive and capacitive losses in power cables cause voltage to decrease slightly the further one goes along a distribution feeder away from a generator, whether a power plant or rooftop PV array. Most networks in developed countries were built without considering the effects of rooftop PV in raising the voltage. Consequently, over-voltage violations are becoming a more common occurrence (Tant et al., 2013).

Mahmud et al. (2016) explored the possibility of solving this problem using domestic PV-battery in combination with EVs that can discharge into the grid as well as charging from it (V2G, vehicle-to-grid). They modelled a hypothetical low-voltage network with 15 houses, 4 of which have an EV (with 24 kWh battery), 5 with rooftop PV (each 20.6 m^2), of which one has both PV and EV and a home battery (sizes 2-8 kWh were tested), the remaining 7 having neither. They designed operating strategies for the battery and V2G, and conducted load flow analysis of the modelled network. They demonstrated a reduction in voltage violations, both over- and under-, but performed no analysis of the economics for the distribution network operator (DNO, who is responsible for ensuring voltage remains within limits), nor the owners of PV, EV and battery.

Crossland et al. (2018) also used load flow analysis but modelled real networks extracted from data held by Electricity Northwest (ENWL, the DNO for the northwest of England). They found the most economical option to prevent over-voltage violations was for the DNO to install 25-kW 3-phase batteries at targeted locations on the network. The same effect could not be achieved by PV-owning homeowners in stochastic locations installing 3.6-kW batteries, even at three times the capacity of DNO-owned batteries, although such a cost would be borne by homeowners themselves rather than the DNO. In both cases, the DNO cannot avoid doing some work to upgrade power lines in future, as more households install rooftop PV over time, but these network upgrade costs can be reduced by the presence of batteries. However, the load flow analysis was only conducted at a single point in time, when electricity consumption is at its minimum and PV generation at its maximum, as that is the worst-case scenario for over-voltage. It was assumed that all batteries on the system could charge from PV at their maximum rate of 3.6 kW at that time, which Crossland et al. (2018) state might require programming into the battery operating algorithm. This is because the Greedy Algorithm very commonly results in the battery being full before noon after charging on excess PV electricity all morning (unless the battery is uneconomically large), meaning it cannot accept more charge to mitigate over-voltage violations on the network at its most problematic times (see Figure 1.1).

Hoppmann et al. (2014), Muenzel et al. (2015) and Bertsch et al. (2017) speculated on another effect that domestic PV-battery systems may have on the wider network: the so-called 'network death spiral'. When the installation of PV-battery allows a household to reduce the electricity it imports from the grid, this reduces the revenue taken by the electricity supplier and therefore the revenue passed on to the body responsible for maintaining the network. (In the UK, this is the DNO, required by law not to trade in electricity for reasons of fair competition, but in some countries the same entity is responsible for both maintaining the network and selling electricity to customers.) In an attempt to recover the lost revenue, electricity bills are increased, stimulating yet more households to install a PV-battery system in order to reduce their exposure to higher electricity prices.

Yu (2018) tested this hypothesis for the French national system, taking a budgeting rather than a detailed modelling approach, due to the prohibitive computational requirements of modelling 18.8 million houses

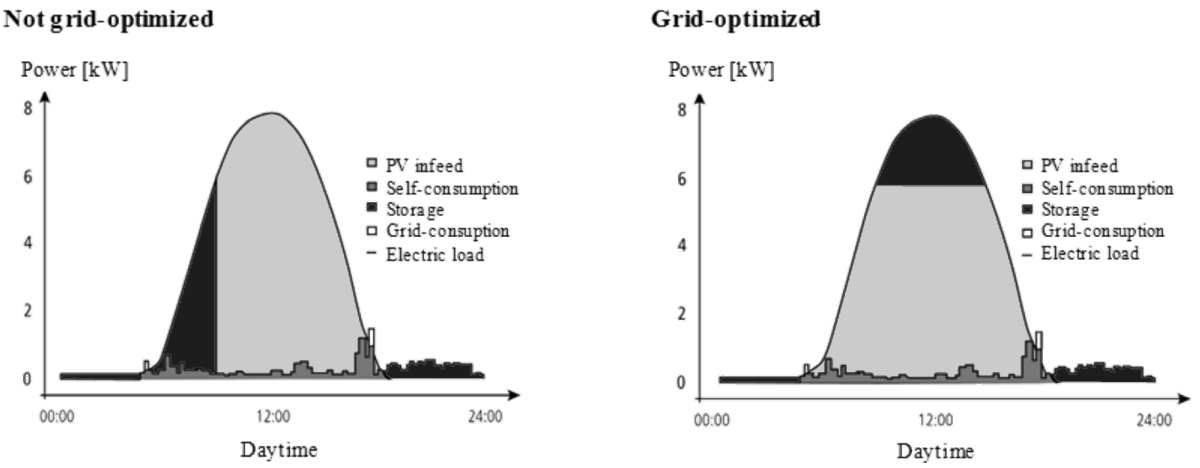

FIGURE 1.1: Illustration of energy stored and energy exported to the grid ('PV infeed') for the Greedy Algorithm (left), and one that limits the power exported to the grid (right) (Kirmas and Madlener, 2017).

individually. Under the extreme case of all 18.8 million installing 3 kW_p of PV, they estimated the costs of integrating this much PV (reinforcing the network, ensuring adequate reserve power and frequency regulation), finding it to be 1-2 billion EUR per year. The worst-case scenario would add roughly 0.005 EUR/kWh to the price of electricity, a 2.8 % increase. However, the costs would be at the lower end of that range if batteries were installed with PV, or if grid export were disallowed. They also estimated the impact on the nuclear generators which currently supply nearly 80 % of France's electricity: they would reduce production during times of high PV generation, as their marginal costs are more than that of PV, to an extent that they would be rendered uneconomical compared to coal and combined cycle gas turbines (CCGT). Some dispatchable plant would still be needed as backup during times of insufficient PV and wind generation, and so to ensure this plant is low-carbon nuclear rather than coal or CCGT, Yu (2018) estimated a carbon price of 93 EUR/ton CO_2 would be required.

Prol and Steininger (2017) conducted a similar budgeting analysis on the Spanish national system. They found the tax/incentives structure made PV-battery an attractive option for industrial consumers, less so for commercial ones, and unattractive to residential ones. They state that the effect of industrial consumers reducing their consumption of grid electricity would ironically have the worst impact on the network, whose operator is heavily indebted. However, they found that eliminating the self-consumption tax for residential consumers would have negligible impact on government tax revenue.

It is worth noting that there are many papers that explore the use of battery operating algorithms other than the Greedy Algorithm. Uddin et al. (2017), for example, made a measurement study rather than a modelling study of a PV-battery system that schedules charge/discharge based on the previous day's consumption, although further details were proprietary. Abdulla et al. (2017) and Muenzel et al. (2015) used dynamic programming to model scheduling the battery charge/discharge over a given rolling time horizon (24 hours in their case) in order to minimise net expenditure on electricity for houses in Australia (New South Wales and Melbourne, respectively). Dynamic programming works by choosing the action (charge or discharge, import or export, by how much) that minimises the cost function at every timestep, working recursively back from the last step within the optimisation horizon. Hassan et al. (2017) used a different optimisation procedure, mixed integer linear programming (MILP), a method to assign values to a vector (battery charge/discharge power requested at each timestep, in this case) in such a way as to minimise an objective function (net costs: electricity on a ToU tariff, minus revenue from FiT and export

payments), subject to linear constraints (power balance between PV, battery, load and grid, power and SoC limits on the battery, etc.). This method was also used by Babacan et al. (2018) with various different objective functions, on which more in the next section, and Li et al. (2015).

The application to which Li et al. (2015) put the MILP method was an aggregator scheduling charging/discharging of storage batteries (50 kW, 150 kWh) and smart charging of EV batteries (50 × 3.3 kW, 24 kWh) in an apartment block with rooftop PV (150 kW_p). The aggregator is an entity that can buy electricity from the grid at lower rates than are available to individual residential consumers, and is given permission by the apartment residents to control their batteries and the rate of charging their EVs, in exchange for selling electricity to them at a lower rate than they can buy it at individually from an electricity supplier, but with a profit margin for the aggregator. Attention is brought to this application because it is possible that individual households may opt to cede control of their own PV-battery to a virtual aggregator in exchange for some benefits, rather than collecting the savings of their individual system directly. With many systems under their control, an aggregator could bid into ancillary service markets that are not open to domestic consumers: frequency response in GB, for example, can only be provided by systems or aggregations of systems exceeding 1 MW in capacity (National Grid, 2016b).

Some experimental work has already been conducted into the concept of aggregation: the 'PowerMatching City' trial in Groningen, Netherlands from 2007-2014 used the ISGAN (2019) software, which enables PV, batteries and consumer appliances to bid into a continuous virtual auction, the results of the auction determining the operational setpoints of the devices. Open Energi (2019) have taken the concept beyond the research phase, using the 'Dynamic Demand' open-source software platform they developed to optimise their clients' generator/storage/load assets on a commercial basis. The interaction of devices coupled with the physical flow of electricity is sometimes referred to as a 'smart grid'.

Before closing this section, it should be noted that nearly all the papers cited have conducted techno-economic analyses of domestic PV-battery systems in developed countries. It is not because such systems are not used in developing countries, but they tend to be used for quite different reasons. In many parts of the world, reliable access to electricity is not available at all times - thus the security of supply afforded by PV-battery, or the use of electricity rather than polluting diesel or kerosene fuels, may be worth more than the savings that could be earned from avoiding grid import, especially if there is no grid connection at all. 14 % of the global population in 2017 had no grid connection, the majority in sub-Saharan Africa (IEA, 2017a). Nerini et al. (2016) analysed the LCoE and cost per household in settlements of varying density in Nigeria and Ethiopia of different options: stand-alone PV-battery systems, micro-grids (individual houses in a locality are interconnected but together have a weak connection to the national electricity network), and establishing mains grid connections to all houses. They found that for household consumption below 224 kWh per year, a stand-alone system was more economical, but as consumption increased, micro-grids proved the lowest-cost option if household density was below around 100 per km^2, and grid connection for denser populations. For household annual consumption above 2195 kWh (still below the average in Europe), a grid connection was most economical regardless of household density. (These calculations were made independently of who bore the costs, whether governments or individuals.)

1.3.3 Existing environmental analyses of domestic batteries

Environmental impacts of domestic PV-battery systems have not been studied as extensively as techno-economic aspects. The conclusion is nearly always that installing PV-battery results in worse life-cycle

impacts than PV alone. Kurland and Benson (2019) made this conclusion based on modelling a 6 kW_p PV system with 12 kWh lithium-iron-phosphate battery ($LiFePO_4$, or LFP, a type of Li-ion) operating the Greedy Algorithm, using hourly weather data and standard load profiles for the USA as input. They found EROI decreased 21 % with a battery compared to PV alone. (Refer to Section 1.2 for definitions of terms specific to environmental impact analysis.) They recommended against installing a battery unless grid export was disallowed, in which case excess PV electricity would be curtailed.

Kabakian et al. (2015) modelled a 1.8 kW_p PV system with 12 kWh PbA batteries in the Lebanon, using the ReCiPe LCA framework, and accounting for the environmental impact intensity of the Lebanese grid whose power plants use mostly diesel and oil. They found the life-cycle impacts with PV alone were reduced compared to the centralised Lebanese grid, 5 times for the human health impact category, 13 times for impacts on ecosystems, and 44 times for impacts on natural resources. However, adding a battery to the system then worsened it by 6.25 % for human health, 3 % for ecosystems, and 4.4 % for natural resources. The global warming potential was 40.2 g CO_2-eq/kWh with batteries compared to 38.9 g CO_2-eq/kWh without. When grid export was disallowed, these figures were respectively 92 and 89 g CO_2-eq/kWh. In contradiction with Kurland and Benson (2019), a battery (at least a PbA one) should not be installed even if grid export is disallowed. It should be stressed that both PV-only and PV-battery were better than the centralised Lebanese grid on all environmental impact categories except ALO.

McKenna et al. (2013) modelled 37 UK households (load profiles and 1.5-3.29 kW_p of PV measured at 5-minute resolution) with PbA batteries of various sizes: 10.08, 20.64 and 27.36 kWh. They operated the Greedy Algorithm and calculated life-cycle impacts in terms of GHG emissions, fossil depletion and metals depletion. Unlike Kurland and Benson (2019) who did not consider grid emissions intensity, and Kabakian et al. (2015) and Uddin et al. (2017) who assumed emissions intensity not to vary throughout the day, McKenna et al. (2013) recognised that a battery could render some positive impact above PV-only if power from the grid were drawn during times of low emissions intensity, and exported to the grid when emissions intensity is high. Otherwise, the battery's efficiency losses and impacts of manufacture obviously could only erode any environmental benefit rendered by PV (Uddin et al., 2017). McKenna et al. (2013) also recognised that it was incorrect to use the average emissions intensity of the grid, as Kabakian et al. (2015) and Uddin et al. (2017) did, because injecting zero-carbon PV electricity into the grid does not displace generator power in the same proportion as being generated at the time (e.g. 20 % nuclear, 20 % wind, 10 % coal, 50 % combined cycle gas turbines, CCGT). Instead, it displaces the generator with highest marginal running costs: this gives rise to the idea of marginal emissions factor (MEF) as opposed to average (AEF). Even so, McKenna et al. (2013) found at the time that PbA batteries still lessened the environmental benefits of PV-only. In fact, adding a battery compared to PV-only was equivalent in CO_2 terms to an average 2009 UK household increasing their consumption by 21 %. Additionally they calculated financial savings of under 100 GBP for annualised costs of up to 1000 GBP, all system configurations they studied being uneconomical.

Babacan et al. (2018) also took care to use the time-varying MEF when modelling a domestic PV-battery system (5 kW_p, 10 kWh) in 16 regions of the USA. Their innovation was in designing operating algorithms based on convex optimisation over a 24-hour horizon assuming perfect forecasting. That is, from day to day, the battery charging/discharging is scheduled based on the forecast load and PV generation in order to minimise the objective function. They analysed the use of financial cost (of electricity on region-specific ToU tariffs) and GHG emissions as the objective functions. They found emissions increased with

cost minimisation as the objective, and cost increased with emissions minimisation as the objective. Re-aligning the incentives would require a CO_2 price of 180-5160 USD/ton (different regions have different technology mixes generating power, and different electricity tariffs).

In contrast to the modelling studies reviewed above, Chowdhury et al. (2018) conducted field trials of 5 houses with PV-battery in the south of England, 3 of which also owned an EV. They measured PV generation and load data at 12-s intervals from 30 May to 30 November 2016, and used GB grid CO_2 intensity data available at 5-minute resolution from GridCarbon (Rogers and Parson, 2019), to calculate and visualise how the CO_2 intensity of the electricity they used varied by time of day, across the week, and from season to season. However, there were some shortcomings to their work: no details were given of which battery products were used nor their operating algorithms, the GridCarbon data were AEF rather than MEF, and considered no environmental impacts besides CO_2, and the benefit of the PV could not be separated out from the effects of the batteries and EVs.

The work of Uddin et al. (2017), a field trial of a house with PV-battery in Loughborough, UK, included a projection of the estimated CO_2 savings. They took grid CO_2 intensity as the AEF values, not varying by time of day, but decreasing from 0.412 kg/kWh in 2016 to 0.244 kg/kWh in 2020. As with Kabakian et al. (2015), they found the addition of a battery eroded the CO_2 savings made by the PV alone, and offered an intuitive explanation: if export to the grid is credited for displacing generation of the same CO_2 intensity as that imported, the energy conversion losses associated with charging and discharging the battery will always result in grid export being reduced more than grid import, and therefore a net burden compared to PV alone.

It can be seen from this survey of the literature on environmental impacts of domestic PV-battery systems that while they render a net benefit relative to using only grid electricity in the USA, UK and Lebanon, the effect of the battery tends to be to lessen the benefits of PV-only. This does not have to be the case, as Babacan et al. (2018) showed with their emissions-minimising algorithm, but this increases the cost of electricity to the consumer. The most notable shortcoming of all the above work is that when they do use time-varying MEF rather than constant AEF, they only consider the electricity grid at the current time in their respective countries: McKenna et al. (2013) and Babacan et al. (2018) examined the UK and USA respectively for only a single year. This is with good reason, as past data were readily available whereas time series of power generation are difficult to predict years into the future, much like forecasting weather or stock markets. However, given that a PV-battery system would last around 25 years, it is worth extending the time-varying MEF analysis at least that far into the future, at least on a statistical basis, for different likely scenarios. After all, the GB grid has seen many changes in the past few years: coal's share of power generation fell three-quarters by 2017 compared to 2012, mostly being replaced by gas (CCGT) and some renewable power, with wind, solar PV and biomass providing one-fifth of demand (Staffell, 2017). Further changes are expected in future, as National Grid (2018b) describe in their Future Energy Scenarios.

Given the difficulty in achieving environmental benefits with domestic PV-battery compared to PV alone, and the role that lower battery costs can play in driving adoption of the technology, the concept of second-life EV batteries offers a promising alternative to using new batteries for domestic applications. The literature on the use of second-life batteries and their economics and environmental impacts are reviewed in the next section.

1.3.4 Second-life electric vehicle batteries in the home

As a battery degrades, over time and with usage, its maximum available capacity decreases and internal resistance increases. For an EV battery, energy density and power density are important design criteria - when these reduce due to battery degradation such that drive performance is severely affected, the battery must be replaced. USABC (1996) recommend this should happen when maximum available capacity has decreased to 80 % of its original value. This typically happens in under 10 years of vehicle use, while the average automobile is over 15 years old by the time it is scrapped, likely having been bought and sold second-hand multiple times first (Bento et al., 2016). The used EV battery, while no longer meeting the energy density and power density requirements for transport applications, may still be used for stationary applications where space and weight are not such crucial considerations. A few companies are already beginning to sell second-life home batteries as a commercial product, Nissan (2018) xStorage and Powervault (2018) 3^{eco} being examples.

Martinez-Laserna et al. (2018) comprehensively reviewed the literature on second-life EV batteries: the processing required to repurpose them for second-life use, the various applications, estimations of market size, the economics of the business model from the point of view of battery repurposing companies, EV owners and manufacturers, and second-life application users, and associated LCAs. The literature pertaining to second-life use in domestic (single home) contexts is reviewed here.

Assunção et al. (2016); Heymans et al. (2014); Kirmas and Madlener (2017) have conducted financial analyses of second-life domestic battery systems. Heymans et al. (2014) considered a Chevrolet Volt battery, originally 16.5 kWh, degraded to 13.2 kWh (80 % of original capacity) and round-trip efficiency 64 %, after 8 years' use in an EV. They modelled its use in a home in Ontario (Canada) with a standard load profile, without PV. The battery is charged during off-peak hours (19:00-07:00) and discharged during peak hours (11:00-17:00 summer weekdays, 07:00-11:00 and 17:00-19:00 winter weekdays; note there is a medium price charged by Ontario electricity suppliers at hours that are neither peak nor off-peak). This operation strategy could achieve savings of 19-38 Canadian dollars (CAD) per year, with greater savings achievable for higher-consuming households. For second-life battery packs costing 38-132 CAD/kWh according to the sources they reviewed, the savings are insufficient to pay back the costs over the 10-year second-use lifetime they considered. However, the NPV (loss) over this period was roughly half that of using the equivalent size of new batteries, and they note that other sources predict longer second-use lifetimes, up to 20 years.

Unlike Heymans et al. (2014), Assunção et al. (2016) included PV (2.4 kW_p) in their system, a domestic PV-battery installation in Portugal operating the Greedy Algorithm. They used standard profiles of PV generation and load, but developed a very detailed battery degradation model, accounting for how DoD, SoC, temperature, and charge/discharge rate affect the capacity and internal resistance. By contrast, Heymans et al. (2014) neglected further degradation of the used EV battery during its second life. Assunção et al. (2016) calculated NPV with discount rate 5 %, finding that both small (10.15 kWh at start of second life) and large (16.8 kWh at start) second-life batteries achieved higher NPV over 10 years than a new 10.2 kWh battery over 20 years: 3119.3, 2727.4, 1251.1 EUR, respectively, relative to a baseline case with PV but no battery. This was assuming a new battery cost 310 EUR/kWh while a second-life battery cost 119 EUR/kWh, this being the highest in the range of second-life prices from their sources. This is in contradiction to the results of Camilo et al. (2017) who found NPV < 0 for a new battery in an equivalent domestic context in Portugal. However, they had considered a gel battery

costing around 500 EUR/kWh and lasting 7 years. The costs and lifetime assumptions used by Heymans et al. (2014) seem overly optimistic even for a Li-ion battery (Uddin et al., 2017).

Kirmas and Madlener (2017) modelled a house in Stuttgart (Germany) with 5 kW_p PV (generation data simulated from hourly weather data), load from standard profiles scaled to an annual consumption of 3892 kWh, and a second-life battery operating the Greedy Algorithm. They took its capacity to decrease from 80 % to 60 % of its original value over 10 years of second-life use, and its internal resistance to increase from 150 % to 320 % of its original value over the same period. They calculated the NPV over 10 years with discount rate 4 %, for different battery sizes (4-8 kWh at start of first life), electricity retail price (increasing 2, 4 or 6 % per year), and FiT (0.1231 EUR/kWh or none), finding what the second-life battery cost would have to be in order for NPV to exceed zero. If the electricity price increases 2 % per year, the second-life battery would need to cost less than 73 EUR/kWh; for a price increase of 4 % per year, the second-life tipping-point cost would be 108 EUR/kWh; for 6 % per year, this would be around 130 EUR/kWh. The NPV-optimal storage size increases from 5.5 kWh at a second-life cost of 117 EUR/kWh, increasing to 7 kWh if the cost decreases to 34 EUR/kWh.

None of the above studies quantify the environmental impacts of second-life batteries; Casals et al. (2017); Faria et al. (2014); Genikomsakis et al. (2013) do, but without quantifying financial sustainability.

Genikomsakis et al. (2013) conducted an LCA using the Eco-indicator 99 framework, which encompasses impact categories: carcinogens, respiratory organics and inorganics, climate change, ionising radiation, ozone layer depletion, ecotoxicity, acidification/eutrophication, land use, minerals depletion, and fossil fuel depletion. Their LCA considered a base case of a 24 kWh Li-ion battery being manufactured and used in an EV for 7 years, before being disposed of and replaced with a new battery of the same specifications up to a total time of 4000 days (roughly 11 years) altogether. This was compared to a case where the used EV battery was not disposed of but sent to a second-life application at a house in Bilbao (Spain) with daily consumption of 10 kWh, assuming battery utilisation of one cycle per day, for the remainder of the 4000 days before being disposed of; and another case where the EV battery was disposed of after its first life and a new smaller battery of 15 kWh was manufactured and used in the house. They took the EV battery capacity and efficiency to both have degraded to 80 % of their original values over the first lifetime, with a further decrease to 60 % and 75 % for the capacity and efficiency respectively over the second lifetime. They found the environmental impacts of the second-life case were more beneficial than the case where a new battery is manufactured for the stationary application, and both were more beneficial than the base case. In particular the life-cycle CO_2 emissions for the second-life case were 16.3 % lower than the base case, but only 9.63 % lower when using the new stationary battery. It is questionable whether these cases offer a fair comparison: surely the EV battery replacement is needed in all cases and cannot be neglected simply when a stationary application is being considered too. However, it would be valid to conclude that the second-life battery offers superior environmental benefits than the new battery, even if these benefits cannot be compared fairly to any other cases.

The LCA of Faria et al. (2014) was conducted under CML2001 (considering abiotic depletion, acidification, eutrophication, global warming), for a used Nissan Leaf battery in peak-shaving and load-shifting applications, not in conjunction with any PV, in domestic settings in Poland, Portugal and France. The battery is charged at night during off-peak hours, and discharged during peak hours in the peak-shaving application, and throughout the day for the load-shifting application. They modelled capacity degradation with both cycling and calendar aging, from a more aggressive baseline than most studies: the capacity is 70 % of its original value at the start of the second life, and degrades to 50 % by the end of

the second life. Unlike most LCAs of second-life domestic batteries, they used time-varying rather than constant AEF. As a result, they found no impacts or negative impacts for the Polish and Portuguese grids, whose CO_2 intensities vary too little throughout the day. On the other hand, the French grid is supplied by varying amounts of low-carbon nuclear and higher-carbon CCGT power, providing sufficient variation for a 2 % benefit on all impact categories in the peak-shaving application, and 4-5 % for load-shifting. Note that they used AEF rather than MEF, for the grid situations at the time with no future projections.

Casals et al. (2017) calculated only GHG emissions in their LCA, for an EV battery used for 10 years in its first life, whose capacity has degraded to 78 % of its original value by the end of its first life. They compared second-life usage in a range of stationary applications against recycling at the end of the first life and either using a new PbA battery in those stationary applications, or no battery. The base case was for a house consuming all its electricity from the grid for 20 years after the dismantling of the EV battery. The stationary applications were: renewable energy support (a house consumes its own PV electricity without a battery for 20 years, or with a used EV battery for sporadic support over 8 years); island generation (the house has no grid connection, and either uses a diesel generator for all its electricity needs over 20 years, or new PbA batteries requiring two replacements over 20 years, or the used EV battery for 20 years without replacement); energy arbitrage (as considered by Heymans et al. (2014), with new PbA batteries requiring two replacements over 8 years, or the used EV battery for 8 years without replacement). Casals et al. (2017) used an energy budgeting rather than modelling approach, estimating daily flows. They took the second-life batteries' capacity to fade with cycling, temperature and charge/discharge rate, to 60 % of the original value by the end of the second lifetime, 8 or 20 years depending on application. They found CO_2 emissions to be 0.7 kg/kWh less when using second-life rather than new PbA batteries in an equivalent application, but consuming renewable energy without batteries was the least CO_2-intensive option when available. New Li-ion batteries were not considered.

One can see that the existing literature uses a wide range of modelling methodologies, assumptions about degradation, and metrics of environmental impact. There are some issues with what is considered a fair comparison too: comparing an EV battery with no second-life use to one with, as Genikomsakis et al. (2013) did, would obviously make second-life use look better than immediate disposal, but does not answer the question of whether a new or second-life battery is better than no battery at all. Casals et al. (2017) did better in this respect but it is not possible to conclude from their work whether second-life batteries are better for the environment, or PbA batteries are simply inferior to Li-ion ones.

There is a gap for research into the financial and environmental sustainability of domestic PV-battery systems, comparing new Li-ion and second-life EV batteries to no batteries (PV only), taking into account the time-varying MEF of grid electricity and how that would change over the 25 years of the system lifetime. To do this requires further review of the literature on second-life batteries, including applications other than domestic ones, and will be conducted in later chapters. Even though frequency response is widely regarded the most lucrative revenue stream, Heymans et al. (2014) estimated the potential market (total kWh) for stationary battery products to be greatest for the residential sector: more than supporting wind and solar parks, offices, light commercial, food distribution, transmission support, and telecommunications towers. The assumptions used in the literature that are in particular need of further examination are the pricing of second-life batteries and the environmental impact of re-purposing used EV batteries.

1.3.5 Summary of existing literature

It has been shown that a great deal of literature exists on the economics of domestic PV-battery systems, especially grid-connected ones operating the Greedy Algorithm. For the most part, net savings are possible according to a wide range of financial metrics, but depend on favourable subsidy schemes, or rapidly rising retail electricity prices, or battery costs decreasing below what they were at the time of the studies reviewed. These conclusions broadly hold for a wide range of locations (with differing solar resource, electricity consumption patterns and tariff structures) and modelling details.

There is some literature into the impact that domestic PV-battery systems may have on the finances of stakeholders other than the homeowner: the DNO in reducing the costs of network upgrade, electricity suppliers who could lose revenue as people consume more of their own PV-generated electricity, and incumbent power generators that may supply less energy but still be required to provide reserve power. Research is being conducted into alternative algorithms involving forecasting and scheduling by optimisation, using EVs as an energy store through V2G or as demand response by smart charging, and aggregating many households to leverage more value out of PV-battery systems.

Grid-connected applications are markedly different from stand-alone and micro-grid systems, in terms of the value derived: saving money on electricity bills, compared to having access to electricity at all. Environmental impact analyses are more common for grid-connected domestic PV-battery systems - this may be due to both the fact that replacing diesel and kerosene fuels in non-grid-connected areas is so obviously good that it is not worth the effort to quantify, and that comparisons are difficult because there would not be an exact kWh-for-kWh substitution of those fuels with electricity, and perhaps not even the same hours of usage for lighting or cooking, for example.

The literature on environmental impacts of grid-connected domestic PV-battery systems nearly all concludes that while impacts are positive, they are not as good as installing PV without batteries, or when they are, the financial costs are higher. Second-life batteries promise lower costs and environmental burdens than manufacturing new batteries, but the assumptions and methodologies used in calculating their financial and environmental impacts make comparison with the literature on new batteries difficult. In all cases, there is an unmet need to address the fact that electricity grids in the future will likely be very different to today: with more renewable power and less dispatchable plant.

1.4 Thesis Structure

The research question decided upon is:

“In what circumstances are domestic PV-battery systems in Great Britain financially and environmentally sustainable?”

This encompasses the sizing of the system components, whether to use a new or second-life battery or none at all, what operating algorithm to use, and in what year to make the initial investment. Although similar questions have been answered before for many parts of the developed world, many of those analyses fall short by failing to account for time-varying marginal emissions from the grid (MEF), and when they do, they do not envisage the MEF profile changing over time. It is also valuable for this field of research to be continually updated, as markets (Goldie-Scot, 2019) and government policy (Ofgem, 2019; UNFCCC, 2018) move very quickly.

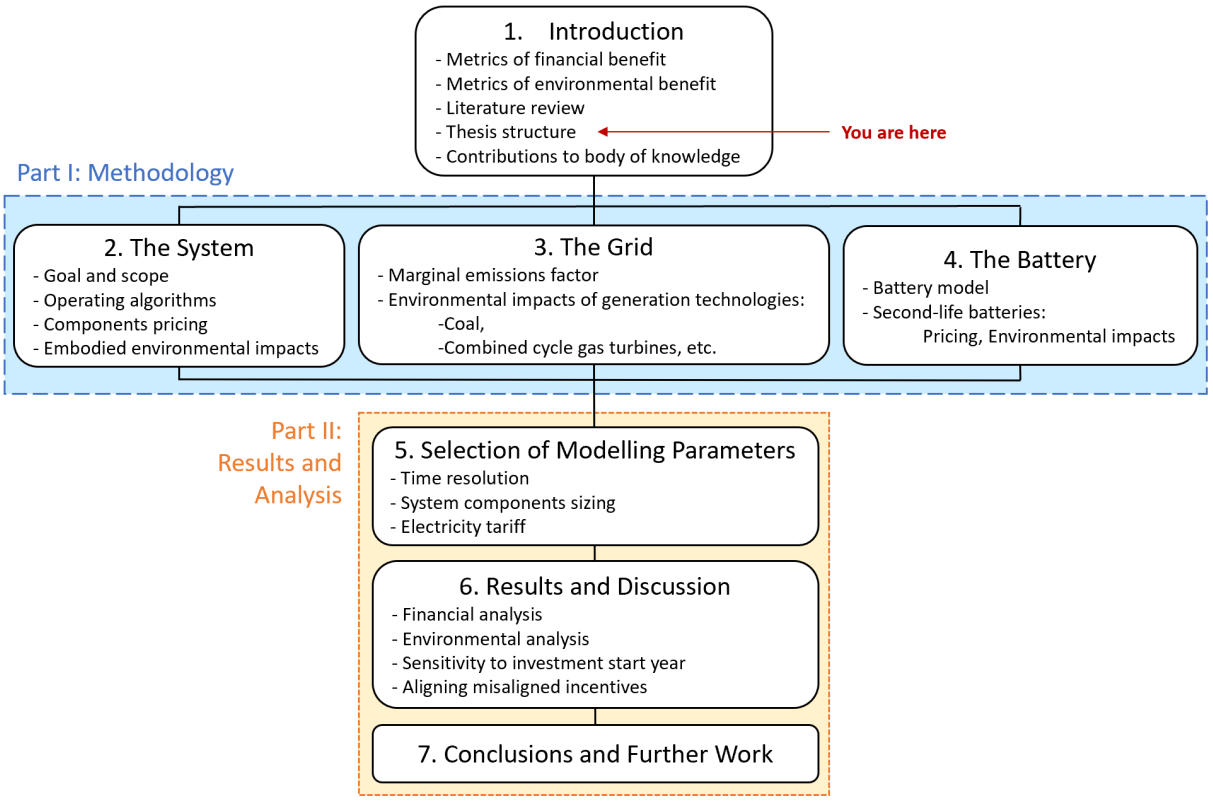

FIGURE 1.2: Structure of the thesis, comprising Introduction (Chapter 1), Part I: Methodology, containing chapters on modelling the system (Chapter 2), the grid (Chapter 3) and the battery (Chapter 4), and Part II: Results and Analysis, containing chapters on selection of modelling parameters (Chapter 5), results and discussion (Chapter 6), and conclusions and further work (Chapter 7).

Part I of the thesis contains details of the improved methodology developed to answer the research question, split into chapters focusing on the PV-battery system itself (including the operating algorithm used), the grid (and how time-varying MEF is projected to 2050), and the battery (how it is modelled accounting for degradation whether new or second-life, and a new projection of how the second-life price may evolve to 2050). Each chapter contains review of literature, some of which is applied directly to the work in the thesis, some of which informs development of better methods; and some intermediate results which are then used as inputs to the main model. The full code and input data to the model described in Part I is available at: `https://doi.org/10.5258/SOTON/D1269`, with file descriptions in Appendix E.

Part II contains Chapter 5 on selection of the specific parameters of the systems being modelled (size, timestep, etc.). Chapter 6 reports results of life-cycle financial analysis and environmental impact analysis using the ReCiPe framework, including dominance and sensitivity analyses, and discussion of what interventions may better re-align financial and environmental incentives. Chapter 7 concludes the thesis and discusses further work that was outside the scope of the study undertaken.

The work undertaken for this thesis follows ISO 14040 and 14044 as far as possible for reasons of quality and transparency. LCA practitioners may recognise the goal and scope in Chapter 2, the LCI in Chapters 2-4, and LCIA and interpretation stages in Chapter 6. But as the thesis does not meet the requirements for external review, it should not be cited as an ISO-compliant LCA.

The scope of the thesis may be criticised for being too narrow: considering GB but not other countries,

the perspective of the homeowner but not the DNO or other stakeholders, battery storage but not other storage types, domestic PV-battery uses but not other stationary applications, nor with aggregation, EV smart charging, or V2G. Such artificial narrowing is necessary if any situation is to be examined to an adequate level of detail. The focus on GB is justified by open access to a high level of detail of all the data needed. Battery storage was chosen as the focus because it is the most mature technology for a domestic context; the fact that customers are already installing such systems in the belief that they are helping the environment should motivate greater scrutiny of the industry, which an academic study can provide in great detail independently of commercial pressures. Even though decarbonising heat and transport currently presents a greater challenge than decarbonising electricity, one pathway to do so is by electrifying them: replacing gas boilers with electric heat pumps, for example, and petrol/diesel vehicles with EVs, as is already starting to happen. The analysis of electrical storage such as batteries, rather than thermal or other storage types, is justified on this basis. And as Heymans et al. (2014) estimated, the potential market for battery products is greatest in the residential sector, even if not the most lucrative. In fact, the marginality of the business case, as shown by the studies reviewed in Section 1.3.2, makes it a particularly interesting problem to try to solve.

Arguably the need for research into improving access to reliable electricity in remote regions of developing countries is greater and more urgent. The only rebuttal to this is that research and development into systems and business models in developed countries may yield knowledge that can be transferred elsewhere: 68 % of the global population is projected to be living in urban areas by 2050, up from 55 % in 2018 (UN, 2018), and as demand for electricity increases in developing countries, connecting to the grid becomes a more economical option than relying on a stand-alone renewable-and-storage system or a micro-grid (Nerini et al., 2016). However, there will remain some settlements that are too remote for a grid connection to ever be viable, and many today that are temporarily in such a state: three-quarters of the additional connections needed in sub-Saharan Africa, according to geospatial modelling reported by IEA (2017a).

1.5 Contributions to Body of Knowledge

While publications in the existing literature have addressed the issue of time-varying (non-constant) grid emissions intensity, and the importance of using marginal rather than average emissions, none have shown the consequences on domestic PV-battery systems of projecting the time-varying marginal emissions intensity into the future across the system lifetime. For the first time, the future development of the GB electricity grid has been explicitly included in a domestic PV-battery model, and this thesis shows its effects on the life-cycle environmental impacts thus calculated (Sun et al., 2019).

With a time varying grid emissions intensity, it becomes possible to use energy storage to reduce emissions by arbitrage. In this study, a novel Emissions Arbitrage Algorithm (EAA) was developed to achieve precisely this, without the need to forecast PV generation, electricity consumption, or market dynamics (Sun et al., 2019). As such, it is less computationally intensive than existing algorithms that use convex optimisation techniques. Nonetheless, the EAA is able to reduce the system's life-cycle CO_2 emissions below that of PV without battery, unlike the standard Greedy algorithm, which is slightly worse than PV without battery.

Literature estimates of EV second-life battery price are often unrepresentative of what a domestic customer might pay, including for installation, and give little indication of how the price might change in

future. This study addressed this need by developing a novel microeconomics-based method to estimate how the second-life battery price evolves in future, in response to demand and supply, new battery price, repurposing cost, and credit available from recycling as an alternative (Sun et al., 2018b). As a consequence, it was found that second-life batteries may not in fact be a reliable source of inexpensive batteries, especially given the increased frequency of replacement required when their degradation is taken into account.

A further issue with the existing literature on financial and environmental impacts of second-life batteries is the lack of standardisation for the cases compared. In this study, the homeowner's perspective is taken, where the configurations compared are with/without PV, and with/without new Li-ion or second-life EV batteries. Care was taken in choosing system parameters appropriate to each household (PV array and new/second-life battery capacities, electricity tariff according to configuration and household consumption pattern, etc.). Environmental impacts of first-life use are attributed to the first-life owner, such that only second-life use and repurposing impacts (or manufacturing impacts, in the case of a new battery) are attributed to the system under study in this thesis. Life-cycle impacts were calculated in 14 ReCiPe midpoint categories, and normalised to EU annual activity data, giving a more holistic and better contextualised picture than any previously.

The result is that second-life use can be effective in restricting the environmental impacts of manufacturing new batteries, especially in categories of metals depletion, freshwater eutrophication, human toxicity, ozone depletion, water depletion and freshwater ecotoxicity. However, they cannot improve on a PV-only system, except in climate change, fossil fuel depletion and ozone depletion categories, for which they must run the EAA in order to do so. Unfortunately, this is the least cost-effective option. This thesis shows how difficult it is to align the financial and environmental incentives. It also raises the question of whether the expected future profitability of PV-battery systems running the Greedy algorithm may incentivise installation of more PV than otherwise, and in that way compensate for reduced environmental benefit relative to PV-only systems.

The contributions of this thesis are not just in the questions answered, but the further questions raised.

Part I

METHODOLOGY

Chapter 2

The System

"...when you can measure what you are speaking about, and express it in numbers, you know something about it; but when you cannot measure it, when you cannot express it in numbers, your knowledge is of a meagre and unsatisfactory kind..."
- Lord Kelvin

Every life cycle assessment begins with a statement of the goal and scope. This encompasses not just the research question, but also how it informs the specifics of the system being studied. A process tree is presented to show what is included and excluded from consideration in calculating the life-cycle impacts of the PV-battery system in question. A schematic of the system is given, along with details of the input data and algorithms used for modelling the operational phase of the life cycle. This is followed by a quantification of the initial costs of each component, comprising the Capex, for use in the financial calculations; and their environmental analogue: the embodied impacts of manufacture and installation.

2.1 Goal and Scope

The goal is to answer the research question,

"In what circumstances are domestic PV-battery systems in Great Britain financially and environmentally sustainable?"

This goal informs all the decisions taken throughout. To start with, generic data for pricing and environmental impact are used as far as possible, as the question pertains to a general case in GB rather than any specific system already installed or proposed. The process tree to be used for the LCA is discussed next, along with considerations of functional unit, temporal and geographic boundaries, environmental impact categories and their accounting. This is followed by more in-depth description of the archetypal domestic PV-battery system under study, with PV capacity in the range 0-8 kW_p and battery 0-20 kWh. (Sizing of the system components is discussed in more detail in Chapter 5.)

The Emissions Arbitrage Algorithm is one of the PV-battery operating algorithms described in this chapter. Its development was first reported in a paper by the author (Sun et al., 2019) in the journal *Energies*.

2.1.1 Process Tree

Every LCA must define a process tree of all the unit processes, or intermediate steps, that contribute to the production of the functional unit in question. The functional unit in this case is 1 kWh of electricity consumed. This means the environmental impacts across the system lifetime are totalled and then divided by the total electricity consumption in that time period, $\sum_t P_d(t)$, to give the impacts per functional unit. Note that $P_d(t)$ is the time series of electrical consumption, independent of whether it is supplied by PV, battery or grid. It is assumed in this study that $P_d(t)$ for each household is constant between all configurations, with/without PV/battery, and is therefore a more meaningful denominator to allow fair comparison between different households than grid import or PV self-consumption, for example. Unchanging $P_d(t)$ is a simplification, as behavioural studies show effects possible in either direction: a rebound effect of increasing $\sum_t P_d(t)$ after installation of PV or battery (Deng and Newton, 2017), or a spillover effect of decreasing $\sum_t P_d(t)$ (Sekitou et al., 2018). Despite this, an argument in favour of using 1 kWh of electricity consumed as the functional unit is that doing so incentivises desirable behaviours: to reduce the impacts per functional unit in the ways this study seeks to find, but also to reduce electrical consumption on the household level, since each household's total impacts are the product of their consumption and their impacts per kWh consumed.

Process trees can be very complex, consisting of many steps from the mining and refining of raw materials, through the processes that combine them eventually into the finished product. Each unit process has associated with it certain inputs (harvested materials, energy, outputs of other processes) and outputs (the product of that process, and also emissions to air, soil and water). This information is contained for many different unit processes in LCA databases such as EcoInvent, which require payment to access. Specialist LCA software such as GaBi or SimaPro can be used to construct process trees, and automatically scale the inputs/outputs of each unit process to be consistent with the functional unit defined by the user. The software can then apply conversion factors to equate the chemical emissions from all steps of the process tree, to environmental impacts under a specified LCA framework such as ReCiPe, CML2001, ILCD and others. (If required, consult Chapter 1 Section 1.2 for a reminder of what the ReCiPe midpoint categories entail.)

Specialist software offers the advantage of a purpose-built way to keep track of the unit processes and their relations, and standardised formatting of results. However, they require inputs in a specific format, and can be difficult to integrate with results from a Matlab model, for example. While standardised formatting is an advantage for an LCA specialist, the processing and results can be difficult to interpret for a non-specialist, and completely opaque to one without access to whichever LCA database is used. Therefore, for greater transparency, it was decided to perform calculations for this study in Matlab, integrated with the system model itself.

This required the process tree (shown in Figure 2.1) to be simple enough to code into Matlab: the more unit processes there are, the greater the chance of making a mistake in scaling their inputs/outputs. LCAs of the different components needed for a PV-battery system already exist, and though they could be improved and updated, the goal was considered better served by focusing efforts on operational and accounting aspects of the system, rather than replicating work that already exists. All the processing steps required for manufacture, transport and installation of PV, battery and balance of system are aggregated into the corresponding unit processes within the System Boundary in Figure 2.1. The existing LCAs which detail inputs and outputs of these processes are reviewed in Section 2.5.

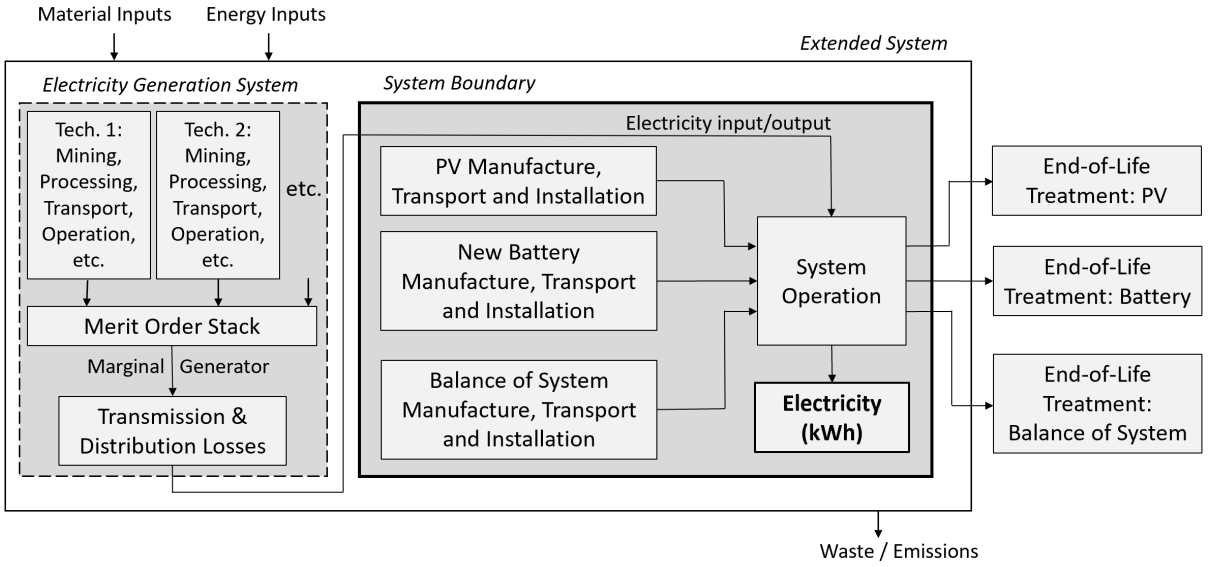

FIGURE 2.1: Process tree for a domestic PV-battery system.

Figure 2.1 shows an interaction between the domestic PV-battery system itself and the national electricity generation system, with generators of different technology types (coal, biomass, nuclear, etc). The time-varying impacts of electricity imported from the grid is debited from the system and that exported to the grid is credited to the system; the net impacts are summed with those of manufacturing all the system components, to give the total impacts, which are divided by the total electricity consumption to give the impacts per kWh consumed by the house. LCAs for the different generator technology types, along with the other elements of that section of the process tree, are reviewed in Chapter 3.

The impacts considered are Climate Change (CC), Ozone Depletion (OD), Human Toxicity (HT), Photochemical Oxidant Formation (POF), Particulate Matter Formation (PMF), Ionising Radiation (IR), Terrestrial Acidification (TA), Freshwater Eutrophication (FE), Marine Eutrophication (ME), Freshwater Ecotoxicity (FET), Land Occupation (LO), Water Depletion (WD), Metal Depletion (MD), Fossil Depletion (FD), under the ReCiPe framework. The categories Marine and Terrestrial Ecotoxicity (MET, TET) are neglected because these data could not be found for all the generator technology types on the GB grid. It is possible that FET may be an inadequate indicator of ecotoxicity in the marine and terrestrial domains, but it was decided to use only FET rather than a weighted sum with MET and TET when those are reported, because doing so would show an unfairly large burden for processes that report them compared to ones that do not. Only a single LO category is used because some sources do not differentiate between Agricultural and Urban Land Occupation (ALO, ULO) and do not report Natural Land Transformation (NLT) at all. When both ALO and ULO are reported, they are summed and NLT is ignored, to give a score for LO.

Note that the balance of system (BoS - power electronic converters, controllers, etc., see Section 2.1.2) is listed as a separate unit process to the battery. This is because the system is compared with new batteries and with second-life EV batteries, both of which require BoS. Furthermore the replacement schedule for new and second-life batteries will differ from each other (see Chapter 4), and may both differ from the BoS replacement schedule.

The end-of-life treatment of PV, battery and BoS are neglected from the life cycle impact analysis (LCIA) calculations. There are some different conventions for allocating burdens and benefits of recycling when all

the data needed are known: allocating half to each the supplier and user of recycled materials, for example (Klöpffer and Grahl, 2014). And while some research has been conducted into the environmental impacts of recycling PV panels and Li-ion batteries, it is not sufficiently detailed to be usable for the work in this thesis. For example, the LCA by Boyden et al. (2016) compares hydrometallurgical and pyrometallurgical recycling, and landfilling, of Li-ion batteries, but only in terms of three impact categories: CC, TET and HT. (Although both recycling processes emitted on the order of 100 times more CO_2 than landfilling, the TET and HT impacts of landfilling were on the order of 1000 times worse than recycling.) The EV LCA by Hawkins et al. (2013) does report on all 18 ReCiPe midpoint impacts, broken down for the EV battery and 'end of life', but this is for end-of-life treatment of the entire EV, not just the battery.

As for PV recycling, some commercial operations are already happening (IRENA, 2016) and some research is being conducted into associated environmental impacts (Latunussa et al., 2016). The PV array in the system under study is very likely to be recycled, as the EU Waste Electronic and Electrical Equipment (WEEE) directive was changed in 2012 to cover PV panels, and was transposed into law in all member countries, including the UK, in 2014 (Solar Waste, 2018). However, the right of the owner of the PV array to have it dismantled and recycled at end-of-life at no cost to themselves (Solar Waste, 2018) justifies the decision to ignore the environmental impacts of recycling. If the financial costs are borne by another entity, which may profit from selling recycled material, that is an argument for allocating the environmental burdens and benefits to that entity also. Indeed, Bekkelund (2013), McManus (2012) and Kabakian et al. (2015) ignore end-of-life treatment in their LCAs of PV, batteries, and PV-battery systems respectively. There is very little information on the environmental impacts of power electronic converter manufacture, let alone their disposal or recycling. This is not an ideal situation, but improving on the existing literature on this issue is outside the scope of this thesis.

The temporal boundary for the LCA is 25 years, the typical warranty period of a PV array which is the longest-lived component of the system (CAT Information Service, 2018). All replacements of the battery and BoS during that time fall within the temporal boundary and therefore the impacts of replacement are included in the LCIA, as indeed are their costs included in the financial analysis. It is common for PV panels to keep generating beyond 25 years albeit at reduced capacity; rather than try to quantify the value remaining in year 25, as Camilo et al. (2017) did by including salvage value of the battery in the system they modelled, the entire system is assumed to keep operating but no longer have its impacts counted. The economic value and environmental benefits calculated would thus be conservative estimates.

The geographic boundary is Great Britain: the load profiles and PV generation used were measured for systems in the UK (see Section 2.2), the national electricity grid with which the system exchanges power is that of GB (more in Chapter 3 - note that the UK includes Northern Ireland, but the Irish electricity grid is not synchronous with the British mainland, hence the references to the 'GB grid' rather than the 'UK grid'), the electricity tariffs considered (in Section 2.4.4) are ones available in the UK, and the system is modelled without subsidy (although possible government interventions in the market are discussed in Chapter 6). The PV and battery products considered for the LCA are commercially available in the UK, with typical pricing listed publicly on price comparison websites, as discussed in Section 2.4. New and innovative technologies such as perovskite PV and aluminium-ion batteries are outside the scope of this work, but could be promising areas for further study.

2.1.2 DC-coupled Domestic PV-Battery System

The distinction between AC-coupled and DC-coupled PV-battery systems is first explained, and the justification for modelling a DC-coupled system for this thesis is then provided. This informs the requirements for power electronics (converters and inverters) which form part of the BoS.

PV cells and batteries are direct-current (DC) devices, whereas the national electricity network transmits alternating current (AC). Therefore most electrical appliances which plug into the mains are designed to be powered by AC electricity of the nominal voltage and frequency in the region it was designed for (230 V, 50 Hz in GB and indeed the rest of Europe). Many modern appliances such as phone chargers, laptop chargers and LED lights actually run on DC and so have a rectifier built in to convert AC mains power to DC of the appropriate voltage to power the device. Some research is being conducted into fully DC micro-grids (Dastgeer et al., 2019), but given the ubiquity of AC-powered appliances, it is assumed that DC power from the PV and battery must be converted to AC power if it is to be used for appliances in the home or exported to the grid. This is in accordance with the geographic boundary defined above.

It used to be common practice for the PV array and battery pack to each have their own inverter (DC-AC) and for the point of coupling to be AC, hence AC-coupled. Such systems were modelled by Bertsch et al. (2017); Hoppmann et al. (2014); Mulder et al. (2013); Naumann et al. (2015); Truong et al. (2016); Weniger et al. (2013), whose work was reviewed in Chapter 1. However, it is possible to couple the PV array and battery pack to each other first, and use a single inverter to convert DC to AC to feed power to household loads or the grid (Muthuvel et al., 2016; Truong et al., 2016). If power is to be imported from the grid to charge the battery directly at times too, the inverter must be bi-directional. Both AC- and DC-coupled configurations are illustrated in Figure 2.2.

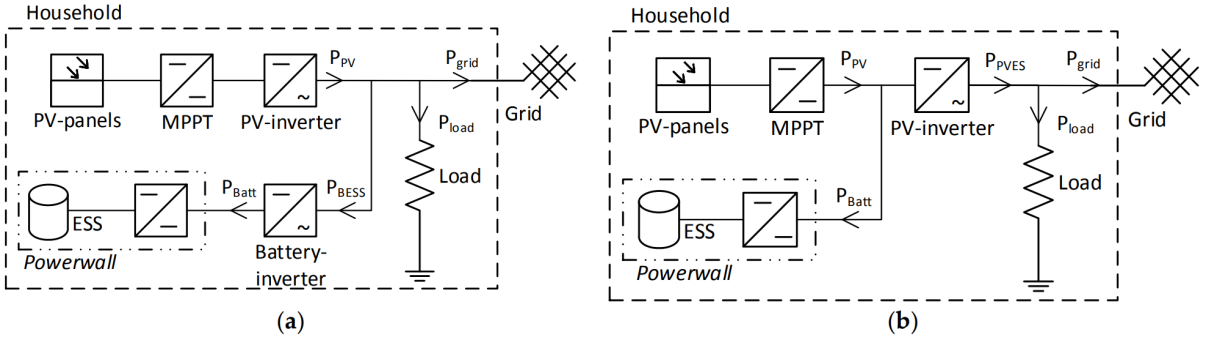

FIGURE 2.2: Schematics illustrating the distinction between (a) AC-coupled and (b) DC-coupled PV array with maximum power point tracking (MPPT), and Powerwall energy storage system (ESS) (Truong et al., 2016).

In the DC-coupled configuration, a DC-DC converter is needed for each, the PV array and the battery pack, to step the voltage from each up or down as appropriate: the PV voltage varies as a function of power generation; the battery voltage varies with state of charge (SoC) as well as temperature, instantaneous charge/discharge rate, and other factors; both must be converted to the voltage of the DC coupling point. Voltage step-up/down is also required upstream of the AC coupling point in AC-coupled systems; it is standard for PV installations to include maximum power point tracking (MPPT), which controls the DC-DC converter to set the PV voltage in real time in order to maximise the power drawn from it at the given irradiance level. The battery DC-DC converter similarly is the hardware that enacts the control logic for when and how much the battery charges and discharges. Given the reduction in components of a DC-coupled system, namely that a separate battery inverter is not needed, overall system efficiency

is higher and costs tend to be lower (Truong et al., 2016). This explains its increasing adoption in the domestic PV-battery market. However, DC-coupled systems must be bought with PV and battery together; it is more straightforward to retro-fit a battery to an existing PV installation by AC-coupling them.

The system to be studied in this thesis is illustrated in Figure 2.3. Note that the utility electricity meter M1 should be a smart meter, which records the time of power flows (grid import or export), unlike a standard meter which only displays the cumulative sum of energy imported. A smart meter is necessary to make use of certain time-of-use (ToU) tariffs being offered, as electricity consumption is billed at different rates depending on time of day (Green Energy, 2017; Octopus, 2019). It is also a requirement of the Emissions Arbitrage Algorithm that has been specially designed in the course of this thesis (see Section 2.3). The UK government has required all energy suppliers to take "reasonable steps" to ensure installation of a smart meter for all their customers by 2020 (BEIS, 2018c). The total at the end of 2018 stands at 12.8 million, out of 25 million households. Customers are not charged for installation of a smart meter, but the costs borne by the energy suppliers are passed on to all their customers in the form of higher electricity and gas bills (BEIS, 2018c). The smart meter cost is therefore ignored in this study.

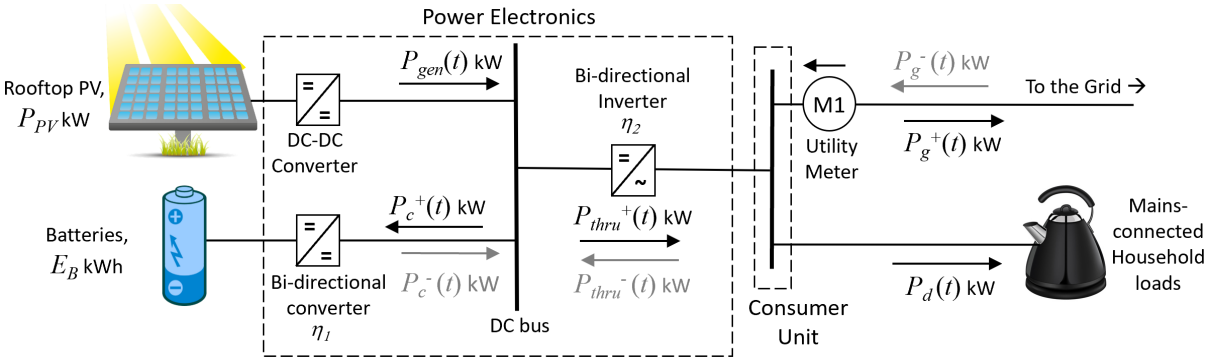

FIGURE 2.3: Schematic of DC-coupled PV array and battery. Refer to Table 2.2 for symbol definitions.

Symbol	Quantity	Unit
	Parameters	
P_{PV}	PV rated capacity	kW_p
E_B	Battery capacity	kWh
	Variables	
$P_{gen}(t)$	PV generation power	kW
$P_c^+(t)$, $P_c^-(t)$	Battery charge, discharge power	kW
$P_{thru}^+(t)$, $P_{thru}^-(t)$	Power flowing forwards (backwards) through DC-AC inverter	kW
η_1	Battery DC-DC converter efficiency	%
η_2	Bi-directional inverter efficiency	%
$P_g^+(t)$, $P_g^-(t)$	Grid export, import power	kW
$P_d(t)$	Household load power, i.e. demand	kW

TABLE 2.2: Definitions of symbols used in Figure 2.3.

The converter and inverter efficiencies η_1 and η_2 are classed as variables rather than parameters in Table

2.2 because they are not fixed values, but vary according to the instantaneous power flowing through them. Examples of this relation are shown in Figure 2.4 for a DC-AC inverter. The same form is found for a DC-DC converter (Mouser, 2019).

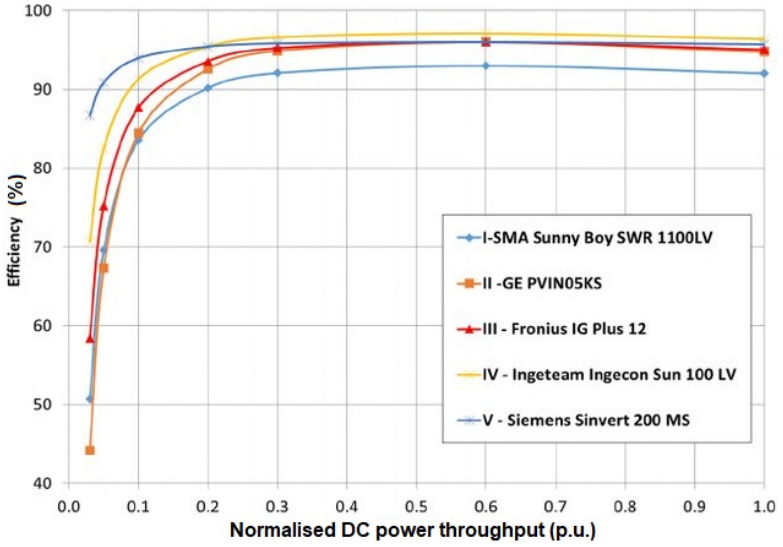

FIGURE 2.4: Efficiency as a function of normalised ('per unit', p.u.) power throughput for 5 commercially available solar inverters (Faranda et al., 2015).

Constant efficiency is an adequate approximation for most levels of power throughput except very low power. Naumann et al. (2015); Truong et al. (2016) recognised that power throughput can sometimes be very low in a domestic PV-battery system (if PV generation only just exceeds load, for example, then very little power flows into charging the battery), and so used a functional form to model the converter and inverter efficiencies:

$$\eta(P, P_0) = \left(k_1 \left(\frac{P}{P_0} \right) + 1 + k_2 \left(\frac{P}{P_0} \right)^{-1} \right)^{-1} \tag{2.1}$$

where P is the instantaneous power flow and P_0 the rated power. Truong et al. (2016) used $k_1 = 0.0345$, $k_2 = 0.0072$. They yield a reasonable representation of the graphs in Figure 2.4, as seen in Figure 2.5. Therefore these values of k_1 and k_2 are also used in this thesis, for both the converter and inverter efficiencies η_1 and η_2.

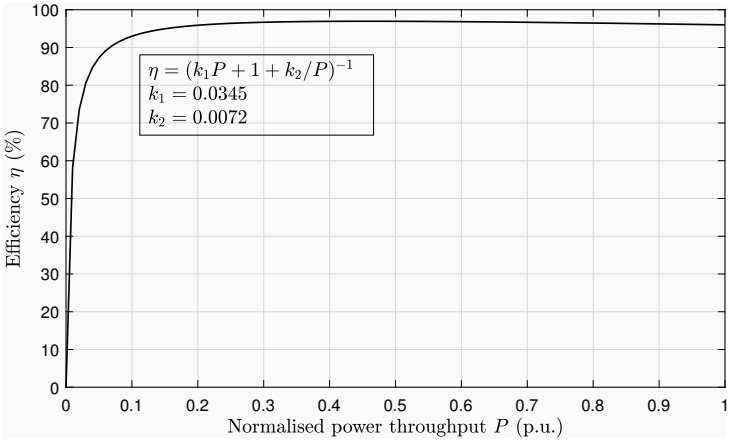

FIGURE 2.5: Efficiency as a function of normalised power throughput as given by the functional form Truong et al. (2016) used.

The efficiency of the DC-DC converter for the PV array does not need to be considered because the PV generation time series used for $P_{gen}(t)$ was measured just downstream of the solar inverter (see Section 2.2.2).

2.2 Input Data Series

PV generation and household load time series were sought that would fulfil the following criteria:

- Real measured data, rather than synthetic or averaged standard profiles,
- Typical of the GB geographic boundary,
- Time resolution as high as possible to ensure accuracy,
- Coverage of at least a full year to account for seasonal effects,
- Showing variation between different households,
- Freely available.

Fulfilment of the criteria were largely successful: some gaps are always present in measured PV and load data, but steps were taken to fill those gaps with plausible data as described below. It was found that the time resolution of the sourced data was actually higher than needed: the trade-off between accuracy and computation time required averaging them to lower resolution for the modelling, as discussed in detail in Chapter 5.

2.2.1 Load profiles

The REFIT electrical load dataset contains measured load time series for 20 houses in the UK logged at an intended sampling interval of 8 s, between September 2013 to July 2015 (Murray et al., 2017). The aggregate active power (over all appliances) consumed at each house was the basis of the input load data used in this work. As the timesteps were in practice irregular, data for the whole of 2014 were averaged to 15-s timesteps, this being close to the time resolution achieved in practice. Missing values were excluded from the averaging. To obtain a full year of data, care was taken to fill in missing time periods with data from a similar time of day, time of year, and weekday/weekend, as load profiles are characteristically different according to these factors (consumption tends to be higher in winter, on weekdays, and in the evening):

Gaps in the data of 5 minutes or less were replaced by the previous value. Gaps of more than half a day had the entire day's values replaced by the corresponding day (weekday or weekend) in 2013, and if still missing, by the corresponding day in 2015. Remaining gaps had missing values replaced by data from 7 days ahead (first half of the year) or 7 days behind (second half). This is repeated once more.

This left 8 houses with fewer than 100 out of 8760 hours still containing missing data, which were then linearly interpolated over. These 8 covered a range of annual total consumption values, in descending order: 6451, 5818, 4714, 4116, 4069, 3982, 3258, 2572 kWh, for respectively houses 5, 8, 7, 6, 2, 1, 12, 19. This almost completely covers the range of typical domestic consumption values for electricity in the UK

(1900-4600 kWh annually for unrestricted domestic customers, 2500-7100 kWh for those on Economy 7 tariffs (Ofgem, 2017)). Only houses 1, 6 and 7 had rooftop PV, but Murray et al. (2017) had made the load measurements to exclude the effects of PV generation. The processing of the load data as described above was done by B. D. Smith, a co-author of (Sun et al., 2020). A sample of the load data for House 1 is shown below in Figures 2.8 and 2.12.

Figure 2.6 shows how each household's consumption is distributed between day (typical sunlight hours, 08:30-17:00), night (Economy 7 night rate hours, 00:00-07:00) and twilight (the morning and evening hours in between), comparing weekdays to weekends and 'winter' (November-April) to 'summer' (May-September). It is clear that winter-time consumption is slightly higher than summer-time, and that twilight consumption tends to be highest, though more evenly distributed between day and twilight at weekends, as is typical for people who are out at work during the day on weekdays. Exceptions are House 5 which has atypically high weekend daytime consumption, and House 8 which consumes more at night. The latter suggests that it may be on an Economy 7 tariff (see Section 2.4.4 below) and actively optimising its consumption pattern accordingly, for example by using a night storage heater.

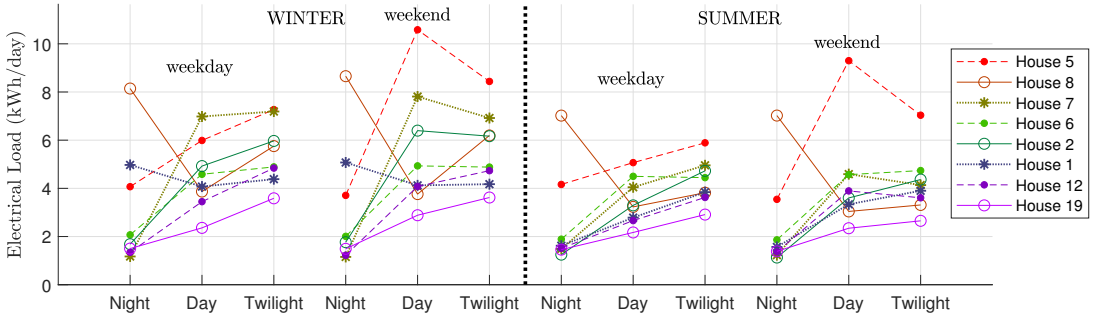

FIGURE 2.6: Each house's electrical load (kWh/day) during hours of night (Economy 7 hours, 00:00-07:00), day (typical sunlight hours, 08:30-17:00) and twilight (07:00-08:30, 17:00-00:00), at weekdays and weekends, and comparing 'winter' (November-April) and 'summer' (May-September).

The same year's data is repeated for each of the 25 years within the temporal boundary, to give $P_d(t)$. There is insufficient reliable data to adjust the load profiles to future years. It is possible that advances in energy efficiency will result in lower consumption; it is also possible that new highly energy-consuming appliances will become the norm. In the case of EVs and electric heat pumps, this is not necessarily bad from an environmental perspective as electricity has so far proven easier to decarbonise than transport or heat (Energy and Climate Change Committee, 2016). The uncertainty in how load profiles will change in future is the key reason why it is so important to model a range of households: variation in electricity consumption today is used as a proxy for variation in possible future scenarios. As discussed above in Section 2.1.1, the simplification is made that $P_d(t)$ remains the same between different configurations (with/without PV/battery) for each household, as there is not a clear consensus on whether it would increase or decrease upon installation of PV or batteries (Deng and Newton, 2017; Sekitou et al., 2018).

2.2.2 PV generation

Generation power (instantaneous values) were logged for a 3.6 kW_p rooftop PV array with 3.6 kW inverter. The system is located in Reading (UK, latitude 51.5° north) and is southeast-facing, inclined roughly 45° from horizontal. Data were logged at intervals of 1-4 s for the period 2 December 2015 to 30 November 2016. The system is owned by D. Hood, who implemented the data logging and made the data available upon request.

It was shown by Weniger et al. (2013) that tilt and azimuth angle had very small effects on a PV-battery system's degree of self-sufficiency: for the system they modelled, were its PV array angled the same as Hood's, its self-sufficiency would be 55 % rather than the optimum of 56 %. Although the use of self-sufficiency as a metric of anything is questionable (Sun et al., 2018a), these results do indicate that it should be unnecessary to adjust Hood's dataset. It is representative enough of a rooftop PV system in the UK.

As the timesteps were irregular, data were averaged to 15-s timesteps, in keeping with load data (see Section 2.2.1). The data logger was known to switch off when PV generation is zero, such as at night - therefore if no data were logged for more than 6 continuous hours according to the timestamps, they are filled in with zero values. Gaps of 5 minutes or less are filled with the previous value. Gaps of between 5 minutes to 6 hours are filled with data from the day ahead (in the first half of the year) or the day behind (in the second half). Any gaps remaining are linearly interpolated over. Any days for which more than 95 % of the values are zero are assumed to be erroneous, as the most likely cause would have been malfunctioning of the data logger rather zero irradiance for over 21 hours. Those days (two of them) are replaced entirely by the previous day's data. Another possibility is that the inverter malfunctioned on those days and no power truly was delivered from the PV; however, given the typical 10-year warranty of PV inverters (Midsummer, 2019), it is unlikely that this occurrence would repeat every year. A sample of the PV data is shown below in Figure 2.8 and 2.12.

The same year's data is used for all houses, scaled to the required capacity P_{PV}, and repeated for all years within the temporal boundary, but reduced linearly by 1.0 % of the original values each year to account for PV degradation (Phinikarides et al., 2014). This gives $P_{gen}(t)$. The degradation rate of 1.0 % is higher than the 0.5 % used by most of the techno-economic literature reviewed in the previous chapter, but they had obtained this value from a less up-to-date study by Jordan and Kurtz (2013). The repeated use of only a single year's PV data may be criticised because solar irradiance varies from year to year, and an effect due to climate change over the 25-year temporal boundary cannot be ruled out: cloud cover may be affected, and temperature is projected to increase which would have a negative impact on PV generation (Dubey et al. (2013) found efficiency was reported to decrease by 0.1-0.6 % per K, from a baseline of roughly 15 %). Furthermore, regional variations in PV output exist even within GB. However, Reading is a fairly central location, the effects of climate change on cloud cover are uncertain, and the effects of temperature are small. Therefore the effects of year-to-year and regional PV output variation are considered out of scope and are topics for further work.

2.3 Operating Algorithms

The Greedy Algorithm has already been introduced in Chapter 1 Section 1.3.2. It is popular for its simplicity, requiring no forecasting but only knowledge of the PV generation $P_{gen}(t)$ and load $P_d(t)$ at the present time, as provided easily by appropriate sensors. By prioritising servicing of the load before charging the battery before exporting to the grid when generation exceeds demand, and using PV generation before discharging the battery before importing from the grid to service the load when demand exceeds generation, the total grid import $\sum_t P_g^-(t)\Delta t$ is minimised. This is equivalent to minimising costs on a flat electricity tariff, and minimising emissions under the assumption of a constant grid emissions intensity (kg CO_2/kWh, or other emissions) - at least, not varying by time of day. While it is possible to recoup savings in this way, as long as the battery cost is low enough and the difference between the

electricity retail price and export payment rate is great enough, it is never possible to recoup the embodied CO_2 of manufacturing the battery if constant grid CO_2 intensity is assumed (Uddin et al., 2017). This is because export must be credited at the same level as import, at the constant CO_2 intensity value multiplied by the energy exported, this being the CO_2 emissions of the grid generation being displaced by the export. Efficiency losses will only worsen the battery's life-cycle CO_2 (and other emissions) costs relative to PV only. (There may be indirect environmental benefits from encouraging more people to install PV who wouldn't otherwise, or from DNOs postponing network reinforcement, but discussion of these is deferred to later.)

However, when time variation of grid CO_2 intensity is taken into account, it becomes possible to assert a difference between CO_2 intensity of import and export, by importing at times of lower marginal CO_2 intensity than when exporting. A similar consideration comes into play when the electricity tariff is ToU rather than flat: the Greedy Algorithm is no longer guaranteed to be cost-minimising, but an opportunity is opened up for scheduling battery charging hours to coincide with low-price hours. For tariffs with pre-defined off-peak hours, such scheduling is straightforward (Farah et al., 2016; Faria et al., 2014; Li et al., 2015; O'Shaughnessy et al., 2018), but when price and indeed CO_2 intensity vary unpredictably, recourse has been sought to optimisation methods, as Li et al. (2015), Hassan et al. (2017), Abdulla et al. (2017) and Babacan et al. (2018) have done. These require forecasting of the relevant variables in order to schedule the battery charging/discharging to minimise the objective function (net cost or emissions) while satisfying all constraints. Babacan et al. (2018); Hassan et al. (2017) assumed perfect forecasting, while Li et al. (2015) simulated a random ± 15 % forecast error.

Abdulla et al. (2017) explored the effects of three different forecasting methods: naive periodic (the next day's load and generation are assumed to be identical to the previous day), multiple linear regression (load and generation are forecast to be a weighted sum of the previous 5 days'), and perfect forecasting. They calculated the "lifetime value" of a 5 kWh domestic battery, which they defined as the total electricity bill net savings compared to having PV only, over the predicted battery lifetime when operating under each forecasting regime. They found the lifetime value to be 3.6 times that achieved with the Greedy Algorithm when using their optimisation procedure with perfect forecasting. But for naive periodic and multiple linear regression forecasts, the benefit was only 2.3 and 2.6 times the Greedy Algorithm baseline, respectively. Breakeven could be achieved with perfect forecasting if the battery cost were below 1000 AUD/kWh, but with imperfect forecasting it would have to be around 750 AUD/kWh or lower.

The development of the Emissions Arbitrage Algorithm was motivated by a wish to avoid forecasting and computation-intensive (Abdulla et al., 2017) optimisation methods for scheduling. Because of this, it should be possible to improve upon it with such methods, but that is a research direction for further work. The logical flow of the simulation of both algorithms, Greedy and Emissions Arbitrage, are presented next. They are coded into the domestic PV-battery system model which constitutes the operation phase of the process tree, Figure 2.1.

2.3.1 Greedy Algorithm

Figure 2.7 shows the logical flow of the Greedy Algorithm. The calculation steps need to be undertaken in the order given to maintain consistency, in other words, not violating the laws of physics by creating or destroying energy, for example. With reference to Figure 2.3, consistency means the following relations must hold at all times (symbols defined in Table 2.3):

1. Charging and discharging cannot occur simultaneously: if $P_c^+(t) > 0$, then $P_c^-(t) = 0$, and if $P_c^-(t) > 0$, then $P_c^+(t) = 0$.

2. Grid export and import cannot occur simultaneously: if $P_g^+(t) > 0$, then $P_g^-(t) = 0$, and vice versa.

3. Power balance at the DC bus: $P_{gen}(t) + P_c^-(t) = P_{thru}^+(t)$ when discharging; $P_{gen}(t) - P_c^+(t) = P_{thru}^+(t)$ when charging.

4. Power balance at the consumer unit: $P_{thru}^+(t) = P_g^+(t) + P_d(t)$ when exporting; $P_{thru}^+(t) + P_g^-(t) = P_d(t)$ when importing.

5. The maximum power that can flow through the battery DC-DC bi-directional converter is its maximum rating P_{conv}, and the power downstream is η_1 times the power upstream (efficiency $\eta_1 < 1$ always).

6. Similarly for the bi-directional DC-AC inverter, power flow is limited to its maximum rating P_{inv}, and power downstream is η_2 times the power upstream ($\eta_2 < 1$ always).

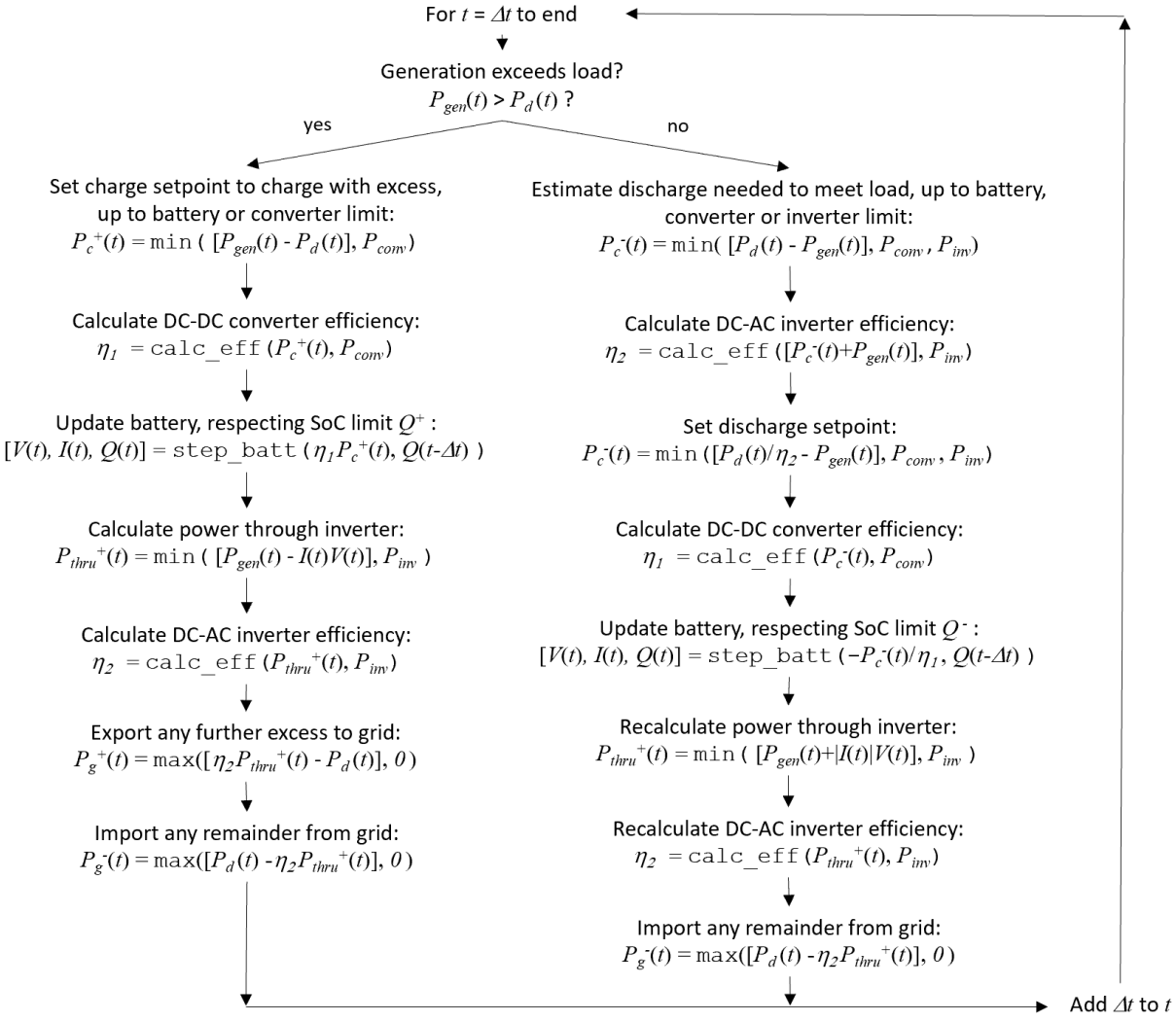

FIGURE 2.7: Logical flow of the simulation of the Greedy Algorithm. Text in `courier font` indicates a Matlab function (whether inbuilt or written by the author). Refer to Table 2.3 for symbol definitions, and Figure 2.8 for an example of the algorithm in (simulated) action.

The variables $P_c^+(t)$, $P_c^-(t)$, $P_g^+(t)$, $P_g^-(t)$, $P_{thru}^+(t)$, $P_{thru}^-(t)$, are initialised at zero for all t. This means if the algorithm (Figure 2.7) does not set their value at a specific timestep, the value at that timestep is zero by default.

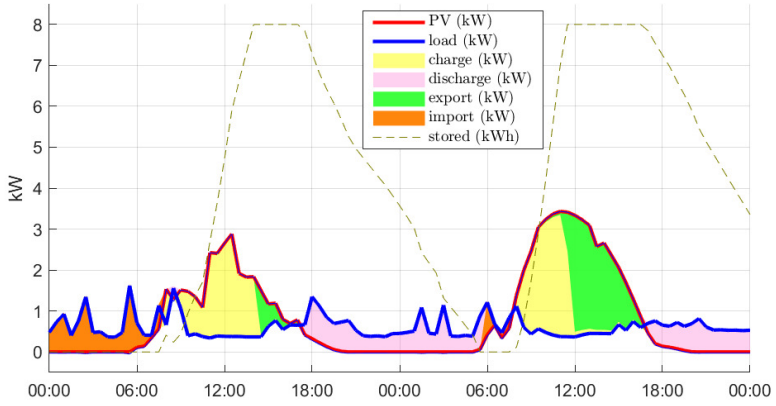

FIGURE 2.8: Operation of the Greedy Algorithm on 12-13 August for House 1 with 4 kW_p PV and 8 kWh battery (sizes chosen for illustrative purposes).

Symbol	Quantity	Unit
	Parameters	
Δt	Timestep	h
P_{conv}	Rated capacity of battery DC-DC converter	kW
P_{inv}	Rated capacity of DC-AC inverter	kW
Q^+, Q^-	Battery upper, lower state-of-charge limits	Ah
	Variables	
t	Time (restarts from 0 each year)	h
$I(t)$	Current entering battery (negative for discharge)	A
$V(t)$	Voltage of battery	kV
$Q(t)$	Charge on battery	Ah
MEF^+, MEF^-	Upper, lower thresholds for marginal emissions factor	kg/kWh
$MEF(t)$	Instantaneous marginal emissions factor	kg/kWh

TABLE 2.3: Definitions of symbols used in Greedy Algorithm, Figure 2.7, and Emissions Arbitrage Algorithm, Figure 2.9.

The function `calc_eff` calculates the converter or inverter efficiency as a function of throughput power and rated power, Equation (2.1). The function `step_batt` updates the battery's current $I(t)$ (positive for flowing in, negative for flowing out), voltage $V(t)$, and charge $Q(t)$, in response to a setpoint charge or discharge power. It respects the battery's SoC limits, not charging above Q^+ nor discharging below Q^-. Details of the function are explained in Chapter 4. More parameters are required for `step_batt` but are omitted from Figure 2.7 for clarity. P_{conv} and P_{inv} are decided upon in Chapter 5, which covers sizing of the system components. The PV converter, which also fulfils the MPPT function, has rated capacity P_{PV} or P_{inv}, whichever is smaller. There is little point in sizing the PV converter capacity to be greater than the inverter capacity, as the inverter would restrict power flow from the PV array anyway. In the early days of domestic PV, the solar inverter would be sized to match the maximum capacity of the PV array, as the cost of PV panels dominated the rest of the system. As the cost of PV panels has

decreased, this is no longer the case: it has become common for cost-saving reasons to use an inverter of slightly lower rating than the PV array, as it would generate at its maximum power for typically only a few hours in the entire year.

2.3.2 Emissions Arbitrage Algorithm

The Emissions Arbitrage Algorithm (EAA) was first introduced in a paper by the author (Sun et al., 2019). Its principle is to schedule the battery charging and discharging to coincide with times of low and high grid CO_2 intensity repectively, thus increasing the system's contribution to reducing net CO_2 emissions beyond what the Greedy algorithm would do. The thresholds for triggering charge/discharge modes are updated continuously based on historic time series of marginal grid CO_2 intensity, thus no forecasting is required for the EAA.

A more detailed discussion of the marginal emissions factor (MEF, a generalisation of marginal grid CO_2 intensity to other pollutant emissions) is deferred to Chapter 3. This includes its distinction from the average emissions factor (AEF) and why it is more valid to use MEF than AEF in this case, how a time series of $MEF_{CC}(t)$ (i.e. MEF in the Climate Change category, unit kg CO_2/kWh) is estimated for the purposes of this study, and the selection of the running-mean time period and deadband (see below). For the remainder of this chapter, the 'CC' subscript will be omitted for conciseness, but $MEF(t)$ should be taken to mean the time series of marginal grid CO_2 intensity.

It is assumed that $MEF(t)$ can be calculated centrally, in real-time in a standardised way, and transmitted to every PV-battery system that requires it as an input. This is not the reality in the UK today. There are many apps and websites that calculate grid CO_2 intensity in real-time (MyGridGB, 2019; Rogers and Parson, 2019), and it should be possible for a government-sanctioned official one to calculate $MEF(t)$ (rather than $AEF(t)$ as Rogers and Parson (2019) and MyGridGB (2019) do), and transmit $MEF(t)$ to consumers' smart meters. The information communications details of how the system would work in practice are outside the scope of the thesis. However, it is a feasible proposition as demonstrated by examples such as WattTime (2020) for the USA.

The EAA sets the battery to charge at its maximum allowed power when instantaneous $MEF(t)$ is below the lower threshold, 0.02 kg CO_2/kWh below the mean $MEF(t)$ of the previous 30 days. The battery is set to discharge at its maximum allowed power when $MEF(t)$ exceeds the upper threshold, 0.02 kg CO_2/kWh above the 30-day mean $MEF(t)$, i.e. a deadband of 0.04 kg CO_2/kWh. When the battery is charging, it does so from PV-generated electricity before importing from the grid; when discharging, it serves the load before exporting to the grid. The simulation of the algorithm must maintain consistency using the same rules as above for the Greedy Algorithm, but rules 3 and 4 are modified because the EAA sometimes allows charging directly from the grid, and therefore backflow of power through the inverter:

3. Power balance at the DC bus: $P_{gen}(t) + P_c^-(t) = P_{thru}^+(t)$ when discharging; $P_{gen}(t) - P_c^+(t) = P_{thru}^+(t)$ when charging and power flows forwards through the bi-directional DC-AC inverter; $P_{gen}(t) + P_{thru}^-(t) = P_c^+(t)$ when charging and power flows back through the inverter.
4. Power balance at the consumer unit: $P_{thru}^+(t) = P_g^+(t) + P_d(t)$ when exporting; $P_{thru}^+(t) + P_g^-(t) = P_d(t)$ when importing and power flows forwards through the inverter; $P_g^-(t) = P_{thru}^-(t) + P_d(t)$ when importing and power flows backwards through the inverter.

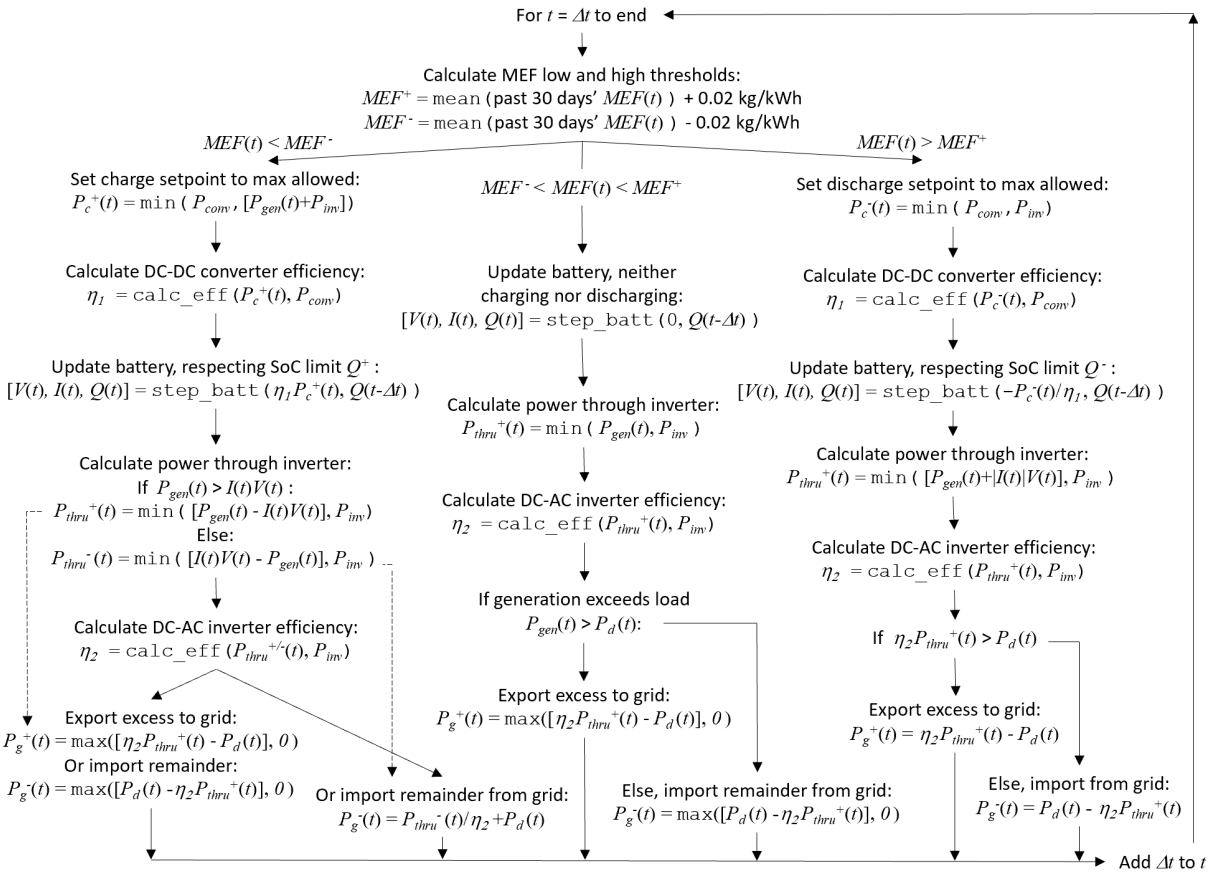

FIGURE 2.9: Logical flow of the simulation of the Emissions Arbitrage Algorithm. Text in `courier font` indicates a Matlab function (whether inbuilt or written by the author). Refer to Table 2.3 for symbol definitions, and Figures 2.10-2.12 for examples of the algorithm in (simulated) action.

For a real EAA programmed into hardware, the thresholds MEF^+ and MEF^- must be re-calculated continuously. A fast way to do this is to update the 30-day mean by adding $\frac{1}{\Delta t} MEF(t)$ to it and subtracting $\frac{1}{\Delta t} MEF(t - [30 \text{ days}])$ from it, every Δt, where Δt is the interval between re-calculations (Kantz and Schreiber, 2003).

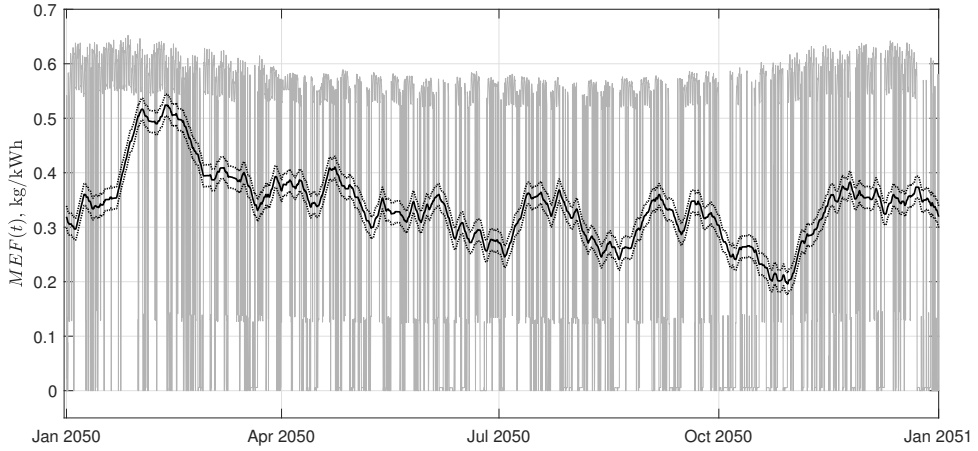

FIGURE 2.10: $MEF(t)$ across the year in an example scenario for 2050, shown with its moving mean of the previous 30 days, and limits MEF^+ and MEF^- which are respectively 0.02 kg/kWh above/below the moving mean.

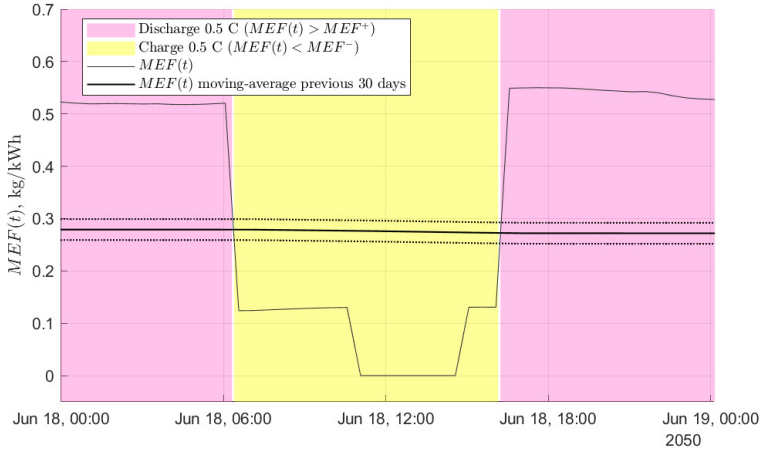

FIGURE 2.11: The above figure, zoomed in to 18 June, showing charge and discharge modes of the battery, defined respectively as when $MEF(t) < MEF^-$ and $MEF(t) > MEF^+$.

See Figure 2.12 for how the charge/discharge modes thus defined in the EAA interact with the real-time PV generation and household electricity consumption. The thin blue line indicates the charge/discharge setpoints relative to the household consumption. A small amount of charging is met by excess PV generation around 06:30 and 07:30, but it is met mostly by importing from a low-CO_2 grid. The battery is full by around 08:00, after which excess PV energy is exported, until discharge mode is entered, around 16:20. The battery then discharges, meeting the household consumption together with PV generation and exporting all excess to a high-CO_2 grid. Once empty, just before 18:00, subsequent consumption during discharge mode must be met by importing from the grid.

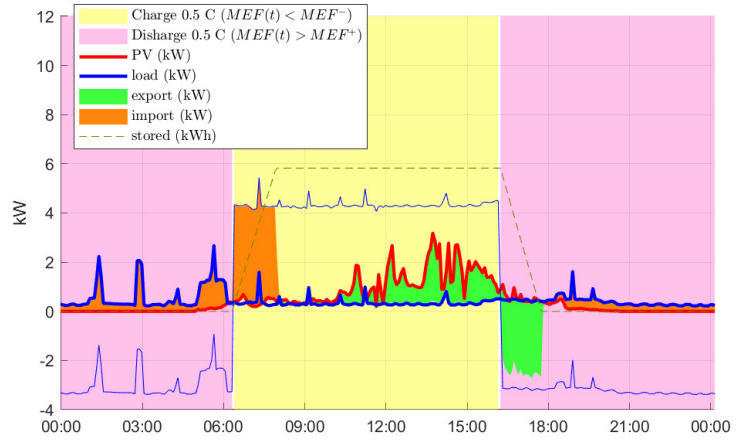

FIGURE 2.12: Operation of the Emissions Arbitrage Algorithm on 18 June for House 1 with 4 kW_p PV and 8 kWh battery (sizes chosen for illustrative purposes; battery degraded to 6 kWh capacity) in an example future scenario.

The decision was taken not to charge nor discharge the battery while $MEF(t)$ is within the deadband. This is because the EAA does not predict whether $MEF(t)$ will rise next, in which case charging would be preferred so that more can be discharged subsequently, or if $MEF(t)$ will fall, in which case discharging would be preferred so that the battery can accept more charge subsequently.

The EAA can easily be modified to perform price arbitrage rather than emissions arbitrage: by inputting

price data for the past 30 days rather than $MEF(t)$ data. The algorithm would work exactly as before, charging the battery when price is low and discharging when price is high. A suitable deadband (in GBP/kWh) would need to be chosen. This configuration is termed the Price Arbitrage Algorithm (PAA). The Greedy algorithm and EAA are compared in this study, but the PAA is discussed in terms of its potential to better align financial and environmental objectives, rather than being applied to any specific existing electricity tariff.

2.4 Pricing

The initial investment, or Capex, comprises the cost of installing P_{PV} kW_p of PV panels, E_B kWh of batteries, and BoS including solar and battery converters and bi-directional inverter in a single unit. The components size parameters P_{PV}, E_B, P_{conv} and P_{inv} are determined in Chapter 5. This section analyses information on the pricing of these components, to find what a UK homeowner would reasonably expect to pay for any size of system.

In addition to this, the homeowner would pay bills every year for the electricity they import from the grid. In the UK, electricity retail is privatised; this means consumers can choose a tariff from a range offered by different electricity supply companies, who in turn purchase from electricity generators the required volumes in the correct time periods to supply all their customers. The most common tariff structures are discussed, along with how they are used to calculate the household electricity bills each year, using grid import results $P_g^-(t)$ produced by the simulation.

2.4.1 PV array pricing

Multicrystalline silicon (also known as polycrystalline, poly-silicon, poly-c Si or multi-c Si) is the most common PV technology type in use, two-thirds of all PV installations globally being of this type (IRENA, 2016). While developments in monocrystalline, thin-film (such as cadmium telluride, CdTe, or copper indium gallium selenium, CIGS), and even newer types, are predicted to bring prices down and expand their market share, it was decided to model a multi-c Si PV array in this thesis as they are likely to still be dominant well past 2030 (IRENA, 2016). This is in keeping with the goal and scope, which is to assess the sustainability of a generic domestic PV-battery system in GB rather than any one specific system.

The UK government department of Business, Energy and Industrial Strategy (BEIS, 2019c) have compiled statistics on the installed costs of small-scale PV systems, but report average GBP cost per kW_p capacity for sizes 0-4 kW_p, 4-10 kW_p and 10-50 kW_p. More disaggregated figures can be found at the websites of Solar Guide (2018) and Clissit (2019). These are plotted in Figure 2.13.

The sources plotted in Figure 2.13 do not specify whether or not value added tax (VAT) is included. Its rate was 5 % for solar PV until October 2019, when it changed to 20 % (Clissit, 2019). The costs do include roof mounting and labour to install. Multi-c Si is the cheapest of PV technologies (IRENA, 2016) so that was why the lower end of the cost range was graphed as well as the midpoint for Clissit (2019). The true cost of a PV installation depends on the specifics of the home's location and its roof, whether more effort would need to go into designing the array to fit the roof (Figure 2.14). Bearing in

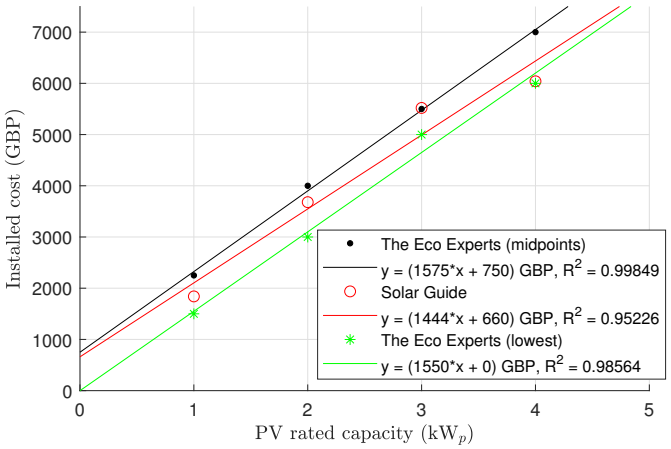

FIGURE 2.13: PV installed cost for different array sizes (Solar Guide (2018), The Eco Experts (Clissit, 2019)), and their linear regression equations.

mind all these considerations, the PV cost C_{PV} is taken to be:

$$C_{PV} = c_{PV,0} + c_{PV,1} P_{PV} \qquad \text{(GBP)} \tag{2.2}$$

where the fixed cost $c_{PV,0} = 700$ GBP, and the size-dependent cost $c_{PV,1} = 1500$ GBP/kW$_p$, for PV size P_{PV} kW$_p$. This is consistent with BEIS (2019c) statistics for 2018/19: median cost 1678 GBP/kW$_p$ and mean cost 1816 GBP/kW$_p$ for a 0-4 kW$_p$ system. Greater precision than this is not justified within the goal and scope.

FIGURE 2.14: PV arrays of differing complexity. Left: requiring 9 triangular panels, 4 square panels, and including a solar thermal panel; right: comparatively simple 8 × 2 array of rectangular panels. Photos by the author.

Solar Guide (2018) also compiled data on PV costs to produce a graph of the cost decline of a 4 kW$_p$ array: from 20 000 GBP in 2010, reaching a plateau at 7000 GBP around 2015. The plateau is consistent with BEIS (2019c) cost data, which shows the plateau continuing to the present day. The PV cost was assumed not to decrease any further in future for the purposes of this thesis. The same is unlikely to be true for newer PV technologies, but these are beyond the scope of this study.

2.4.2 Battery pricing

A home battery can only be purchased from a discrete set of possible sizes, however there are so many suppliers in the market and most of them offer modular batteries which can be connected together, that an almost continuous range of sizes is readily available. This thesis will focus on Li-ion batteries as these are the most common type being installed in domestic PV-battery systems in GB, in accordance with the goal and scope.

Naked Solar (2019) surveyed the installed costs of a range of home battery products (all Li-ion, including battery inverter and installation labour, 5 % VAT excluded). GreenMatch (2019) gave estimated prices for a range of Li-ion battery sizes (usable capacity, not stated whether VAT was included or not). The costs from both these sources are plotted against battery capacity in Figure 2.15.

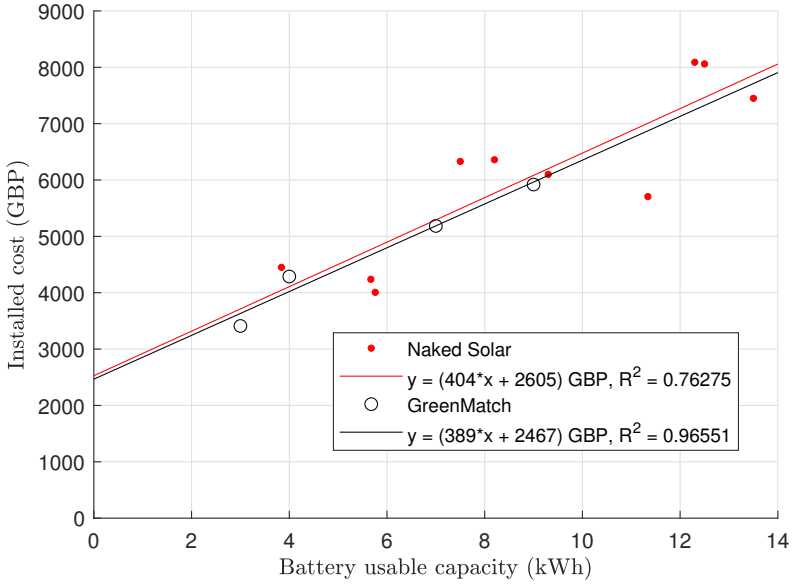

FIGURE 2.15: Battery installed cost for different sizes (GreenMatch, 2019; Naked Solar, 2019), and their linear regression equations.

The size-dependent costs found by linear regression of these data are 404 GBP/kWh (Naked Solar, 2019) and 389 GBP/kWh (GreenMatch, 2019). They are towards the lower end of what EnergySage (2019) claim, that battery costs (excluding inverter and labour) are 400-750 USD/kWh (exchange rate 0.8 GBP/USD at time of writing). It was found that the rather low goodness of fit $R^2 = 0.76$ for the Naked Solar (2019) data could be improved, firstly by excluding the SolaX Hybrid X1 TriplePower 6.3 kWh and 12.6 kWh from the dataset because they both have a warranty of 5 years, and thus are not directly comparable to all the others which had warranty 10 years. And secondly, by regressing cost against both battery capacity (kWh) and maximum discharge power (kW). The goodness of fit R^2 increases to 0.85: this is to be expected, as a higher claimed power limit implies a higher rating of power electronics (converter or inverter), which would be reflected in the cost. The best-fit equation of this multiple linear regression is $y = (404x_1 + 16x_2 + 2605)$ GBP, where y is the total cost, x_1 is battery capacity (kWh) and x_2 is battery discharge power limit (kW). The remaining cost variation may be caused by other variables such as battery chemistry (Li-ion encompasses a range of cathode chemistries), or details in the organisation of the supplier companies.

These findings can be compared to the average costs Goldie-Scot (2019) found for EV batteries. They stood at 176 USD/kWh in 2019, much lower than for home battery products despite being a very similar

product. Tesla (2018) in fact use the same size-18650 cylindrical batteries across their entire operation, for transport and stationary applications. As Goldie-Scot (2019) explained, a likely explanation is that large car manufacturers can command a much lower price due to the size of their orders compared to in other applications. It can be expected that if the home battery market expands in future, their costs will also decrease. For this study it is assumed that the size-dependent portion of battery cost decreases at the same rate as Goldie-Scot (2019) found for EV batteries, 18 % per year, to an eventual minimum of 50 GBP/kWh, as Berckmans et al. (2017) estimated this to be the cost for Li-ion battery raw materials. The fixed portion of the cost is taken not to change over time, as they represent labour and fixed overheads from running a battery supplier business. As with PV, different factors may affect the pricing of any individual battery system.

The pricing of second-life batteries is analysed separately in Chapter 4. Because they may need to be replaced more frequently than new batteries, the second-life battery replacement schedule may not coincide with the inverter replacement schedule. This is why the pricing and environmental impacts of battery and BoS are treated separately in this thesis. To separate out the BoS fixed and size-dependent costs, the foregoing must be considered together with the next section.

2.4.3 Balance of System pricing

BoS refers to all the additional equipment needed for the PV array and battery to function as required. This includes the power electronics (DC-DC converters for each PV and battery, and DC-AC inverter) shown in Figure 2.3, but also refers to sensors and micro-controllers which enact the control logic of the operating algorithm and keep the system within specified operating conditions. For example, the battery's life is reduced if its voltage, current, SoC and temperature are not kept within the limits it was designed for (the mechanisms for degradation are discussed in Chapter 4). While most EVs have a heater to warm up the battery when it is needed after a cold night, temperature control is far from ubiquitous for home batteries. In regions that experience extreme heat, such as California (USA) and Australia, a home battery may be fitted with a cooling system (fans or liquid coolant in a refrigeration cycle). Cooling is also common for larger, MW-scale battery systems, even in temperate climates, as the operation of so many batteries packed closely together can generate sizeable quantities of heat. It is assumed that the system under study does not include any active temperature control equipment, as its costs would outweigh the small benefit it could give in GB's temperate climate.

As found in the previous section, a multiple linear regression of Naked Solar (2019) battery cost against kWh capacity and kW discharge power limit gives a power-dependent cost of 16 GBP/kW. This is a reasonable estimate for the size-dependent portion of the battery power converter cost, but there is no indication of how much of the 2605 GBP fixed cost can be attributed to the battery and how much to the BoS. EnergySage (2019) state that the Tesla Powerwall 2.0 (13.5 kWh, with built-in inverter) has a list price of 6700 USD, while the LG Chem RESU (9.3 kWh, excluding inverter) is typically sold for 6000-7000 USD. Even taking the lowest price in that range, there would appear to be no cost difference between including or excluding an inverter, as the 700 USD difference could be accounted for by the difference in capacity.

However, a clue can be found in the prices for a SolaX hybrid inverter (excluding battery) listed at Midsummer (2019): 1336.5, 1417.5, 1498.5 GBP for rated capacity of 3, 4, 5 kW respectively. This is consistent with a fixed price of 1093.5 GBP and a size-dependent cost of 81 GBP/kW. It is the closest

product to a complete BoS for a DC-coupled PV-battery system on the website, the others being PV inverters and converters, smart EV chargers, and other products.

In consideration of all the above, the battery cost C_B and BoS cost C_{BoS} are taken as:

$$C_B = c_{B,0} + c_{B,1} E_B \qquad \text{(GBP)} \tag{2.3}$$

$$C_{BoS} = c_{BoS,0} + c_{BoS,1}(P_{conv} + P_{inv} + \texttt{min}[P_{inv}, P_{PV}]) \qquad \text{(GBP)} \tag{2.4}$$

where the battery fixed cost $c_{B,0} = 1500$ GBP, its size-dependent cost $c_{B,1} = 390$ GBP/kWh for a battery of usable capacity E_B kWh; BoS fixed cost $c_{BoS,0} = 1000$ GBP, its size-dependent cost $c_{BoS,1} = 25$ GBP/kW for battery converter rated at P_{conv} kW, bi-directional inverter rated at P_{inv} kW, and PV converter rated at $\texttt{min}[P_{inv}, P_{PV}]$ kW (as explained in Section 2.3.1). This is justified by the fact that DC-DC converters and DC-AC inverters have very similar hardware, both being circuit boards with switches (MOSFETs or IGBTs) and heat sinks; the difference is in the circuit topology and switching sequences. Equations (2.3) and (2.4) with these values provide an adequate approximation to the price data reported by Naked Solar (2019), though they could not be made perfectly consistent with every source of information used.

It is assumed that the entire BoS is replaced once during the system lifetime, for the same price, in year 13 (halfway to $N = 25$ years). This is slightly above the 10-year warranty offered by SolaX for its hybrid inverter (Midsummer, 2019), but not unreasonable: companies tend to set a warranty period one or two standard deviations below the expected mean lifetime of a product, in order to reduce the risk of them bearing the cost of a repair or replacement within the warranty period. Indeed, Hoppmann et al. (2014) took the inverter lifetime to be 15 years, though Camilo et al. (2017) only took it to be 11 years. No replacement of the PV array is required as $N = 25$ years was chosen for being the typical warranty period of a PV array. Replacement of the battery will be analysed separately in Chapter 4. The O & M costs are taken to be zero, as most if not all of any repairs would take place within the warranty period of all components of the system. Maintenance such as PV panel cleaning is assumed to be done by the homeowner rather than as a paid-for service.

It is interesting to compare this survey of PV-battery system component costs to the values used in the literature. As expected, declining costs mean papers published more than a few years ago reported much higher costs: Tant et al. (2013) took Li-ion battery costs as 1000 EUR/kWh plus 270 EUR/kW, Mulder et al. (2013) 1476 EUR/kWh (12 400 EUR for 8.4 kWh), Hassan et al. (2017) used surprisingly high figures of 990 USD/kWh for the battery and 3.752 USD/W_p for PV, given their year of publication. A worrying trend in the existing literature is for fixed costs to be ignored: the previous three cited; the PV and battery costs Hoppmann et al. (2014) used were reasonable for the time (PV 1.7 EUR/W_p, PbA battery 171 EUR/kWh and 172 EUR/kW), but they took the inverter to cost only 170 EUR/kW; Naumann et al. (2015) similarly assumed batteries and inverters to decline in cost to 200-500 EUR/kWh and 40-300 EUR/kW respectively in 2034, but with no fixed costs; Parra et al. (2016) used the figure 350 GBP/kWh for Li-ion battery cost, which was optimistic at the time, but 1100 GBP/kW for the inverter, which is so high that it probably mostly cancelled the error. Truong et al. (2016) avoided this problem by focusing on a specific battery product, the Tesla Powerwall (6250 EUR for the 6.4 kWh AC-coupled model, of which 1385 EUR was fixed installation cost and 1250 EUR for the inverter, and 5000 EUR for the 6.4 kWh DC-coupled model). Camilo et al. (2017) appear to have done similarly, quoting prices separately for every size of system they analysed. Bertsch et al. (2017) too included a 1330 EUR fixed installation cost in addition to PV at 1130 EUR/kW_p and batteries at 500 EUR/kWh.

It is important to account for fixed and size-dependent costs correctly, otherwise this will cause errors if the system components are sized to optimise for a financial objective function (IRR, MCoE, etc.).

2.4.4 Electricity pricing

The most common electricity tariffs in the UK are flat-rate and Economy 7. In both cases there is a fixed standing charge component, charged to the customer daily. On a flat-rate tariff, the customer is charged a constant GBP/kWh rate for each unit (kWh) of electricity they consume, regardless of when during the day. On an Economy 7 tariff, the customer is charged a lower night rate for each unit consumed during 7 hours of the night, typically 00:00-07:00, and a higher day rate during all other hours. This is to encourage a shift in demand to night-time for those who are able to do so, such as homes with night storage heating. (Of the 8 houses in the dataset used in this thesis, only House 8, the second-highest-consuming, fits this description.) Demand tends to be lower at night time, so if the daily variation can be smoothed out, generator plants can run with less ramping up or down, and therefore more efficiently. Many customers opt for a 'dual fuel' tariff, which includes both gas and electricity. Only electricity is considered in this thesis, and so only single-fuel electricity tariffs are considered.

The UK government department of Business, Energy and Industrial Strategy (BEIS, 2019a) collect statistics on household electricity bills. The 2018 UK average charges are given in Table 2.4. They are for customers who pay by direct debit, and as such are a conservative estimate of what a homeowner might have to pay, as paying by standard credit or pre-payment meter are more expensive.

	Standing charge (GBP/day)	**Standard/day rate (GBP/kWh)**	**Night/low rate (GBP/kWh)**	**High rate (GBP/kWh)**
Flat-rate	0.1904	0.1537	_	_
Economy 7	0.2085	0.1861	0.08952	_
Tide	0.2970	0.1627	0.0791	0.3255

Table 2.4: UK average electricity tariffs for flat-rate and Economy 7 customers paying by direct debit in 2018 (BEIS, 2019a, QEP 2.2.4), and the Green Energy (2019) Tide tariff (applicable until 30 September 2020).

It is possible for individual customers to obtain better deals than the values given in Table 2.4, as is the nature of average values. However, a lower standing charge is often coupled with higher per-unit charges, and vice versa. The former case would favour a household with lower annual consumption, and the latter a household with higher annual consumption. For simplicity this distinction is neglected in this study.

In addition to flat-rate and Economy 7, electricity suppliers are beginning to offer more complex tariff structures. The Green Energy (2017) Tide tariff is a time-of-use (ToU) tariff like Economy 7, but also features a much higher rate on weekday evenings (16:00-19:00) as well as lower rate at night-time (23:00-06:00, weekdays and weekends). The theory is to incentivise load-shifting away from peak periods, as with Economy 7, but with more rate levels, now that consumers have increasing load-shifting capability thanks to home batteries and EV smart charging. Octopus (2019) take this further with their Agile tariff, which is dynamic time-of-use. This means there is not a fixed weekly pattern of charges in peak/off-peak periods, but a dynamically changing per-unit charge, communicated to the customer's mobile phone a day in advance.

For this thesis, an export tariff is paid to the homeowner for all electricity exported to the grid, at a rate of 0.05 GBP/kWh in 2019. This is in line with the export tariff offered in the FiT scheme before it was discontinued (Ofgem, 2019), and that currently being offered by Octopus and Green Energy, amongst other suppliers, for PV export.

The change in electricity bills over the temporal boundary of the system is informed by (BEIS, 2019a, QEP 2.2.2). The average increase for flat-rate direct debit customers was 3.4 % per year in the period 1998-2018, but had increased to 5.5 % per year for 2008-2018. In the latter period, the average increase was 6.7 % per year for Economy 7 direct debit customers. For simplicity, the rate of 5.5 % per year is applied to all tariffs and all components (standing charge, per-unit rates, export rate) in this thesis. Note that these increases do not account for inflation (they are nominal rather than real-terms increases). The inflation rate (consumer prices index including owner-occupiers' housing costs, CPIH) averaged 2.1 % in the period 2008-2018 (ONS, 2019), meaning there was also a real-terms increase in electricity bills, as 5.5 % is higher than this.

The electricity bill in each year is calculated as:

$$C_g = 365 \cdot c^-_{g,0} + \begin{cases} \sum_t \left[c^-_{g,1} \cdot P^-_g(t) - c^+_{g,1} \cdot P^+_g(t)\right] & \text{Flat} \\ \sum_{day} \left[c^-_{g,1} \cdot P^-_g(t)\right] + \sum_{night} \left[c^-_{g,2} \cdot P^-_g(t)\right] - \sum_t \left[c^+_{g,1} \cdot P^+_g(t)\right] & \text{Economy 7} \end{cases} \tag{2.5}$$

where $c^-_{g,0}$ is the daily standing charge, $c^+_{g,1}$ the export rate, $c^-_{g,1}$ the per-unit standard/day rate, and $c^-_{g,2}$ the per-unit night rate, appropriate to the tariff (flat or Economy 7) as discussed above. The Green Energy Tide tariff is calculated similarly to the Economy 7 tariff, but rather than two sums over day (07:00-00:00) and night (00:00-07:00), there are three sums: standard (weekdays 06:00-16:00 and 19:00-23:00, and weekends 06:00-23:00), low (23:00-06:00), and high (weekdays 19:00-23:00), with the prices appropriate to each as given in Table 2.4. This is illustrated for one weekday in Figure 2.16

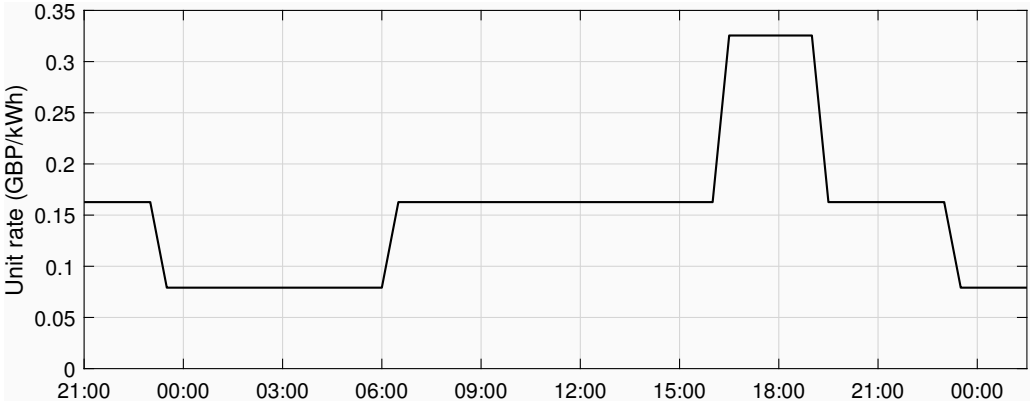

FIGURE 2.16: The time-of-use unit rate (GBP/kWh) across a weekday for the Green Energy Tide (2020) tariff, showing the low period during the night (23:00-06:00), the high one in the evening (16:00-19:00), and standard rate the rest of the time.

The price rates $c^-_{g,0}$, $c^-_{g,1}$, $c^-_{g,2}$, $c^+_{g,1}$, all increase at 5.5 % per year relative to the 2018 values in Table 2.4.

2.4.5 Discount rate and inflation

As discussed in Chapter 1 Section 1.1, the discount rate r is a measure of the decrease in value of a cash flow in future compared to the present, due to uncertainty and the missed opportunity cost of investing in some alternative. It is used in calculating NPV, RoI and MCoE. For a homeowner, the most likely alternative to investing in a PV-battery system is to put their money in a savings account. Brett (2019) has compared the returns from cash ISAs and stocks and shares ISAs (individual savings accounts) in the UK in the period 1999-2018, finding annual real-terms returns averaging 0.6 % and 2.9 % respectively (nominal returns 2.6 % and 5.0 %). This is in line with the discount rates ranging from 1-6 % used in the literature when calculating financial returns for a domestic PV-battery system. Brett (2019) also found the total amount of money held in cash ISAs to be consistently higher than in stocks and shares ISAs. In light of this, and the fact that 4 % is the most commonly used nominal discount rate in the literature for developed European countries, 4 % is used in this study.

The inflation rate is a measure of the decrease in each unit of currency (such as GBP) over time. The UK Office for National Statistics (ONS, 2019) measure various indices of inflation by comparing the nominal costs from year to year of a variety of commonly bought goods. Their foremost index CPIH averaged 2.1 % in the period 2008-2018. The effect of inflation cannot be neglected over a temporal boundary as long as 25 years. This study accounts for inflation thus:

- Cash flows are calculated first in nominal rather than real terms (e.g. electricity tariff rates increase at 5.5 % rather than the inflation-adjusted value),
- Future cash flows are then inflation-adjusted by dividing by 102.1 % for each year from 2019 (i.e. cash flows in 2020 are divided by 102.1 %, in 2021 by 104.244 %, etc.), to give all values in units of 2019 GBP,
- The nominal discount rate of 4 % is inflation-adjusted by 2.1 % according to Equation (1.2) in Chapter 1, to give a real discount rate of 1.86 % - this is the discount rate used in calculating NPV, RoI, MCoE, after cash flows have been inflation-adjusted.

Note that for the component costs found above, all changes over time are described in nominal rather than real terms. Therefore, a PV array for example, which nominally costs the same purchased in 2019 as in any future year, is in real-terms cheaper when purchased in future due to the effect of inflation. That is, the costs of PV and BoS, and the fixed portion of the battery cost, are assumed to decrease in real terms while remaining constant in nominal terms.

For this study, the investment start year is taken to be 2020 for the baseline case. Sensitivity to the investment start year is analysed in Chapter 6. Costs of PV, battery and BoS as found above are assumed to include VAT, although it is not clear from the sources if they always do so. This uncertainty is also discussed in Chapter 6.

2.5 Components Embodied Environmental Impact

Embodied, or cradle-to-gate, impacts refer to the impacts of manufacturing a product, as far back as mining and harvesting all the raw materials needed, before it reaches its operational phase. Embodied impacts are the environmental analogy to Capex in the financial calculations.

As well as deciding on central estimates for each ReCiPe midpoint impact category, for PV, battery and BoS, an uncertainty value is estimated for each as well. This uncertainty encompasses both the true variance found in real systems, and the variation in methodologies used to quantify the environmental impacts of their manufacture and installation.

Because there were too few data sources from which standard deviation could robustly be calculated, an uncertainty estimate is defined here for each midpoint category of each component as 1/4 the difference between the highest and lowest values from all the sources, or the central estimate itself, whichever is smaller. The reasoning behind this is that for a normally distributed random variable, 95 % of all values measured are expected to fall within two standard deviations either side of the mean (Kennedy and Neville, 1966). Thus the difference between the highest and lowest values is estimated as covering four standard deviations.

Sometimes this estimator of standard deviation is greater than the central estimate itself. This happens because the central estimate is not always taken as the mean of all the values from different sources: if one source is particularly comprehensive and reliable, it is used for the central estimates of all ReCiPe midpoint impacts, as consistency is deemed most important. When the uncertainty estimator is greater than the central estimate itself on any impact category, it would imply that the likelihood of negative values is non-negligible. To reduce this effect, the uncertainty value is taken to be equal to the central estimate value in such cases. The implication is that the mean value minus one standard deviation for that impact is zero, and the mean plus one standard deviation is twice the central estimate.

There is an undeniable degree of subjectivity in this method; the strongest defence is that it is more statistically informative than using only a single source for each set of environmental impact values, as is the case when using an LCA database.

2.5.1 PV array environmental impacts

A typical manufacturing process for multi-c Si PV panels (Bekkelund, 2013) is described qualitatively first, followed by quantitative data on the impacts per kW_p installed.

Metallurgical-grade Si is obtained by reduction of silicon dioxide from sand in an electric arc furnace, using carbon as the reducing agent. The molten Si tapped off from the furnace must be further purified to solar-grade, commonly by mixing it in powdered form with hydrogen chloride (HCl) gas in a fluidised bed reactor at 300 °C. The resultant trichlorosilane gas is reduced with hydrogen gas, leading to deposition of Si on to high-purity Si rods placed in the reactor chamber. The HCl and other gaseous by-products are recovered and reused. Chunks of solar-grade Si thus grown are melted in quartz crucibles and cooled from the bottom up to form ingots. The ingots are sawn into square wafers by multi-wire sawing, with a kerf loss of typically 150-180 μm thickness per 180-200 μm-thick wafer. The wafers are cleaned with hydroxides and acids, doped with boron (to make p-type Si) and selectively doped with phosphorus (to make p-n junctions). Silver and aluminium back contacts are applied by screen printing, a silicon nitride anti-reflective coating is applied by chemical vapour deposition on to the front surface, and the individual solar cells are connected together with electrically conductive copper into a module. The module is encapsulated in transparent thermoplastic polymer (such as ethylene vinyl acetate) with glass to provide rigid support, and a foil (tedlar or mylar) backing. Each module, or panel, requires a junction box for the electrical connections and the roof mounting is typically aluminium.

The process is very energy-intensive, especially the steps that require temperatures high enough to melt silicon. The breakdown provided by Bekkelund (2013) indicates the silicon production and processing steps to be the greatest contributors to nearly all impact categories. An exception is MD (metals depletion), which is mostly due to the silver and copper needed for the electrical connections. Also of note is the use of various chemicals for purifying, cleaning, and for functionality of the solar panels, which despite efforts to keep within closed loops, can leak into the environment in small quantities.

The sources of data used for PV array manufacture and installation impacts were: Bekkelund (2013), Palanov (2014), Hertwich et al. (2015), Frischknecht (2017). They are collated in Table 2.5 below. Impacts were desired per kW_p installed so they could be multiplied by the PV capacity P_{PV} to give the total impact. Unlike financial cost, there is assumed to be zero fixed portion to the embodied environmental impact. This convention is standard in LCAs of mass-manufactured products, as the same plant (equipment, machinery, etc.) is used to make typically millions of units, and so the impacts of the plant are spread out over so many units as to be negligible (Klöpffer and Grahl, 2014).

All these sources reported impacts per kWh electricity generated as the functional unit, except Bekkelund (2013) who reported them per m^2 installed. These had to be converted using data given within each of the sources, and where needed, converted also to the units appropriate to the ReCiPe 2008 framework. Although they include impacts of shipping, roof mounting and inverter, unfortunately none of them include impacts of recycling or disposal.

Because Bekkelund (2013) reported impacts under ReCiPe 2008 already, theirs was the most complete LCA. Midpoint values for multi-c Si PV made by the Siemens process were used as the central estimates of PV embodied impact, these being the most directly comparable to values given in the other sources. The conversion for array area to rated power was given as 0.0227 kW_p/m^2 (Bekkelund, 2013, p.108), so the midpoint values given were all divided by this factor to give the values in Table 2.5. As explained in Section 2.1.1, ALO and ULO are summed to give a single value for LO.

Palanov (2014) analysed a roof-mounted monocrystalline silicon PV array, and so care should be taken when comparing to multi-c Si, which is around 15 % efficient compared to 20 % for mono-c Si (and is accordingly cheaper) but otherwise very similar. They reported impacts under CML2001: CC, OD, ME, HT, IR, TA, LO, WD, FD, and MD were given, but PMF, POF, FE, FET, MET, TET, ALO, NLT were omitted. Their functional unit was kWh generated; for the 3 kW_p system they analysed, 77 487 kWh were assumed to be generated over its lifetime. This means every midpoint impact value given must be multiplied by 77487/3 to bring the functional unit to kW_p. Additionally, ME had to be multiplied by 0.039 to convert from units of kg NO_x to kg N, FD by 0.072 to convert from kWh to kg oil, and IR by 9.3×10^7 to convert from DALY to kg U235. Other impact values were already given in the units required. The conversion factors used were given by Goedkoop et al. (2008b) for converting to ReCiPe units from other LCA frameworks. Raw data from Frischknecht (2017); Hertwich et al. (2015); Palanov (2014) are given in Appendix A1.

Both Bekkelund (2013) and Palanov (2014) give a detailed breakdown of which processes in PV manufacture and installation contribute to each midpoint impact, which Hertwich et al. (2015) and Frischknecht (2017) do not do. The latter two analysed roof-mounted multi-c Si arrays in North America and Belgium respectively, amongst other electricity generation technologies.

Hertwich et al. (2015) reported ReCiPe midpoint impacts, but omitted OD, ME, IR, FD, and they aggregated ecotoxicity into a single category, and likewise land use. They assumed 22 000 kWh generated

per kW_p installed over the system lifetime, so midpoint values were multiplied by 22 000.

Frischknecht (2017) reported impacts under the ILCD framework. These were converted to ReCiPe units using conversion factors given by Owsianiak et al. (2014) - note that human toxicity cancer and non-cancer effects were summed for HT, and non-renewable CED was used for FD. The ILCD impacts had been calculated for a 3 kW_p rooftop system generating 880 $kWh/kW_p/y$ for 30 years. To convert from a functional unit of kWh generated to kW_p installed, impacts were multiplied by $30 \times 880 = 26\ 400$.

		Palanov (2014)	**Hertwich et al. (2015)**	**Frischknecht (2017)**	**Central Estimate (Bekkelund, 2013)**	**Uncertainty**
CC	kg CO_2/kW_p	1.26×10^3	1.27×10^3	1.65×10^3	1.15×10^3	1.25×10^2
OD	kg CFC11/kW_p	5.11×10^{-4}	-	6.02×10^{-5}	7.88×10^{-5}	7.88×10^{-5}
HT	kg DCB/kW_p	2.26×10^3	1.79×10^3	8.50×10^3	1.94×10^3	1.68×10^3
POF	kg NMVOC/kW_p	-	4.25	6.85	4.08	6.93×10^{-1}
PMF	kg PM10/kW_p	-	2.71	2.07	2.66	1.48×10^{-1}
IR	kg U235/kW_p	3.47×10^2	-	9.00×10^1	5.70×10^2	1.20×10^2
TA	kg SO_2/kW_p	5.95	9.90	7.84	8.66	9.88×10^{-1}
FE	kg P/kW_p	-	9.79×10^{-1}	3.46×10^{-1}	1.18	2.09×10^{-1}
ME	kg N/kW_p	1.31×10^{-1}	-	2.17	1.40	5.10×10^{-1}
FET	kg DCB/kW_p	-	8.10×10^1	3.31	8.16×10^1	1.96×10^1
LO	m^2·a/kW_p	5.39×10^1	3.85×10^1	2.68×10^2	3.64×10^1	6.72
WD	m^2·a/kW_p	2.18×10^1	-	1.44	7.69	5.09
MD	kg Fe/kW_p	4.23×10^2	2.86×10^2	8.12	2.70×10^2	1.04×10^2
FD	kg oil/kW_p	1.75×10^2	-	5.24×10^2	3.51×10^2	8.73×10^1

TABLE 2.5: Converted ReCiPe midpoint impact values for manufacture and installation of 1 kW_p roof-mounted multi-c Si PV (except mono-c Si in the case of Palanov (2014)).

Fu et al. (2015) and Chen et al. (2016) conducted LCAs of multi-c and mono-c Si PV panels respectively. These were not used in the analysis here because they do not include impacts of the roof mounting.

Note that all sources used in this section include the impacts of the solar inverter, whereas the domestic PV-battery system in question has an inverter, and DC-DC converters for each the PV array and battery bank, which are all counted as part of the BoS, separately to the PV array itself. The inverter impacts should thus be subtracted from the corresponding values in Table 2.5, so as not to double-count them. More details are given below in Section 2.5.3. With the inverter impacts subtracted, the PV embodied impacts in category i (= CC, OD, HT, etc.) are referred to as $c_{PV,i}$ per kW_p installed, and for the whole PV array:

$$C_{PV,i} = c_{PV,i} P_{PV}. \tag{2.6}$$

2.5.2 Battery environmental impacts

LCAs of sufficient detail could only be found for EV batteries (specifically nickel manganese cobalt oxide, Li-NMC) rather than Li-ion batteries for stationary applications. This is not ideal, but as mentioned

in Section 2.4.2, it is an adequate approximation. The Li-ion battery manufacture process described by Ellingsen et al. (2014) proceeds thus:

The negative electrode paste (graphite) is screen-printed or doctor-bladed on to copper foil. The positive electrode paste (a lithium-containing metal oxide, whose formulation contains nickel, manganese, cobalt, aluminium, or others in combination, along with carbon black and a binder such as polytetrafluoroethylene, PTFE, or polyvinylidene difluoride, PVDF) is similarly applied to aluminium foil. The electrodes are baked to evaporate any solvents, and cut to size. A porous polymer separator maintains electrical insulation of electron current between the electrodes while allowing ion conduction, these ions being Li^+ dissolved in the electrolyte, an organic solvent containing mainly a lithium salt such as $LiPF_6$. The electrodes and separator may be formed into a pouch, flooded with electrolyte, and electrically conductive tabs welded on; or the layers (the separator soaked in electrolyte, sandwiched between the electrode-coated current collectors) may be rolled into a cylinder. The cells (pouch, cylindrical, or otherwise) are electrically connected together with copper and aluminium busbars, packed into a steel tray with foam for protection, aluminium plates to dissipate heat, and nylon or steel screws and washers to seal the package.

According to Ellingsen et al. (2014), most of the energy used in the battery manufacturing process is for maintaining dry conditions in the rooms where the cells are made and tested. Note that the quantities of lithium used are small compared to the other high-value metals in the positive electrode, and the lower-value metals used in large quantity in the packaging and for electrical connections. Together they form a sizeable contribution to the MD (metals depletion) impact.

While Hawkins et al. (2013) report ReCiPe midpoint impact values for both lithium iron phosphate ($LiFePO_4$, or LFP) and Li-NMC battery chemistries, their Li-NMC values are taken as the central estimates for battery embodied impacts. This is because Ellingsen et al. (2014); McManus (2012), the only other sources to give nearly the same level of detail in their LCAs, focus on Li-NMC. LFP is likely to become dominant for home battery applications due to its long lifetime and superior safety characteristics, but as Hawkins et al. (2013) found, environmental impacts per kWh of battery capacity do not differ by more than 30 % between them for most categories. Exceptions are POF, FE and FD, which are 8-10 times less for LFP, and IR, which is nearly 13 times more for LFP. This is worth bearing in mind, however confirmation could not be found from other sources. It should also be noted that NMC encompasses many further sub-types according to the ratios in which nickel, manganese and cobalt are combined in the positive electrode.

McManus (2012) gave upper- and lower-bound values for the production impacts of Li-NMC batteries for EVs. They used the ReCiPe framework but omitted TA, ME, FE, FET, MET, TET. (This may be indicative of a greater focus on the human health and natural resources endpoint impacts than natural ecosystems.) Impacts were reported per MJ of battery capacity and so had to be multiplied by 3.6 to convert to a functional unit of per kWh capacity. This is so the impacts can be multiplied by battery capacity E_B (kWh) to give the total embodied impacts. As with PV, there is assumed to be no fixed portion to the embodied impacts. Raw data for McManus (2012) are given in Appendix A2. Data from Ellingsen et al. (2014) are already in the form required and so are given directly in Table 2.6, and Hawkins et al. (2013) too save for a factor of 24, as they reported impacts per EV, for an EV with 24 kWh battery.

Ellingsen et al. (2014) included a cooling system and battery management system (BMS) in their LCA of a Li-NMC EV battery. It would be preferred to disaggregate the battery's embodied impacts from those of the BMS, as a second-life battery would only incur the impacts of repurposing a used EV battery (as

discussed in Chapter 4) but would still require the same BoS as a new battery. McManus (2012) exclude BoS impacts, while Hawkins et al. (2013) exclude the battery charger but include packaging. Ellingsen et al. (2014) reported on all ReCiPe midpoint categories except IR, ALO, ULO, NLT and WD. They gave lower-bound, average and asymptotic values for each impact category, and recommended taking the lower-bounds as more representative of what could be achieved with greater economies of scale in mass-manufacturing. This recommendation is followed here.

		McManus (2012)		**Ellingsen et al. (2014)**	**Central Estimate (Hawkins et al., 2013)**	**Uncertainty**
		Lower	Upper	Lower		
CC	kg CO_2/kWh	6.12×10^{1}	9.72×10^{1}	1.72×10^{2}	1.93×10^{2}	4.64×10^{1}
OD	kg CFC11/kWh	1.20×10^{-3}	1.88×10^{-3}	1.10×10^{-5}	1.97×10^{-3}	6.40×10^{-4}
HT	kg DCB/kWh	1.08×10^{1}	1.80×10^{1}	5.96×10^{2}	6.25×10^{2}	1.86×10^{2}
POF	kg NMVOC/kWh	1.08×10^{-1}	1.80×10^{-1}	6.8×10^{-1}	4.96×10^{-1}	1.57×10^{-1}
PMF	kg PM10/kWh	1.08×10^{-1}	1.44×10^{-1}	5.8×10^{-1}	4.54×10^{-1}	1.18×10^{-1}
IR	kg U235/kWh	9.72	1.48×10^{1}	-	5.21	5.21
TA	kg SO_2/kWh	-	-	1.9	1.54	1.79×10^{-1}
FE	kg P/kWh	-	-	3.0×10^{-1}	3.43×10^{-1}	7.44×10^{-2}
ME	kg N/kWh	-	-	2.4×10^{-1}	2.87×10^{-1}	2.93×10^{-2}
FET	kg DCB/kWh	-	-	9.6	7.04	6.40×10^{-1}
LO	m^2·a/kWh	1.33	2.43	-	4.39	7.65×10^{-1}
WD	m^2·a/kWh	4.36×10^{-1}	6.88×10^{-1}	-	4.46	1.30
MD	kg Fe/kWh	1.01×10^{2}	1.58×10^{2}	1.54×10^{2}	1.45×10^{2}	1.44×10^{1}
FD	kg oil/kWh	7.92	1.22×10^{1}	4.95×10^{1}	4.10×10^{1}	1.11×10^{1}

TABLE 2.6: Converted ReCiPe midpoint impact values for manufacture of 1 kWh of Li-NMC battery.

The central estimate values in Table 2.6 are referred to as $c_{B,i}$ for impact category i. The embodied impacts $C_{B,i}$ in category i of manufacturing a battery of size E_B kWh would thus be:

$$C_{B,i} = c_{B,i} E_B. \tag{2.7}$$

2.5.3 Balance of System environmental impacts

There is a distinct lack of LCA data on PV-battery BoS, and power electronics in general. A qualitative description of the construction of a power converter is given here based on the work of Popović-Gerber et al. (2011) and Sharkh et al. (2014):

A power converter in general, whether it converts DC to DC, DC to AC or vice versa, operates by switching a number of switches in a circuit at high frequency (tens or hundreds of kHz) according to a specific sequence to route the input power flow into the form required at output. The switches themselves are Si semiconductor devices (MOSFETS or IGBTs), and employ similar techniques for their production as for that of Si PV cells (see Section 2.5.1). The micro-controller, which controls the switching sequence, is also formed of Si semiconductor devices. The purity requirements for Si in semiconductor devices are much more stringent than for PV cells, but much less Si is needed to make a 1 kW power converter

compared to 1 kW_p of solar panels (requiring 5-6 m^2). The Si devices are mounted on printed circuit boards (PCBs) which are themselves made of glass epoxy and copper. The semiconductor switches generate heat which must be dissipated by aluminium heat plates in order to maintain optimal operating conditions, and the output of the switching sequence requires filtering by electrolytic capacitors and inductors in order to meet requirements. These, along with the steel and plastic housing for the BoS, place further requirements on the materials and processing needed.

Central estimates of BoS environmental impacts are achieved here by taking the mean of the values given by Bekkelund (2013) and Palanov (2014) for the PV inverter and electrical installation, and Hawkins et al. (2013) for the EV battery inverter and charge controller. The inverters for a PV array and an EV battery are not directly representative of the BoS for a PV-battery system, but they are the best approximation currently available. Raw data are given in Appendix A3, while data converted to ReCiPe midpoint impacts and a functional unit of kW are given in Table 2.7.

		Bekkelund (2013)	**Palanov (2014)**	**Hawkins et al. (2013)**	**Central Estimate**	**Uncertainty**
CC	kg CO_2/kW	8.13×10^1	8.27×10^1	2.70×10^1	6.37×10^1	1.39×10^1
OD	kg CFC11/kW	5.37×10^{-6}	7.47×10^{-6}	1.89×10^{-6}	4.91×10^{-6}	1.39×10^{-6}
HT	kg DCB/kW	6.54×10^2	4.22×10^2	3.26	3.60×10^2	1.63×10^2
POF	kg NMVOC/kW	4.26×10^{-1}	-	1.03×10^{-1}	1.76×10^{-1}	8.09×10^{-2}
PMF	kg PM10/kW	3.35×10^{-1}	-	9.95×10^{-2}	1.45×10^{-1}	5.88×10^{-2}
IR	kg U235/kW	2.63×10^1	8.02×10^1	7.88	3.81×10^1	1.81×10^1
TA	kg SO_2/kW	8.59×10^{-1}	8.76×10^{-1}	1.98×10^{-1}	6.45×10^{-1}	1.71×10^{-1}
FE	kg P/kW	3.32×10^{-1}	-	6.01×10^{-2}	1.31×10^{-1}	6.79×10^{-2}
ME	kg N/kW	1.45×10^{-1}	1.38×10^{-2}	3.31×10^{-2}	6.40×10^{-2}	3.29×10^{-2}
FET	kg DCB/kW	7.85	-	1.34	3.06	1.63
LO	m^2·a/kW	5.56	5.80	7.54×10^{-1}	4.04	1.26
WD	m^2·a/kW	6.39×10^{-1}	9.36×10^{-1}	1.82×10^{-1}	5.86×10^{-1}	1.89×10^{-1}
MD	kg Fe/kW	2.05×10^2	4.89×10^1	7.42×10^1	1.09×10^2	3.90×10^1
FD	kg oil/kW	2.49×10^1	2.79×10^1	7.33	2.00×10^1	5.14

TABLE 2.7: Converted ReCiPe midpoint impact values for manufacture and installation per kW of power electronics.

To find the total BoS impacts, for a bi-directional inverter rated at P_{inv} kW, a battery converter at P_{conv} kW and a PV converter at $\texttt{min}[P_{inv}, P_{PV}]$, some approximations need to be made. Each of these three modules of the BoS are assumed to have equal embodied impacts. A PV inverter, such as Bekkelund (2013) and Palanov (2014) include in their LCAs, comprises two modules of equal power rating: a DC-DC converter to enact the MPPT function and a DC-AC inverter so that power from the PV array can be used in the home and exported to the grid. The power electronics in an EV also comprises two modules of equal power rating: a DC-DC converter for controlling battery charge/discharge, and a bi-directional inverter so power can be fed to the AC motor, and accepted from the (AC) grid for recharging the battery.

Referring to the central estimate values in Table 2.7 as $c_{BoS,i}$ in ReCiPe midpoint category i, the total BoS impact $C_{BoS,i}$ in category i is thus:

$$C_{BoS,i} = \frac{1}{2} c_{BoS,i}(P_{conv} + P_{inv} + \texttt{min}[P_{inv}, P_{PV}]). \tag{2.8}$$

The factor 1/2 is to account for the fact that data comes from sources which consider two modules. In reality, a DC-DC converter has a quite different circuit topology to a DC-AC inverter (Sharkh et al., 2014): the former would typically have one semiconductor switch while the latter would have four (in the case of an H-bridge inverter, though other topologies are sometimes used). However, both would require circuit boards, ceramic capacitors and wire-wound inductors for filtering, micro-controllers to control switcing sequences, cabling, and heat sinks. For similar efficiencies in particular, similar energy losses through conversion to heat can be expected, and therefore similar requirements of the heat sink. Of course the real material requirements would need to be determined through a rigorous design process for the required application, and may result in a different division between the modules for each impact category. Without going through such a process, the foregoing is the best approximation that can be achieved.

The central estimate values $c_{BoS,i}$ in Table 2.7 are subtracted from those in Table 2.5 to give $c_{PV,i}$, so as not to double-count the PV inverter.

2.6 Summary

This chapter has laid out the foundations of the modelling work undertaken in this study. The goal and scope was defined in relation to the research question, to find the circumstances in which domestic PV-battery systems in GB are financially and environmentally sustainable. The process tree was given, the functional unit (1 kWh electricity consumed) and LCIA framework (ReCiPe 2008, excluding MET, TET, NLT, and merging ALO and ULO into a single category LO) were chosen, the geographic and temporal boundaries defined (GB, 25 years), and the decision to exclude impacts of disposal/recycling was justified. A schematic was given of the system under study, with definitions of symbols used throughout the rest of this work.

Details were given of the input data used: real measured PV generation and load time series from dwellings in the UK, and further processing that was done to them to yield $P_{gen}(t)$ and $P_d(t)$. The PV-battery operating algorithms were described: the Greedy, Emissions Arbitrage (EAA) and Price Arbitrage Algorithms (PAA), including the logical flow of how they are simulated for this study.

Different sources of data were then examined to find how to account for the initial (and replacement) costs of each component depending on its size, and the environmental analogue of these, the embodied impacts of their manufacture and installation. In summary, these are:

- PV array cost:

$$C_{PV} = c_{PV,0} + c_{PV,1} P_{PV} \qquad \text{(GBP)} \tag{2.2}$$

  where $c_{PV,0} = 700$ GBP, $c_{PV,1} = 1500$ GBP/kW$_p$,

- Battery cost:

$$C_B = c_{B,0} + c_{B,1} E_B \qquad \text{(GBP)} \tag{2.3}$$

where $c_{B,0} = 1500$ GBP, $c_{B,1} = 390$ GBP/kWh, and for the purpose of calculating the replacement cost, $c_{B,1}$ decreases at 18 % per year to an eventual minimum of 50 GBP/kWh,

- BoS cost:
$$C_{BoS} = c_{BoS,0} + c_{BoS,1}(P_{conv} + P_{inv} + \texttt{min}[P_{inv}, P_{PV}]) \qquad \text{(GBP)} \tag{2.4}$$
where $c_{BoS,0} = 1000$ GBP, $c_{BoS,1} = 25$ GBP/kW.
These are all 2019 costs, and are assumed to include the relevant taxes.

- PV array embodied impacts, in ReCiPe midpoint category i:
$$C_{PV,i} = c_{PV,i} P_{PV}, \tag{2.6}$$

- Battery embodied impacts:
$$C_{B,i} = c_{B,i} E_B, \tag{2.7}$$

- BoS embodied impacts:
$$C_{BoS,i} = \frac{1}{2} c_{BoS,i}(P_{conv} + P_{inv} + \texttt{min}[P_{inv}, P_{PV}]). \tag{2.8}$$

The central estimates of $c_{PV,i}$, $c_{B,i}$ and $c_{BoS,i}$, and their uncertainties, are given in Tables 2.5, 2.6 and 2.7 respectively. Note that $c_{PV,i}$ refers not to the values in Table 2.5, but those values after subtracting $c_{B,i}$. The values of $c_{B,i}$ and $c_{BoS,i}$ are assumed not to change over time. This is a conservative approximation, as developments in technology and process efficiency are likely to reduce them by the time the battery and BoS are replaced.

The electricity bill in each year is calculated as the sum of:

- A daily standing charge, times 365 days,
- A per-unit charge, which may depend on time of day, for all electricity imported from the grid,
- Minus the export payment, for all electricity exported to the grid.

$$C_g = 365 \cdot c^-_{g,0} + \begin{cases} \sum_t \left[c^-_{g,1} \cdot P^-_g(t) - c^+_{g,1} \cdot P^+_g(t)\right] & \text{Flat} \\ \sum_{day} \left[c^-_{g,1} \cdot P^-_g(t)\right] + \sum_{night} \left[c^-_{g,2} \cdot P^-_g(t)\right] - \sum_t \left[c^+_{g,1} \cdot P^+_g(t)\right] & \text{Economy 7} \end{cases} \tag{2.5}$$

All elements of the electricity bill are taken to increase at 5.5 % per year. The baseline case analyses a system with investment start date 2020, with all costs adjusted accordingly, nominal discount rate 4 %, and inflation rate 2.1 %. Cash amounts are inflation-adjusted to units of 2019 GBP.

The calculation of the environmental analogue of the electricity bills is discussed in the next chapter. It describes how the time-varying marginal emissions factor $MEF(t)$ is calculated, and how the environmental impacts per kWh are quantified for each different power generation technology type. Part I concludes in the chapter after, which is a detailed discussion of how the battery is modelled.

Chapter 3

The Grid

"It is interesting to contemplate a tangled bank, clothed with many plants of many kinds, with birds singing on the bushes, with various insects flitting about, and with worms crawling through the damp earth, and to reflect that these elaborately constructed forms, so different from each other, and dependent upon each other in so complex a manner, have all been produced by laws acting around us."
- Charles Darwin, *On the Origin of Species*

In this chapter the modelling of the GB electricity grid is described in detail. It begins with a discussion of the marginal emissions factor (MEF, also known as grid CO_2 intensity, in kg/kWh), its importance both as an input to the Emissions Arbitrage Algorithm (EAA) and in calculating the contribution of the domestic PV-battery system's interaction with the grid to its life-cycle environmental impacts. Existing methods of evaluating MEF are reviewed and justification is given for the choice of methods used in this thesis, namely the need to obtain $MEF(t)$ at sufficient time resolution, and representing changes likely to occur in demand and generation on the grid to 2050 and beyond. Some intermediate results are given to illustrate the application of these methods. The analysis of 2017 GB data, and synthesis of data for 2030 and 2050, first appeared in a paper by the author, Sun et al. (2019). Minor developments have been made since its publication in the journal *Energies*.

Most of the second half of this chapter details how the ReCiPe midpoint environmental impact intensities (per kWh of electricity generated) are obtained for the different generator types currently on the GB grid and projected to be constructed in future. These are: coal, combined cycle gas turbines (CCGT), biomass, carbon capture and storage (CCS), nuclear, imports and exports, and renewable power. Many different sources of data were used to pinpoint a quantitative estimate of each generator type's impact intensity in each ReCiPe midpoint category (see Chapter 1 Section 1.2), and the uncertainty in those values. With these data, it is then a case of debiting the impacts of imports from the grid to the PV-battery system and crediting grid exports, over the system lifetime; when added to the embodied impacts of the PV, battery, BoS (and their replacements) found in the previous chapter, this gives the total life-cycle impacts. Then when divided by the total electricity consumed by the household over the system lifetime, this gives the impacts per kWh consumed.

The chapter finishes by detailing how the uncertainties of the environmental impacts for each individual system component and generator type are combined to give a total uncertainty (error bars, in other words) in each life-cycle impact category.

3.1 Marginal Emissions Factor

The time-varying marginal emissions factor $MEF(t)$ is important for two reasons: firstly it is the input to the Emissions Arbitrage Algorithm (EAA) which determines whether the battery is in charge, discharge or idle mode (Chapter 2 Section 2.3.2); secondly its evaluation forms the basis of how grid import and export are debited and credited to the system in the LCA.

MEF is distinct from the average emissions factor AEF, defined as the grid CO_2 intensity (kg/kWh) found by dividing the total CO_2 emissions (kg) in a given time interval by the total energy generated (kWh) in that interval (Rogers and Parson, 2019). AEF was used by Casals et al. (2017); Chowdhury et al. (2018); Faria et al. (2014); Genikomsakis et al. (2013); Kabakian et al. (2015); Uddin et al. (2017) in their analyses of the environmental impacts of domestic PV-battery systems. However, using AEF implies that every kWh imported from the grid conceptually causes an increase in generation (compared to not importing) by all the different generator types in the country in proportion to what they are currently generating, and every kWh exported decreases the generation in the same proportion. In reality, it is the generator lowest in the merit order (typically the one with the highest running costs) that increases or decreases its output, in other words the marginal generator.

Furthermore, a constant value (MEF or AEF) is only an approximation to reality: the marginal (or average) generator is not the same plant throughout the day, and not necessarily even of the same type (coal, nuclear, biomass, etc.). Uddin et al. (2017) used an AEF that decreased from one year to the next, but crucially they credited grid export in each year at the same CO_2 intensity as they debited grid import. They pointed out that under this assumption of non-time-varying CO_2 intensity, a home battery could only reduce any benefit rendered by rooftop PV, due to energy losses in charging and discharging the battery. This is why it is crucial to use a time-varying series $MEF_{CC}(t)$[1] rather than a constant value, otherwise there is no scope to render any environmental benefit above PV alone by using algorithms like the EAA.

While Faria et al. (2014) did consider sub-daily variations of grid CO_2 intensity in their LCA of a home battery in peak-shaving and load-shifting applications in France, Portugal and Poland, they used $AEF(t)$. Studies have shown that using AEF rather than MEF can cause errors of up to 25 % in the results being examined (Bettle et al., 2006; Hawkes, 2010; McKenna et al., 2017; Siler-Evans et al., 2012).

3.1.1 Review of Existing Methods

The problem is to calculate the marginal emissions factor $MEF(t)$, or better yet, the marginal generator response $MGR_j(t)$, so that ReCiPe midpoint impacts other than CC (Climate Change) can be calculated (using Equation (3.1) below). $MGR_j(t)$ is defined here as the power increase (MW) of generator type j (= coal, nuclear, biomass, etc.) in response to a demand increase of 1 MW. The existing literature is reviewed against this goal. The main difficulty is that it is a hypothetical situation that is being considered: for a hypothetical increase or decrease in total demand (such as from operating a PV-battery system), what would the power generators do differently from otherwise? As the hypothetical situation doesn't exist in historical data, the solution lies in finding appropriate proxies.

[1] $MEF(t)$ refers generically to the marginal emissions factor in any environmental impact category; the subscript 'CC' (Climate Change) means $MEF_{CC}(t)$ refers specifically to the CO_2-equivalent emissions.

Bettle et al. (2006) derived a fixed merit order by analysing historical electricity generation. They formed load duration curves for each power plant in England and Wales in the year 2000 (sorting power output in each half-hour settlement period in descending order), and ranked the power plants according to how much of the time they output closer to their maximum rated power. Baseload plants output close to their maximum most of the time and were thus higher in the merit order. Plants that output their maximum for less of the time were identified as load-following, or for even less of the time, as peaker plants, and occurred lower in the merit order. The national demand in each moment was assumed to be met by the plants in merit order, and the lowest-merit plant needed to fulfil the demand was identified as the marginal generator. This approximation works to some extent because there are markets for power generation (Elexon, 2015), which tend to accept offers at lower prices first, hence the inverse relationship between running costs and merit order. In reality, the merit order is not fixed but depends dynamically on running costs, electricity price, physical constraints such as whether a plant can ramp up quickly enough, and other factors. Recent changes in the generator technology mix on the GB grid (Staffell, 2017) have rendered much of the work by Bettle et al. (2006) obsolete.

Hawkes (2010) also used historical data but performed a linear regression of the hour-to-hour change in total CO_2 emissions (ΔE) against the hour-to-hour change in total demand (ΔD) of the GB grid, to derive MEF as the gradient $\Delta E / \Delta D$ (kg/kWh). In essence, they used real changes in demand ΔD at different times across the year, as a proxy for hypothetical changes. McKenna et al. (2017) applied this method to the Irish grid by binning the data by total demand D and performing linear regressions separately within each bin. This allowed them to produce time series of marginal CO_2 intensity. Siler-Evans et al. (2012) did similarly for various grids in the USA, producing time series of marginal SO_2 and NO_x as well as CO_2 intensity.

Olkkonen and Syri (2016) took a different approach, using the energy dispatch model EnergyPLAN to simulate operation of the Nordic grid. They ran the model once for a real year, and again for a hypothetical year with demand constantly greater than in the real year to a total of 1 TWh, finding the MEF from the difference in resultant CO_2 emissions between them. This is similar to one of the methods used by LCP and EnAppSys (2014), who ran the Department of Energy and Climate Change Demand Dispatch Model (DECC DDM) rather than EnergyPLAN. LCP and EnAppSys (2014) compared this method to another three using historical data for determining the marginal generator response $MGR_j(t)$:

- Merit order by running cost: all plants intending to generate in a particular settlement period must submit a final physical notification of volume (MWh) and price accepted (GBP/MWh), to the transmission system operator National Grid an hour before the settlement period begins (gate closure), from which the plant with highest price was identified,
- Identifying the load-following plant: the one that increases or decreases output most closely in line with demand at the time interval in question and up to three half-hour periods before and after,
- Highest bid or offer in the Balancing Mechanism (BM), a continuous auction chaired by National Grid where generators offer to change their final physical notification at short notice after gate closure, in case of unexpected imbalances between supply and demand.

There were discrepancies between all four methods when applied to GB historic data, owing in part to plants running 'out of merit'. For example, running overnight despite high running costs because the costs of startup/shutdown are even greater. LCP and EnAppSys (2014) judged the BM method the best: its prices were most representative of running costs at the time of delivering power.

As for applications to environmental analysis of domestic PV-battery systems, McKenna et al. (2013) and Babacan et al. (2018) used the method of Hawkes (2010) and Siler-Evans et al. (2012) to account for the impacts of importing from and exporting to the grid. However, they were constrained by historical data, which may not be representative of the grid (of GB and in the USA respectively) in future. Given the 25-year temporal boundary chosen for this study, some representation of the future grid is essential. The only way to achieve this is through modelling, as Olkkonen and Syri (2016) did, and LCP and EnAppSys (2014) using the DECC DDM, although neither projected more than a few years into the future. The next sections explain:

- How the method of Hawkes (2010), with adaptations by Siler-Evans et al. (2012), was applied to the GB grid,
- Merit order dispatch modelling of the future GB grid,
- Interpolation to find results for any given year to 2050 and beyond.

3.1.2 Siler-Evans' Adaptation to Hawkes' Method

Although the method of Hawkes (2010) can only be used on historical data, it is instructive to examine its application to the GB grid. Two adaptations by Siler-Evans et al. (2012) are applied to data from 2017:

Firstly, rather than linearly regressing the change in emissions ΔE from one time step to the next against the change in demand ΔD, the change in power from each generator type was taken as the dependent variable. That is, ΔP_j was regressed against ΔD, where P_j is generated power (MW) from j = {coal, CCGT (combined cycle gas turbines), bio (biomass), nuc (nuclear), hy (hydroelectric), Fr (French interconnector), Du (Dutch interconnector)}, these being the most significant generator types in GB, together supplying over 97 % of the total demand (Gridwatch, 2018). Thus it is possible to apply conversion factors to obtain not just CC impacts (CO_2), but also OD (CFC11), TA (SO_2), and other marginal emissions impacts according to the ReCiPe midpoint categories.

Secondly, in addition to binning the data by total demand $D(t)$, they were further binned by month. That is, instead of performing the linear regression on all the data in 2017, separate values of the gradient regressing ΔP_j on ΔD were obtained for each month and each demand bin ($D < 20$ GW, 20 GW $\leq D <$ 22.5 GW, ..., $D >$ 52.5 GW). This way it was possible to capture seasonal effects, notably the decreased usage of coal in summer compared to winter. Note that to improve linear fit quality, run-of-river and pumped hydroelectric were summed to give the single category 'hydroelectric'. To capture more granularity in the changes in $MGR_j(t)$ throughout the year it is desirable to perform the linear regression on shorter time periods, but the shorter the time periods the less data in each one and the lower the fit quality. Only CCGT showed sufficient fit quality to perform the linear regression on single months; for the other generator types, the temporal bins are two-month periods (see Figure 3.1). This informs the selection of 30 days as the time period over which to calculate the mean $MEF_{CC}(t)$ to use as input to the EAA: it is the shortest time period with enough data to capture the characteristic generation patterns of that time of year.

From the gradients $\Delta P_j/\Delta D$ are derived time series of marginal generator response $MGR_j(t)$ (MW/MW). The time series of marginal emissions intensity in ReCiPe midpoint category i is then given by:

$$MEF_i(t) = \sum_j c_{j,i} \cdot \lambda(t) \cdot MGR_j(t) \qquad \text{(kg/kWh)} \tag{3.1}$$

where $c_{j,i}$ is the intensity of emissions in category i from generator type j (quantified in Section 3.2), and $\lambda(t)$ is a time-dependent multiplicative factor to take into account the losses from transmitting and distributing the generated electricity to the home (see Section 3.2). For example, in the climate change category i = CC, $c_{j,i}$ would be the CO_2 intensity (kg/kWh) of generator type j.

For the study reported by the author (Sun et al., 2019), generated power (MW) and total demand (MW) in GB at 5-minute resolution for the year 2017 were downloaded from the GridWatch website (Gridwatch, 2018). This data source was chosen as being reliable, being synthesised from Elexon BM reports (Elexon, 2018), but more easily accessible (any desired time period from 2011 onwards can be downloaded freely as a CSV spreadsheet). The power generation data are aggregated by type: coal, CCGT, biomass, nuclear, hydroelectric, wind, and various interconnectors. This was considered a suitable level of granularity for application of the adapted Hawkes' method. To reduce the impact of missing data points, the GridWatch data were averaged from 5-min to half-hourly resolution. This left 97.5 hours of data still missing out of a total 8760 in 2017. Missing data were replaced by linear interpolation.

Figure 3.1 shows the goodness of fit R^2 for the linear regressions of ΔP_j against ΔD binned by month and demand $D(t)$, for each generator type j. $R^2 > 0.8$ is typical for CCGT, indicating a close correlation between changes in demand and changes in CCGT power in response. Exceptions occur in very low- and high-demand bins where there is little data (Figure 3.2). Especially in the summer months, $D(t) < 40$ GW typically, so there is no data at all in higher bins. A moderately good fit ($R^2 = 0.5$ to 0.8) is obtained for coal power response in winter. The poor correlation in summer is likely due to most coal plants outputting very low or zero power, so that they cannot ramp down further in response to decreasing $D(t)$. The goodness of fit is similar for hydroelectric power but throughout the year. Biomass, nuclear, and French and Dutch interconnector responses are poorly correlated with changes in demand. This is as expected for nuclear power, which generates at an almost constant level throughout the year (Gridwatch, 2018), almost completely independently of demand. Biomass and the interconnectors contribute little power (1-2 GW each to a demand ranging around 20-50 GW) and are unlikely to greatly distort the $MEF_{CC}(t)$ results. They are included for completeness.

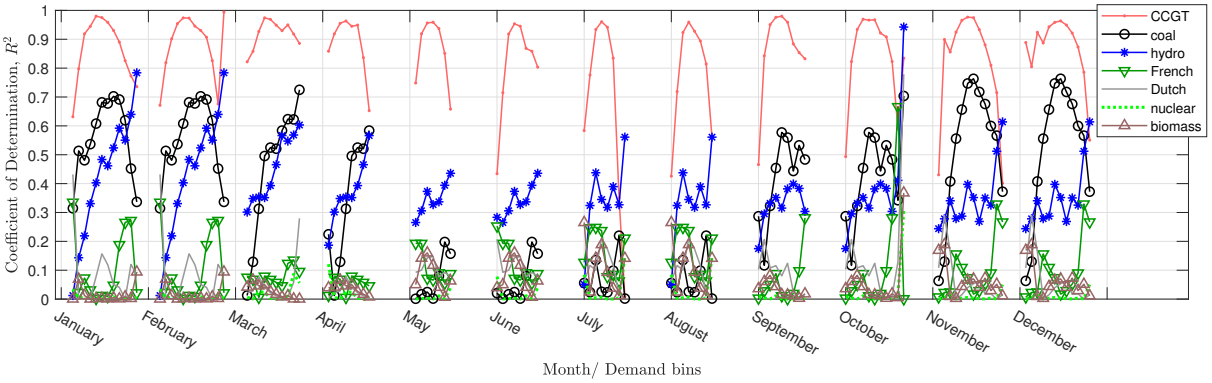

FIGURE 3.1: R^2 values for linear regressions of ΔP_j against ΔD, for j = CCGT, coal, hydroelectric, French and Dutch interconnectors, nuclear and biomass, binned by month and by demand D (< 20 GW, in 2.5 GW steps, to > 52.5 GW).

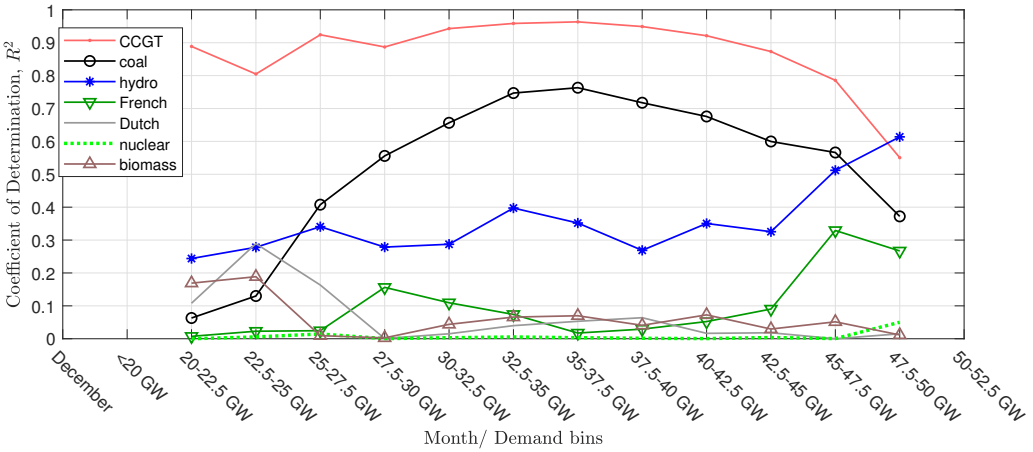

FIGURE 3.2: Figure 3.1, zoomed in on December to show the demand bins. These bins are the same for all months but for clarity are not marked on Figure 3.1.

Samples of the $MGR_j(t)$ of the 7 generator types in summer and winter are shown in Figure 3.3. $MGR_{CCGT}(t)$ is high, cycling around 0.75 MW/MW, indicating most load-following is done by CCGT. The rest of the load-following is mostly contributed by coal and hydroelectric power, and intermittently by the French interconnector. Note that $MGR_{Fr}(t)$ sometimes going below zero does not necessarily indicate power export to France. It may mean an increase in export, or a reduction in import despite $D(t)$ *in*creasing at that moment in GB, or vice versa despite GB $D(t)$ *de*creasing. This often happens because patterns of daily life cause some correlation between demand in France and GB, so power in the interconnector flows in the direction dictated by price (typically towards the region with greater instantaneous demand), not in response to demand in GB only.

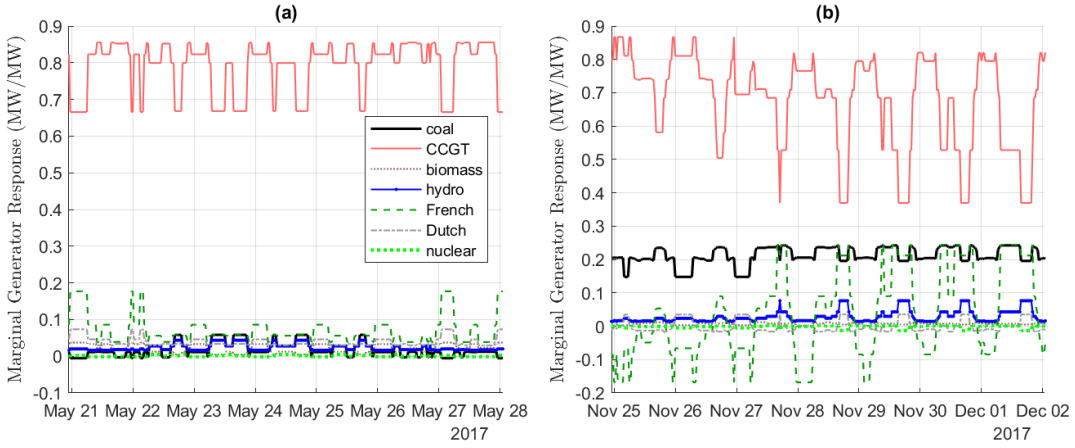

FIGURE 3.3: $MGR_j(t)$ of coal, CCGT, biomass, hydroelectric, French and Dutch interconnectors, and nuclear, for (a) 21-28 May 2017, and (b) 25 November - 2 December 2017.

To illustrate the effects on $MEF_{CC}(t)$, Figure 3.4 shows for the same time periods as Figure 3.3 the results of applying CO_2 intensities for each generator type ($c_{j,CC}$, see Section 3.2 below) to these $MGR_j(t)$ series and summing them together as in Equation (3.1), setting $\lambda(t) = 1$ for illustrative purposes. Variation can be between 0.46 and 0.67 kg/kWh in winter. Taking the average across the whole year of the MEF in each half-hour period of the day results in the average day's $MEF_{CC}(t)$, also shown repeated each day in Figure 3.4. It varies < 10 % away from the mean 0.5 kg/kWh, because the patterns of low and high $MEF_{CC}(t)$ vary from day to day. This is consistent with the prediction by LCP and EnAppSys

(2014) that in the next few years the daily variation in $MEF_{CC}(t)$ would reduce to close to zero, and appears to justify the use of a single value of MEF_{CC} in CO_2 abatement studies (Casals et al., 2017; Genikomsakis et al., 2013; Kabakian et al., 2015; Uddin et al., 2017). As seen from Figure 3.4, however, the average day's $MEF_{CC}(t)$ masks the variation that is present on other days.

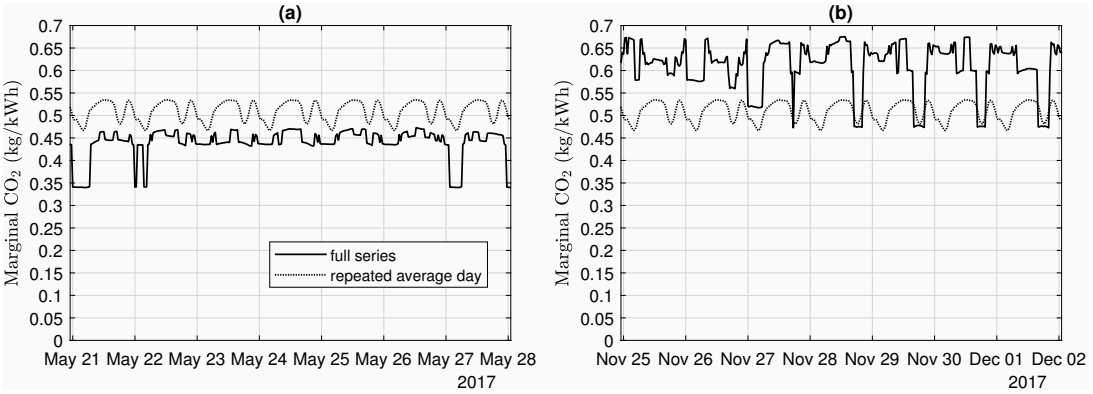

FIGURE 3.4: $MEF_{CC}(t)$ and its average across 2017 for each half-hour period of the day, for (a) 21-28 May 2017, and (b) 25 November - 2 December 2017.

After explaining how $MGR_j(t)$ and $MEF_i(t)$ are calculated in future scenarios, there follows a discussion of how these are used along with the same from 2017, to derive emissions impact intensities for all the years to 2050 and beyond, so that the crediting/debiting of grid export/import can be calculated for the domestic PV-battery system in question.

3.1.3 Future Grid Scenarios

To derive $MGR_j(t)$ for future scenarios, the 2018 edition of Future Energy Scenarios (FES) produced by National Grid (2018b) was used. They built their scenarios using the electricity markets modelling software BID3, which takes account of fuel prices, ramping constraints, electricity prices in interconnected regions, and other factors that can affect the merit order. Ideally the adapted Hawkes' method described above could be applied to the BID3 results for future years, treating them as if they were historical data. Unfortunately the hourly-resolution BID3 results for power generation and demand could not be made available upon request, and so a method more akin to that used by Olkkonen and Syri (2016) and LCP and EnAppSys (2014) had to be applied. That is, the scenarios outlined by National Grid (2018b) formed the basis of a fixed merit-order generator dispatch model (GDM), which was run once for a future year to obtain a baseline, and again with national demand $D(t)$ constantly 1 MW higher, to find the resulting difference in output for each generator type j, and hence the marginal generator response $MGR_j(t)$.

FES 2018 (National Grid, 2018b) presented four scenarios with different characteristics in terms of degree of centralisation and speed of decarbonisation. This study limits itself to analysing the two scenarios with fastest decarbonisation, as only these allow the UK to meet its Paris Agreement target (UNFCCC, 2018) to limit global temperature increase to below 2 °C: the more decentralised one is termed 'Community Renewables' (CR) and the more centralised one 'Two Degrees' (TD). Their demand characteristics and generator total capacities are given in Table 3.2, for 2030 and 2050, and also 2017 (National Grid, 2018a).

Note that the present-day GB grid consists of almost constant nuclear power as baseload, augmented by coal in winter. Despite significant wind and PV capacities, most GB electricity is still generated by CCGT, which performs most of the load-following, aided by a small amount of hydroelectric power.

There is a move to replace coal with biomass, whose capacity remains small. Power can flow in the interconnectors to France, the Netherlands and Ireland, in either direction as determined by prices in each region (Gridwatch, 2018). The CR scenario is characterised by a roughly five-fold increase in wind and PV capacity; while TD also anticipates a great increase in renewable generation (almost four-fold), it features a greater reliance on nuclear power and carbon capture and storage (CCS) than CR does.

	2017	**CR30**	**TD30**	**CR50**	**TD50**
Total demand (TWh)	297	302	293	441	373
Peak demand (GW)	59	62	64	83	79
Wind [(a)] (GW)	17.6	47.0	39.4	83.2	65.7
PV [(b)] (GW)	12.4	33.0	24.3	66.2	43.7
Biomass (GW)	3.3	6.2	5.9	5.8	3.7
Nuclear (GW)	9.2	9.2	9.0	9.0	18.6
CCS (GW)	0	0	0.9	0	12.1
Hydroelectric, Marine and Other Renewables [(c)] (GW)	3.6	7.3	8.2	11.2	13.9
CCGT (GW)	34.9	31.7	30.7	22.8	9.5
Coal (GW)	12.7	0	0	0	0
Interconnector (GW)	4	16.5	19.8	16.5	19.8
V2G (GW)	0	1.1	1.0	20.6	17.9
Other Storage (GW)	2.9	9.0	8.9	29.0	17.3

TABLE 3.2: Demand characteristics and generator capacities in 2017 and the Community Renewables (CR) and Two Degrees (TD) scenarios of FES 2018, in 2030 (CR30, TD30) and 2050 (CR50, TD50) (National Grid, 2018a).

(a) Onshore and offshore wind are summed together.

(b) As all PV is connected at distribution level, it is netted off from demand $D(t)$ rather than being its own category of generator in the GDM.

(c) The 'Other Renewables' category in FES 2018 is here aggregated with hydroelectric and marine power. The simplification is made that some combination of them can always be dispatched up to their total capacity.

A rule-based dispatch was used within these parameters to produce time series of power output by each generator type. The simplification of a fixed merit order was used for the future scenarios, going from low-CO_2 to higher-CO_2 generator types until the demand in that period $D(t)$ is satisfied. CO_2 intensities $c_{j,CC}$ for generator types j are given in Section 3.2. The equating of merit order with inverse CO_2 order is justified by an anticipated increase in the CO_2 price. Staffell (2017) has studied the effects of the UK's CO_2 price floor, which taxes power generation according to its emissions: CCGT has effectively displaced coal in the merit order compared to as recently as 2012.

In practice the fixed merit order is implemented thus in the GDM:

- If the sum of wind, PV and nuclear baseload exceeds the national demand in any half-hour period, nuclear power is ramped down by up to 25 % (according to Stamford and Azapagic (2012) the average ramp-down rate is 0.83 % per minute), and any further excess is exported internationally,

- If interconnector capacity is insufficient, the remaining excess is assumed to be curtailed,
- If the national demand is not met by wind, PV and nuclear power, then 'hydroelectric, marine and other renewable' power is dispatched up to their maximum capacity,
- If insufficient, then nuclear power is ramped up by up to 5 % (according to Stamford and Azapagic (2012) the average ramp-up rate is 0.17 % per minute) up to its maximum capacity,
- If still insufficient, then biomass, CCS, then CCGT are dispatched in that order up to their respective maximum capacities,
- If still insufficient, power is imported internationally,
- If interconnector capacity is insufficient, the remaining shortfall is assigned to 'Other', whose accounting is discussed at the end of Section 3.2.7.

As total demand time series for each of the future scenarios was presently unavailable upon request, the demand for 2017, $D_{17}(t)$, is scaled and shifted such that the annual total and peak demand match those given in Table 3.2 for each scenario:

$$D_x(t) = a_x + b_x \cdot D_{17}(t) \tag{3.2}$$

for each scenario x = CR30, TD30, CR50, TD50. Parameters a_x and b_x are obtained by solving simultaneous equations:

$$\text{Total demand (GWh)} = 8760 \text{ h} \times a_x + 297\,000 \text{ GWh} \times b_x \tag{3.3}$$

$$\text{Peak demand (GW)} = a_x + 59 \text{ GW} \times b_x. \tag{3.4}$$

Total demand and peak demand for each scenario x are given in the first two rows of Table 3.2. These are respectively 297 000 GWh and 59 GW in 2017, hence their multiplication by scaling factor b_x in Equations (3.3) and (3.4), and there are 8760 hours in a year, hence its multiplication by the shift factor a_x in Equation (3.3). The solutions of these simultaneous equations are given in Table 3.3.

x :	**2017**	**CR30**	**TD30**	**CR50**	**TD50**
Total demand (TWh)	297	302	293	441	373
Peak demand (GW)	59	62	64	83	79
a_x (GW)	0	−2.71	−7.83	+6.22	−6.62
b_x	1	1.10	1.22	1.30	1.45

TABLE 3.3: Shifting and scaling parameters a_x and b_x to transform 2017 demand series $D_{17}(t)$ into series appropriate for future scenarios in terms of total and peak demand.

Wind and PV time series are taken from the 2017 Gridwatch data and scaled in proportion to their capacities in the future scenarios. In FES 2018 (National Grid, 2018b) it is assumed that power flows across interconnectors are only limited by total capacity, when in reality they depend on prices in the two interconnected regions. This simplification is kept in this study. Two example weeks output from the GDM for the CR50 scenario are shown in Figure 3.5, and the resulting $MEF_{CC}(t)$ for those weeks in Figure 3.6. As can be seen, there is greater variation in $MEF_{CC}(t)$ in CR50 compared to 2017 (Figure 3.4). This is exploited by the EAA to achieve greater CO_2 savings.

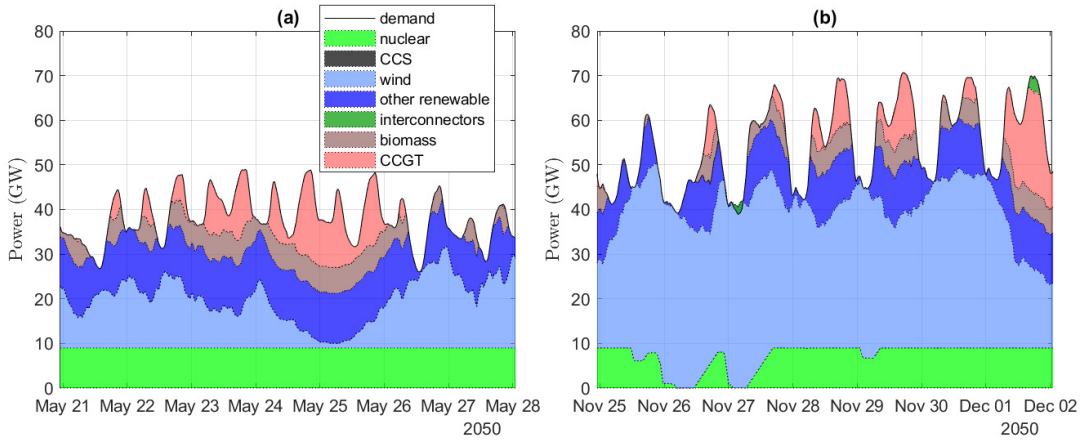

FIGURE 3.5: Generators dispatched in Community Renewables scenario, for (a) 21-28 May 2050, and (b) 25 November - 2 December 2050.

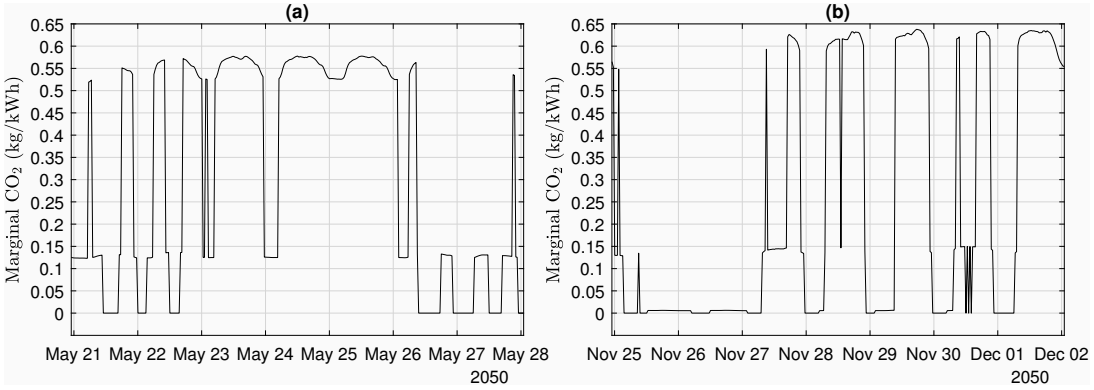

FIGURE 3.6: $MEF_{CC}(t)$ in Community Renewables scenario, for (a) 21-28 May 2050, and (b) 25 November - 2 December 2050.

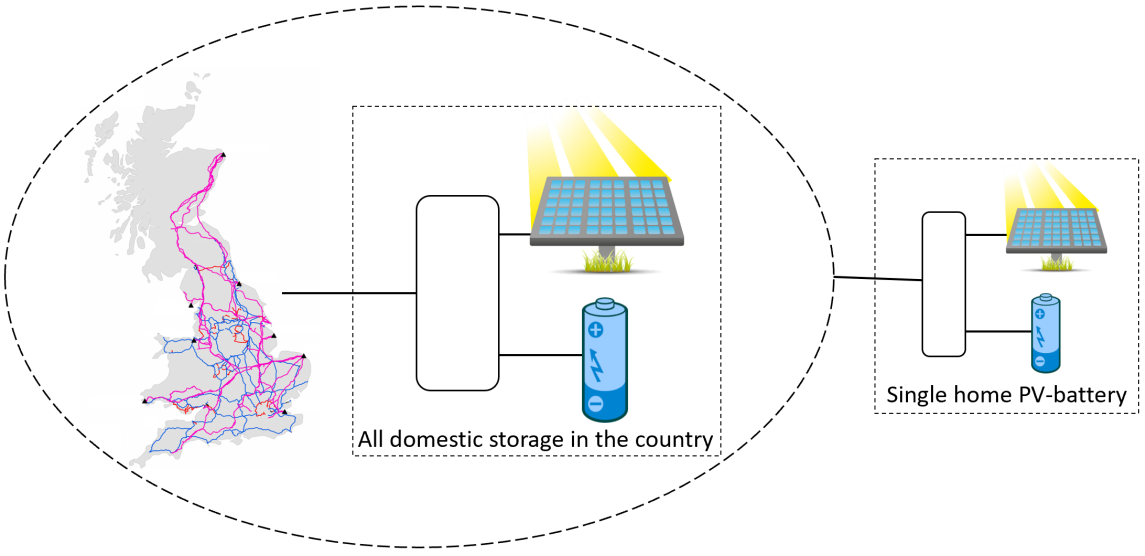

FIGURE 3.7: Conceptual schematic of how storage is incorporated when calculating $MGR_j(t)$: first all the storage in the country is treated as a single storage unit responding to a grid with no storage; then the PV-battery system interacts with this storage-adjusted grid.

Only nominal power (GW) of energy storage and vehicle-to-grid (V2G) were given in FES 2018 (National Grid, 2018b), but not their energy storage capacities (GWh). As such, there was not enough information to incorporate storage directly in the GDM in this study. Instead, storage is considered as an aggregation of home batteries. There is precedent for making such an approximation: EnergyPLAN, for example, treats the totality of EV batteries in a country as a single battery with capacity equal to the sum of all the individual ones (Lund and Thellufsen, 2018).

First, the GDM is run with no storage, and again with national demand $D(t)$ greater by 1 MW constantly. The difference between them gives a no-storage $MGR_j(t)$ from which $MEF_{CC}(t)$ is calculated. This $MEF_{CC}(t)$ is *not* used as input to the EAA for a single domestic PV-battery system: each such system interacts with a grid that includes all other such systems, not a grid with no storage. Instead, the no-storage $MEF_{CC}(t)$ is fed into the PV-battery simulation along with a portion of $D(t)$ and PV generation in each scenario, as detailed in Table 3.4 below. This single PV-battery system representing all the domestic batteries in the country is simplified as operating on only one algorithm (Greedy, EAA or PAA), when in reality there would likely be a distribution of algorithms in operation. The simulation output is used to adjust $D(t)$ to account for the presence of all the PV-battery systems. (Details of how the battery is modelled in the simulation are given in Chapter 4.)

The sizing of the single PV-battery system representing all the domestic batteries in the country was achieved thus: first, the 'Other Storage' values in Table 3.2 were divided by 3.3 kW to find an approximate number of participating PV-battery systems (the first row of Table 3.4), 3.3 kW being the most common charge/discharge power limit of home batteries surveyed by Naked Solar (2019). This number is multiplied by 2.8 kW_p, the average rooftop PV capacity in the UK (BEIS, 2020), giving the total PV capacities that are part of PV-battery systems, in the second row of Table 3.4. The third row of Table 3.4 is the fraction of the whole country's PV capacity (Table 3.2) that is coupled with batteries. An estimate is found for what fraction of the total national demand is associated with such systems by multiplying the number of them (first row of Table 3.4) by 3800 kWh (the average UK household annual electricity consumption (Ofgem, 2017)), and dividing by the total electricity consumed nationwide in the corresponding year. These demand fractions are given in the fourth row of Table 3.4. This assumes the profile of electrical loads participating in PV-battery systems is the same shape as total demand (that is, residential, commercial and industrial loads participate proportionally to their presence nationally).

	CR30	**TD30**	**CR50**	**TD50**
Participating PV-battery systems (approx.)	2.73 mill.	2.70 mill.	8.79 mill.	5.24 mill.
Participating PV capacity (GW)	7.64	7.56	24.6	14.7
PV fraction	0.231	0.311	0.372	0.335
Demand fraction	0.035	0.036	0.078	0.055

TABLE 3.4: Parameters involved in the demand adjustment due to energy storage in the future scenarios.

The national demand $D_x(t)$ is scaled down to the demand fraction and used as an input to the simulation of the aggregate national PV-battery system, whose PV capacity is equal to the second row of Table 3.4, and whose battery capacity is equal to 8 kWh times the number of participating systems. (8 kWh is the median capacity of home batteries surveyed by Naked Solar (2019).) While not every such system will have 2.8 kW_p PV and 8 kWh batteries, all that matters is that this ratio of PV to battery is roughly

correct, on average. 'V2G' values in Table 3.2 are ignored for consistency, as EV charging was not included in the modelling of future demand reported in FES 2018 (National Grid, 2018b).

The adjustment of national demand $D(t)$ to account for storage is achieved thus: grid import to the aggregate PV-battery system is added to $D(t)$ (minus the fraction involved in the aggregate system) and export from it is then subtracted. The PV capacity used in the rest of the GDM must then be less than the national total by the amount included in the aggregate system, so as not to double-count it.

The GDM is then run again with the storage-adjusted demand as input. When compared against the situation with no storage, this can already give one interesting set of results: the impacts of having domestic batteries in the country up to the 'Other Storage' values in Table 3.2, compared to having none (all PV systems are PV-only). These impacts can be combined with the embodied impacts of this much PV, battery, BoS and component replacements over 25 years, to give the total national impacts of the batteries over this time period.

Once the results of the GDM with storage-adjusted $D(t)$ are obtained, the GDM is run again with the storage-adjusted $D(t)$ constantly 1 MW greater, to find the storage-adjusted $MGR_j(t)$. This then forms the basis of a (storage-adjusted) $MEF_{CC}(t)$ which can be used as input to a single home's PV-battery system running the EAA, and storage-adjusted $MEF_i(t)$ for accounting for the impacts of grid import to/export from the single home's PV-battery system. This concept is illustrated in Figure 3.7.

While treating all storage in the country as a single aggregate unit is an adequate approximation if they are all running the Greedy algorithm, a complication arises if they all run the EAA. Because the EAA takes $MEF_{CC}(t)$ as an input, such a system is affected *by* as well as itself *affecting* all other such systems in the country. Short of modelling every single one of the millions of PV-battery systems in the country, some way is needed to represent this endogeneity. This was done by treating the country's storage as not one, but N_d aggregate systems. The corresponding PV and demand are also divided between them. Each aggregate system, or 'division' as they are termed here, interacts with the grid adjusted by the previous division, and the first division interacts with the grid without storage. This is illustrated in Figure 3.8.

A test was then conducted to see how many divisions are needed to represent a fully storage-adjusted grid. The number of divisions N_d was incremented and each time, the dispatched power $P_j(t)$ was found for each generator type j in 2030 and 2050, in CR and TD scenarios. The difference was taken between the sum $\sum_t P_{CCGT}(t)\Delta t$ without storage, and fully storage-adjusted. This is shown in Figure 3.9: $N_d = 1$ is indeed adequate to model the country's storage all running the Greedy algorithm, as the battery scheduling only depends on instantaneous load and PV generation; each PV-battery system is not affected by any others on the grid. With the EAA, convergence of CCGT generation difference can be seen from around $N_d = 10$ in the 2030 cases, and even before that in TD 2050, but $N_d = 50$ is required for the CR 2050 results to converge. $N_d = 50$ is taken for initialisation of all the EAA cases, to ensure convergence (the initialisation only needs to be run once, and results are loaded in for each iteration of the model).

It is interesting to note that the impact battery storage has on reducing CCGT generation is greatest in the CR 2050 scenario, and especially so if all operate on the EAA. But running the Greedy algorithm, battery storage can even cause more CCGT to be dispatched in the TD 2030 scenario. The effect of N_d can also be seen on the differences of generation dispatched for other generator types. Discussion of the other types is deferred to Chapter 6; all that is relevant here is that they all converge by $N_d = 50$.

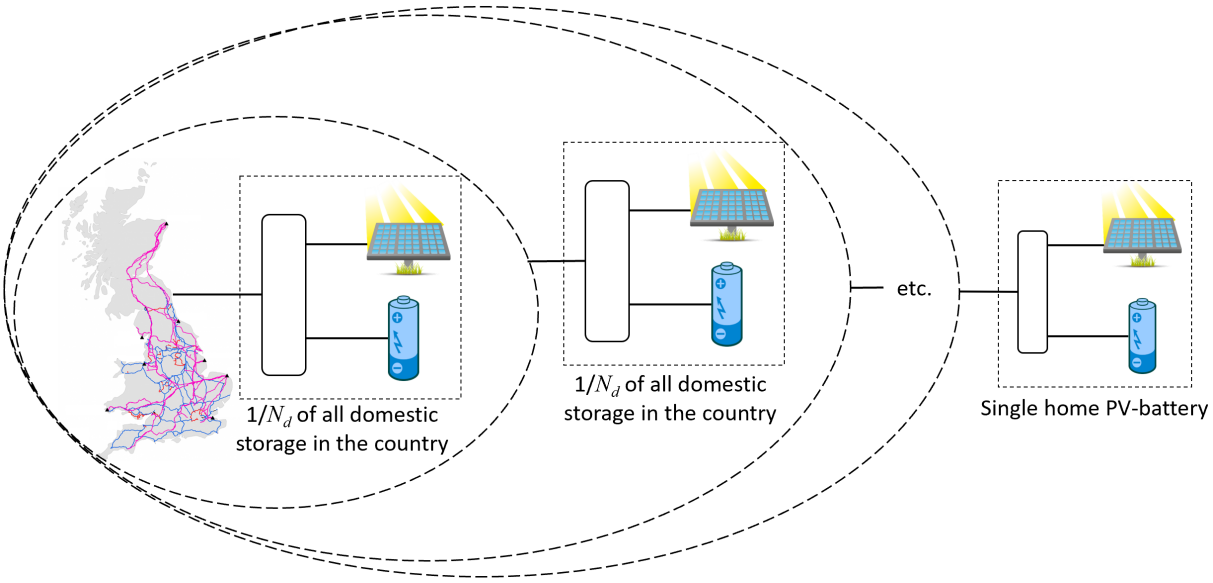

FIGURE 3.8: Conceptual schematic of how storage is incorporated when calculating $MGR_j(t)$: all the storage in the country is divided between N_d equal divisions, each division interacting with the grid adjusted by the previous division; then the PV-battery system interacts with this fully storage-adjusted grid.

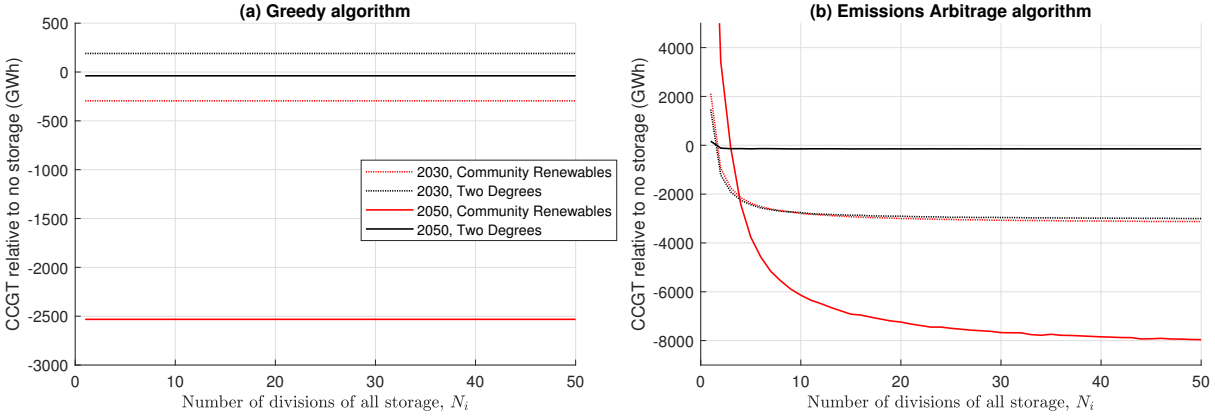

FIGURE 3.9: Annual CCGT generation (GWh) with storage relative to without, in 2030 and 2050, in CR and TD future grid scenarios, for (a) all storage in the country operating on the Greedy algorithm, and (b) all operating on the EAA; showing convergence as number of divisions N_d is increased.

The treatment of electricity storage as an aggregate system, or many aggregate systems, with which the single system in question interacts, is necessarily an approximation. The method used in this thesis does not make manifest any instabilities which may result if, for example, the national demand is only just low enough to be met without any CCGT: this may induce all the EAA-operating PV-battery systems to start charging from the low-CO_2 grid electricity; the resultant increase in demand may then cause a CCGT plant to ramp up, which could be enough to push the PV-battery systems into discharge mode; the resultant decrease in net demand may be enough to push the CCGT plant into switching off; and so the cycle may continue. The modelling of dynamic effects such as this are neglected in this work, but are of great importance to the national electricity system, and worthy of further study.

3.1.4 Interpolation to 2050

Lacking the hourly-resolution BID3 results for power generation and demand produced for FES 2018, some means had to be found of accounting for the years in between 2017, 2030 and 2050. The 2017 $MGR_j(t)$ are obtained with the adapted Hawkes' method applied to historical data whereas those for 2030 and 2050 are from running the fixed merit order GDM. As such, there is not an obviously correct way to obtain $MGR_j(t)$ in the years in between, especially as the adapted Hawkes' method on 2017 yielded significantly different results to running the GDM with that year's demand $D_{17}(t)$ as input (it identifies coal as the marginal generator type whenever there is any coal generating, when in reality coal power only contributes to around a quarter of load-following, according to Figure 3.3). That is, the GDM could not simply be run for every year between 2017 and 2050 with power generation capacities of each technology type j adjusted appropriately.

Instead, a linear interpolation method is deployed. Before beginning the simulation, $MGR_j(t)$ and $MEF_{CC}(t)$ are determined for the years 2017, 2030 and 2050, using the adapted Hawkes' and GDM methods as appropriate. Then for each year of the simulation for the domestic PV-battery system in question, that same year is run up to twice: if between 2017 and 2030, it is run once for the 2017 grid and again for the 2030 grid, and similarly if between 2030 and 2050. In this way two sets of grid export/import series $P_g^{+/-}(t)$ are obtained: one set for the system interacting with the 2017 grid, and another for it interacting with the 2030 grid (and similarly if between 2030 and 2050). In the case of the EAA, they differ because the different grid generation mixes in each year would result in different $MEF_{CC}(t)$ input to the EAA, and so different resultant $P_g^{+/-}(t)$. (For the Greedy algorithm and PAA, import and export are only determined by electrical consumption and PV generation of the house, and by electricity price respectively, not what else is on the grid, and so they do not need to be run twice because $P_g^{+/-}(t)$ will be the same in each year.) The grid export credits and import debits are then calculated for each of those years (2017 and 2030 in this example):

$$C_{g,i} = \sum_t \left(MEF_i(t) \cdot [P_g^-(t) - P_g^+(t)] \right) \Delta t \tag{3.5}$$

where $C_{g,i}$ is the net debit in ReCiPe midpoint impact category i of interacting with the grid, and $MEF_i(t)$ is the marginal emissions factor for category i as defined in Equation (3.1). Remember that grid import cannot be simultaneous with export: $P_g^-(t) = 0$ when $P_g^+(t) > 0$ and $P_g^+(t) = 0$ when $P_g^-(t) > 0$.

The grid import/export net debits $C_{g,i}$ for the two years (2017 and 2030, for example) are then combined in a weighted sum. The weights are given in Figure 3.10, i.e. a linear interpolation. In the example in Figure 3.10, the 2028 grid import/export net debit is found by combining $C_{g,i}$ from 2017 and 2030 in the ratio 0.1538 : 0.8462.

The choice of linear interpolation can rightly be questioned, as can the use of results for a 2050 grid for all years subsequent to 2050 (in the cases where initial investment is delayed until after 2025). It is possible that decarbonisation might accelerate or decelerate up to 2050, in which case a nonlinear interpolation would be required. Should the information to constrain the model in the intervening years and after 2050 become available, it would be simple to modify the weightings in Figure 3.10, or indeed not to need to take a weighted sum at all if $MEF_i(t)$ can be calculated for every model year. But in the absence of such information, a linear interpolation and subsequent persistence of the 2050 grid are assumed in this thesis. In reality, a further decrease in CCGT capacity after 2050 is likely, amongst other changes,

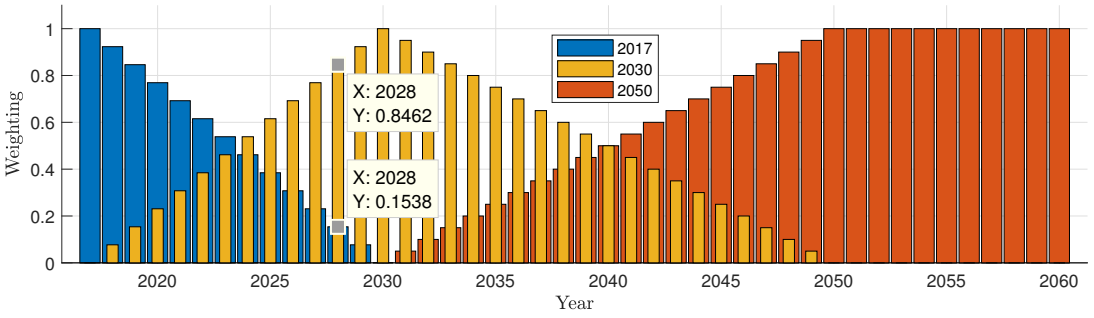

FIGURE 3.10: Weightings of each run (2017, 2030, 2050) for combining them for each simulated year: for the 2017 run, linearly 1 to 0 from 2017 to 2030; for the 2030 run, 0 to 1 from 2017 to 2030 and then to 0 again in 2050; for the 2050 run, 0 to 1 from 2030 to 2050 and then 1 for all years subsequently.

and is necessary if the UK is to meet the target of net zero CO_2 emissions set out by the Committee on Climate Change (2019).

With the foregoing, all the conceptual elements are in place for calculating the life-cycle environmental impacts of the domestic PV-battery system in question. The embodied impacts for PV, $C_{PV,i}$, battery, $C_{B,i}$, and BoS, $C_{BoS,i}$, discussed in Chapter 2 are summed, along with the embodied impacts of battery and BoS replacements (schedule of replacement discussed in Chapter 4), and the grid import/export net debits $C_{g,i,y}$ for each year y of the $N = 25$ years in the temporal boundary. The total impacts are then divided by the household's total electricity consumption $N \cdot \sum_t P_d(t)\Delta t$ over the system lifetime, to give the impacts c_i per functional unit (per kWh consumed) in each ReCiPe midpoint category i, as in Equation (3.6). These per-kWh results are compared for different system configurations: with/without PV/battery, with second-life rather than new batteries, and the two future grid scenarios CR and TD.

$$c_i = \frac{C_{PV,i} + C_{B,i} + C_{BoS,i} + \sum_y^N \left(u_{B,y} \cdot C_{B,i,y} + u_{BoS,y} \cdot C_{BoS,i} + C_{g,i,y}\right)}{N \cdot \sum_t P_d(t)\Delta t} \tag{3.6}$$

where $u_{B,y}$ and $u_{BoS,y}$ are binary variables, equal to 1 if the battery or BoS respectively are replaced in year y, or 0 otherwise.

Unlike with cash flows, environmental impacts incurred in future are not discounted in this thesis. There is some debate on whether or not this is appropriate: some advocate discounting of future CO_2 emissions at rates as high as 6 % (Smith and Braathen, 2015, Section 2.3). The effect of higher discount rate is to incentivise actions with short-term gains and long-term losses (to the environment, in this case). As Smith and Braathen (2015) explain, this is motivated by some different reasons: a valuation of future populations as less important than present ones; that future populations will be richer, more technologically advanced and better equipped to tackle environmental degradation than at present; and the non-zero risk that the collapse of human civilisation will be brought about by other means before environmental degradation of the types considered in the LCA. The other side of the argument, which advocates lower or even zero discount rate for environmental impacts, is motivated both physically and morally. Physically, CO_2 accumulates in the atmosphere with effects persisting many centuries into the future, such that 1 kg emitted today leads to effects physically equivalent to 1 kg emitted many years from now; morally, it can be argued that if all people are to be valued equally, then harm inflicted on future populations is no less than harm inflicted on present ones. It is conventional for LCAs not to discount future environmental impacts, and that convention is followed in this thesis (Klöpffer and Grahl, 2014). Further discussion of this point can be found in Chapter 6.

Before examining the quantitative environmental impacts of different generator technology types in the next section, it is worth saying a few words about attributional and consequential LCA. Masanet et al. (2013) explain attributional LCA as a way of answering the question of what environmental impacts can be attributed to a product, all else being equal; whereas consequential LCA includes impacts of changes in the surrounding system to accommodate that product or process. The former is useful to an environmentally-conscious customer deciding between products to purchase; the latter to policy-makers who need to know the consequences of potential policies to incentivise certain products or processes. There is an analogy between attributional LCA and AEF on the one hand, and consequential LCA and MEF on the other. However, to be truly consequential, the LCA conducted in this thesis would have to take account of changes in the national electricity generation and transmission/distribution system brought about by and/or to accommodate domestic PV-battery systems. McKenna and Darby (2017) discuss this issue in relation to demand-response technology, whose effects are negligible or even slightly negative, unless accounting for the fact that they may reduce peak demand to the extent that new peaker power stations do not need to be built, or old polluting power stations can be shut down early. While the CR and TD future grid scenarios are compared in this thesis, and the whole GB with storage is compared to without, these situations are imposed exogenously. Accounting for endogenous changes in power generation capacities is left to further work.

3.2 Environmental Impacts of Generation Technologies

So far the environmental impacts of importing grid electricity and displacing grid generation by exporting have been discussed on an abstract level. This section quantitatively examines in turn the different generation technologies in the present-day and future electricity system of GB. ReCiPe midpoint impacts are required per kWh generated by these different technologies. As with embodied impacts for PV, battery and BoS, many data sources were analysed and a central estimate $c_{j,i}$ and uncertainty value were synthesised for each impact category i and technology type j. Again, the uncertainty value is given by 1/4 the difference between the highest and lowest values in all the sources considered, or the central estimate itself, whichever is lower. As well as these quantitative values, a qualitative description of the supply chain is given for each technology type.

Where possible, the construction and decommissioning impacts were separated out from the operating impacts. The reasoning behind this is that a single domestic PV-battery system, importing from or exporting to the grid, would only affect the operation of those power plants: some more natural gas is burnt, or some is saved from burning, for example. The PV-battery system cannot affect whether or not the plant itself is built. (However a whole country's worth of PV-battery systems may do - but taking account of this effect endogenously, as for a fully consequential LCA, is deferred to further work.)

It should be noted that power generation LCAs typically take the functional unit to be a unit of electricity generated (kWh, MJ, MWh, etc.) whereas the functional unit for this thesis is 1 kWh consumed. Therefore the central estimates given in the tables below need to be increased by a factor $\lambda(t)$ (introduced in Equation (3.1)) taking account of transmission and distribution (T & D) losses: 1 kWh consumed in the home requires slightly more than 1 kWh to be generated at the power station as some is lost along the way. T & D losses vary by location (higher losses occur through distribution to very remote areas) and time of day (when power flow is high, such as in the evening, the greater current in the power lines increases losses through ohmic heating). Since sub-daily variations in electricity generation dynamics

are pivotal to the work of this thesis, it would be remiss to neglect such variations in T & D losses. An estimate for the time-varying T & D factor, $\lambda(t)$, is found using these facts:

1. T & D losses were 8.7 % when averaged across 2015 (according to Western Power (2019a), 338 TWh generated and 311 TWh consumed); this figure is taken to be unchanged in 2017,
2. Of the roughly 7 % technical losses (the rest being theft or unmetered consumption), 1/4 to 1/3 are fixed losses while 2/3 to 3/4 vary with power flow (Western Power, 2019b),
3. Ohmic losses are proportional to the square of the current, itself proportional to power (Western Power, 2019b).

From condition 3, the parameters m_1, m_2 are varied in Equation (3.7):

$$\lambda(t) = 100\% + m_1 + m_2[D_{17}(t)]^2 \tag{3.7}$$

until conditions 1 and 2 are fulfilled, respectively:

$$\texttt{mean}[\lambda(t)] = 108.7\% \tag{3.8}$$

$$\texttt{min}[\lambda(t)] = 104\% \tag{3.9}$$

(Equation (3.9) follows from condition 2 because the 1.7 % non-technical losses, plus 1/3 of 7 %, are fixed losses at roughly 4 %.)

These equations are satisfied by $m_1 = 1.8$ % and $m_2 = 6.0 \times 10^{-11}$ MW^{-2}, as found by iterative adjustment of the m_1 and m_2 values. The result is $\lambda(t)$ varies between 104 % to 110 % in summer, and 107 % to 118 % in winter. The values of m_1 and m_2 will almost certainly change in future as the electricity network is upgraded to accommodate electric heat pumps and EV charging. These upgrades are assumed to keep $\lambda(t)$ the same in every year throughout the temporal boundary of the domestic PV-battery system under study. This is a simplification, as the effects of network upgrades are irregular: the yearly average T & D loss has been as low as 7.6 % in 1993 and as high as 10.6 % in the following year, although it has remained 8-9 % in recent years (Trading Economics, 2019). It is beyond the scope of this thesis to account for regional variations in T & D losses.

Note that $\lambda(t)$ applies for both import and export: obviously grid import must be debited by the amount correct for each kWh consumed rather than each kWh generated, but for grid export, the reason is less straightforward. The electrical energy exported to the grid from one house is typically all consumed by other houses on the same distribution feeder. This results from demand diversity (Konstantelos et al., 2014), meaning not all houses have identical load profiles, such that one whose PV generation exceeds its own load is likely to be connected to ones with higher net loads at that instant on the same feeder. Therefore energy export from one house to the grid would displace some grid power generation that was otherwise destined for that house's neighbours. Being close by, $\lambda(t)$ would apply almost equally to grid export (power generation *and T & D to neighbours* displaced) as to grid import. The situation becomes more complicated when so many houses on the same feeder have rooftop PV that not all exported energy can be consumed close by, and it flows to higher voltage levels and further away, incurring more losses. This is rare in GB, where houses are typically close together (spatially and electrically). However, it is

currently unknown what level of house remoteness and rooftop PV penetration would invalidate the use of the same $\lambda(t)$ for both import and export. This would be an interesting subject for further study.

Finally, it is assumed that the $c_{j,i}$ values do not change throughout the course of the 25-year temporal boundary. This may be valid for mature technologies which are no longer developing much, but not for new ones that are still innovating. But without being able to predict the course of technological development, no better accuracy can be achieved at present than with this approximation.

3.2.1 Coal

A qualitative description of electricity generation by coal combustion is given based on that by Ryberg et al. (2015) and Schakel et al. (2014), followed by quantitative life-cycle environmental impact data. A reminder of ReCiPe midpoint category abbreviations can be found in Chapter 1 Section 1.2.

The coal mining process requires energy and water, and results in some contamination of the soil and waterways (all with associated environmental impacts) and entails a non-natural use of land (LO). The mined coal is transported by freight and train (to the UK mostly from Russia and to a lesser extent from the USA, according to (BEIS, 2018a, DUKES G.2)). The coal is pulverised by hammer mills and the resulting coal powder is combusted in a power plant. The heat generated by combustion heats water into steam to drive a turbine-generator, to generate electricity. CO_2 is a product of combustion and contributes to CC when released to the atmosphere. The carbon that comprises nearly the entirety of coal and that is released in the form of CO_2 is fossil carbon: it had been accumulated through millions of years of heat and pressure acting on dead organic matter. Some nitrogen oxides are also produced through heat driving reactions between oxygen and nitrogen in the air. Sulphur impurities in the coal react with oxygen in the air to produce sulphur oxides. Most of the nitrogen oxides and sulphur oxides are chemically scrubbed out of the flue gas before release to the atmosphere, though some non-zero impact on POF and TA respectively is unavoidable (amongst other impacts). The chemical scrubbing process itself requires water to dilute contaminants in the effluent before it is released into waterways, though again non-zero impacts are unavoidable. Some ash is left in the combustion chamber and is typically landfilled, with resultant environmental impacts. In addition to mining and chemical scrubbing, WD occurs through evaporation of water used to cool the plant to keep it at working temperature.

These operational impacts dominate the life cycle of a coal power plant; construction and decommissioning of the plant contribute at most 14 % to the full life cycle for the MD impacts, and only 3 % averaged across all impact categories (Stamford and Azapagic, 2012). LCAs that don't disaggregate construction and decommissioning from operation are included in this analysis, as they incur negligible error. Schakel et al. (2014) conducted LCAs of coal combustion with and without CCS, and co-firing with biomass; their ReCiPe midpoint impacts for combustion of pulverised coal without CCS nor biomass are given in Table 3.5. Hertwich et al. (2015) conducted LCAs of many different generator technologies; their ReCiPe midpoint impacts for subcritical[2] coal without CCS are used here, although they are specific to a coal power plant in China. Frischknecht (2017) did similarly, but reporting impacts under the ILCD framework. Their results for a hard coal plant in Germany were used.

[2]Newer coal plants are often supercritical rather than subcritical, the former achieving higher efficiency of up to 40 % by keeping water at higher pressure and temperature in the steam cycle. Most GB coal plants are of the subcritical type.

These results are given in Table 3.5 along with central estimates ($c_{coal,i}$, the means of all the sources) and uncertainty values. Raw data from Stamford and Azapagic (2012) and Frischknecht (2017) are given in Appendix B1 along with their conversions from CML2001 and ILCD respectively to ReCiPe.

		Stamford and Azapagic (2012)	**Schakel et al. (2014)**	**Hertwich et al. (2015)**	**Frischknecht (2017)**	**Central Estimate**	**Uncertainty**
CC	kg CO_2/kWh	1.07	9.03×10^{-1}	9.33×10^{-1}	1.09	1.00	4.73×10^{-2}
OD	kg CFC11/kWh	4.13×10^{-9}	6.88×10^{-9}	-	1.85×10^{-9}	4.29×10^{-9}	1.26×10^{-9}
HT	kg DCB/kWh	7.50×10^{-2}	2.41×10^{-1}	1.11×10^{-1}	4.25×10^{-1}	2.13×10^{-1}	8.76×10^{-2}
POF	kg NMVOC/kWh	5.00×10^{-5}	1.45×10^{-3}	8.09×10^{-4}	1.13×10^{-3}	8.59×10^{-4}	3.50×10^{-4}
PMF	kg PM10/kWh	-	5.96×10^{-4}	3.35×10^{-4}	8.17×10^{-5}	3.38×10^{-4}	1.29×10^{-4}
IR	kg U235/kWh	6.53×10^{-2}	1.57×10^{-2}	-	4.59×10^{-3}	2.85×10^{-2}	1.52×10^{-2}
TA	kg SO_2/kWh	1.77×10^{-3}	1.80×10^{-3}	1.10×10^{-3}	8.36×10^{-4}	1.38×10^{-3}	2.41×10^{-4}
FE	kg P/kWh	6.93×10^{-5}	3.87×10^{-4}	4.82×10^{-4}	3.70×10^{-5}	2.44×10^{-4}	1.11×10^{-4}
ME	kg N/kWh	-	5.74×10^{-4}	-	3.91×10^{-4}	4.82×10^{-4}	4.58×10^{-5}
FET	kg DCB/kWh	1.55×10^{-2}	5.51×10^{-3}	-	4.75×10^{-5}	7.03×10^{-3}	3.87×10^{-3}
LO	m^2·a/kWh	2.72×10^{-2}	1.03×10^{-2}	2.04×10^{-2}	5.04×10^{-2}	2.71×10^{-2}	1.00×10^{-2}
WD	m^2·a/kWh	-	8.13×10^{-4}	-	3.41×10^{-4}	5.77×10^{-4}	1.18×10^{-4}
MD	kg Fe/kWh	7.74×10^{-7}	4.66×10^{-3}	9.90×10^{-4}	2.40×10^{-6}	1.41×10^{-3}	1.16×10^{-3}
FD	kg oil/kWh	3.02×10^{-1}	2.17×10^{-1}	-	3.03×10^{-1}	2.74×10^{-1}	2.15×10^{-2}

TABLE 3.5: Converted ReCiPe midpoint impact values for generation of 1 kWh electricity by coal combustion.

The uncertainty in $c_{coal,CC}$ and $c_{coal,FD}$ is small (5 % and 8 % respectively) compared to the other impact categories. These others depend on impurities naturally occurring in different coal deposits, and processes used to remove them or mitigate their impacts. The capacity factor of generation (the equivalent percentage of time for which power output is at maximum) affects the ratio of operational to non-operational impacts in all categories: a plant running very rarely and/or at below its nominal power most of the time has lower capacity factor and would have a lower proportion of operational impacts over its lifetime compared to a plant with higher capacity factor. Lower capacity factor is increasingly becoming a reality for all of GB's fossil-fuelled generators, and in other countries with increasing shares of renewable energy, where the function of fossil-fuelled generators is shifting from baseload to reserve, or backup power. Stamford and Azapagic (2012) took a capacity factor of 62 %, Schakel et al. (2014) took it as 85 %, and Hertwich et al. (2015) took it as decreasing from 60 % to 30 % from 2007 to 2050. The fact that capacity factor is likely to decrease in future does not invalidate the usage of these data, as only operational impacts are within the scope of this study (the split between operational and non-operational is out of scope).

3.2.2 Combined Cycle Gas Turbines

The UK has some natural gas (methane, CH_4) reserves of its own under the North Sea, but is increasingly reliant on imported gas (BEIS, 2018a, DUKES G.5), 75 % of which by pipeline from Norway. Natural gas occurs naturally in under-sea gas fields along with crude oil, another fossil fuel. It is extracted by

pumping from a well that has been drilled into the gas field, and must be separated from impurities and other hydrocarbons. As well as transportation by pipe, natural gas may be liquefied first and transported by tanker: Qatar is the dominant origin of such imports to the UK (BEIS, 2018a, DUKES G.5). As explained by Wärtsilä (2019), the combustion of CH_4 produces CO_2 and water vapour at high velocity and temperature. The kinetic energy of the combustion products drives one turbine-generator directly, and the heat generated by combustion heats water via a heat exchanger. The steam thus produced drives another turbine-generator, cooling down and being cycled back through the heat exchanger repeatedly, hence 'combined cycle'. Like coal, CH_4 combustion also releases CO_2 and also requires flue gas scrubbing and water for cooling. However, the efficiency is higher (up to 60 %, compared to around 30 % for coal) due to the combined cycles making more use of the energy released in CH_4 combustion, and there are no solid waste products to dispose of. The result is lower impacts in nearly all categories.

Again, data from Stamford and Azapagic (2012) is used, excluding construction and decommissioning impacts. The operational impacts are still dominant in the CCGT life cycle (13 % non-operational, averaged across all impacts), except for HT, FET, and MD, for which they are almost equal to non-operational impacts. However, this was decided to be insufficient grounds to exclude or adjust the other sources of LCA data which did not disaggregate operational from non-operational impacts. The uncertainty values for HT, FET and MD are an expectedly large proportion of the central estimates in those categories.

Singh et al. (2011) conducted an LCA of CCGT (which they refer to as NGCC, natural gas combined cycle) with and without CCS; their baseline results without CCS are given in Table 3.6. Also given are the results of Hertwich et al. (2015) for NGCC without CCS (for a plant in China), and Frischknecht (2017) for a natural gas power plant in Germany. Raw data from Stamford and Azapagic (2012) and Frischknecht (2017) are given in Appendix B2 along with their conversions from CML2001 and ILCD respectively to ReCiPe midpoint impacts. Note that because only Frischknecht (2017) reported any results for WD, the uncertainty in that category was taken to be the same as the central estimate itself. This implies a range between zero and twice the central estimate in the WD category. There is not enough information to further constrain the central estimate, nor even its uncertainty.

		Singh et al. (2011)	**Stamford and Azapagic (2012)**	**Hertwich et al. (2015)**	**Frischknecht (2017)**	**Central Estimate**	**Uncertainty**
CC	kg CO_2/kWh	4.59×10^{-1}	3.78×10^{-1}	5.27×10^{-1}	5.37×10^{-1}	4.75×10^{-1}	3.98×10^{-2}
OD	kg CFC11/kWh	-	1.26×10^{-8}	-	8.19×10^{-8}	4.73×10^{-8}	1.73×10^{-8}
HT	kg DCB/kWh	1.39×10^{-3}	2.34×10^{-3}	8.80×10^{-2}	7.27×10^{-2}	4.11×10^{-2}	2.17×10^{-2}
POF	kg NMVOC/kWh	7.01×10^{-4}	9.59×10^{-6}	6.17×10^{-4}	6.51×10^{-4}	4.95×10^{-4}	1.73×10^{-4}
PMF	kg PM10/kWh	1.74×10^{-4}	-	7.57×10^{-4}	2.79×10^{-5}	3.20×10^{-4}	1.82×10^{-4}
IR	kg U235/kWh	-	2.42×10^{-2}	-	3.50×10^{-4}	1.23×10^{-2}	5.97×10^{-3}
TA	kg SO_2/kWh	4.53×10^{-4}	1.42×10^{-4}	3.78×10^{-3}	3.02×10^{-4}	1.17×10^{-3}	9.09×10^{-4}
FE	kg P/kWh	-	1.98×10^{-5}	5.40×10^{-6}	4.30×10^{-7}	8.54×10^{-6}	4.84×10^{-6}
ME	kg N/kWh	6.75×10^{-5}	-	-	1.73×10^{-4}	1.19×10^{-4}	2.68×10^{-5}
FET	kg DCB/kWh	4.96×10^{-6}	1.72×10^{-3}	-	8.56×10^{-6}	5.78×10^{-4}	4.29×10^{-4}
LO	m^2·a/kWh	-	5.96×10^{-4}	4.88×10^{-4}	4.73×10^{-2}	1.61×10^{-2}	1.17×10^{-2}
WD	m^2·a/kWh	-	-	-	3.18×10^{-5}	3.18×10^{-5}	3.18×10^{-5}
MD	kg Fe/kWh	-	1.61×10^{-7}	2.56×10^{-4}	1.20×10^{-6}	8.58×10^{-5}	6.40×10^{-5}
FD	kg oil/kWh	-	1.15×10^{-1}	-	2.21×10^{-1}	1.68×10^{-1}	2.66×10^{-2}

TABLE 3.6: Converted ReCiPe midpoint impact values for generation of 1 kWh electricity by CCGT combustion.

3.2.3 Biomass

The majority of biomass burned for power in GB today is in the form of wood pellets imported from North America (BEIS, 2018a, DUKES G.6), co-fired with coal. North American forestry for wood and paper results in off-cuts which are processed into wood pellets, dried, and shipped to the UK. This arrangement may be unsustainable in the long term, especially if North American demand for biomass increases, biomass for the UK may need to be sourced from elsewhere.

The term 'biomass' encompasses a wide range of sources and applications (Cherubini and Strømman, 2011): in addition to forestry residue wood pellets, biomass can refer to the processing of food, farm or gardening waste in anaerobic digestors to produce CH_4 for burning in CCGT plants, or the farming of crops specifically for such processing. The bio-methane can alternatively be used as a heating fuel, or in combined heat and power plants, and a different process can produce bio-ethanol from these inputs, for use as a transport fuel. In the case of farming biomass crops, environmental impacts depend on farming practices (use of water, pesticides and fertilisers) and alternative uses of the land (whether it is marginal land or displaces farming of other crops or livestock). While the combustion of wood releases more CO_2 per kWh than coal combustion (due to lower efficiency from higher water content), each kWh generated means more CO_2-absorbing crops are grown that would not otherwise have been, or methane emission from rotting forestry residue or farm waste is avoided. Biomass LCAs tend to subtract these CO_2 mitigation impacts from the direct emissions. It is considered valid to include life-cycle impacts of the source of biomass as part of the operational impacts.

Stamford and Azapagic (2014) conducted an LCA comparing combustion of different types of biomass for power generation in the UK. Their results for imported wood (excluding construction and decommissioning of the biomass power plant) were best representative of biomass power as it is currently used in the UK. Operational impacts dominated the life cycle, like for coal and CCGT. Non-operational impacts constitute on average 7 % of the full life-cycle impacts, and in the worst case 40 % of MD is from non-operational impacts. Therefore it was considered acceptable to use LCAs that did not disaggregate operational and non-operational impacts.

Vázquez-Rowe et al. (2014) analysed scenarios for producing bio-methane from an increase in maize crop production in Luxembourg with different potential effects on other crops, livestock, and meadow land. As they reported ReCiPe midpoint impacts per MJ bio-methane produced, these values were multiplied by 3.6 MJ/kWh and divided by 0.5 to give values per kWh electricity produced (Singh et al. (2011) used a CCGT power generation efficiency of 55 %, Frischknecht (2017) 43.7 %, Wärtsilä (2019) quoted 60 %). The mean of the converted results of Vázquez-Rowe et al. (2014) are given in Table 3.7, and only the mean is used in calculating the central estimates, so as not to skew them towards the results of Vázquez-Rowe et al. (2014) and away from the results from other data sources. However, the uncertainty values take account of all five 'C' scenarios (from the policy-makers' perspective) that they analysed.

Using results from only Stamford and Azapagic (2014) and Vázquez-Rowe et al. (2014) would be undesirable, as Stamford and Azapagic (2014) did not report impacts for PMF, ME, or WD, which would mean only one data source being used for those categories. It was difficult to find LCAs that took energy production as a functional unit (as opposed to tons of waste treated, for example), or that analysed biomass for electricity production as opposed to heating or transport fuels. Moretti et al. (2016) compared a biomass-fuelled heating and cooling system for a building, to a natural gas boiler with electric heat pumps. Although this is a very different application to electricity generation in a power plant, an approximation can be found by taking the ratio of biomass impacts to natural gas impacts that Moretti et al. (2016) calculated, and multiplying them by the central estimates for CCGT, $c_{CCGT,i}$. This is valid because both biomass and CCGT generation impacts are dominated by their fuels, and heat and electricity are both forms of energy.

The result of processing the Moretti et al. (2016) data in this way is that PMF, ME and WD are very close to the values that Vázquez-Rowe et al. (2014) calculated, these being the categories missing from Stamford and Azapagic (2014). At the same time, FE is two orders of magnitude lower and LO two orders of magnitude higher than the values given by other sources. Excluding the results of Moretti et al. (2016) would significantly under-estimate the uncertainty in those categories.

Appendix B3 contains raw CML2001 impacts from Stamford and Azapagic (2014) and their conversion to ReCiPe midpoint impacts, Vázquez-Rowe et al. (2014) data in all five of their 'C' scenarios, and Moretti et al. (2016) data for natural gas and biomass heating of a building.

		Stamford and Azapagic (2014)	**Vázquez-Rowe et al. (2014)**	**Moretti et al. (2016)**	**Central Estimate**	**Uncertainty**
CC	kg CO_2/kWh	1.04×10^{-1}	8.31×10^{-2}	1.51×10^{-1}	1.13×10^{-1}	2.55×10^{-2}
OD	kg CFC11/kWh	9.48×10^{-9}	4.43×10^{-9}	2.01×10^{-9}	5.31×10^{-9}	1.30×10^{-9}
HT	kg DCB/kWh	6.09×10^{-2}	1.07×10^{-2}	1.17×10^{-1}	6.29×10^{-2}	2.68×10^{-2}
POF	kg NMVOC/kWh	8.20×10^{-5}	2.45×10^{-4}	1.42×10^{-3}	5.83×10^{-4}	3.35×10^{-4}
PMF	kg PM10/kWh	-	3.48×10^{-4}	8.61×10^{-4}	6.05×10^{-4}	1.33×10^{-4}
IR	kg U235/kWh	4.02×10^{-2}	4.21×10^{-3}	1.08×10^{-2}	1.48×10^{-2}	9.02×10^{-3}
TA	kg SO_2/kWh	2.84×10^{-3}	2.18×10^{-3}	2.05×10^{-3}	2.36×10^{-3}	2.01×10^{-4}
FE	kg P/kWh	1.21×10^{-4}	1.26×10^{-5}	8.54×10^{-6}	4.73×10^{-5}	2.71×10^{-5}
ME	kg N/kWh	-	3.04×10^{-4}	3.38×10^{-4}	3.21×10^{-4}	1.29×10^{-5}
FET	kg DCB/kWh	1.91×10^{-2}	4.81×10^{-4}	9.22×10^{-4}	6.82×10^{-3}	4.65×10^{-3}
LO	m^2·a/kWh	2.82×10^{-1}	1.75×10^{-3}	6.66	2.37	1.63
WD	m^2·a/kWh	-	1.70×10^{-4}	5.09×10^{-5}	1.10×10^{-4}	7.53×10^{-6}
MD	kg Fe/kWh	4.06×10^{-7}	4.14×10^{-3}	1.71×10^{-4}	1.44×10^{-3}	1.08×10^{-3}
FD	kg oil/kWh	2.55×10^{-2}	1.01×10^{-2}	4.00×10^{-2}	2.52×10^{-2}	7.54×10^{-3}

TABLE 3.7: Converted ReCiPe midpoint impact values for generation of 1 kWh electricity by biomass combustion.

3.2.4 Carbon Capture and Storage

As Schreiber et al. (2012) explain, CCS typically refers to post-combustion CO_2 capture, where it is separated from nitrogen in the air by amine scrubbing. Other methods include pre-combustion capture and oxyfuel combustion, which alter the composition of gases in the combustion chamber in such a way as to facilitate CO_2 separation from the other reaction products. It is not stated in FES 2018 which technology is referred to by CCS, nor what specifically happens to the captured CO_2. It can be transported to geologically stable underground sites and sealed from release to the atmosphere, or used to make new products such as limestone for building materials. In both cases a small amount of CO_2 leakage to the atmosphere over time can be expected to occur. For this thesis, post-combustion CO_2 capture with subsequent underground storage is assumed to be the predominant mode of CCS in future scenarios.

It is implied in FES 2018 that natural gas will be the predominant fuel in CCS plants: no CCS is deployed in the CR scenario but 12.1 GW of CCS capacity are by 2050 in TD, whose CCGT capacity by then is less than that of CR50 by roughly the same amount. This suggests that some CCGT plants are expected to be retrofitted with carbon capture technology.

Two LCAs fitting this description of CCGT with post-combustion CCS and subsequent compression and storage are those by Singh et al. (2011) and Hertwich et al. (2015). Both analysed the use of monoethanolamine as the CO_2 capture reagent; Singh et al. (2011) considered compression to 110 bar and transport 500 km by pipeline to a geological formation represented by the Utsira saline aquifer 800 m below the sea floor; Hertwich et al. (2015) specified compression to 150 bar, transport 150 km by pipeline

and storage in an underground formation at 1200 m depth. These two data sources are insufficient, as between them they give no values for OD, IR, WD, FD impacts.

Other LCAs of CCS only examined the use of coal as fuel. As these tend to compare coal combustion with and without CCS, it is still possible to find an approximation to CCGT with CCS: the ratio of the coal power impacts with and without CCS is multiplied by the impacts of CCGT, $c_{CCGT,i}$. The coal LCAs used are by Koornneef et al. (2008) (supercritical coal combustion without and with CCS, cases 2 and 3 in their nomenclature) and Schakel et al. (2014) (pulverised coal with and without CCS), as given in Appendix B4. This is valid because the carbon capture process decreases electricity generation efficiency, meaning more fuel is needed per kWh, and both CCGT and coal combustion impacts are dominated by the impacts associated with their fuels. The with-to-without CCS ratios from Koornneef et al. (2008) and Schakel et al. (2014), multiplied by the CCGT impacts central estimates, are given in Table 3.8 along with the results of Singh et al. (2011) and Hertwich et al. (2015).

After this, there was still only one source for the IR, WD and FD categories (Schakel et al., 2014). With no other information available, the uncertainty in those categories was taken to be equal to the central estimates themselves.

		Singh et al. (2011)	**Hertwich et al. (2015)**	**Koornneef et al. (2008)**	**Schakel et al. (2014)**	**Central Estimate**	**Uncertainty**
CC	kg CO_2/kWh	1.67×10^{-1}	2.47×10^{-1}	1.38×10^{-1}	1.22×10^{-1}	1.69×10^{-1}	3.12×10^{-2}
OD	kg CFC11/kWh	-	-	7.32×10^{-8}	6.57×10^{-8}	6.95×10^{-8}	1.89×10^{-9}
HT	kg DCB/kWh	3.11×10^{-3}	1.12×10^{-1}	1.15×10^{-1}	5.68×10^{-2}	7.18×10^{-2}	2.81×10^{-2}
POF	kg NMVOC/kWh	8.51×10^{-4}	7.68×10^{-4}	6.26×10^{-4}	6.72×10^{-4}	7.29×10^{-4}	5.63×10^{-5}
PMF	kg PM10/kWh	2.31×10^{-4}	9.16×10^{-4}	-	3.98×10^{-4}	5.15×10^{-4}	1.71×10^{-4}
IR	kg U235/kWh	-	-	-	1.71×10^{-2}	1.71×10^{-2}	1.71×10^{-2}
TA	kg SO_2/kWh	6.48×10^{-4}	4.68×10^{-3}	1.71×10^{-3}	1.53×10^{-3}	2.14×10^{-3}	1.01×10^{-3}
FE	kg P/kWh	-	1.01×10^{-5}	1.54×10^{-5}	1.18×10^{-5}	1.24×10^{-5}	1.32×10^{-6}
ME	kg N/kWh	8.85×10^{-5}	-	-	1.67×10^{-4}	1.28×10^{-4}	1.97×10^{-5}
FET	kg DCB/kWh	1.32×10^{-5}	-	8.44×10^{-4}	7.99×10^{-4}	5.52×10^{-4}	2.08×10^{-4}
LO	m^2·a/kWh	-	6.75×10^{-4}	-	2.24×10^{-2}	1.15×10^{-2}	5.42×10^{-3}
WD	m^2·a/kWh	-	-	-	4.42×10^{-5}	4.42×10^{-5}	4.42×10^{-5}
MD	kg Fe/kWh	-	5.21×10^{-4}	1.15×10^{-4}	1.23×10^{-4}	2.53×10^{-4}	1.02×10^{-4}
FD	kg oil/kWh	-	-	-	2.32×10^{-1}	2.32×10^{-1}	2.32×10^{-1}

TABLE 3.8: Converted ReCiPe midpoint impact values for generation of 1 kWh electricity by CCGT with CCS.

3.2.5 Nuclear

All nuclear power plants currently in operation in GB are pressurised water reactors (PWR). Whether any nuclear new-build in future will be of the same scale or in the form of many smaller reactors is uncertain. The operation of a PWR is described qualitatively here, based on the description by EIA (2019).

Nuclear fuel for a PWR requires processing (and therefore energy expenditure, with associated environmental impacts) to make it usable in power plants. Uranium ore is mined and refined, and then must be enriched to increase the concentration of fissile U235 (non-fissile U238 is the more common isotope). At the power plant, the fuel rods are inserted into the reactor where they are bombarded by neutrons; the fission of U235 releases more neutrons, enabling a chain reaction. Much of the complexity of a PWR is in keeping the chain reaction rate stable rather than having it slow to a stop or accelerate uncontrollably, and in safety measures to prevent endangerment to human life if normal operation fails. Heat generated by U235 fission drives a steam turbine-generator in much the same way as heat from coal combustion. There are analogous requirements for cooling water, but no CO_2 is emitted from the nuclear reaction itself. The waste products are solid radioactive elements which must be securely contained to eliminate leakage and reduce ionising radiation, and transported to a safe storage site where it must be monitored for hundreds of years.

The embodied impacts associated with construction of a nuclear PWR plant tend to be high due to the concrete needed to shield the reactor to reduce leakage of ionising radiation to the outside. Much less nuclear fuel is needed than fossil fuels compared by mass due to the greater quantities of energy released by nuclear fission than by combustion. As a result, the operational impacts comprise a lower proportion of a nuclear plant's life-cycle impacts compared to coal and CCGT, at 80.6 % on average according to Stamford and Azapagic (2012).

The only other LCA for nuclear power that analyses other impacts in addition to CC is by Frischknecht (2017), but it does not disaggregate operational and non-operational impacts. Because the latter comprise a significant proportion of the life-cycle impacts in all categories, the decision was taken to reduce the impacts reported by Frischknecht (2017) accordingly. Because Stamford and Azapagic (2012) did not analyse impacts for PMF, ME and WD, those impacts reported by Frischknecht (2017) were reduced to the average of 80.6 % of their full life-cycle values. The other impacts were reduced to the corresponding percentage calculated by Stamford and Azapagic (2012) in each category. Details are given in Appendix B5; the results are given below in Table 3.9.

Using only one paper (Stamford and Azapagic, 2012) as the source of all operational/non-operational adjustment factors raises questions of reliability. But as no other nuclear power LCAs of sufficient detail could be found, this option was considered to yield more accurate data than using the Frischknecht (2017) data for full life-cycle impacts without adjustment, and preferable to excluding the Frischknecht (2017) data completely and ignoring PMF, ME and WD categories. With only one source (Frischknecht, 2017) for PMF, ME, WD values, the uncertainty in those categories was taken to be the same as the central estimates, as that is the only information available.

		Stamford and Azapagic (2012)	**Frischknecht (2017)**	**Central Estimate**	**Uncertainty**
CC	kg CO_2/kWh	4.38×10^{-3}	5.40×10^{-3}	4.89×10^{-3}	2.53×10^{-4}
OD	kg CFC11/kWh	4.66×10^{-10}	1.61×10^{-8}	8.28×10^{-9}	3.91×10^{-9}
HT	kg DCB/kWh	1.08×10^{-1}	2.98×10^{-2}	6.89×10^{-2}	1.96×10^{-2}
POF	kg NMVOC/kWh	1.52×10^{-6}	3.40×10^{-5}	1.77×10^{-5}	8.11×10^{-6}
PMF	kg PM10/kWh	-	4.39×10^{-6}	4.39×10^{-6}	4.39×10^{-6}
IR	kg U235/kWh	1.88	4.72	3.30	7.10×10^{-1}
TA	kg SO_2/kWh	3.63×10^{-5}	2.86×10^{-5}	3.25×10^{-5}	1.93×10^{-6}

		Stamford and Azapagic (2012)	Frischknecht (2017)	Central Estimate	Uncertainty
FE	kg P/kWh	3.25×10^{-6}	3.87×10^{-7}	1.82×10^{-6}	7.16×10^{-7}
ME	kg N/kWh	-	1.25×10^{-5}	1.25×10^{-5}	1.25×10^{-5}
FET	kg DCB/kWh	1.95×10^{-2}	2.52×10^{-5}	9.78×10^{-3}	4.88×10^{-3}
LO	m^2·a/kWh	2.55×10^{-4}	1.64×10^{-3}	9.49×10^{-4}	3.47×10^{-4}
WD	m^2·a/kWh	-	9.84×10^{-5}	9.84×10^{-5}	9.84×10^{-5}
MD	kg Fe/kWh	4.96×10^{-7}	3.30×10^{-5}	1.68×10^{-5}	8.13×10^{-6}
FD	kg oil/kWh	1.19×10^{-3}	2.22×10^{-1}	1.12×10^{-1}	5.53×10^{-2}

TABLE 3.9: Converted ReCiPe midpoint impact values for generation of 1 kWh electricity by nuclear power.

3.2.6 Imports and Exports

International imports and exports of electricity (not to be confused with grid import to/export from a single house) are achieved physically through high-voltage interconnectors, under-sea in the case of an island like GB. As explained by Strbac et al. (2014), the owner of an interconnector profits by buying electricity in the lower-price region and selling it in the higher-price region; thus electricity market prices determine the direction of power flow in interconnectors. The consumers in the higher-price region benefit from access to a greater supply (which lowers the price), and producers in the lower-price region benefit from access to a greater market (which increases the price they are paid). Conversely, consumers in the lower-price region cannot enjoy electricity at as low a price as it would be without the interconnector, and producers in the higher-price region face greater competition from the region to which they are interconnected.

GB has interconnections to France (2 GW), the Netherlands (1 GW), and the Republic of Ireland (0.5 GW), as well as under-sea connections between England and Scotland, and England and Northern Ireland. Interconnections to Spain, Norway, Denmark, Germany, and Belgium are also anticipated in FES 2018 (National Grid, 2018b), but the individual capacities of each are not revealed due to commercial sensitivity.

If the hourly-resolution BID3 modelling results for electricity import/export were available, the ideal would be to apply the adapted Hawkes' method to find $MGR_j(t)$, and assign emissions impact factors $c_{j,i}$ to import/export according to the generator types operating in the regions to which GB is interconnected. As it is, BID3 results are not available, and even if they were, the problem soon becomes one of modelling the entire European electricity grid to find the marginal generator in each country. While the European grid has been modelled by some such as Bussar et al. (2014), it is a level of detail uncalled for by the goal and scope of this thesis.

Instead, imports/exports via the French and Dutch interconnectors in 2017 are associated with impacts according to the average generation mix in each country in 2016: for France (IEA, 2018a), 73 % nuclear, 6 % CCGT, 2 % coal; for the Netherlands (IEA, 2018b), 47 % CCGT, 34 % coal, 6 % biomass, 3 % nuclear. (The remainder in each case is renewable energy, whose impacts are ignored as explained in the next section.)

For 2030 and 2050, an approximation is made based on the correlations in demand and renewable energy supply that exist throughout Europe. Any export from GB in future is likely to result from an excess of wind and PV generation, from weather patterns affecting Europe too, and will likely displace or curtail wind and PV elsewhere on the European grid. Imports to GB will likely occur at times of low wind and PV generation, when hydroelectric, nuclear, biomass, and other generators are outputting their maximum power but still cannot meet demand. Assuming such a situation would occur throughout Europe, imports to GB would likely be met by CCGT (the next most CO_2-intense generator after coal, which is planned to be phased out by 2030 (Beyond Coal, 2018) in all the countries to which GB is or will be interconnected).

Therefore when exporting in 2030 and 2050, all interconnectors have zero impacts associated with them (see Section 3.2.7), and when importing, their emissions impacts are equivalent to CCGT generation. The interpolation between 2017 and 2030, and 2030 and 2050 was described above in Section 3.1.4. This is necessarily an approximation. Its implications are discussed in further work, Chapter 7.

3.2.7 Wind, Solar, Hydroelectric, and Other

The approximation is made that zero impacts are associated with wind, solar PV, and 'hydroelectric, marine and other renewables'. This is motivated by the decision to count only operating impacts but to exclude construction and decommissioning impacts from the calculation of $MEF_i(t)$, as each kWh imported from or exported to the grid can only increase or displace some operating impacts but, within the scope of this study, cannot cause or prevent a power plant to be built.

The first point to note is that operating impacts of renewable power are around four orders of magnitude lower than their embodied impacts of construction (Stamford and Azapagic, 2012). Maintenance requires some fuel to transport technicians to the site once or a few times each year, and some small impacts are associated with water use to clean PV panels, for example. Secondly, the O & M impacts cannot be reduced by curtailing renewable generation. This is markedly different to fuel-burning generators (nuclear and biomass included): reducing power generation for a time period reduces the fuel consumption and all associated impacts of extracting and processing the fuel. It makes sense to associate impacts per kWh of electricity used or displaced from these generator types, but not in the case of wind, solar PV, and 'hydroelectric, marine and other renewables'.

Finally, there is a generator type 'Other', not to be confused with 'hydroelectric, marine and other renewables'. Generation from 'Other' is not so much real physical generation but an indicator that there is not enough capacity from all other generator types, including international import. In the worst case (CR50), 'Other' comprises 15 GWh out of 441 TWh total generation in that year (0.003 %). It may be even less in reality, when national demand is not pre-determined but responds to price. Electricity prices would be high in such supply-short periods, encouraging industrial and commercial, if not domestic consumers, to reduce their demand. While notionally incorrect, assigning CCGT as the marginal generator in such situations ensures robustness of modelling: the EAA should make home batteries discharge when national demand exceeds supply, which it will do because CCGT is the most CO_2-intense generator type in the future scenarios.

3.2.8 Combining Uncertainties

The uncertainties in environmental impact intensities of each electricity generator type and system component arise as a result of both methodological differences between the LCAs examined, and true physical variation between different manufacturers of PV arrays, between different coal-burning power stations, and so on. The uncertainties for each of these, in each ReCiPe midpoint impact category, propagate through to an uncertainty in the total life-cycle environmental impacts of the domestic PV-battery system.

Because the propagation of these uncertainties is far from straightforward to analyse, it may not be appropriate to use a partial-derivative approach, where the final uncertainty is a sum of contributions from linearising the different sources of uncertainty input. Instead, the Monte Carlo method (Sobol, 1975) is used in this work: the total life-cycle impact c_i in each category i is re-calculated multiple times assuming different impact intensities for electricity generation and system components. All impact intensities are allowed to vary simultaneously, independently, and stochastically within distributions defined for every impact intensity $c_{j',i}$ in each ReCiPe midpoint category i, of each generator type and manufacture of each system component j'. (Note that the index i runs from 1 to 14, for the 14 ReCiPe midpoint impact categories considered in this study, and j' runs from 1 to 10: the set {coal, CCGT, biomass, CCS, nuclear, French interconnector, Dutch interconnector, PV, battery, BoS} has 10 elements in total.) The result is a distribution in resultant values of c_i.

To conduct the Monte Carlo analysis, a distribution shape must be chosen to represent the uncertainties in electricity generation and system component impact intensities, and the number of iterations chosen to adequately capture the distribution shape. If enough data could be found for every impact intensity $c_{j',i}$, it would be possible to fit a distribution shape to them, whether Gaussian, Poisson, Weibull, etc. This was not the case in this study, nor was there enough information to choose a distribution uniquely based on the physical process giving rise to the uncertainty.

The recommendation of ISO 14044 (ISO, 2006b) in such situations is to use a Gaussian distribution (also known as the normal distribution):

$$N(\mu, \sigma) = \frac{1}{\sqrt{(2\pi\sigma^2)}} \exp\left(-\frac{(x-\mu)^2}{2\sigma^2}\right) \tag{3.10}$$

where the Gaussian-distributed random variable x has mean μ and standard deviation σ. The reasoning is that due to the Central Limit Theorem, a Gaussian is the asymptotic result of combining many independent random variables, regardless of the distribution shape of each of them (Kennedy and Neville, 1966). A Gaussian shape is therefore a reasonable approximation since all that is needed is a way to propagate the mean and variance of the input uncertainties through to the final life-cycle impact uncertainties. This method cannot give accurate information on the skewness or higher moments of the distribution.

The central estimates $c_{j',i}$ found above and in the previous chapter for the impact intensity in each ReCiPe midpoint category i, of each generator type and manufacture of each system component j', are used as μ for each Gaussian distribution. Their corresponding uncertainty estimate is used as σ. The Matlab function `normrnd` is used with these inputs to generate a large number of Gaussian-distributed random values of $c_{j',i}$ for use in the Monte Carlo iterations. A hypothetical example is shown in Figure

3.11 (a) with $\mu = 10$ and $\sigma = 2$ (shown with 10 000 data points, but the choice of this number is discussed further below).

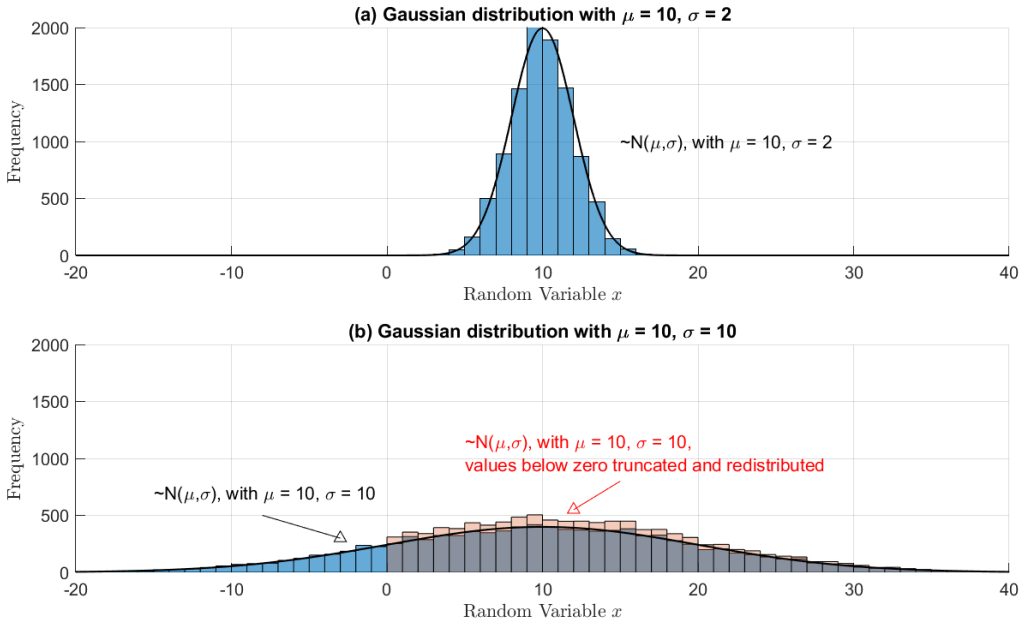

FIGURE 3.11: Histograms of Gaussian-distributed random variable x with mean $\mu = 10$ and standard deviation (a) $\sigma = 2$, and (b) $\sigma = 10$, and with below-zero values truncated and redistributed.

A problem arises from the fact that a Gaussian-distributed random variable has finite probability of having below-zero values. (An extreme example with $\mu = 10$, $\sigma = 10$, is shown in Figure 3.11 (b).) But there is a finite, above-zero impact to every process in the set j' considered in this study, since credits from recycling are excluded. To resolve this contradiction, the below-zero values of each distribution are truncated and redistributed by calling `normrnd` again twice more, and any remaining below-zero values are assigned the value zero. This process mostly preserves the mean and standard deviation, but does distort the skewness of the distribution.

The number of Monte Carlo iterations performed must be sufficient to capture the variation in each of the impact intensities $c_{j',i}$. One approach is to consider that each of the 10 $c_{j',i}$ values in a given impact category i can take on a 'small' or 'large' value within their respective distributions - there are then $2^{10} = 1024$ ways in which 'small' and 'large' can be combined for the 10 elements of set j' (generators and system components). 1024 Monte Carlo iterations should then cover all these combinations, as the impact intensities are allowed to vary independently and simultaneously. While it is typical for applications of the Monte Carlo method to use 10 000 iterations (Sobol, 1975), it was found that smooth distributions in the results (Chapter 6) were already obtained with only 1024. A RAM upgrade to the device performing the computations would be needed to increase the number of iterations beyond this. Given that the Gaussian shape is only being used as a vehicle to propagate uncertainties through to the results, with no great confidence placed in the specific distribution shape, 1024 was considered a sufficient number of Monte Carlo iterations for the purposes of this study.

Sensitivity of results to system configuration (with/without PV/battery), size, second-life battery degradation rate, and household load are discussed in later chapters.

3.3 Summary

To achieve the goal of this study, marginal emissions factor time series $MEF(t)$ were required for whole years at sub-daily resolution, to 2050 and beyond. After reviewing existing methods of calculating $MEF(t)$, Siler-Evans' adaptation to Hawkes' method (linear regression of historical data binned by month and national demand level) was chosen and applied to 2017 data from Gridwatch (2018). But as $MEF(t)$ was required for future years too, and existing modelled generation data for those years in GB was unavailable, a fixed merit-order generator dispatch model (GDM) was developed for this purpose. The Community Renewables and Two Degrees scenarios were selected from National Grid's FES 2018 document, and their predicted generator capacities in 2030 and 2050 were imposed on the GDM exogenously. Battery storage in the country was approximated as 50 divisions of an aggregated system, with which the domestic PV-battery system in question interacts. The linear interpolation to find results in years between 2017, 2030 and 2050 was described.

Existing LCAs of coal, CCGT, biomass, CCS and nuclear power were then analysed to find central estimates and uncertainty values of the ReCiPe midpoint environmental impact intensities (per kWh of electricity generated) for each of them.

Using the adapted Hawkes' method and GDM, the marginal generator response $MGR_j(t)$ could be found, this being the power response of each generator type j to each MW increase in the national demand $D(t)$. The marginal emissions factor in each impact category i is then the weighted sum of $MGR_j(t)$, weighted by each generator type's impact intensity $c_{j,i}$:

$$MEF_i(t) = \sum_j c_{j,i} \cdot \lambda(t) \cdot MGR_j(t) \qquad \text{(kg/kWh)} \tag{3.1}$$

where $\lambda(t)$ is a factor taking account of transmission and distribution losses at each timestep. It increases with current due to ohmic heating, approximated by a dependence on the square of the national demand $D(t)$. It is given by:

$$\lambda(t) = 100\% + m_1 + m_2[D_{17}(t)]^2 \tag{3.7}$$

where $m_1 = 1.75$ % and $m_2 = 6.5 \times 10^{-11}$ MW^{-2}.

With $MEF_i(t)$ thus defined, the operation of the domestic PV-battery system in question is simulated for each year within the temporal boundary. Electricity imported to the household from the grid $P_g^-(t)$, and exported to the grid $P_g^+(t)$, are used to calculate the environmental net debit $C_{g,i}$ in category i, of the system interacting with the grid:

$$C_{g,i} = \sum_t \left(MEF_i(t) \cdot [P_g^-(t) - P_g^+(t)] \right) \Delta t \tag{3.5}$$

For each year y within the temporal boundary, the net debits $C_{g,i,y}$ are summed across the system lifetime and added to embodied impacts of PV, battery, BoS and their replacements. The impacts per kWh are then found by dividing this quantity by the total electricity consumed during the N years of the system lifetime:

$$c_i = \frac{C_{PV,i} + C_{B,i} + C_{BoS,i} + \sum_y^N \left(u_{B,y} \cdot C_{B,i,y} + u_{BoS,y} \cdot C_{BoS,i} + C_{g,i,y} \right)}{N \cdot \sum_t P_d(t) \Delta t} \tag{3.6}$$

The uncertainty in the total life-cycle impact c_i in each impact category i, is found by the Monte Carlo method: Gaussian distributions are defined for each generator type and system component, using the central estimates and uncertainty estimates as respectively the mean and standard deviation. The calculation of c_i is repeated for 1024 iterations, in which the impact intensities are all varied simultaneously, independently, and randomly within their distributions. Thus the uncertainty in impact intensities of power generation and system component manufacture is propagated through to uncertainty in total life-cycle impact c_i.

So far the battery operation has only been discussed at a higher level; the next chapter describes how the battery itself is modelled within the operational simulation, including its degradation with repeated charge/discharge cycling. The pricing and environmental impacts of re-purposing a used EV battery for second-life are also discussed next.

Chapter 4

The Battery

"I am subject to aging, have not gone beyond aging.
I am subject to illness, have not gone beyond illness.
I am subject to death, have not gone beyond death."
- The Buddha, *Upajjhatthana Sutta*

The Greedy algorithm and Emissions Arbitrage Algorithm were introduced in Chapter 2. However, details of how the charge/discharge power setpoints set by these algorithms are used to update the current, voltage and state of charge of the battery, were deferred until this chapter. Likewise, the costs of PV, battery and balance of system were quantified and the accounting of replacement costs were described, with details of how the replacement schedule is calculated, deferred to this chapter.

Environmental impacts, defined in Chapter 1, were quantified for a new Li-ion domestic battery in Chapter 2; here, costs (both financial and environmental) are estimated for a second-life battery too. As discussed in Chapter 1, a second-life battery is an EV battery that has degraded beyond usefulness for transport applications (usually taken as when energy capacity has degraded to 80 % of its value when new), and been repurposed for a stationary application. The literature on this topic is largely positive about the economic and environmental advantages of second-life batteries. However, as some of the assumptions used to reach such conclusions did not seem valid, they are re-examined in this chapter.

A new method for quantifying the time evolution of second-life battery price was developed by the author (Sun et al., 2018b). It was published in *Journal of Energy Storage*, and an abridged and updated version of it forms the basis of Section 4.3.

4.1 Battery Modelling

The battery model used in this study was required to provide an accurate representation of both the short-term operation and long-term degradation, as these impact on the grid export/import time series $P_g^{+/-}(t)$ which ultimately affect the accounting of financial and environmental costs and benefits for the system. The degradation also affects when the battery reaches the end of its life, and therefore its replacement schedule and costs.

As well as providing accurate results, the model must run fast enough to obtain results within the timeframe of this study. In practice, this meant including the minimum of features necessary to represent the functioning of the battery. What constitutes the minimum necessary is discussed below based on evidence in the existing literature. Before continuing, the basic structure of a lithium-ion battery must be understood. Those familiar with both battery chemistry and battery systems may skip to Section 4.1.2.

4.1.1 Battery chemistry and battery systems background

A battery cell comprises two electrodes (positive and negative) separated by an ion-conducting electrolyte and insulating separator. The electrodes of a Li-ion cell are solid structures capable of intercalating lithium ions (Li^+): graphite for the negative electrode (with advances being made in silicon and lithium titanate as alternative materials), and a metal oxide for the positive electrode, common ones being iron phosphate (in LFP, or $LiFePO_4$, batteries), cobalt oxide (LCO, or $LiCoO_2$), nickel-manganese-cobalt oxide (NMC), and nickel-cobalt-aluminium oxide (NCA). The separator is typically a polymer and the electrolyte an organic solvent. The composition of each component is tuned to achieve multiple goals such as longer lifetime, higher power capability, functionality at extreme temperatures (Cherry, 2016).

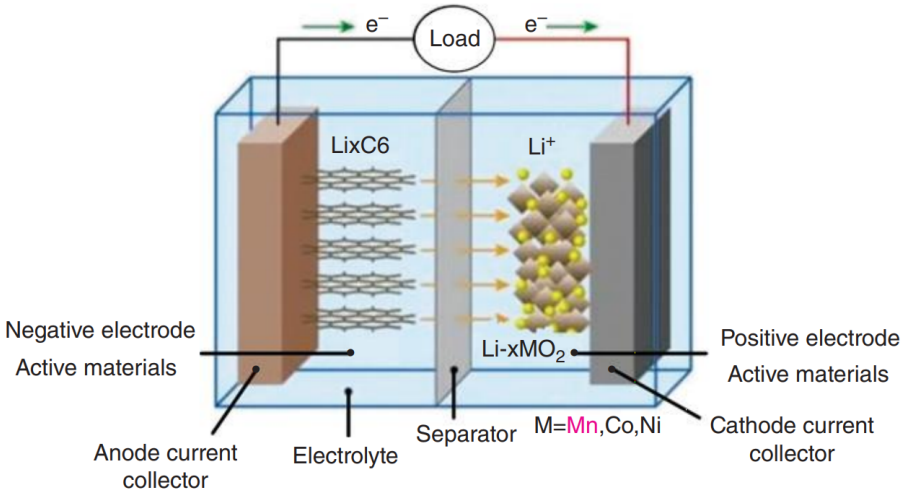

FIGURE 4.1: Schematic of a Li-ion battery taken with permission from Jiang and Zhang (2015), showing negative and positive electrode active materials deposited on current collectors, with a separator in between, flooded with electrolyte. Battery discharging is shown, with electrons flowing from the negative electrode through the load of the external circuit, to the positive electrode. (By convention, electron flow is in the opposite direction to current.)

When discharging, a current flows out of the cell into the external circuit, supplying higher-energy electrons to the load from the negative electrode and recovering lower-energy electrons at the positive electrode. Electrons entering the positive electrode neutralise Li^+ transported through the electrolyte from the negative electrode, intercalating lithium into the positive electrode structure (using LCO as an example here):

$$CoO_2 + Li^+ + e^- \rightleftharpoons LiCoO_2$$

At the negative electrode, lithium is de-intercalated, giving up electrons to the external circuit (using graphite as an example):

$$LiC_6 \rightleftharpoons C_6 + Li^+ + e^-$$

The reverse of these reduction-oxidation (redox) reactions occur when the cell charges. Thus the current flows from the external circuit into the cell, transferring electrical energy to the cell.

The electrode materials take the form of microscopic grains cemented together with binder (usually polyvinylidene difluoride, PVDF, or similar) in a porous structure, to a current collector such as copper foil. Experiments are ongoing to improve upon this structure, increasing the surface area and efficiency of lithium intercalation, for example by forming the electrode materials as nanoparticles or tubes (Wang et al., 2010; Wu et al., 2012). The layers (current collector, negative electrode, separator soaked in electrolyte, positive electrode, current collector) may be rolled up and encased in a cylindrical package, or stacked together to form a pouch cell, or with even more layers in a rigid casing, a prismatic cell (Baczyńska et al., 2018).

The voltage of a cell is the ratio of power to current, that is, energy transferred per unit of charge transferred. For a Li-ion cell, voltage is typically 3-4 V, meaning each 1 A of current would transfer power at a rate of 3-4 W. Cells are connected in series to increase the voltage, and strings of cells are connected in parallel to increase the energy capacity of the battery module (DiOrio et al., 2015). Further increases in voltage and capacity are achieved by connecting modules in series or parallel respectively (Figure 4.9).

A control system, sometimes called a battery management system (BMS), is implemented through power electronics. It sets setpoints for battery power, current, state of charge (SoC) or voltage according to the scheduling algorithm, and, using sensors in a feedback loop, constrains the battery within operational limits of voltage, current and temperature. These limits are for both safety and performance reasons: to prevent short-circuit or thermal runaway which may endanger lives nearby, and to slow down degradation mechanisms which shorten battery lifetime.

Some characteristic features and behaviours of Li-ion batteries are described in detail next. Although they are not all represented in the model developed for this study, it is necessary to understand them in order to decide which must be included and which can be ignored with minimal consequences to accuracy of results. The features are:

- Voltage variation with state of charge and current,
- Capacity dependence on temperature,
- Finite diffusion time effects,
- Degradation of capacity and efficiency.

4.1.1.1 Voltage variation with state of charge and current

Cell terminal voltage (that measured across the terminals of the cell, where it connects to the external circuit) tends to be higher when state of charge (SoC) is higher, with a plateau at intermediate SoC (Jiang and Zhang, 2015). The function of voltage with SoC, also known as the voltage profile, depends on the thermodynamics of the particular battery chemistry. An example is given in Figure 4.2. A consequence is that the battery efficiency is reduced at lower SoC: when voltage is lower, more current is required

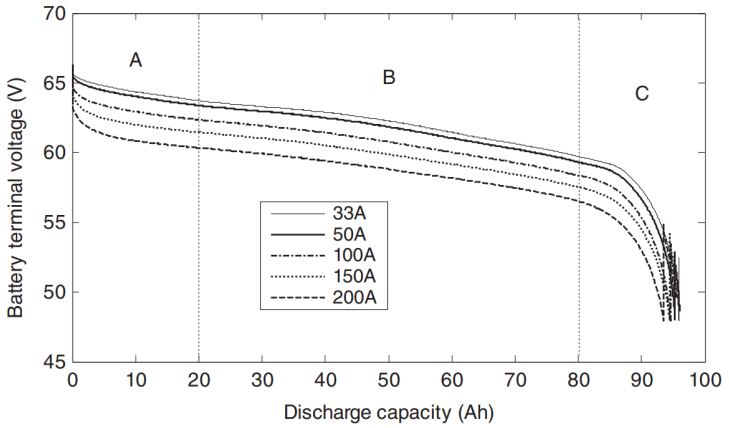

FIGURE 4.2: Li-ion EV battery terminal voltage against discharge, at discharge currents ranging from 33 A - 200 A. 'A', 'B' and 'C' mark respectively the exponential zone, plateau zone, and finishing zone (Jiang and Zhang, 2015).

to transfer a given power, thus increasing the ohmic losses in the resistive elements of the cell (binder, electrolyte, separator).

For practical purposes, a battery manufacturer sets high and low voltage limits which mark when the battery is full and empty respectively. Although nothing would physically stop one discharging a battery beyond the low voltage limit, it becomes so inefficient as to be useless, and there are risks to safety and long-term performance due to both ohmic heating and certain side reactions that become more energetically favourable at low voltage. It is important to remember that an 'empty' battery does not necessarily have a fully lithiated positive electrode and fully de-lithiated negative electrode, and there is no standard for what the voltage limits are, as the nominal (plateau) voltage varies depending on battery chemistry. This means that any discussion in the literature of SoC, depth of discharge (DoD) and full cycles must be considered relative to the voltage limits (and other conditions) defined in each particular study. For example, a hypothetical battery supplier may claim a product can achieve 100 % DoD within the voltage limits they impose; a different supplier may hypothetically impose identical limits on an identical product but claim 80 % DoD relative to a wider voltage range. The latter boasts a larger nominal capacity, but both have the same usable capacity.

The terminal voltage is increased at higher charging current and decreased at higher discharging current. This is because the voltage dropped across the internal resistance increases with current (voltage dropped equals IR), as shown in Figure 4.3. A consequence of ohmic losses by the cell's internal resistance is that efficiency of both charging and discharging are reduced at higher charge/discharge rates (Jiang and Zhang, 2015).

4.1.1.2 Capacity dependence on temperature

Raising the temperature improves the kinetics of the cell redox reactions, generally increasing the available capacity (Figure 4.4). However, this is at the cost of battery lifetime (see below) and capacity does not increase much above room temperature, or the temperature range for which a particular battery chemistry was designed.

A complication is that not only the ambient temperature has an effect: heat is generated within the battery due to its internal resistance, and the distribution of that heat depends on the type (pouch, prism,

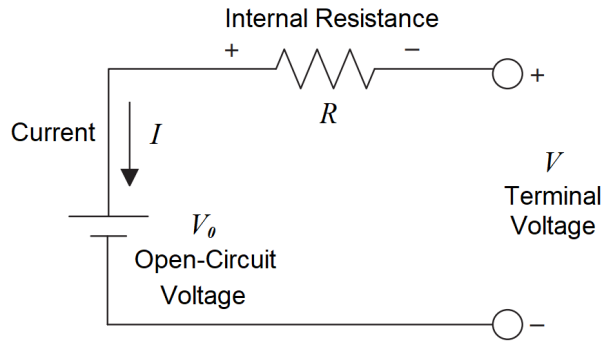

FIGURE 4.3: Rint equivalent circuit model, where the voltage V between the battery terminals is given by the open-circuit voltage (OCV), V_0, plus the voltage drop IR across the internal resistance R, for a given charging current I (Jiang and Zhang, 2015).

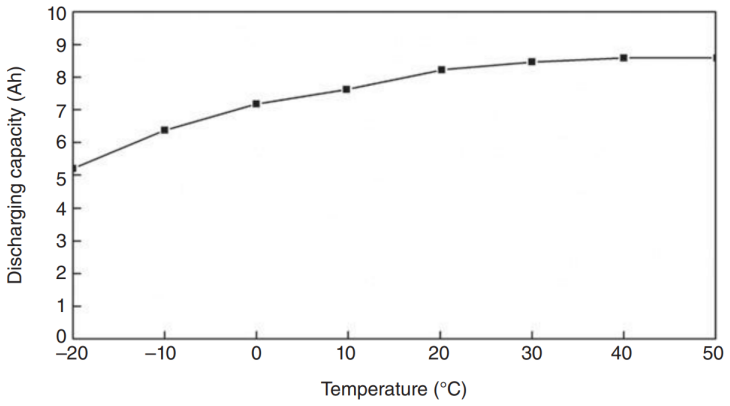

FIGURE 4.4: Discharging capacity of a Li-ion battery designed for power applications, as a function of ambient temperature (Jiang and Zhang, 2015).

cylindrical) and spatial arrangement of the cells, and the cooling mechanism if there is one. Multi-physics models, which numerically solve the heat diffusion equations, are used when such details are needed, such as when diagnosing localised heat-related cell failures or designing battery pack arrangement for optimal heat distribution and cooling efficiency. The long time needed to run multi-physics models is judged not to be worth the increased accuracy, given the nature of this study as an LCA.

The foregoing considerations show why a constant battery efficiency may be an inadequate assumption, despite being used in many of the studies of domestic PV-battery systems reviewed in Chapter 1. Efficiency depends on SoC, charge/discharge rate, and temperature. Furthermore, the BMS may stop the battery charging or discharging when a pre-defined voltage cut-off (high and low, respectively) is reached. Thus charging and discharging may stop before the SoC high/low limits are reached, due to operational conditions modifying the voltage profile. On the other hand, a BMS can be programmed to vary the voltage cut-off limits in response to temperature and other conditions.

One method of accounting for the dependency of voltage on SoC, charge/discharge rate and temperature is to measure the cell voltage across a range of possible conditions, forming a lookup table. Being very time- and resource-intensive, this method is the reserve of industrial companies with the resources to dedicate to it. Alternatively, battery models are available from Matlab Simulink, and National Renewable Energy Laboratory's System Advisor Model (NREL SAM, DiOrio et al. (2015)), which incorporate these empirical data. For example, the Shepherd equation (4.1) gives the dependence of voltage, V, on SoC, $\int I dt$, and charge current, I (negative for discharge). However, the empirical relationships require real

measurements to parameterise them (to find V_0 K, a and B in Equation (4.1)), otherwise they may not accurately represent the battery system in question.

$$V = V_0 - RI - K\left(\frac{Q^+}{Q^+ - \int Idt}\right) + a\exp\left(-B\int Idt\right) \tag{4.1}$$

4.1.1.3 Finite diffusion time effects

Mobile phones, power tools and EVs typically charge at constant-current constant-voltage (CCCV). This means the battery is charged at a constant pre-defined current until a pre-defined voltage level is reached, after which the charger is maintained at a slightly higher voltage, trickle-charging the battery until its voltage equalises with the charger. CCCV is often used in battery testing, for both charge and discharge. This explains a discrepancy between results reported in the literature, where some claim that cell capacity is reduced when charging or discharging at higher rate, and others that there is almost no dependence (Cherry, 2016; Jiang and Zhang, 2015).

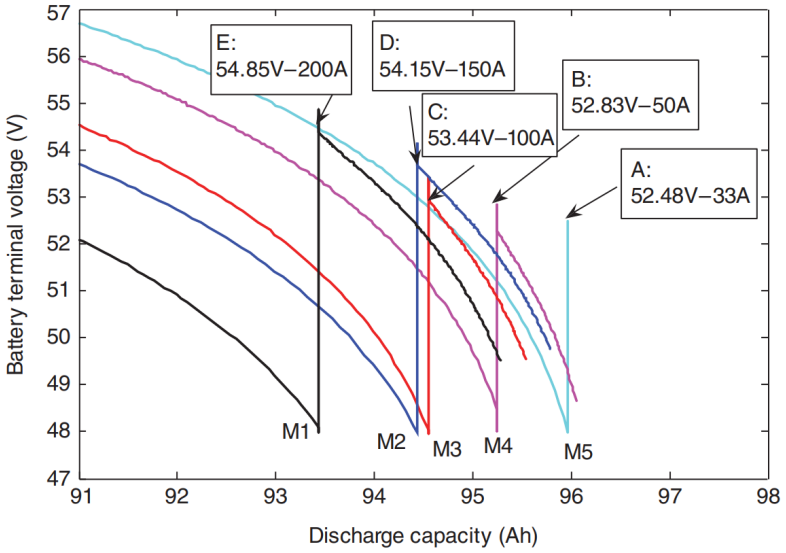

FIGURE 4.5: Voltage profiles of Figure 4.2, zoomed in to show discharge to a 48-V cut-off and subsequent voltage recovery and further discharge. Labels A-E indicate the maximum recovered voltage after relaxation, and the discharge current (Jiang and Zhang, 2015).

In CCCV mode, the cell is fully charged or fully emptied; in a real operation mode, there might not be enough time for this to occur, as it takes a finite time for Li^+ to be transported within the electrolyte and to diffuse into/out of the electrodes. Thus a voltage cut-off may be reached before the cell fully empties (or fully charges), as in Figure 4.5. The effect becomes more pronounced at higher current (the discharge capacity to cut-off is lower) because Li^+ ions are required to intercalate at a greater rate. Some modellers take account of this effect by making the cell internal resistance vary as a function of SoC: a higher resistance at lower SoC (Jiang and Zhang, 2015). There is experimental evidence to support the validity of doing so, as measured by Dubarry et al. (2009) for a commercial LFP cell and shown in Figure 4.6.

The phenomenon of voltage relaxation recovery occurs when a battery discharged at high rate is then left for several minutes without charging or discharging. The voltage rises slightly, or *recovers* while the battery *relaxes*. Afterwards the battery can be discharged further than seemed possible before the voltage

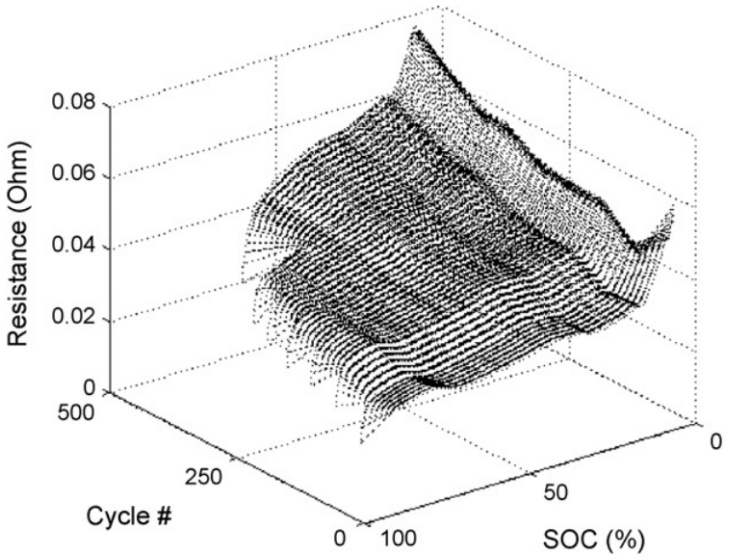

FIGURE 4.6: Internal resistance of a LFP cell as a function of SoC and cycles at rate C/3, showing a higher resistance at low SoC, and resistance increasing with cycling (Dubarry et al., 2009).

relaxation recovery (Jiang and Zhang, 2015). The same occurs in reverse when a battery is charged at high rate: the voltage decreases slightly upon relaxation, and further charging is then possible. Physically, this happens because high-rate discharging transports Li^+ from negative to positive electrode through the electrolyte faster than Li^+ can diffuse into the positive electrode particles' bulk from the surface (and out of the negative electrode particles' bulk to the surface; and the reverse for high-rate charging). It may appear that the battery has fully discharged because there is no more lithium at the negative electrode surface, or no more lithium vacancies at the positive electrode surface. But letting the battery relax allows more lithium to diffuse from the negative electrode bulk to its surface, and to diffuse from the positive electrode surface into the bulk. Discharging can then continue further, the effect being more pronounced at higher discharge rates (Figure 4.5).

The mass transport of Li^+ through the electrolyte and its diffusion and migration within the electrodes can be described with partial differential equations. The simplest case is the single particle model, where each electrode is treated as a collection of identical non-interacting spheres, so that the equations for diffusion into and out of only one sphere need to be solved (Pinson and Bazant, 2013). Equations can be derived and solved numerically for more complex cases, with electrode particles of different sizes distributed across the current collector surfaces. An interesting development is the use of x-ray computed tomography to scan real electrodes, to input them as boundaries to a set of partial differential equations (Babu et al., 2015). This route requires data on, and outputs results for, a specific battery system, contrary to the goal and scope of this study, to analyse a generic system.

A different approach is to model the cell as an equivalent circuit with RC (resistance-capacitance) branches. An example is the Thevenin cell (Figure 4.7). The RC branch buffers the cell's charging/discharging, emulating the effect of finite-time Li^+ diffusion in the electrodes. The R and C values can be found by electro-impedance spectroscopy (EIS) where an oscillating voltage of varying frequency is put across the cell (alternately charging and discharging it by small amounts) and the current through the cell is measured. The impedance Z, as a function of frequency, is a complex number equal to the voltage divided by the current, taking account of the phase difference between them. An equivalent circuit is then fit to the data. A better fit can be achieved by including more components, and so care must be

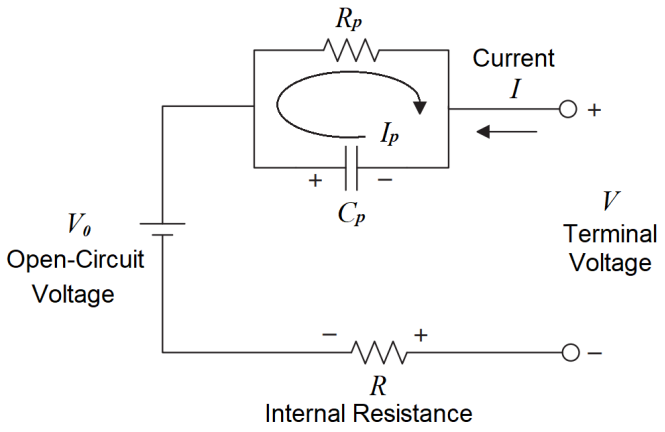

FIGURE 4.7: Thevenin equivalent circuit model, where an RC branch buffers the charging/discharging for a finite time after charge/discharge rate is changed suddenly. Adapted from Jiang and Zhang (2015).

taken not to over-fit but only to use as many components and branches as have a corresponding meaning in physical reality (Jiang and Zhang, 2015). Again, this approach is more suited for study of a specific system rather than a generic one.

4.1.1.4 Degradation of capacity and efficiency

As a battery ages, its capacity and efficiency decrease as a result of several phenomena (Cherry, 2016):

1. Irreversible side reactions at the solid-electrolyte interface (SEI) of the electrodes permanently remove active material (Li^+ and electrode materials) - this decreases the cell capacity and increases internal resistance due to growth of the poorly conducting SEI layer,
2. High temperature accelerates the reaction kinetics of all side reactions, not just the desired redox reactions,
3. Gases produced by side reactions can cause the electrodes to expand, cracking and delaminating pieces from them and thus reducing the capacity,
4. Decomposition of binder and active materials over time can lead to loss of active material from the electrodes and hence loss of capacity,
5. Current collector corrosion, enhanced by low voltage, increases internal resistance and therefore reduces efficiency,
6. Electrolyte breakdown, enhanced by high voltage, also increases internal resistance.

In addition, high voltage and low temperature enhance lithium plating: dendritic growth of lithium out from the electrodes can pierce the separator and short-circuit the battery (Cherry, 2016). This is not so much an aging phenomenon as a sudden failure mechanism.

Pinson and Bazant (2013) used the single particle model to analytically derive relationships for how SEI thickness depends on time, cycling, and temperature, which they compared to measured experimental data in the literature. They found a $\sqrt{t}$ dependence of SEI thickness, and hence also internal resistance (which increases proportionally to SEI thickness) and capacity loss (due to loss of active material to the

SEI-forming reaction). The dependence they found on cycling was linear: in their model, the negative electrode expands when charging, exposing fresh surface area for SEI growth, and contracts on discharging, compacting and dislodging some of the SEI, so that more fresh surface area is exposed each cycle. The temperature dependence they found was a basic Arrhenius relation: the diffusion constant (which relates the flux of a chemical species to the concentration gradient driving its diffusion) is proportional to $\exp(-E_{act}/k_B T)$, where E_{act} is the activation energy of the SEI-forming reaction, k_B is Boltzmann's constant and T is temperature.

The nature of the degradation mechanisms makes it difficult to predict the capacity loss and resistance increase of an individual battery pack: stress can keep building up over time, with cycling, and in response to physical vibration and temperature fluctuations, until another piece of electrode delaminates - but when, from where, and how much, is subject to some degree of randomness. A common approach is to test some cells or packs, cycling them under different conditions of rate, DoD, average SoC, and temperature, and measuring the voltage profile, capacity, and internal resistance at regular intervals. From this, empirical correlations can be found between the battery parameters and the factors driving its degradation. Some of this work is reviewed below in Section 4.2; general trends are that high rate, high DoD, and both high and low SoC and temperature, all exacerbate battery degradation.

Even knowing empirical relationships between driving factors and degradation parameters (capacity loss and resistance increase), the question of how to combine the impacts for a realistic battery use case is a challenging one. Omar et al. (2014) for example measured the capacity loss and resistance increase of cylindrical LFP cells as a function of cycling at different discharge rates (1 C to 15 C) and temperatures (-18 °C to 40 °C), and used their data to parameterise a Matlab Simulink model to predict the battery's cycle life. However, they did not reveal details of their model.

Muenzel et al. (2015) took a technology-agnostic approach, hypothesising that the various driving factors of battery degradation are independent of one another, such that their separate effects on the battery cycle life can be combined multiplicatively to obtain a prediction of the battery cycle life. The quantitative effects of the driving factors on the cycle life must be obtained from datasheets or further lab tests. In a realistic setting, the impacts change across the battery cycles, unlike lab tests where a range of temperatures, charge/discharge rates, etc. are tested but often held constant throughout the cycling within each test. (Sometimes temperature cycling and realistic charge/discharge profiles are applied during testing, but not every single possible combination of changes can be tested with finite time and resources.) To sum the changing impacts across the battery cycles, Muenzel et al. (2015) used rainflow counting, a technique originally developed to model fatigue of a solid component caused by stress-cycling it. Rainflow counting accounts for cycles of different depths (e.g. shallow charge/discharge cycles within a deep cycle), as opposed to counting energy or charge throughput, which do not distinguish between multiple shallow cycles and few full cycles. Rainflow counting is also used in NREL's SAM, which models PV-battery systems incorporating degradation (DiOrio et al., 2015), and work by Fernández et al. (2013), Stroe et al. (2016), Truong et al. (2016), amongst others.

A final general feature of battery degradation worth noting here is the aging knee: while capacity loss and resistance increase tend to decelerate over the battery lifetime, there comes a point known as the aging knee, where they accelerate. The aging knee can occur over a range of remaining capacity values (70-90 %, as discussed below in Section 4.2), and can occur at different times even for identical cells subjected to identical cycling regimes (Figure 4.8, showing capacity degradation of 48 Sanyo/Panasonic UR18650E cylindrical Li-NMC cells, cycled at 25 °C between 3.5 and 3.9 V, 30 minutes each for charge

and discharge, corresponding to 1 Ah per cycle average throughput (Baumhöfer et al., 2014)). As such, the occurrence of the aging knee is difficult to predict. Not every experimental study of battery degradation has the time to cycle a battery until it reaches its aging knee, meaning the phenomenon is still poorly understood. While its causes are uncertain, some believe the aging knee to be associated with gas production from side reactions within the battery, as batteries have been observed to swell at a faster rate after the aging knee (Martinez-Laserna et al., 2018). This can occur to such an extent that the battery can no longer operate within its packaging, and the supplier often recommends replacing the battery at this point, for fear that further use will increase risk of explosion.

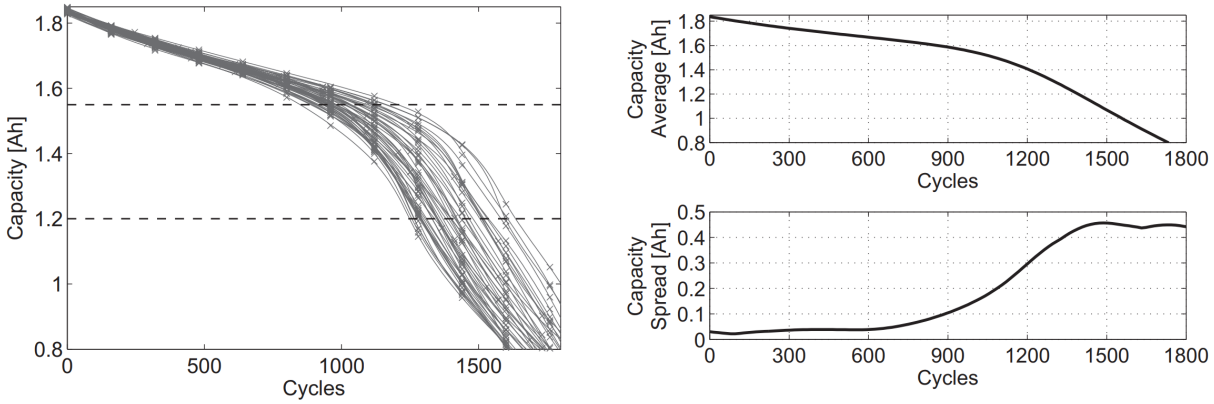

FIGURE 4.8: Left: capacity of 48 identical cells, cycled identically, showing a knee point from 84 % capacity (1000-1200 cycles), and a useful life cut-off at 65 % (1250-1700 cycles). Right: average capacity and capacity spread across the 48 cells, with cycling, showing the spread starts to increase around the same time as the knee point (Baumhöfer et al., 2014).

The USABC (1996) recommendation to replace EV batteries once they have degraded to 80 % of their original capacity ensures that the aging knee is rarely reached while the battery is still within the EV. Domestic battery suppliers tend to be less stringent, taking 70 % or even 60 % as end of life (EoL). This could be because domestic batteries tend to be formulated to delay the aging knee, or because a post-aging-knee battery is not as critical in a domestic context, compared to an EV which requires high energy density and power density, may not have space to accommodate a swelling battery, and could leave driver and passengers stranded if the battery does explode unexpectedly.

Sathre et al. (2015) took a markedly different approach in their budgeting calculation of the CO_2 benefit of using second-life batteries in the electricity grid of California. Rather than factoring in all the different driving factors of battery degradation, they constructed functional forms for the batteries' degrading capacity with energy throughput, including the aging knee. They captured the variety of degradation states by using low, medium and high values for the knee point (as a percentage of original capacity) and degradation rates pre-knee and post-knee. Although Truong et al. (2016) used a rainflow counting procedure rather than energy throughput, they also explored different aging scenarios by applying two degradation regimes: baseline and 'strong' aging.

4.1.2 Battery modelling applications

The variety of approaches to modelling battery operation and degradation can be explained by the variety of goals that these models are required to achieve. Some try to predict the remaining lifetime of a battery asset (Muenzel et al., 2015; Omar et al., 2014; Stroe et al., 2016) so that its owner can plan and

budget for its replacement to a tighter schedule; some output to a 'charge remaining' gauge on an EV for example (known as SoC estimation (Nejad et al., 2016)), so the driver can better plan journeys with recharging stops; some seek to better understand the fundamental physical chemistry of the degradation mechanisms themselves (Märker et al., 2019).

These uses of battery models, especially the latter two, require accuracy even in the short-term. For calculating lifetime costs and benefits of a system, this is not so crucial, as long as short-term errors do not accumulate to an extent that they unduly impact the total lifetime results. It is likely for this reason that most of the techno-economic analyses of domestic PV-battery systems reviewed in Chapter 1 use nothing more complex than a 'storage tank' model, where energy is injected and extracted at constant efficiency within the fixed capacity limits of the 'tank'.

An exception is McKenna et al. (2013), who took efficiency of charging and discharging a PbA battery as the product of voltage efficiency (with losses caused by the fact that charge is injected at higher voltage than it is extracted when discharging) and coulombic efficiency (more charge must be injected than it is possible to remove upon discharging). They parameterised their model with experimental measurements. Note that coulombic efficiency tends to be close to 100 % in Li-ion batteries, whereas they measured it to drop below 60 % for discharge rates as low as 0.1 C in their PbA batteries. More complex models of Li-ion batteries include that of Zhang et al. (2017), who modelled a PV-battery system for a block of flats in Sweden (50-200 kW_p, up to 800 kWh, much larger than considered in this thesis), and NREL SAM (DiOrio et al., 2015) which was designed as a tool to help owners and investors in PV-battery systems calculate the potential financial returns. Both use the Shepherd equation (4.1) to model the battery's voltage profile. SAM additionally models the impact of temperature (ambient and self-generated by ohmic heating) on operational capacity, and reduces the battery capacity with cycling. Zhang et al. (2017) used rainflow counting of the battery cycles to determine when it would need to be replaced, but did not explicitly alter the performance of the modelled battery as it ages.

Of the techno-economic analyses of domestic PV-battery systems reviewed in Chapter 1, only Naumann et al. (2015) and Truong et al. (2016) included the effects of battery degradation on performance, and even then only the effects of cycling on capacity loss, not on internal resistance increase. But as Uddin et al. (2017) showed with their measurements of a commercial home battery product operating coupled with rooftop PV, capacity had already decreased by around 20 % and resistance had almost doubled within 5 years. These are not negligible effects.

In the case of second-life batteries, the effects of degradation are even more crucial to model, as demonstrated by a series of papers on the use of second-life batteries to provide peaking power to the electricity grid in Ontario, Canada (Ahmadi et al., 2014a,b, 2017). Although this is a different application to the one studied in this thesis, there is no reason to doubt the applicability of the lessons that can be learned from it. When Ahmadi et al. (2017) included the effects of a 20 % fade (exponential and then linear) in energy efficiency during the EV lifetime and a further 15 % fade during the battery's second life, the CC (Climate Change) impact increased by 47 % and 67 % in the first and second lives respectively, and FD (Fossil Depletion) increased by 17 % and 25 %, compared to when they neglected the effects of efficiency fade.

These results raise the question of whether it was valid for Naumann et al. (2015) and Truong et al. (2016) to ignore the increase of internal resistance, which is what leads to efficiency fade. It is a particular concern for second-life batteries because if the efficiency is so low, and the degradation so fast that they must be replaced often, could these effects outweigh the environmental benefits of avoiding the manufacture

of new batteries? For this reason it is imperative to include the effects of capacity loss and resistance increase in a plausible if not realistic manner. Meaning that the results need not be correct at every single timestep throughout the system lifetime, nor for a specific battery product (and even a single product can be subject to sizeable variation, as Figure 4.8 shows), but that they are correct enough to indicate what aspects of the generic system need further work to improve the financial and environmental sustainability, in accordance with the research question.

The possibility of using NREL SAM was considered, as it models the operation and degradation of a PV-battery system to beyond an appropriate degree of plausibility, as discussed above. However, it is too restrictive in terms of the operating algorithm (no straightforward way could be found of programming the EAA into it), and it requires so many input parameters for the Shepherd equation of voltage profile and for the thermal and degradation models, that the system becomes too specific for the goal and scope of this thesis. The same issue arises with using or adapting the Matlab Simulink battery module.

An approach more in keeping with the goal and scope is to use the Rint model (Figure 4.3), which represents the battery as a constant voltage source with internal resistance, combined with the approach of Sathre et al. (2015) where a range of functional forms are used to encompass the range of probable degradation pathways, for both capacity and resistance. This is described in detail in the next section. Advantages of this approach are that few parameters are needed (nominal voltage, internal resistance, and range for knee point and degradation rates pre- and post-knee), efficiency variation with charge/discharge rate is represented in a computationally fast way, and the effect of increasing internal resistance is made manifest in the less efficient performance of the battery throughout its lifetime. A limitation is that using essentially a flat voltage profile, as opposed to the Shepherd equation or other more realistic profile, means the effect of SoC on efficiency is neglected (as described in Section 4.1.1.1). The effects of finite diffusion time are also neglected, but they are only captured by the most detailed equivalent circuit or physico-chemical models, and not necessary except for accurate real-time SoC estimation or fundamental studies into degradation mechanisms. The approach chosen is still an improvement on the many studies that only use a storage tank model while ignoring degradation.

4.2 The Battery Model

In light of the literature reviewed above, the battery model developed for use in this study is described in this section. It is a Rint equivalent circuit model, with degradation modelled by decreasing the charge capacity and increasing the internal resistance with cycling. The `step_batt` function is described, which updates the charge stored in the battery at each timestep according to the power setpoint requested (these are set by the operating algorithm, see Chapter 2). The decreasing capacity and increasing resistance which result from cycling the battery, are updated after each simulated year and fed through to the `step_batt` function. Thus operation drives degradation and degradation affects operation. Many information sources were drawn upon to parameterise the model in a plausible but generic way.

4.2.1 Voltage Source with Internal Resistance

The Rint model depicted in Figure 4.3 forms the basis of the battery operational model in this thesis. It assumes a constant voltage source in series with an internal resistance. Reasonable values for the nominal voltage V_0 and initial internal resistance R are needed. From V_0, the maximum charge Q^+

can be calculated as E_B/V_0, where the battery's usable capacity E_B is decided by a sizing procedure described in the next chapter. For simplicity, the minimum charge Q^- is taken as zero (i.e. 100 % DoD) and charging/discharging is stopped when $Q^{+/-}$ is reached, as an approximation to stopping when voltage end-of-charge/discharge limits are reached.

For the whole battery pack, V_0 was chosen as 48 V as this is the typical voltage of battery packs for historic reasons. It must be voltage-stepped up by the battery DC-DC converter (Figure 2.3 in Chapter 2), in order to feed into or charge up from the grid, whose mains voltage is typically 240 V in GB. Internal resistance R is rarely given in datasheets for complete home battery products - the round-trip efficiency is more commonly reported, but it includes losses in the power electronics. The approach taken by NREL SAM (DiOrio et al., 2015) is to model the pack as a parallel-series string of individual cells (Figure 4.9). The total resistance R is then:

$$R = \left(n_{\parallel} \cdot (n_{\perp} R')^{-1}\right)^{-1} \tag{4.2}$$

where R' is the resistance of each cell, $n_{\perp}$ the number of cells in series, and $n_{\parallel}$ the number of strings in parallel.

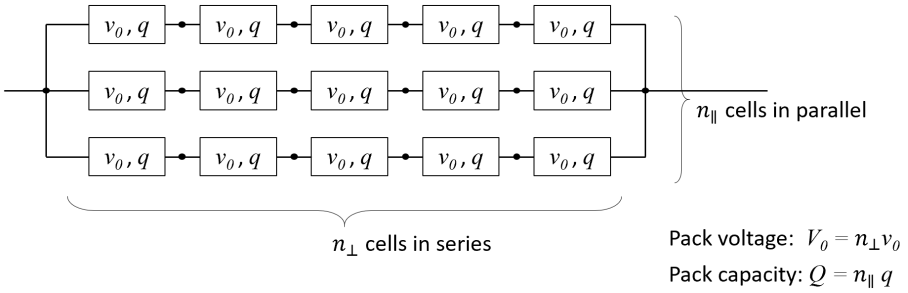

FIGURE 4.9: Series-parallel connection of cells. This example shows $n_{\perp} = 5$ cells in series in each string, and $n_{\parallel} = 3$ strings in parallel, giving a nominal pack voltage of $V_0 = 5v_0$, a pack capacity of $Q = 3q$, and energy capacity $E_B = 15qv_0$ (DiOrio et al., 2015).

$n_{\perp}$ is chosen so as to bring the pack voltage up to 48 V as required:

$$V_0 = 48 \text{ V} = n_{\perp} v_0 \tag{4.3}$$

where v_0 is the nominal voltage of a single cell, and $n_{\parallel}$ is chosen to bring the pack capacity up to E_B:

$$E_B = n_{\parallel} q V_0 \tag{4.4}$$

where q is the charge capacity of a single cell. From this, $Q^+ = n_{\parallel} q$. The problem of parameterising the battery pack is reduced to one of finding v_0, q and R' for a cell that can plausibly be connected together as in Figure 4.9 to give the voltage and capacity required. Some examples of rechargeable Li-ion cells were surveyed, from papers by Baczyńska et al. (2018) and Hesse et al. (2017), and datasheets found online using a search engine (EEMB, 2010; Kim, 2017; LG Chem, 2018b; PylonTech, 2016). These are tabulated in Table 4.2; the code used to refer to them is given in the key below the table. This is not an exhaustive survey, but indicates the voltage, resistance and other parameters typical of Li-ion cells used in domestic and EV applications.

	NMC1	**NMC2**	**NMC3**	**NCA1**	**LFP1**	**NMC4**	**NMC5**	**NMC6**	**LFP2**
Cell chemistry	NMC	NMC	NMC	NCA	LFP	NMC?	NMC?	NMC?	LFP?
Shape	Pouch	Pouch	Prismatic	Cylinder	Cylinder	Cylinder	Cylinder	Pouch	Pouch
Voltage (V)	3.6	3.65	3.7	3.6	3.2	3.7	3.63	3.6	3.2
Capacity (Ah)	37	60	94	3.2	3.0	2.5	3.33[(a)]	64.6	25
Resistance (ohm)	0.006	0.013	-	-	-	≤0.07	0.036 ± 0.006	0.00135-0.0116[(b)]	≤ 0.0025
Charge retention[(c)]	-	-	-	-	-	80 %	90 %	98 %	-
Cycle life[(d)]	-	-	5000	320	6000	300	1000	1000	6000

TABLE 4.2: A web survey by the author of some rechargeable Li-ion cells technical specifications. The key to the codes used to refer to the different cells is given below. Charge retention data are used to determine self-discharge rate, and cycle life to parameterise the degradation rate.

Key to Li-ion cell reference codes in Table 4.2:

- NMC1, NMC2: the two cells (models IXP74/212/269PA and LG60AH-3.6 V/60 Ah respectively) designed for transport applications, tested by Baczyńska et al. (2018),
- NMC3, NCA1, LFP1: the three cells (Samsung SDI94Ah, Panasonic NCR18650B, Murata US26650FTC1 respectively) designed for home battery applications, reviewed by Hesse et al. (2017),
- NMC4: EEMB model LIR18650 2600mAh (EEMB, 2010) - the cell chemistry is not specified in this datasheet but is presumed to be NMC based on similarity to cells in the other data sources,
- NMC5: LG Chem model INR18650 M36T 12.50Wh (Kim, 2017) - as above, presumed NMC,
- NMC6: LG Chem model E63 (LG Chem, 2018b) - as above, presumed NMC,
- LFP2: PylonTech model PF25N, designed for transport applications (PylonTech, 2016).

(a) Estimate given by 12.10 Wh, divided by 3.63 V (Kim, 2017).

(b) Resistance was given at different SoC levels, and for charge and discharge - the lowest resistance is for discharge at 50 % SoC, the highest for discharge at 0 % SoC (LG Chem, 2018b).

(c) The capacity left in the cell after storing it at room temperature (25 °C) for 28 days in the case of NMC4, 30 days for NMC5, and 1 month at 45 °C for NMC6. This gives information on the cell's self-discharge rate.

(d) The number of cycles to degrade the cell capacity to 80 % of its original value. Hesse et al. (2017) did not specify the cycling regimes used, but for the others, all were cycled at 100 % DoD, at different rates and between different limits: 1.3 A charge and discharge for NMC4; 0.3 C charge, 10 minutes rest, 0.5 C discharge, 20 minutes rest, for NMC5; 21.6 A charge and 32.5 A discharge with 60 minutes rest after each for NMC6; 0.8 C charge and discharge for LFP2.

LFP batteries are more commonly used in home batteries due to their design prioritising long life and safety (Naked Solar, 2019) over energy density, which is more important in transport applications. However, the embodied environmental impact data reviewed in Chapter 2 were for NMC batteries, as not enough sources could be found for LFP embodied impact data. It should not be a problem to model the battery as more NMC-like, as it is still fairly common in domestic battery products: the Samsung SDI94Ah reviewed by Hesse et al. (2017), the Tesla (2018) Powerwall, and LG Chem (2018a) RESU are known to use NMC cells.

From the above, it was decided to take $v_0 = 3.6$ V, $R' = 0.05$ ohm, $q = 3$ Ah. The requirement that $n_\perp$ and $n_\parallel$ be whole numbers means that V_0 doesn't generally equal exactly 48 V, nor does $n_\parallel q V_0$ equal exactly E_B. For the values used here, $n_\perp = 48/3.6 = 13.333... \approx 13$ cells in series, from Equation (4.3), meaning $V_0 = 13 \times 3.6 = 46.82$ V. If $E_B = 8$ kWh for example, this means from Equation (4.4) that $n_\parallel = E_B/(qV_0) = 56.98... \approx 57$ strings in parallel. Thus $Q^+ = n_\parallel q = 57 \times 3 = 171$ Ah. From Equation (4.2), the total internal resistance $R = 0.0114$ ohm.

These values of q and R' are typical of a cylindrical cell, whereas the pouch and prismatic cells reviewed tend to have larger capacity and lower resistance. The capacity can of course be controlled in the design and manufacturing process, for example by using electrodes of larger surface area. If many (specifically 13) large-capacity cells are connected in series to bring V_0 up to 48 V, the total energy capacity of a single string could be larger than is typical of a domestic battery module. For the values of v_0, q and R' given above, a single string has energy capacity $qV_0 = 0.140$ kWh. The total capacity E_B can only be integer multiples of this.

As well as the advantage of the Rint model in keeping the system more generic, it also requires less computation to solve at each timestep than, for example, the Shepherd equation which is nonlinear and requires iterative solving, using a lookup table for the voltage profile, or including an RC branch in the equivalent circuit. The equations of the Rint model form the basis of the `step_batt` function introduced in Chapter 2, used in the Greedy Algorithm and EAA (Jiang and Zhang, 2015):

$$V = V_0 + IR \tag{4.5}$$

$$P_{set} = IV \tag{4.6}$$

Given a charge setpoint P_{set} (it is negative for discharge), Equations (4.5) and (4.6) are solved simultaneously to obtain the terminal voltage, V, and the current inflow, I (negative for discharge):

$$V = \frac{1}{2}V_0 + \sqrt{V_0^2 + 4P_{set}R} \tag{4.7}$$

$$I = P_{set}/V \tag{4.8}$$

Graphically, this is equivalent to finding the intersection between the straight line $V = V_0 + IR$, and the contour $P_{set} = IV$, in Figure 4.10. The Shepherd equation does not have an analytical solution like this.

Note that at very high discharge rate, the contour might never intersect the straight line. In fact, as the battery degrades and its resistance increases, the straight line becomes steeper and this further limits the maximum discharge power, a phenomenon known as power fade. A discharge power setpoint higher than the battery can achieve, manifests as a complex-valued V in Equation (4.7). In such a case only the real part, $\frac{1}{2}V_0$, would be used further in the `step_batt` function, Figure 4.11.

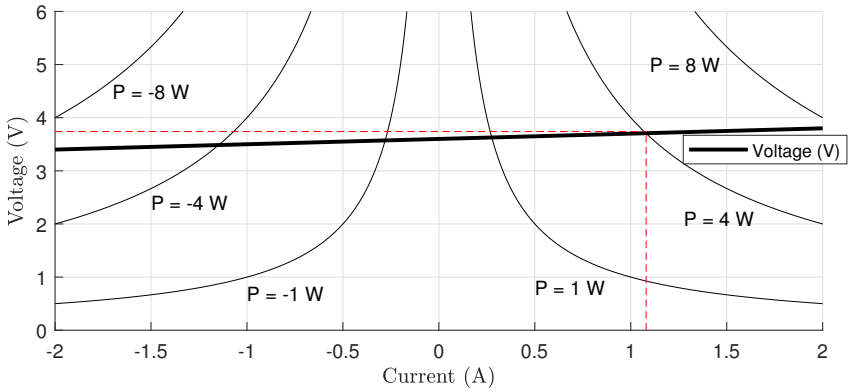

FIGURE 4.10: Voltage-current characteristic of a cell with nominal voltage $V_0 = 3.6$ V, internal resistance $R = 0.1$ ohm (for illustrative purposes). Shown with constant-power contours ($P > 0$: charging; $P < 0$: discharging). For example, charging at $P = 4$ W requires injecting $I = 1.08$ A current, and results in the cell terminal voltage being $V = 3.74$ V.

From Table 4.2 it can be seen that at most 20 % of the charge on a cell is lost over 28 days as a result of self-discharge. This happens when no cycling occurs but as a result of the separator not being a perfect insulator of electrons, so some charge leaks through it all the time. 20 % in 28 days equals a self-discharge rate of C/3360, that is, the cell would fully discharge in 3360 hours, which is 5 times 28 days. For a battery even as large as 20 kWh, this equates to 6 W, and is likely less given that this is for the worst charge retention in Table 4.2.

The control system of the BoS (balance of system) draws a small amount of power, roughly 5 W according to personal communication with Moixa (2016). It is assumed in this thesis that an auxiliary drain P_{drain} occurs on the battery all the time, encompassing both the BoS drain and battery self-discharge, at a rate of 5 W plus C/6000 (that is, it depends on E_B). P_{drain} reduces the SoC of the battery at each timestep, or if it is empty, P_{drain} is drawn from the PV generation, or if that is insufficient, by importing from the grid. Figure 4.11 shows the logical flow of the `step_batt` function, calculating V and I given a power setpoint P_{set}, while respecting the battery's charge limits, and adjusting for P_{drain}.

The power adjustment P_{adj} is subtracted from the PV generation, leading to less power P^{+}_{thru} flowing through the inverter (see Chapter 2), or more power P^{-}_{thru} flowing back through the inverter, imported from the grid. Over the course of a simulated year, voltage and current time series $V(t)$ and $I(t)$ are obtained from running `step_batt` at every timestep. The power into the battery is given by multiplying them element-wise (when the result is negative, power is flowing out of the battery).

Simulating constant-current test cycles for the hypothetical 48 V, 8 kWh battery described above, the round-trip efficiency is 91.6 % at rate 1 C (fully charge in 1 hour, fully discharge in 1 hour) and 97.2 % at C/4 (fully charge and discharge in 4 hours each). Including the DC-DC converter described in Chapter 2, the system round-trip efficiency is 84 % at 1 C and 90 % at C/4, which is typical for products on the market today.

The number of cycles n is taken to be:

$$n = \frac{\sum_t |I(t) \cdot V(t)| \Delta t}{2E_B}. \tag{4.9}$$

That is, the two-way energy throughput divided by twice the battery's energy capacity (once for charge, once for discharge), following the example of Sathre et al. (2015). The number of cycles is used in the

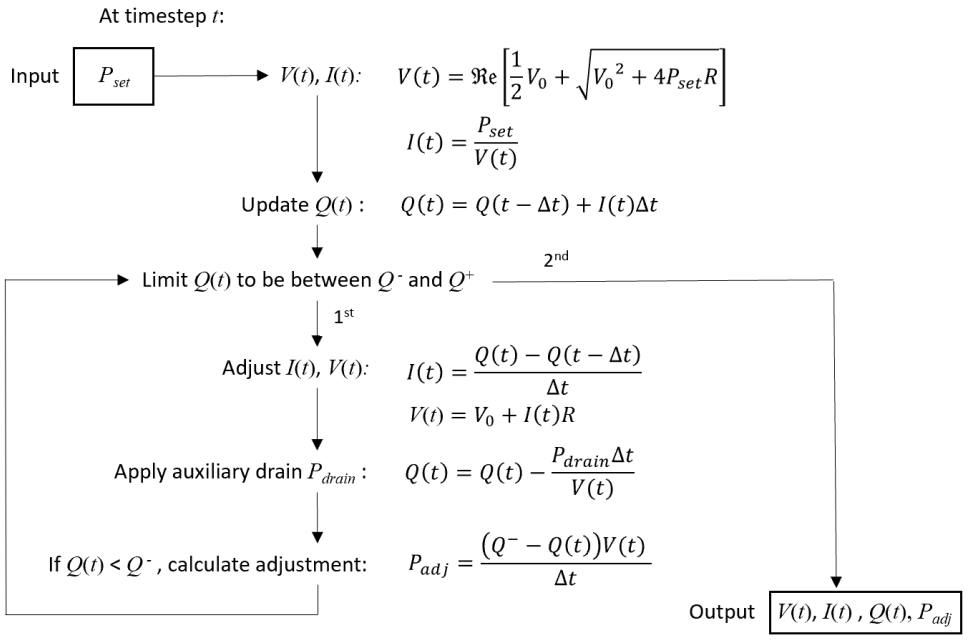

FIGURE 4.11: Logical flow of the `step_batt` function, which takes the setpoint power P_{set} as input ($P_{set} < 0$ means discharge required), and calculates the resulting battery terminal voltage $V(t)$, current inflow $I(t)$, and charge stored $Q(t)$.

next section to calculate degradation in the form of capacity loss and resistance increase.

4.2.2 Application of Sathre's Method

The method Sathre et al. (2015) used in their calculation of the CO_2 benefit of second-life batteries in the Californian grid involved representing the capacity degradation as a function of battery cycles, n. The normalised capacity, referred to here as $Q_t(n)$, experiences a (close to) square-root decrease to the knee point, Q_{knee}, followed by a power-law decrease capturing the shape of the aging knee.

Sathre et al. (2015) did not consider the effect of cycling on resistance increase, but it is a logical extension to form similarly a normalised resistance function $R_t(n)$. For the study in this thesis, the cycles n are counted up according to Equation (4.9) and accumulated after every simulated year, and the battery's internal resistance R and charge limits $Q^{+/-}$ are updated to their original values multiplied by $R_t(n)$ and $Q_t(n)$ respectively. These updated values are fed through for use in the `step_batt` function for the following simulated year (though lacking specific quantitative data, V_0 does not change). Thus the degradation of the battery influences its performance.

Apart from the study by Wang et al. (2011), the parameters used for the function $Q_t(n)$ were only estimated by Sathre et al. (2015) to cover a realistic expected range, without reference to other sources. For this thesis, the following sources were consulted:

- Wang et al. (2011), who found for a LFP cell that at low charge/discharge rate (C/2, typical of domestic applications) capacity degradation is dominated by cycling (specifically, charge throughput) and temperature, with negligible impact from DoD. The aging knee tended to occur when capacity had degraded to 70-80 % of its original value, and until then, capacity loss was directly proportional to charge throughput raised to the power of 0.55,

- Omar et al. (2014), who took capacity and resistance measurements of LFP cells with cycling at different rates, temperatures and DoD. The aging knee appeared to occur around 90 % capacity, while resistance never increased beyond 1.56 times the original value, although no measurements were taken below 80 % capacity. For the 1 C discharge rate example, the 90 % and 80 % capacity points occurred around 2000 and 2900 cycles respectively,
- Ecker et al. (2014), who found for a NMC cell that the aging knee tended to occur around 80 % capacity, over which time the resistance increased to 1.5-2 times the original value. This took roughly 500 cycles at 100 % DoD, and a further 200 or so cycles to 50 % capacity, 3 times the resistance, when the cells failed,
- Baumhöfer et al. (2014), who measured 48 identical NMC cells under an identical cycling regime, finding the aging knee occurred at 84 % capacity after 1000-1200 cycles, with a roughly fourfold steeper decline in capacity subsequently,
- Uddin et al. (2017), who measured a NCA cell and an operational domestic battery made of such cells, finding resistance increased almost in step with capacity degradation, reaching 1.9 times the original value when capacity had degraded to 80 % of its original value,
- Ning et al. (2003), who measured capacity loss with cycling for a LCO cell at different discharge rates. They found capacity loss depends on rate (16.9 % lost over 300 cycles at 3 C compared to 9.5 % lost at 1 C over the same number of cycles). However, these rates are higher than the BoS would typically allow in a domestic battery product (Naked Solar, 2019).

From these, it was decided to take the following form as the capacity degradation with cycling, of a new stationary battery:

$$Q_t(n) = \begin{cases} 1 - D_1 \cdot n^{0.55} & \text{for } Q_t(n) < Q_{knee} \\ Q_{knee} - D_3 \cdot (1.006^{D_2(n-n_{knee})} - 1) & \text{otherwise} \end{cases} \tag{4.10}$$

based on the equations developed by Sathre et al. (2015), but where $Q_{knee} = 0.75$, n_{knee} is the number of cycles at the knee point (i.e. $Q_t(n_{knee}) = Q_{knee}$), $D_1 = 0.0025$, $D_2 = 0.15$. D_3 is determined by the constraint that before and after the knee point, both the function $Q_t(n)$ and its gradient must be continuous. This leads to:

$$D_3 = 0.55 \cdot D_1 \left(\frac{1 - Q_{knee}}{D_1} \right)^{-0.45/[0.55 D_2 \ln(1.006)]}$$

With these parameters, battery end of life is reached around 6000 cycles, consistent with the warranties of most home battery products listed by Naked Solar (2019). Of the batteries surveyed in Table 4.2, the ones which gave graphs of capacity as a function of cycling show no sign of an aging knee up to 80 % capacity, nor does the product measured by Uddin et al. (2017). However, the aging knee was reached sooner than this according to the measurements by Baumhöfer et al. (2014); Ecker et al. (2014); Omar et al. (2014), suggesting that even if the aging knee is not reached by 80 %, it will occur soon after. This informed the choice of $Q_{knee} = 0.75$.

From the sources listed above, resistance increase can be seen to be subject to much uncertainty. Only an approximation can be hoped for; roughly the correct shape (see Figure 4.12) is achieved by taking:

$$R_t(n) = 4Q_t(n) - 3. \tag{4.11}$$

End of life is taken as when capacity degrades to 60 % of the original value, or after 15 years, whichever comes first. Unlike Naumann et al. (2015) and Truong et al. (2016), this study does not superpose the effects of calendar aging and cyclic aging. This is justified by the following: in the sources listed above, cycling tests necessarily had to happen over time, often several months, so it is not straightforward to separate the effects of cyclic and calendar aging; it only really matters if algorithms resulting in vastly different cycling frequencies are being compared, then degradation might be over-estimated for one where the battery cycles very many times each year, or under-estimated if the battery cycles few times, and that is not the case in this study; a similar approach (applying whichever is the shorter out of a calendar-life or cycle-life cut-off) is used by Bertsch et al. (2017); Mulder et al. (2013); Weniger et al. (2013).

As Neubauer et al. (2015) showed, EV battery degradation is strongly dependent on factors besides cycling, such as local climate and driver aggression. Rather than accounting for all these factors in detail, it better serves the goal of this study to analyse only the best and worst cases likely to enter the second-life battery market. For the best-case second-life battery, Equation (4.10) is used as given; for the worst case, it is used with $Q_{knee} = 0.85$, $D_1 = 0.0035$, $D_2 = 0.2$, and D_3 set so as to keep both $Q_t(n)$ and its gradient continuous. Equations (4.10) and (4.11) for all cases (new, best-case second-life, worst-case second-life) are shown in Figure 4.12.

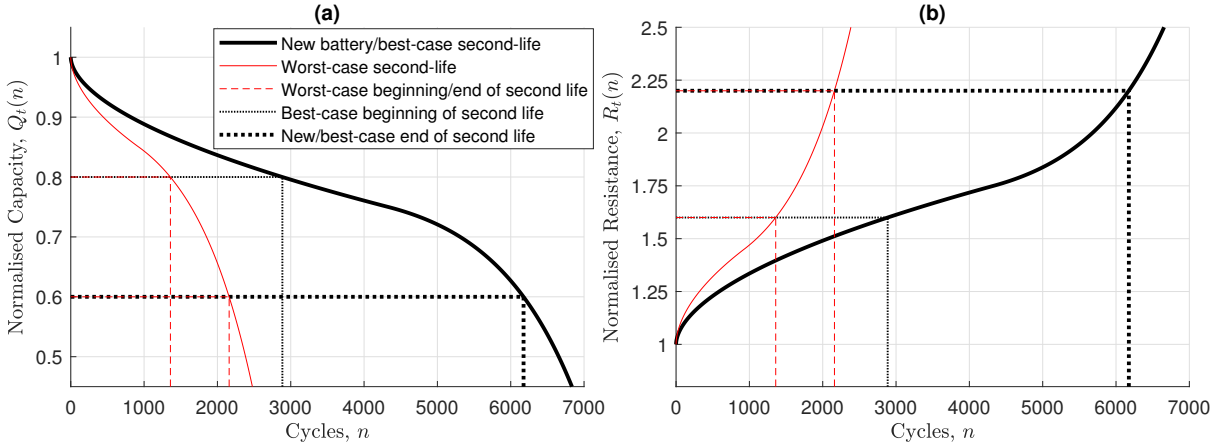

FIGURE 4.12: (a) Capacity loss $Q_t(n)$ and (b) resistance increase $R_t(n)$ as a function of cycling, n, as given by Equations (4.10) and (4.11) respectively, for a new battery and best- and worst-case second-life batteries.

In both best- and worst-case, the second-life battery begins the simulation with 80 % of its original (first-life) capacity and continues degrading from there, until it reaches 60 % of original capacity (75 % of what its capacity was at the beginning of its second life). It is replaced at this point, or after 15 years, whichever comes first. EV usage is generally regarded as a greater strain on the battery than domestic usage (Casals et al., 2017; Martinez-Laserna et al., 2018; Neubauer et al., 2015), given the high charge rate associated with fast-charging and high discharge required for acceleration, whereas domestic batteries are typically limited to C/2 by their BoS. This is why the best-case second-life EV battery is taken as following the same degradation pathway as a new stationary battery, where roughly 3000 cycles can be expected between 80 % and 60 % capacity, in which time resistance increases from 1.6 to 2.2 times its original value (Figure 4.12).

In the worst case, only 1300 cycles have been performed in the EV before capacity has degraded to 80 %, and a further 800 or so are possible in the second life (Figure 4.12). The use of 80 % and 60 % as the first- and second-life capacity cut-off points is conservative compared to 75 % and 50 % used

by Neubauer and Pesaran (2011), and 70 % and 30 % used by Sathre et al. (2015). However, the existing literature on battery degradation suggests their figures may be too optimistic: while some NMC cells tested by Ecker et al. (2014) continued working until their capacity had degraded to 50 %, some experienced sudden failure soon after reaching 80 %; 80 % is the first-life cut-off officially recommended by USABC (1996); most home battery products are warrantied to 70 % remaining capacity, so although some usage can be expected after this, it is unlikely to be much; and as Uddin et al. (2017) pointed out, there are performance issues with continuing to use a degraded battery even if it does not experience sudden failure.

For simplicity, best- and worst-cases for the new battery are not considered. In any case they are unlikely to diverge as much as for an EV battery. In fact, for all households in the dataset, simulated with a new battery, the 15-year cut-off was reached before the 60 % capacity cut-off. Although local climates differ enough even within GB that the effect of extremely cold ambient temperature may accumulate over the battery lifetime and cause significantly different results compared to warmer local climates (Uddin et al., 2017), the effects of regional variation are outside the scope of this thesis.

4.3 Second-Life Batteries Pricing

The cost of new batteries was discussed in Chapter 2. As with new batteries, second-life ones incur a cost initially and every time they are replaced over the system's temporal boundary, $N = 25$ years. This cost is taken to comprise both a fixed portion $c_{B,0} = 1500$ GBP, and a size-dependent portion $c_{B,1}$ GBP/kWh. The fixed portion represents installation costs and fixed overheads for the company supplying the home battery, which are unlikely to be any lower for a second-life battery than a new one. Determining the size-dependent cost of second-life batteries is the subject of this section. Once obtained, it is multiplied by the usable energy capacity of the second-life battery (not its original first-life capacity) and added to $c_{B,0}$, to give the total second-life battery cost.

Because the battery needs to be replaced at least once during the temporal boundary, it is necessary to find not just the cost of a second-life battery today, but an estimate of its likely cost in future. Some existing methods of doing this are reviewed next, followed by a description of the microeconomics-driven method of projecting second-life battery price developed by the author (Sun et al., 2018b). Second-life battery pricing is an active research topic, as it has implications not just for potential buyers and users of second-life batteries, but also potential sellers and companies specialising in repurposing used EV batteries. The results of the author's microeconomics-driven pricing model are discussed in this context.

4.3.1 Existing methods of quantifying second-life battery price

Estimates of the price range of second-life batteries can be obtained by searching for second-hand EV battery packs offered on online auction sites (CEC, 2015). These may be far from indicative of second-life prices, which may be lower due to economies of scale, or indeed higher as labour will be paid whereas an informal seller may not factor in their own labour. Furthermore, auction sites only offer a snapshot price, whereas what is required is the time evolution of the price.

Casals et al. (2014) have estimated the costs of repurposing used EV batteries, that is, preparing them for resale into the second-life market, involving shipping and testing the packs. This gives a lower bound

to the second-life battery price, as they must be sold at higher price than their processing costs if any profit is to be made. Repurposing cost does in fact turn out to be a strong determinant of second-life battery price, as shown later in this section, but Casals et al. (2014) do not demonstrate this. Again, what they offer is a snapshot of costs rather than a time evolution.

Neubauer and Pesaran (2011) have attempted to predict the evolution of second-life battery price by assuming the price of the battery as new is reduced according to its degraded state of health, reduced again by a 'second-hand discount factor', and with the refurbishment cost subtracted. The second-hand discount factor is arbitrary: they analysed scenarios 50 % and 75 %. Even after accounting for state of health and repurposing cost, there is no reason to believe that the second-life price would vary proportionally to the new battery price.

An alternative for potential second-life users is to design the system under a range of different battery cost scenarios, and pick an option passively in response to the market, as done by Kirmas and Madlener (2017); Wolfs (2010). This may be adequate for a one-off investment, but not if batteries must be replaced over the system lifetime, as for the second-life use case in this study.

The new methodology developed by the author (Sun et al., 2018b) uses principles of microeconomics to account for changing supply of and demand for second-life batteries. It factors in the cost of or income available from immediate recycling (without second-life usage), and both niche and mass-market stationary applications. It offers the following improvements over existing methods:

- An estimate of second-life battery price evolution to 2050, rather than a snapshot,
- Account taken of many driving forces in the market: different EV uptake scenarios, new battery costs, repurposing costs, recycling net credit, elasticity of supply, and size of demand.

For example, where Neubauer and Pesaran (2011) assume a fixed second-life market and find it would rapidly be saturated by spent EV batteries, this methodology models a more realistic situation, where a larger supply of second-life batteries would reduce the price and thus expand the market for them.

4.3.2 Microeconomics-driven model setup

The modelled system and its constituent parts are defined here, with a description of the calculation methodology. This is followed by the assumptions used, with some justification of their validity, and then more details of how the microeconomics-driven model was parameterised. The results are presented afterwards.

4.3.2.1 System Definition

System Boundary: In this work, calculations are done on a global basis. Since battery recycling is a global business, with used batteries being transported to plants in only a few countries, and recycled materials being exported worldwide (Casals et al., 2014), it stands to reason that battery repurposing (preparing a used EV battery for the second-life market) would be similarly global.

Sellers of second-life batteries include EV owners but predominantly EV manufacturers, given the trend for battery leasing, where the EV owner does not own the battery outright but pays a monthly fee to rent

it from the manufacturer (Green Car Guide, 2017; Jiao and Evans, 2016). The results presented in this work are independent of who the sellers are. The competing alternative to selling onto the second-life market is to send the battery to recycling straight away.

Buyers of second-life batteries are suppliers of batteries for stationary applications. The competing alternative to buying second-life is to buy new stationary batteries. The supplier may further re-package, market, distribute and install the batteries (new or second-life), with a markup to the end customer. It should be noted that companies specialising in battery repurposing may be created in future (Klör et al., 2015). These companies would act as middlemen between sellers and buyers. This complication is avoided here by attributing the repurposing costs solely to sellers (as if the repurposing companies are subsidiaries of the EV manufacturers, for example).

Calculation Methodology:
The higher the price of second-life batteries, the greater the incentive to sell. The lower the price, the greater the incentive to buy. These tendencies are quantified respectively in the price-supply and price-demand curves, $p_{sup}(E, y)$ and $p_{dem}(E, y)$, which are the prices (GBP/kWh) that sellers would accept and buyers would bid respectively, in year y as a function of quantity bought and sold, E (kWh). The price-supply curve is generally a monotonically increasing function of E, while the price-demand curve decreases monotonically with E (see Figure 4.13). They both change from year to year in response to the changing supply of used EV batteries, developments in battery recycling, etc. Quasi-static equilibrium is assumed, whereby the price-quantity equilibrium is converged upon each year. Equilibrium is the crossing point of the price-supply and price-demand curves: an above-equilibrium price would be lowered by sellers competing to attract more buyers, and a below-equilibrium price would be bid upwards by competing buyers (Harvey, 1994). Price-quantity equilibria are found for every year from 2017 to 2050, giving the time evolution of second-life price, $p_{eqm}(y)$, and total quantity sold, $E_{eqm}(y)$.

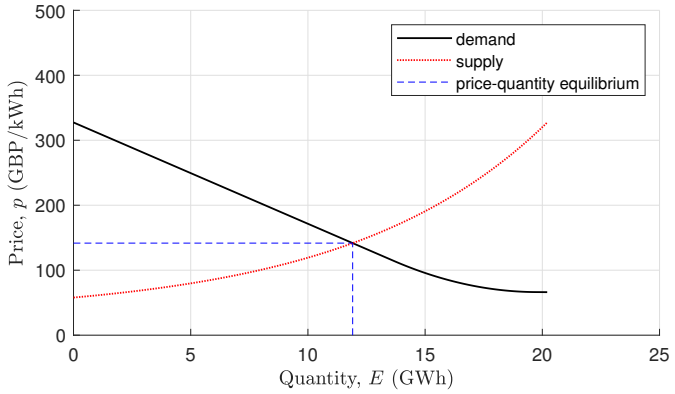

FIGURE 4.13: Example price-supply curve $p_{sup}(E)$ and price-demand curve $p_{dem}(E)$ in year $y = 2020$, as calculated by the procedure described below in Section 4.3.2.3. The curves' intersection is the price-quantity equilibrium for that year, (E_{eqm}, p_{eqm}).

The price-supply curve $p_{sup}(E, y)$ at each year y is constrained thus:

- Price can never exceed the cost of a new stationary battery in year y, as there is no reason to buy a second-life battery for more than a new one ($p_{sup}(E, y) < c_{B,1,y}$),
- Quantity sold, E, can never exceed the quantity of used EV batteries $f_{EV}(y)$ reaching end of first life in year y ($E < f_{EV}(y)$),

- Price must always be above the sum of the repurposing cost $c_{repur}(y)$ and recycling net income $c_{recyc}(y)$: sale on to the second-life market is only done if the profit (price minus repurposing cost) exceeds the net income possible from the competing alternative, immediate recycling: $p_{sup}(E, y) - c_{repur}(y) > c_{recyc}(y)$.

In the absence of a global survey of all possible stationary applications and their corresponding net present values and market sizes, from which to form price-demand curves, the curve $p_{dem}(E, y)$ for each year y is approximated as two linear segments joined by a quadratic polynomial to smooth the joint (see Appendix C4 for details). The reasoning behind this is that there is likely to be a lucrative but limited niche applications market, and a larger but cheaper mass market (Eyer and Corey, 2010). The linear coefficients are set to follow these constraints:

- $p_{dem}(E, y)$ can never exceed $c_{B,1,y}$, as there is no reason to buy a second-life battery for more than a new one,
- $p_{dem(mass)}(E_{max}(y), y) = 0$, that is, the highest possible annual demand $E_{max}(y)$ (in kWh) can only be reached when price goes to zero,
- $p_{dem(niche)}(E, y)$ and $p_{dem(mass)}(E, y)$ join at the point (E^*, p^*_{dem}): it is set by the size of the niche market and the maximum price that would be paid in the mass market.

The mass-market segment decreases linearly from the point (E^*, p^*_{dem}) to $(E_{max}, 0)$, to account for diversity in mass-market uses and household incomes around the world: even if a home battery recoups its own costs over its lifetime, the initial investment may still be too much for lower-income households, even if paying by instalments. Home battery suppliers could not then sell their product to these households, and would not buy so many second-life batteries to keep in stock. Note that the potential second-life buyers are battery suppliers, not homeowners, as the latter would likely buy a value-added product including power electronics and installation service.

The price-supply and price-demand curves, $p_{sup}(E, y)$ and $p_{dem}(E, y)$, require quantification of the used EV battery supply $f_{EV}(y)$, repurposing cost $c_{repur}(y)$, recycling net income $c_{recyc}(y)$, niche market size E^*, mass market maximum price p^*_{dem}, and maximum demand $E_{max}(y)$. These are discussed after listing the assumptions used in the microeconomics-driven model.

4.3.2.2 Assumptions

No Stockpiling:
The stockpiling of used batteries is neglected. However, this assumption may not hold under some circumstances: for example, if the batteries' value as material for recycling increases faster than the annual warehousing costs. Such analysis is outside the scope of this thesis. The only two choices assumed to be available to the owner of a used EV battery are to recycle immediately, or sell into second-life. Illegal dumping is ruled out (Ongondo et al., 2011; The Basel Convention, 1989).

Frictionless International Trade:
Import/export tariff barriers are neglected, as are subsidies and taxes which may vary between countries unless an international agreement can be reached. The current political climate would suggest that this cannot be taken for granted, but detailed analysis is outside the scope of this thesis.

Perfect Competition:
The assumption of quasi-static equilibrium is valid under perfect competition: large numbers of buyers and sellers (no monopoly) with perfect knowledge of the market, operating rationally and freely with no collusion to fix prices (Harvey, 1994). While there are many EV manufacturers and potential second-life battery users, today's situation is far from perfect competition. However, new electronic trading platforms and future regulations may improve knowledge availability to buyers and sellers (Klör et al., 2015).

As long as changes in new battery price, recycling income, supply of used EV batteries, etc., are slow compared to the timescale on which second-life prices converge to equilibrium, quasi-static equilibrium may be reasonably assumed. However, with a yearly interval, some features are not captured: sudden step changes in technology, economic boom-and-bust cycles, sub-yearly dynamics such as new product launches and seasonal variations.

EV Sales unaffected by Second-life Market:
Some pose the question of whether the second-life sale of used EV batteries can allow a discount on new EV batteries, thus driving EV sales. The conclusion is most commonly that the second-life price would be insufficient to bring this about (Neubauer and Pesaran, 2011). Therefore, the feedback is not modelled here, but nonetheless a number of different EV uptake scenarios were investigated.

Sufficient Battery Repurposing Capacity:
It is assumed that the processing capacity of battery repurposing plants will be sufficient at every time step. Good market research and forecasting should ensure that adequate investment is made in repurposing capacity. In such a case, second-life sales quantities are driven by market dynamics as modelled in this study, rather than ignorance, poor analysis, or poor decision-making.

Second-Life Price Variance:
The same price per kWh is unlikely to be paid for every second-life battery. Even if all EV batteries are removed once they degrade to 80 % of their original capacity, there may still be variations in performance and remaining life. These could be due to differences in battery chemistry and first-life usage patterns as discussed above (Neubauer et al., 2015), while the second-life application will affect the remaining second lifetime (Strickland et al., 2014). It is beyond the scope of this work to account for the variance in second-life price likely to come about due to all these differences. Thus the price found, $p_{eqm}(y)$, is not *the* equilibrium second-life price, but the *average* equilibrium second-life price.

4.3.2.3 Constructing price-supply and price-demand curves

The used EV battery supply, $f_{EV}(y)$ (in kWh), is required for the upper bound of quantity of second-life batteries sold in each year. An adaptation of the Bass (1969) model of innovation diffusion is used to estimate $f_{EV}(y)$. EV sales data from IEA (2017b) and EV Volumes (EV Volumes, 2014, 2016a,b) are used to parameterise the model.

The original Bass model considers the rate of uptake of a new technology, $\dot{F}(t)$, relative to the population yet to adopt it, $1 - F(t)$, to vary linearly with the fraction of the population that has already adopted it, $F(t)$ (the integral of $\dot{F}(t)$):

$$\frac{\dot{F}(t)}{1 - F(t)} = p + qF(t). \tag{4.12}$$

The parameters p and q have natural interpretations as the spontaneous uptake of the technology by early adopters (the 'coefficient of innovation'), and the influence of those who have already become users of the technology on those who have not yet ('coefficient of imitation'), respectively (Bass, 1969). Solving (4.12), the adoption rate $\dot{F}(t)$ follows the form given in (4.13), growing as the technology gains popularity, then peaking and declining as the market saturates (Bass, 1969):

$$\dot{F}(t) = \frac{(p+q)^2 \exp\left(-(p+q)t\right)}{p(1+\frac{q}{p}\exp\left(-(p+q)t\right))^2} \tag{4.13}$$

The amount of first-time EV sales is hypothesised to follow the form given in Equation (4.13), see Figure 4.14. To find the coefficients of innovation and imitation, p and q, data from IEA (2017b) on the cumulative global fleet of battery electric vehicles (BEV - that is, with no internal combustion engine, or ICE) and plug-in hybrid electric vehicles (PHEV - typically diesel vehicles with an onboard battery to power most driving except long stretches of cruising), were used. But as battery capacity varies between different makes of BEVs and PHEVs, sales data from EV Volumes (EV Volumes, 2014, 2016a,b) were used to estimate their average capacities from 2013-2016, and a linear extrapolation was assumed for previous years to 2010. Total annual EV battery sales are then given as BEV annual sales multiplied by the respective average battery capacity for that year, added to the same for PHEVs. Finding the battery sales in kWh obviates the need to extrapolate separately the sales figures for BEV and PHEV units and average battery capacities (see Appendix C1). Only the total kWh data need be extrapolated.

The Bass model curve, Equation (4.13), was fit to the total annual (kWh) sales data by a least-squares regression. As there are so few data points, the goodness of fit R^2 can exceed 0.999 for extremely different outcomes depending on the initial values of p and q given to the fitting procedure (see Appendix C2). However, as reported by the author (Sun et al., 2018b), the second-life price was found not to be sensitive to the used battery supply $f_{EV}(y)$. This was true for scenarios ranging from 'Low', equivalent to a global EV fleet of roughly 15 million, to 'High', where all cars (2 billion by 2040 (Smith, 2016)) are fully electric, each with a 40 kWh battery. 'Medium' corresponds to an eventual EV penetration of 45 %, guided by the projections of Wills (2016). It is taken as the most likely scenario of first-time EV sales, denoted here by $r_0(y)$.

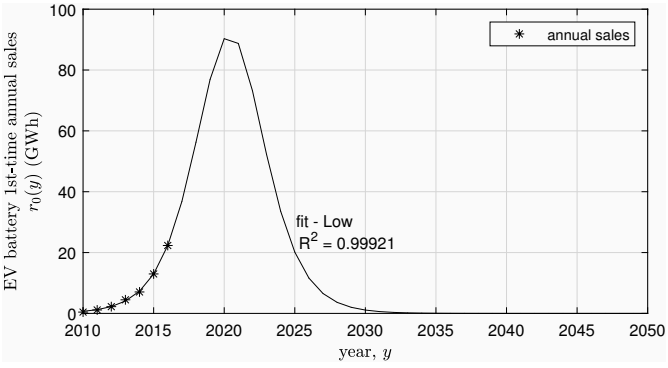

FIGURE 4.14: EV annual sales and extrapolated Low scenario, which peaks in 2020 at 91 GWh. The Medium and High scenarios (not shown) peak respectively in 2028 and 2029, at 5 TWh and 11 TWh.

Olson and Choi (1985) adapted the Bass model to include replacement purchases of durable goods with finite lifetimes, finding their version predicted sales figures for televisions and fridges with better accuracy than the Bass model alone. Their methods should be applicable to EV battery replacement purchases:

EVs may soon go from novelty to essential commodity, where nearly all purchases now are first-time purchases, but in future nearly all may be replacement purchases.

Following Olson and Choi (1985), a Rayleigh distribution $Ra(\tau)$ is used for the distribution of product lifetime, as it requires only one parameter (the mean lifetime, μ):

$$Ra(\tau) = \frac{\pi}{2\mu^2}\tau \exp\left(-\frac{\pi\tau^2}{4\mu^2}\right). \tag{4.14}$$

Olson and Choi (1985) found distribution choice to have little influence on results. The lifetime before removal and replacement of an EV battery is influenced by mileage, ambient temperature, driver aggression, usage in vehicle-to-grid, amongst other factors (Neubauer et al., 2015). Thus it is reasonable to expect a spread around the mean lifetime, as shown in Figure 4.15.

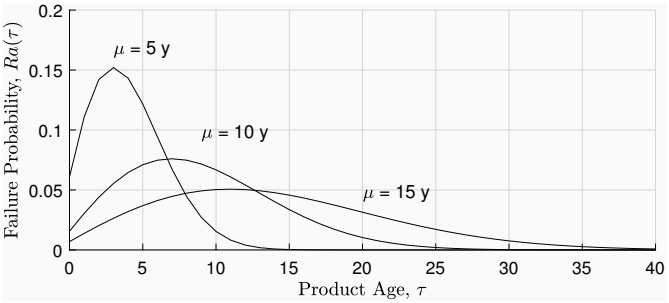

FIGURE 4.15: Rayleigh distributions of battery failure probability in year τ, for a range of mean lifetimes, $\mu = 5, 10, 15$ years.

Neubauer and Pesaran (2011) use 8 years (no spread) as the EV battery's first lifetime, while Foster et al. (2014) use a uniform distribution between 3 to 10 years. With improvements in understanding of battery chemistry and battery management systems, further increases in lifetime may be achieved.

The removal rate of used EV batteries, $f_{EV}(y)$, is given by the sum of all replacement purchases in year y. The replacement of the first-time sales is referred to here as the 'first-generation replacement', $r_1(y)$. The eventual replacement of these replacement purchases is the 'second-generation replacement', $r_2(y)$, and so on ad infinitum. Replacement of EVs themselves occurs too, but the focus is on their batteries. The amount (kWh) of batteries removed and replaced in year y of generation j is given by the sum from the beginning of the series up to year y, of the previous generation's sales in year τ multiplied by the failure probability of a battery of that age, $(y - \tau)$ years (Olson and Choi, 1985):

$$r_j(y) = \sum_{\tau=0}^{y} r_{j-1}(\tau) \cdot Ra(y - \tau). \tag{4.15}$$

The generation previous to the first-generation replacement is the first-time sales, $r_0(y)$. As $r_j(y)$ cannot be summed to $j \to \infty$, the sum is truncated at $j = 14$. The reason for this is that the sum of replacement purchases up to $j = 14$ is indistinguishable from the sum to $j = 13$ over the time period considered, 2017 to 2050, to within machine precision, as increasingly few units reach their j^{th} replacement before 2050 as j is increased. As computational run-time was so short as to not be an issue, no further work was

done to decide where to truncate the sum:

$$f_{EV}(y) = 0.8 \sum_{j=1}^{14} r_j(y). \tag{4.16}$$

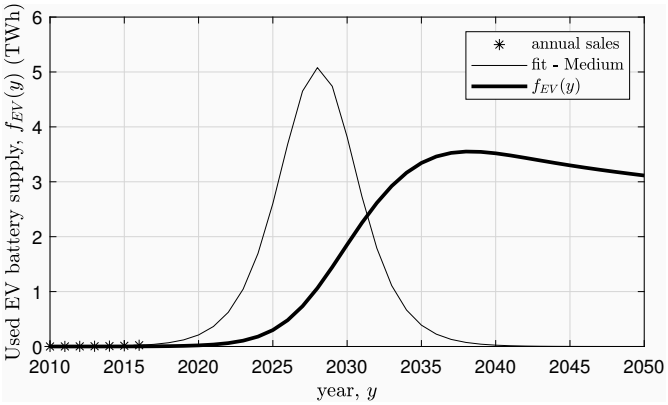

FIGURE 4.16: First-time EV sales $r_0(y)$, and supply of used EV batteries $f_{EV}(y)$. 'Medium' scenario, with mean battery lifetime increasing from 8 to 20 years.

The factor 0.8 is to account for the average remaining capacity of a used EV battery being 80 % of its capacity when new. An increasing mean lifetime is approximated by using a different μ in the term $Ra(y-\tau)$ in Equation (4.15) for each generation. A longer mean lifetime results in lower rate of battery removal, simply because they last longer. For mean lifetime increasing linearly from $\mu = 8$ years in generation $j = 1$ to $\mu = 20$ years in generation $j = 14$, the supply of used batteries declines slightly after an initial rise (Figure 4.16). The choice of 8 to 20 years is guided by past and current trends in battery development, and the fact that 20 years may be close to the average lifetime before scrappage of a vehicle in 2050 (in the USA, it has increased from 12.2 to 15.6 years in the period 1969 to 2014 (Bento et al., 2016)). This is an optimistic estimate of EV battery lifetimes, but the only effect of shorter lifetimes is faster replacement and larger $f_{EV}(y)$. This was found by the author (Sun et al., 2018b) to result in a slightly faster decline in second-life price up to around 2025, but almost negligible effect on the price subsequently. It is also possible that $f_{EV}(y)$ may be smaller if some fraction of used EV batteries fail testing and cannot be repurposed into second-life batteries (Richa et al., 2017).

There is a tendency for existing estimates of used EV battery supply (Foster et al., 2014; PV Europe, 2016; Sathre et al., 2015; Tokash and Dehamma, 2016; Wills, 2016) not to plateau like in this work, with the exception of the 'pessimistic' scenario analysed by Foster et al. (2014). It may be that a plateau will occur later than the timeframes examined (most often up to 2030). It is also possible that these publications only extrapolate exponential growth, which clearly cannot continue indefinitely. Furthermore, the tendency is to predict what is probable, rather than what is necessary to tackle urban air pollution (Asthana and Taylor, 2017) and to meet targets such as net zero GHG emissions from the UK by 2050, set by the Committee on Climate Change (2019). This might explain why the predictions in the literature tend to fall between the Low and Medium scenarios in this thesis.

The repurposing cost and recycling net income, $c_{repur}(y)$ and $c_{recyc}(y)$ (in GBP/kWh), form the lower bound of price in the price-supply curve $p_{sup}(E, y)$. Neubauer and Pesaran (2011) quoted repurposing costs of 250-1000 USD per pack, meaning 10-40 USD/kWh (8-33 GBP/kWh), assuming capacity 25 kWh, as was common at the time (EV Volumes, 2014). Williams and Lipman (2012) calculated the repurposing cost in more detail, taking account of shipping, dismantling and testing the EV battery packs.

They concluded a cost of 111-248 USD/kWh (91-203 GBP/kWh), of which roughly 100 USD/kWh for shipping. Casals et al. (2014) performed an updated calculation, placing the cost at 87-360 EUR/kWh (80-330 GBP/kWh, the lower end assuming less dismantling, and greater automation and economies of scale). For this study, an estimate was taken of the repurposing cost starting from 300 GBP/kWh in 2010, a minimum eventual cost of 10 GBP/kWh and an 18 % rate of decline, the same as for battery costs themselves. It is reasonable to suppose that the economies of scale and organisational efficiencies that are reducing battery costs may also be applicable to repurposing processing. The present-day repurposing cost is widely cited to be around 50 EUR/kWh (46 GBP/kWh) (Reid and Julve, 2016).

As for $c_{recyc}(y)$, the Commission for Environmental Cooperation (CEC, 2015) reported that many battery recycling plants charge for their service (that is, $c_{recyc} < 0$), but return a credit according to the value of the material recovered. Businesses were reluctant to reveal their exact charges and credits. Toyota offered bounties of 100-500 USD for the return of used batteries, suggesting c_{recyc} in the region 2-41 GBP/kWh, assuming batteries of capacity 10-30 kWh. Ma et al. (2018) estimated potential profits of 3394 CNY/ton (Chinese yuan per 1000 kg) for recycling LFP batteries and 17 571 CNY/ton for NMC (396 and 2052 GBP/ton, or $c_{recyc} = 4$ and 20 GBP/kWh respectively, considering the energy density of packs that Baczyńska et al. (2018) reviewed). On the other hand, Battery University (2019) estimated lithium-ion recycling to cost 4000-5000 USD/ton, meaning a negative c_{recyc}, roughly -40 GBP/kWh. The net credit from recycling may rise with increasing efficiency of recycling processes and scarcity of raw materials, or indeed *decrease* over time if new battery chemistries are invented using lower-cost materials (CEC, 2015). In any case battery recycling cannot become more profitable than the cost of a new battery, as the latter requires material input, whether recycled or virgin raw materials, which sets a lower bound to the cost. Lacking any more reliable information, $c_{recyc}(y) = 0$ is taken for all years y.

The price-supply curve must be monotonically increasing. This is not possible if the new battery cost falls below the sum of repurposing cost and recycling net credit ($c_{B,1} < c_{recyc} + c_{repur}$). In such a case, the buyer would prefer to buy a new battery for their stationary application, and the potential seller of a second-life battery would have to immediately recycle their product instead. There would then be no second-life sales in that year ($E_{eqm}(y) = 0$).

The new battery per-kWh cost $c_{B,1,y}$ is taken to decrease exponentially from 390 GBP/kWh in 2019 to a minimum eventual cost of 50 GBP/kWh, at a rate 18 % per year (see Chapter 2). Cost is extrapolated backwards at the same rate for previous years. Varying the new battery cost evolution was found to have little impact on second-life price (Sun et al., 2018b).

The price-supply curve for second-life batteries is approximated as an exponential (more details in Appendix C3). It is bound from below by ($c_{recyc} + c_{repur}$), from above by $c_{B,1}$, and its domain is from $E = 0$ to $E = f_{EV}$. This still gives it a degree of freedom within these constraints: the curve may be shallow for most of the domain and increase steeply as $E \to f_{EV}$, or the curve may be closer to a straight line. The former case represents high elasticity, where a small change in price results in a large change in quantity sold (for most of the domain), and the latter lower elasticity. Elasticity of the price-supply curve was found to have negligible effect on second-life price (Sun et al., 2018b). The curve for 2020 is shown above in Figure 4.13.

The niche market size, E^*, is taken as 16.7 GWh, based on the analysis of stationary battery markets by Eyer and Corey (2010) and used by Neubauer and Pesaran (2011) to constitute their fixed market for second-life applications:

- Area regulation: battery net present value 1050-2650 USD/kWh for potential USA market size of 700 MWh,
- Power quality and reliability: 700-1800 USD/kWh for 10 GWh in USA,
- Transmission and distribution upgrade deferral: 400-500 USD/kWh for 6 GWh in USA.

Although Eyer and Corey (2010) calculated market size for applications in the USA rather than the world, suggesting 16.7 GWh is an under-estimate, it was for a potential total market rather than on an annual basis, so in fact 16.7 GWh would be a reasonable order-of-magnitude estimate. E^* is assumed not to vary with time: the niche market encompasses applications that are already using batteries, and there is little room for market expansion as is the nature of niche markets, though this is of course a simplification.

The mass market maximum price, p^*_{dem}, is taken as 67 GBP/kWh, assuming the mass market will consist mainly of home batteries. While home batteries today are still a luxury product, a drastic decrease in their price, as may be achieved by using second-life batteries, could change that. Kirmas and Madlener (2017) calculated 73 EUR/kWh (67 GBP/kWh) to be a conservative estimate of the price at which a home battery recoups its own costs by increasing onsite consumption of rooftop PV energy, thus making savings on a German homeowner's electricity bills, for 10 years. The retail cost of electricity is relatively high in Germany, so the breakeven price may be lower in other parts of the world (Heymans et al., 2014).

The maximum demand, $E_{max}(y)$, may be expected to follow a similar form as $f_{EV}(y)$, since second-life batteries in a stationary application are durable goods with finite lifetime, like EV batteries in their first lifetime. The function is approximated by the same form as the solution $F(t)$ of Equation (4.12):

$$E_{max}(y) = A_{max}\left(\frac{1-e^{-(p_{max}+q_{max})y}}{1+\frac{q_{max}}{p_{max}}e^{-(p_{max}+q_{max})y}}\right) \tag{4.17}$$

where $A_{max} = 3 \times 10^9$ kWh, $p_{max} = 0.0013$ per year, $q_{max} = 0.35$ per year. Though this form is usually used for the cumulative sales of a product, here it is used to approximate the annual demand including replacements (Figure 4.17). The parameters were chosen to make $E_{max}(y)$ plateau at a plausible maximum level for all the home batteries in the world, $A_{max} = 3$ TWh being equivalent to 2 billion households replacing a 15 kWh battery every 10 years. Another consideration was to make the cumulative sum of $E_{max}(y)$ roughly follow the projection of Wills (2016) for global battery fleet up to 2025 (Figure 4.17). Logically the cumulative sum of $E_{max}(y)$ should exceed these values, as demand must always exceed actual sales, since not all demand can be satisfied.

The price-demand curve $p_{dem}(E)$, in each year y, goes linearly from $p_{dem} = c_{B,1}$ at $E = 0$, to (E^*, p^*_{dem}), then another linear segment to $(E_{max}, 0)$. The curve is truncated at $E = f_{EV}$, as no more second-life batteries can be sold than the supply of used EV batteries. More details are given in Appendix C4. The curve for 2020 is shown above in Figure 4.13.

4.3.3 Second-life battery price results

The foregoing method is summarised in Figure 4.18, which shows for illustrative purposes the price-supply and price-demand curves for 2017, 2019 and 2021. Such pairs of curves were found for each year from

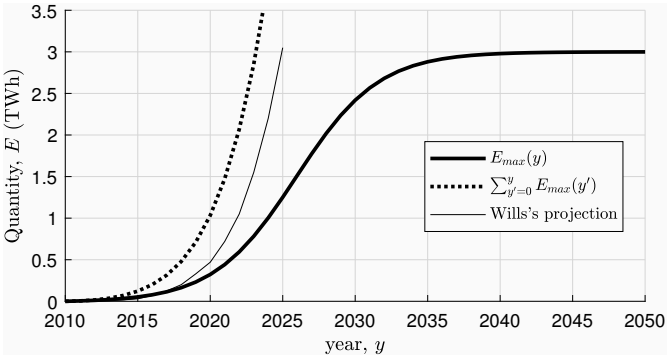

FIGURE 4.17: Maximum possible demand $E_{max}(y)$ (TWh worldwide, annually), shown with its cumulative sum, and the projection of Wills (2016) for global stationary battery fleet.

2017 to 2050, and their intersections give the price-quantity equilibrium in each year, $(E_{eqm}(y), p_{eqm}(y))$. These are plotted in Figure 4.19.

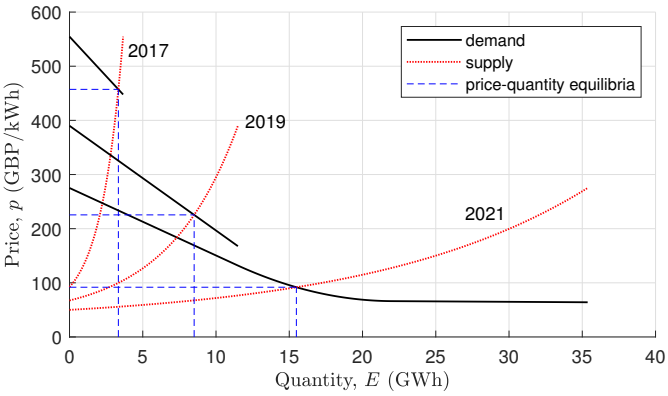

FIGURE 4.18: Price-supply and price-demand curves in 2017, 2019 and 2021, showing their intersections in each year.

In the paper by the author (Sun et al., 2018b), many different driving factors were varied to find the sensitivity of the second-life price and quantity sold to each of them. New battery price, EV uptake (and therefore used battery supply), elasticity of supply, and price-demand curve parameters were found to have little impact on the second-life price. The most significant driving factor was found to be the sum of battery repurposing cost and recycling net income, $(c_{recyc} + c_{repur})$. In the few years up to around 2022, when the cost of a new stationary battery is still much higher than the repurposing cost of a used EV battery, the second-life price decreases rapidly; there is a plateau in price for a few years while demand for stationary batteries accelerates, and subsequently the second-life price remains not far above $(c_{recyc} + c_{repur})$. This prediction is similar to what has been observed for many other products and business models: there is an initial period when very high 'super-normal' profits can be made by the few companies that are able to supply the innovative new product (second-life batteries in this case), followed by a decline to 'normal' profits as competition outpaces expansion of demand (Harvey, 1994).

By contrast, the quantity of second-life batteries sold globally is sensitive to all the driving factors tested. Fortunately only the price is needed for this study. It is on the basis that the second-life battery price is insensitive to most driving factors, that the approximations used in determining it are justified. The exception is the sum of battery repurposing cost and recycling net income, $(c_{recyc} + c_{repur})$, which must be quantified more accurately and precisely in further work.

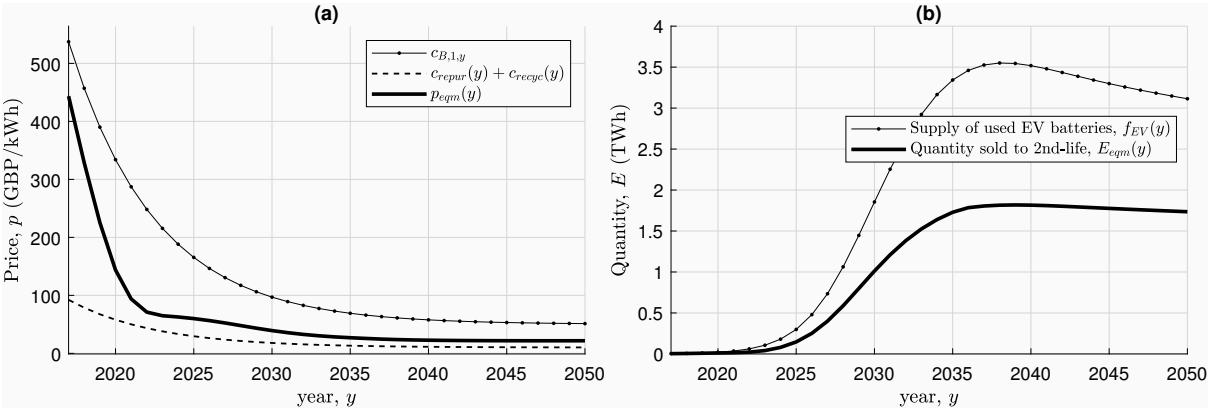

FIGURE 4.19: Time evolution of (a) equilibrium second-life battery price, shown between the bounds of new battery cost from above and repurposing cost plus recycling net income from below; and (b) quantity of second-life batteries sold globally each year, shown against the annual supply of used EV batteries.

In the process of estimating the time evolution of the second-life battery price, some interesting auxiliary observations were made:

Firstly, if ICEs are to be phased out completely, as many governments are announcing (Asthana and Taylor, 2017) and as will be necessary to meaningfully tackle air pollution and climate change (Committee on Climate Change, 2019), the global supply of used EV batteries will likely be greater than anything the literature has predicted. (The exception would be if ICEs are replaced by something other than EVs, such as hydrogen vehicles, or greatly expanded electric rail transport.)

Secondly, if this huge supply of used batteries is to be saved from immediate recycling, if recycling technology and capacity cannot expand quickly enough for example, the mass market for second-life batteries must increase rapidly and the product must be sold at higher prices. This means more lucrative value propositions need to be made available to ordinary householders, if they are not to be mis-sold.

Thirdly, the cost of new stationary batteries is decreasing so rapidly that even if repurposing costs are pushed down further, the gap between them will eventually be so small that there will be little surplus value to share out between EV manufacturers, EV owners, second-life battery suppliers and users, as so much of the research is promising (Martinez-Laserna et al., 2018). The surplus value would be further eroded if EV battery recycling becomes more lucrative, as sources such as Ma et al. (2018) suggest.

The method used here to estimate the second-life battery price evolution was applied in the absence of government intervention in the form of taxes or subsidies. These could be tested in further work by modifying the price-supply and price-demand curves. However, it is important to ask what government intervention should attempt to achieve. For example, a tax on battery recycling might lower the second-life battery price and increase the quantity sold, as it would then be a more attractive proposition than recycling; but given the environmental burdens of manufacturing and landfilling batteries, an intervention to disincentivise battery recycling would be a risky policy. This is especially true given how small a proportion of the used EV battery supply is sold into the second-life market (Figure 4.19), and how little difference second-life use would make in delaying the stream of batteries sent to recycling globally (the author (Sun et al., 2018b) estimated a delay of 1 year).

It should be noted that many of the other assumptions used - perfect competition between rational actors, frictionless international trade, quasi-static equilibrium of supply and demand - are less straightforward

to address. The best that can be said for the equilibrium second-life price, $p_{eqm}(y)$, is that it is an approximation that can be used for the size-dependent portion of second-life battery cost, $c_{B,1,y}$, in the financial analysis of the domestic PV-battery system under study in this thesis.

4.4 Battery Repurposing Environmental Impacts

For cases where a second-life battery rather than a new one is used in the domestic PV-battery system, there are environmental impacts associated with the repurposing process. These are used in place of the battery manufacturing impacts each time the second-life battery is replaced in the calculation of life-cycle impacts (see the process tree in Chapter 2).

To quantify the impacts of repurposing a used EV battery for a second-life application, guidance was sought first from the existing literature. A range of impact values were used, from Faria et al. (2014) who did not mention the repurposing impacts at all, to Ahmadi et al. (2014b) who assumed them to be half the impacts of manufacturing a new battery, with no further justification given.

Although Williams and Lipman (2012) did not give environmental impact data, they were more specific in describing what battery repurposing might entail. They found the dominant financial cost to be shipping of the used battery packs from EV dealerships where they would be deposited, to repurposing facilities, and of newly repurposed packs to battery suppliers. At a repurposing facility, the used EV batteries would need to be dismantled and tested according to USABC recommendations with different charge-discharge cycles to a total of four cycles. It is uncertain what level of dismantling, and how much repair and replacement of parts, would be considered economical.

Casals et al. (2017) analysed some different possibilities in this regard - the most economical process they considered would be not to dismantle packs at all, to test each pack in its entirety, and issue a simple pass/fail, where any failed packs are sent for recycling with no effort made to isolate and repair the failure. Whatever the level of dismantling and repair, the GHG emissions are dominated by shipping and electricity use in battery testing. They stated CO_2 emissions of 11.5 kg (27 kWh in a typical EU grid mix) for testing the used EV battery, plus 317 kg for 1000 km shipping, per battery pack (8-25 kWh).

By contrast, Bobba et al. (2018) assumed only 100 km of transport, though they also included the energy cost of manufacturing new trays and foam for securing the battery modules. They considered battery testing to require only one charge-discharge cycle, consuming 8.72 kWh to test a used EV battery with 11.4 kWh remaining usable capacity.

Both of these cases assume a smaller energy requirement for testing than Williams and Lipman (2012) did. On the other hand, Richa et al. (2017) considered the testing of 450 kWh of cells to require 4812 kWh in total, the equivalent of nearly 11 full cycles. They also took shipping to be 1000 km.

From these sources, it is clear that shipping cannot be neglected in calculating the battery repurposing impacts. The distance and mode of transport depends on where repurposing facilities will be located globally. In this study, 1000 km shipping is considered via container ship running on heavy fuel oil (HFO). This is a conservative estimate, as other less polluting transport modes exist, such as container ships running on liquefied natural gas (LNG), or over land in diesel trucks.

Following Williams and Lipman (2012), testing is taken to consist of four charge-discharge cycles, that is, 4 kWh of electricity per kWh of usable battery capacity. A GB average grid mix for 2017 is assumed for

this electricity. Battery repurposing may take place in countries whose electricity generation is dominated by more polluting technologies; on the other hand, adoption of cleaner technologies may render this an over-estimate when the second-life battery needs to be replaced in future.

The impacts of manufacturing new parts, as Bobba et al. (2018) considered, are taken in this study to be negligible in comparison to all the uncertainties described above. However, the BoS is replaced on its own schedule (see Chapter 2) independently of the second-life battery replacements. This is guided by the work of Richa et al. (2017), who considered a new BMS to be necessary for the repurposed EV battery. It is assumed here that if the second-life batteries must be replaced more often than the BoS, the replacements can be integrated with the existing BoS so that a new BoS is not needed every time the batteries are replaced.

Appendix C5 gives details of how the impacts of shipping and testing are calculated. They are summed together to give the total impacts per usable kWh for the battery repurposing process, in Table 4.3. These are used in this study as the central estimates, and also the uncertainty values, as there is so much uncertainty in the repurposing process.

Battery repurposing impacts		
CC	2.97	kg CO_2/kWh
OD	2.96×10^{-7}	kg CFC11/kWh
HT	3.22×10^{-1}	kg DCB/kWh
POF	4.04×10^{-2}	kg NMVOC/kWh
PMF	2.26×10^{-2}	kg PM10/kWh
IR	3.62	kg U235/kWh
TA	5.45×10^{-2}	kg SO_2/kWh
FE	1.57×10^{-4}	kg P/kWh
ME	4.94×10^{-3}	kg N/kWh
FET	1.70×10^{-2}	kg DCB/kWh
LO	5.70×10^{-1}	m^2·a/kWh
WD	1.07×10^{-3}	m^3/kWh
MD	6.33×10^{-3}	kg Fe/kWh
FD	1.08	kg oil/kWh

Table 4.3: Battery repurposing ReCiPe midpoint impacts per usable kWh of used EV battery, using data from Øberg (2013), Laugen (2013), Baczyńska et al. (2018), and Gridwatch (2018), with details in Appendix C5.

It is interesting to note that the CC impact of shipping, calculated as described here, is much lower than the figure Casals et al. (2017) gave. 317 kg CO_2 per 8-25 kWh battery pack is equivalent to at least 12.7 kg CO_2/kWh, contrasted with 1.69 kg CO_2/kWh (see Appendix C5). This may be explained by the assumption Casals et al. (2017) used, that battery repurposing is of such a small scale that a separate delivery vehicle is used to transport every single pack. Even if this turns out to be true in the long-term, it is likely that used and newly-repurposed EV batteries would be transported along with other goods. In that case it would be unfair to attribute the entire vessel's impacts solely to the battery pack, rather than distributing them across the tonnage of all goods transported.

4.5 Summary

The chapter began with some theory and background on the physical characteristics of Li-ion batteries, specifically the factors affecting their efficiency and capacity during operation in the short-term, and due to degradation mechanisms in the long-term.

Although the Rint equivalent circuit model does not capture some of the behaviours described, it was selected as the basis of the battery model in this study for its relative simplicity (which aids computation speed), its ability to still represent the important effect of charge/discharge rate on efficiency, and its flexibility to incorporate degradation effects. These are the decrease in capacity and increase in internal resistance, which are modelled as following pre-defined functions of battery cycling; one for a new battery and best-case second-life battery, and one for a worst-case second-life battery. This follows the work of Sathre et al. (2015) but draws on many other publications to parameterise these functions and the battery equivalent circuit. The battery is replaced when its capacity has degraded to 60 % of its original value (its first-life original value, in the case of second-life batteries) or after 15 years if it hasn't degraded as far as that yet. This occurs separately to the BoS replacement schedule.

The time-evolving cost of second-life batteries is needed for the financial calculations. Finding the existing literature on this topic insufficient, a method based on microeconomics was developed to quantify this. It involves constructing price-supply and price-demand curves to represent the willingness of potential sellers and potential buyers respectively to make a transaction, as a function of second-life battery quantity (kWh), in each year. The equilibrium second-life price $p_{eqm}(y)$ (GBP/kWh) and quantity sold $E_{eqm}(y)$ (kWh) in each year is the intersection of the price-supply and price-demand curves. $p_{eqm}(y)$ is then used for second-life batteries in the financial calculations (see later chapters) in place of $c_{B,1,y}$, the size-dependent cost of new home batteries. The fixed cost is taken as $c_{B,0} = 1500$ GBP for both new and second-life batteries.

The environmental impacts of the battery repurposing process are estimated, as these are needed for the calculation of life-cycle environmental impacts. There is much uncertainty in the literature on this topic, so an estimate is made here to include the impacts of shipping by HFO-fuelled container ship across 1000 km in total, and testing involving four charge-discharge cycles, powered by electricity whose generation impacts equal those of GB generation in 2017.

This concludes Part I: Methodology. The remainder of the thesis is devoted to reporting the application of the methodology developed thus far to various simulated configurations of domestic PV-battery systems, and discussing the results obtained.

Part II

RESULTS AND ANALYSIS

Chapter 5

Selection of Modelling Parameters

"One pill makes you larger and one pill makes you small
And the ones that mother gives you, don't do anything at all..."
- Jefferson Airplane, *White Rabbit*

In Part I, the elements of the PV-battery model developed in this thesis were described:

- An inventory was given of the system components - PV, battery, converter, inverter - along with their costs and embodied environmental impacts of manufacture (Chapter 2),
- Input data for PV generation and household load were sourced from real measured data (Chapter 2),
- Logical flows were defined for the battery operating strategies: the Greedy algorithm, and the Emissions Arbitrage Algorithm, the latter of which was developed in the course of this study (Chapter 2),
- The method of obtaining time-varying environmental impact intensities for grid electricity was elucidated: using the adapted Hawkes' method on GB generation data from 2017, a merit order dispatch model and National Grid's Future Energy Scenarios for 2030 and 2050, and linear interpolation in years in between (Chapter 3),
- Life-cycle environmental impact data were obtained for operation of the different generator technologies currently on the GB grid and expected to be on the grid by 2050 (Chapter 3),
- A Rint equivalent circuit model was chosen for the battery itself, and parameterised in terms of initial internal resistance, and how capacity and internal resistance change with cycling as the battery degrades (Chapter 4),
- A microeconomics-driven model was developed to provide an estimate of how second-life battery price will vary to 2050 (Chapter 4),
- Estimates of environmental impacts for the battery repurposing process were obtained (Chapter 4).

The full code and input data to the model described in Part I of this thesis is available at: `https://doi.org/10.5258/SOTON/D1269`, with file descriptions in Appendix E.

These elements are brought together in Part II, to calculate the financial and environmental life-cycle impacts across the 25-year system temporal boundary. These financial and environmental metrics were defined in Chapter 1: the various metrics used by businesses to assess investment options, and the ReCiPe 2008 midpoint environmental impact categories, against a functional unit of 1 kWh electricity consumed.

Before this can be done and the different configurations compared (with/without new/second-life battery), there is the matter of the time resolution at which the modelling should be conducted, and the sizing of the system for each house. The literature on time resolution effects in PV-battery systems only considered systems running the Greedy algorithm, and less relevant contexts such as micro-grids, and so it was necessary to run some tests to find the trade-off between accuracy and computational speed for the EAA as well. This is reported in a conference paper by the author (Sun et al., 2020) and developed further in this chapter.

After reviewing the many different optimisation procedures available for sizing the system components, a direct search method was chosen. This was applied to the lowest- and highest-consuming houses in the dataset, finding how life-cycle CO_2 intensity and financial metrics depend on capacity of PV, battery, battery DC-DC converter, and DC-AC inverter, for the different algorithms and future grid scenarios (Community Renewables, CR, and Two Degrees, TD). From these results some heuristic rules were developed to size the components in relation to each household's annual consumption, and the lowest-cost electricity tariff was found for each house and configuration. The heuristic rules do not give an exact global optimum for system component sizes, but are a reasonable representation of a real sizing procedure that a PV/battery installer might undertake.

5.1 Time Resolution of Input Data and Model

As discussed in Chapter 1 Section 1.3.2, techno-economic analyses of domestic PV-battery systems in the existing literature differ in many ways. One of these is the time resolution of input data (PV generation and load profiles) and modelling timestep. At finer resolution there is an advantage in accuracy. However, this must be traded off against the challenges of acquiring and storing data at higher resolution, and the increased computing run-time required for modelling.

Such trade-offs have been investigated in the existing literature, and this is discussed next. But as such investigations have been limited in terms of battery operating strategies tested, it was necessary to replicate their analyses for the Emissions Arbitrage Algorithm (EAA) developed in this thesis. The results of these analyses are presented afterwards.

5.1.1 Literature review of time resolution effects

Some of the existing analyses of time resolution effects on domestic PV-battery modelling only investigated operational effects (import/export, self-consumption, etc.), as opposed to the finances or environmental impacts of the system. Nonetheless it is instructive to consider them.

Wright and Firth (2007) used 1-minute resolution data measured at 8 houses in England, studying the effect on electrical import and export of averaging the data to lower resolutions. However, they assumed constant generation power and no storage, and only studied 2 houses in detail for week-long periods.

Wyrsch et al. (2013) improved on this by using 6-s load data and 1-minute PV data measured in Switzerland to model and calculate the self-consumption ratio (SCR, the proportion of PV-generated energy that is consumed in the home, see Chapter 1 Section 1.1) with different battery capacities. They found less error from low time resolution when a battery is present. Their explanation for this is thus: as time resolution is lowered (timestep lengthened), peaks in load and PV generation become smeared out, over-stating the overlap in load and generation. This causes an over-estimation in the amount of load that can be served by PV generation, when in fact the peaks in each do not coincide as often at higher time resolution. This leads to errors in SCR. With a battery operating on the Greedy algorithm, its effect is to absorb excess PV energy and supply unfulfilled demand when it is able. In other words, it has a similar peak-smearing effect as lowering the time resolution, but in physical reality rather than erroneously. This is why the presence of a battery reduces the errors caused by lower time resolution.

Beck et al. (2016) found similarly, using 2-s load data and 10-s PV data measured in Germany. The error in SCR could be kept below 5 % in PV-only cases with PV resolution 15-minute and load resolution 1-minute, but this is achievable at load resolution 5-minute if there is a battery too. In addition, Beck et al. (2016) studied the effects of time resolution on optimal sizing of the system (to minimise costs), recommending 5-minute resolution or better for sizing the battery power (kW), but finding negligible effects of time resolution on sizing the PV capacity (kW_p) nor battery capacity (kWh).

In contrast, Hittinger et al. (2015) had found optimal battery size 236 % higher at 1-minute modelling resolution compared to hourly. This could be due to the different context: a stand-alone micro-grid on a Southeast Asian island, whereas others have studied grid-connected houses. Hittinger et al. (2015) also studied the effects on levelised cost of electricity (LCoE - see Chapter 1 Section 1.1), finding a 25 % under-estimation for a PV-diesel micro-grid modelled at hourly resolution compared to 1-minute, and 3 % under-estimation when a lead-acid battery is added to the system.

Quoilin et al. (2016) modelled domestic PV-battery systems in many EU countries, finding an unusually low error of 1.5 % in the self-sufficiency values at hourly compared to 1-minute resolution. (Self-sufficiency ratio, SSR, is the proportion of household load that is supplied by PV and battery rather than by the grid, see Chapter 1 Section 1.1.) This was for PV-only systems, and the error decreases further as the battery capacity is increased.

None of these studies gave an indication of how the computing run-time changes with modelling time resolution. This is understandable as run-time is dependent on details of the code and the programming language and operating system on which it is run. Furthermore, it is reasonable to suppose that run-time would double if timestep is halved, for example, as that would double the number of operations the machine must carry out. All the same, it is necessary to know specifically how much time each run takes for the system studied in this thesis in order to decide what timestep to use and how many different configurations can be investigated within the timeframe of the study.

Apart from lengthening the timestep, other more complex techniques exist for reducing the time domain of the model and therefore the computation run-time. However, one must look beyond the context of PV-battery systems to find these. For example, time-slicing, namely running the code on selected slices of input data rather than for the whole year, is an option given in the energy dispatch model Temoa

(Hunter et al., 2013), amongst others. Due to patterns in daily and weekly electricity usage (greater consumption in the evening, and less at weekends), it is necessary to take week-long slices to ensure the time-sliced data are still representative of the original data. Another consideration is that the slices be distributed over the whole year in order to capture seasonal effects in load and PV generation. For example, using alternate weeks as input would roughly halve the run-time; using one week in every month would reduce it to roughly a quarter, given the same timestep. No quantitative information was given by Hunter et al. (2013) on the errors introduced by time-slicing.

Pfenninger (2017) also considered time-slicing as well as down-sampling (simply reducing the resolution by lengthening the timestep) in their comparison of time reduction methods. Their application was the GB electricity system in hypothetical scenarios with 50-90 % renewable energy penetration. They used Calliope, an investment and dispatch model, to calculate the system-wide LCoE under different constraints, and how LCoE error varied with different time reduction methods. They found the best methods (lowest product of error and run-time) to be statistical clustering combined with keeping extreme days (with minimum/maximum wind/PV generation). Statistical clustering involves grouping periods (for example, days) of the data into a number of clusters that are similar within themselves but different to each other. For each cluster, the day of original data that most closely resembles the cluster centroid is selected, and these data are strung together to form a reduced-time input series. Clustering requires clear definition of a similarity measure, which is used by one of the various clustering algorithms that exist (k-means, hierarchical, etc.) to divide the original data into clusters. As Pfenninger (2017) themselves pointed out, the suitability of any time reduction method is contingent on the context being modelled and the research question being asked. Their specific results are therefore unlikely to apply to the domestic PV-battery modelled in this thesis.

5.1.2 Time resolution effects on study data

The domestic PV-battery system model as described in Part I of this thesis was run at different timesteps: 15-s, 1-minute, 5-minute, 30-minute, 1-hour. The results at 15-s resolution were taken as true, and for longer timesteps, the input data were coarsened by averaging. That is, the first PV and load data-points at 1-minute resolution are the mean of the first 4 at 15-s resolution, the next are the mean of the next 4, and so on. The capacity of PV, battery and converters are not important for testing time-resolution, so they were simply fixed for all houses at: 3.6 kW_p PV, 8 kWh battery, 3.6 kW for each the battery DC-DC converter and the DC-AC inverter, and the electricity tariff used was Economy 7. The metrics recorded were defined in Chapter 1 Section 1.1:

- Mean cost of electricity (MCoE) - the total expenditure on the system and electricity bills over the system lifetime, divided by the total electricity consumed during that time (cash flows discounted, electricity flows not),
- Internal rate of return (IRR) - the equivalent interest rate that makes the total savings pay back the total expenditure,
- Self-sufficiency ratio (SSR) - the proportion of household load that is served by PV and battery rather than grid import, across the whole system lifetime,
- CO_2 intensity - defined analogously to MCoE but with embodied CO_2 of manufacture and marginal CO_2 intensity of grid generation rather than financial Capex and bills (discount rate zero; this

definition means zero CO_2 intensity equates to carbon neutrality; CO_2 being used as an indicator to help parameterise the model before results are found for other environmental impact categories in the next chapter).

In Sun et al. (2020), the load and PV resolutions were varied in turn while keeping the other at 15-s, and running at 15-s timestep. Figure 5.1 shows greater errors on all metrics as load resolution is decreased, compared to when PV resolution is decreased. This confirms the relative importance of high load resolution compared to PV resolution as reported by Wyrsch et al. (2013), Beck et al. (2016), Hittinger et al. (2015) and Quoilin et al. (2016). Their finding that the system appears better at lower resolution is also confirmed: for the most part, bill savings, IRR and SSR are higher, while battery cycling, MCoE and CO_2 emissions (for the Greedy algorithm) are lower.

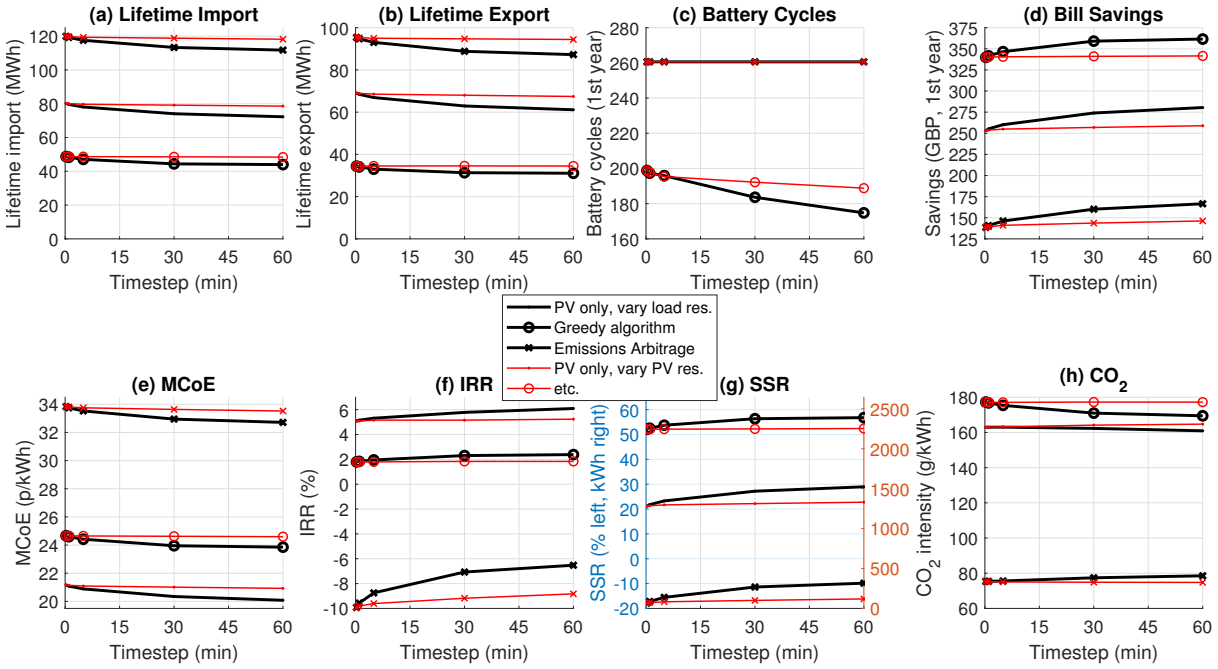

FIGURE 5.1: The effect of time resolution of PV and load input data for House 2 (4069 kWh), on the lifetime grid import and export, number of battery cycles and amount saved in bills in the first year (Economy 7 tariff), MCoE, IRR, SSR and CO_2 emissions. PV-battery Greedy and Emissions Arbitrage algorithms are compared, along with PV and no battery.

An exception is that battery cycling is unaffected by time resolution when running the EAA: this is as expected because charging/discharging is determined by the CO_2 intensity of the grid, rather than any property of the load or PV generation. The grid data were used at half-hourly resolution, and were not super-resolved for the runs at higher resolution.

While the errors caused by lower time resolution were less when there was a battery running the Greedy algorithm compared to the same system with PV but no battery, this was not so for the EAA. In most cases, the time resolution errors were in fact greater for EAA than for PV only. Therefore it is not true that the presence of a battery always reduces errors associated with lower time resolution; the operating strategy matters.

For the next tests, PV and load resolution and timestep were varied together. For example, 'hourly timestep' means both PV generation and load profiles have been averaged to hourly resolution, and a timestep of 1 hour is used for the modelling.

Figure 5.2 shows the absolute error in SSR, CO_2 emissions, IRR and MCoE at different time resolutions, averaged across all 8 houses. (The unusual behaviour of CO_2 emissions for EAA beyond half-hourly resolution is likely due to the fact that the EAA scheduling depends on grid data which are at half-hourly resolution.) The general trend is for the error to increase sharply at first as timestep is lengthened, but more slowly at longer timesteps.

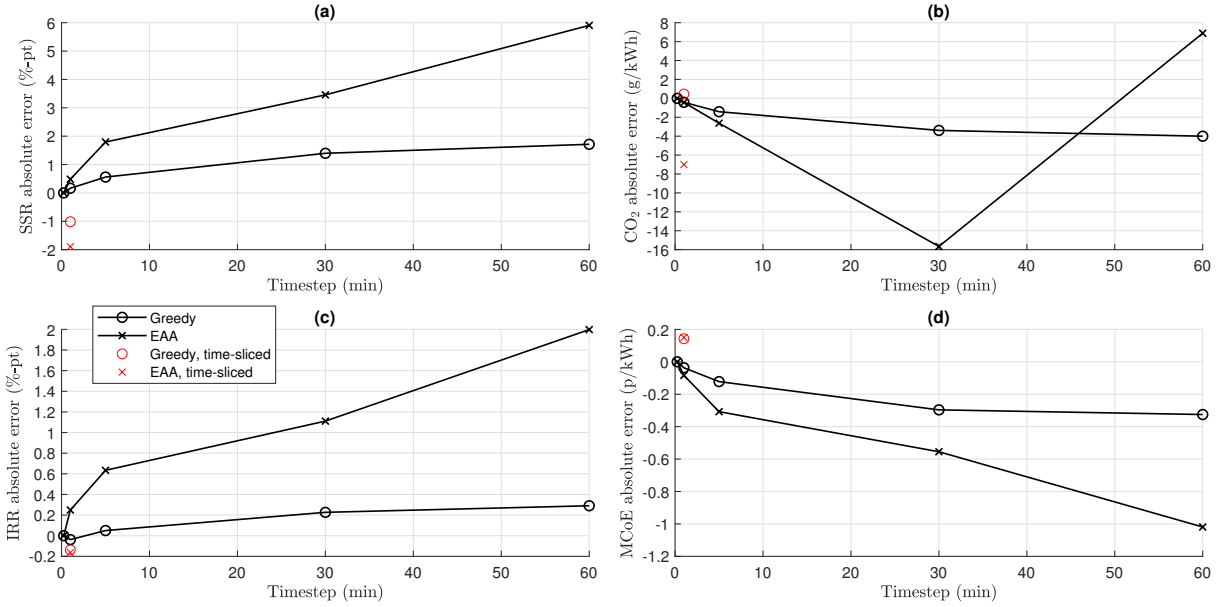

FIGURE 5.2: Coarsened by averaging: absolute error in SSR, CO_2 emissions, IRR, MCoE, as a function of timestep, averaged across all houses, comparing Greedy and Emissions Arbitrage algorithms. Also marked: errors at 1-minute resolution time-sliced by alternate weeks.

Figure 5.3 shows the computation run-time averaged across all 8 houses as timestep is varied. The run-time includes the time to initialise, simulate 25 years, and calculate the metrics required. The code is run in Matlab R2018a on a Windows 10 device with 8 GB RAM. As can be seen in Figure 5.3, the reduction in run-time diminishes at longer timestep. In other words, better accuracy can be achieved at shorter timestep, but at greater cost in terms of run-time.

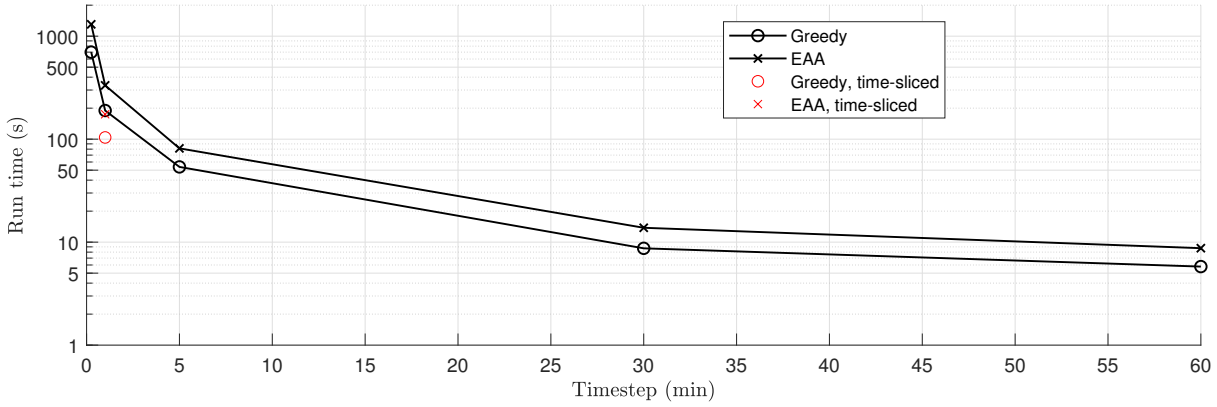

FIGURE 5.3: Computation run-time as a function of timestep, averaged across all houses, comparing Greedy and Emissions Arbitrage algorithms. Also marked: run-time at 1-minute resolution time-sliced by alternate weeks.

While the product of error and run-time seems an objective way of determining quantitatively the optimal timestep (Pfenninger, 2017), there is still room for subjectivity: is absolute or relative error

more relevant? Why should each only be raised to the power of unity in the product, why not error-squared times run-time, or any other way of weighting them? Bearing this in mind, 5-minute resolution was chosen as a reasonable compromise between accuracy and speed (Figures 5.2 and 5.3).

Figure 5.4 shows the relative errors at 5-minute resolution compared to 15-s. It is clear firstly that the average errors in Figure 5.2 mask a large variation between the houses in the dataset: -8 to +47 % relative error in SSR for the EAA-running systems, -0.8 to -8 % in CO_2 emissions, and so on. And secondly that the absolute error is in some cases a large fraction of the metric's value itself: in the worst case, House 1 running the Greedy algorithm has a -26 % relative error in IRR, despite the average absolute error (across all houses) being 0.05 %-points.

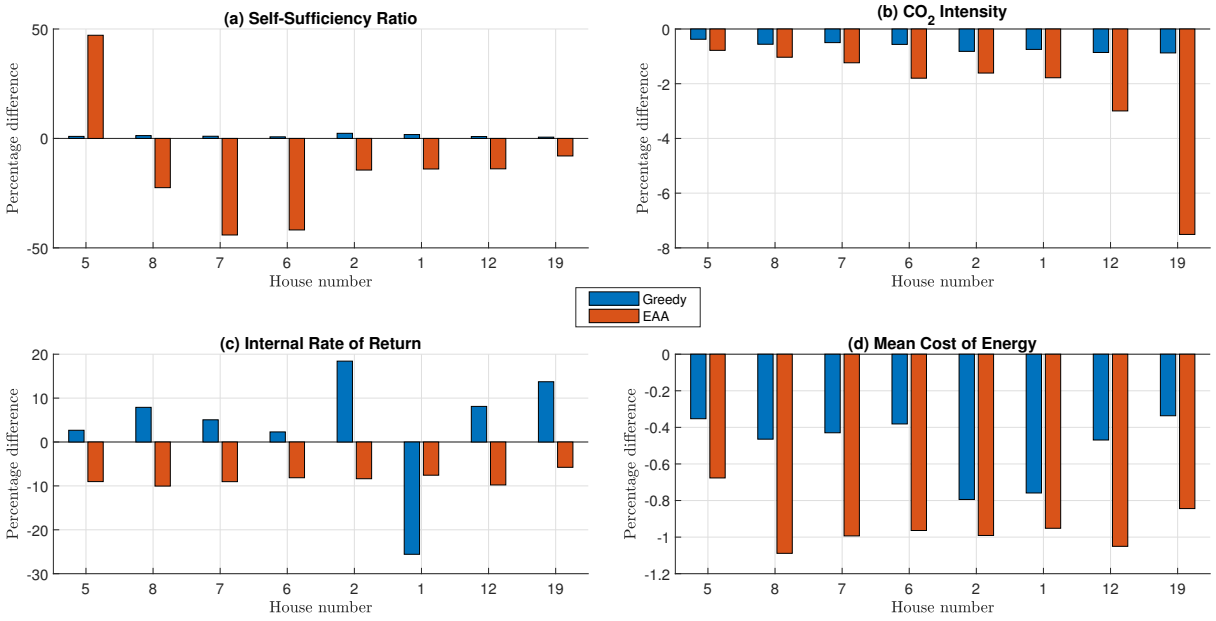

FIGURE 5.4: Coarsened by averaging: relative errors (%) in SSR, CO_2 emissions, IRR, MCoE, for each house, at 5-min resolution compared to 15-s, comparing Greedy and Emissions Arbitrage algorithms.

In fact, IRR is close to zero for all houses. Given that the economic case is so marginal, either the time resolution needs to be high enough that associated errors do not tip the results, or IRR cannot be used as a metric of financial benefit. When running the EAA, IRR is below zero for all houses. In other words, 3.6 kW_p PV and 8 kWh battery running the EAA is less economical than having no PV and no battery, although this cannot yet be concluded to hold for all sizes of PV and battery.

Note that SSR < 0 for 7 out of 8 houses when running the EAA, and the magnitude of this negative SSR is decreased by lengthening the timestep (hence negative relative errors in Figures 5.4 and 5.5). SSR < 0 means more electricity is imported from the grid than is consumed by the house. The excess is exported back to the grid at times of higher grid CO_2 intensity, as the EAA is designed to do.

Time-slicing was investigated as a way of reducing computation run-time, whether 1-minute resolution accuracy could be achieved in run-times closer to that for 5-minute resolution. The processing was thus:

- Select alternate weeks (days 8-14, 22-28, 36-42, etc.) of these time series: PV generation $P_{gen}(t)$, household load $P_d(t)$, national load $D_{17}(t)$, $D_{30}(t)$ and $D_{50}(t)$, in years 2017, 2030 and 2050 respectively (from which marginal generator response $MGR_x(t)$ is calculated, and from that, environmental costs of grid-generated electricity),

- For each of these time-sliced series, multiply them by the ratio of the means of the original and time-sliced series (this normalisation is necessary (Pfenninger, 2017) because time-slicing can change the mean value by chance, leading to systematic error in subsequent calculations),
- Run the model to find grid import and export, $P_g^-(t)$ and $P_g^+(t)$, and number of battery cycles, $\frac{1}{2}\sum_t |I(t) \cdot V(t)|\Delta t/E_B$, in each year, resulting from these time-sliced inputs,
- Multiply these results by 2.0055 (the factor by which a full year of 365 days is greater than a time-sliced year of 26 weeks, or 182 days) to correct for alternate-week time-slicing (Pfenninger, 2017),
- Calculate all required metrics (SSR, CO_2, IRR, MCoE) using these corrected results.

As expected, the run-time for the 1-minute resolution alternate-week time-sliced data was roughly half that for the full data (Figure 5.3). While the absolute error in IRR was less for the time-sliced 1-minute data than the full 5-minute data, the comparison was less favourable for SSR, MCoE, and especially CO_2 (Figure 5.2). Figure 5.5 directly compares the relative errors for all 8 houses, between time-sliced 1-minute and full 5-minute data.

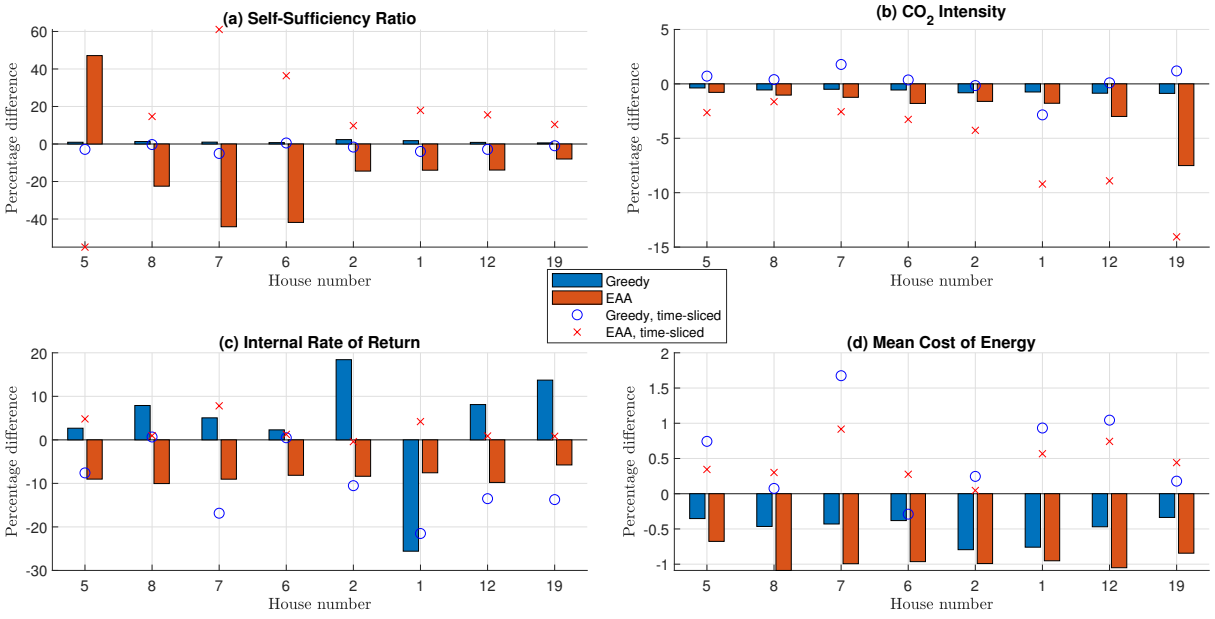

FIGURE 5.5: As in Figure 5.4 but also showing errors for 1-minute resolution time-sliced by alternate weeks, relative to 15-s resolution full data.

Given how inaccurate the results were for time-sliced 1-minute data, particularly for CO_2 intensity, the time-slicing tests were abandoned. Even alternate-week time-slicing could not achieve accuracy nor speed as high as when using the full 5-minute resolution data. Although time-slicing one week in four can halve the run-time again compared to alternate-week (one week in two) 1-minute data, even worse accuracy would be expected. Pfenninger (2017) describes a 'discontinuity effect' which can occur when discontinuous time periods are sliced together, as with alternate-week time-slicing. It can particularly affect systems with energy storage, because state of charge should only change as a result of charging/discharging the storage (and a small amount of self-discharge), and is otherwise physically required to be continuous from one timestep to the next. It cannot be claimed with certainty that this is the cause of the poor performance of 1-minute alternate-week time-slicing compared to full data at

5-minute resolution, but it is beyond the scope of this thesis to find the cause. Whether more advanced time reduction methods involving clustering can improve accuracy and run-time is left to further work. 5-minute resolution without time-slicing was used for all subsequent runs of the model.

5.2 System Components Sizing

In Chapter 1 Section 1.3.4, a number of techno-economic and life cycle analyses of second-life EV batteries in domestic applications were reviewed. They tended not to give much justification for the battery capacities they considered, beyond that specific makes of EV had batteries of that capacity. The work of Kirmas and Madlener (2017) stood out as they modelled systems with different battery capacities, showing how the optimum depends on the second-life battery cost. This sort of sensitivity analysis was much more common in the techno-economic PV-battery literature that considers new batteries (Chapter 1 Section 1.3.2).

In principle, when an LCA compares different products or processes, they must be compared on an equal footing. For example, comparing drinks cans against tetrapak cartons, the most appropriate functional unit would be a quantity of beverage contained, such as 1000 litres beverage (Klöpffer and Grahl, 2014). This focuses on the function of the products being compared, to contain beverages, unlike comparing the environmental impacts of the packaging types per unit weight or volume of packaging, for example. Even so, it cannot be assumed that the LCA results would scale with beverage quantity independently of how the functional unit is composed, that is, whether considering the manufacture of one thousand 1-litre cartons or four thousand 250-ml cartons. The cans and tetrapak cartons in this hypothetical example must be considered on a like-for-like basis in terms of the individual unit sizes as well as the functional unit.

Applying these ideas to domestic PV-battery systems, 8 different houses are being compared in this study, on the basis of the same functional unit, 1 kWh electricity consumption. As detailed in Chapter 2, and below in Table 5.2, the annual consumption varies from 2572 kWh to 6451 kWh across the dataset. The same PV, battery, converter and inverter capacities were used for all houses in the previous section to test the errors that result from reduced time resolution. But to find results for financial and environmental impacts, this unrealistic assumption cannot hold. Each homeowner would in reality be trying to install the best size system for their own house. What 'best' means is of course subjective, and involves some compromise between multiple objectives. The guiding principle in this study is that amongst all the configurations (no PV and no battery, PV only, battery only, with PV and new or second-life battery), the best should be compared to the best. This is the like-for-like basis on which the different configurations are compared, and the range of households gives an indication of the realistic variation that may be expected in the results.

The next section reviews existing literature on optimisation procedures in the context of sizing renewable energy systems. Most of these methods are more complex and computationally intensive than can be justified within the scope of this thesis. A direct search method was chosen and used to develop heuristic rules to size PV-battery systems for houses outside of the small subset tested. The results of this procedure are then shown, concluding the section.

5.2.1 Literature review of system optimisation

The problem of sizing the system components can be expressed as an optimisation problem: how should the **decision variables** (PV, battery, converter and inverter capacity, electricity tariff) be chosen in order to minimise the **objective functions** (environmental burdens, in terms of CO_2 or other impact categories, and financial costs, by any of the metrics defined in Chapter 1)?[1]

The most common optimisation method used in the techno-economic literature on domestic PV-battery systems is the direct search (Hoppmann et al., 2014; Muenzel et al., 2015; Mulder et al., 2013; Naumann et al., 2015; Truong et al., 2016; Weniger et al., 2013): the decision variable is varied and the resulting effects on the metrics, or dependent variables, are found. In the case of two decision variables such as PV capacity and battery capacity, they may be varied independently one at a time, or together to form a 2-dimensional domain. Weniger et al. (2013) did the latter, forming contour plots of self-sufficiency ratio (SSR) and mean cost of electricity (MCoE) against the axes of PV and battery capacities.

The direct search method is simple and transparent, and often categorised as a sensitivity analysis rather than an optimisation procedure. That is, answering the question "what happens to the objective function when the decision variables are varied in this way?" rather than "what values of the decision variables will optimise the objective function?" Direct search can become unwieldy when many decision variables must be considered simultaneously.

An alternative procedure that is particularly suitable in cases where linear programming is already being used for scheduling the battery, is to include the PV and battery capacities in the set of decision variables along with the battery state-of-charge at each timestep. This is what Beck et al. (2016) did, and called the 'investment and operation' mode of their model, as opposed to 'operation' mode, for which PV and battery capacity were fixed and only battery SoC allowed to vary. The EAA was designed to avoid computationally intensive scheduling procedures such as linear programming, and so this sizing method is not applicable to this study.

Many more methods exist for solving optimisation problems, as reviewed by Baños et al. (2011) in the context of renewable energy systems, beyond domestic PV-battery. PV and battery capacities commonly appear as decision variables to be optimised, in addition to other components in a micro-grid, such as wind turbines, fuel cells and diesel generators, which must also be sized. Different studies optimise for different objectives: self-sufficiency, self-consumption, peak demand reduction, emissions reduction, cost (MCoE or LCoE) minimisation, NPV maximisation, and so on.

Baños et al. (2011) categorised the optimisation methods broadly as trajectory-based or population-based. In the former category, a set of decision variables is iteratively varied and the objective function(s) calculated; the progress in approaching the objective(s) determines how the decision variables are changed in the next iteration, to bring them closer to an optimum. Examples of trajectory-based methods include hill climbing, simulated annealing, tabu search, variable neighbourhood search, and iterated local search. These differ in the details of how the decision variables are changed from one iteration to the next.

For example, hill climbing keeps track of the gradient of the trajectory towards the objective (imagining it as maximising the height one can travel to on a landscape), and directs the solution towards the steepest ascent in each iteration. By contrast, neighbourhood or local searches calculate the objective function

[1] Scheduling the battery charging/discharging can also be regarded as an optimisation problem, where the decision variables are the charge/discharge power at each timestep. This was discussed with reference to some examples in Chapter 1 Section 1.3.2, but this section is concerned with sizing rather than scheduling.

for different combinations of the decision variables close to the current set, without prior assumptions about which direction will lead the solution closer to the objective. Tabu search improves computational efficiency by forbidding calculation of the objective function for sets of decision variables that are too similar to ones that have already been calculated, assuming these would be redundant calculations. Simulated annealing allows non-monotonic progress towards the objective, with decreasing probability of accepting worse solutions as the number of iterations grows. This mimics annealing, a controlled cooling process which improves the hardness of metals, by 'shaking' the solution out of any local minima, and increasing the chance of converging on a global minimum.

In contrast, population-based methods proceed by initialising a population of sets of decision variables, and in each 'generation' changing the values of each member's decision variables until the population converges on an optimal solution. With a whole population each following a trajectory towards an optimum, more of the parameter space can be explored and it is more likely a global optimum is found. Convergence towards a local rather than global optimum is a risk of trajectory-based methods, but greater computational effort is required for population-based methods, as the objective function(s) must be calculated for every member of the population. This can be mitigated by parallelising the computation, since the calculations can be performed independently for each member within one generation. By contrast, the results of each trajectory-based iteration depend on the results of the previous iteration.

Examples of population-based methods include genetic algorithms, particle swarm optimisation, and optimisations inspired by various ecological phenomena such as ant and bee colonies (Baños et al., 2011). For example, the genetic (also known as evolutionary) algorithm mimics natural selection: only the (user-defined) fraction of the population that is closest to the objective will 'breed', or 'cross-over', to produce the next generation, whose decision variables are a random blend of those of their 'parents'. Convergence to the optimum population is improved by allowing some degree of 'mutation', or random changes in the decision variables not inherited from either 'parent', and some 'elite' fraction of the population to 'clone' themselves, or to continue unchanged into the next generation (Crossland et al., 2018). Some effort is required to tune the cross-over, mutation and elite fractions, to improve convergence speed; other optimisation methods similarly require tuning.

Baños et al. (2011) additionally reviewed the various approaches to dealing with multiple objectives, for example, minimising both MCoE and CO_2 emissions. One approach is to form a single objective function that is a weighted sum of all the objectives. This introduces the problem of how the weights should be decided. Another approach avoids this issue by framing the optimisation problem as a search not for a single optimal solution (set of decision variables), but an optimal set (of sets of decision variables). When the optimal set is plotted in objective space (a space whose dimensions are each one of the multiple objectives), the result is a Pareto front. This quantifies how an improvement in one objective comes at the cost of another objective.

To illustrate these abstract concepts, consider the example of the PV-battery system for a Swedish block of flats analysed by Zhang et al. (2017). The PV capacity was fixed at 150 kW_p, and they modelled three different operating strategies which scheduled battery charging/discharging in response to dynamic electricity price. Their decision variables were the battery capacity, and the operating parameters: price thresholds and start/end times for switching between the different modes of operation they defined. Their objective functions were NPV and SSR.

Figure 5.6 shows the Pareto fronts produced by Zhang et al. (2017) for two of their operating strategies. In both cases, the shape is convex: a diminishing increase in SSR is achieved at accelerating reduction

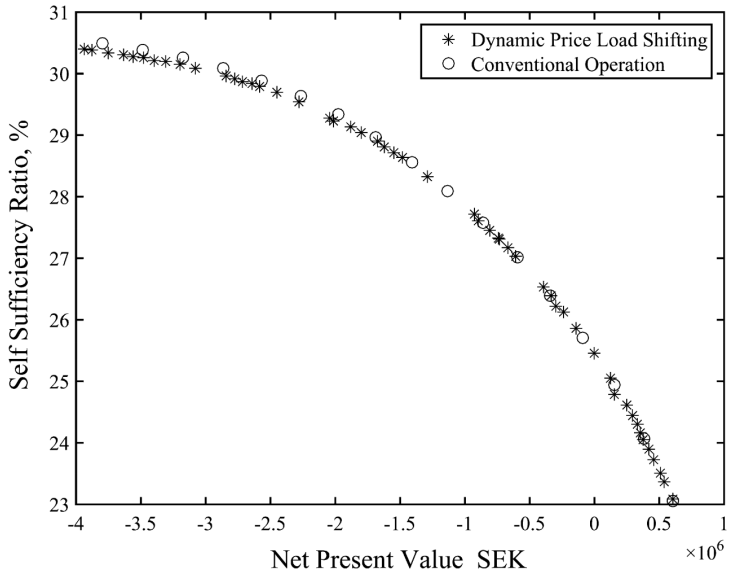

FIGURE 5.6: Pareto fronts for the Conventional Operation and Dynamic Price Load Shifting strategies, where each point represents a set of decision variables, plotted at the self-sufficiency ratio and net present value that result from that set. Taken with permission from Zhang et al. (2017).

in NPV, and vice versa. Higher SSR and lower (more negative) NPV result from larger battery capacity (shown elsewhere in their paper).

The problem with the optimisation methods described above is whether the computational effort is justified with reference to the goal and scope of this thesis. There are 8 houses, 2 grid scenarios (CR and TD), 2 algorithms (Greedy and EAA), and 3 battery types (new, best-case second-life, worst-case second-life), meaning $8 \times 2 \times 2 \times 3 = 96$ situations altogether. If, for example, a multi-objective genetic algorithm is to be run for each situation, using a population of 50 for (a conservative estimate) 100 generations (Zhang et al., 2017), that is $96 \times 50 \times 100 = 480\,000$ iterations. At 5-minute resolution, the run-time is on the order of 1 minute, meaning 333 days of continuous computation are required. This can be reduced by parallelisation and use of a supercomputing cluster such as IRIDIS at the University of Southampton (2019). While feasible, the question becomes whether or not such effort is justified.

For a real household deciding whether and how much PV and battery to install, it is unlikely that they would carry out such modelling themselves, or even that they would have acquired their own load data measured at sufficient resolution over a year. The company supplying their PV array and home battery are also unlikely to run an in-depth optimisation for every single one of their customers, given the number of customers they would be serving. Instead, they use some heuristics, or 'rules of thumb', to estimate suitable sizes of PV, battery and power electronics, based on information such as the household's annual electricity consumption.

In this context, it is not crucial that a global optimum of system component sizes be found for each house, grid scenario and battery type. Some deviation from the global optimum is to be expected when using rules of thumb, and this sub-optimality will be plausibly represented in the simulations in this study. What is more useful within the goal and scope of the thesis, is to find trends in how changing the system component sizes affect the various financial and environmental metrics.

5.2.2 Sizing the system under study

Each decision variable is subjected to a direct search one after the other, namely the capacity of PV, battery, DC-DC converter, DC-AC inverter, and choice of electricity tariff. Each one is varied while the others are held fixed. This is more decision variables than are typically considered with a direct search, but in light of the literature review above, it was judged the most suitable method in relation to the goal and scope of the thesis. The CO_2 emissions, mean cost of electricity (MCoE), payback period (PP) and return on interest (RoI) are calculated for each combination of grid scenario (CR or TD) and operating algorithm (Greedy or EAA). At this stage, a starting year of 2020 is assumed for all runs. For MCoE and RoI, cash flows are discounted at a nominal rate of 4 %; all monetary sums are inflation-adjusted at annual rate 2.1 % to 2019 GBP.

Strictly speaking, other environmental impact categories besides climate change (CC) ought to be calculated as well, but it is difficult to conceptualise so many metrics simultaneously. Instead, CC impact minimisation is taken as one of the objectives, and the resultant effects on the other impact categories are reported in the next chapter.

PP was not calculated in the time resolution testing because the way it is defined (Chapter 1 Section 1.1), PP is an integer number of years, and this is insufficient granularity to show the effects of varying time resolution. The effects of varying the aforementioned decision variables are comparatively larger, and so it is worthwhile to consider PP as one of the financial metrics. Cash flows are not discounted in calculating PP, and replacement costs for battery and BoS are excluded. The result is therefore an under-estimate of how long it can be expected to take for savings to fully pay back the initial Capex, but is nonetheless a useful indicator of how much longer the battery lifetime needs to be.

To save time, only the highest- and lowest- consuming houses (5 and 19 respectively) are tested in this section. All tests are run at 5-minute resolution. In this way heuristic rules for component sizing are developed to encompass the other houses too.

5.2.2.1 PV Capacity

To begin with, the other parameters are set arbitrarily thus:

- Battery capacity: $E_B = \frac{\text{[Annual electricity consumption]}}{1000}$ kWh,
- Battery DC-DC converter rating: $P_{conv} = (\frac{E_B}{5 \text{ hours}})$, i.e. C/5,
- DC-AC inverter rating: 3 kW,
- Electricity tariff: flat-rate.

This means 6.45 kWh of battery with a 1.29 kW converter for House 5 (annual consumption 6451 kWh), and 2.57 kWh/ 0.51 kW for House 19 (2572 kWh).

The greater the PV capacity, the less the CO_2 emissions per kWh consumed, for both algorithms, both grid scenarios, and both houses (Figures 5.7 and 5.8). If minimising CO_2 emissions were the only objective, the solution would be to install as much PV as the roof can support.

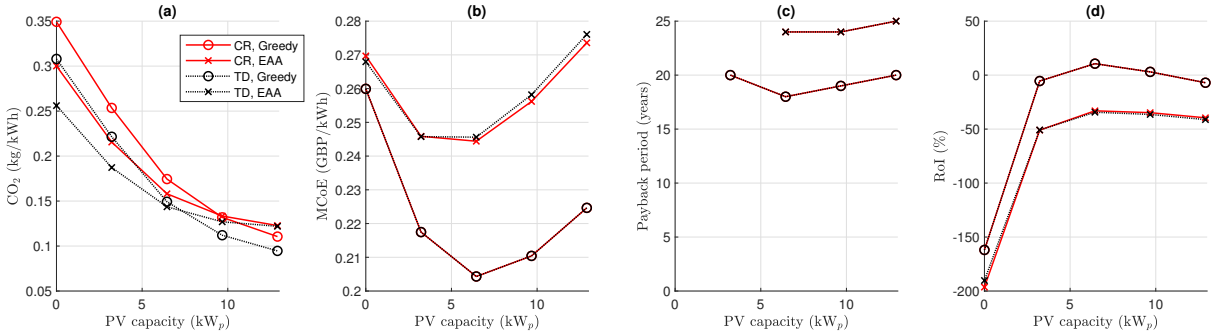

FIGURE 5.7: House 5's (a) CO_2 emissions intensity, (b) MCoE, (c) PP, (d) RoI, as a function of PV capacity, given a 6.45 kWh/ 1.29 kW battery, 3 kW inverter, and flat-rate tariff.

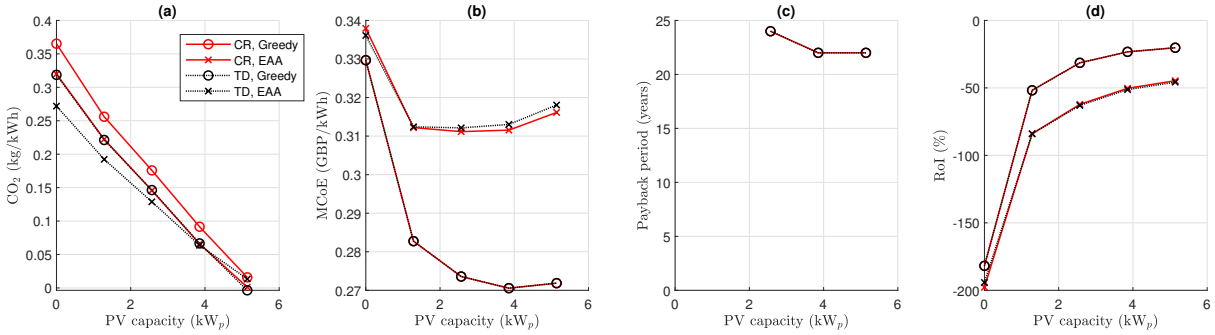

FIGURE 5.8: House 19's (a) CO_2 emissions intensity, (b) MCoE, (c) PP, (d) RoI, as a function of PV capacity, given a 2.57 kWh/ 0.51 kW battery, 3 kW inverter, and flat-rate tariff.

For House 5, the minimal MCoE and PP and maximal RoI occur around 6.45 kW_p; for House 19, around 4 kW_p, although minimising MCoE favours a slightly smaller array compared to optimising for PP or RoI. (PP longer than the 25-year temporal boundary are excluded from the graphs.) It is not surprising that an optimum exists for financial metrics but not environmental ones (at least not CO_2 emissions): PV export to the grid is rewarded at a lower rate than the cost of electricity (0.05 GBP/kWh compared to 0.157 GBP/kWh), whereas the environmental costs of importing grid electricity are the same per kWh as the costs displaced by exporting to the grid. This means from a CO_2 perspective, the more PV the better; but financially, PV is most effective when it is helping the household to avoid grid import rather than when it is exporting. As PV capacity is increased, an increasing proportion of generation is exported rather than consumed onsite, and so accrue diminishing returns compared to the increasing cost of installing more PV.

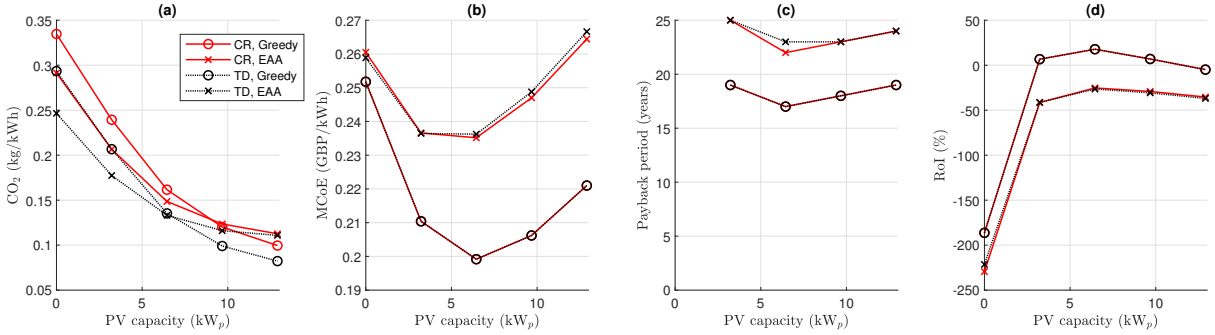

FIGURE 5.9: House 5 with a best-case second-life battery: (a) CO_2 emissions intensity, (b) MCoE, (c) PP, (d) RoI, as a function of PV capacity, given a 6.45 kWh/ 1.29 kW battery, 3 kW inverter, and flat-rate tariff.

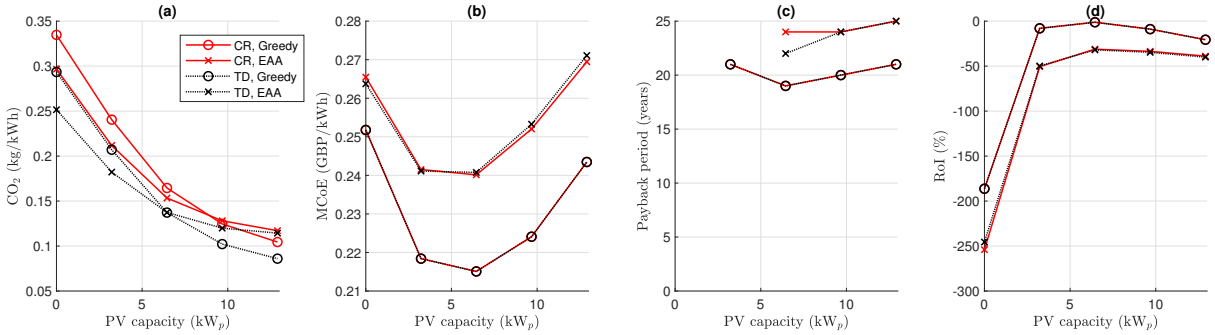

FIGURE 5.10: House 5 with a worst-case second-life battery: (a) CO_2 emissions intensity, (b) MCoE, (c) PP, (d) RoI, as a function of PV capacity, given a 6.45 kWh/ 1.29 kW battery, 3 kW inverter, and flat-rate tariff.

Although the values of MCoE, PP and RoI are different when considering second-life rather than new batteries, the trends are the same for House 5, whose finances are still optimised around 6.45 kW_p. For House 19, finances are optimised around 4 kW_p of PV with a new or best-case second-life battery.

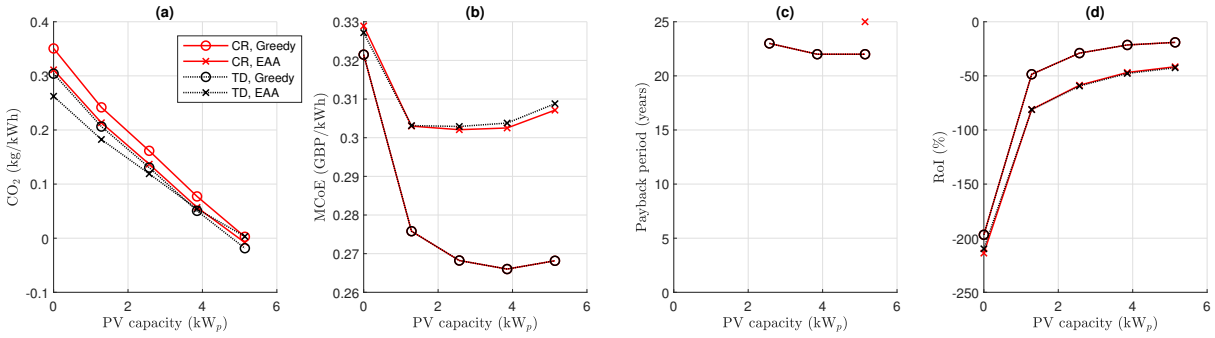

FIGURE 5.11: House 19 with a best-case second-life battery: (a) CO_2 emissions intensity, (b) MCoE, (c) PP, (d) RoI, as a function of PV capacity, given a 2.57 kWh/ 0.51 kW battery, 3 kW inverter, and flat-rate tariff.

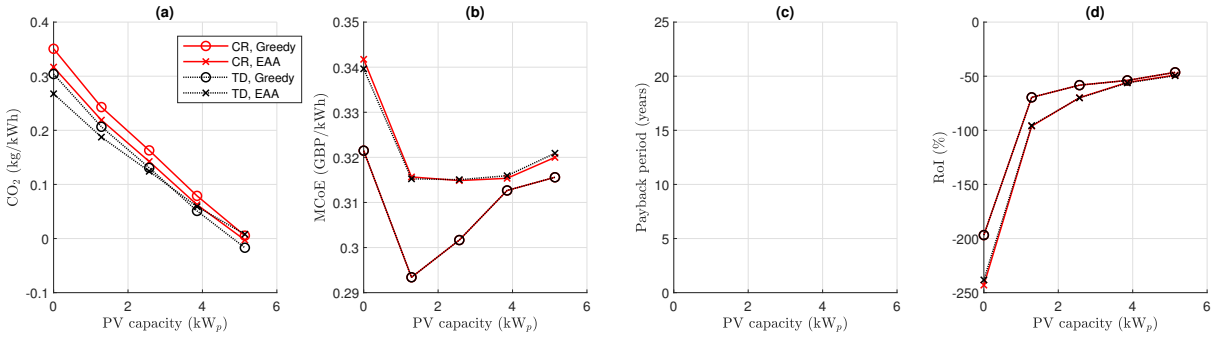

FIGURE 5.12: House 19 with a worst-case second-life battery: (a) CO_2 emissions intensity, (b) MCoE, (c) PP (none shown because all cases exceed 25 years), (d) RoI, as a function of PV capacity, given a 2.57 kWh/ 0.51 kW battery, 3 kW inverter, and flat-rate tariff.

But for a worst-case second-life battery running the Greedy algorithm, MCoE is minimised around 1.2 kW_p of PV. However, 4 kW_p is still a better option when considering RoI. No PP data are shown in Figure 5.12 (c) because the investment is not paid back within the 25-year temporal boundary for House 19 in any cases.

In consideration of these facts, the following heuristic rule for PV array sizing is adopted:

$$P_{PV} = \left(2 + \frac{[\text{Annual electricity consumption in kWh}]}{2000}\right) \quad \text{kW}_p. \tag{5.1}$$

For House 5 this means PV capacity 5.23 kW_p; for House 19, 3.29 kW_p. It is assumed that the homeowner does not know beforehand whether the second-life battery they purchased is closer to a best-case or worst-case one, and so cannot make any sizing decisions based on this piece of information.

5.2.2.2 Battery Capacity

Using the arbitrary default parameters defined for the PV capacity sizing, but with PV capacity itself set by the heuristic rule (5.1), the battery capacity E_B is now varied.

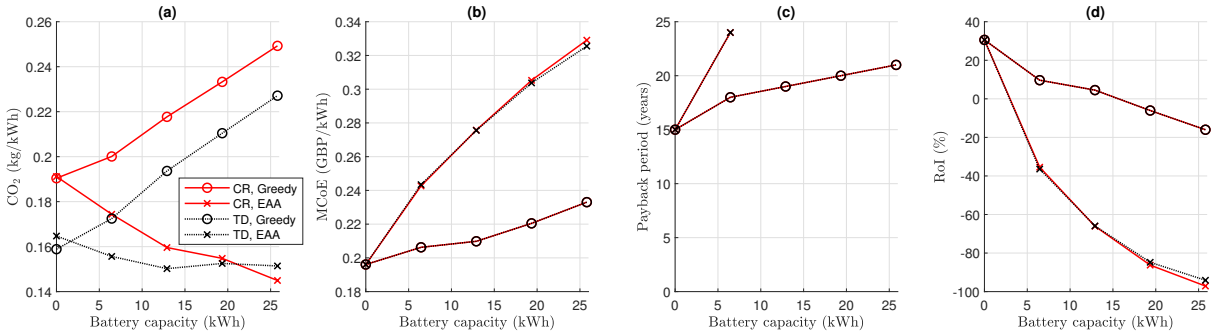

FIGURE 5.13: House 5's (a) CO_2 emissions intensity, (b) MCoE, (c) PP, (d) RoI, as a function of battery capacity, given a 0.2 C-rate battery converter, 5.23 kW_p PV, 3 kW inverter, and flat-rate tariff.

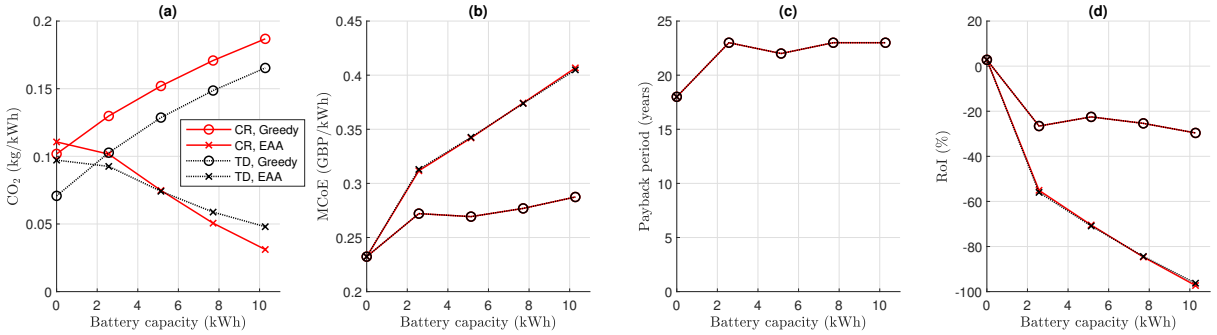

FIGURE 5.14: House 19's (a) CO_2 emissions intensity, (b) MCoE, (c) PP, (d) RoI, as a function of battery capacity, given a 0.2 C-rate battery converter, 3.29 kW_p PV, 3 kW inverter, and flat-rate tariff.

For both houses, grid scenarios and algorithms, MCoE and PP increase and RoI decreases with increasing battery capacity (Figures 5.13 and 5.14). From a financial perspective, the optimal size of battery is zero. With the Greedy algorithm, CO_2 emissions are also minimised by zero battery. But with the EAA, CO_2 emissions are reduced by increasing battery capacity.

In consideration of these facts, the following heuristic rule is adopted for sizing the new battery pack:

$$E_B = \left(3 + \frac{[\text{Annual electricity consumption}]}{2000}\right) \quad \text{kWh}. \tag{5.2}$$

For House 5 this means battery capacity 6.23 kWh; for House 19, 4.29 kWh. With the EAA, it is not possible to optimise for CO_2 emissions and finances simultaneously, but having this size of battery allows for exploration of the relationship between financial and environmental costs. These sizes are also used with the Greedy algorithm, to quantify how much worse it is than PV only, in terms of CO_2 emissions. But as found by the author (Sun et al., 2020), PV-battery running the Greedy algorithm can actually save CO_2 relative to PV-only, if the system is installed later in future. The sensitivity to investment start date is analysed in the next chapter.

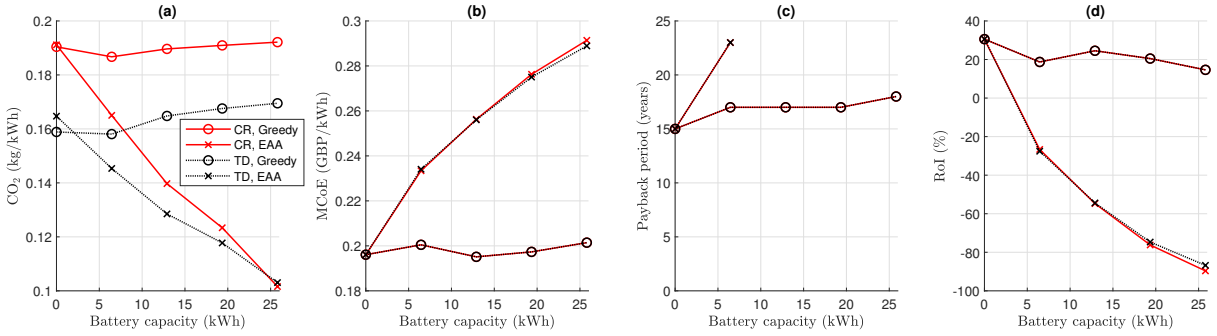

FIGURE 5.15: House 5 with a best-case second-life battery: (a) CO_2 emissions intensity, (b) MCoE, (c) PP, (d) RoI, as a function of battery capacity, given a 0.2 C-rate battery converter, 5.23 kW_p PV, 3 kW inverter, and flat-rate tariff.

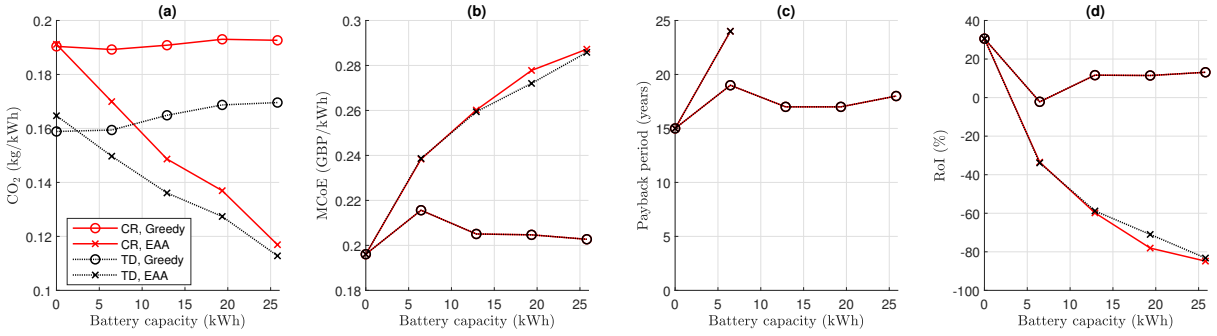

FIGURE 5.16: House 5 with a worst-case second-life battery: (a) CO_2 emissions intensity, (b) MCoE, (c) PP, (d) RoI, as a function of battery capacity, given a 0.2 C-rate battery converter, 5.23 kW_p PV, 3 kW inverter, and flat-rate tariff.

For House 5 with a second-life battery running the Greedy algorithm, CO_2 emissions are minimised at 6.45 kWh (original first-life) capacity, at which point all financial metrics are maximally bad (locally for a best-case second-life battery, Figure 5.15, and globally for a worst-case one, Figure 5.16). MCoE is minimised at 12.9 kWh for a best-case second-life battery running the Greedy algorithm, but PP and RoI are optimised at zero battery. With the EAA, the more battery the less emissions, for second-life as for new batteries. This is also true for House 19, for which all financial metrics are optimised at zero battery, no matter the algorithm and whether new or second-life, best-case or worst-case.

To allow fair comparison between new and second-life batteries, equivalent sizes of each must be used. What 'equivalent' means is not straightforward: should this study compare new and second-life batteries of equal usable capacity, equal initial cost, or some other measure of equivalence? If comparing batteries of equal usable capacity, such batteries are still not equivalent because the second-life ones would have greater internal resistance (lower efficiency) than the new one. If sizing on the basis of equal initial costs, this is not necessarily a guarantee of equal value.

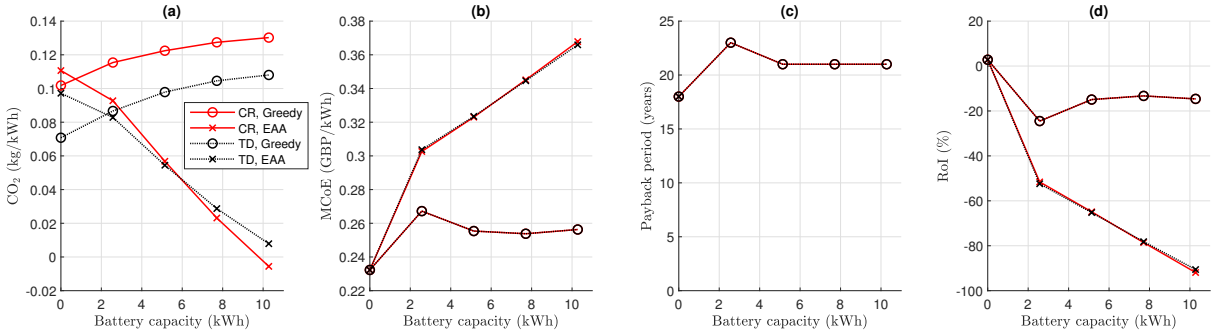

FIGURE 5.17: House 19 with a best-case second-life battery: (a) CO_2 emissions intensity, (b) MCoE, (c) PP, (d) RoI, as a function of battery capacity, given a 0.2 C-rate battery converter, 3.29 kW_p PV, 3 kW inverter, and flat-rate tariff.

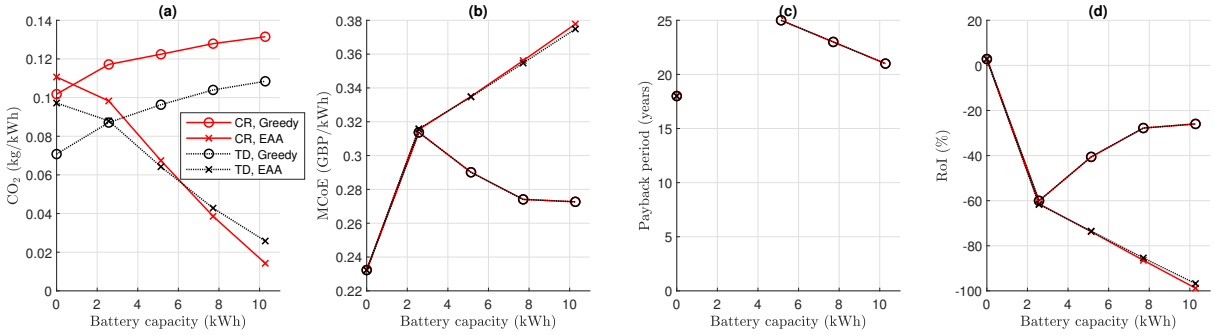

FIGURE 5.18: House 19 with a worst-case second-life battery: (a) CO_2 emissions intensity, (b) MCoE, (c) PP, (d) RoI, as a function of battery capacity, given a 0.2 C-rate battery converter, 3.29 kW_p PV, 3 kW inverter, and flat-rate tariff.

Logically, the fairest comparison would be between the optimal size of new battery, and the optimal size of second-life battery: in a hypothetical situation where the homeowner has all the required information, they would compare the best that each can offer. This would not necessarily lead to new and second-life batteries of equal usable capacity or equal initial cost. The problem, as has been demonstrated so far, is that there is conflict between the different metrics and therefore no single optimal size of new nor second-life battery.

As a compromise, for this study, the second-life battery is sized thus:

$$E_{B,2} = E_{B,1} \times \left(1 + \frac{[\text{Annual electricity consumption}]}{6000}\right) \quad \text{kWh.} \tag{5.3}$$

where $E_{B,1}$ is the capacity of a new battery as set by rule (5.2), and $E_{B,2}$ the capacity of the second-life battery to be compared. For House 5, this means a second-life battery capacity of 12.9 kWh (original size, or 10.3 kWh usable at the start of the second life); for House 19, 6.12 kWh (original, 4.90 kWh usable). This avoids the local peak in MCoE and PP and the local trough in RoI associated with using a second-life battery of the same capacity as the new battery. The other consideration was that lower-consuming households suffer a greater financial penalty from over-sizing their battery: so while House 5 compares a second-life battery of roughly double the capacity of a new one, House 19 compares one only 1.4 times the capacity of a new one, according to rule (5.3).

Note that with a best-case second-life battery, typically one replacement is needed within the 25-year temporal boundary, as is also the case with a new battery. With a worst-case second-life battery, two or

three replacements are needed in that time. The fixed cost of 1500 GBP (see Chapter 2 Section 2.4.2) is incurred with each replacement.

5.2.2.3 Battery DC-DC Converter Rating

Using the default parameters defined for the PV capacity sizing, but with PV and battery capacities set by the heuristic rules (5.1)-(5.3), the battery DC-DC converter rating P_{conv} is now varied.

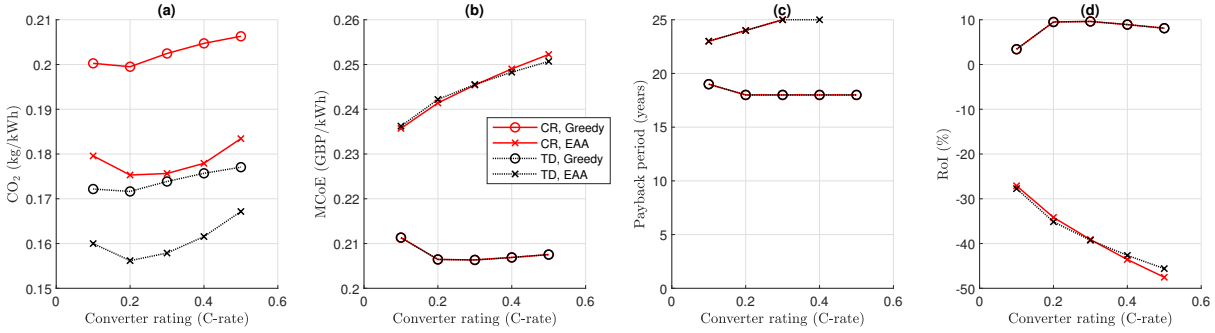

FIGURE 5.19: House 5's (a) CO_2 emissions intensity, (b) MCoE, (c) PP, (d) RoI, as a function of battery converter rating, given 5.23 kW_p PV, 6.23 kWh battery, 3 kW inverter, and flat-rate tariff.

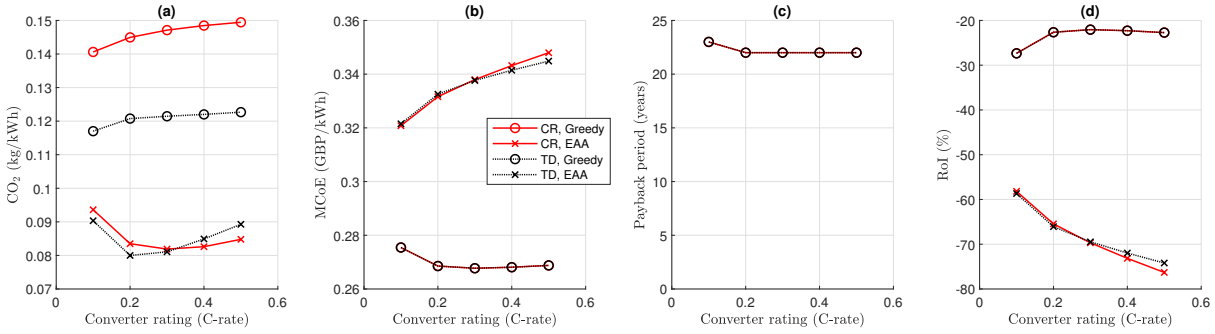

FIGURE 5.20: House 19's (a) CO_2 emissions intensity, (b) MCoE, (c) PP, (d) RoI, as a function of battery converter rating, given 3.29 kW_p PV, 4.29 kWh battery, 3 kW inverter, and flat-rate tariff.

The first observation from Figures 5.19 and 5.20 is that the effects of varying the converter rating are small compared to those of varying the other component sizes. This is unsurprising as the embodied environmental cost and the size-dependent portion of the converter cost is small compared to that of the PV and battery (see Chapter 2 Section 2.4). The second observation is that with the Greedy algorithm, all metrics, financial and environmental, can be optimised for House 5 by setting $P_{conv} = (0.2E_B)$ kW. With the EAA, this converter rating also tends to minimise CO_2 emissions; but financial metrics are improved by lower converter rating. The same is true for House 19 except that, in the case of the Greedy algorithm, there is little difference in the financial metrics above $P_{conv} = (0.2E_B)$ kW, and CO_2 emissions with the Greedy algorithm are minimised at lower converter rating.

With second-life batteries, for House 5, CO_2 emissions are minimised by lowering the converter rating in all cases. With the EAA, financial metrics are again improved by lowering the converter rating. But with the Greedy algorithm, there is still a small optimum in the financial metrics around $P_{conv} = (0.2E_B)$ kW.

Similar observations are made for second-life batteries for House 19, except that $P_{conv} = (0.2E_B)$ kW does minimise CO_2 emissions for the EAA, and MCoE and RoI are improved at lower converter rating.

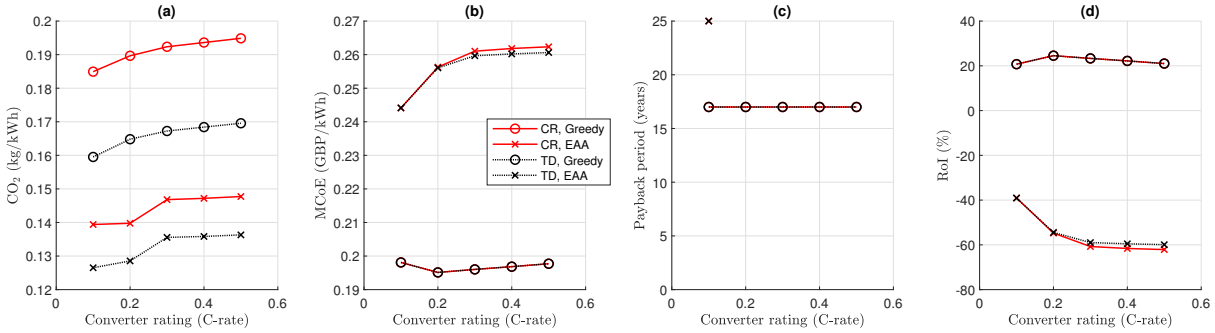

FIGURE 5.21: House 5 with a best-case second-life battery: (a) CO_2 emissions intensity, (b) MCoE, (c) PP, (d) RoI, as a function of battery converter rating, given 5.23 kW_p PV, 12.9 kWh battery (10.3 kWh usable), 3 kW inverter, and flat-rate tariff.

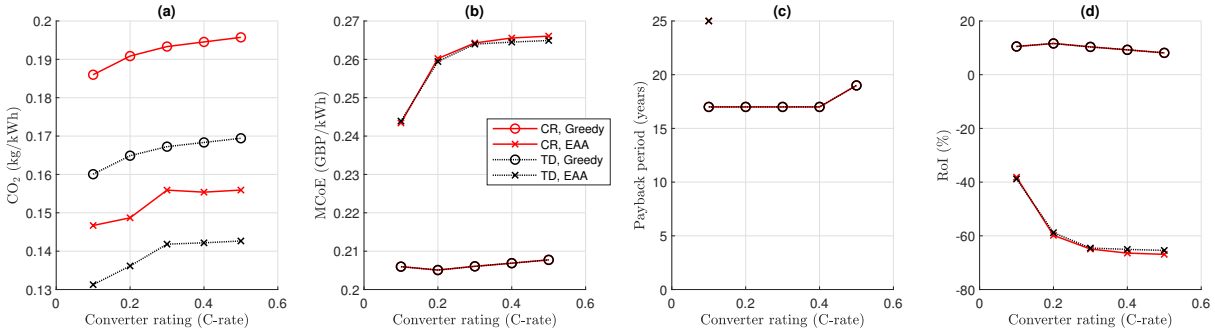

FIGURE 5.22: House 5 with a worst-case second-life battery: (a) CO_2 emissions intensity, (b) MCoE, (c) PP, (d) RoI, as a function of battery converter rating, given 5.23 kW_p PV, 12.9 kWh battery (10.3 kWh usable), 3 kW inverter, and flat-rate tariff.

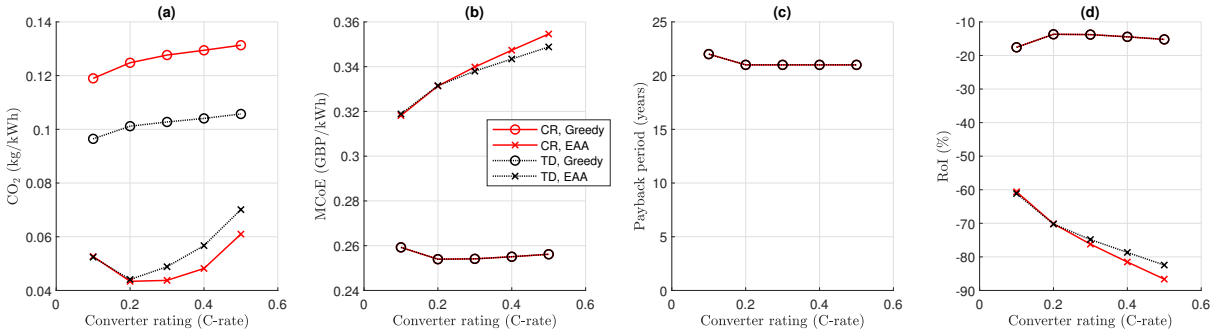

FIGURE 5.23: House 19 with a best-case second-life battery: (a) CO_2 emissions intensity, (b) MCoE, (c) PP, (d) RoI, as a function of battery converter rating, given 3.29 kW_p PV, 6.12 kWh battery (4.90 kWh usable), 3 kW inverter, and flat-rate tariff.

The differences are not large in any case, and so the battery DC-DC converter is sized thus:

$$P_{conv} = \left(\frac{E_B}{5 \text{ hours}} \right) \text{ kW}. \tag{5.4}$$

5.2.2.4 DC-AC Inverter Rating

A range of DC-AC inverter ratings P_{inv} were tested, for a system sized according to heuristic rules (5.1)-(5.4) for PV, battery and DC-DC converter. The DC-AC inverter rating is capped at 3.68 kW. This is because of Engineering Recommendation G98 (ENA, 2018), which governs the installation of low-voltage

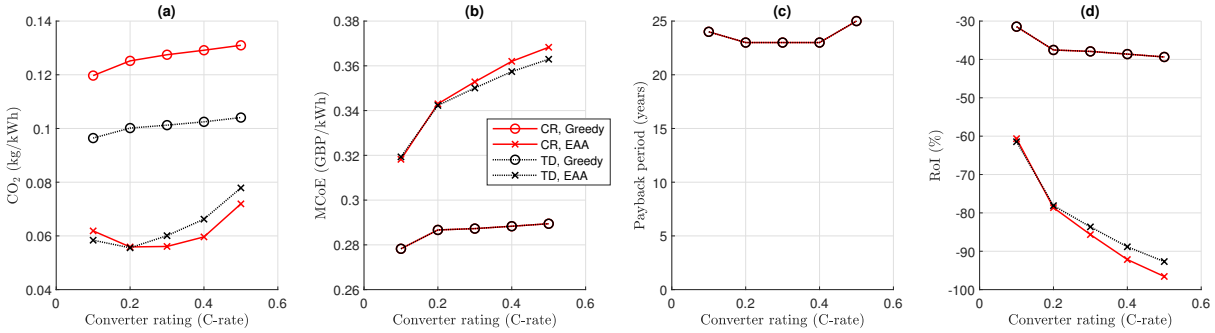

FIGURE 5.24: House 19 with a worst-case second-life battery: (a) CO_2 emissions intensity, (b) MCoE, (c) PP, (d) RoI, as a function of battery converter rating, given 3.29 kW_p PV, 6.12 kWh battery (4.90 kWh usable), 3 kW inverter, and flat-rate tariff.

micro-generation systems feeding not more than 16 A (3.68 kW) into the grid. Such systems must comply with all the regulations in G98 before they are allowed to connect to the distribution network. One way to demonstrate compliance is by using only equipment on the approved list of G98-compliant products. For larger systems, permission to connect can be sought from the distribution network operator (DNO), but is not guaranteed. Therefore for simplicity, the 3.68 kW cap is applied at the level of the inverter.

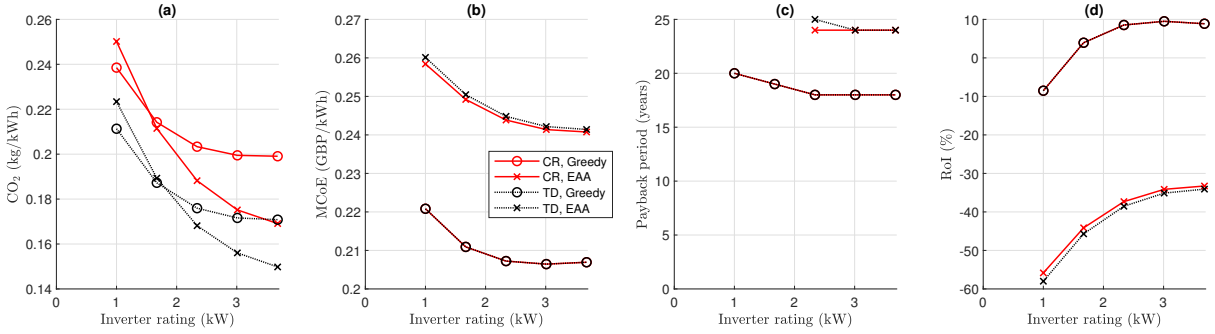

FIGURE 5.25: House 5's (a) CO_2 emissions intensity, (b) MCoE, (c) PP, (d) RoI, as a function of inverter rating, given 5.23 kW_p PV, 6.23 kWh/ 1.25 kW battery, and flat-rate tariff.

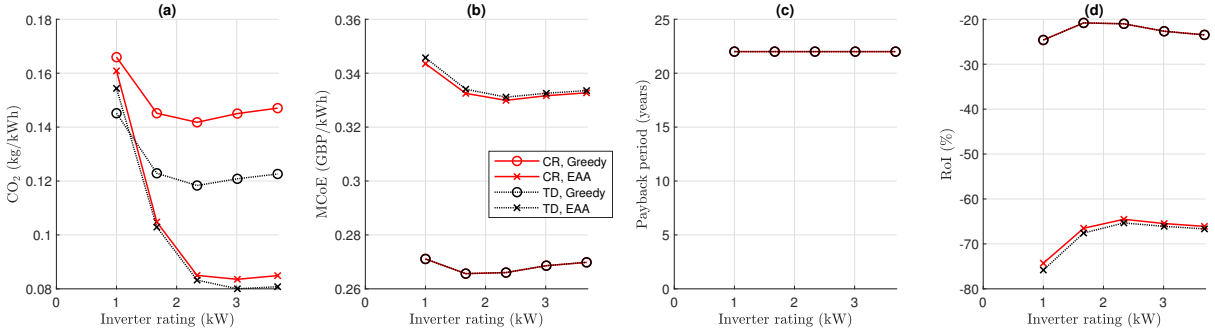

FIGURE 5.26: House 19's (a) CO_2 emissions intensity, (b) MCoE, (c) PP, (d) RoI, as a function of inverter rating, given 3.29 kW_p PV, 4.29 kWh/ 0.86 kW battery, and flat-rate tariff.

For House 5, all metrics, financial and environmental, are improved by increasing the inverter rating up to the 3.68 kW cap (Figure 5.25), although there is little difference above 3 kW. For House 19, all metrics, financial and environmental, are optimised around $P_{inv} = 2$ kW (Figure 5.26). This is true for both algorithms and both grid scenarios. That there is an optimum is not surprising because there is a cost to over-sizing the inverter: a small financial one, but also a loss in efficiency, as power

electronics efficiency is greatest when power throughput is close to maximum. Even though 4.15 kW could theoretically be required to flow through the inverter, when the 3.29 kW_p PV is generating at its maximum simultaneously to the battery discharging at its maximum 0.86 kW, this would be over-sizing because PV arrays at GB latitudes rarely generate at their maximum rating. Figure 5.26 shows that above $P_{inv} = 2$ kW, the benefits of reduced curtailment of PV generation are outweighed by costs associated with decreasing efficiency due to over-sizing the inverter.

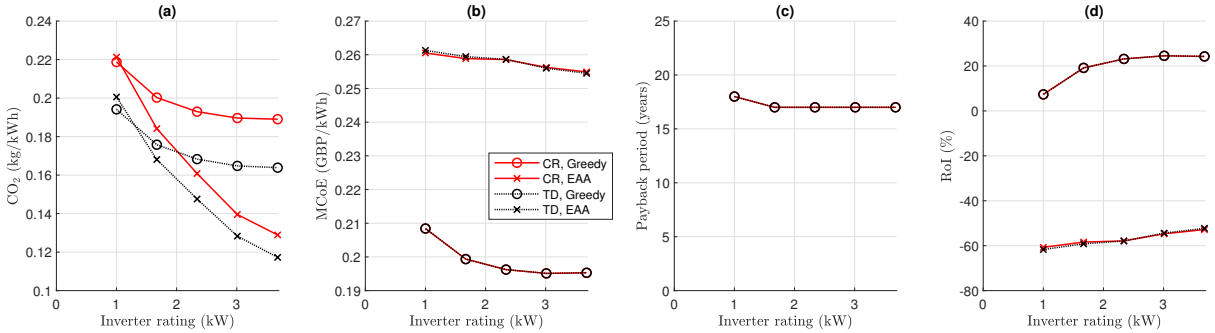

FIGURE 5.27: House 5 with a best-case second-life battery: (a) CO_2 emissions intensity, (b) MCoE, (c) PP, (d) RoI, as a function of inverter rating, given 3.29 kW_p PV, 12.9 kWh (10.3 kWh usable)/ 2.58 kW battery, and flat-rate tariff.

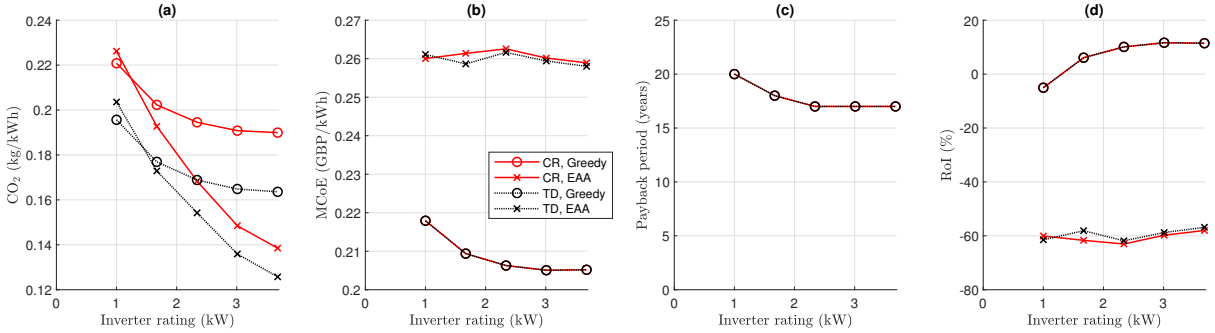

FIGURE 5.28: House 5 with a worst-case second-life battery: (a) CO_2 emissions intensity, (b) MCoE, (c) PP, (d) RoI, as a function of inverter rating, given 3.29 kW_p PV, 12.9 kWh (10.3 kWh usable)/ 2.58 kW battery, and flat-rate tariff.

The optimal inverter ratings for House 5 and House 19 are similar for second-life batteries (Figures 5.27-5.30) as for new.

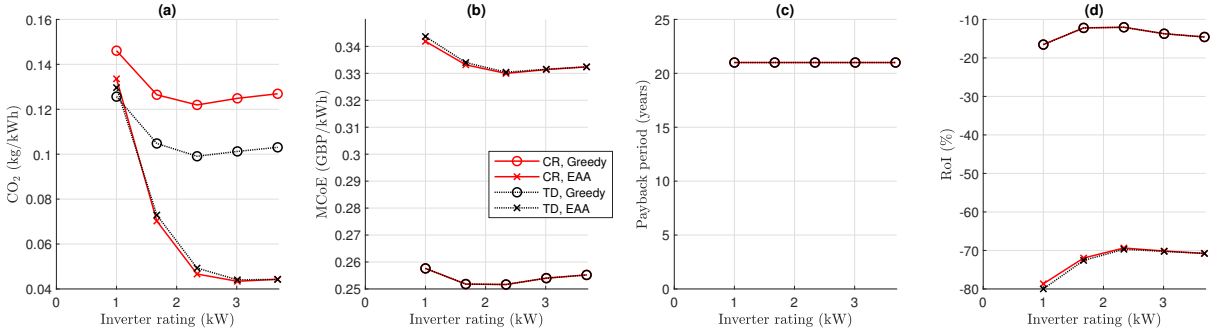

FIGURE 5.29: House 19 with a best-case second-life battery: (a) CO_2 emissions intensity, (b) MCoE, (c) PP, (d) RoI, as a function of inverter rating, given 3.29 kW_p PV, 6.12 kWh (4.90 kWh usable)/ 1.22 kW battery, and flat-rate tariff.

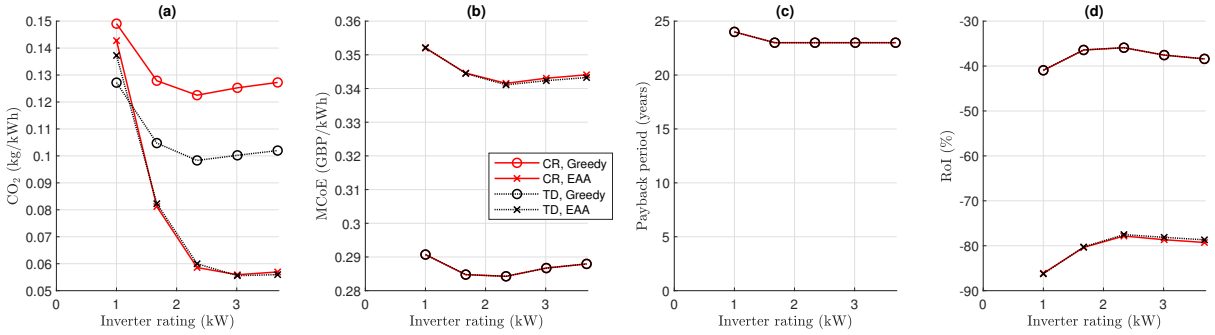

FIGURE 5.30: House 19 with a worst-case second-life battery: (a) CO_2 emissions intensity, (b) MCoE, (c) PP, (d) RoI, as a function of inverter rating, given 3.29 kW_p PV, 6.12 kWh (4.90 kWh usable)/ 1.22 kW battery, and flat-rate tariff.

Bearing in mind the dependence of the optimal inverter rating on both the PV capacity and the battery DC-DC converter rating, the following heuristic rule is developed:

$$P_{inv} = \texttt{min}\left(\left[3.68 \text{ kW}, 0.5(P_{PV} + P_{conv})\right]\right). \tag{5.5}$$

This means P_{inv} capped at 3.68 kW for House 5 with a second-life battery (otherwise it would be 3.90 kW). For House 19, P_{inv} is 2.07 kW for a new battery, or 2.25 kW for a second-life battery. For the PV-only configuration, which is run for each house to provide a comparison for PV-battery, the DC-AC inverter rating is taken as:
$P_{inv} = \texttt{min}\left(\left[3.68 \text{ kW}, 0.8 \cdot P_{PV}\right]\right)$.

These findings for battery DC-DC converter and DC-AC inverter ratings were repeated at 15-s resolution for confirmation, because Beck et al. (2016) had shown that the optimal power rating is more sensitive to time resolution errors than the optimal PV and battery capacities. The findings at 5-minute were confirmed at 15-s resolution. As Beck et al. (2016) recommended, 5-minute is in fact sufficiently high resolution to size the system's power rating.

5.2.2.5 Electricity Tariff

So far the financial metrics have been calculated on the basis of a flat-rate tariff. In reality, the homeowner can choose from a range of tariffs. While it may appear fair to compare different configurations (with/without new/second-life battery) on the same tariff, it may be that different tariffs minimise costs for different configurations. For example, a PV-battery system on Economy 7 may save money compared to without PV nor battery, on Economy 7, but cost more than the no-PV-no-battery system on a flat-rate tariff. In such a case, the PV-battery system would be more costly than no PV and no battery, but the opposite conclusion would be found if they were compared only on the Economy 7 tariff. Therefore this thesis compares the different configurations based on the lowest-cost tariff for each. For simplicity, the choice of tariffs is restricted to flat-rate, Economy 7 and Green Energy (2019) Tide, as described in Chapter 2 Section 2.4.4.

Each house was run with the components of the PV-battery system optimised according to heuristic rules (5.1)-(5.5), with the Greedy algorithm and the EAA in CR and TD scenarios. In each case, MCoE is calculated on each of the three tariffs. These are plotted in Figure 5.31 for a new battery, 5.32 for

a best-case second-life battery, and 5.33 for a worst-case second-life battery. MCoE is used rather than IRR, RoI or PP, because the way the latter three are defined, they calculate savings compared to having no PV and no battery assuming the same tariff. The environmental impacts are independent of the electricity tariff, and are not considered in this section.

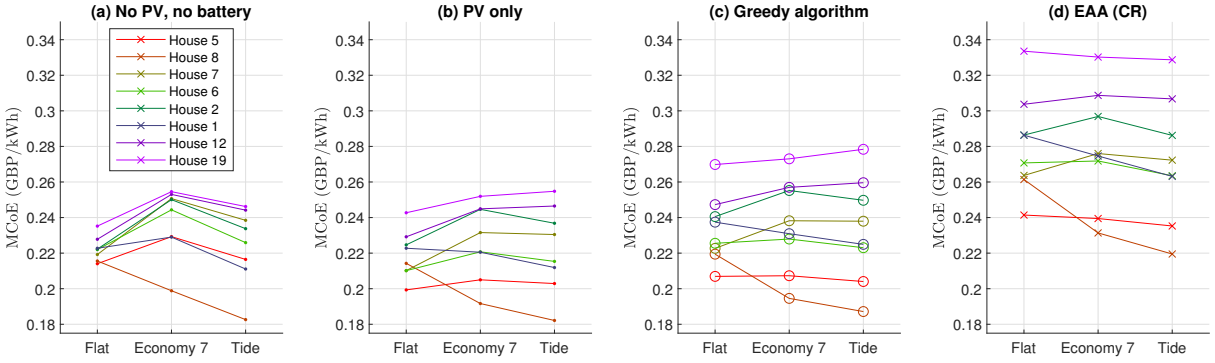

FIGURE 5.31: MCoE comparing flat-rate, Economy 7 and Tide tariffs (new battery), for (a) no PV and no battery, (b) PV only, (c) optimised PV-battery running the Greedy algorithm, (d) running the EAA under CR grid scenario.

Figures 5.31-5.33 also show MCoE for all houses with no PV and no battery, and with PV only, alongside the PV-battery cases. (Despite the fact the first two graphs are the same in all three figures, they are included for ease of comparison). Since the Greedy algorithm schedules the battery according to instantaneous PV generation and household load, it is the same between the CR and TD grid scenarios. On the other hand, the EAA schedules the battery according to marginal grid CO_2 intensity, which differs between CR and TD scenarios. Nonetheless, the difference in MCoE values between CR and TD is small and the trends identical, and so EAA under only CR is shown.

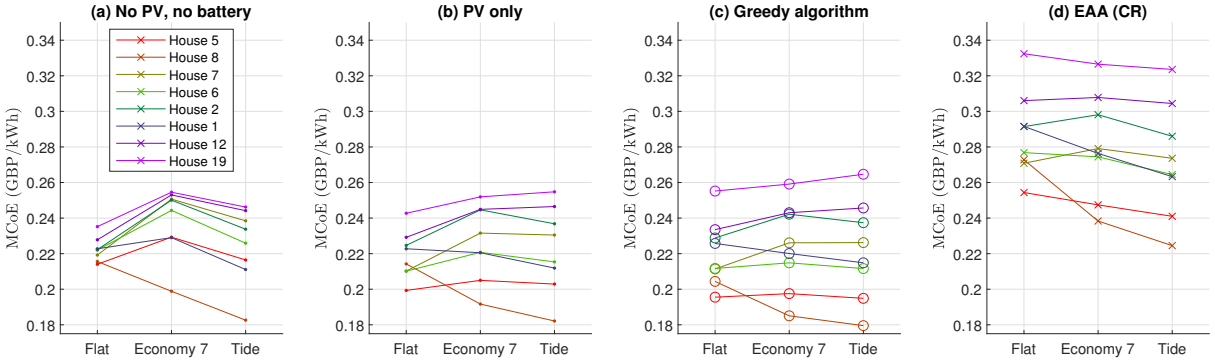

FIGURE 5.32: MCoE comparing flat-rate, Economy 7 and Tide tariffs (best-case second-life battery), for (a) no PV and no battery, (b) PV only, (c) optimised PV-battery running the Greedy algorithm, (d) running the EAA under CR grid scenario.

In nearly all cases, the Economy 7 tariff leads to higher MCoE than with a flat-rate tariff. The exception is House 8, which according to Figure 5.34, regularly consumes more of its electricity at night than the other houses, perhaps using a night storage heater. This suggests that the real house from which the data were taken may already be on Economy 7 and have actively made arrangements to make best use of the tariff. The Tide tariff is structured similarly to Economy 7 but with an additional higher rate on weekday afternoons; it is not surprising that House 8, which makes such good use of Economy 7, could save even more money on the Tide tariff.

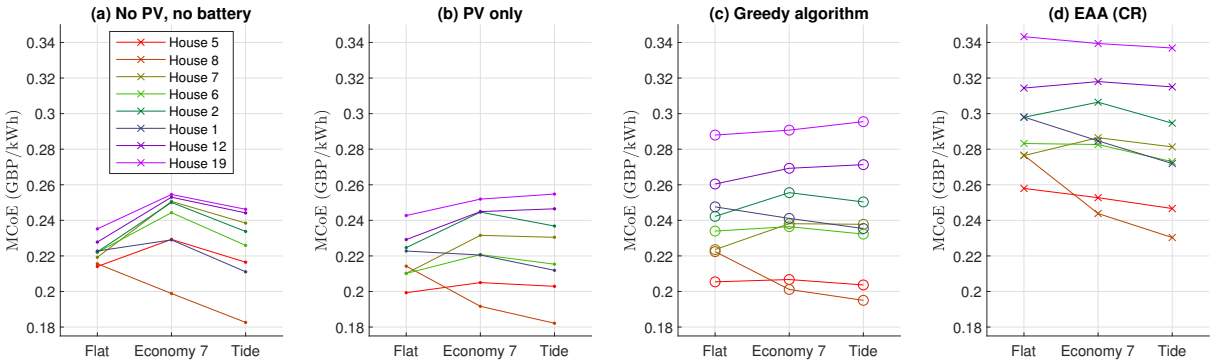

FIGURE 5.33: MCoE comparing flat-rate, Economy 7 and Tide tariffs (worst-case second-life battery), for (a) no PV and no battery, (b) PV only, (c) optimised PV-battery running the Greedy algorithm, (d) running the EAA under CR grid scenario.

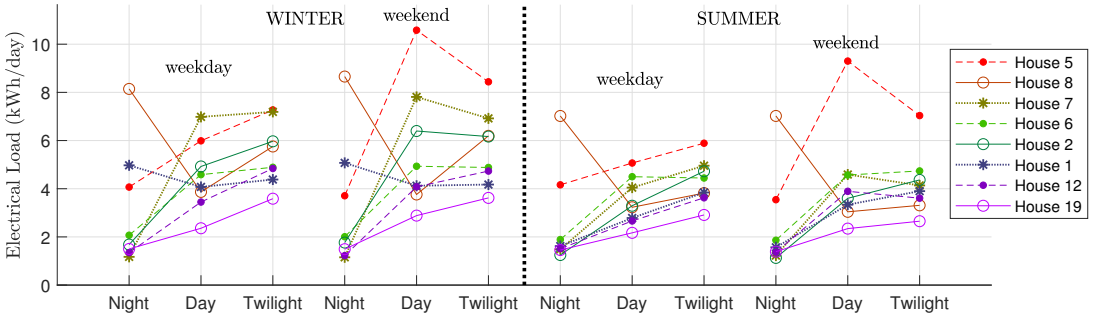

FIGURE 5.34: Each house's electrical load (kWh/day) during hours of night (Economy 7 hours, 00:00-07:00), day (typical sunlight hours, 08:30-17:00) and twilight (07:00-08:30, 17:00-00:00), at weekdays and weekends, and comparing 'winter' (November-April) and 'summer' (May-September).

With no battery and no PV, the cheapest tariff is flat-rate for all houses except 8 and 1, for which the Tide tariff is cheapest. In this configuration, MCoE occupies a narrow range 0.215-0.237 GBP/kWh with the flat-rate tariff. This is larger than the 2018 average unit rate of 0.1537 GBP/kWh reported in Chapter 2 Section 2.4.4, because electricity prices are projected to increase faster than inflation. The reason that MCoE is not identical for all houses on a flat-rate tariff is because the standing charge occupies a different proportion of their total bills relative to the per-kWh charges: a greater proportion for lower-consuming houses, and a smaller proportion for higher-consuming ones.

Adding PV but no battery, the cheapest tariff for each house is the same as before. Economy 7 still tends to be worse than the flat-rate tariff, but to a lesser extent than without PV, and is actually better than flat-rate in the case of House 1 (though Tide is still even better). This observation can be explained by the fact that the least electricity consumption occurs during the night (except for House 8, and House 1 on winter nights, see Figure 5.34), and the day-time unit rate on Economy 7 is higher than the flat-rate unit rate. Because of this, PV generation displacing some grid import during the day reduces households' exposure to the higher day-time unit rate, making a more dramatic saving on Economy 7 than on the flat-rate tariff.

With a battery running the Greedy algorithm, the cheapest tariff for each house is the same as before, with the exception of House 5. MCoE is almost the same regardless of which tariff it is on, but the Tide tariff is the cheapest.

With a battery running the EAA, the cheapest tariff is Tide for every house except Houses 7 and 12,

for which the flat-rate tariff is still cheapest. It is unsurprising that for most houses, Tide would be the cheapest tariff with an EAA-running battery. The EAA schedules discharging of the battery and therefore reduced grid import during times of high grid CO_2 intensity, and vice versa at times of low grid CO_2 intensity. There is some correlation between CO_2 intensity and electricity price on the Tide tariff: the highest-price periods are weekday afternoons, when national demand tends to be highest (Gridwatch, 2018) and low-carbon generators may not be sufficient to meet it. More high-carbon generating power is called upon in those high-price periods, pushing up the marginal grid CO_2 intensity. In the case of Houses 7 and 12, it could be that because more of their consumption occurs during daylight hours compared to the other houses (Figure 5.34), they are less exposed to high evening prices on the Tide tariff - and thus don't stand to save as much from using a battery to shift that consumption.

Based on these observations, the tariffs are optimised thus:

House	Annual consumption (kWh)	Lowest-cost Tariff			
		No PV, no battery	PV only	With battery (Greedy)	With battery (EAA)
5	6451	Flat	Flat	Tide	Tide
8	5818	Tide	Tide	Tide	Tide
7	4714	Flat	Flat	Flat	Flat
6	4116	Flat	Flat	Flat	Tide
2	4069	Flat	Flat	Flat	Tide
1	3982	Tide	Tide	Tide	Tide
12	3258	Flat	Flat	Flat	Flat
19	2572	Flat	Flat	Flat	Tide

Table 5.2: The cheapest electricity tariff for each house and each configuration.

From Figures 5.31-5.33, it can already be seen that the most economical option open to most homeowners is to install PV without battery, and that running the EAA on a PV-battery system is significantly more costly than running the Greedy algorithm. This is developed further in the next chapter, alongside discussion of the environmental impacts.

5.2.2.6 Application of heuristic rules to all houses

The component sizes chosen based on the above heuristic rules are summarised in Table 5.3 for a new battery, and Table 5.4 for a second-life battery.

House	Annual consumption (kWh)	PV capacity (kW_p)	Battery capacity (kWh)	DC-DC converter rating (kW)	DC-AC inverter rating (kW)
5	6451	5.23	6.23	1.25	3.23
8	5818	4.91	5.91	1.18	3.05
7	4714	4.36	5.36	1.07	2.71
6	4116	4.06	5.06	1.01	2.54
2	4069	4.04	5.04	1.01	2.52
1	3982	3.99	4.99	1.00	2.49
12	3258	3.63	4.63	0.93	2.28
19	2572	3.29	4.29	0.86	2.07

TABLE 5.3: System component sizes for each house with a new battery in its PV-battery system.

House	Annual consumption (kWh)	Battery capacity (kWh)	Usable capacity (kWh)	DC-DC converter rating (kW)	DC-AC inverter rating (kW)
5	6451	12.9	10.3	2.58	3.68
8	5818	11.6	9.31	2.33	3.62
7	4714	9.56	7.65	1.91	3.13
6	4116	8.53	6.83	1.71	2.88
2	4069	8.45	6.76	1.69	2.86
1	3982	8.30	6.64	1.66	2.83
12	3258	7.15	5.72	1.43	2.53
19	2572	6.12	4.90	1.22	2.25

TABLE 5.4: System component sizes for each house with a second-life battery in its PV-battery system.

The same PV capacities are used for both new and second-life batteries, and the PV-only systems. The optimal PV size does depend on whether or not the system includes a battery, but the literature indicates that this effect is small and in this case likely to be dominated by the sub-optimality inherent in the heuristic rules.

The system component sizes in Tables 5.3 and 5.4 are unlikely to be installed exactly because standard modules may not exist in sizes that can be connected together to give exactly these totals. Furthermore, PV capacity is likely to be restricted by roof space, and so in real cases may be lower than the values given in Table 5.3, especially for the higher-consuming houses. On the other hand, there are some correlations between electricity consumption, wealth (White et al., 2012), and house size (Foye, 2017), so it is possible that they can support such large PV arrays.

It is interesting to note that the heuristically optimised PV capacities found here tend to be higher than the UK average domestic array size of 2.8 kW_p (BEIS, 2020). Note that this is even with curtailment of any export above the DC-AC inverter ratings in Table 5.3, or in the PV-only cases, 0.8 times the PV array capacity, capped at 3.68 kW. This could be either because most roofs cannot support a PV array as large as would be financially optimal, or because most homeowners cannot afford the Capex on such a large array.

Data could not be found for average battery installation sizes in GB households, but the heuristically optimised capacities found here for new batteries tend to be lower than the median capacity of 8 kWh of the home battery products listed by Naked Solar (2019). Furthermore, C/5 is a considerably lower charge/discharge limit than those of the products they listed. Considering how small the size-dependent portion of the BoS cost is compared to the fixed portion (25 GBP/kW vs. 1000 GBP), one might expect an optimal converter rating much larger than C/5.

A possible reason for such a low optimal rating is thus: with a higher converter rating, say C/2, there are many periods throughout the year where the battery would quickly charge to full and then be unable to charge further until the next time it is scheduled to discharge, and many periods where it would quickly empty and be unable to discharge further until it is next scheduled to charge. The revenues/savings are therefore not adversely impacted by reducing the converter capacity, in fact they are improved by slowing down the battery charging/discharging across such periods because the efficiency losses are much reduced. (Ohmic losses of I^2R increase proportionally to the square of the charge/discharge rate.) With less energy lost in ohmic heating, there is more energy to use in the home (displacing grid import) or to export to the grid for payment. It is outside the scope of this thesis to investigate this hypothesis further, but it would have interesting implications for the design of home battery products.

5.3 Summary

In this chapter, preliminary tests were conducted to decide the time resolution of modelling and the system component sizes that would be examined in the main analysis.

The input data time resolution was coarsened by averaging, and resultant errors found in SSR, CO_2 intensity, IRR and MCoE, relative to the highest resolution of 15-s. The literature finding, that the presence of a battery lessens the impact of coarser time resolution, was confirmed for a PV-battery system running the Greedy algorithm, but with the EAA, the errors were of a similar magnitude to the corresponding PV-only system (Sun et al., 2020). A timestep of 5 minutes was chosen for the remainder of this study, as a compromise between accuracy and computation speed: CO_2 intensity errors below 8 % (<2 g/kWh average absolute error) and MCoE errors below 1 % (<0.3 p/kWh average absolute error) in all cases, for a run-time averaging 60 s for the Greedy algorithm and 80 s for the EAA.

Time-slicing was tested but ruled out because it could not achieve better results than using the full 5-minute resolution data. At 1-minute resolution time-sliced by alternate weeks, the run-time was still more than double the full 5-minute resolution runs, and errors were worse, particularly errors in CO_2 intensity. More complex time reduction methods involving statistical clustering were considered but ruled out; they are deferred to further work.

For sizing of the system components, the guiding principle is that like-for-like comparison is achieved by comparing the best to the best: fixing PV, battery, converter and inverter capacities across all the houses would be unrealistic, when each household would be trying to optimise their own system. At the same time, a mathematical optimisation procedure such as a genetic algorithm would take too long to apply to every single house and configuration; both in this study and in a realistic context where a PV/battery installer would be serving too many customers to acquire input data and run a detailed optimisation for each of them.

Instead, a direct search method was applied to the highest- and lowest-consuming houses, and heuristic rules developed for sizing PV, battery, converter and inverter capacities based on each house's annual electricity consumption. These rules are:

- PV capacity:

$$P_{PV} = \left(2 + \frac{[\text{Annual electricity consumption in kWh}]}{2000}\right) \quad \text{kW}_p. \tag{5.1}$$

- Battery capacity:

$$E_B = \left(3 + \frac{[\text{Annual electricity consumption}]}{2000}\right) \quad \text{kWh}. \tag{5.2}$$

  for a new battery, and

$$E_{B,2} = E_{B,1} \times \left(1 + \frac{[\text{Annual electricity consumption}]}{6000}\right) \quad \text{kWh}. \tag{5.3}$$

  for a second-life battery $E_{B,2}$ (whose usable capacity actually begins at 0.8 times this, due to degradation in its first life), relative to a new battery capacity $E_{B,1}$,

- Battery DC-DC converter rating:

$$P_{conv} = \left(\frac{E_B}{5 \text{ hours}}\right) \text{ kW}. \tag{5.4}$$

  in other words, C/5 charge/discharge limit (for both new and second-life batteries - meaning a converter at 1.4-2.1 times the rating for second-life compared to new),

- DC-AC inverter rating:

$$P_{inv} = \texttt{min}\left(\left[3.68 \text{ kW}, 0.5(P_{PV} + P_{conv})\right]\right). \tag{5.5}$$

These rules do not yield an exact global optimum system for each house; nor can an exact global optimum be expected in reality when buying from a PV/battery installer. The numerical values found by applying the rules to each house are given in Tables 5.3 and 5.4.

These rules inevitably contain some subjectivity because the multiple objectives (environmental impact, represented by life-cycle CO_2 emissions intensity, and financial impact, represented by MCoE, PP and RoI) are not all aligned and decisions needed to be made in trading them off against each other. However, the effects of these decisions can be seen in the next chapter, where comparisons are made between these PV-battery systems, and PV-only systems with the equivalent PV capacity, and battery-only systems with the equivalent battery capacity.

Finally, all 8 houses were run with their heuristically optimised component sizes, and the MCoE calculated under different electricity tariffs. The options were flat-rate, Economy 7 and Green Energy Tide (details in Chapter 2 Section 2.4.4). Each household is free to choose any electricity tariff available to them, and so the lowest-cost one in each configuration is chosen for them in this study, in keeping with the principle of comparing the best against the best. When there is no PV and no battery, or PV only, the flat-rate tariff is to be used for all houses except 8 and 1; for Houses 8 and 1, the Tide tariff is to be used in those

cases. With a battery too, running the Greedy algorithm, only House 5 is taken to switch from flat-rate to Tide. But running the EAA, all are taken to switch to the Tide tariff, except Houses 7 and 12 which remain on flat-rate.

The results are carried forward to the next chapter, where the (heuristically) optimally sized systems are compared against each other, in terms of financial metrics MCoE, RoI, IRR, PP, and the 14 midpoint impact categories of ReCiPe 2008.

Chapter 6

Results and Discussion

"Markets make a good servant, a bad master and a worse religion."
- Amory Lovins

In the previous chapters, a model was developed of a domestic PV-battery system, including the novel Emissions Arbitrage Algorithm (EAA) for battery operation scheduling, and a microeconomics-based method to estimate future replacement costs of second-life batteries. Using the parameters selected in the previous chapter (modelling timestep and system component sizes), the model was run for each of the 8 houses in the dataset, for the two future grid scenarios (Community Renewables, CR, and Two Degrees, TD), in 10 different configurations:

- No PV and no battery,
- PV only (no battery),
- Battery only (no PV), running the Greedy algorithm,
- PV with new battery, running the Greedy algorithm,
- PV with best-case second-life battery, running the Greedy algorithm,
- PV with worst-case second-life battery, running the Greedy algorithm,
- Battery only (no PV), running the EAA,
- PV with new battery, running the EAA,
- PV with best-case second-life battery, running the EAA,
- PV with worst-case second-life battery, running the EAA.

This chapter reports, for all these cases, the life-cycle financial results as represented by four of the metrics defined in Chapter 1 Section 1.1: mean cost of electricity, return on investment, internal rate of return, payback period; and the life-cycle environmental impacts according to fourteen of the ReCiPe 2008 midpoint indicators described in Chapter 1 Section 1.2: climate change, ozone depletion, human toxicity, photochemical oxidant formation, particulate matter formation, ionising radiation, terrestrial

acidification, freshwater eutrophication, marine eutrophication, freshwater ecotoxicity, land occupation, water depletion, metals depletion, fossil fuel depletion.

Thus comparisons are made, in terms of financial and environmental impacts, for:

- PV-only against the baseline (no PV nor battery),
- PV-battery against PV-only,
- Second-life batteries against new,
- EAA against the Greedy algorithm,
- TD future grid scenario against CR.

These comparisons are discussed, for an investment starting in 2020 and in 2030. The use of carbon pricing and dynamic time of use electricity tariffs are considered as means of aligning the misaligned financial and environmental incentives. Ultimately, this was found not to be straightforward, requiring further work to design regulations or market-based incentive structures to achieve alignment of the financial and environmental goals.

6.1 Financial Analysis

In this section, the various different configurations of PV-battery systems, heuristically optimised in the previous chapter, are compared on the basis of four financial metrics:

- Mean Cost of Electricity (MCoE), calculated by a discounted cash flow analysis of expenditure on system installation and electricity bills over the system lifetime, divided by the total electricity consumed in that time period,
- Return on Investment (RoI), where the total savings relative to the baseline system with no PV and no battery, as found by the discounted cash flow analysis, are reported relative to the Capex,
- Internal Rate of Return (IRR), the equivalent annual percentage return on Capex yielded by savings relative to the baseline system,
- Payback Period (PP), the time taken for savings to fully pay back the Capex, without discounting future cash flows, and neglecting component replacement costs.

All the metrics are defined for each house and system configuration with the most cost-effective (lowest MCoE) tariff as found in the previous chapter (Table 5.2). RoI, IRR and PP are defined in terms of savings relative to the baseline system with no PV and battery, on the most cost-effective tariff for each house with no PV and battery. Thus the best tariff is compared to the best in each case.

This section presents results for an investment starting in 2020, with all cash flows inflation-adjusted to 2019 currency. Results for an investment starting in 2030 are presented for comparison in Section 6.3.

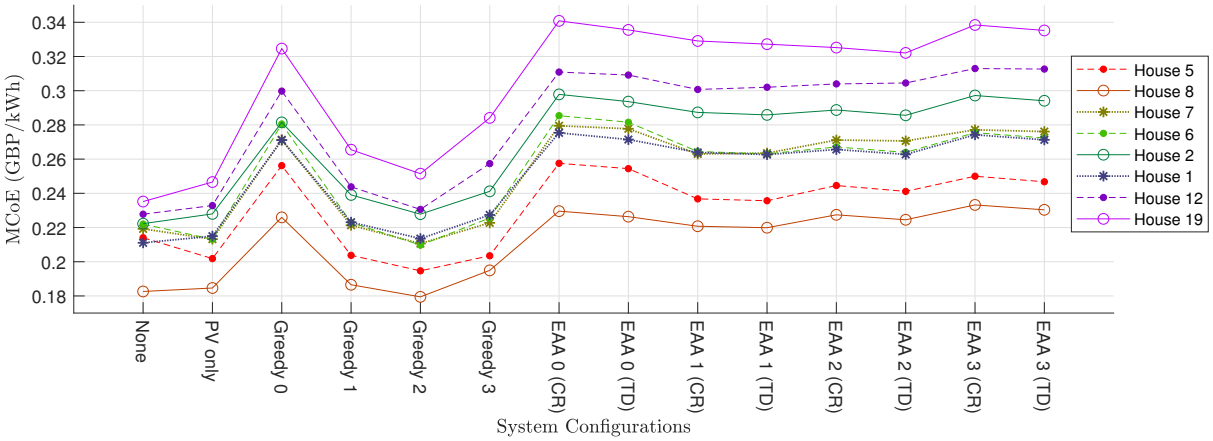

FIGURE 6.1: Mean Cost of Electricity for each house in each configuration (and future grid scenarios 'Community Renewables', CR, or 'Two Degrees', TD), start year 2020.

6.1.1 Mean Cost of Electricity

Figure 6.1 shows the MCoE for each of the 8 houses, in each configuration: 'None' (the baseline, no PV and no battery), PV only, 'Greedy' (the battery operates the Greedy algorithm; '0' meaning battery with no PV, '1' meaning PV with a new battery, '2' and '3' meaning PV with a best-case and worst-case second-life battery respectively), and 'EAA' (the battery operates the Emissions Arbitrage Algorithm; '0', '1', '2' and '3' signifying the same as for the 'Greedy' configurations). In each configuration where PV and/or battery (new or second-life) are present, their capacities are optimised for each house according to the heuristic rules developed in the previous chapter.

The lines joining each data point do not signify progression; they are present only to assist the eye in seeing which house each data point belongs to. Markers and linestyles have no significance other than to assist in distinguishing between households represented by similar colours. It is clear from Figure 6.1 that there is a tendency for each house, whether it is at the low, middle or high end of the MCoE range in one configuration, to occupy a similar place relative to the other houses in all configurations.

The future grid scenario (Community Renewables, CR, or Two Degrees, TD) only affects the operation of the EAA but not any of the other configurations; thus MCoE is the same between CR and TD for those configurations, and only differ for the EAA configurations. While the TD cases tend to have lower MCoE than the equivalent CR case, this difference is small and in many cases smaller than the 0.003 GBP/kWh error expected due to the lower time resolution used for the simulations (5-minute rather than 15-s, see previous chapter).

Further observations are that the EAA configurations all have higher MCoE than the baseline cases, and this is not helped by having a second-life battery. The battery-only configuration running the Greedy algorithm ('Greedy 0') is also much less cost-effective than the baseline cases. Only Houses 5, 7 and 6 lower their MCoE compared to the baseline by installing PV; the others raise their MCoE. Considering PV-battery running the Greedy algorithm, only Houses 5, 8 and 6 can lower their MCoE below that for PV-only by installing a best-case second-life battery ('Greedy 2'). The same is not true with a new battery ('Greedy 1') nor a worst-case second-life battery ('Greedy 3'). Without knowing beforehand if a particular second-life battery is closer to the best-case or worst-case, it is a risky strategy to try to lower MCoE by installing PV with a second-life battery running the Greedy algorithm.

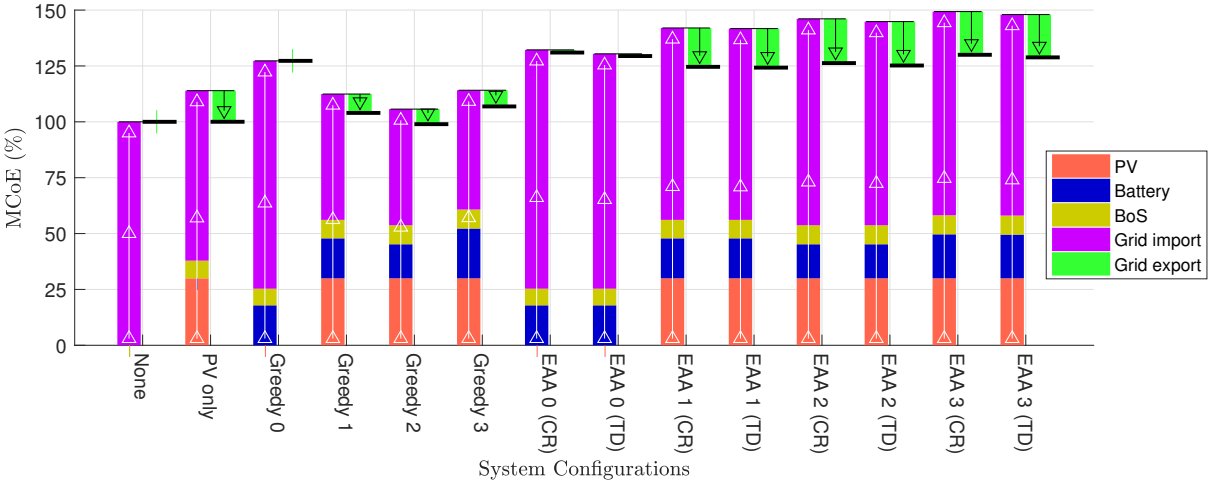

FIGURE 6.2: Mean breakdown of contributions to Mean Cost of Electricity in each configuration, start year 2020.

Figure 6.2 shows the MCoE in each configuration (the mean taken across the 8 houses) broken down into contributions from expenditure on installation of PV, battery and BoS, and on grid import and export. Battery and BoS expenditure include replacement costs. Grid export results in a payment to the homeowner, hence the downward arrows on those bars; taken together with expenditure on grid import, they comprise the electricity bills. All are normalised relative to the mean MCoE of the baseline case, with the thick black horizontal line denoting total mean MCoE in each configuration.

In the PV-only case, the expenditure on grid import is reduced, and together with the payment received from grid export, almost cancel the expenditure on installing the PV.

The battery-only case running the Greedy algorithm ('Greedy 0') is only included for completeness, as the battery never actually charges or discharges. This is due to the way the Greedy algorithm operates, the battery only charges from excess PV and never directly from the grid (Chapter 2 Section 2.3.1) - without any PV, the battery does nothing. The lifetime electricity bills are the same as the baseline case, and the MCoE is increased solely by expenditure on battery and BoS which do nothing. (The tariffs used for all the battery-only cases are the same as for the corresponding PV-battery cases.)

With PV and battery running the Greedy algorithm, grid export is reduced compared to the PV-only case, but so too is grid import. However, this reduction is insufficient to pay back the expenditure on PV, battery and BoS in most cases. When the battery is second-life ('Greedy 2' and '3'), the expenditure on grid import is reduced compared to a new battery ('Greedy 1') because the second-life batteries considered are larger-capacity, as heuristically optimised in the previous chapter. While expenditure on a best-case second life battery ('Greedy 2') is less than on a new battery, it is greater for a worst-case second life battery ('Greedy 3'). This is because the worst-case second-life battery needs to be replaced more frequently; as seen in Figure 6.3, the Capex on a second-life battery is slightly less than a new one ('Greedy 2' and '3' compared to '1'), even though the second-life battery capacity considered is up to twice that of a new one.

Referring again to Figure 6.2: the battery-only case running the EAA ('EAA 0'), unlike the battery-only case running the Greedy algorithm, does export power to the grid as well as importing. However, the power export is small and almost imperceptible in the chart. Grid import is on the order of 1 %-point less in the TD future grid scenarios compared to CR. This is unsurprising because the more centralised TD

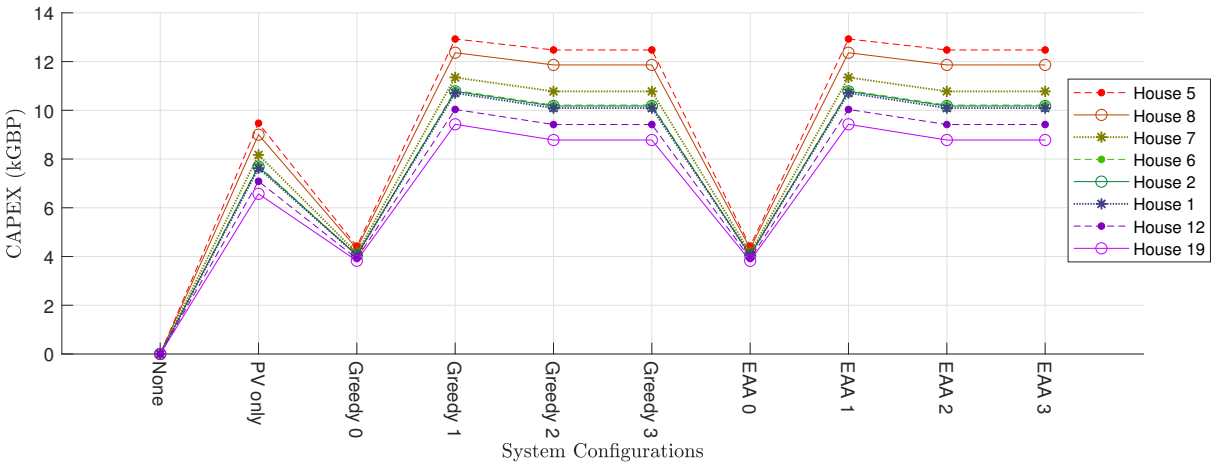

FIGURE 6.3: Capital expenditure for each house in each configuration, start year 2020.

scenario leaves less scope for decentralised assets such as domestic PV-battery to operate. Homeowners should take heart that the difference is so small, in other words, their returns are not strongly affected by the future evolution of the grid, which they as individuals cannot influence.

Unlike the PV-battery cases running the Greedy algorithm, a larger battery capacity running the EAA leads to increased grid import and export. This effect means MCoE is higher with a second-life battery than a new one, although the effect size is small, on the order of 1 %-point. Overall the EAA configurations lead to MCoE on average around 25 % higher than the baseline case average.

6.1.2 Return on Investment

Figure 6.4 shows the RoI in each configuration, where returns are defined as the savings relative to the baseline case ('None'), comparing the best tariff for each house in each case against the best tariff for each house with no PV and no battery. The battery-only configurations ('Greedy 0', 'EAA 0') are the least economic by this measure, with RoI below -140 %. In contrast to considering the MCoE, by which the 'EAA 0' cases are only slightly costlier than the other 'EAA' cases, 'EAA 0' has markedly lower RoI than the other 'EAA' cases. This is because despite similar life-cycle costs, the Capex on a battery-only installation is around 4000 GBP compared to 8500-13000 GBP for PV and battery (see Figure 6.3 above). The 'EAA 0' cases thus incur a similar loss, but relative to a smaller initial investment.

Figure 6.5 zooms in to show the RoI closer to the zero level. From this information, similar conclusions are drawn as when examining MCoE: PV-only is profitable only for Houses 5, 7 and 6 (RoI 9-21 %); PV-battery is profitable when running the Greedy algorithm on a best-case second-life battery for Houses 5, 8, 7 and 6 (RoI 4-25 %), but this is a risky strategy if it is not known beforehand whether the battery is closer to best-case or worst-case, as only House 5 stands to profit regardless (RoI 13-25 %).

All cases running the EAA are loss-making (RoI -27 % to -76 % with PV and battery), the losses being slightly less bad in TD scenarios compared to CR, and slightly worse with (the larger-capacity) second-life batteries compared to new ones. As with MCoE, there is a tendency for higher-consuming households to make more savings (or incur smaller losses) in all configurations. However, the correlation is not perfect: for example, House 8 is the second highest-consuming but only the third or fourth most profitable. While

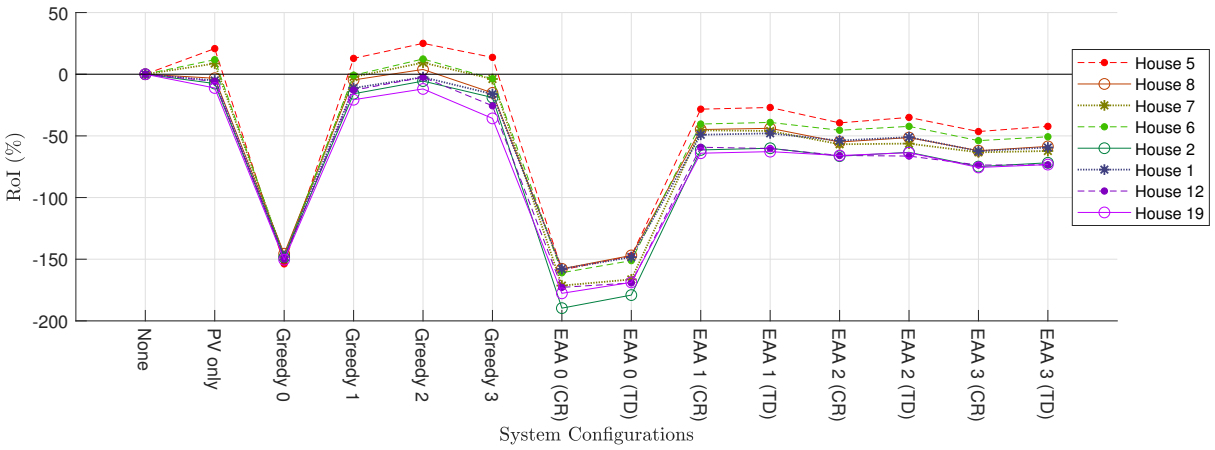

FIGURE 6.4: Return on Investment for each house in each configuration, start year 2020.

House 8 has the lowest MCoE in all configurations, followed by House 5, it is House 5 that has the highest RoI, followed by House 6.

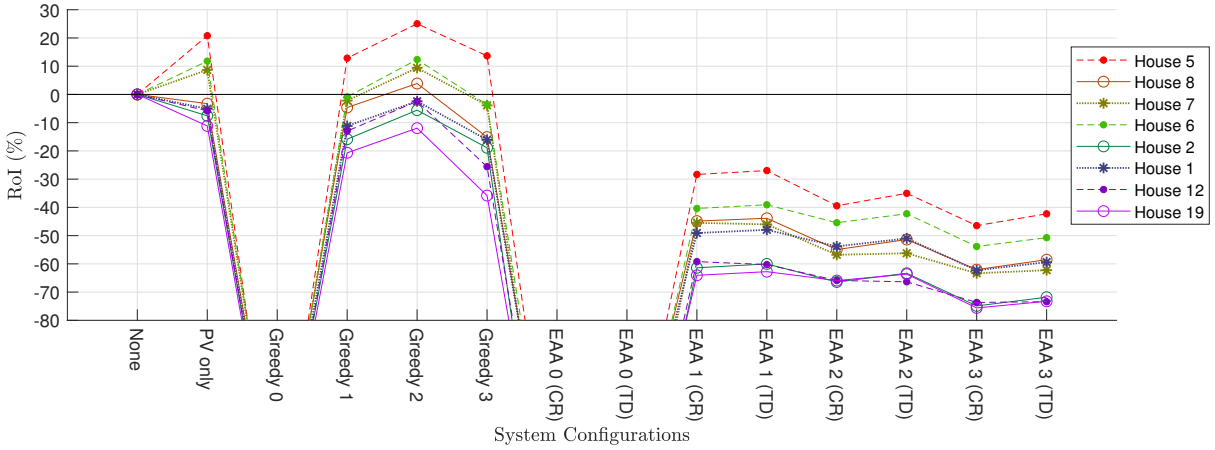

FIGURE 6.5: Zoom in of Figure 6.4, Return on Investment for each house in each configuration, start year 2020.

6.1.3 Internal Rate of Return

Figure 6.6 shows the IRR in each configuration, where again, returns are defined as savings relative to the baseline case ('None'), comparing the best tariff for each house in each case against the best tariff for each house with no PV and no battery. IRR was below -100 % for the battery-only configurations ('Greedy 0', 'EAA 0') and are thus omitted from the chart.

All 8 houses have IRR above zero in the PV-only configuration (0.9-3.8 %) and PV with best-case second-life battery running the Greedy algorithm ('Greedy 2'; IRR 0.8-3.9 %). Whether this counts as a profitable investment depends on each household's attitude to risk and the alternative investment options available to them, that is, a more risk-averse homeowner or one with access to higher-earning investment options would set a higher hurdle rate. Conversely, one whose best alternative option is a savings bank with below-inflation interest rate may choose to invest in a configuration with IRR of zero or even lower.

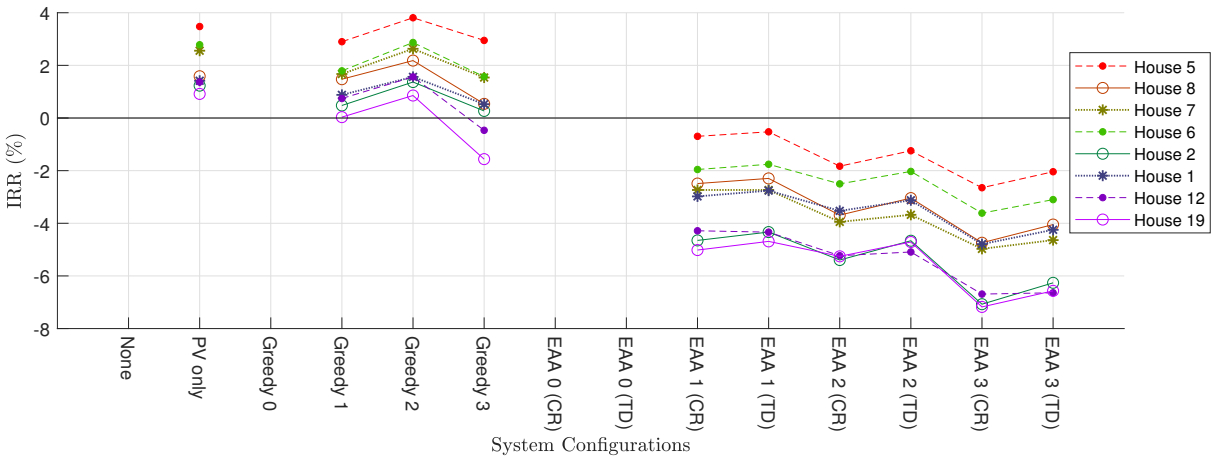

FIGURE 6.6: Internal Rate of Return for each house in each configuration, start year 2020. Values below -100 % are excluded from the chart.

Again, all cases running the EAA are the least profitable (IRR -0.3 % to -7.2 % with PV and battery), the losses being slightly less bad in TD scenarios compared to CR, and slightly worse with (the larger-capacity) second-life batteries compared to new ones. Like with RoI but unlike with MCoE, House 5 has the highest IRR, followed by House 6.

6.1.4 Payback Period

Care must be taken in interpreting the PP results in Figure 6.7, as they are calculated from cash flows without discounting, and excluding replacement costs of batteries and BoS. PPs higher than the system temporal boundary of 25 years are excluded from the chart.

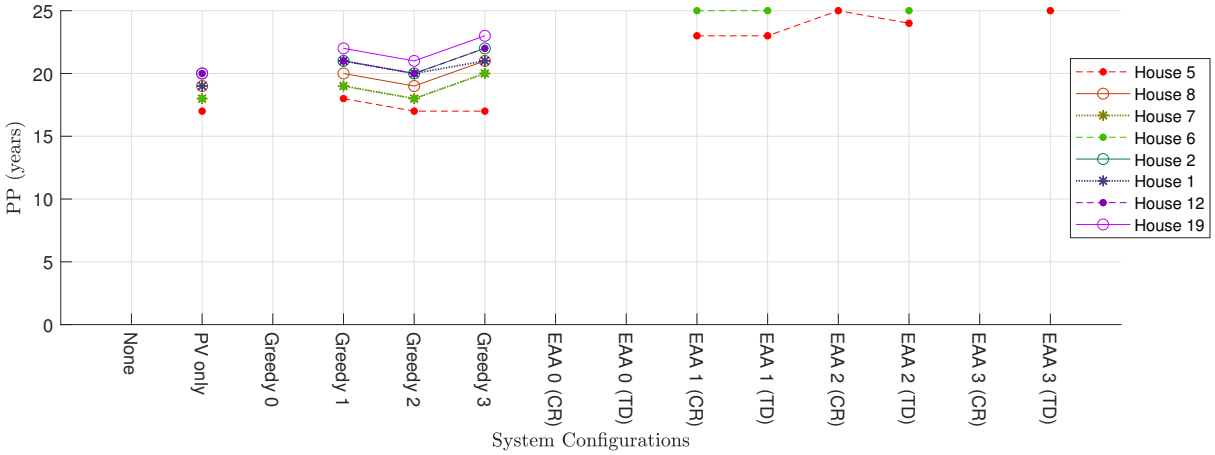

FIGURE 6.7: Payback Period for each house in each configuration, start year 2020. Values above 25 years are excluded from the chart.

Even without discounting future cash flows, the investment in a PV-only system takes 17-20 years to accrue enough savings to fully pay itself back. This is well within the working lifetime of a PV array, but under the assumptions of this study (no subsidies, cost 700 GBP plus 1500 GBP/kW$_p$), it is still a serious long-term investment. Note that the 17-20-year payback was calculated including a PV capacity degradation of 1 % per year (Chapter 2 Section 2.2.2).

Throughout this thesis, a maximum working lifetime of 15 years is assumed for the battery packs; the PP in all cases is above 15 years. This indicates the need for an increase in battery lifetime, or decrease in battery costs, before such systems become profitable.

These life-cycle financial results are all discussed together with environmental results in Section 6.4.

6.2 Environmental Impact Analysis

This section begins with a discussion of how the life-cycle environmental impact data are presented, using the Climate Change (CC) ReCiPe midpoint impact category as an example. (Refer to Chapter 1 Section 1.2 for definitions of the 14 ReCiPe midpoint impact categories used in this thesis.)

Questions are raised as to how to normalise the data to yield useful information. A normalisation to activity in the EU is chosen and explained next. There then follows a detailed breakdown of the environmental impacts for each system configuration, in each impact category, in decreasing order of magnitude according to the normalisation procedure.

6.2.1 Presentation of Environmental Impact Results

Figure 6.8 shows distribution plots of total life-cycle impacts in the Climate Change category, per kWh electricity consumed, in CR and TD future grid scenarios. The width of the distribution shapes indicates the relative frequency of data at the given y-axis value, and the mean and inter-standard deviation range is marked in white on each shape. When comparing distributions between different cases, a difference is considered **significant** if the mean of one lies outside the inter-standard deviation range of the other. The distributions in Figure 6.8 are based on the 1024 Monte Carlo iterations which randomise the impact intensities (of electricity generation by each generator type, and embodied emissions of manufacturing PV, battery and BoS) within the distributions defined in Chapter 3 Section 3.2.8, for each of the 8 houses in the dataset. A CC impact of zero would signify carbon neutrality of the household electricity over the 25-year system lifetime.

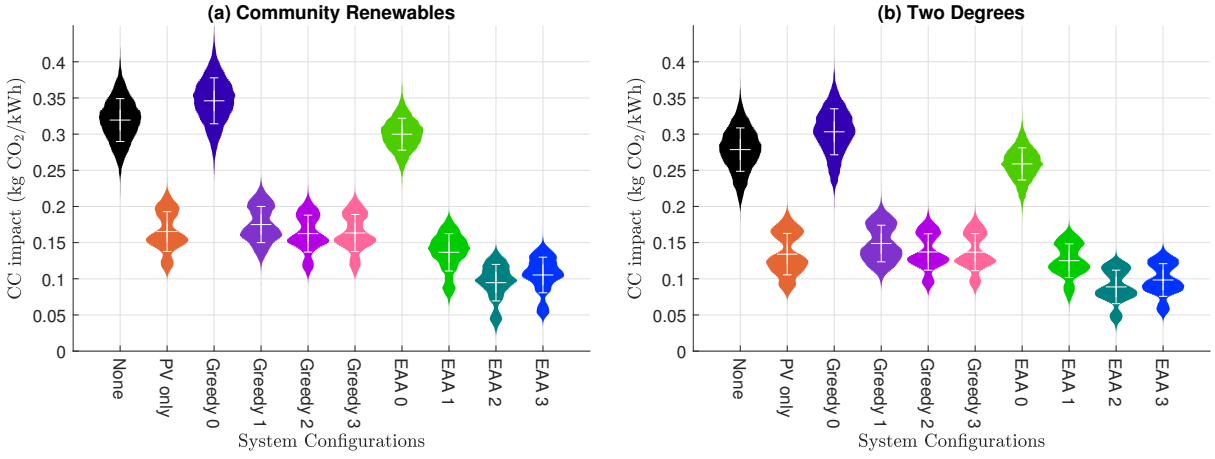

FIGURE 6.8: Distribution plots of Climate Change impact in each configuration, showing variation across houses and due to uncertainties in power generation impacts and embodied impacts of component manufacture.

By contrast, Figure 6.9 uses for the distributions only the 8 houses in the dataset, using mean values only for each impact intensity value input to the calculations. The spread of the distributions is similar, indicating that most of the variation in CC results is due to variation in household electricity consumption, rather than uncertainty or variation in CC impact intensities of electricity generation and system component manufacture.

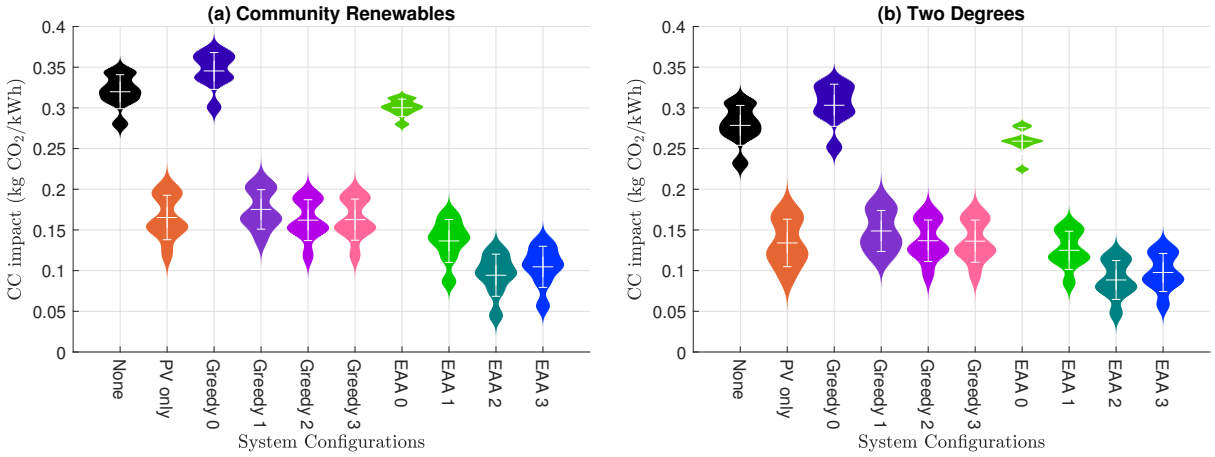

FIGURE 6.9: Distribution plots of Climate Change impact in each configuration, showing variation across the 8 houses.

The distributions for the baseline and battery-only configurations ('None', 'Greedy 0', 'EAA 0') are smooth bell-curve shapes in Figure 6.8, whereas they are multi-lobed in Figure 6.9. All other distributions are multi-lobed in both figures. It is not surprising that they should be multi-lobed in Figure 6.9, when the distribution contains only 8 data points, as this is generally too small a dataset to give a smooth distribution shape.

The fact that the distributions remain multi-lobed with the 8×1024 Monte Carlo iterations indicates that the uncertainties in the CC impact intensity values input to the calculation are small compared to variation between the houses - except for the baseline and battery-only configurations, where the input uncertainties are sufficient to smooth out the lobes in Figure 6.8. From Figure 6.27 below, it can be seen that grid import contributes a greater proportion of the CC impact in the baseline and battery-only configurations than in the other configurations. This would imply a greater uncertainty in the electricity generation CC impact intensities compared to those of system components manufacture; this fact can be verified by referring to the tables in Chapters 2 and 3.

From the above discussion, it was considered superfluous to present distribution plots of only the 8 houses, as opposed to the 8×1024 Monte Carlo iterations. The latter still yields information on the relative contributions of house-to-house and input uncertainties to the total variance, according to how smooth or lobed the distributions are. With Figure 6.8 as it is, the different configurations in the CR and TD future grid scenarios can easily be compared against each other. These comparisons are discussed in detail below in Section 6.2.3.

But while one can say, for example, that a PV-battery system running the EAA can reduce a household's life-cycle CC impact to between a third and a half of what it would be with neither, the figures so far give no indication of how important an impact that is. For example, domestic electricity use is responsible for a fraction of global CO_2 emissions; a halving of such emissions may equate to a very small improvement indeed.

An attempt is made to address this issue next, using data on annual activity in the EU for normalisation. Normalised data are then presented for each ReCiPe midpoint impact category. For raw (un-normalised) results, see Appendix D.

6.2.2 Normalisation of Environmental Impact Results

Benini et al. (2014) report on the environmental impacts of all activity within the EU in one year, under the ILCD framework. By dividing these values by 3198 TWh (the electricity generation in the EU in 2010 (Eurostat, 2019), this being the year from which most of the Benini et al. (2014) data originate), one obtains the impacts per kWh. These are not strictly the impact intensities of electricity generation because they include impacts from other activities within the EU economy too. Nonetheless, they form a basis for normalisation: the raw data for life-cycle environmental impacts (per kWh) calculated in this thesis (Appendix D) are divided by the impacts-per-kWh EU data. The mean impact of the baseline (no PV, no battery) configuration in the CR future grid scenario is then subtracted from all the data. All the normalised results are thus referenced against the baseline CR scenario, and the magnitude indicates how important it is relative to all other activity in the EU.

The method outlined above is far from ideal:

- The EU is not representative of the entire world, which is especially an issue for processes involved in the manufacture and operation of PV-battery systems that take inputs primarily from outside the EU, such as mining of lithium and cobalt. Although such data exist for the world (Sala et al., 2017), it is not reported in a form that can reliably be converted to the ReCiPe framework;
- The Benini et al. (2014) data are only for activity internal to the EU. While they did attempt to adjust for imports and exports to give a consumption-based rather than production-based perspective, they themselves do not place high confidence in its reliability, and so their adjustments were not used in this thesis;
- The Benini et al. (2014) data provide a snapshot of one year, whereas this is likely to change across the 25-year system lifetime;
- It is unlikely that all the electricity consumption in the EU could be coupled with a PV-battery system like the one analysed in this study, so care should be taken when interpreting the normalised data: they do not necessarily represent a likely result of an actionable policy; rather, they indicate the relative contribution of PV-battery systems operation compared to other activities within the EU that also contribute to environmental impacts.

For these reasons, the numerical values of the following normalised results should not be taken as accurate. They provide context, and allow for rank ordering of the 14 impact categories considered in this study.

6.2.3 Environmental Impact Results

The midpoint impact category with the largest range when normalised against the EU activity data is Terrestrial Acidification. Figure 6.10 shows that a PV-only system and PV with second-life battery running the Greedy algorithm (‘Greedy 2’ and ‘3’) give the greatest improvement compared to the

baseline. The magnitude of improvement, around 150× below zero (-15 000 %) appears physically impossible, as a continent's TA impacts cannot be reduced below -100 % (unless using processes that capture SO_2 and other acidifying gases out of the air, which are not considered in this study). Similarly it seems impossible that a range of over 20 000 % be encompassed within one standard deviation of the mean for the baseline ('None') scenarios.

There is reason to believe that there is an inconsistency in the data: consider that the majority of electricity generation in the EU is CCGT, with TA intensity of 1.17 g SO_2/kWh (see Chapter 3). The total annual TA impact of electricity generation can be estimated by multiplying this by 3198 TWh, the total electricity generation of the EU in 2010 (Eurostat, 2019), which gives 3.7×10^9 kg SO_2. The total annual TA impact would be higher than this because it includes run-off from fertiliser and other processes too (Benini et al., 2014). But the number reported by Benini et al. (2014) is 2.36×10^{10} mol H^+, which when converted from ILCD to ReCiPe (Owsianiak et al., 2014), is 1.17×10^7 kg SO_2. This is less than 1/300 of the value of 3.7×10^9 kg SO_2 estimated here for the TA impact solely of electricity generation. The source of the inconsistency could not be identified, whether a mistake in the Benini et al. (2014) data, or the conversion factors given by Owsianiak et al. (2014), although the same conversion factors were used in Chapter 3.

In any case, the TA category should perhaps come third or fourth in the rank order, rather than first. Leaving this aside, some inferences can still be made from Figure 6.10: installing PV significantly reduces (improves) the total life-cycle TA impact compared to the baseline, this reduction is smaller in magnitude if a battery is added to the PV, but similar again if the battery is second-life rather than new, and the reduction is smaller in magnitude for configurations running the EAA compared to the Greedy algorithm in the CR future grid scenario, but similar between Greedy and EAA in the TD scenario.

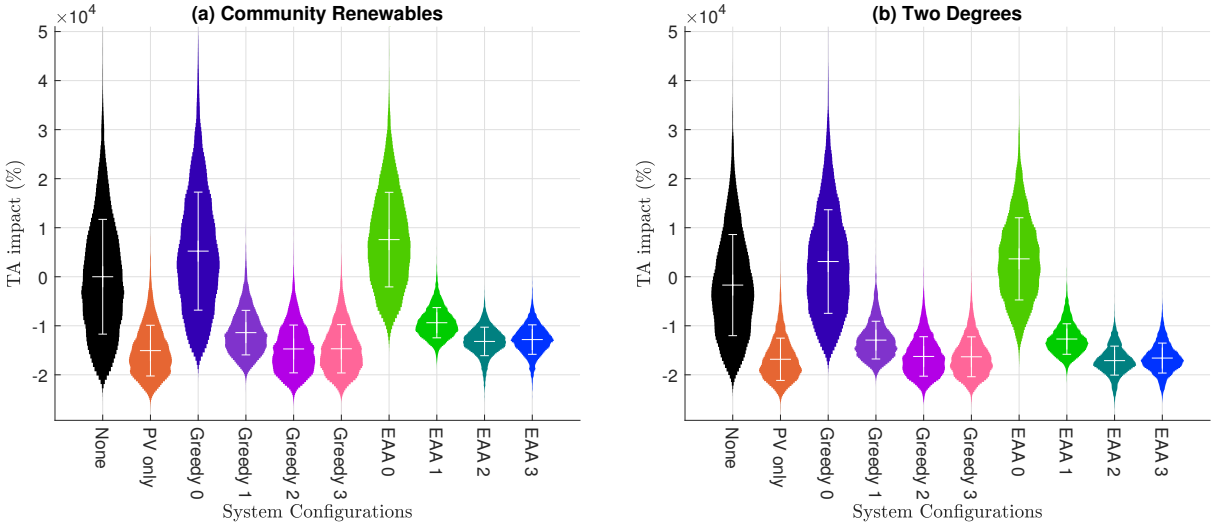

FIGURE 6.10: Distribution plots of Terrestrial Acidification impact in each configuration, normalised to EU impact in this category.

Figure 6.11 shows that grid import is the dominant contributor to the life-cycle TA impact, although the contribution of PV manufacture is also sizeable, at around 30 % of the baseline TA impact.

Metals Depletion is expected to increase as a result of manufacture of PV, batteries and BoS. The magnitude of the increase is up to 78× (7800 %) when comparing PV with new batteries against the baseline (Figure 6.13), and up to around 200× (20 000 %) when normalised against the EU activity data

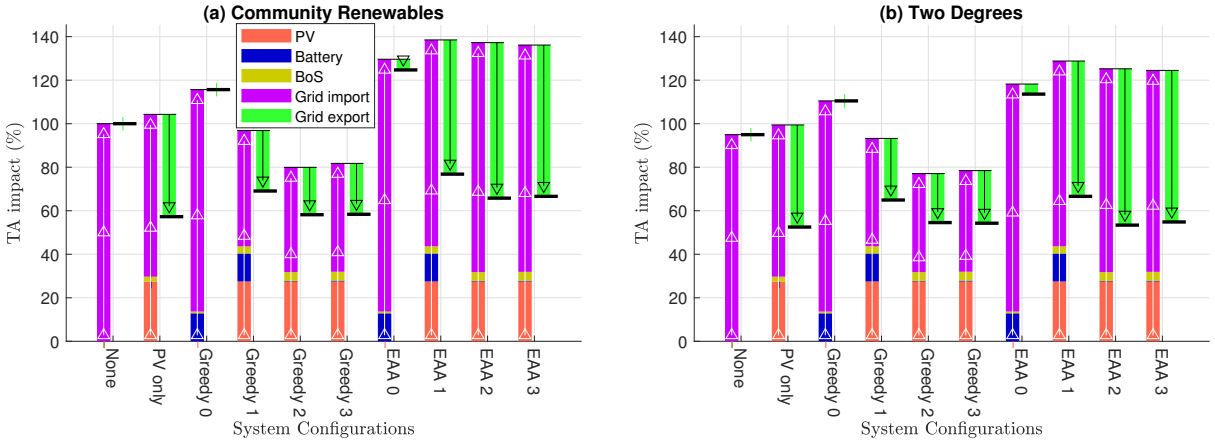

FIGURE 6.11: Breakdown of contributions to Terrestrial Acidification impact in each configuration, normalised to the baseline case in the Community Renewables grid scenario.

(Figure 6.12). The fact is that expansion of PV-battery systems globally would put an enormous strain (on the order of 78×) on mining operations for the metals used in the manufacture of such systems. (The disproportionately large impact when normalised against EU activity is an artifact of the fact that most mining for and manufacture of PV and batteries occurs outside the EU, and the Benini et al. (2014) data used do not account for international imports. However, the global activity data collected by Sala et al. (2017) indicates that global MD impact is only an order of magnitude more than in the EU, and so is likely to be substantially affected by expansion of PV-battery systems.)

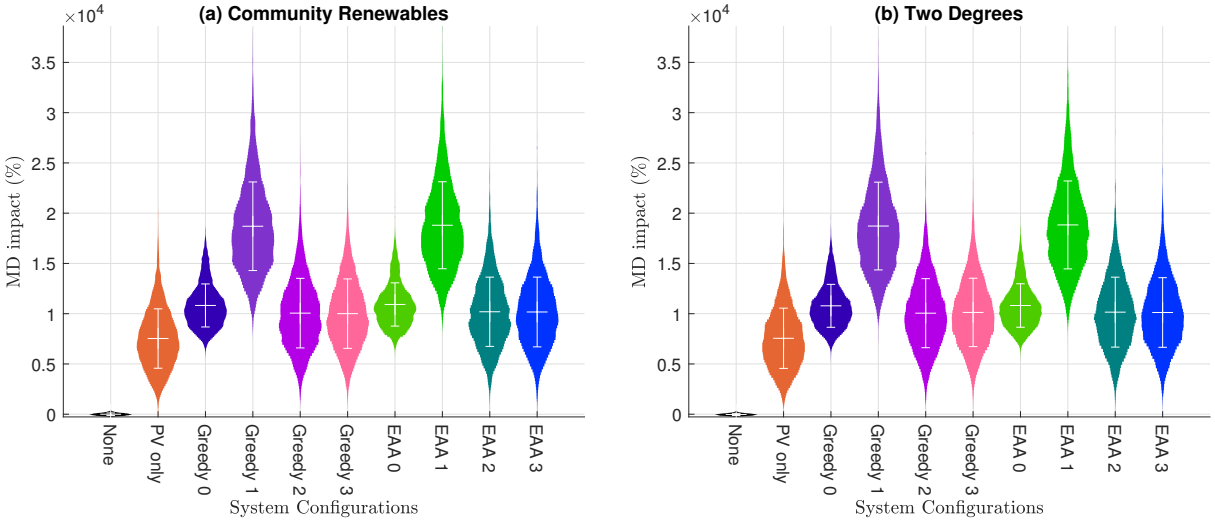

FIGURE 6.12: Distribution plots of Metals Depletion impact in each configuration, normalised to EU impact in this category.

Because MD impacts are dominated by manufacture of the system components (see Figure 6.13), the life-cycle MD impacts are almost identical between CR and TD future grid scenarios, and comparing equivalent configurations running the Greedy algorithm as opposed to the EAA (Figure 6.12). Using second-life rather than new batteries can reduce MD impacts by around a half, but the best option from an MD perspective is to not install any battery at all. In other words, the baseline configuration has lowest MD impact, or considering the other negative impacts it leads to, the next-best choice is PV-only.

Some interesting observations can be made from Figure 6.14 regarding the Ionising Radiation impacts:

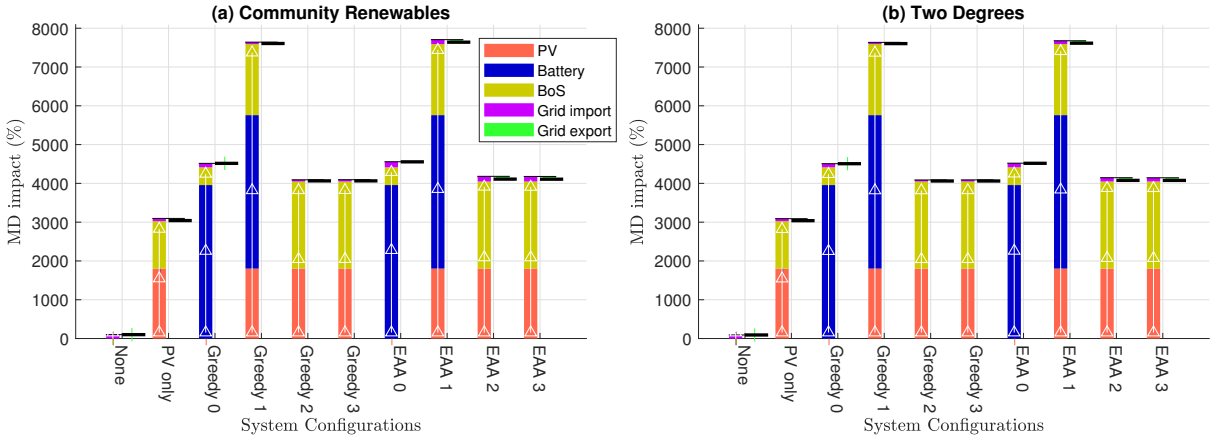

FIGURE 6.13: Breakdown of contributions to Metals Depletion impact in each configuration, normalised to the baseline case in the Community Renewables grid scenario.

the configurations without PV ('Greedy 0' and 'EAA 0') do not show improvement in IR compared to the baseline ('None') and are smooth bell-curve shapes, whereas the other configurations show improvements centering around -200 to -250 % and are multi-lobed. In fact, there is a 100 % worsening in baseline IR in the TD scenario compared to CR, which makes sense as the nuclear capacity in TD is larger than (roughly double) that in CR.

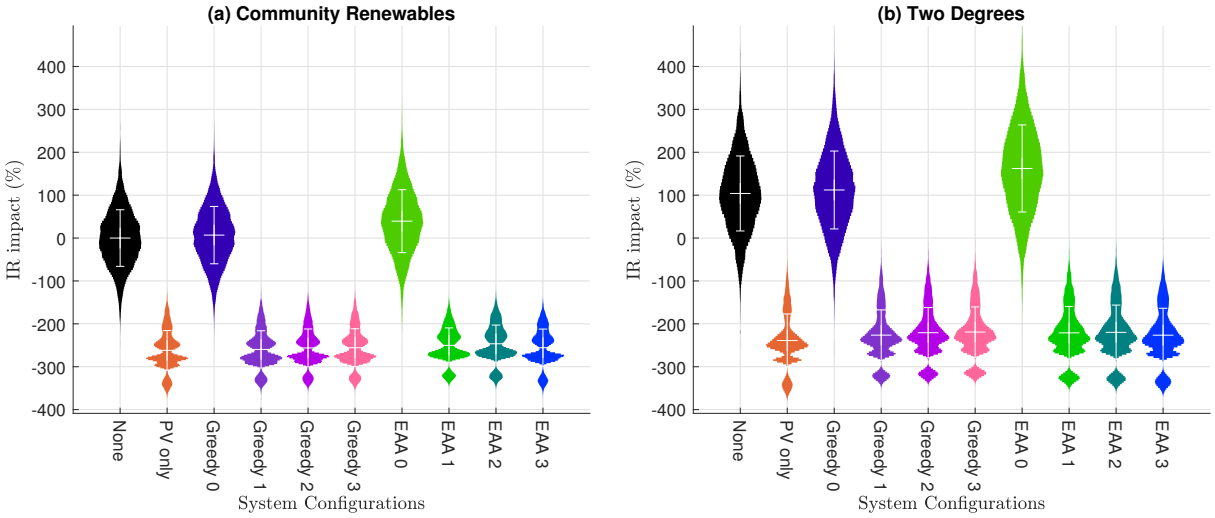

FIGURE 6.14: Distribution plots of Ionising Radiation impact in each configuration, normalised to EU impact in this category.

The dominant contributor to IR impacts is nuclear power generation, at 3.3 (±0.7) kg U235/kWh, two orders of magnitude higher than any other generation type (see Chapter 3). It should also be remembered that power imported from France is 73 % nuclear, though this reduces to zero in future years under the assumption that power imported into GB is wholly CCGT. The relatively large uncertainty of 0.7 kg U235/kWh (22 % of the central estimate) in nuclear power IR intensity accounts for the smooth bell-curve in configurations where IR impact is dominated by grid import.

For the others, grid export is responsible for reducing the IR impact by -200 to -250 % (Figure 6.14), with PV manufacture contributing about 5 % to the total life-cycle IR impact (Figure 6.15). The impossibly large IR reduction in these configurations is likely due to the fact that little nuclear power was used

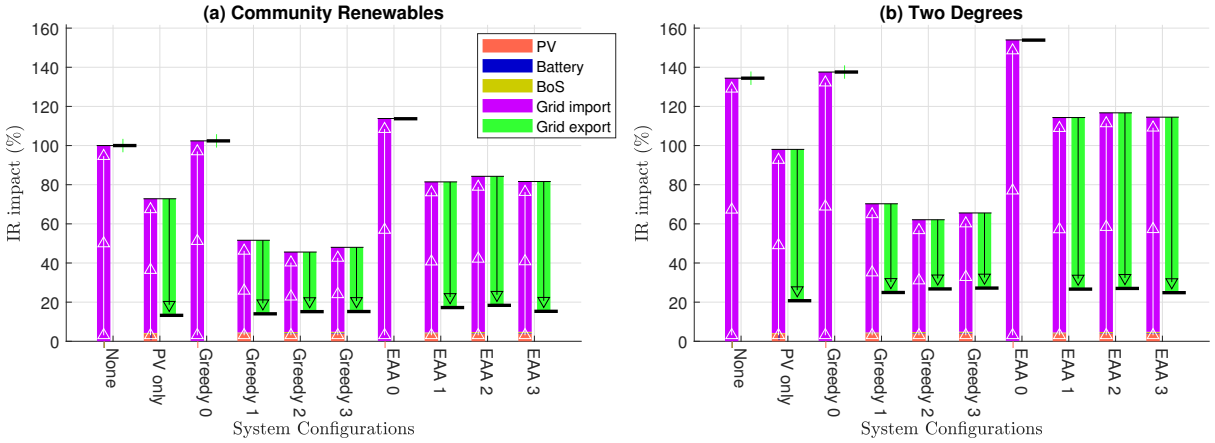

FIGURE 6.15: Breakdown of contributions to Ionising Radiation impact in each configuration, normalised to the baseline case in the Community Renewables grid scenario.

across the EU in 2010 compared to what has been modelled as being used in GB in this study; the normalisation procedure could then result in impacts of magnitude greater than 100 %.

Figure 6.15 shows grid export contributing greatly to reducing IR impact in the PV-only and PV-battery cases. It is an interesting coincidence that despite differing levels of grid import in the PV-only and PV-battery cases (especially with the Greedy algorithm compared to the EAA), the grid export in each case brings the total impact down to a very similar level, regardless of algorithm and battery type (new, second-life or none).

Freshwater Ecotoxicity impacts are subject to large uncertainty in all elements contributing to it, resulting in smooth bell-curves for all the cases in Figure 6.16. There is some increase in FET impact for PV-only compared to the baseline, and further (worse) for PV-battery, further again if running the EAA, but less if the battery is second-life rather than new. Despite the magnitude of these changes being large (up to 100 % in the EAA cases, an implied doubling of FET burden for the EU), the uncertainty is so large that only the configurations running the EAA can be said to be significantly worse than the baseline. This is likely due to the increase of grid imports during times when biomass is the marginal generator: despite having low CO_2 intensity, the FET intensity of biomass is the second-highest of the generation types considered (the highest being nuclear, see Chapter 3).

According to Figure 6.17, the majority of FET life-cycle impacts are due to PV manufacture, although the presence of PV offsets this somewhat by reducing grid import and increasing grid export, which are the next largest contributors. Improvements in the PV manufacturing process or new PV materials that reduce FET impact would be most fruitful in mitigating harm from this category.

Figure 6.18 shows that Fossil fuel Depletion is significantly reduced compared to the baseline by installing PV, by -50 % or more. There is small and insignificant change from adding a battery (new or second-life) if running the Greedy algorithm, but a significant reduction in FD impact from running the EAA with a second-life battery ('EAA 2' and '3'). Since the FD impact of battery manufacture contributes so little to the total (Figure 6.19), this can be surmised as due to the increased capacity of the second-life battery increasing grid exports at times of high marginal CC intensity and thus displacing more high-carbon generation.

The smoothness of all the distributions implies variation in FD intensities input to the calculation dominates over house-to-house variation. The variance is greatest (around ±40 %) for the baseline

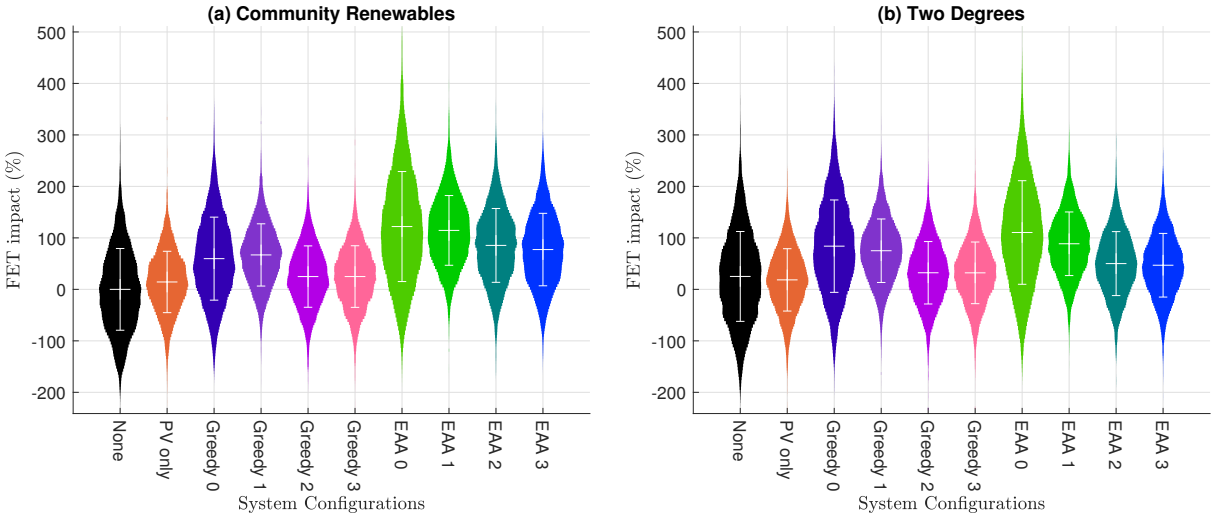

FIGURE 6.16: Distribution plots of Freshwater Ecotoxicity impact in each configuration, normalised to EU impact in this category.

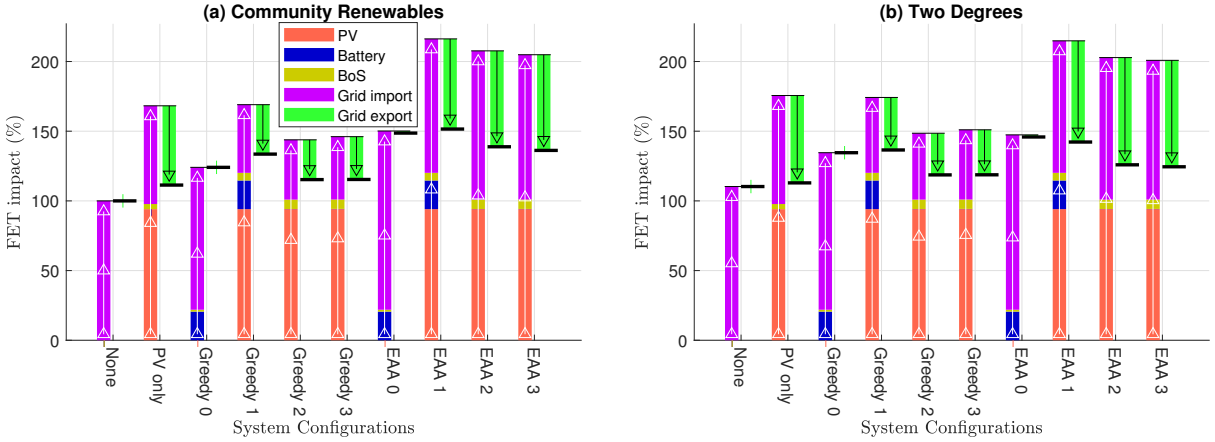

FIGURE 6.17: Breakdown of contributions to Freshwater Ecotoxicity impact in each configuration, normalised to the baseline case in the Community Renewables grid scenario.

and battery-only configurations. Figure 6.19 shows that FD impact is dominated by grid import and export.

Figure 6.20 shows that Land Occupation is significantly reduced compared to the baseline by installing PV, by around -40 %. There is almost no change when a battery (new or second-life) running the Greedy algorithm is added, and the improvement is reduced if the battery is running the EAA. As with FET, running the EAA increases grid import during times of high biomass generation, which though low-carbon, has the highest LO intensity of the generation types (see Chapter 3).

As expected, Figure 6.21 shows grid import to be the dominant contributor to LO impacts. These results show how important it is that any biomass used in future for power generation must be sourced through processes that minimise the exploitation of natural land or high-quality agricultural land.

Figure 6.22 shows that Particulate Matter Formation is significantly reduced compared to the baseline by installing PV, by -20 %. Adding a new battery to the installation, running the Greedy algorithm, reduces this benefit; it is recovered again if a second-life rather than new battery is used instead. Comparing the EAA to the Greedy algorithm in the CR future grid scenario, the PMF reduction is less (-10 to -17 %

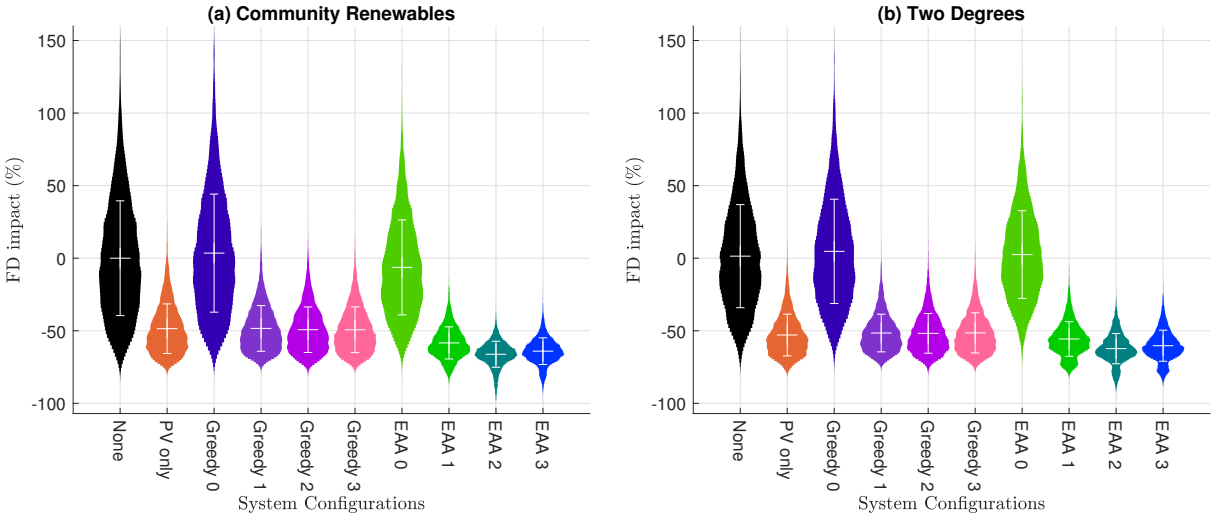

FIGURE 6.18: Distribution plots of Fossil fuel Depletion impact in each configuration, normalised to EU impact in this category.

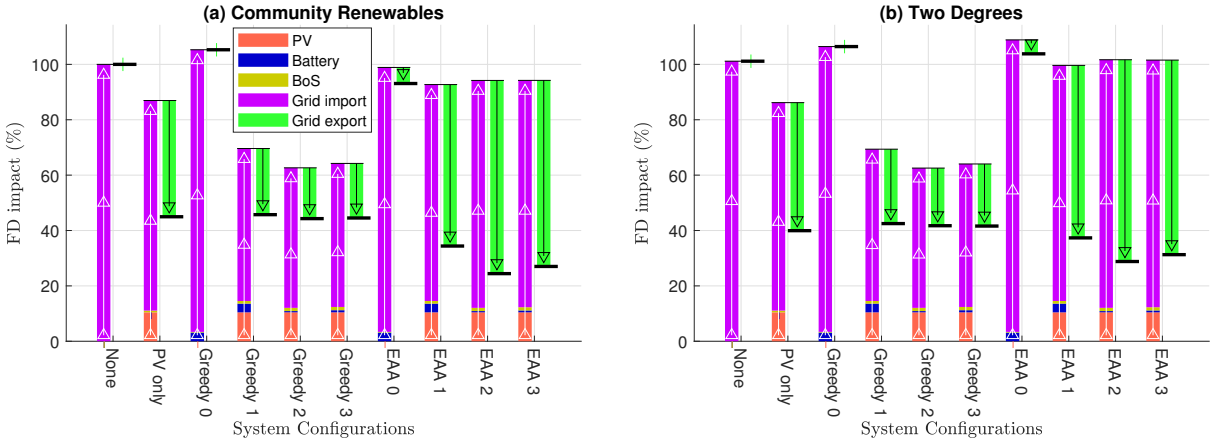

FIGURE 6.19: Breakdown of contributions to Fossil fuel Depletion impact in each configuration, normalised to the baseline case in the Community Renewables grid scenario.

rather than -13 to -20 %) in EAA cases, whereas they are similar between EAA and Greedy algorithms in the TD scenario. In fact, with a second-life battery ('EAA 2' and '3') in the TD scenario, the PMF reduction is even greater, around -24 %. In all cases the distributions are smooth bell curves, indicating that the variation in input PMF intensities dominates over the house-to-house variation.

Figure 6.23 shows a sizeable contribution to PMF from the manufacture of the PV array, at 35 % of the total PMF impact in the baseline CR case. However, the greatest contribution comes from grid import. The generator type with largest PMF intensity is biomass, closely followed by CCS and CCGT (see Chapter 3). It is interesting that biomass and CCS are both low-CO_2 generators, and thus fairly likely to be the marginal generator at times when the EAA schedules the battery to charge (though they are not the marginal generator as often as wind, PV, hydroelectric or other renewables, which are assumed zero-CO_2). There is more biomass in the CR scenario and more CCS in TD, with no CCS in CR - and yet the high PMF intensity of biomass (0.605 g PM10/kWh) leads to a smaller PMF reduction (smaller benefit) in the CR scenario when comparing EAA to Greedy cases, whereas in the TD scenario, the high PMF intensity of CCS (0.515 g PM10/kWh) *in*creases the PMF reduction.

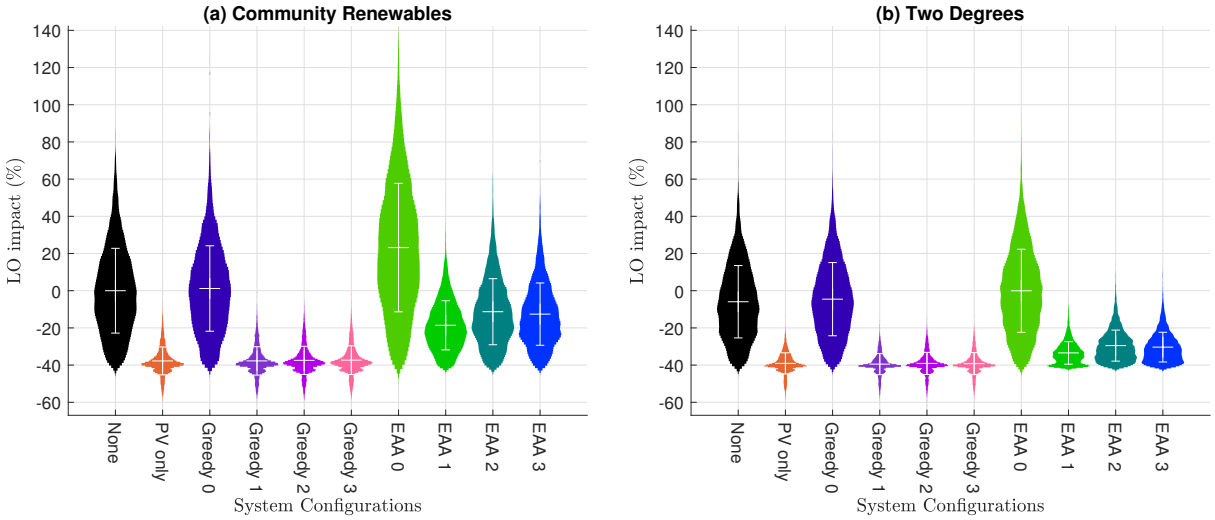

FIGURE 6.20: Distribution plots of Land Occupation impact in each configuration, normalised to EU impact in this category.

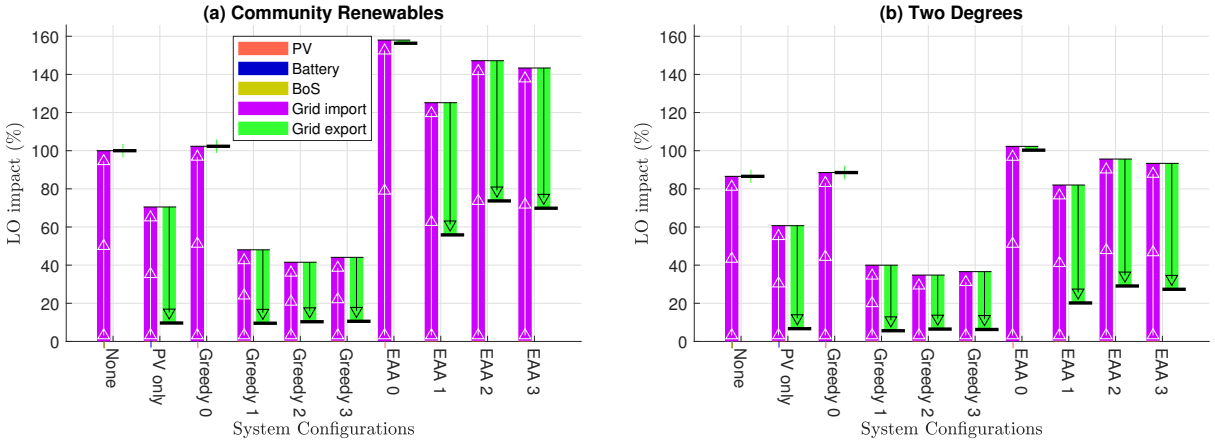

FIGURE 6.21: Breakdown of contributions to Land Occupation impact in each configuration, normalised to the baseline case in the Community Renewables grid scenario.

Freshwater Eutrophication is worsened the greater the capacity of PV and battery installed (Figure 6.24), although at an increase of up to 31 % when normalised to EU activity, it may be considered a lower priority than Metals Depletion, for example. The variation is dominated by uncertainty in FE intensities of the inputs rather than house-to-house variation, as indicated by the smooth bell-curve shapes. While sizeable, this variation is still small enough that it may be inferred that a PV installation leads to significantly higher life-cycle FE impact than the baseline, and a new battery to significantly higher life-cycle FE impact than second-life.

Figure 6.25 shows that the total life-cycle FE impacts are dominated by manufacture of the PV-battery system. Improving the processes or material choices for both PV and battery, and even BoS, would be worthwhile to attempt, as indeed would encouraging the use of second-life rather than new batteries be.

The Climate Change impact category is a special case because the EAA was designed specifically to reduce CC impacts, by scheduling the battery to charge at times of low marginal CC intensity on the grid, and vice versa. The EAA could equally be used to reduce impacts in other categories, but this was not studied in this thesis. CC comes 9th out of 14 in the rank ordering of impact categories,

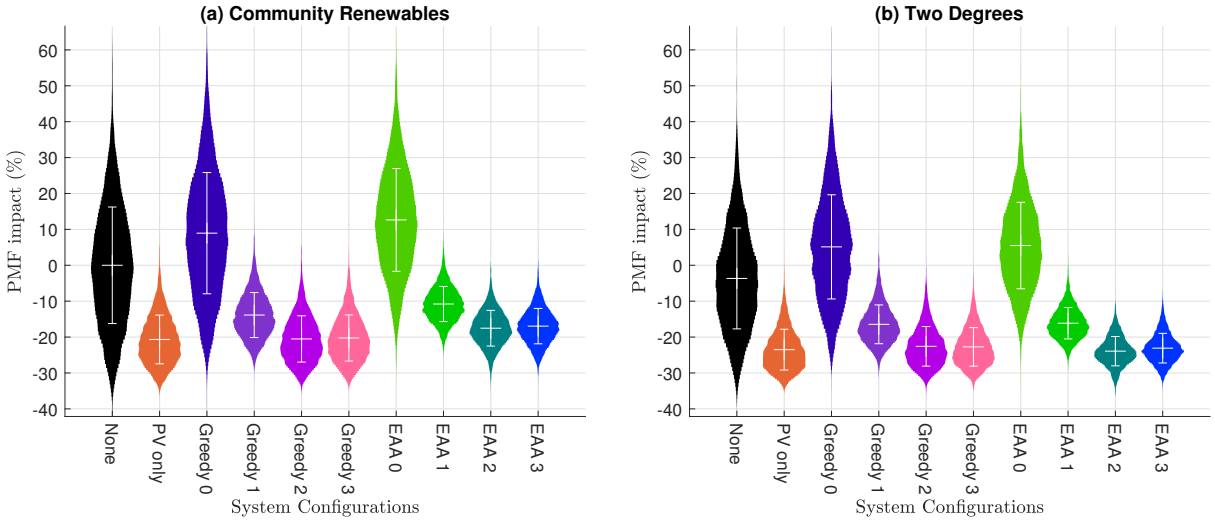

FIGURE 6.22: Distribution plots of Particulate Matter Formation impact in each configuration, normalised to EU impact in this category.

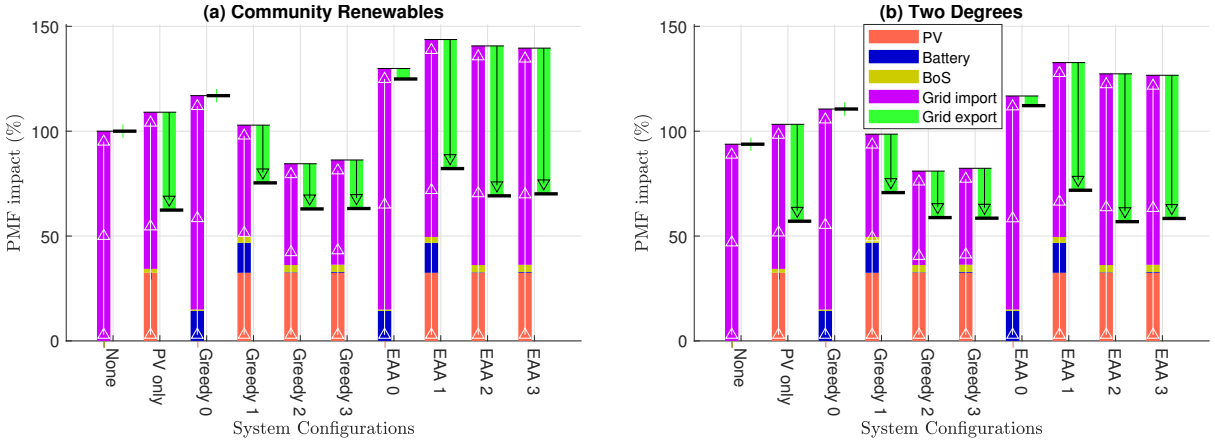

FIGURE 6.23: Breakdown of contributions to Particulate Matter Formation impact in each configuration, normalised to the baseline case in the Community Renewables grid scenario.

despite being the focus of the EAA. The fact is that so many different activities contribute to climate change that any one of them, such as domestic electricity use, forms only a small part of the whole. The normalisation procedure used in this chapter, while contextualising the magnitude of impacts from different PV-battery configurations, cannot give a complete perspective without information on how close the EU is to breaching any of the ecological boundaries represented by the impact categories. This would be a useful direction for further work; for now, climate change can be regarded as important due to the attention given it by the IPCC (2018) and in the Paris Agreement (UNFCCC, 2018). Then the impact categories that rank higher than it should be the subject of special concern, as impacts to mitigate in the course of taking (policy) action against climate change.

Figure 6.26 shows that a small reduction of -3 % in life-cycle CC impact can be achieved without doing anything, if the grid evolves along the Two Degrees scenario rather than Community Renewables. The former features a doubling of nuclear capacity to 18 GW, and the presence of 12 GW of CCS plants. But in both scenarios, a highly significant reduction in life-cycle CC impact results from installing PV (-11 % in CR, -13 % in TD, though from the reduced baseline of -3 %). This benefit is reduced (though not significantly) by adding a new battery running the Greedy algorithm, but restored if the battery is

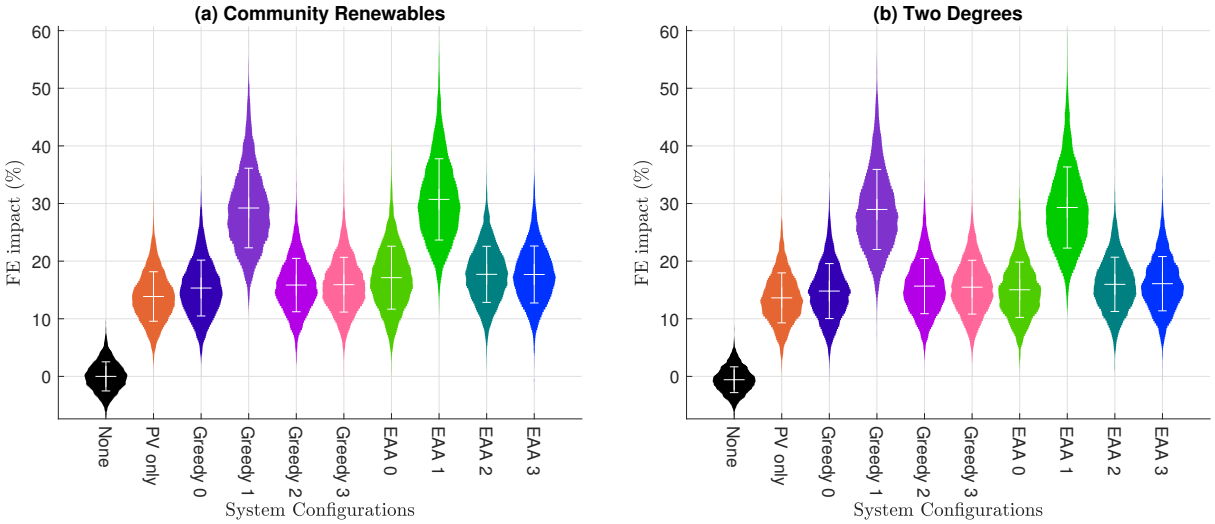

FIGURE 6.24: Distribution plots of Freshwater Eutrophication impact in each configuration, normalised to EU impact in this category.

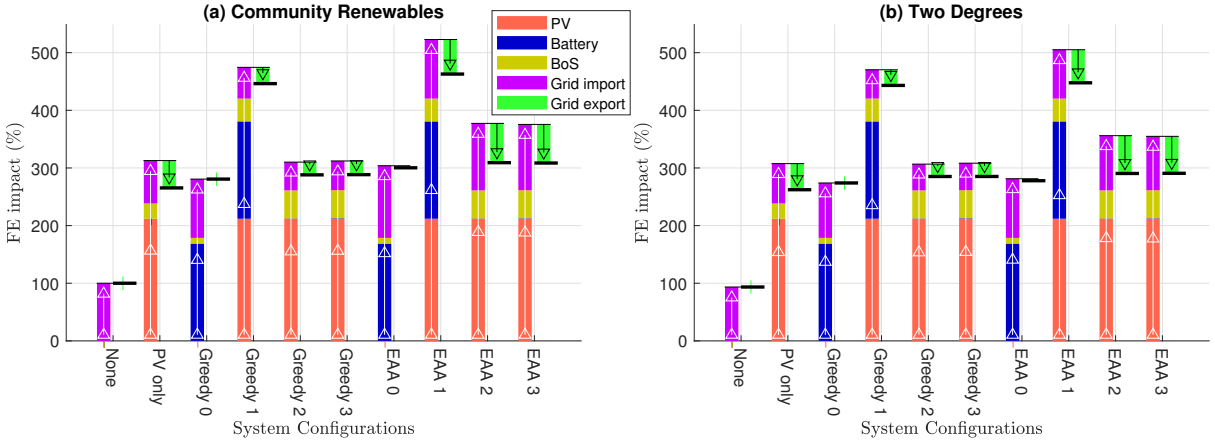

FIGURE 6.25: Breakdown of contributions to Freshwater Eutrophication impact in each configuration, normalised to the baseline case in the Community Renewables grid scenario.

second-life. The benefit is enhanced by running the EAA on the PV-battery system instead, and even further to around -16 % if the battery is second-life.

The battery-only configuration running the EAA ('EAA 0') gives a small and insignificant benefit, and is a poor option considering the financial cost (see Figure 6.1). The multi-lobed distribution shapes of the configurations with PV show that their variation is dominated by house-to-house variation. Indeed, the contribution of PV manufacture to the total life-cycle impact (around 15 % of the baseline impact in Figure 6.27) is a greater proportion of the total in the configurations with PV. This, combined with the relatively low uncertainty in PV manufacture impacts (1.15 ± 0.125 ton CO_2/kW_p, from Chapter 2), and the strong dependence of PV capacity on household electricity consumption (Chapter 5), would explain the dominance of the house-to-house variation.

Human Toxicity impacts are subject to a great degree of uncertainty, and so although Figure 6.28 shows them to be increased (worsened) by installing PV and/or battery, the changes are only just significant. As the changes are of magnitude a few percent, they may not be of great concern compared to other activity within the EU. This is despite them doubling or more in all configurations relative to the baseline

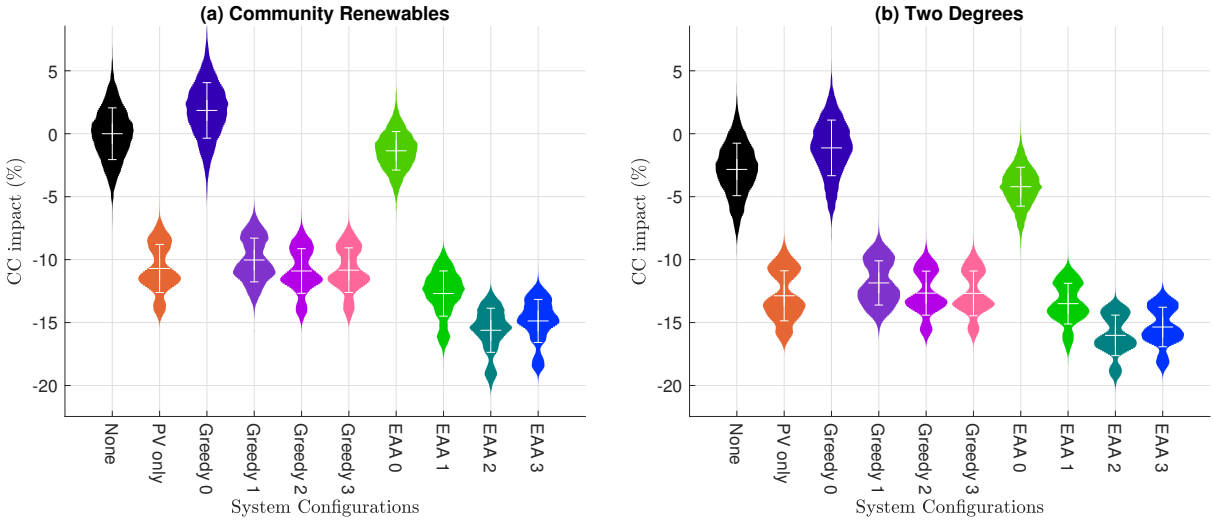

FIGURE 6.26: Distribution plots of Climate Change impact in each configuration, normalised to EU impact in this category.

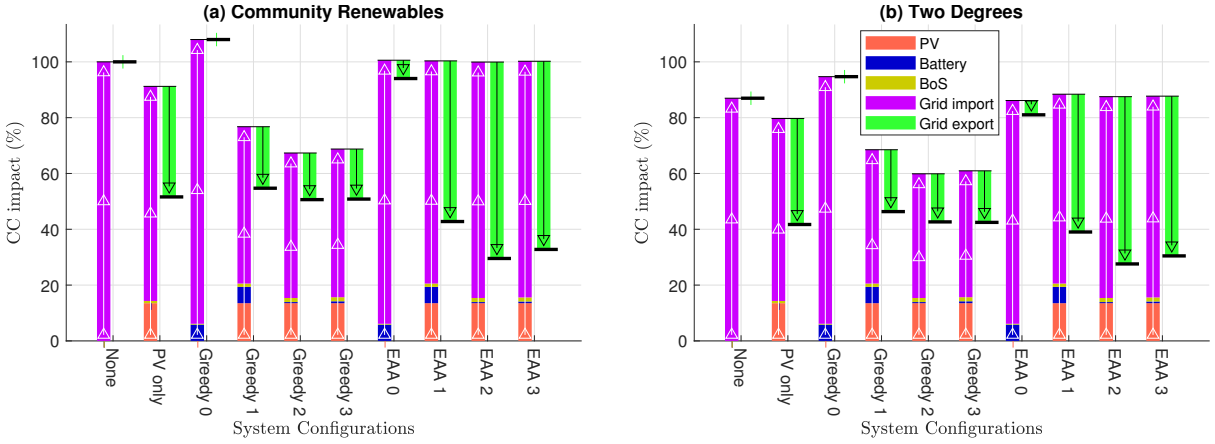

FIGURE 6.27: Breakdown of contributions to Climate Change impact in each configuration, normalised to the baseline case in the Community Renewables grid scenario.

(Figure 6.29).

Figure 6.29 shows the HT impacts to be dominated by manufacture of the system components. Improvements in the processing and materials used for PV, battery and BoS, are all worthwhile to attempt.

Figure 6.30 shows that the configurations with a new battery ('Greedy 0' and '1', 'EAA 0' and '1') significantly increase the Ozone Depletion impact relative to the baseline. However, the magnitude is small, around 5 %, indicating there are other activities of greater concern contributing to OD within the EU. The uncertainty is also large, the inter-standard deviation range spanning around 5 %-points. By contrast, the uncertainty range is vastly smaller for the PV-only configuration and those with second-life batteries. These all reduce the life-cycle OD impacts relative to the baseline, though only by -1 %.

Figure 6.31 shows that the roughly 7-fold increase in OD impact with a new battery compared to the baseline is almost wholly a result of battery manufacture. There is some evidence (Vandepaer et al., 2017) to suggest that the specific sub-process responsible is the production of PTFE binder used in cementing the electrode active material to the current collectors. Not all batteries use PTFE (Vandepaer et al.,

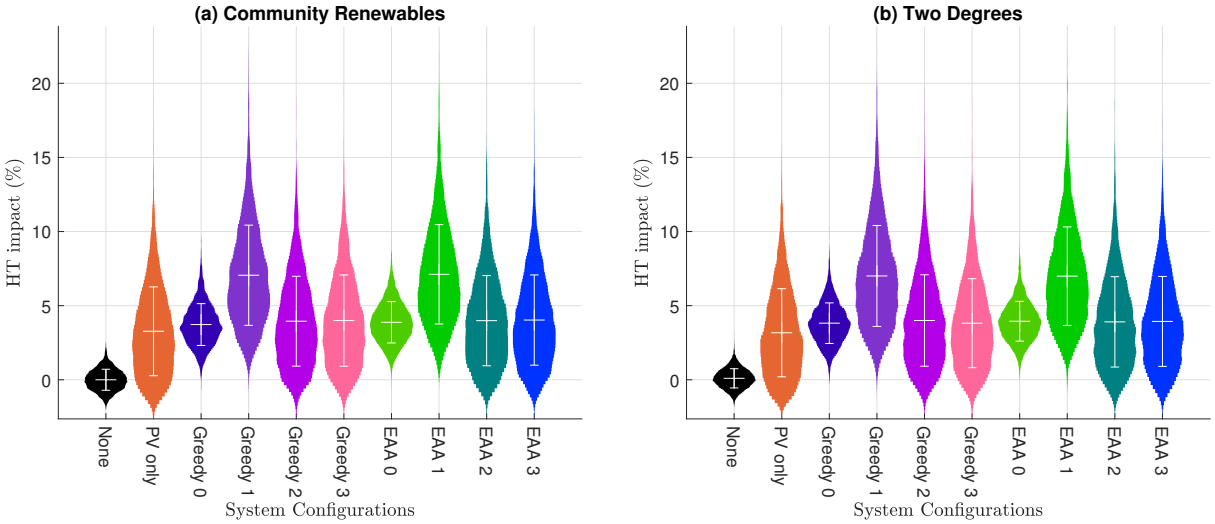

FIGURE 6.28: Distribution plots of Human Toxicity impact in each configuration, normalised to EU impact in this category.

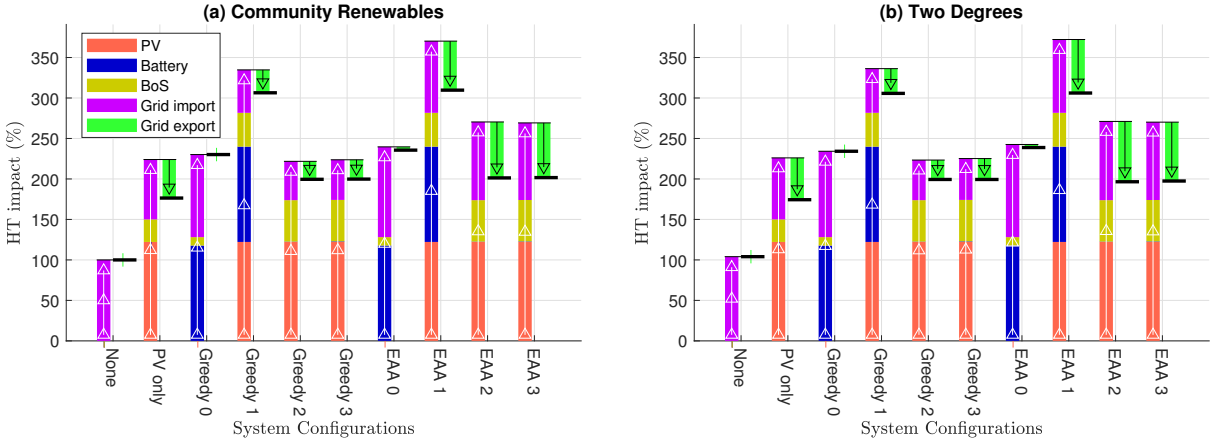

FIGURE 6.29: Breakdown of contributions to Human Toxicity impact in each configuration, normalised to the baseline case in the Community Renewables grid scenario.

2017), which would explain at least some of the sizeable variation in OD impact for the configurations with a new battery.

Figure 6.32 shows that while installing PV significantly increases (worsens) the Water Depletion impact, and while PV-battery cases with a new battery are significantly worse than the others, the large uncertainty range reduces the confidence with which any other inferences can be made. Furthermore, the magnitude of the changes is small, a few %, indicating low concern for the EU relative to other water-depleting activities.

The small magnitude of changes in normalised WD impact is despite the large changes relative to the baseline (up to 11-fold), shown in Figure 6.33. Battery manufacture dominates the WD impact, closely followed by PV manufacture.

Figure 6.34 shows that installing PV can reduce Photochemical Oxidant Formation by up to -3 %, but only just significantly. The benefits rendered by PV with a second-life battery are at a similar level. This benefit is less for PV with a new battery ('Greedy 1' and 'EAA 1') but not significantly so. The small magnitude of the changes indicates low concern for the EU relative to other activites that lead to POF.

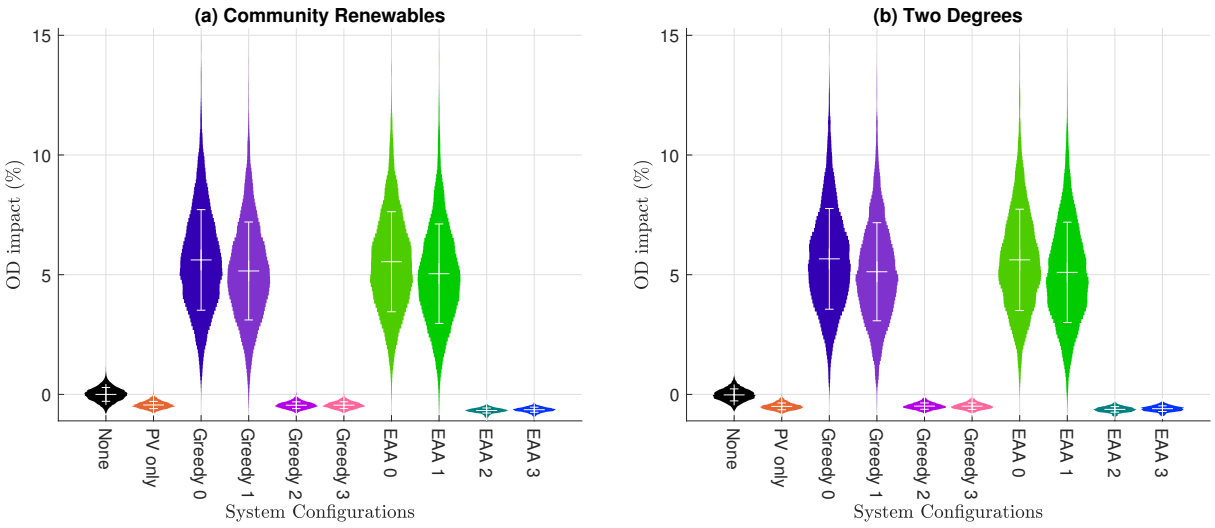

FIGURE 6.30: Distribution plots of Ozone Depletion impact in each configuration, normalised to EU impact in this category.

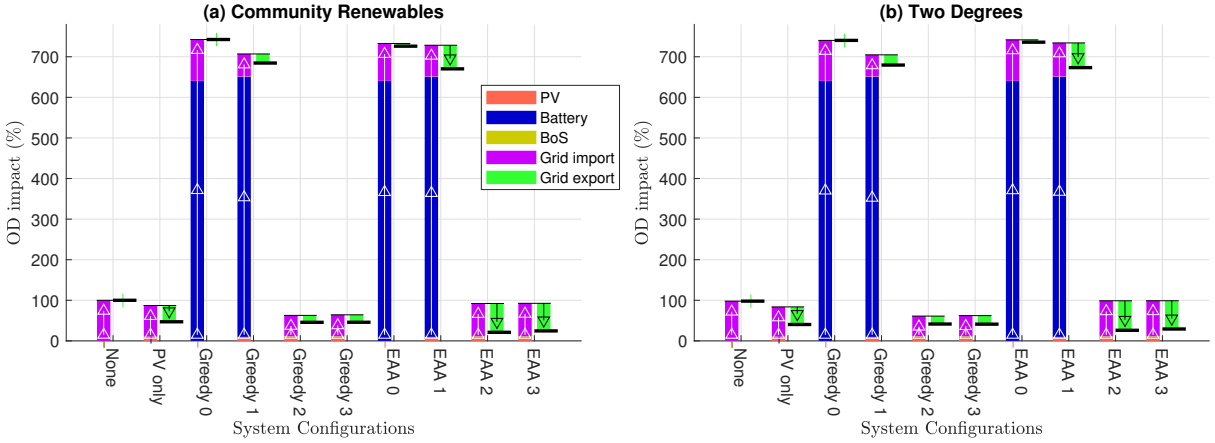

FIGURE 6.31: Breakdown of contributions to Ozone Depletion impact in each configuration, normalised to the baseline case in the Community Renewables grid scenario.

POF impact is dominated by grid import and where applicable, PV manufacture, according to Figure 6.35.

Figure 6.36 shows that installing PV can reduce Marine Eutrophication impacts by up to -2 %, but only just significantly. The benefits rendered by PV with a second-life battery are at a similar level in the TD future grid scenario, but in CR, PV with a second-life battery running the EAA renders less benenfit, -1 %. This benefit is also less for PV with a new battery ('Greedy 1' and 'EAA 1'), only just significantly. The small magnitude of the changes indicates low concern for the EU relative to other activites that lead to ME.

ME impact is dominated by grid import and where applicable, PV manufacture, according to Figure 6.37.

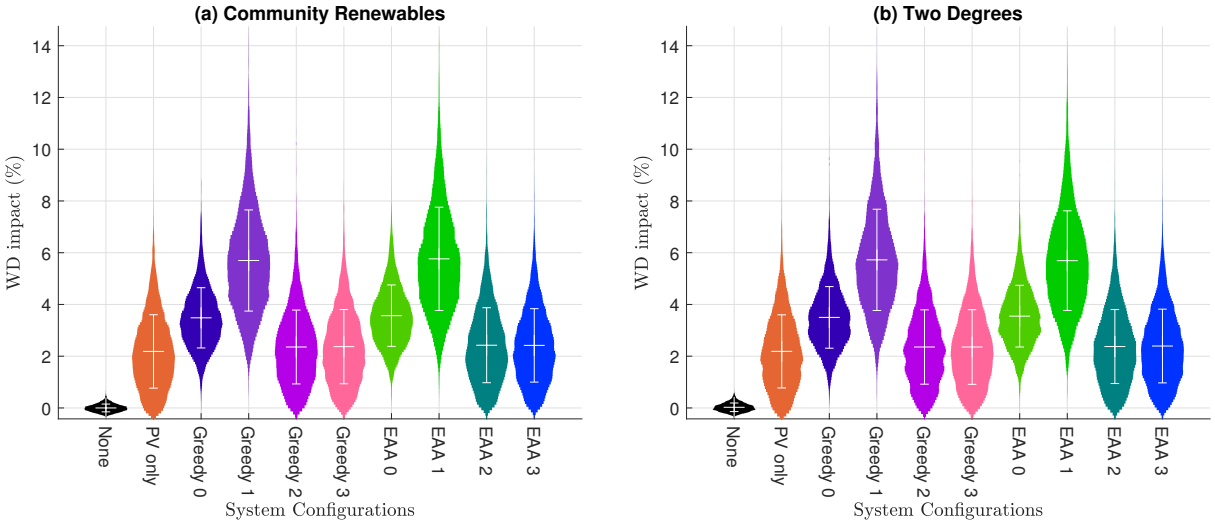

FIGURE 6.32: Distribution plots of Water Depletion impact in each configuration, normalised to EU impact in this category.

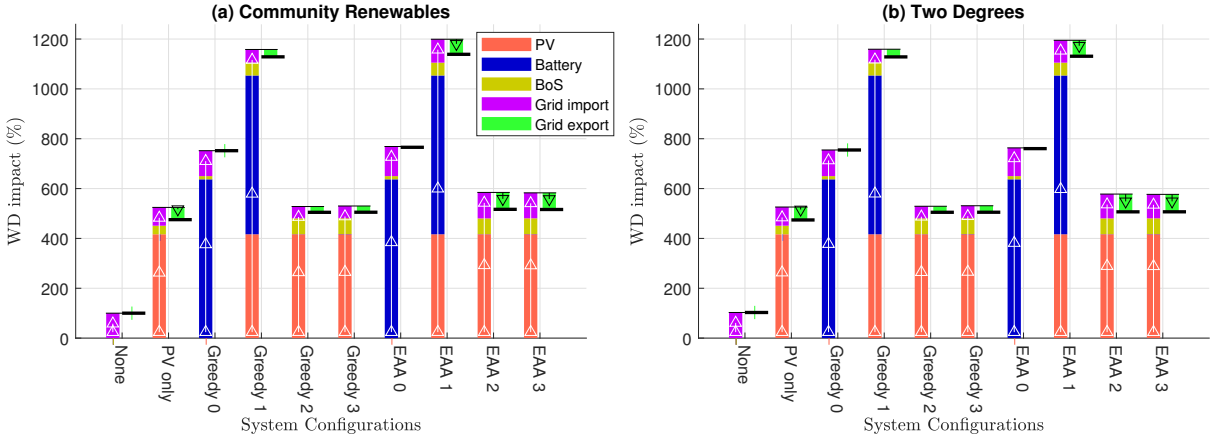

FIGURE 6.33: Breakdown of contributions to Water Depletion impact in each configuration, normalised to the baseline case in the Community Renewables grid scenario.

6.2.4 Discussion of Environmental Impact Results

When considering the foregoing environmental impact results, it is useful to bear in mind the different factors being compared:

- PV-only against the baseline (no PV nor battery),
- PV-battery against PV-only,
- Second-life batteries against new,
- EAA against the Greedy algorithm,
- TD future grid scenario against CR.

Regarding the Climate Change impacts, which are the focus of the EAA in this thesis, a highly significant improvement is achieved compared to the baseline simply by installing PV. Adding a battery does not

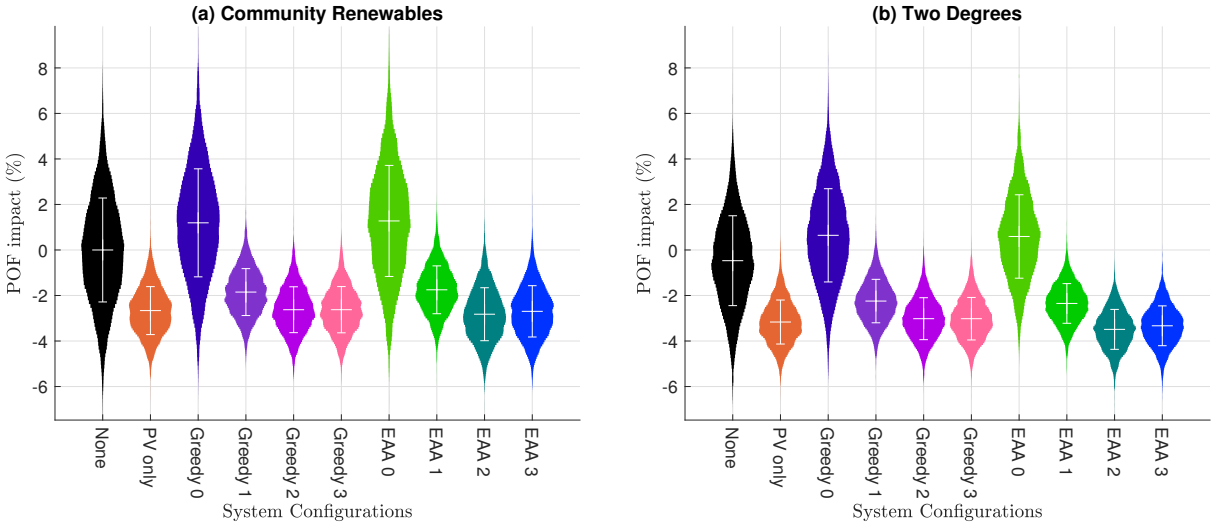

FIGURE 6.34: Distribution plots of Photochemical Oxidant Formation impact in each configuration, normalised to EU impact in this category.

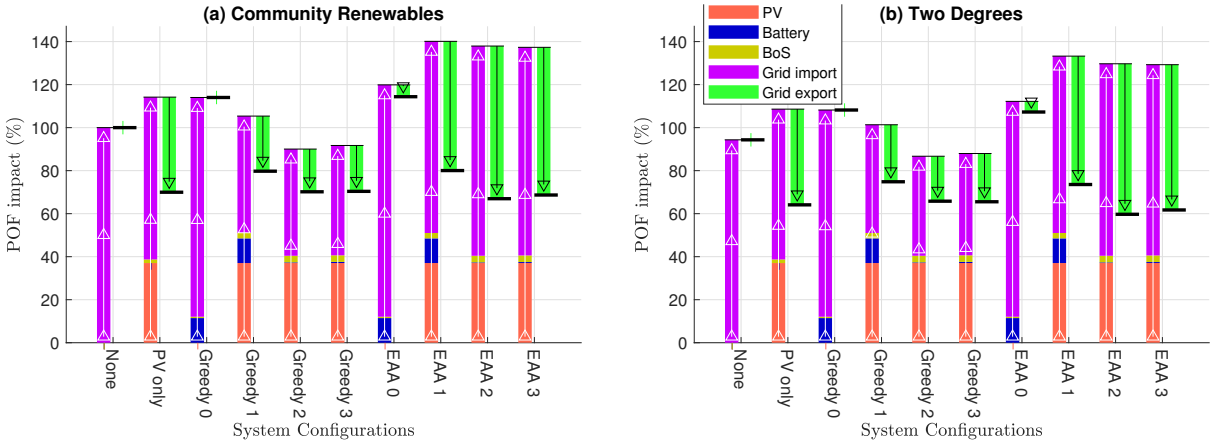

FIGURE 6.35: Breakdown of contributions to Photochemical Oxidant Formation impact in each configuration, normalised to the baseline case in the Community Renewables grid scenario.

increase the improvement significantly, unless it is a second-life battery running the EAA. Second-life batteries achieve greater reduction in CC impact than their new counterparts, though this is insignificant with the Greedy algorithm. Greater improvements are achieved in the TD scenario than in CR when normalised against EU activity, but it can also be argued that the improvements are *smaller* in TD when referenced against the TD baseline rather than the CR baseline.

As well as the rank ordering of impact categories in the previous section, by importance relative to other activity within the EU, some alternative divisions can be observed. For instance, some of the impact categories are dominated by embodied impacts of manufacturing the system components (MD, FE, HT, OD, WD, and to some extent FET) while others are dominated by impacts of grid generation (IR, LO, FD, CC, and to some extent POF). The remaining categories (TA, ME, PMF) fall in between them.

Manufacturing-dominated categories are characterised by a worsening of the impact relative to the baseline when adding PV, batteries, or both. As such, the effect of using second-life batteries rather than new, is to reduce the magnitude of this environmental burden. This is a strong point in favour of second-life batteries, although they never bring the impacts down below the level of the PV-only configuration,

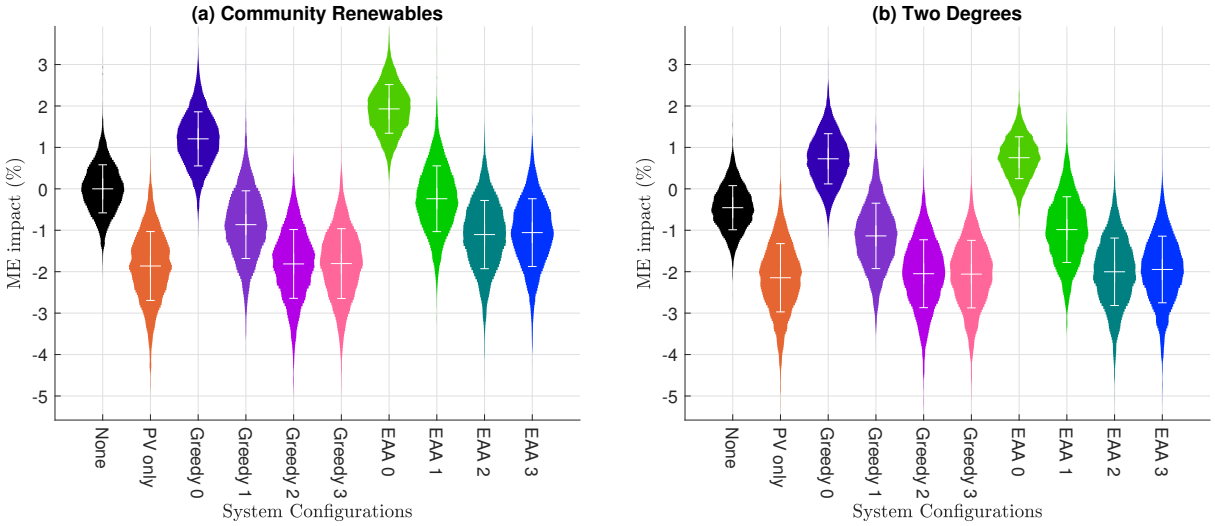

FIGURE 6.36: Distribution plots of Marine Eutrophication impact in each configuration, normalised to EU impact in this category.

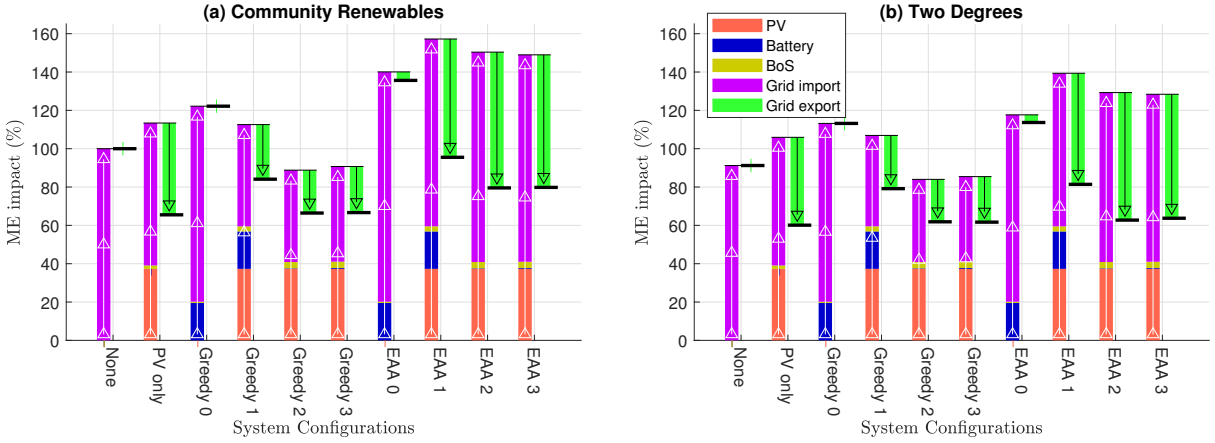

FIGURE 6.37: Breakdown of contributions to Marine Eutrophication impact in each configuration, normalised to the baseline case in the Community Renewables grid scenario.

with the exception of the OD category. OD is a special case because the contribution from battery manufacture is so disproportionately large - unlike for the other manufacturing-dominated categories, the PV-only and PV with second-life battery configurations reduce rather than worsen OD impacts relative to the baseline.

Grid-dominated categories are characterised by a reduction (improvement) of the impact relative to the baseline when installing PV or PV-battery. For IR and LO, a second-life battery is not significantly better than a new one; for FD and POF, a second-life battery is better but insignificantly so, and for CC, a second-life battery is significantly better only when comparing configurations running the EAA.

Another way of dividing the impact categories is by whether a PV-battery system reduces or increases the impact when running the EAA rather than the Greedy algorithm. The EAA is significantly better than the Greedy algorithm when considering FD, CC, OD (though significantly only when considering the second-life battery cases), and better but insignificantly for POF. The EAA is significantly worse than the Greedy algorithm when considering LO. For ME, TA, IR, and PMF, the EAA is worse than the Greedy algorithm, but insignificantly so.

The key conclusions that can be drawn from this are:

- where possible, PV-only is the configuration that strikes the best balance between reducing life-cycle environmental impacts in grid-dominated categories (IR, LO, FD, CC, POF) and restricting harms in manufacturing-dominated categories (MD, FE, HT, WD, OD, FET); and while adding a battery to the installation can enhance the grid-dominated impact reductions, these improvements are mostly small to insignificant, and tend to worsen the manufacturing-dominated impacts;
- Second-life batteries restrict the harm in manufacturing-dominated impact categories, with small to insignificant effects in other categories;
- Running the EAA on a PV with second-life battery system enhances life-cycle environmental impact reductions relative to the Greedy algorithm in FD, CC and OD categories, with insignificant side-effects in other categories (except for LO, in which the EAA is significantly worse);
- These conclusions are robust between CR and TD future grid scenarios; the differences between them tend to be differences in quantity rather than sign.

There are promising synergies possible between the EAA and second-life batteries: together, they do more to reduce environmental impacts in the grid-dominated categories and to restrict the increase in manufacturing-dominated impacts, than each feature on its own (that is, running the EAA on a new battery, or running the Greedy algorithm on a second-life battery). However, the financial analysis of Section 6.1 shows that running the EAA on a PV system with second-life batteries results in close to the lowest profitability out of all the configurations. Some possibilities for addressing this are discussed in Section 6.4, but from the foregoing, the best balance between financial and environmental benefit to the homeowner is the PV-only configuration. This is true only where installation of a PV-only system is possible - the increase in voltage violation problems for distribution networks may change the situation (Crossland et al., 2018; Tant et al., 2013), but further analysis is beyond the scope of the thesis.

From the perspective of the battery industry, this study provides evidence contributing to a roadmap to designing in greater sustainability. While second-life usage is one way to restrict the increase in manufacturing-dominated environmental impacts of an expanding battery market, it is far from the only way. Recycling, if processes can be improved to the extent that valuable but low-quantity materials can be recovered, could go a long way towards tackling Metals Depletion especially (Harper et al., 2019). In the ReCiPe framework, the MD category is considered a harm to commodity prices, as mining finite resources leads to a need to expand exploration into lower-grade deposits where the resources are more difficult and costly to extract. This would stymie the growth of the battery market, if the raw materials become so expensive, but additionally poses a humanitarian concern for mine workers who often labour in unsafe and unhealthy conditions (McManus, 2012).

A complementary route to improving sustainability is to substitute less problematic materials at the manufacturing stage, and to better control the processes and waste streams. For example, OD could be reduced almost single-handedly by substituting a less ozone-depleting binder material for PTFE. Of the manufacturing-dominated impact categories, three of them relate to water: Water Depletion, Freshwater Ecotoxicity and Freshwater Eutrophication. This supports a recommendation of better standards in the use and disposal of water in battery manufacturing processes. It is beyond the scope of this study to quantify the financial effects of making any of these changes.

The results of this section offer evidence to support recommendations to the PV industry as well as the battery industry. In nearly all of the manufacturing-dominated impact categories, the manufacture and installation of PV contributes more than the battery. Reducing these impacts by improving processes, substituting materials, and increasing material recovery and recycling rates, would improve the sustainability of all PV-only and PV-battery configurations. As such, PV-only may still be the best choice for a homeowner in terms of balancing financial and environmental benefits. Note that the majority of MD impact comes from battery manufacture, but even the PV contribution is not so much from the PV cells themselves, but the silver and copper used as electrical conductors to join the cells together.

From the perspective of electricity generation on the grid, a particularly interesting effect of the use of the EAA in domestic PV-battery systems is that they increase the demand for biomass generation, to the extent that Land Occupation life-cycle impacts are worse than when running the Greedy algorithm. Options for mitigating this impact are: incentivise or enforce standards on biomass production to be only from waste (food waste, farm waste, forestry residue) or crops grown on land unsuitable for other purposes; restrict biomass-fuelled generating capacity on the grid (indeed, it is less in the TD scenario, where the LO impact is less bad than in CR); adapt the EAA to schedule battery operation based on factors other than the marginal CC intensity on the grid. The last option raises questions of which factors should be combined and how, and whether and how any standards can be enforced or incentivised. These issues are discussed further in Section 6.4.

6.3 Sensitivity to Investment Start Year

The results so far have all been for a system temporal boundary of 25 years beginning in the year 2020. The model was run again with a start year of 2030, and the results presented here. The delay of 10 years means that within the assumptions of the study, battery costs have fallen, electricity prices have risen, PV and BoS costs have held steady in numerical terms (declined with inflation in real terms), and the GB grid is further along one of two routes to decarbonisation (CR and TD future grid scenarios). Sensitivity to Capex and electricity retail price increase were also analysed separately, to disentangle their contributions to the different financial results in 2030 compared to 2020. The heuristic optimisation of Chapter 5 was not performed again for the 2030 start year, but it cannot be assumed that the heuristically optimal system sizes for an initial investment in 2020 will still apply in 2030.

6.3.1 Effect of Investment Start Year on Finances

With a start year of 2030, the baseline MCoEs (Figure 6.38) are higher than for 2020 (Figure 6.1, above) due to the above-inflation increase in electricity prices, 5.5 % annually compared to 2.1 % inflation. Unlike for the 2020 start year, all 8 houses can decrease their MCoE by installing PV in 2030. While the battery-only configurations ('Greedy 0' and 'EAA 0') are still poor investments, a PV-battery system running the Greedy algorithm can now achieve even lower MCoE than a PV-only system.

The EAA still cannot compete with the Greedy algorithm on MCoE, but in some cases can compete with the baseline ('None'). These cases are: House 5 (all), and Houses 8, 7, 6, 1 (new battery in either future grid scenario, or TD only if second-life). The TD scenario again tends to result in lower MCoE than CR for configurations running the EAA, but the MCoE now tends to be slightly higher with second-life rather than new batteries, for best-case as well as worst-case. Contrast this with a start year of 2020,

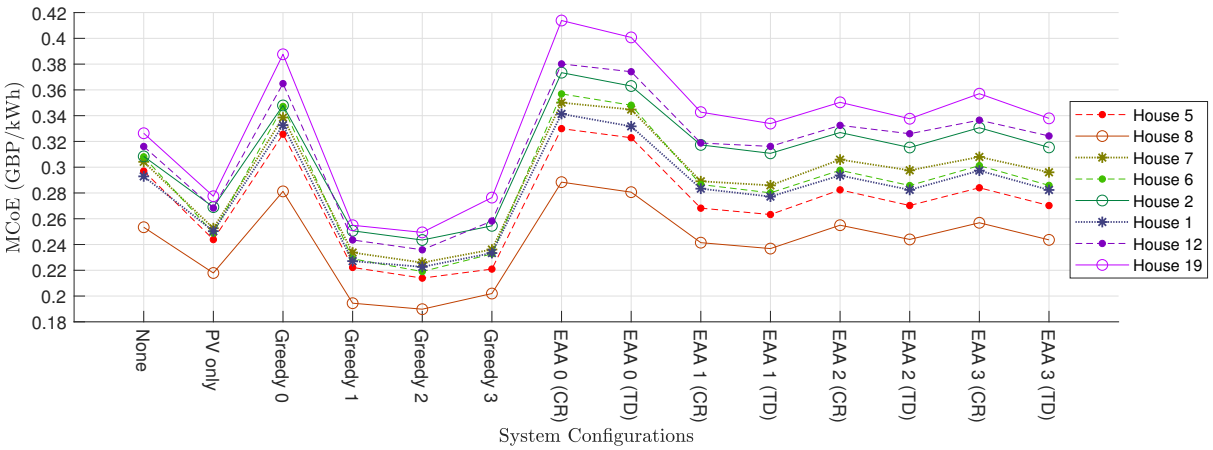

FIGURE 6.38: Mean Cost of Electricity for each house in each configuration, start year 2030.

where the best-case second-life battery tended to result in similar or lower MCoE than a new one, and the worst-case second-life battery led to higher MCoE.

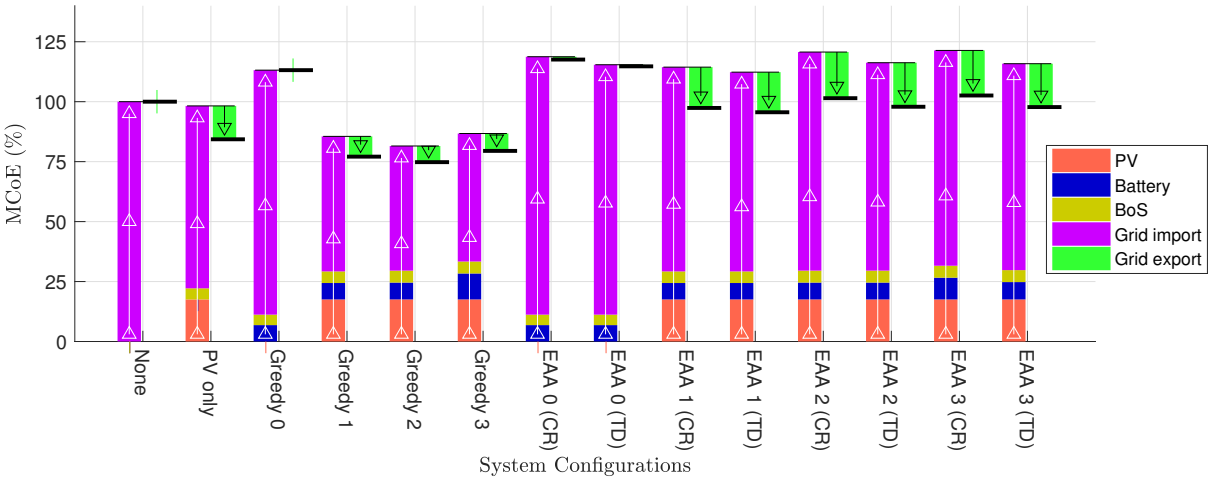

FIGURE 6.39: Mean breakdown of contributions to Mean Cost of Electricity in each configuration, start year 2030.

Figure 6.39 shows the combined effects of a real-terms increase in electricity prices and real-terms decreases in the costs of PV, battery and BoS: the former comprise an even larger proportion of the total MCoE when the initial investment is made in 2030 compared to 2020. Again, the worst-case second-life battery comprises more of the MCoE than when using a new or best-case second-life battery due to the costs of more frequent replacement.

The evolution of new and second-life battery prices (see Chapter 4 Section 4.3) is such that the difference between new and second-life is less in 2030 than in 2020. The result is that in contrast to the Capex on a PV-battery system being slightly less when investing in a (larger-capacity) second-life battery compared to a new one in 2020 (Figure 6.3), the Capex is almost identical and for Houses 5 and 8 slightly higher when investing in a second-life battery in 2030 ('Greedy/EAA 2' and '3' compared to '1' in Figure 6.40). The price differential between new and second-life batteries has been predicted in this thesis to narrow in future. This leads one to question the financial value of second-life batteries in domestic applications, as they are likely to become a worse proposition over time.

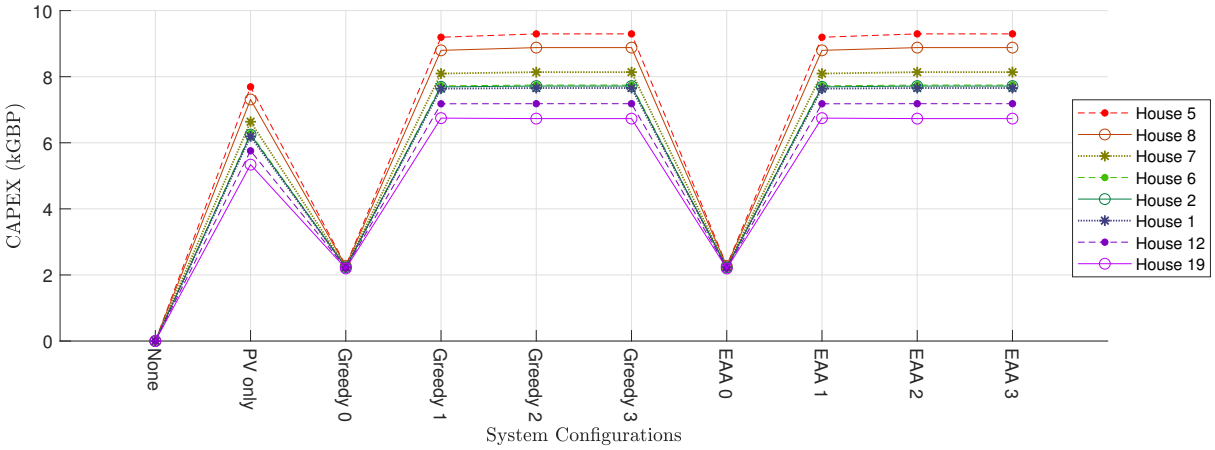

FIGURE 6.40: Capital expenditure for each house in each configuration, start year 2030.

The effect of differing cost decline rates between PV and battery can also be observed in Figure 6.40 compared to Figure 6.3: the Capex on the PV-only configurations in 2030 are around 80 % of what they were in 2020 (in real terms), whereas on the PV-battery systems, they are around 70 % of what they were, and on the battery-only systems, are around half. If batteries do decrease in cost faster than PV arrays, one can expect a comparatively larger battery pack to be optimal in future. This should be investigated in further work, specifically how the optimal capacities of each system component might change over time in response to their changing costs, and the effects of allowing the capacity to change at each replacement. (In this study, each time the BoS and batteries were replaced, it was with components of the same capacity as originally installed.)

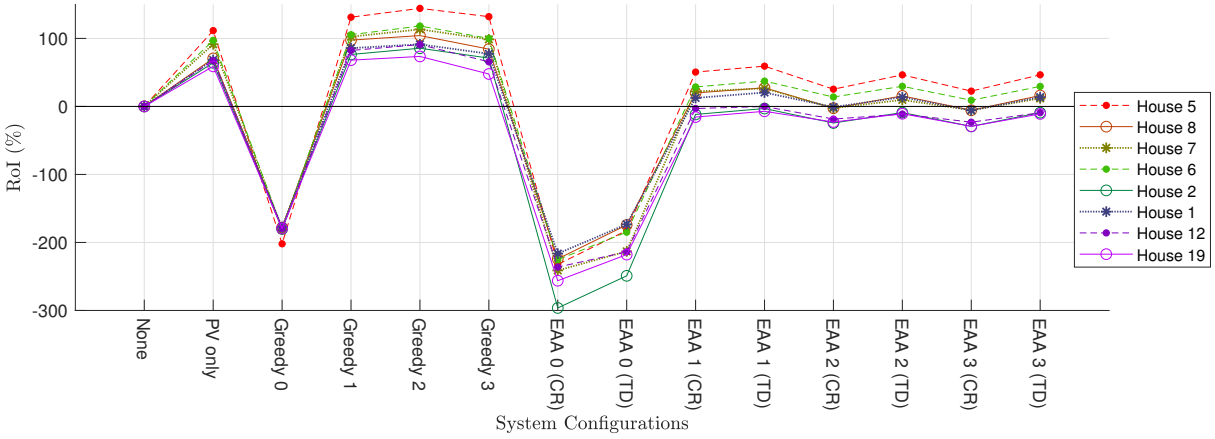

FIGURE 6.41: Return on Investment for each house in each configuration, start year 2030.

Examining the RoI (Figure 6.41), IRR (Figure 6.42) and PP (Figure 6.43) for an investment start year of 2030 confirms the findings deduced from the MCoE. The savings achieved relative to the baseline by installing PV results in RoI of 60-110 %, IRR of 6.1-9.3 %, and PP of 9-11 years. Adding a new battery to the installation, running the Greedy algorithm, the savings are increased resulting in RoI 70-130 %, IRR 6.8-11 %, and PP 8-10 years. The results are even better with a best-case second-life battery but not as good with a worst-case one. In these cases the PP is always below 15 years, the typical working lifetime of a battery. This is a good sign that battery costs in 2030 would have decreased to a level that they are a worthwhile investment. (Note that no improvement in battery lifetime as technology progresses has been accounted for in this study.) The same cannot be said for PV-battery systems running the

EAA, whose PP comes below 15 years only for the highest-consuming houses, if they use new rather than second-life batteries, and in some cases if the grid evolves along the TD scenario rather than CR.

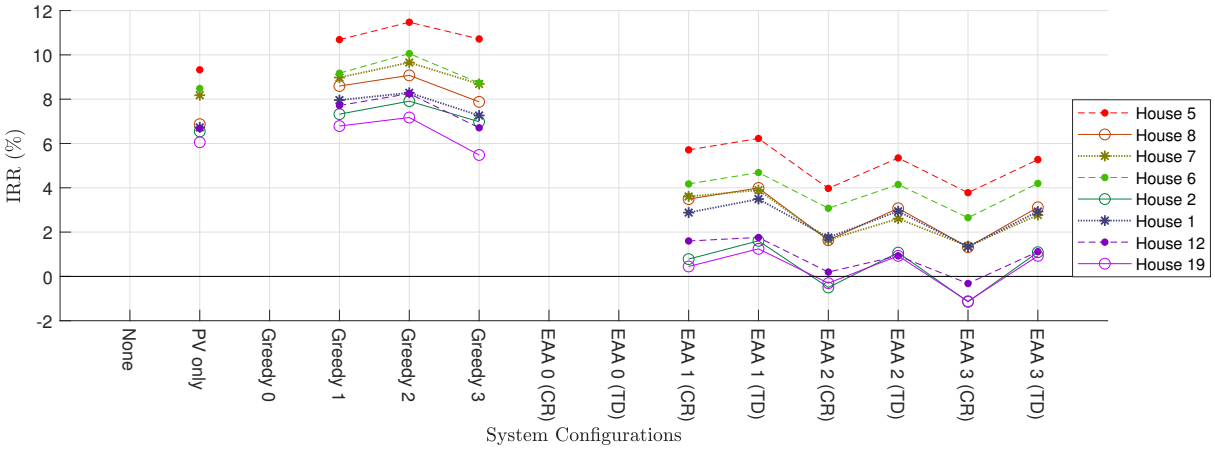

FIGURE 6.42: Internal Rate of Return for each house in each configuration, start year 2030. Values below -100 % are excluded from the chart.

Similarly, the RoI is smallest for the configurations running the EAA, even dropping below zero for Houses 19, 12 and 2 (Figure 6.41). IRR is also smaller for the EAA configurations, although it remains above zero for all cases except Houses 19, 12 and 2 with second-life batteries in the CR scenario. Note that this does not necessarily mean a profitable investment for the other houses, but would depend on their attitude to risk and the other investment options available to them.

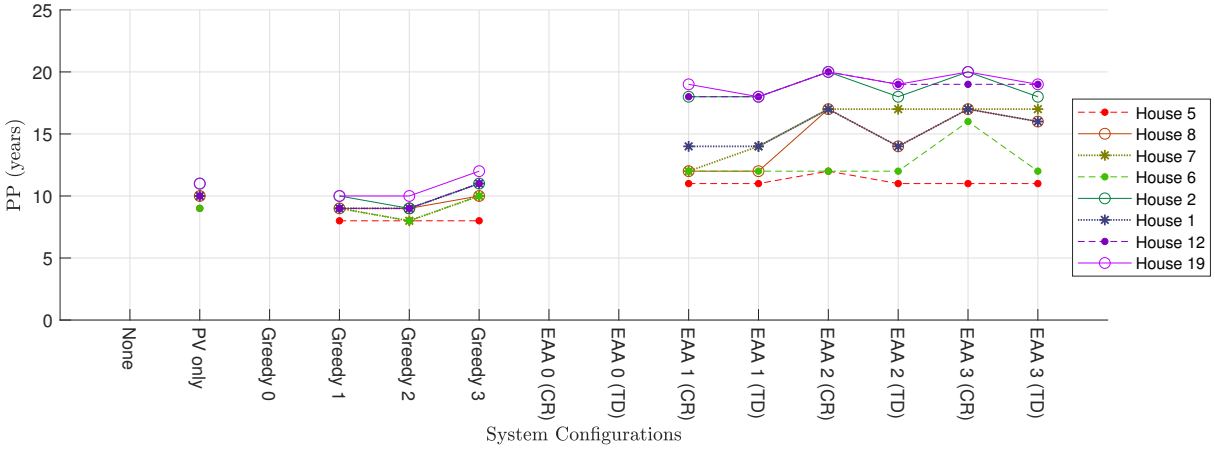

FIGURE 6.43: Payback Period for each house in each configuration, start year 2030. Values above 25 years are excluded from the chart.

While these results strongly indicate that delaying the initial investment would improve financial returns, there is a danger to interpreting this as advice or a recommendation. If the potential market for home battery products were to delay investment, this could restrict the industry's opportunity for learning by installing more products and possibly result in battery costs not declining as quickly as expected. This may lead to decisions to further delay investment, further restriction to the battery industry's learning opportunities, and even slower cost declines, in a vicious cycle.

Instead, these results are more useful to battery suppliers as one piece of evidence among many which indicate a target to aim for. That is, reduce costs and improve efficiencies to a level that allows them to charge 2030 prices for their products (as used in this study), and the PV-battery proposition will become

objectively more profitable than PV-only for a wide range of households. With appropriate marketing, this could lead to a rapid increase in sales.

To explore this more quantitatively, the 8 households were simulated again with the baseline configuration, with PV-only, and PV with new battery running the Greedy algorithm, for a start year of 2020. The electricity price annual rise and the relative Capex were varied independently: the former between -0.5 % to 9.5 %, the latter between 60 % to 140 % (affecting all components equally: PV, battery, BoS and their replacements, and both fixed and size-dependent portions of cost). Figure 6.44 shows, across this parameter space, the proportion of the 8 houses for which PV-only is a better investment than the baseline. With a 5.5 % nominal annual increase in electricity price and Capex as used in this study, only 3 out of 8 of the houses improve their MCoE and RoI by installing PV-only, although all improve their IRR and PP (relative to a low bar of 0 % IRR and 25 years PP). A Capex decrease of only 20 % could render PV arrays worthwhile investments for all houses considered, although a steeper discount is required if electricity price is expected to increase less quickly: roughly 10 % in Capex for every 1 % in electricity price.

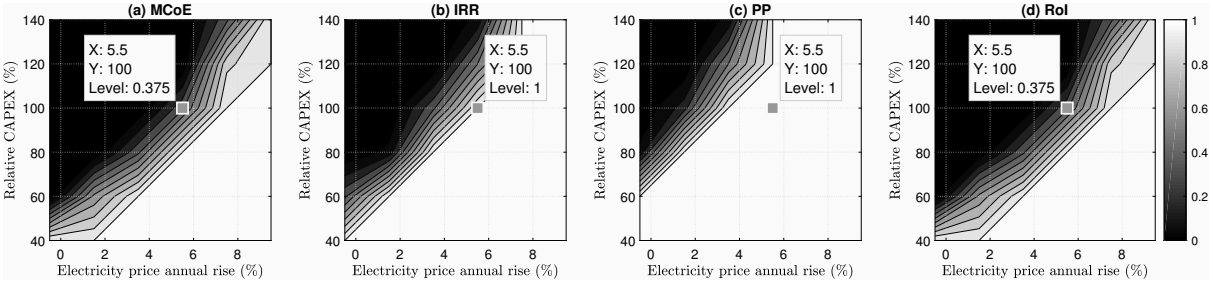

FIGURE 6.44: Proportion of houses for which PV-only is a better investment than the baseline, as a function of Capex and electricity price increase rate, according to a) Mean Cost of Electricity, b) Internal Rate of Return, c) Payback Period, d) Return on Investment.

Figure 6.45 shows the proportion of the 8 houses for which PV with new battery running the Greedy algorithm is a better investment than PV-only. Again, a Capex decrease of only 20 % could tip the balance in favour of PV-battery systems. In this case, the balance is less sensitive to the electricity price increase. Interestingly, when considering payback period, it seems that if electricity price increases too slowly, a PV-battery system would not be worthwhile at any price above 40 % of the Capex used in this study.

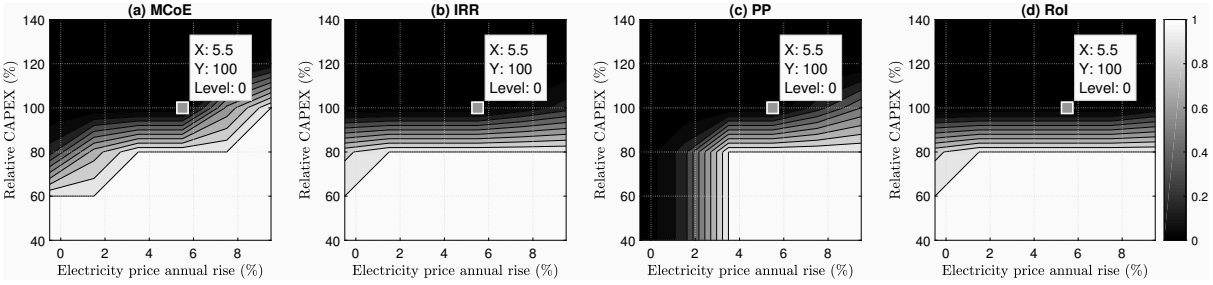

FIGURE 6.45: Proportion of houses for which PV-battery ('Greedy 1') is a better investment than PV-only, as a function of Capex and electricity price increase rate, according to a) Mean Cost of Electricity, b) Internal Rate of Return, c) Payback Period, d) Return on Investment.

One may ask what electricity price increase rate is reasonable to assume, whether the historic rate of 5.5 % will continue in future? GB must invest in its generation infrastructure going forward regardless of the specific form that that infrastructure will take: whether vast expansion in wind, PV and other

renewables, replacement and expansion of the aging nuclear capacity, or replacement of aging CCGT plants (Deane et al., 2015). These costs may be passed on to electricity bill-payers, although it cannot be said whether they will lead to a faster increase in the variable (per-kWh) costs or the standing charge (the former would render PV-battery systems more profitable, for avoiding these costs, whereas the standing charge cannot be avoided). Alternatively, these costs may be recovered through general taxation, leading to less of an increase in electricity prices. This would require a complete reversal of the privatised model of electricity generation and supply that has dominated for the past three decades, although it should not be discounted as impossible.

6.3.2 Effect of Investment Start Year on Environmental Impacts

These financial results must be considered in tandem with the changing environmental impact results. The ones given below should be taken as provisional, because they assume the embodied impacts of manufacturing PV, battery and BoS not to change over time, when in fact technological progress will almost certainly lead to changes. As such, the life-cycle impacts in the manufacturing-dominated categories (MD, FE, HT, WD, OD, FET) are almost identical for start year 2030 compared to 2020, under the simplification of this study. However, one example of the effects of the evolving electricity grid are clear to see from Figure 6.46:

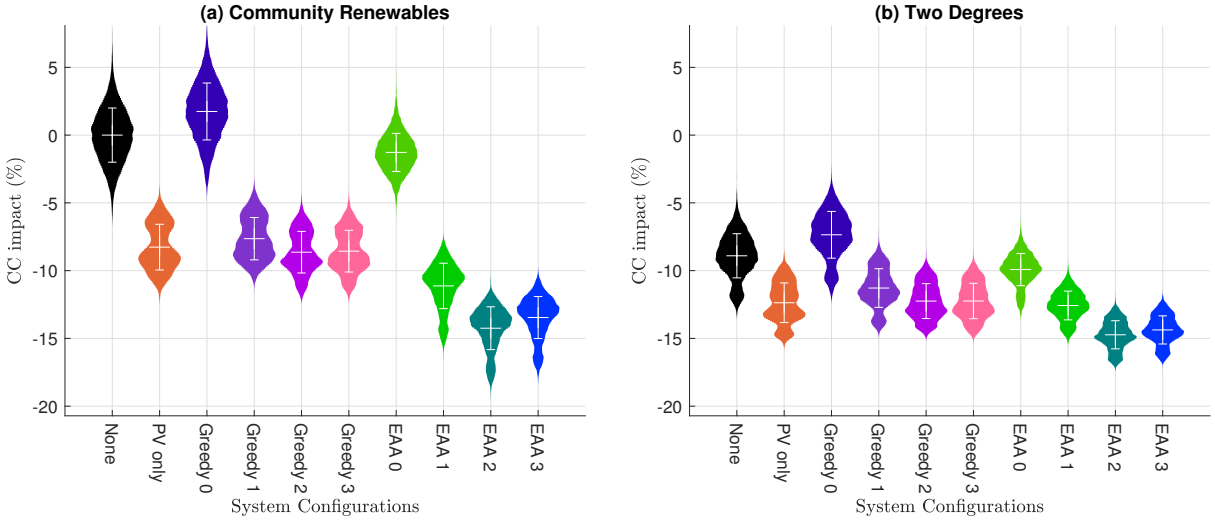

FIGURE 6.46: Distribution plots of Climate Change impact in each configuration, normalised to EU impact in this category, start year 2030.

The life-cycle CC impact reductions (normalised against EU activity) are smaller in magnitude for a start year of 2030 than for 2020. In the TD scenario, the reductions achievable by the PV-battery systems are similar or larger in magnitude relative to the CR baseline, but much more similar to each other and to the TD baseline. This is because for a later start year, the grid as a whole is lower-carbon for the 25-year duration of the system in question, and even lower-carbon if the grid evolves along TD rather than CR. That is, not installing PV nor battery can still save CO_2 emissions as long as the grid decarbonises in a more centralised way.

In a lower-carbon future, each individual PV-battery system has less effect as it is shifting import and export to a grid that is less CO_2-intense. In the extreme case of a zero-carbon grid, with no CO_2-intensity differential between different times of day, a home battery is of course no use at all in arbitraging

emissions (though it may offer other environmental benefits such as those associated with aggregated ancillary services, which are beyond the scope of this study to analyse).

On the other hand, the PV with second-life battery running the EAA is still the configuration with lowest CC impact (greatest reduction compared to the baseline). If a projection of EU activity into the future were available to use in the denominator of the normalisation, rather than the Benini et al. (2014) data, the magnitude of the impacts in Figure 6.46 may well be larger, especially if the EU is likely to make progress in decarbonisation.

Such issues make the development of meaningful metrics extremely fraught, that is, metrics that promote desirable actions and behaviours while avoiding being gamed by vested interests. For example, the battery industry might lobby for a country to follow a pathway with more decentralised renewable generation such as CR, because that makes battery systems seem more effective relative to the baseline. But when the whole system is analysed, this might not lead to lower CO_2 emissions (or other environmental impacts) than following a more centralised pathway. On the other hand, a more centralised pathway such as TD could be more susceptible to free riding: there is less incentive for individuals to install PV and batteries since they are less effective relative to the baseline, so more of the infrastructure cost is borne by government or industry. Whether that is a good or bad thing is, of course, debatable.

The environmental impact results of Figure 6.46 and Figures 6.10-6.37 were calculated by debiting impacts from marginal grid generation response (grid import) from the system and crediting impacts of avoided marginal generation (grid export) to the system. As discussed in Chapter 3, this is not the best approximation to a consequential LCA, which would compare, for example, the CO_2 emissions of the entire GB grid over 25 years with up to 29 GW of home batteries, against the grid with no home batteries. In fact, the method of accounting for interactions between the nation's home batteries and the grid as described in Chapter 3, provides an approximate answer to this very question:

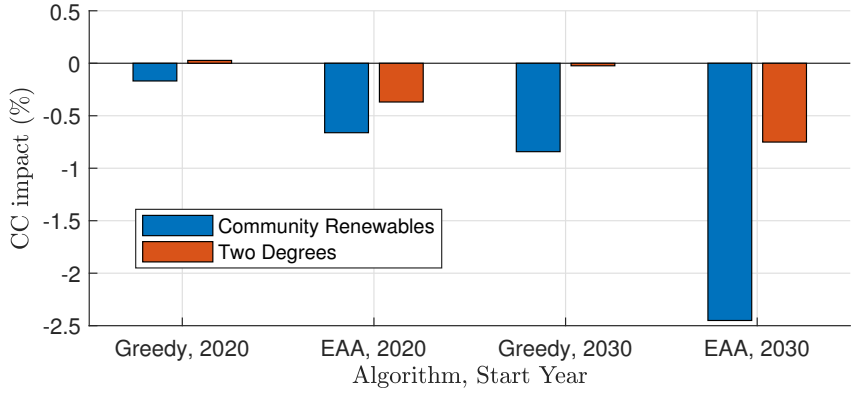

FIGURE 6.47: Climate Change impact to the UK of having PV-battery systems, starting from 2020 or 2030, running either the Greedy algorithm or EAA, in CR and TD future grid scenarios, relative to PV-only.

Figure 6.47 shows that the effect of adding home batteries to rooftop PV arrays is small, less than 2.5 % of the UK's projected CO_2 emissions during each time period (2020-2045 and 2030-2055). Note that the projected emissions are estimated based on a linear decrease from 400 Mton (4×10^{11} kg) in 2015 (BEIS, 2018b) to zero in 2050, and so should be interpreted as giving context rather than as accurate values. These assumptions lead to an estimate of 5000 Mton emitted across 2020-2045 and 2290 Mton across 2030-2055. In agreement with the calculations using marginal generator responses, Figure 6.47 shows a smaller CC impact from PV-battery compared to PV-only in the TD scenario than in CR. This

is further evidence that could motivate the battery industry to lobby for more decentralised generation, despite higher overall CO_2 emissions, because their products have a greater effect in the CR scenario.

On the other hand, the calculations using marginal generator responses all show PV-battery running the Greedy algorithm to have higher (worse) CC impact than PV-only. But comparing the whole GB with and without home batteries, Figure 6.47 shows that even the Greedy algorithm can reduce the nation's CO_2 emissions. However, it does so to a smaller extent than the EAA (which was designed for this purpose, whereas the Greedy algorithm was not), and in the TD scenario even increases CO_2 emissions relative to PV-only over the period 2020-2045. Furthermore, while the CC impact (per-kWh) reduction is less in absolute terms for a 2030 start than 2020, these reductions are a greater proportion of the whole country's CO_2 emissions, as the annual emissions rate decreases over time.

The small magnitude of the effects of PV-battery relative to PV-only are due to the fact that many factors besides domestic electricity use contribute to CO_2 emissions: transport, gas heating, land use emissions, to name a few. To put Figure 6.47 into context, consider the contribution of 10 GW_p of rooftop PV arrays to avoiding emissions from electricity generation. (10 GW_p was the 2030 estimate for how much rooftop PV would be associated with batteries in Chapter 3, and is equivalent to around 2.7 million households.) Supposing an average output equivalent to 800 hours/year for 25 years, displacing grid generation that is on average 0.3 kg CO_2/kWh:

$$10\ \text{GW}_p \times 800\ \text{hours/year} \times 25\ \text{years} \times 0.3\ \text{kg CO}_2\text{/kWh} = 67\ \text{Mton CO}_2.$$

This is 1.3 % of the 5000 Mton estimated to be emitted across 2020-2045. Again, this should be interpreted as giving context, not as an accurate value. The point is that the contribution of a battery to enhancing a PV array's CO_2-saving capability is likely less than the contribution of the PV array alone, but is nonetheless a non-negligible contribution, and especially so if running the EAA in a highly decentralised grid.

A similar effect to that seen in Figure 6.46 for the CC impact category is also observed for PMF, POF, and to some extent ME. That is, the impact magnitude across all configurations is less for a 2030 start year than 2020; the TD baseline is lower (better) than the CR baseline; and the system configurations in the TD scenario show less impact reduction relative to the TD baseline than their analogues in the CR scenario relative to the CR baseline. Graphs of these impacts can be found in Appendix D.

It is worth noting that the FET baseline is higher (worse) in TD than in CR by over 100 % (normalised to EU activity). This is much starker for the 2030 start year than 2020, where the FET baseline in TD is only around 25 % higher than in CR. Similarly, the IR baseline in TD is higher than in CR by 400 % for a 2030 start, compared to it being higher by 100 % for a 2020 start. In both categories, FET and IR, this effect is due to the fact that nuclear capacity remains stable in the CR scenario whereas it doubles in TD relative to the present-day. Nuclear is the generator type with highest IR intensity (by two orders of magnitude) and highest FET intensity (by less than one order of magnitude), and so as the CR and TD future grid scenarios diverge from each other, the difference in their FET and IR baselines becomes larger.

6.4 Aligning Misaligned Incentives

In this chapter, it has been shown that the financial and environmental incentives do not neatly align when a homeowner comes to choosing between the different PV-battery configurations available. Notably the PV with second-life battery system running the EAA consistently offers the greatest savings in CO_2 and fossil fuels, with embodied emissions in the manufacturing-dominated categories similar to those of PV-only, but consistently poor financial returns, beaten to last place only by the battery-only configurations. This is consistent with the findings of Babacan et al. (2018), that an algorithm to minimise CO_2 emissions is more costly while one that minimises cost leads to more CO_2 emissions.

There is also the interesting issue of how the incentives differ between the households studied. For example, investing in a PV-only system in 2020 can lower the MCoE for a higher-consuming household, but tends to increase it for a lower-consuming one. This is consistent with the findings of Truong et al. (2016) and Bertsch et al. (2017). Without intervention, the likely outcome would be that higher-consuming, and generally wealthier (White et al., 2012), households invest in PV. That could be interpreted as a good thing, that wealthier households bear more of the cost of decarbonising the country; or as a bad thing, that poorer households are priced out of the opportunity to contribute to the country's decarbonisation. This becomes less of an issue over time, as the expected rise in electricity prices lead to PV installation becoming more profitable than the baseline for all households studied. However, the Capex of 5000-8000 GBP may still pose a barrier to poorer households, and there is the separate issue of the effects of rising electricity prices on fuel poverty.

Another issue arising from the changing dynamics between the financial and environmental incentives, is how they influence the decision to invest in PV-battery running the Greedy algorithm rather than PV-only. For investment in 2020, the former option is costlier than the latter for all households, except the highest-consuming, and only then if they are lucky enough to buy a second-life battery closer to best-case than worst-case. In this situation, the financial and environmental incentives actually do align, because the environmental benefit of PV-battery running the Greedy algorithm relative to PV-only, ranges from negligible (Figure 6.47) to negative (Figures 6.10-6.37). However, this situation changes when battery costs have declined and electricity prices risen so much that PV-battery running the Greedy algorithm is more profitable than PV-only for all households. This could be seen as a disaster, as the financial and environmental incentives have come out of alignment; or as a blessing, that batteries can now offer even more savings compared to the baseline, that perhaps more homeowners will invest in a PV-battery system, resulting in greater PV uptake than there would otherwise be.

It must be remembered that some people place a high importance on sustainability such that they are willing to bear some financial loss, whether real or an opportunity cost. Conversely, the findings of Agnew and Dargusch (2017) suggest there are many who prioritise saving money above environmental impacts. However, there is no need to accept the situation as it is: there is a growing consensus around the world and across the political spectrum in favour of carbon pricing (World Bank, 2019). What follows is a summary of what carbon pricing is, the forms it has already taken in some jurisdictions, and a discussion of how it might help to align the misaligned incentives in the specific case of domestic PV-battery systems.

6.4.1 Carbon Pricing to solve Negative Externalities

In classical economic theory, an activity may give rise to side effects that negatively affect society at large but without imposing a cost on the originator. This is termed a negative externality, and the emission of GHGs from burning fossil fuels is one example. One solution is to regulate the negative externality through law; another is to impose a tax, to 'internalise the externality' (Harvey, 1994).

The EU Emissions Trading Scheme (ETS) combines the two approaches by setting a cap on how much CO_2 can be allowed to be emitted each year, allocating permits to companies, and allowing a free market in these permits to set their price (Sandbag, 2019). Companies that emit more CO_2 than allowed by the permits they hold must buy more permits, and companies that emit less can sell their surplus permits. This creates an economic incentive to decarbonise. The ETS has come under criticism for allowing the permit price to fall as low as 3 EUR/ton CO_2, as a result of the recession of 2012 onwards reducing economic activity and therefore reducing demand for emissions permits. With some re-structuring of the ETS mechanism, the price has risen to 25 EUR/ton CO_2 at the time of writing (Sandbag, 2019).

de Boer et al. (2018) reviewed the various consumption taxes and subsidies in place in the UK and compared them in terms of their equivalent carbon price. For example, the carbon price floor (CPF) is a tax levied on electricity generators, currently at 18 GBP/ton CO_2, as a surcharge on the EU ETS permit price (Hirst and Keep, 2018). In contrast, fuel duty applies to all purchases of petrol and diesel for road vehicles - the duty charged per litre divided by the CO_2 emissions per litre, implies a much higher carbon price than the CPF. A subsidy on renewable electricity generation also implies a carbon price, in terms of value placed on avoiding emissions rather than a cost charged on emitting. de Boer et al. (2018) found substantial variation in equivalent carbon prices across different economic sectors. They recommended some options for the UK to harmonise the carbon price across sectors, from applying a tax on all fuels produced or imported, with costs passed on downstream to the customers purchasing goods produced using the energy from these fuels, to applying the tax directly on consumer goods according to the embodied emissions of their manufacture. They highlighted issues of transparency in the application of the carbon price, measures needed to prevent its impact falling disproportionately on poorer members of society, and the need for a 'border carbon adjustment' levied on goods imported from countries with lower or no carbon price.

Some form of carbon pricing is scheduled or already implemented in 57 countries, covering 20 % of global GHG emissions (World Bank, 2019). But like the different sectors internal to the UK, there is much variation between mechanisms used and carbon prices set. The question of how to set the level of a carbon price has been a hot topic of research (van den Bergh and Botzen, 2014). There is the ETS approach, which is susceptible to disincentivising improvements above a pre-defined target rate of decarbonisation, as happened in the EU when ETS permit prices fell during the recent economic recession.

In contrast, there is the concept of the social cost of carbon (SCC), the monetary cost caused by climate-related damages as a result of each ton of CO_2 emitted (Smith and Braathen, 2015). SCC is subject to uncertainty in the climate sensitivity (what temperature rise is caused by each doubling of atmospheric CO_2), the physical consequences of global warming (flooding, heat waves, hurricanes, etc.), and the accounting of economic costs incurred by them. In particular, the choice of discount rate for climate-related costs incurred in future attracts debate and controversy, as does the evaluation of human suffering, which may be greater in a densely populated developing country but less economically significant than in a country with highly developed and costly infrastructure. Some estimates put the SCC as low as

8 USD/ton CO_2 (van den Bergh and Botzen, 2014), while others put it higher, such as Ricke et al. (2018) who found a median of 417 USD/ton CO_2. Ricke et al. (2018) also found the SCC to vary between 177-805 USD/ton CO_2 in different countries, as a result of the differences in each country's vulnerability to climate change.

Rather than setting a level for a carbon price first and then seeing if a particular action (such as installing domestic PV-battery systems) is thus incentivised, the question can be posed the other way round: what carbon price is necessary to incentivise a particular action? Babacan et al. (2018) estimated this by dividing the CO_2 savings differential between their cost-minimising and emissions-minimising algorithms, by the financial cost differential between them, across one year. The result was 180-5160 USD/ton CO_2. The high end of this range exceeds even the estimates of Ricke et al. (2018), and suggest that PV-battery systems are simply not the most cost-effective decarbonisation option in certain regions.

A difficulty arises when considering how in practice a carbon price may be applied in a way that will incentivise PV-battery systems, or more specifically, second-life batteries and the EAA. A subsidy could be offered for second-life batteries, in accordance with the avoided externalities (in Climate Change and other environmental impact categories) of new battery manufacture. An increase to the UK's CPF charged to electricity generators would sooner or later be passed on to customers. But supposing most of the customers are on a flat-rate tariff, an increase in the flat per-kWh rate would make the PV-battery system with the Greedy algorithm a more cost-effective option, as it reduces a customer's exposure to the cost of grid import. This is precisely what is seen in Figures 6.38-6.43 for an investment starting in 2030 compared to 2020.

To incentivise the EAA above the Greedy algorithm, a hypothetical CPF increase would need to be concentrated at times of higher grid CO_2 intensity. In the extreme case, this would make the EAA and PAA (price arbitrage algorithm) one and the same; there would be no need to send out real-time grid CO_2 intensity data; home batteries could be scheduled on price signals alone. In other words, a dynamic time-of-use (dToU) tariff is needed.

6.4.2 Dynamic Time-of-Use Tariffs

In contrast to the Green Energy (2019) Tide tariff used in this thesis as an example of a static ToU tariff, dToU prices do not change in a repeating pattern. Rather, they are set dynamically by the energy supplier, who informs their customers of low- and high-price periods in the day ahead, for example by daily text message (Schofield, 2015). An example of a dToU already in commercial operation is the Octopus (2019) Agile tariff, for which 3 days of prices are shown in Figure 6.48.

Each day shows a pricing peak lasting 3 hours around 18:00, but at a different level each day, capped at 0.35 GBP/kWh on 10 December. Note also the period of negative pricing, where customers were paid for consuming electricity, around 05:00 on 8 December. The price tends to be higher in winter, but for the whole period of data supplied by Wall (2019) (19 February 2018 to 3 June 2019), the mean price was 0.1137 GBP/kWh, compared to 0.1537 GBP/kWh for an average flat-rate tariff in the same time period (BEIS, 2019a). (The standing charge is 0.21 GBP/day, similar to the average.) 0.1137 GBP/kWh is not the mean price a customer pays, unless they shift their electricity consumption to a constant level 24 hours a day. The other reason a dToU supplier can charge such low prices is because they pass the price signals they receive on to their customers: when the price is high on the wholesale market, the cost of purchasing that electricity is recovered through the higher price charged to customers in those

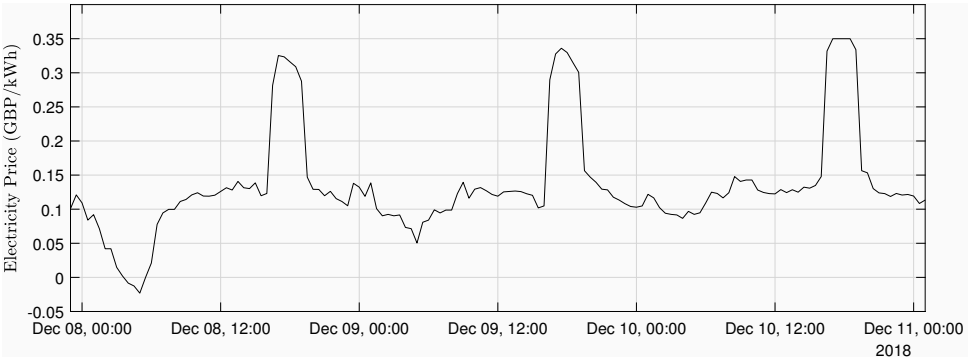

FIGURE 6.48: Dynamic time-of-use pricing charged to a retail customer on an Octopus (2019) Agile tariff, for 8-11 December 2018. Data provided by Wall (2019) using the Octopus API.

periods; furthermore, the high retail price incentivises a shift in consumption so that the supplier need not purchase as much high-cost electricity on the wholesale market or from a generator in the first place.

Octopus takes their dToU tariff a step further by changing the level of payment they make to households for PV export dynamically in line with wholesale electricity prices. They call this offering 'Outgoing Agile', and benefit by reducing their exposure to wholesale prices if they can buy instead from their customers, who have been incentivised to shift their export (using a battery or otherwise) to higher-price periods. This raises the question of what might happen to export payments in lower-price periods - with a much elevated CPF, these would be periods of high generation by zero-carbon generators, including rooftop PV. If export payments are lower during times of high PV generation, could this make the PV-only configuration less profitable than calculated in this study, where export payments have been assumed to rise in line with electricity prices? On the one hand, export payments do not reflect their contribution to lowering life-cycle CC impact: 15-70 % of the total baseline CC impact in Figure 6.27, compared to only 10-20 % of the total baseline MCoE in Figure 6.2. On the other hand, it is possible that an increase in rooftop PV installations to the extent that excess PV electricity will no longer be used by a neighbour but sent to higher levels of the network, incurring more losses (see Chapter 3), could reduce the environmental benefit to a level that reductions in export payments over time are justified.

No systematic analysis has been conducted into whether a dToU can incentivise the use of the EAA above the Greedy algorithm, and what price levels would be needed to do this. In theory, what is needed is a sufficiently large price differential, with low- and high-price periods well correlated with respectively low and high CO_2 intensity. (It would also be possible to include a component of pricing to disincentivise consumption during periods of high biomass generation, if land occupation for biomass is a concern.) Unfortunately, such tariff structures also favour the Greedy algorithm: the battery charging/discharging it schedules is less well correlated with grid CO_2 intensity than the EAA scheduling, but the Greedy algorithm's advantage is that it minimises grid import and therefore exposure to all electricity pricing. It is concerning that the more CO_2-intense option, the Greedy algorithm, is so difficult to make less financially attractive than the less CO_2-intense option, the EAA. On the other hand, it is unknown if the small to negative impact of the Greedy algorithm is compensated by its capability to increase PV uptake.

6.5 Summary

The financial results indicated by mean cost of electricity, return on investment, internal rate of return, and payback period largely agree - for an investment starting in 2020:

- Installing PV without battery is a worthwhile investment for Houses 5, 7 and 6, but for the others are costlier than the baseline;
- PV-battery running the Greedy algorithm is costlier than PV-only;
- A second-life battery in that configuration may be more costly or less than a new one over the life-cycle, depending on whether it is a worst-case or best-case second-life battery;
- Running the Emissions Arbitrage Algorithm is costlier than the Greedy algorithm, PV-only, and the baseline, whether with new or second-life batteries;
- The battery-only systems are the costliest;
- The Community Renewables and Two Degrees future grid scenarios lead to very similar results, with CR being slightly costlier than TD in corresponding configurations;
- It tends to be higher-consuming households that stand to profit the most, or incur the least loss, although the correlation is not perfect: House 8 has the lowest MCoE, whereas House 5 followed by House 6 are the most lucrative in terms of RoI, IRR and PP (the order from highest- to lowest-consuming is: 5, 8, 7, 6, 2, 1, 12, 19).

These results are consistent with the literature reviewed in Chapter 1, which found the financial case for PV and batteries to be marginal, but stronger for higher-consuming households. It will be interesting to see whether society trends towards higher electricity consumption in future, with electrification of heating and transport, or towards lower consumption, with improved efficiency in appliances and in provision of services such as thermal comfort, lighting, cooking and mobility. The range of outcomes between best-case and worst-case second-life batteries demonstrates a need for better monitoring of EV batteries in their first life and prediction of their degradation and subsequent value.

As for environmental impact results for investment starting in 2020:

- Climate Change impacts are reduced by installing a PV-only system, slightly worsened again by adding a battery running the Greedy algorithm, restored similar to PV-only when the battery is second-life, significantly improved if the EAA is run instead of the Greedy algorithm, and improved further still if the battery is second-life rather than new;
- Similar results were found in the other grid-dominated impact categories: Fossil fuel Depletion, Ozone Depletion, Particulate Matter Formation, Photochemical Oxidant Formation and Marine Eutrophication;
- Manufacturing-dominated impact categories (Metals Depletion, Freshwater Ecotoxicity, Freshwater Eutrophication, Human Toxicity, Water Depletion and Ozone Depletion) are worsened the more PV and new batteries are manufactured;
- Second-life usage is an option for reducing these manufacturing-dominated impacts, but never achieves as low impacts as PV-only;

- While a PV system with second-life battery running the EAA tends to be the best option in terms of Climate Change, Fossil fuel Depletion and Ozone Depletion, with insignificant side-effects in Terrestrial Acidification, Ionising Radiation and Particulate Matter Formation, the Land Occupation side-effects can be significant if care is not taken in sourcing or dispatching biomass generation on the grid.

Bearing these points in mind, a PV-only system would be the best compromise between financial and environmental benefits. The environmental benefits rendered by PV with second-life batteries running the EAA are due in part to the avoided impacts of manufacturing new batteries, but also the larger capacity of second-life batteries used (as decided by the heuristic rules developed in Chapter 5).

For an investment starting in 2030:

- Installing PV without battery becomes worthwhile for all houses, due to a real-terms increase in electricity prices (and therefore to the baseline costs);
- PV-battery running the Greedy algorithm becomes more profitable than PV-only, as a result of the expected fall in battery prices and the rise in electricity prices;
- Improvements in Climate Change, Fossil Fuel Depletion, Particulate Matter Formation, Photochemical Oxidant Formation and Marine Eutrophication from installing PV and batteries, are smaller in absolute terms because the electricity grid has made more progress towards decarbonisation, but the improvements form a larger proportion of these reduced emissions;
- PV-battery systems render a greater benefit in a more decentralised grid (CR compared to TD), and when running the EAA compared to the Greedy algorithm.

Note that while a more decentralised grid would be favoured by PV-battery suppliers, it may not necessarily be the best option from the perspective of an environmentally conscious society. It is outside the scope of this thesis to comment whether decentralisation is desirable from the perspective of society at large, the government, homeowners, or network operators.

There is significant misalignment in the financial and environmental incentives:

- A PV system with second-life battery running the EAA is the best option for reducing grid-dominated environmental impacts, but is one of the costliest configurations;
- A PV-battery system running the Greedy algorithm installed between 2020-2030 is the most profitable configuration, despite reducing the environmental benefits rendered by PV-only (or not increasing them as much as the EAA would).

A carbon price was discussed as an option for aligning the financial and environmental incentives, but it is imperative that the implementation accounts for timing (marginal grid CO_2 intensity changing throughout the day), and passes this price signal through to the domestic consumer. The obvious way to achieve this is with a dynamic time of use tariff. While such a tariff can reduce the MCoE of systems running the EAA, it is not straightforward to design a tariff that will do so without further reducing the MCoE of systems running the Greedy algorithm too. A systematic study of tariff structure and levels would be needed, and is deferred to further work.

There remains the question of how much it matters that the financial and environmental incentives are misaligned for the Greedy algorithm, whether its profitability stimulates the uptake of domestic PV to an extent that compensates the environmental burdens of installing and operating a battery in addition.

Chapter 7

Conclusions and Further Work

It is time to return to the original research question:

"In what circumstances are domestic PV-battery systems in Great Britain financially and environmentally sustainable?"

This chapter presents the conclusions drawn from the work of this thesis in answering this question, firstly in the context of the existing literature, and secondly in terms of recommendations to different stakeholders: homeowners, the PV-battery supply chain, policy makers, and the research community. These include suggestions for work to extend this research further.

7.1 Conclusions in relation to the existing literature

7.1.1 PV-battery systems, running an emissions-minimising algorithm, can be more sustainable than PV-only

The findings of Kabakian et al. (2015); Kurland and Benson (2019); Uddin et al. (2017), that a PV-battery system leads to more GHG emissions and generally worse environmental impacts than PV-only, were confirmed for the Greedy algorithm. The results found in this thesis were consistent with the findings of Babacan et al. (2018), that a cost-minimising algorithm tended to increase emissions while an emissions-minimising algorithm increased costs, despite the differences in context and methodology: a convex optimisation scheduling, applied across a single year, in 16 regions of the USA, on the one hand (Babacan et al., 2018), and the EAA, simulated for 25 years of operation in GB, on the other (Sun et al., 2019). In the previous chapter (Figure 6.26), a 8-15 % reduction in CO_2 emissions brought about by a PV system (normalised to EU activity; most of this variation being house-to-house variation) was found to be reduced (improved) a further 1-2 %-points by adding a battery running the EAA (2-4 %-points if second-life), but increased (worsened) 1 %-point above the PV-only level if the battery is new and runs the Greedy algorithm.

Whereas the existing literature did not take account of the time-varying nature of grid emissions (Kabakian et al., 2015; Uddin et al., 2017), or used average rather than marginal emissions factors (Faria et al., 2014), this study has followed the example of McKenna et al. (2013) and Babacan et al. (2018), by

modelling the time-varying marginal emissions intensity of the grid (in GB, in this case). And further, this study models not just the present-day grid but plausible future scenarios, as defined by National Grid (2018b) Future Energy Scenarios.

While it is common practice in the techno-economic literature to analyse the sensitivity of financial outcomes to delaying the initial investment, taking account of decreasing costs in battery technology and increasing electricity prices (Hoppmann et al., 2014; Muenzel et al., 2015; Mulder et al., 2013; Naumann et al., 2015; Truong et al., 2016; Weniger et al., 2013), the corresponding effects on environmental impacts are not as widely studied. There is good reason, as even present-day environmental impacts of PV/battery manufacturing and electricity generation are highly uncertain (see Chapters 2 and 3), and multiple possible future scenarios cannot all be validated as the present evolves into only one future. Nonetheless, it was considered an informative thought experiment to perform. The main findings were:

- With wind and PV capacity increasing in GB, there can be a sufficient differential in the marginal grid CO_2 intensity to be exploited by emissions-minimising algorithms such as the EAA, to achieve lower life-cycle emissions than a PV-only system. This is not in agreement with the findings of McKenna et al. (2013), although this may be only partly due to the accounting of a future GB grid in this thesis; developments in battery technology may also have contributed;
- The degree of centralisation matters: in a grid dominated by decentralised generators (wind and PV), each PV-battery system is more effective at helping reduce the grid's emissions than in a more centralised grid (with greater nuclear, and carbon capture and storage capacity). The effect is not so pronounced for a temporal boundary of 2020-2045, but becomes sizeable for 2030-2055, when the two future grid scenarios studied have diverged from each other to a greater extent.

This study did not take account of future changes to manufacturing processes and materials used in PV, batteries and power electronics, nor of recycling of any of the components at end-of-life. But in doing so, it has highlighted the need for improvements in materials, manufacturing and recycling. Metals Depletion is likely the largest side-effect of increased PV-battery installation, with the most contribution from the battery and power electronics, and the most urgent focus of recycling. Freshwater Ecotoxicity, Freshwater Eutrophication and Water Depletion all affect watercourses as a result of chemical processes. Human Toxicity and Ozone Depletion must also be reduced by selection of alternative materials and process improvements.

7.1.2 Second-life batteries can limit harms from system manufacture, but may require financial support

The existing literature on second-life batteries is varied in its approach to quantifying costs, revenues, and environmental impacts. Assunção et al. (2016); Heymans et al. (2014); Kirmas and Madlener (2017) conducted techno-economic studies without analysing environmental impacts, while Casals et al. (2017); Faria et al. (2014); Genikomsakis et al. (2013) conducted life-cycle environmental analyses without considering financial aspects. And while Martinez-Laserna et al. (2018) reviewed both financial and environmental aspects of second-life battery use in the literature, no study until now has examined both for the same domestic PV with second-life battery system.

In agreement with Genikomsakis et al. (2013) and Casals et al. (2017), this study found the life-cycle environmental impacts to be reduced with second-life batteries compared to new, for the Greedy algorithm and EAA, in a wide range of categories: the 14 ReCiPe midpoint impacts used in this thesis, compared to the Eco-indicator 99 impacts used by Genikomsakis et al. (2013) and GHG emissions only in the case of Casals et al. (2017). However, as Casals et al. (2017) alluded to, the majority of the benefit rendered by PV with second-life batteries is contributed by the PV array itself. Especially in the manufacturing-dominated ReCiPe impact categories (Metals Depletion, Freshwater Ecotoxicity, Freshwater Eutrophication, Human Toxicity, Water Depletion and Ozone Depletion), second-life batteries cannot bring the impacts below the level of a PV-only system.

In Climate Change and Fossil fuel Depletion categories, the greatest advantage of a second-life battery is realised by the EAA: the EAA is more effective at reducing those impacts the larger the battery, and the heuristic rules developed in Chapter 5 optimise a second-life battery at a larger capacity than a new one in the corresponding configuration.

However, this study was less optimistic than Heymans et al. (2014) and Assunção et al. (2016) on the financial benefits of second-life batteries compared to new. While it was possible to reduce the mean cost of electricity and payback period, and increase return on investment and internal rate of return by using a second-life battery on a best-case degradation trajectory, the reverse is true if it is closer to the worst-case. Heymans et al. (2014) did not model any degradation of the battery during its second life, while Assunção et al. (2016) modelled a single degradation trajectory according to what they measured experimentally on one setup. But as Baumhöfer et al. (2014) showed, even identical cells, cycled identically, can diverge in their rate of capacity degradation.

Therefore, this study followed the approach of Sathre et al. (2015) and Truong et al. (2016) in modelling different degradation rates but, taking note of the findings of Ahmadi et al. (2014a), also included the effects of cycling on internal resistance increase as well as capacity degradation. The result was that the worst-case second-life battery in most cases needed to be replaced twice over the 25-year system lifetime, whereas a new or best-case second-life battery required only one replacement. In this study, a fixed installation cost was incurred for each replacement, in addition to a capacity-dependent cost, whereas this is neglected in much of the techno-economic literature on second-life batteries.

Furthermore, the assumptions on capacity-dependent costs of second-life batteries in the literature were questionable. Using a microeconomics-based method newly developed specifically to estimate the future costs of second-life battery replacements (Sun et al. (2018b), and Chapter 4), it was found that while the second-life price is likely to fall rapidly in the 2020s, it will subsequently be strongly determined by the sum of the repurposing cost and recycling net credit available. There is much uncertainty in what this sum will be, but it is likely that the price difference between new and second-life batteries will become narrower in future. The result is the economic case for second-life batteries weakens if the initial investment is delayed to 2030.

7.2 Recommendations for Stakeholders

7.2.1 For the homeowner

This work has produced some clear recommendations for homeowners in GB who currently have neither PV nor battery and are considering what configuration, if any, to install. A PV-only system offers the best balance between financial and environmental benefits, although with a 17-20 year payback time, it is very much a long-term investment at today's prices. A PV and large second-life battery system running an emissions-reducing algorithm such as the EAA has scope for greater CO_2 emissions reduction, but at greater cost, and is not yet widely available as a commercial product. A PV-battery system running the Greedy algorithm, on the other hand, while not yet cost-effective for the majority of households, may become so after a modest reduction in Capex. Such a system tends to slightly erode the environmental benefits compared to a PV-only system, and should only be recommended if it makes the difference between installing, and being unable to afford any system with PV at all.

These are very general statements, and a real homeowner must consider their individual circumstances - for example, if they can obtain a quote much lower than the Capex considered in this thesis, or if they live in a remote location with weak grid connection, these may tip the balance in favour of installing more PV or battery capacity.

Furthermore, the vast majority of the nearly one million domestic PV arrays in GB (BEIS, 2020) are not yet coupled to a battery. A natural question for the owners of these arrays is whether it would be worthwhile to retrofit a battery. Bearing in mind that this study did not model such a situation, it can only be inferred from comparing the PV-only and PV-battery cases, that retrofitting a battery is unlikely to render a significant benefit to an existing PV array. Additionally, a retrofitted battery would likely need to be AC-coupled to the PV, a setup that is less efficient and more costly than DC-coupling (see Chapter 2). Retrofitting a battery would likely only be worthwhile financially if the installation cost were to reduce greatly compared to that considered in this study. However, it would be interesting to extend this modelling study to explicitly consider such decisions: whether or not to retrofit a battery to an existing PV array, and whether to expand the battery capacity in future rather than replacing the battery pack with one of identical capacity at end-of-life, as was modelled here.

Another question that is natural for potential PV-battery customers to ask, is how the financial and environmental benefits compare to other measures that their money could be spent on. The framework of this study unfortunately does not lend itself well to making this type of comparison, due to the use of 1 kWh electricity consumed as the functional unit. This assumes the annual total consumption of the household does not change upon installation of PV and/or battery, whereas measures such as home insulation, heat pumps and EV purchase, do change the household energy consumption, *by design*.

However, it is simple enough to multiply the MCoE or environmental impacts per kWh obtained in this study, by household electricity consumption $\sum_t P_d(t)$, and subtract from the baseline (no PV, no battery), to give a household-level benefit, for example in terms of kg CO_2 saved annually. A greater complication is that synergies are possible by combining different measures: smart-charging an EV at times of high PV generation may be more beneficial than simply the sum of installing PV and replacing a petrol vehicle with an EV. Nonetheless, a household has limits to its cash flow and must decide whether to install PV first and then save up for an EV to replace their petrol vehicle some years later (for example), or vice versa, or purchase both PV and EV immediately on credit. While such decisions are commercial

by nature, academic research still has a role to play in evaluating them in order to offer impartial advice, along both financial and environmental dimensions.

Although the national smart meter rollout has not been as comprehensive as planned (see Chapter 2), smart meters offer at least one exciting opportunity to homeowners considering purchasing a PV-battery system. If a year's worth of high-quality (relatively gap-free) electricity consumption data can be measured by a smart meter at half-hourly intervals, it would be possible to run a direct search optimisation (as in Chapter 5) to provide that household a bespoke recommendation for what capacity of PV and battery to install, what electricity tariff to switch to, with an estimate of financial and environmental benefit. This could be a great advantage to outlier households which, by some quirk, would receive a highly sub-optimal result from using the heuristic rules of Chapter 5, which size the PV-battery system only according to the household's annual electricity consumption. Obstacles to the use of smart meters for bespoke PV-battery sizing include: over-stated benefits from using input data at resolution as coarse as half-hourly (as discussed in Chapter 5 and Sun et al. (2020), although the sizing should not be greatly affected), the fact that downloading a year of one's own consumption data is not yet a standard functionality of smart meters, and privacy concerns of sharing that data, as consumption patterns can reveal personal lifestyle details.

Another exciting opportunity open to homeowners who have purchased a PV array is participation in peer-to-peer (P2P) trading (Gao et al., 2018). In essence, a PV owner can sell the energy they generate directly to a consumer elsewhere on the grid rather than receiving an export payment from their energy supplier. As P2P trading is an accounting mechanism and does not change the physics of the system, it would be a simple matter to run the model developed in this thesis with the P2P price (which may be time-varying) instead of the fixed export payment, additionally to any fees incurred by participating in a P2P scheme. (They may also buy electricity from a peer at times rather than from their energy supplier.) Without having run the model with these parameters, it is hard to conclude much. However, since P2P prices tend to be higher than export payments offered by energy suppliers (otherwise PV owners would not participate), the tendency is to favour PV-only rather than PV-battery systems. This is because the latter offer greater value when the price of grid import is much higher than the payment receivable from grid export, making it more worthwhile to store PV energy to displace later consumption, while P2P trading reduces the price differential between import and export.

A related but separate concept is solar cryptocurrency (in that both it and P2P trading rely on blockchain technology). An example is SolarCoin: PV generators who have signed up receive one SolarCoin for every MWh they generate. To spend any solar cryptocurrency, it must be exchanged for fiat currency. At the time of writing, the cryptocurrency exchange site CoinMarketCap (2020) offer a rate of 0.015326 USD per SolarCoin, equivalent to a feed-in tariff of 0.000012 GBP/kWh. Whether signing up and exchanging solar cryptocurrency is worth the small benefit and the satisfaction of participating in the technology, is a personal decision that only a PV owner can make for themselves. It is a simple matter to enter a FiT rate of 0.000012 GBP/kWh into the model, but it would have negligible effect on results.

7.2.2 For the PV-battery supply chain

This group of stakeholders includes primarily the manufacturers of PV panels, batteries, power electronics, their materials suppliers, companies involved in installing PV-battery systems, and in developing them, including control software.

The results of Chapter 6 highlight the midpoint categories of ReCiPe environmental impacts which are dominated by the effects of manufacturing: Metals Depletion, Freshwater Ecotoxicity, Freshwater Eutrophication, Human Toxicity, Water Depletion and Ozone Depletion. Reducing these impacts, especially Metals Depletion, must be a priority not just for battery manufacturers, but PV and power electronics too, as the manufacture of these components contribute significantly. How these aims are to be enacted is down to the ingenuity of researchers both in these industries and in academia. The main approaches are: use less material more efficiently, substitute problematic materials for more benign ones, make products more durable and so longer-lasting, and recycle at end-of-life.

This study restricted itself to only the most common types of PV and batteries, with the most LCA data available. However, there are many types already commercially available (monocrystalline Si, amorphous Si, cadmium telluride PV; Aquion 'salt-water' batteries, older chemistries such as PbA, and other storage types altogether, including the Sunamp (2019) thermal storage 'heat battery' and flywheel products like the Amber Kinetics (2019) flywheel), as well as new technologies still in research and development, such as perovskite PV and aluminium-ion batteries.

In selecting alternative materials for the system components, it is important to bear in mind which environmental impact categories are being targeted for reduction, and what side-effects might result in other categories. For example, Al-ion batteries might be hoped to reduce the Metals Depletion impact compared to Li-ion, but how much of the impact is caused by lithium compared to other metals used in the positive electrode, such as nickel and cobalt? As another example, the manufacture of Aquion batteries is less harmful than that of Li-ion in most environmental impact categories when compared on a per-kg basis, but the reduced energy density of Aquion means it is almost as harmful on a per-kWh basis, and over twice as harmful in the Climate Change category (Peters and Weil, 2017). This is a pitfall of designing batteries for stationary applications, where high energy density is not required operationally but is useful from a material consumption point of view.

In the same vein, perovskite PV is a thin-film material, and so has the potential to reduce embodied environmental impacts in many categories from the reduced material usage, as well as reduced energy usage from the lower temperatures required for processing compared to Si PV. However, the Metals Depletion impact of PV manufacture comes mostly not from the cell itself, but the silver paste used to form electrical contacts (Bekkelund, 2013). This is still needed for perovskite PV. Where perovskite technology has the potential to reduce Metals Depletion, is in the ease with which it can be formed into tandem cells (Leijtens et al., 2018): the band-gap of the perovskite material can be tuned, to make PV cells in layers with different band-gaps, which can absorb a greater proportion of the energy in incoming solar radiation. The greater efficiency of tandem cells means a smaller area is needed per kW_p of capacity, and therefore less silver paste (amongst other inputs) per kW_p.

It is particularly difficult to draw conclusions around the power electronic components (converters and inverters) as there is so little LCA data available. If the manufacturers of such systems were to collaborate more closely with impartial LCA specialists (inside or outside of academia), this would be a great boon to the research community.

On the financial side, this thesis has shown in Chapter 6 that PV-battery systems become financially worthwhile for all the households in the dataset when Capex is reduced by 20 % from the values used in this study. This gives suppliers and installers of PV and battery systems an aim for cost reductions, in order to access the mass market of domestic customers. It may be challenging to balance these cost reductions with the aforementioned requirements for more comprehensive recycling and selection of more

sustainable materials, and there are of course marketing considerations, to communicate to potential customers the benefits of the improved products.

While the work of this thesis in developing the EAA is largely hypothetical, the PAA (and even more sophisticated algorithms to take advantage of variable pricing) are already commercial reality, e.g. the Powervault (2018) smart controller. To apply these innovations to reducing emissions of CO_2 and other pollutants instead of or as well as bills, is not so much a technical challenge but one of data availability and dissemination, and incentivising uptake, as discussed more in the next section.

An interesting and somewhat surprising result from Chapter 5 is the heuristic optimisation of converter and inverter ratings at such low values compared to products currently available commercially (Naked Solar, 2019). It could be that a more sophisticated algorithm than the EAA can schedule charging and discharging at power values well below the maximum possible most of the time, reserving maximum charge/discharge for times when it is most valuable. Another possibility is customer perception of higher-power products as superior, in the absence of information on what converter and inverter ratings are optimal for their household. (What use is higher power, of course, if a small energy capacity is emptied quickly?) Therefore it is recommended that battery suppliers take into account the efficiency losses of higher-power operation, both in the design of the control software and of the power electronics sizing, and communicate this more effectively to potential customers.

7.2.3 For the policy maker

The work of this thesis has assumed little by way of policy interventions above what already exists or is planned - for example the National Grid (2018b) Future Energy Scenarios, the typical grid export payment resulting from the BEIS (2019b) Smart Export Guarantee, and the effect of the Carbon Price Floor, if any, on domestic electricity tariffs today and in future. However, as discussed in Chapter 6, there is a misalignment in financial and environmental incentives which may require intervention to correct. That is, adding a battery running the Greedy algorithm to a PV array slightly worsens the environmental impacts, especially in the manufacturing-dominated categories if the battery is new, whereas this configuration could become the most lucrative before long as Capex decreases and electricity tariffs increase. If the battery is second-life and running the EAA on the other hand, a substantial improvement can be achieved in terms of Climate Change, Fossil fuel Depletion and Ozone Depletion, with small side-effects in the other categories, but it is one of the costliest configurations.

There is much literature on carbon pricing in its various forms, as reviewed in Chapter 6, but it is an open question if any form of carbon tax is enough on its own to cause energy suppliers en masse to offer dynamic time-of-use tariffs that align prices with real-time marginal CO_2 intensity on the grid. In theory, a perfect correlation between pricing and emissions intensity should achieve the desired outcome. However, there is the complication that such a tariff would need to favour PV with second-life battery running the EAA, not only compared to the other configurations on the same tariff, but the others on any tariff the homeowner may choose. Additionally, this tariff would need to be profitable for any electricity supplier offering it. A systematic study is needed to design a dToU tariff that meets these objectives. If the market cannot be relied on to deliver the desired outcomes, regulatory policies may be required: for example, a law stating that all energy suppliers must offer at least one dToU tariff with high/low-price periods corresponding to real-time marginal grid CO_2 intensity and a price differential above some specified minimum, as determined by independent research. Another possibility is that more sustainable

configurations and operating strategies may become more socially desirable, despite the higher costs. In both cases, transmission of standardised information on the real-time marginal grid CO_2 intensity is needed, similar to WattTime (2020) in the USA.

As for the environmental advantage and financial disadvantage of second-life batteries, a case could be made for a subsidy to incentivise their uptake. The microeconomics-based model could be adapted to calculate the consequences of different levels of subsidy, and so help design such a policy. However, such a subsidy would have to increase the demand for second-life batteries by many times if it is to have a non-negligible impact on the stream of used battery packs that will be removed from EVs in future (Sun et al., 2018b). Alternatively, the expansion of the global electric car fleet could be constricted, preferably (from an environmental point of view) by improved provision of other low-carbon transport options rather than continuing to manufacture internal combustion vehicles. In any case, it is imperative that recycling facilities for EV batteries be improved and expanded to meet the need across the next decade, whether to process batteries after their first life in an EV or after their second life in a stationary application. If the market cannot be relied on to deliver, even with a surcharge at point of sale to help finance development and scale-up of recycling plants, government grants or loans may be needed.

It should be noted that the vast difference in results between best-case and worst-case second-life batteries (Chapter 6) indicates a need for some way to distinguish between them, and grades of battery in between. This would require monitoring of the battery in its first life, making that data available for assessment, and communicating this information to customers in some form of certification. (The market could then settle on different prices for different quality second-life batteries.) The organisation Flexi-Orb (2020) already performs these functions to some extent at zero cost to customers or taxpayers, and are well placed to monitor and certify second-life batteries. The government may wish to promote or endorse their work, and only consider mandating installers to register with Flexi-Orb or similar if voluntary registration proves insufficient.

7.2.4 For the research community

In order to better serve the various stakeholders as discussed above, the work of this thesis requires some refinement. This includes:

- collection of more and better LCA data for the system components and electricity generation technologies,
- inclusion of recycling burdens and benefits in the LCA,
- use of PV generation and household electrical consumption data that spans more than a year (as Pfenninger (2017) showed, significant year-to-year variation in PV and wind generation may require over a decade of data to give accurate results),
- instead of repeating a single year's input data, project how electrical consumption patterns may change in future as a result of broader societal changes (Boßmann and Staffell, 2015) and of behavioural changes after installing PV and battery (Deng and Newton, 2017; Sekitou et al., 2018),
- investigation of downsampling and statistical clustering techniques (Pfenninger, 2017) to reduce computing run-time, as alternatives to coarsening input data by averaging,

- more sophisticated modelling of the future GB grid than a fixed merit order dispatch (models such as Calliope, Temoa, EnergyPLAN, etc. exist but require significant work to parameterise; the ideal would be to apply the adapted Hawkes' method of Chapter 3 to the hourly generator dispatch results National Grid (2018b) obtained for their Future Energy Scenarios document from running the BID3 model, to derive marginal generator responses for every year modelled to 2050 - perhaps National Grid could be persuaded to save their hourly BID3 results and release them for academic research, if not to the public, in future editions of their Future Energy Scenarios),
- better accounting for the location-dependent nature of transmission and distribution losses and constraints, including the effects of high localised PV penetration,
- making the LCA fully consequential, that is, where capacity of power plants constructed in future respond endogenously to installation and operation of the various configurations of PV-battery systems (McKenna and Darby, 2017), and relatedly whether enough PV uptake could result from the greater profitability of PV-battery running the Greedy algorithm relative to PV-only, to outweigh the environmental impacts of adding a battery to that PV,
- further investigation into the costs of repurposing second-life batteries and the credit available from recycling them instead, as their sum is the strongest determinant of how second-life battery price will evolve,
- quantifying the environmental impact results not just in relation to EU or global activity, but also their severity and urgency - this would require input from the research into Earth systems known as planetary boundaries (Steffen et al., 2015), illustrated in Figure 7.1.

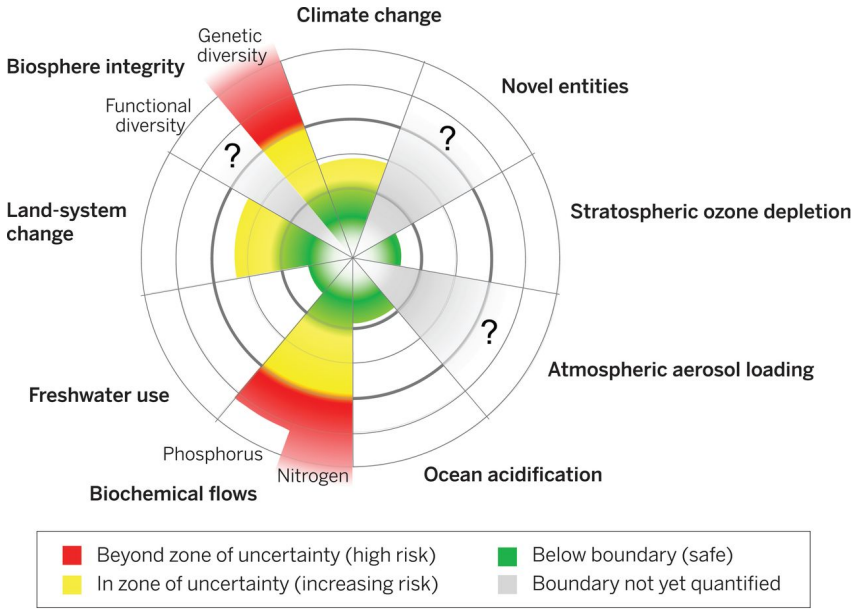

FIGURE 7.1: The nine planetary boundaries defined by Steffen et al. (2015): climate change (increasing risk), novel entities (boundary not yet quantified), stratospheric ozone depletion (safe), atmospheric aerosol loading (boundary not yet quantified), ocean acidification (safe but verging on increasing risk), biochemical flows (comprising nitrogen and phosphorus, both high risk), freshwater use (safe), land-system change (increasing risk), and biosphere integrity (comprising genetic diversity, at high risk, and functional diversity, not quantified).

As well as the questions raised in previous sections - how PV-battery systems compare to other energy-saving investments a homeowner could make, whether to retrofit a battery to existing PV and/or expand

battery capacity in future, how to manufacture the components more sustainably, what algorithms to program into them, the design of electricity tariff structures, and how best to incentivise second-life usage - there are many other stakeholders who stand to benefit from the expansion of this research. It is possible to adapt the modelling framework for different systems of renewable energy and storage: other load types such as office buildings, supermarkets, schools, universities, apartment buildings, factories, which differ in consumption patterns as well as total amount; alternative business models including those without an explicit load, where the PV-battery asset trades electricity in the wholesale and/or ancillary service markets (Moreno et al., 2015; Sun et al., 2018c; Zeng et al., 2018); coupling to wind power (Stroe et al., 2016) instead of or additionally to PV (PV is guaranteed not to generate for some 12 hours every day, whereas the wind might blow strongly for many days at a time, as well as there being lulls lasting many days (Gridwatch, 2018)).

All these examples would require significant additional work: designing operating algorithms, programming them into the model, and optimising system component sizes. This could be done independently to adapting the model to apply to different national contexts. For that, the grid modelling would need to be edited to have the appropriate generator technology mix and dispatch pattern, the input PV and household load profiles must be changed to ones appropriate to the geographic region, and the pricing of component installation and electricity tariffs must be changed to the appropriate values and currency. Although there are commonalities in the existing literature on PV-battery in different countries (for example, the addition of a battery running the Greedy algorithm tended to reduce the environmental benefit of a PV-only system, in GB as found in this study and by McKenna et al. (2013), in the USA (Babacan et al., 2018), and Lebanon (Kabakian et al., 2015)), caution should be exercised in extrapolating the results of this study to other countries outside of GB before explicitly modelling them.

Finally, there is a promising opportunity for closer collaboration between battery researchers and energy systems modellers. While the work of this thesis would benefit greatly from a better understanding of battery degradation, its drivers, and especially the aging knee phenomenon, the simulated battery charging/discharging power time series output from this type of modelling work could also be used as an input to experimental battery degradation tests. The variety of potential use cases described above could be simulated and fed into accelerated aging experiments, as an option between unrealistic constant-current charge-discharge profiles, and installing such systems for real and measuring them for many years. These other options still yield useful information, nonetheless it is important for those researching battery degradation in its own right to stay up-to-date with realistic applications as they develop; the likely returns of such research could pave the way to longer-lasting, better-performing batteries.

7.3 Summary

Finally, to answer the question:

"In what circumstances are domestic PV-battery systems in GB financially and environmentally sustainable?"

- Financial sustainability can be achieved for PV-only systems and PV with new battery running the Greedy algorithm with decreasing costs of PV and balance of systems but especially battery costs, and increasing costs of electricity, which is likely to happen by 2030 for a wide range of GB households;

- Environmental sustainability is best achieved over the greatest range of impact categories by a PV-only system, although with second-life batteries running the EAA, can further reduce fossil fuel depletion, ozone depletion and climate change impacts, with small to negligible side-effects in other categories;
- Improvements are needed in material selection and recycling of all system components, especially to mitigate the impacts of metals depletion, and more care should be taken around the use and treatment of contaminated water in manufacturing processes;
- No configuration could be found that simultaneously maximised both financial and environmental sustainability, although this does not preclude its existence, especially in other contexts and applications, and with more work on designing market structures that incentivise environmental sustainability.

The conclusions were then framed as recommendations to homeowners, PV-battery manufacturers and installers, policy-makers, and the community of battery researchers and energy systems modellers. To aid further research efforts, the full code and input data to the model described in this thesis are freely available at: `https://doi.org/10.5258/SOTON/D1269`, with file descriptions in Appendix E.

References

Abdulla, K., Hoog, J. D., Muenzel, V., Suits, F., Steer, K., Wirth, A., and Halgamuge, S. (2017). Optimal operation of energy storage systems considering forecasts and battery degradation. *IEEE Transactions on Smart Grid*, PP(99):1–1.

Agnew, S. and Dargusch, P. (2017). Consumer preferences for household-level battery energy storage. *Renewable and Sustainable Energy Reviews*, 75:609 – 617.

Ahmadi, L., Fowler, M., Young, S. B., Fraser, R. A., Gaffney, B., and Walker, S. B. (2014a). Energy efficiency of li-ion battery packs re-used in stationary power applications. *Sustainable Energy Technologies and Assessments*, 8:9 – 17.

Ahmadi, L., Yip, A., Fowler, M., Young, S. B., and Fraser, R. A. (2014b). Environmental feasibility of re-use of electric vehicle batteries. *Sustainable Energy Technologies and Assessments*, 6:64 – 74.

Ahmadi, L., Young, S. B., Fowler, M., Fraser, R. A., and Achachlouei, M. A. (2017). A cascaded life cycle: reuse of electric vehicle lithium-ion battery packs in energy storage systems. *The International Journal of Life Cycle Assessment*, 22(1):111–124.

Amber Kinetics (2019). M32 data sheet. `https://www.amberkinetics.com/wp-content/uploads/2019/10/AK-Datasheet-M32.pdf`. [Online; accessed 14-Dec-2019].

Assunção, A., Moura, P. S., and de Almeida, A. T. (2016). Technical and economic assessment of the secondary use of repurposed electric vehicle batteries in the residential sector to support solar energy. *Applied Energy*, 181:120 – 131.

Asthana, A. and Taylor, M. (2017). Britain to ban sale of all diesel and petrol cars and vans from 2040. `https://www.theguardian.com/politics/2017/jul/25/britain-to-ban-sale-of-all-diesel-and-petrol-cars-and-vans-from-2040`. [Online; accessed 1-Dec-2017].

Babacan, O., Abdulla, A., Hanna, R., Kleissl, J., and Victor, D. G. (2018). Unintended effects of residential energy storage on emissions from the electric power system. *Environmental Science & Technology*, 52(22):13600–13608. PMID: 30335994.

Babu, S. K., Mohamed, A. I., Whitacre, J. F., and Litster, S. (2015). Multiple imaging mode x-ray computed tomography for distinguishing active and inactive phases in lithium-ion battery cathodes. *Journal of Power Sources*, 283:314 – 319.

Baczyńska, A., Niewiadomski, W., Gonçalves, A., Almeida, P., and Luís, R. (2018). Li-NMC batteries model evaluation with experimental data for electric vehicle application. *Batteries*, 4(1).

Baños, R., Manzano-Agugliaro, F., Montoya, F., Gil, C., Alcayde, A., and Gómez, J. (2011). Optimization methods applied to renewable and sustainable energy: A review. *Renewable and Sustainable Energy Reviews*, 15(4):1753 – 1766.

Bass, F. (1969). A new product growth model for product diffusion. *Management Science*, 15(5):215–227.

Battery University (2019). Battery recycling as a business. `https://batteryuniversity.com/learn/article/battery_recycling_as_a_business`. [Online; accessed 20-Aug-2019].

Baumhöfer, T., Brühl, M., Rothgang, S., and Sauer, D. U. (2014). Production caused variation in capacity aging trend and correlation to initial cell performance. *Journal of Power Sources*, 247:332 – 338.

Beck, T., Kondziella, H., Huard, G., and Bruckner, T. (2016). Assessing the influence of the temporal resolution of electrical load and PV generation profiles on self-consumption and sizing of PV-battery systems. *Applied Energy*, 173:331 – 342.

BEIS (2018a). Digest of UK energy statistics (DUKES): foreign trade statistics. `https://www.gov.uk/government/statistics/dukes-foreign-trade-statistics#history`. [Online; accessed 19-Jul-2019].

BEIS (2018b). Final UK greenhouse gas emissions national statistics: 1990-2016. `https://www.gov.uk/government/statistics/final-uk-greenhouse-gas-emissions-national-statistics-1990-2016`. [Online; accessed 24-Nov-2019].

BEIS (2018c). Smart metering implementation programme: Progress report for 2018. `https://assets.publishing.service.gov.uk/government/uploads/system/uploads/attachment_data/file/767128/smart-meter-progress-report-2018.pdf`. [Online; accessed 30-Jun-2019].

BEIS (2019a). Annual domestic energy bills. `https://www.gov.uk/government/statistical-data-sets/annual-domestic-energy-price-statistics`. [Online; accessed 07-Jun-2019].

BEIS (2019b). New laws to guarantee payment for solar homes providing excess electricity. `https://www.gov.uk/government/news/new-laws-to-guarantee-payment-for-solar-homes-providing-excess-electricity`. [Online; accessed 19-Jun-2019].

BEIS (2019c). Solar photovoltaic (PV) cost data. `https://www.gov.uk/government/statistics/solar-pv-cost-data`. [Online; accessed 03-Jul-2019].

BEIS (2020). Solar photovoltaics deployment. `https://www.gov.uk/government/statistics/solar-photovoltaics-deployment`. [Online; accessed 06-Jun-2020].

Bekkelund, K. (2013). A comparative life cycle assessment of PV solar systems. `https://brage.bibsys.no/xmlui/handle/11250/235329`. [Online; accessed 29-Sep-2018].

Benini, L., Mancini, L., Sala, S., Manfredi, S., Schau, E. M., and Pant, R. (2014). Normalisation method and data for environmental footprints. `https://ec.europa.eu/environment/eussd/smgp/pdf/JRC_Normalisation_method_and_data_EF_web.pdf`. [Online; accessed 30-Sep-2019].

Bento, A., Roth, K., and Zuo, Y. (2016). Vehicle lifetime trends and scrappage behavior in the U.S. used car market. `http://faculty.sites.uci.edu/kevinroth/files/2011/03/Scrappage_18Jan2016.pdf`. [Online; accessed 15-Nov-2017].

Berckmans, G., Messagie, M., Smekens, J., Omar, N., Vanhaverbeke, L., and Van Mierlo, J. (2017). Cost projection of state of the art lithium-ion batteries for electric vehicles up to 2030. *Energies*, 10:1314–1333.

Bertsch, V., Geldermann, J., and Lühn, T. (2017). What drives the profitability of household PV investments, self-consumption and self-sufficiency? *Applied Energy*, 204:1 – 15.

Bettle, R., Pout, C., and Hitchin, E. (2006). Interactions between electricity-saving measures and carbon emissions from power generation in England and Wales. *Energy Policy*, 34(18):3434 – 3446.

Beyond Coal (2018). Overview: National coal phase-out announcements in Europe. `https://beyond-coal.eu/wp-content/uploads/2018/09/Overview-of-national-coal-phase-out-announcements-Europe-Beyond-Coal-September-2018.pdf`. [Online; accessed 26-Jul-2019].

Bobba, S., Mathieux, F., Ardente, F., Blengini, G. A., Cusenza, M. A., Podias, A., and Pfrang, A. (2018). Life cycle assessment of repurposed electric vehicle batteries: an adapted method based on modelling energy flows. *Journal of Energy Storage*, 19:213 – 225.

Boßmann, T. and Staffell, I. (2015). The shape of future electricity demand: Exploring load curves in 2050s Germany and Britain. *Energy*, 90:1317 – 1333.

Boyden, A., Soo, V. K., and Doolan, M. (2016). The environmental impacts of recycling portable lithium-ion batteries. *Procedia CIRP*, 48:188 – 193. The 23rd CIRP Conference on Life Cycle Engineering.

Brett, D. (2019). Cash ISA vs stock market ISA: which has returned the most? `https://www.cityam.com/cash-isa-vs-stock-market-isa-which-has-returned-most/`. [Online; accessed 17-Sep-2019].

Bussar, C., Moos, M., Alvarez, R., Wolf, P., Thien, T., Chen, H., Cai, Z., Leuthold, M., Sauer, D. U., and Moser, A. (2014). Optimal allocation and capacity of energy storage systems in a future European power system with 100 % renewable energy generation. *Energy Procedia*, 46:40 – 47. 8th International Renewable Energy Storage Conference and Exhibition (IRES 2013).

Callendar, G. S. (1938). The artificial production of carbon dioxide and its influence on temperature. *Quarterly Journal of the Royal Meteorological Society*, 64(275):223–240.

Camilo, F. M., Castro, R., Almeida, M., and Pires, V. F. (2017). Economic assessment of residential PV systems with self-consumption and storage in Portugal. *Solar Energy*, 150:353 – 362.

Carbajales-Dale, M., Barnhart, C. J., and Benson, S. M. (2014). Can we afford storage? A dynamic net energy analysis of renewable electricity generation supported by energy storage. *Energy & Environmental Science*, 7(5):1538–1544.

Casals, L. C., García, B., and González Benítez, M. (2014). A cost analysis of electric vehicle batteries second life businesses. In *XVIII Congreso Internacional de Dirección e Ingeniería de Proyectos*.

Casals, L. C., García, B. A., Aguesse, F., and Iturrondobeitia, A. (2017). Second life of electric vehicle batteries: relation between materials degradation and environmental impact. *The International Journal of Life Cycle Assessment*, 22(1):82–93.

CAT Information Service (2018). How long do solar electric PV panels last? http://info.cat.org.uk/questions/pv/life-expectancy-solar-PV-panels/. [Online; accessed 12-Mar-2018].

CEC (2015). Environmentally sound management of end-of-life batteries from electric-drive vehicles in North America. http://www.cec.org/islandora/en/item/11637-environmentally-sound-management-end-life-batteries-from-electric-drive-vehicles-en.pdf. [Online; accessed 2-Nov-2017].

Chen, W., Hong, J., Yuan, X., and Liu, J. (2016). Environmental impact assessment of monocrystalline silicon solar photovoltaic cell production: a case study in China. *Journal of Cleaner Production*, 112:1025 – 1032.

Cherry, J. (2016). Battery durability in electrified vehicle applications: A review of degradation mechanisms and durability testing. https://wiki.unece.org/download/attachments/29884985/EVE-18-04e.pdf?api=v2. [Online; accessed 24-May-2017].

Cherubini, F. and Strømman, A. H. (2011). Life cycle assessment of bioenergy systems: State of the art and future challenges. *Bioresource Technology*, 102(2):437 – 451.

Chowdhury, N., Price, B. A., Smith, A., Gooch, D., and v. d. Linden, J. (2018). 50 shades of green and brown: Comparing grid carbon intensity with consumption for households with PV generation and battery storage. In *2018 IEEE Conference on Technologies for Sustainability (SusTech)*, pages 1–8.

Climate Action Tracker (2018). Warming projections global update. https://climateactiontracker.org/documents/507/CAT_2018-12-11_Briefing_WarmingProjectionsGlobalUpdate_Dec2018.pdf. [Online; accessed 15-Jun-2019].

Clissit, C. (2019). Solar panel costs 2019. https://www.theecoexperts.co.uk/solar-panels/cost. [Online; accessed 03-Jul-2019].

CoinMarketCap (2020). SolarCoin markets. https://coinmarketcap.com/currencies/solarcoin/markets/. [Online; accessed 20-Jun-2020].

Committee on Climate Change (2019). Net Zero: The UK's contribution to stopping global warming. https://www.theccc.org.uk/wp-content/uploads/2019/05/Net-Zero-The-UKs-contribution-to-stopping-global-warming.pdf. [Online; accessed 26-Jul-2019].

Crossland, A. F., Jones, D., Wade, N. S., and Walker, S. L. (2018). Comparison of the location and rating of energy storage for renewables integration in residential low voltage networks with overvoltage constraints. *Energies*, 11(8).

Dastgeer, F., Gelani, H. E., Anees, H. M., Paracha, Z. J., and Kalam, A. (2019). Analyses of efficiency/energy-savings of DC power distribution systems/microgrids: Past, present and future. *International Journal of Electrical Power & Energy Systems*, 104:89 – 100.

de Boer, F., Johnson, M., McCullough, A., and de Oliveira, C. (2018). Rethinking decarbonisation incentives. https://es.catapult.org.uk/news/five-options-to-tackle-carbon-pricing/. [Online; accessed 24-Nov-2019].

Deane, P., Fitzgerald, J., Valeri, L. M., Tuohy, A., and Walsh, D. (2015). Irish and British electricity prices: what recent history implies for future prices. *Economics of Energy & Environmental Policy*, 4(1):97–112.

Deichmann, U. and Zhang, F. (2013). Growing green: the economic benefits of climate action. http://documents.worldbank.org/curated/en/501061468283462662/pdf/Growing-green-the-economic-benefits-of-climate-action.pdf. [Online; accessed 30-May-2019].

Deng, G. and Newton, P. (2017). Assessing the impact of solar PV on domestic electricity consumption: Exploring the prospect of rebound effects. *Energy Policy*, 110:313 – 324.

DiOrio, N., Dobos, A., Janzou, S., Nelson, A., and Lundstrom, B. (2015). Technoeconomic modeling of battery energy storage in SAM. https://www.osti.gov/biblio/1225314. [Online; accessed 30-Aug-2017].

Dreyer, L. C., Niemann, A. L., and Hauschild, M. Z. (2003). Comparison of three different LCIA methods: EDIP97, CML2001 and Eco-indicator 99. *The International Journal of Life Cycle Assessment*, 8(4):191–200.

Dubarry, M., Vuillaume, N., and Liaw, B. Y. (2009). From single cell model to battery pack simulation for Li-ion batteries. *Journal of Power Sources*, 186(2):500 – 507.

Dubey, S., Sarvaiya, J. N., and Seshadri, B. (2013). Temperature dependent photovoltaic (PV) efficiency and its effect on PV production in the world - a review. *Energy Procedia*, 33:311 – 321. PV Asia Pacific Conference 2012.

Ecker, M., Nieto, N., Käbitz, S., Schmalstieg, J., Blanke, H., Warnecke, A., and Sauer, D. U. (2014). Calendar and cycle life study of Li(NiMnCo)O2-based 18650 lithium-ion batteries. *Journal of Power Sources*, 248:839 – 851.

EEMB (2010). Lithium-ion battery datasheet. https://www.ineltro.ch/media/downloads/SAAItem/45/45958/36e3e7f3-2049-4adb-a2a7-79c654d92915.pdf. [Online; accessed 16-Aug-2019].

EIA (2019). Nuclear explained: The nuclear fuel cycle. https://www.eia.gov/energyexplained/index.php?page=nuclear_fuel_cycle. [Online; accessed 19-Jul-2019].

Elexon (2015). The electricity trading arrangements. https://www.elexon.co.uk/guidance-note/beginners-guide/. [Online; accessed 19-Jun-2017].

Elexon (2018). Balancing Mechanism reporting service (BMRS). https://www.bmreports.com/bmrs/?q=help/about-us. [Online; accessed 02-Dec-2018].

Ellingsen, L. A.-W., Majeau-Bettez, G., Singh, B., Srivastava, A. K., Valøen, L. O., and Strømman, A. H. (2014). Life cycle assessment of a lithium-ion battery vehicle pack. *Journal of Industrial Ecology*, 18(1):113–124.

ENA (2018). Engineering Recommendation G98 issue 1. http://www.ena-eng.org/ENA-Docs/D0C3XTRACT/ENA_EREC_G98_Extract_180902050358.pdf. [Online; accessed 16-Sep-2019].

Energy and Climate Change Committee (2016). 2020 renewable heat and transport targets. https://publications.parliament.uk/pa/cm201617/cmselect/cmenergy/173/173.pdf. [Online; accessed 10-Aug-2017].

EnergySage (2019). How much does solar storage cost? understanding solar battery prices. https://www.energysage.com/solar/solar-energy-storage/what-do-solar-batteries-cost/. [Online; accessed 03-Jul-2019].

Eurostat (2019). Electricity production, consumption and market overview. https://ec.europa.eu/eurostat/statistics-explained/index.php/Electricity_production,_consumption_and_market_overview. [Online; accessed 18-Nov-2019].

EV Volumes (2014). Global Sales. http://www.ev-volumes.com/news/global-ev-phev-volumes-december-2014-and-full-year/. [Online; accessed 9-Nov-2017].

EV Volumes (2016a). Global Sales. http://www.ev-volumes.com/news/global-plug-in-sales-for-2016/. [Online; accessed 9-Nov-2017].

EV Volumes (2016b). Global Sales. http://www.ev-volumes.com/news/global-electric-vehicle-sales-2016-q1/. [Online; accessed 9-Nov-2017].

Eyer, J. and Corey, G. (2010). Energy storage for the electricity grid: Benefits and market potential assessment guide. http://www.sandia.gov/ess/publications/SAND2010-0815.pdf. [Online; accessed 19-Jun-2017].

Fajardy, M. and Mac Dowell, N. (2017). Can BECCS deliver sustainable and resource efficient negative emissions? *Energy Environ. Sci.*, 10:1389–1426.

Farah, S., Whaley, D., and Saman, W. (2016). Control strategies of domestic electrical storage for reducing electricity peak demand and life cycle cost. *International Journal of Hydrogen Energy*, 41(45):20939 – 20949.

Faranda, R. S., Hafezi, H., Leva, S., Mussetta, M., and Ogliari, E. (2015). The optimum PV plant for a given solar DC/AC converter. *Energies*, 8:4853–487.

Faria, R., Marques, P., Garcia, R., Moura, P., Freire, F., Delgado, J., and de Almeida, A. T. (2014). Primary and secondary use of electric mobility batteries from a life cycle perspective. *Journal of Power Sources*, 262:169 – 177.

Fernández, I., Calvillo, C., Sánchez-Miralles, A., and Boal, J. (2013). Capacity fade and aging models for electric batteries and optimal charging strategy for electric vehicles. *Energy*, 60:35 – 43.

Flexi-Orb (2020). Flexible energy register. https://www.flexi-orb.com/services/flexible-energy-register/. [Online; accessed 20-Jun-2020].

Foster, M., Isely, P., Standridge, C. R., and Hasan, M. M. (2014). Feasibility assessment of remanufacturing, repurposing, and recycling of end of vehicle application lithium-ion batteries. *Journal of Industrial Engineering and Management*, 7(3):698–715.

Foye, C. (2017). The relationship between size of living space and subjective well-being. *Journal of Happiness Studies*, 18(2):427–461.

Frischknecht, R. (2017). Life cycle assessment and human health impacts of electricity production. http://treeze.ch/fileadmin/user_upload/downloads/Publications/Case_Studies/Energy/617_LCA_of_electricity_Frischknecht_170526_v2.01.pdf. [Online; accessed 27-Jan-2019].

Frölicher, T. L., Winton, M., and Sarmiento, J. L. (2014). Continued global warming after CO_2 emissions stoppage. *Nature Climate Change*, 4(1):40–44.

Fu, Y., Liu, X., and Yuan, Z. (2015). Life-cycle assessment of multi-crystalline photovoltaic (PV) systems in China. *Journal of Cleaner Production*, 86:180 – 190.

Gao, C., Ji, Y., Wang, J., and Sai, X. (2018). Application of blockchain technology in peer-to-peer transaction of photovoltaic power generation. In *2018 2nd IEEE Advanced Information Management, Communications, Electronic and Automation Control Conference (IMCEC)*, pages 2289–2293.

Genikomsakis, K. N., Ioakimidis, C. S., Murillo, A., Trifonova, A., and Simic, D. (2013). A life cycle assessment of a li-ion urban electric vehicle battery. In *2013 World Electric Vehicle Symposium and Exhibition (EVS27)*, pages 1–11.

Goedkoop, M., Heijungs, R., Huijbregts, M., De Schryver, A., Struijs, J., and Van Zelm, R. (2008a). ReCiPe 2008: A life cycle impact assessment method which comprises harmonised category indicators at the midpoint and the endpoint level. `https://www.rivm.nl/en/Topics/L/Life_Cycle_Assessment_LCA/Downloads`. [Online; accessed 24-Feb-2018].

Goedkoop, M., Heijungs, R., Huijbregts, M., De Schryver, A., Struijs, J., and Van Zelm, R. (2008b). Recipe 2008 characterization and normalisation factors. `https://www.rivm.nl/en/Topics/L/Life_Cycle_Assessment_LCA/Downloads`. [Online; accessed 20-Nov-2017].

Goldie-Scot, L. (2019). A behind the scenes take on lithium-ion battery prices. `https://about.bnef.com/blog/behind-scenes-take-lithium-ion-battery-prices/`. [Online; accessed 20-Jun-2019].

Green, R. and Staffell, I. (2014). The impact of government interventions on investment in the GB electricity market. `http://ec.europa.eu/competition/state_aid/studies_reports/green_staffell_en.pdf`. [Online; accessed 27-Jun-2018].

Green Car Guide (2017). Renault leases 100,000 electric vehicle batteries. `https://www.greencarguide.co.uk/2017/03/renault-leases-100000-electric-vehicle-batteries/`. [Online; accessed 1-Dec-2017].

Green Energy (2017). A new and better way to control home energy bills. `https://www.greenenergyuk.com/PressRelease.aspx?PRESS_RELEASE_ID=76`. [Online; accessed 12-Jul-2019].

Green Energy (2019). Tariff information. `https://www.greenenergyuk.com/TariffInfoLabel.aspx?TARIFF_ID=4&IS_TWO_RATE=False&IS_DUAL_FUEL=True&GAS=False&ELECTRICITY=True`. [Online; accessed 24-Sep-2019].

GreenMatch (2019). Solar battery storage system cost & advantages. `https://www.greenmatch.co.uk/blog/2018/07/solar-battery-storage-system-cost`. [Online; accessed 03-Jul-2019].

Gridwatch (2018). About the Gridwatch site. `https://www.gridwatch.templar.co.uk/about.html`. [Online; accessed 11-May-2018].

Harari, D. (2009). Vehicle scrappage scheme. `https://researchbriefings.parliament.uk/ResearchBriefing/Summary/SN05177`. [Online; accessed 10-Aug-2017].

Harper, G., Sommerville, R., Kendrick, E., Driscoll, L., Slater, P., Stolkin, R., Walton, A., Christensen, P., Heidrich, O., Lambert, S., Abbott, A., Ryder, K., Gaines, L., and Anderson, P. (2019). Recycling lithium-ion batteries from electric vehicles. *Nature*, 575(7781):75–86.

Harvey, J. (1994). *Mastering Economics*. Macmillan Master Series, 4th edition. ISBN: 9780333617038.

Hassan, A. S., Cipcigan, L., and Jenkins, N. (2017). Optimal battery storage operation for PV systems with tariff incentives. *Applied Energy*, 203:422 – 441.

Hawkes, A. (2010). Estimating marginal CO_2 emissions rates for national electricity systems. *Energy Policy*, 38(10):5977 – 5987. The socio-economic transition towards a hydrogen economy - findings from European research, with regular papers.

Hawkins, T. R., Singh, B., Majeau-Bettez, G., and Strømman, A. H. (2013). Comparative environmental life cycle assessment of conventional and electric vehicles. *Journal of Industrial Ecology*, 17(1):53–64.

Hertwich, E. G., Gibon, T., Bouman, E. A., Arvesen, A., Suh, S., Heath, G. A., Bergesen, J. D., Ramirez, A., Vega, M. I., and Shi, L. (2015). Integrated life-cycle assessment of electricity-supply scenarios confirms global environmental benefit of low-carbon technologies. *Proceedings of the National Academy of Sciences*, 112(20):6277–6282.

Hesse, H. C., Schimpe, M., Kucevic, D., and Jossen, A. (2017). Lithium-ion battery storage for the grid - a review of stationary battery storage system design tailored for applications in modern power grids. *Energies*, 10(12).

Heymans, C., Walker, S. B., Young, S. B., and Fowler, M. (2014). Economic analysis of second use electric vehicle batteries for residential energy storage and load-levelling. *Energy Policy*, 71:22 – 30.

Hirst, D. and Keep, M. (2018). Carbon price floor (CPF) and the price support mechanism. `https://researchbriefings.parliament.uk/ResearchBriefing/Summary/SN05177`. [Online; accessed 24-Nov-2019].

Hittinger, E., Wiley, T., Kluza, J., and Whitacre, J. (2015). Evaluating the value of batteries in microgrid electricity systems using an improved energy systems model. *Energy Conversion and Management*, 89:458 – 472.

Hoppmann, J., Volland, J., Schmidt, T. S., and Hoffmann, V. H. (2014). The economic viability of battery storage for residential solar photovoltaic systems - a review and a simulation model. *Renewable and Sustainable Energy Reviews*, 39:1101–1118.

Huijbregts, M. A. J., Steinmann, Z. J. N., Elshout, P. M. F., Stam, G., Verones, F., Vieira, M., and Van Zelm, R. (2016). ReCiPe 2016: A life cycle impact assessment method which comprises harmonised category indicators at the midpoint and the endpoint level. `https://www.rivm.nl/en/Topics/L/Life_Cycle_Assessment_LCA/Downloads`. [Online; accessed 04-Mar-2018].

Hunter, K., Sreepathi, S., and DeCarolis, J. F. (2013). Modeling for insight using Tools for Energy Model Optimization and Analysis (Temoa). *Energy Economics*, 40:339 – 349.

IEA (2017a). Energy access outlook 2017. `https://www.iea.org/access2017/`. [Online; accessed 27-Jun-2019].

IEA (2017b). Global EV Outlook. `https://www.iea.org/publications/freepublications/publication/GlobalEVOutlook2017.pdf`. [Online; accessed 15-Nov-2017].

IEA (2018a). Statistics data browser. `https://www.iea.org/statistics/?country=FRANCE&year=2016&category=Electricity&indicator=ElecGenByFuel&mode=chart&dataTable=ELECTRICITYANDHEAT`. [Online; accessed 31-Jul-2019].

IEA (2018b). Statistics data browser. https://www.iea.org/statistics/?country=NETHLAND&year=2016&category=Electricity&indicator=ElecGenByFuel&mode=chart&dataTable=ELECTRICITYANDHEAT. [Online; accessed 31-Jul-2019].

IEA (2019). Global energy & CO_2 status report. https://www.iea.org/geco/electricity/. [Online; accessed 20-Jun-2019].

IPBES (2018). Global assessment report on biodiversity and ecosystem services of the Intergovernmental Science-Policy Platform on Biodiversity and Ecosystem Services. https://www.un.org/sustainabledevelopment/blog/2019/05/nature-decline-unprecedented-report/. [Online; accessed 07-Feb-2019].

IPCC (2018). Summary for policymakers. in: Global warming of 1.5°C. an IPCC special report on the impacts of global warming of 1.5°C above pre-industrial levels and related global greenhouse gas emission pathways, in the context of strengthening the global response to the threat of climate change, sustainable development, and efforts to eradicate poverty. https://www.ipcc.ch/sr15/chapter/summary-for-policy-makers/. [Online; accessed 07-Feb-2019].

IRENA (2016). End-of-life management - solar photovoltaic panels. http://www.irena.org/DocumentDownloads/Publications/IRENA_IEAPVPS_End-of-Life_Solar_PV_Panels_2016.pdf. [Online; accessed 29-Sep-2018].

IRENA (2017). Electricity storage and renewables: Costs and markets to 2030. https://www.irena.org/publications/2017/Oct/Electricity-storage-and-renewables-costs-and-markets. [Online; accessed 11-Jun-2019].

IRENA (2018). Global energy transformation: A roadmap to 2050. https://www.irena.org/-/media/Files/IRENA/Agency/Publication/2018/Apr/IRENA_Report_GET_2018.pdf. [Online; accessed 14-Jun-2019].

IRENA (2019). Renewable capacity statistics. https://www.irena.org/publications/2019/Mar/Renewable-Capacity-Statistics-2019. [Online; accessed 20-Jun-2019].

ISGAN (2019). Netherlands: Powermatching city. http://www.iea-isgan.org/cee-case08-netherlands/. [Online; accessed 27-Jun-2019].

ISO (2006a). ISO 14040:2006 - Environmental management - Life cycle assessment - Principles and framework. http://www.iso.org/standard/37456.html. [Online; accessed 26-Jun-2018].

ISO (2006b). ISO 14044:2006 - Environmental management - Life cycle assessment - Requirements and guidelines. https://www.iso.org/standard/38498.html. [Online; accessed 26-Jun-2018].

Jiang, J. and Zhang, C. (2015). *Fundamentals and application of lithium-ion batteries in electric drive vehicles*. John Wiley & Sons, Inc. ISBN: 9781118414781.

Jiao, N. and Evans, S. (2016). Business models for sustainability: The case of second-life electric vehicle batteries. *Procedia CIRP*, 40(Supplement C):250–255. 13th Global Conference on Sustainable Manufacturing – Decoupling Growth from Resource Use.

Jordan, D. C. and Kurtz, S. R. (2013). Photovoltaic degradation rates - an analytical review. *Progress in Photovoltaics: Research and Applications*, 21(1):12–29.

Kabakian, V., McManus, M., and Harajli, H. (2015). Attributional life cycle assessment of mounted 1.8kWp monocrystalline photovoltaic system with batteries and comparison with fossil energy production system. *Applied Energy*, 154:428 – 437.

Kantz, H. and Schreiber, T. (2003). *Nonlinear time series analysis*. Cambridge Universtiy Press, 2nd edition. ISBN: 0521 551447.

Kennedy, J. B. and Neville, A. (1966). *Basic statistical methods for engineers and scientists*. IEP, 2nd edition. ISBN: 0700224807.

Kim, Y.-H. (2017). Product specification: Rechargeable lithium ion battery, model: INR18650 M36T 12.50Wh. `http://www.nkon.nl/sk/k/m36.pdf`. [Online; accessed 16-Aug-2019].

Kirmas, A. and Madlener, R. (2017). Economic viability of second use electric vehicle batteries for energy storage in residential applications. *Energy Procedia*, 105(Supplement C):3806–3815. 8th International Conference on Applied Energy, ICAE2016, 8-11 October 2016, Beijing, China.

Klimstra, J. (2014). *Power Supply Challenges*. Wärtsilä Finland Oy. ISBN: 978-952-93-3635-7.

Klöpffer, W. and Grahl, B. (2014). *Life cycle assessment: A guide to best practice*. John Wiley & Sons, Inc, 1st edition. ISBN: 9783527655656.

Klör, B., Beverungen, D., Bräuer, S., Plenter, F., and Monhof, M. (2015). A market for trading used electric vehicle batteries - theoretical foundations and information systems. In *Twenty-Third European Conference on Information Systems (ECIS)*.

Konstantelos, I., Sun, M., and Strbac, G. (2014). Quantifying demand diversity of households. `https://spiral.imperial.ac.uk/bitstream/10044/1/30567/2/LCL%20ICL%20Quantifying%20Demand%20Diversity%20of%20Households%20FINAL.PDF`. [Online; accessed 30-Jul-2019].

Koornneef, J., van Keulen, T., Faaij, A., and Turkenburg, W. (2008). Life cycle assessment of a pulverized coal power plant with post-combustion capture, transport and storage of CO_2. *International Journal of Greenhouse Gas Control*, 2(4):448 – 467. TCCS-4: The 4th Trondheim Conference on CO_2 Capture, Transport and Storage.

Kurland, S. D. and Benson, S. M. (2019). The energetic implications of introducing lithium-ion batteries into distributed photovoltaic systems. *Sustainable Energy Fuels*, 3:1182–1190.

Latunussa, C. E., Ardente, F., Blengini, G. A., and Mancini, L. (2016). Life cycle assessment of an innovative recycling process for crystalline silicon photovoltaic panels. *Solar Energy Materials and Solar Cells*, 156:101 – 111. Life cycle, environmental, ecology and impact analysis of solar technology.

Laugen, L. (2013). An environmental life cycle assessment of LNG and HFO as marine fuels. `https://pdfs.semanticscholar.org/e010/ee462106f4581be5c744d3a48035020fd191.pdf`. [Online; accessed 23-Aug-2019].

LCP and EnAppSys (2014). Analysis of the marginal emission factor (MEF). `https://assets.publishing.service.gov.uk/government/uploads/system/uploads/attachment_data/file/357753/MEF_Analysis_-_Report_FINAL.pdf`. [Online; accessed 06-Sep-2018].

Leijtens, T., Bush, K. A., Prasanna, R., and McGehee, M. D. (2018). Opportunities and challenges for tandem solar cells using metal halide perovskite semiconductors. *Nature Energy*, 3(10):828–838.

LG Chem (2018a). ESS battery. `http://www.lgchem.com/global/ess/ess/product-detail-PDEC0001`. [Online; accessed 20-Aug-2018].

LG Chem (2018b). Product specification: Rechargeable lithium ion battery E63. `http://queenbattery.com.cn/index.php?controller=attachment&id_attachment=109`. [Online; accessed 17-Aug-2019].

Li, J., Wu, Z., Zhou, S., Fu, H., and Zhang, X. (2015). Aggregator service for PV and battery energy storage systems of residential building. *CSEE Journal of Power and Energy Systems*, 1(4):3–11.

Lund, H. and Thellufsen, J. Z. (2018). EnergyPLAN: Advanced energy systems analysis computer model. `https://www.energyplan.eu/wp-content/uploads/2018/11/EnergyPLAN-Documentation-Version14_final.pdf`. [Online; accessed 26-Jul-2019].

Luo, X., Wang, J., Dooner, M., and Clarke, J. (2015). Overview of current development in electrical energy storage technologies and the application potential in power system operation. *Applied Energy*, 137:511–536.

Ma, X., Ma, Y., Zhou, J., and Siqin, X. (2018). The recycling of spent power battery: Economic benefits and policy suggestions. *IOP Conference Series: Earth and Environmental Science*, 159:012017.

Mahmud, K., Morsalin, S., Kafle, Y. R., and Town, G. E. (2016). Improved peak shaving in grid-connected domestic power systems combining photovoltaic generation, battery storage, and V2G-capable electric vehicle. In *2016 IEEE International Conference on Power System Technology (POWERCON)*, pages 1–4.

Märker, K., Reeves, P. J., Xu, C., Griffith, K. J., and Grey, C. P. (2019). Evolution of structure and lithium dynamics in LiNi0.8Mn0.1Co0.1O2 (NMC811) cathodes during electrochemical cycling. *Chemistry of Materials*, 31(7):2545–2554.

Martinez-Laserna, E., Gandiaga, I., Sarasketa-Zabala, E., Badeda, J., Stroe, D.-I., Swierczynski, M., and Goikoetxea, A. (2018). Battery second life: Hype, hope or reality? a critical review of the state of the art. *Renewable and Sustainable Energy Reviews*, 93:701 – 718.

Masanet, E., Chang, Y., Gopal, A. R., Larsen, P., Morrow, W. R., Sathre, R., Shehabi, A., and Zhai, P. (2013). Life-cycle assessment of electric power systems. *Annual Review of Environment and Resources*, 38(1):107–136.

McKenna, E., Barton, J., and Thomson, M. (2017). Short-run impact of electricity storage on CO_2 emissions in power systems with high penetrations of wind power: A case-study of Ireland. *Proceedings of the Institution of Mechanical Engineers, Part A: Journal of Power and Energy*, 231(6):590–603.

McKenna, E. and Darby, S. (2017). How much do smart appliances reduce CO_2 emissions? assessing the environmental impact of domestic demand response technologies. European Council for an Energy-Efficiency Economy.

McKenna, E., McManus, M., Cooper, S., and Thomson, M. (2013). Economic and environmental impact of lead-acid batteries in grid-connected domestic PV systems. *Applied Energy*, 104:239 – 249.

McManus, M. (2012). Environmental consequences of the use of batteries in low carbon systems: The impact of battery production. *Applied Energy*, 93:288 – 295. (1) Green Energy; (2) Special Section from papers presented at the 2nd International Enery 2030 Conf.

Merchant, E. F. (2019). Tesla Powerwalls are in high demand, installers just don't have them. https://www.greentechmedia.com/articles/read/tesla-powerwalls-but-installers-dont-have-them. [Online; accessed 05-Jun-2019].

Midsummer (2019). SolaX power battery storage systems. https://midsummerwholesale.co.uk/buy/solax. [Online; accessed 03-Jul-2019].

Moixa (2016). Tech Specs. http://www.moixa.com/products/. [Online; accessed 18-Mar-2018].

Moreno, R., Moreira, R., and Strbac, G. (2015). A MILP model for optimising multi-service portfolios of distributed energy storage. *Applied Energy*, 137:554 – 566.

Moretti, E., Barbanera, M., Foschini, D., Buratti, C., and Cotana, F. (2016). Energy and environmental performance analysis of biomass-fuelled combined cooling and heating system for commercial building retrofit: An Italian case study. *Energy Procedia*, 101:376 – 383. ATI 2016 - 71st Conference of the Italian Thermal Machines Engineering Association.

Mouser (2019). ABB embedded power QSxW050A0B DC/DC converter power modules. https://www.mouser.co.uk/new/GE-Critical-Power/ge-critical-power-qsxw050a0b-dc-dc-modules/. [Online; accessed 01-Jul-2019].

Muenzel, V., de Hoog, J., Brazil, M., Vishwanath, A., and Kalyanaraman, S. (2015). A multi-factor battery cycle life prediction methodology for optimal battery management. In *Proceedings of the 2015 ACM Sixth International Conference on Future Energy Systems*, e-Energy '15, pages 57–66, New York, NY, USA. ACM.

Muenzel, V., Mareels, I., de Hoog, J., Vishwanath, A., Kalyanaraman, S., and Gort, A. (2015). PV generation and demand mismatch: Evaluating the potential of residential storage. In *2015 IEEE Power Energy Society Innovative Smart Grid Technologies Conference (ISGT)*, pages 1–5.

Mulder, G., Six, D., Claessens, B., Broes, T., Omar, N., and Mierlo, J. V. (2013). The dimensioning of PV-battery systems depending on the incentive and selling price conditions. *Applied Energy*, 111:1126 – 1135.

Murray, D., Stankovic, L., and Stankovic, V. (2017). An electrical load measurements dataset of United Kingdom households from a two-year longitudinal study. *Scientific Data*, 4(160122).

Muthuvel, P., Daniel, S. A., and Yazhini, D. (2016). Retrofitting domestic appliances for PV powered DC nano-grid and its impact on net zero energy homes in rural India. *Engineering Science and Technology, an International Journal*, 19(4):1836 – 1844.

MyGridGB (2019). MyGridGB dashboard. https://www.mygridgb.co.uk/dashboard/. [Online; accessed 15-Jul-2019].

Naked Solar (2019). Solar batteries & storage. https://nakedsolar.co.uk/storage/. [Online; accessed 03-Jul-2019].

National Grid (2016a). Enhanced Frequency Response: Invitation to tender for pre-qualified parties. https://www.nationalgrid.com/sites/default/files/documents/Enhanced%20Frequency%20Response%20ITT%20v2_2%20clean.pdf. [Online; accessed 25-Jan-2018].

National Grid (2016b). Future requirements for balancing services. https://www.nationalgrid.com/sites/default/files/documents/Requirements%20Report%202016.pdf. [Online; accessed 25-Jan-2018].

National Grid (2018a). Future energy scenarios data workbook. http://fes.nationalgrid.com/media/1366/2018-fes-charts-v2_as-published.xlsx. [Online; accessed 01-Oct-2018].

National Grid (2018b). Future energy scenarios modelling methods. http://fes.nationalgrid.com/media/1360/modelling-methods-v20.pdf. [Online; accessed 01-Oct-2018].

National Grid (2018c). Short term operating reserve (STOR). https://www.nationalgrid.com/uk/electricity/balancing-services/reserve-services/short-term-operating-reserve-stor?technical-requirements. [Online; accessed 25-Jan-2018].

Naumann, M., Karl, R. C., Truong, C. N., Jossen, A., and Hesse, H. C. (2015). Lithium-ion battery cost analysis in PV-household application. *Energy Procedia*, 73:37 – 47. 9th International Renewable Energy Storage Conference, IRES 2015.

Nejad, S., Gladwin, D., and Stone, D. (2016). A systematic review of lumped-parameter equivalent circuit models for real-time estimation of lithium-ion battery states. *Journal of Power Sources*, 316:183 – 196.

Nerini, F. F., Broad, O., Mentis, D., Welsch, M., Bazilian, M., and Howells, M. (2016). A cost comparison of technology approaches for improving access to electricity services. *Energy*, 95:255 – 265.

Neubauer, J. and Pesaran, A. (2011). The ability of battery second use strategies to impact plug-in electric vehicle prices and serve utility energy storage applications. *Journal of Power Sources*, 196(23):10351–10358.

Neubauer, J. S., Wood, E., and Pesaran, A. (2015). A second life for electric vehicle batteries: Answering questions on battery degradation and value. *SAE International Journal of Materials and Manufacturing*, 8(2):544–553.

Ning, G., Haran, B., and Popov, B. N. (2003). Capacity fade study of lithium-ion batteries cycled at high discharge rates. *Journal of Power Sources*, 117(1):160 – 169.

Nissan (2018). Energy storage: Why own xStorage. https://www.nissan.co.uk/experience-nissan/electric-vehicle-leadership/xstorage-by-nissan.html. [Online; accessed 18-Aug-2018].

Øberg, M. M. (2013). Life cycle assessment of fuel choices for marine vessels. https://pdfs.semanticscholar.org/f2d4/19ceefba4ba5f0b99145c5a3bf12b3f23c5b.pdf. [Online; accessed 23-Aug-2019].

Octopus (2019). Introducing Agile Octopus. https://octopus.energy/agile/. [Online; accessed 12-Jul-2019].

Ofgem (2017). Typical domestic consumption values. https://www.ofgem.gov.uk/gas/retail-market/monitoring-data-and-statistics/typical-domestic-consumption-values. [Online; accessed 12-Jul-2019].

Ofgem (2019). Feed-in tariff (FIT) rates. https://www.ofgem.gov.uk/environmental-programmes/fit/fit-tariff-rates. [Online; accessed 19-Jun-2019].

Olkkonen, V. and Syri, S. (2016). Spatial and temporal variations of marginal electricity generation: the case of the Finnish, Nordic, and European energy systems up to 2030. *Journal of Cleaner Production*, 126:515 – 525.

Olson, J. and Choi, S. (1985). A product diffusion model incorporating repeat purchases. *Technological Forecasting and Social Change*, 27(4):385–397.

Omar, N., Monem, M. A., Firouz, Y., Salminen, J., Smekens, J., Hegazy, O., Gaulous, H., Mulder, G., Van den Bossche, P., Coosemans, T., and Van Mierlo, J. (2014). Lithium iron phosphate based battery - assessment of the aging parameters and development of cycle life model. *Applied Energy*, 113:1575–1585.

Ongondo, F., Williams, I., and Cherrett, T. (2011). How are WEEE doing? A global review of the management of electrical and electronic wastes. *Waste Management*, 31(4):714–730.

ONS (2019). CPIH annual rate 00: All items 2015=100. `https://www.ons.gov.uk/economy/inflationandpriceindices/timeseries/l55o/mm23`. [Online; accessed 01-Sep-2019].

Open Energi (2019). Dynamic demand 2.0. `https://www.openenergi.com/technology/`. [Online; accessed 27-Jun-2019].

O'Shaughnessy, E., Cutler, D., Ardani, K., and Margolis, R. (2018). Solar plus: Optimization of distributed solar PV through battery storage and dispatchable load in residential buildings. *Applied Energy*, 213:11 – 21.

Owsianiak, M., Laurent, A., Bjørn, A., and Hauschild, M. Z. (2014). IMPACT 2002+, ReCiPe 2008 and ILCD's recommended practice for characterization modelling in life cycle impact assessment: a case study-based comparison. *The International Journal of Life Cycle Assessment*, 19(5):1007–1021.

Palanov, N. (2014). Life-cycle assessment of photovaltaic systems. `http://www.byfy.lth.se/fileadmin/byfy/files/TVBH-5000pdf/TVBH-5074NP_web.pdf`. [Online; accessed 06-Mar-2018].

Parra, D., Walker, G. S., and Gillott, M. (2016). Are batteries the optimum PV-coupled energy storage for dwellings? techno-economic comparison with hot water tanks in the UK. *Energy and Buildings*, 116:614 – 621.

Peters, J. F. and Weil, M. (2017). Aqueous hybrid ion batteries – an environmentally friendly alternative for stationary energy storage? *Journal of Power Sources*, 364:258 – 265.

Petroff, A. (2017). These countries want to ditch gas and diesel cars. `https://money.cnn.com/2017/07/26/autos/countries-that-are-banning-gas-cars-for-electric/index.html`. [Online; accessed 10-Aug-2017].

Pfenninger, S. (2017). Dealing with multiple decades of hourly wind and PV time series in energy models: A comparison of methods to reduce time resolution and the planning implications of inter-annual variability. *Applied Energy*, 197:1 – 13.

Phinikarides, A., Kindyni, N., Makrides, G., and Georghiou, G. E. (2014). Review of photovoltaic degradation rate methodologies. *Renewable and Sustainable Energy Reviews*, 40:143 – 152.

Pinson, M. B. and Bazant, M. Z. (2013). Theory of SEI formation in rechargeable batteries: capacity fade, accelerated aging and lifetime prediction. *Journal of the Electrochemical Society*, 160(2):A243–A250.

Popović-Gerber, J., Ferreira, J. A., and v. Wyk, J. D. (2011). Quantifying the value of power electronics in sustainable electrical energy systems. *IEEE Transactions on Power Electronics*, 26(12):3534–3544.

Powervault (2018). Why choose powervault? environmental benefits. `https://www.powervault.co.uk/powervault-to-store-your-solar-energy/`. [Online; accessed 18-Aug-2018].

Prol, J. L. and Steininger, K. W. (2017). Photovoltaic self-consumption regulation in Spain: Profitability analysis and alternative regulation schemes. *Energy Policy*, 108:742 – 754.

PV Europe (2016). Energy storage: 10 GWh used EV batteries by 2025 for second life stationary storage. `http://www.pveurope.eu/News/Energy-Storage/Energy-storage-10-GWh-used-EV-batteries-by-2025-for-second-life-stationary-storage`. [Online; accessed 30-Nov-2017].

PylonTech (2016). PF25N energy type cell. `http://www.pylontech.com.cn/pro_detail.aspx?id=108&cid=26`. [Online; accessed 16-Aug-2019].

Quoilin, S., Kavvadias, K., Mercier, A., Pappone, I., and Zucker, A. (2016). Quantifying self-consumption linked to solar home battery systems: Statistical analysis and economic assessment. *Applied Energy*, 182:58 – 67.

Reid, G. and Julve, J. (2016). Second life-batterien als flexible speicher für erneuerbare energien. `https://www.bee-ev.de/fileadmin/Publikationen/Studien/201604_Second_Life-Batterien_als_flexible_Speicher.pdf`. [Online; accessed 25-Apr-2018].

Richa, K., Babbitt, C. W., Nenadic, N. G., and Gaustad, G. (2017). Environmental trade-offs across cascading lithium-ion battery life cycles. *The International Journal of Life Cycle Assessment*, 22(1):66–81.

Ricke, K., Drouet, L., Caldeira, K., and Tavoni, M. (2018). Country-level social cost of carbon. *Nature Climate Change*, 8(10):895–900.

Rogers, A. and Parson, O. (2019). GridCarbon. `http://www.cs.ox.ac.uk/people/alex.rogers/gridcarbon/`. [Online; accessed 15-Jul-2019].

Ryberg, M. W., Owsianiak, M., Laurent, A., and Hauschild, M. Z. (2015). Power generation from chemically cleaned coals: do environmental benefits of firing cleaner coal outweigh environmental burden of cleaning? *Energy Environ. Sci.*, 8:2435–2447.

Sala, S., Crenna, E., Secchi, M., and Pant, R. (2017). Global normalisation factors for the environmental footprint and life cycle assessment. `https://publications.jrc.ec.europa.eu/repository/bitstream/JRC109878/kjna28984enn_global_norm_factors.pdf`. [Online; accessed 18-Nov-2019].

Sandbag (2019). Carbon price viewer. `https://sandbag.org.uk/carbon-price-viewer/`. [Online; accessed 24-Nov-2019].

Sathre, R., Scown, C. D., Kavvada, O., and Hendrickson, T. P. (2015). Energy and climate effects of second-life use of electric vehicle batteries in California through 2050. *Journal of Power Sources*, 288(Supplement C):82–91.

Schakel, W., Meerman, H., Talaei, A., Ramírez, A., and Faaij, A. (2014). Comparative life cycle assessment of biomass co-firing plants with carbon capture and storage. *Applied Energy*, 131:441 – 467.

Schofield, J. (2015). Dynamic time-of-use electricity pricing for residential demand response: design and analysis of the Low Carbon London smart-metering trial. https://openknowledge.worldbank.org/handle/10986/31755. [Online; accessed 30-Jul-2016].

Schreiber, A., Zapp, P., and Marx, J. (2012). Meta-analysis of life cycle assessment studies on electricity generation with carbon capture and storage. *Journal of Industrial Ecology*, 16(s1):S155–S168.

Sekitou, M., Tanaka, K., and Managi, S. (2018). Household electricity demand after the introduction of solar photovoltaic systems. *Economic Analysis and Policy*, 57:102 – 110.

Sharkh, S. M., Abu-Sara, M. A., Orfanoudakis, G. I., and Hussain, B. (2014). *Converter Topologies*. IEEE. ISBN: 9780470824054.

Siler-Evans, K., Azevedo, I. L., and Morgan, M. G. (2012). Marginal emissions factors for the U.S. electricity system. *Environmental Science & Technology*, 46(9):4742–4748. PMID: 22486733.

SimpliPhi (2018). PHI 2.7 Battery. https://simpliphipower.com/product/phi-2-7-battery/. [Online; accessed 20-Aug-2018].

Singh, B., Strømman, A. H., and Hertwich, E. (2011). Life cycle assessment of natural gas combined cycle power plant with post-combustion carbon capture, transport and storage. *International Journal of Greenhouse Gas Control*, 5(3):457 – 466. The 5th Trondheim Conference on CO_2 Capture, Transport and Storage.

Smith, M. N. (2016). The number of cars worldwide is set to double by 2040. https://www.weforum.org/agenda/2016/04/the-number-of-cars-worldwide-is-set-to-double-by-2040. [Online; accessed 15-Nov-2017].

Smith, S. and Braathen, N. A. (2015). Monetary carbon values in policy appraisal: An overview of current practice and key issues. https://www.oecd-ilibrary.org/content/paper/5jrs8st3ngvh-en. [Online; accessed 26-Jul-2019].

Sobol, I. M. (1975). *The Monte Carlo Method*. Mir Publishers, English translation edition. ISBN: 9780226767499.

Solar Guide (2018). How much does it cost to install solar panels in the UK? https://www.solarguide.co.uk/how-much-does-it-cost-to-install-solar-panels/. [Online; accessed 03-Jul-2019].

Solar Waste (2018). European WEEE directive. http://www.solarwaste.eu/collection-and-recycling/. [Online; accessed 29-Sep-2018].

SolarWatt (2018). MyReserve. https://www.solarwatt.com/solar-batteries/myreserve. [Online; accessed 20-Aug-2018].

SolaX Power (2018). Home. https://www.solaxpower.com/en/home/. [Online; accessed 20-Aug-2018].

Staffell, I. (2017). Measuring the progress and impacts of decarbonising British electricity. *Energy Policy*, 102:463 – 475.

Stamford, L. and Azapagic, A. (2012). Life cycle sustainability assessment of electricity options for the UK. *International Journal of Energy Research*, 36(14):1263–1290.

Stamford, L. and Azapagic, A. (2014). Life cycle sustainability assessment of UK electricity scenarios to 2070. *Energy for Sustainable Development*, 23:194 – 211.

Stamford, L. and Azapagic, A. (2018). Environmental impacts of photovoltaics: The effects of technological improvements and transfer of manufacturing from Europe to China. *Energy Technology*, 6(6):1148–1160.

Steffen, W., Richardson, K., Rockström, J., Cornell, S. E., Fetzer, I., Bennett, E. M., Biggs, R., Carpenter, S. R., de Vries, W., de Wit, C. A., Folke, C., Gerten, D., Heinke, J., Mace, G. M., Persson, L. M., Ramanathan, V., Reyers, B., and Sörlin, S. (2015). Planetary boundaries: Guiding human development on a changing planet. *Science*, 347(6223).

Strbac, G., Pollitt, M., Konstantinidis, C. V., Konstantelos, I., Moreno, R., Newbery, D., and Green, R. (2014). Electricity transmission arrangements in Great Britain: Time for change? *Energy Policy*, 73:298 – 311.

Strickland, D., Chittock, L., Stone, D. A., Foster, M. P., and Price, B. (2014). Estimation of transportation battery second life for use in electricity grid systems. *IEEE Transactions on Sustainable Energy*, 5(3):795–803.

Stroe, D., Swierczynski, M., Stroe, A., Laerke, R., Kjaer, P. C., and Teodorescu, R. (2016). Degradation behavior of Lithium-ion batteries based on lifetime models and field measured frequency regulation mission profile. *IEEE Transactions on Industry Applications*, 52(6):5009–5018.

Sun, S., Kiaee, M., Norman, S., and Wills, R. (2018a). Self-sufficiency ratio: an insufficient metric for domestic PV-battery systems? *Energy Procedia*, 151:150 – 157. 3rd Annual Conference in Energy Storage and Its Applications, 3rd CDT-ESA-AC, 11–12 September 2018, The University of Sheffield, UK.

Sun, S. I., Chipperfield, A. J., Kiaee, M., and Wills, R. G. (2018b). Effects of market dynamics on the time-evolving price of second-life electric vehicle batteries. *Journal of Energy Storage*, 19:41 – 51.

Sun, S. I., Crossland, A. F., Chipperfield, A. J., and Wills, R. G. A. (2019). An emissions arbitrage algorithm to improve the environmental performance of domestic PV-battery systems. *Energies*, 12(3).

Sun, S. I., Kiaee, M., Chipperfield, A. J., and Wills, R. G. A. (2018c). Techno-economic and environmental analysis of second-life batteries compared to new in a revenue-stacking network-constrained solar PV farm. In *Energy Systems Conference 2018*.

Sun, S. I., Smith, B. D., Wills, R. G. A., and Crossland, A. F. (2020). Effects of time resolution on finances and self-consumption when modeling domestic PV-battery systems. Under review. 4th Annual Conference in Energy Storage and Its Applications, 4th CDT-ESA-AC, 9-10 July 2019, The University of Southampton, UK.

Sunamp (2019). Heating your home and hot water. `https://www.sunamp.com/residential/#intro`. [Online; accessed 26-Jun-2019].

Tant, J., Geth, F., Six, D., Tant, P., and Driesen, J. (2013). Multiobjective battery storage to improve PV integration in residential distribution grids. *IEEE Transactions on Sustainable Energy*, 4(1):182–191.

Tesla (2018). Powerwall. `https://www.tesla.com/powerwall`. [Online; accessed 18-Mar-2018].

The Basel Convention (1989). On the control of transboundary movements of hazardous wastes and their disposal. `http://www.basel.int/TheConvention/Overview/TextoftheConvention/tabid/1275/Default.aspx`. [Online; accessed 5-Dec-2017].

Tokash, W. and Dehamma, A. (2016). Alternative revenue models for advanced batteries. https://www.navigantresearch.com/wp-assets/brochures/RB-ARM-16-Executive-Summary.pdf. [Online; accessed 27-Oct-2017].

Trading Economics (2019). United Kingdom - transmission and distribution losses. https://tradingeconomics.com/united-kingdom/transmission-and-distribution-losses-percent-wb-data.html. [Online; accessed 06-Sep-2019].

Truong, C. N., Naumann, M., Karl, R. C., Müller, M., Jossen, A., and Hesse, H. C. (2016). Economics of residential photovoltaic battery systems in Germany: The case of Tesla's Powerwall. *Batteries*, 2(2).

Uddin, K., Jackson, T., Widanage, W. D., Chouchelamane, G., Jennings, P. A., and Marco, J. (2017). On the possibility of extending the lifetime of lithium-ion batteries through optimal V2G facilitated by an integrated vehicle and smart-grid system. *Energy*, 133:710 – 722.

UN (2018). 68% of the world population projected to live in urban areas by 2050, says UN. https://population.un.org/wup/Publications/Files/WUP2018-PressRelease.pdf. [Online; accessed 07-Jul-2019].

UNFCCC (2018). The Paris Agreement. https://unfccc.int/process-and-meetings/the-paris-agreement/the-paris-agreement. [Online; accessed 06-Aug-2018].

University of Southampton (2019). The Iridis compute cluster. https://www.southampton.ac.uk/isolutions/staff/iridis.page. [Online; accessed 01-Oct-2019].

USABC (1996). Electric vehicle battery test procedures manual, revision 2. https://avt.inl.gov/sites/default/files/pdf/battery/usabc_manual_rev2.pdf. [Online; accessed 09-Aug-2018].

van den Bergh, J. C. J. M. and Botzen, W. J. W. (2014). A lower bound to the social cost of CO_2 emissions. *Nature Climate Change*, 4(4):253–258.

Vandepaer, L., Cloutier, J., and Amor, B. (2017). Environmental impacts of lithium metal polymer and lithium-ion stationary batteries. *Renewable and Sustainable Energy Reviews*, 78:46 – 60.

Vázquez-Rowe, I., Marvuglia, A., Rege, S., and Benetto, E. (2014). Applying consequential LCA to support energy policy: Land use change effects of bioenergy production. *Science of The Total Environment*, 472:78 – 89.

Wall, M. (2019). Personal communication. https://www.energy-stats.uk/.

Wang, J., Liu, P., Hicks-Garner, J., Sherman, E., Soukiazian, S., Verbrugge, M., Tataria, H., Musser, J., and Finamore, P. (2011). Cycle-life model for graphite-LiFePO4 cells. *Journal of Power Sources*, 196(8):3942 – 3948.

Wang, Y., Li, H., He, P., Hosono, E., and Zhou, H. (2010). Nano active materials for lithium-ion batteries. *Nanoscale*, 2:1294–1305.

Wärtsilä (2019). Combined cycle plant for power generation: Introduction. https://www.wartsila.com/energy/learn-more/technical-comparisons/combined-cycle-plant-for-power-generation-introduction. [Online; accessed 19-Jul-2019].

WattTime (2020). Grid emissions intensity by electric grid. https://www.watttime.org/explorer/#3/41.23/-97.64. [Online; accessed 06-Jun-2020].

Weniger, J., Tjaden, T., and Quaschning, V. (2013). "Sizing and grid integration of residential PV battery systems", proceedings of the 8th International Renewable Energy Storage Conference and Exhibition (IRES 2013). *Berlin, Germany*, 18:20.

Western Power (2019a). Losses. https://www.westernpower.co.uk/our-network/losses/electrical-losses. [Online; accessed 18-Jul-2019].

Western Power (2019b). What causes losses. https://www.westernpower.co.uk/our-network/losses/what-causes-losses. [Online; accessed 18-Jul-2019].

Which? (2018). Solar panels and energy storage. https://www.which.co.uk/reviews/solar-panels/article/solar-panels/solar-panels-and-energy-storage. [Online; accessed 05-Jun-2019].

White, V., Roberts, S., and Preston, I. (2012). "Beyond average consumption". https://www.ofgem.gov.uk/ofgem-publications/75556/beyond-average-consumption-pdf. [Online; accessed 01-Oct-2019].

Williams, B. and Lipman, T. (2012). Analysis of the combined vehicle- and post-vehicle value of lithium-ion plug-in vehicle propulsion batteries: Second life applications and value of "traction" lithium batteries. http://www.energy.ca.gov/2013publications/CEC-500-2013-088/CEC-500-2013-088.pdf. [Online; accessed 08-Jul-2018].

Wills, R. (2016). Going clean tech. http://www.raywills.net/rtwtechadopt.html. [Online; accessed 25-Nov-2017].

Wilson, I. G., Rennie, A. J., Ding, Y., Eames, P. C., Hall, P. J., and Kelly, N. J. (2013). Historical daily gas and electrical energy flows through Great Britain's transmission networks and the decarbonisation of domestic heat. *Energy Policy*, 61:301 – 305.

Wolfs, P. (2010). An economic assessment of "second use" lithium-ion batteries for grid support. In *2010 20th Australasian Universities Power Engineering Conference*, pages 1–6.

World Bank (2018). World Bank Group commits 1 billion USD for battery storage to ramp up renewable energy globally. https://www.worldbank.org/en/news/press-release/2018/09/26/world-bank-group-commits-1-billion-for-battery-storage-to-ramp-up-renewable-energy-globally. [Online; accessed 11-Jun-2019].

World Bank (2019). State and trends of carbon pricing 2019. https://openknowledge.worldbank.org/handle/10986/31755. [Online; accessed 24-Nov-2019].

World Health Organisation (2019). Air pollution. https://www.who.int/airpollution/en/. [Online; accessed 20-Jun-2019].

Wright, A. and Firth, S. (2007). The nature of domestic electricity-loads and effects of time averaging on statistics and on-site generation calculations. *Applied Energy*, 84(4):389 – 403.

Wu, H., Chan, G., Choi, J. W., Ryu, I., Yao, Y., McDowell, M. T., Lee, S. W., Jackson, A., Yang, Y., Hu, L., and Cui, Y. (2012). Stable cycling of double-walled silicon nanotube battery anodes through solid-electrolyte interphase control. *Nature Nanotechnology*, 7:310.

Wyrsch, N., Riesen, Y., and Ballif, C. (2013). Effect of the fluctuations of PV production and electricity demand on the PV electricity self-consumption. *Proceedings of the 28th European Photovoltaic Solar Energy Conference and Exhibition*, pages 4322–4324. IMT-NE Number : 733.

Yu, H. J. J. (2018). A prospective economic assessment of residential PV self-consumption with batteries and its systemic effects: The French case in 2030. *Energy Policy*, 113:673 – 687.

Zeng, H., Sun, F., Ge, W., Su, A., Gao, K., Ge, Y., Li, T., Zhu, Y., Shao, B., Xu, T., Liu, G., Whng, J., Duan, Y., Quan, X., Yue, L., Xu, K., Sun, M., Tang, J., Jiang, F., Cui, D., Feng, Z., and Liu, A. (2018). Introduction of Australian 100MW storage operation and its enlightenment to China. In *2018 China International Conference on Electricity Distribution (CICED)*, pages 2895–2900.

Zhang, Y., Lundblad, A., Campana, P. E., Benavente, F., and Yan, J. (2017). Battery sizing and rule-based operation of grid-connected photovoltaic-battery system: A case study in Sweden. *Energy Conversion and Management*, 133:249 – 263.

Appendix A

System Components Embodied Environmental Impact Data

A1 Rooftop PV Array

Palanov (2014) analysed a roof-mounted monocrystalline silicon PV array, and so care should be taken when comparing to multi-c Si. They reported impacts under CML2001: CC, OD, ME, HT, IR, TA, LO, WD, FD, and MD were given, but PMF, POF, FE, FET, MET, TET, ALO, NLT were omitted. Their functional unit was kWh generated; for the 3 kW_p system they analysed, 77 487 kWh were assumed to be generated over its lifetime. This means every midpoint impact value given must be multiplied by 77487/3 to bring the functional unit to kW_p. Additionally, ME had to be multiplied by 0.039 to convert from units of kg NO_x to kg N, FD by 0.072 to convert from kWh to kg oil, and IR by 9.3×10^7 to convert from DALY to kg U235. Other impact values were already given in the units required. The conversion factors used were given by Goedkoop et al. (2008b) for converting to ReCiPe units from other LCA frameworks.

	Palanov (2014)		**Converted to ReCiPe units per kW_p**	
CC	4.89×10^{-2}	kg CO_2/kWh	1.26×10^3	kg CO_2/kW_p
OD	1.98×10^{-8}	kg CFC11/kWh	5.11×10^{-4}	kg CFC11/kW_p
HT	8.76×10^{-2}	kg DCB/kWh	2.26×10^3	kg DCB/kW_p
POF	-		-	
PMF	-		-	
IR	1.45×10^{-10}	DALY/kWh	3.47×10^2	kg U235/kW_p
TA	2.30×10^{-4}	kg SO_2/kWh	5.95	kg SO_2/kW_p
FE	-		-	
ME	1.30×10^{-4}	kg NO_x/kWh	1.31×10^{-1}	kg N/kW_p
FET	-		-	
LO	2.09×10^{-3}	m^2·a/kWh	5.39×10^1	m^2·a/kW_p
WD	8.45×10^{-4}	m^3/kWh	2.18×10^1	m^3/kW_p
MD	1.64×10^{-2}	kg Fe/kWh	4.23×10^2	kg Fe/kW_p
FD	9.42×10^{-2}	kWh/kWh	1.75×10^2	kg oil/kW_p

TABLE A1: Raw CML2001 enviromental impact values from Palanov (2014), and their conversion to ReCiPe units and a functional unit of kW_p installed.

Hertwich et al. (2015) reported ReCiPe midpoint impacts, but omitted OD, ME, IR, WD, FD, and they aggregated ecotoxicity into a single category, and likewise land use. Their single ecotoxicity value is taken here as FET. They assumed 22 000 kWh were generated per kW_p installed over the system lifetime, so midpoint values given had to be multiplied by 22 000.

	Hertwich et al. (2015)		**Converted to ReCiPe units per kW_p**	
CC	5.75×10^{-2}	kg CO_2/kWh	1.27×10^{3}	kg CO_2/kW_p
OD	-		-	
HT	8.14×10^{-2}	kg DCB/kWh	1.79×10^{3}	kg DCB/kW_p
POF	1.93×10^{-4}	kg NMVOC/kWh	4.25	kg NMVOC/kW_p
PMF	1.23×10^{-4}	kg PM10/kWh	2.71	kg PM10/kW_p
IR	-		-	
TA	4.50×10^{-4}	kg SO_2/kWh	9.90	kg SO_2/kW_p
FE	4.45×10^{-5}	kg P/kWh	9.79×10^{-1}	kg P/kW_p
ME	-		-	
FET	3.68×10^{-3}	kg DCB/kWh	8.10×10^{1}	kg DCB/kW_p
LO	1.75×10^{-3}	m^2·a/kWh	3.85×10^{1}	m^2·a/kW_p
WD	-		-	
MD	1.30×10^{-2}	kg Fe/kWh	2.86×10^{2}	kg Fe/kW_p
FD	-		-	

TABLE A2: Raw ReCiPe midpoint impact values from Hertwich et al. (2015), and their conversion to a functional unit of kW_p installed.

Frischknecht (2017) reported impacts under the ILCD framework. These were converted to ReCiPe units using conversion factors given by Owsianiak et al. (2014) - note that human toxicity cancer (1.15 $nCTU_h$) and non-cancer (14.75 $nCTU_h$) effects were summed for HT, and non-renewable CED was taken to be equal to FD. The ILCD impacts had been calculated for a 3 kW_p rooftop system generating 880 $kWh/kW_p/y$ for 30 years. To convert from a functional unit of kWh generated to kW_p installed, the impacts had to be multiplied by $30 \times 880 = 26400$.

	Frischknecht (2017)		**Converted to ReCiPe units per kW_p**	
CC	6.24×10^{1}	g CO_2/kWh	1.65×10^{3}	kg CO_2/kW_p
OD	2.28	μg CFC11/kWh	6.02×10^{-5}	kg CFC11/kW_p
HT	1.59×10^{1}	$nCTU_h$/kWh	8.50×10^{3}	kg DCB/kW_p
POF	2.59×10^{2}	mg NMVOC/kWh	6.85	kg NMVOC/kW_p
PMF	7.85×10^{1}	mg PM2.5/kWh	2.07	kg PM10/kW_p
IR	3.41	Bq U235/kWh	9.00×10^{1}	kg U235/kW_p
TA	6.0×10^{-1}	molc H^+/kWh	7.84	kg SO_2/kW_p
FE	1.31×10^{1}	mg P/kWh	3.46×10^{-1}	kg P/kW_p
ME	8.23×10^{1}	mg N/kWh	2.17	kg N/kW_p
FET	1.23×10^{2}	$mCTU_e$/kWh	3.31	kg DCB/kW_p

LO	9.84×10^1	g C deficit/kWh	2.68×10^2	m^2·a/kW_p
WD	5.45×10^1	cm^3/kWh	1.44	m^3/kW_p
MD	3.33×10^1	mg Sb/kWh	8.12	kg Fe/kW_p
FD	8.30×10^{-1}	MJ oil/kWh	5.24×10^2	kg oil/kW_p

TABLE A3: Raw ILCD environmental impact values from Frischknecht (2017), and their conversion to ReCiPe units and a functional unit of kW_p installed.

A2 Home Battery

McManus (2012) gave upper- and lower-bound values for the production impacts of Li-NMC batteries for EVs. They used the ReCiPe framework but omitted TA, ME, FE, FET, MET, TET. (This may be indicative of a greater focus on the human health and natural resources endpoint impacts than natural ecosystems.) ALO ($0.15 - 0.23$ m^2·a/MJ) and ULO ($0.22 - 0.34$ m^2·a/MJ) were summed to give a value for a single LO category. Impacts were reported per MJ of battery capacity and so had to be multiplied by 3.6 to convert to a functional unit of per kWh capacity.

	(McManus, 2012)			**Converted to ReCiPe units per kWh**		
	Lower	Upper		Lower	Upper	
CC	1.7×10^1	2.7×10^1	kg CO_2/MJ	6.12×10^1	9.72×10^1	kg CO_2/kWh
OD	3.34×10^{-4}	5.23×10^{-4}	kg CFC11/MJ	1.20×10^{-3}	1.88×10^{-3}	kg CFC11/kWh
HT	3	5	kg DCB/MJ	1.08×10^1	1.80×10^1	kg DCB/kWh
POF	3×10^{-2}	5×10^{-2}	kg NMVOC/MJ	1.08×10^{-1}	1.80×10^{-1}	kg NMVOC/kWh
PMF	3×10^{-2}	4×10^{-2}	kg PM10/MJ	1.08×10^{-1}	1.44×10^{-1}	kg PM10/kWh
IR	2.7	4.1	kg U235/MJ	9.72	1.48×10^1	kg U235/kWh
TA	-	-		-	-	
FE	-	-		-	-	
ME	-	-		-	-	
FET	-	-		-	-	
LO	3.7×10^{-1}	5.7×10^{-1}	m^2·a/MJ	1.33	2.43	m^2·a/kWh
WD	1.21×10^{-1}	1.91×10^{-1}	m^3/MJ	4.36×10^{-1}	6.88×10^{-1}	m^3/kWh
MD	2.8×10^1	4.4×10^1	kg Fe/MJ	1.01×10^2	1.58×10^2	kg Fe/kWh
FD	2.2	3.4	kg oil/MJ	7.92	1.22×10^1	kg oil/kWh

TABLE A4: Lower- and upper-bound values of midpoint impacts for lithium-ion (Li-NMC) batteries (McManus, 2012).

A3 Balance of System

Palanov (2014) report a disaggregation of the CML2001 impacts of a rooftop PV array. Table A5 gives those impacts for the PV inverter and electrical installation. They are summed, multiplied by 77 487, and divided by 3, to convert from the impacts per kWh to per kW, as explained in Section A1. This assumes the power electronics are rated the same as the PV array itself, as was common at the time. The conversion factors used in Section A1 to go from CML2001 to ReCiPe are also applied here.

	Palanov (2014)			**Converted to ReCiPe units per kW**	
	Inverter	Installation			
CC	4.76×10^{-3}	1.64×10^{-3}	kg CO_2/kWh	8.27×10^{1}	kg CO_2/kW
OD	5.29×10^{-10}	5.00×10^{-11}	kg CFC11/kWh	7.47×10^{-6}	kg CFC11/kW
HT	1.87×10^{-2}	1.40×10^{-2}	kg DCB/kWh	4.22×10^{2}	kg DCB/kW
POF	-	-		-	
PMF	-	-		-	
IR	4.61×10^{-11}	6.55×10^{-12}	DALY/kWh	8.02×10^{1}	kg U235/kW
TA	4.36×10^{-5}	2.43×10^{-5}	kg SO_2/kWh	8.76×10^{-1}	kg SO_2/kW
FE	-	-		-	
ME	1.97×10^{-5}	7.69×10^{-6}	kg NO_x/kWh	1.38×10^{-2}	kg N/kW
FET	-	-		-	
LO	4.04×10^{-4}	4.55×10^{-5}	m^2·a/kWh	5.80	m^2·a/kW
WD	6.01×10^{-5}	1.24×10^{-5}	m^3/kWh	9.36×10^{-1}	m^3/kW
MD	3.00×10^{-2}	7.86×10^{-4}	kg Fe/kWh	4.89×10^{1}	kg Fe/kW
FD	2.27×10^{-2}	7.28×10^{-3}	kWh/kWh	2.79×10^{1}	kg oil/kW

TABLE A5: Raw CML2001 enviromental impact values from Palanov (2014) for PV inverter and electrical installation, and their conversion to ReCiPe units and a functional unit of kW installed.

The ReCiPe midpoint impacts given by Hawkins et al. (2013) for the charge controller and inverter of an EV are given in Table A6 (ALO and ULO are summed to give a value for the single category LO). The EV battery has capacity 24 kWh and the power electronics are sized to allow discharge at a maximum rate of 1 C, i.e. 24 kW. The charge controller and inverter impacts are summed and then divided by 24, to obtain the impacts per kW.

	Hawkins et al. (2013)			**Converted to units per kW**	
	Charge controller	Inverter			
CC	7.18	6.41×10^{2}	kg CO_2/EV	2.70×10^{1}	kg CO_2/kW
OD	8.75×10^{-7}	4.46×10^{-5}	kg CFC11/EV	1.89×10^{-6}	kg CFC11/kW
HT	5.47×10^{1}	2.36×10^{1}	kg DCB/EV	3.26	kg DCB/kW
POF	3.68×10^{-2}	2.43	kg NMVOC/EV	1.03×10^{-1}	kg NMVOC/kW
PMF	1.83×10^{-2}	2.37	kg P10/EV	9.95×10^{-2}	kg PM10/kW
IR	1.00	1.88×10^{2}	kg U235/EV	7.88	kg U235/kW
TA	4.16×10^{-2}	4.72	kg SO_2/EV	1.98×10^{-1}	kg SO_2/kW
FE	3.24×10^{-2}	1.41	kg P/EV	6.01×10^{-2}	kg P/kW
ME	1.25×10^{-2}	7.81×10^{-1}	kg N/EV	3.31×10^{-2}	kg N/kW
FET	6.69×10^{-1}	3.15×10^{1}	kg DCB/EV	1.34	kg DCB/kW
LO	3.58×10^{-1}	1.77×10^{1}	m^2·a/EV	7.54×10^{-1}	m^2·a/kW
WD	5.34×10^{-2}	4.31	m^3/EV	1.82×10^{-1}	m^3/kW
MD	3.06×10^{1}	1.75×10^{3}	kg Fe/EV	7.42×10^{1}	kg Fe/kW
FD	2.86	1.73×10^{2}	kg oil/EV	7.33	kg oil/kW

TABLE A6: Raw ReCiPe midpoint impact values from Hawkins et al. (2013) for EV battery charge controller and inverter, and their conversion to a functional unit of kW installed.

Appendix B

Grid Generation Environmental Impact Data

B1 Coal

Stamford and Azapagic (2012) analysed a coal power station in the UK with efficiency 36 % and capacity factor 62 %. They reported impacts under CML2001: CC, OD, HT, POF, IR, TA, FE, FET, MET, TET, LO, MD and FD were given, but PMF, ME and WD were omitted. POF had to be multiplied by 0.36 to convert from units of kg C_2H_4 to kg NMVOC, IR by 9.3×10^7 to convert from DALY to kg U235, FE by 0.033 to convert from kg PO_4^{3-} to kg P, MD by 9.24 to convert from kg Sb to kg Fe, and FD by 0.02 to convert from MJ to kg oil. Other impact values were already given in the units required. The conversion factors used were given by Goedkoop et al. (2008b) for converting to ReCiPe units from other LCA frameworks. Conversion was applied only to the operational impacts; total impacts were ignored but are given in Table B1 for completeness.

	Stamford and Azapagic (2012)			**Converted to ReCiPe units per kWh**	
	Operational	Total			
CC	1.07	1.07	kg CO_2/kWh	1.07	kg CO_2/kWh
OD	4.13×10^{-9}	4.25×10^{-9}	kg CFC11/kWh	4.13×10^{-9}	kg CFC11/kWh
HT	7.50×10^{-2}	7.77×10^{-2}	kg DCB/kWh	7.50×10^{-2}	kg DCB/kWh
POF	1.39×10^{-4}	1.40×10^{-4}	kg C_2H_4/kWh	5.00×10^{-5}	kg NMVOC/kWh
PMF	-	-		-	
IR	7.05×10^{-10}	7.10×10^{-10}	DALY/kWh	6.53×10^{-2}	kg U235/kWh
TA	1.77×10^{-3}	1.78×10^{-3}	kg SO_2/kWh	1.77×10^{-3}	kg SO_2/kWh
FE	2.10×10^{-4}	2.15×10^{-4}	kg PO_4^{3-}/kWh	6.93×10^{-5}	kg P/kWh
ME	-	-		-	
FET	1.55×10^{-2}	1.67×10^{-2}	kg DCB/kWh	1.55×10^{-2}	kg DCB/kWh
LO	2.72×10^{-2}	2.73×10^{-2}	m^2·a/kWh	2.72×10^{-2}	m^2·a/kWh
WD	-	-		-	
MD	8.38×10^{-8}	9.72×10^{-8}	kg Sb/kWh	7.74×10^{-7}	kg Fe/kWh
FD	1.51×10^{1}	1.51×10^{1}	MJ/kWh	3.02×10^{-1}	kg oil/kWh

TABLE B1: Raw CML2001 enviromental impact values from Stamford and Azapagic (2012) for coal power, and their conversion to ReCiPe units.

Frischknecht (2017) reported impacts under the ILCD framework for a 36 %-efficient hard coal power station in Germany. These were converted to ReCiPe units using conversion factors given by Owsianiak et al. (2014) - note that human toxicity cancer (1.32 $nCTU_h$) and non-cancer (19.68 $nCTU_h$) effects were summed for HT, and non-renewable CED was taken to be equal to FD.

	Frischknecht (2017)		**Converted to ReCiPe units per kWh**	
CC	1.09×10^3	g CO_2/kWh	1.09	kg CO_2/kWh
OD	1.85	μg CFC11/kWh	1.85×10^{-9}	kg CFC11/kWh
HT	2.10×10^1	$nCTU_h$/kWh	4.25×10^{-1}	kg DCB/kWh
POF	1.13×10^3	mg NMVOC/kWh	1.13×10^{-3}	kg NMVOC/kWh
PMF	8.17×10^1	mg PM2.5/kWh	8.17×10^{-5}	kg PM10/kWh
IR	4.59	Bq U235/kWh	4.59×10^{-3}	kg U235/kWh
TA	1.69	molc H^+/kWh	8.36×10^{-4}	kg SO_2/kWh
FE	3.70×10^1	mg P/kWh	3.70×10^{-5}	kg P/kWh
ME	3.91×10^2	mg N/kWh	3.91×10^{-4}	kg N/kWh
FET	4.66×10^1	$mCTU_e$/kWh	4.75×10^{-5}	kg DCB/kWh
LO	4.90×10^2	g C deficit/kWh	5.04×10^{-2}	m^2·a/kWh
WD	3.41×10^2	cm^3/kWh	3.41×10^{-4}	m^3/kWh
MD	2.60×10^{-1}	mg Sb/kWh	2.40×10^{-6}	kg Fe/kWh
FD	1.27×10^1	MJ oil/kWh	3.03×10^{-1}	kg oil/kWh

TABLE B2: Raw ILCD environmental impact values from Frischknecht (2017) for hard coal power, and their conversion to ReCiPe units.

B2 Combined Cycle Gas Turbines

Stamford and Azapagic (2012) analysed a CCGT power station in the UK with capacity factor 63 %. Conversion factors from CML2001 to ReCiPe midpoint impacts are as given above in Section B1. Conversion was applied only to the operational impacts; total impacts were ignored but are given in Table B3 for completeness.

	Stamford and Azapagic (2012)			**Converted to ReCiPe units per kWh**	
	Operational	Total			
CC	3.78×10^{-1}	3.79×10^{-1}	kg CO_2/kWh	3.78×10^{-1}	kg CO_2/kWh
OD	1.26×10^{-8}	1.27×10^{-8}	kg CFC11/kWh	1.26×10^{-8}	kg CFC11/kWh
HT	2.34×10^{-3}	5.44×10^{-3}	kg DCB/kWh	2.34×10^{-3}	kg DCB/kWh
POF	2.66×10^{-5}	2.73×10^{-5}	kg C_2H_4/kWh	9.59×10^{-6}	kg NMVOC/kWh
PMF	-	-		-	
IR	2.61×10^{-10}	2.63×10^{-10}	DALY/kWh	2.42×10^{-2}	kg U235/kWh
TA	1.42×10^{-4}	1.48×10^{-4}	kg SO_2/kWh	1.42×10^{-4}	kg SO_2/kWh
FE	6.00×10^{-5}	6.23×10^{-5}	kg PO_4^{3-}/kWh	1.98×10^{-5}	kg P/kWh

ME	-	-		-	
FET	1.72×10^{-3}	2.58×10^{-3}	kg DCB/kWh	1.72×10^{-3}	kg DCB/kWh
LO	5.96×10^{-4}	6.33×10^{-4}	m^2·a/kWh	5.96×10^{-4}	m^2·a/kWh
WD	-	-		-	
MD	1.74×10^{-8}	2.83×10^{-8}	kg Sb/kWh	1.61×10^{-7}	kg Fe/kWh
FD	5.74	5.75	MJ/kWh	1.15×10^{-1}	kg oil/kWh

Table B3: Raw CML2001 enviromental impact values from Stamford and Azapagic (2012) for CCGT power, and their conversion to ReCiPe units.

Frischknecht (2017) reported impacts under the ILCD framework for a 43.7 %-efficient natural gas power station in Germany. These were converted to ReCiPe units using conversion factors given by Owsianiak et al. (2014) - note that human toxicity cancer (0.59 $nCTU_h$) and non-cancer (3.00 $nCTU_h$) effects were summed for HT, and non-renewable CED was taken to be equal to FD.

	Frischknecht (2017)		**Converted to ReCiPe units per kWh**	
CC	5.37×10^2	g CO_2/kWh	5.37×10^{-1}	kg CO_2/kWh
OD	8.19×10^1	μg CFC11/kWh	8.19×10^{-8}	kg CFC11/kWh
HT	3.59	$nCTU_h$/kWh	7.27×10^{-2}	kg DCB/kWh
POF	6.51×10^2	mg NMVOC/kWh	6.51×10^{-4}	kg NMVOC/kWh
PMF	2.79×10^1	mg PM2.5/kWh	2.79×10^{-5}	kg PM10/kWh
IR	3.50×10^{-1}	Bq U235/kWh	3.50×10^{-4}	kg U235/kWh
TA	6.10×10^{-1}	molc H^+/kWh	3.02×10^{-4}	kg SO_2/kWh
FE	4.30×10^{-1}	mg P/kWh	4.30×10^{-7}	kg P/kWh
ME	1.73×10^2	mg N/kWh	1.73×10^{-4}	kg N/kWh
FET	8.39	$mCTU_e$/kWh	8.56×10^{-6}	kg DCB/kWh
LO	4.60×10^2	g C deficit/kWh	4.73×10^{-2}	m^2·a/kWh
WD	3.18×10^1	cm^3/kWh	3.18×10^{-5}	m^3/kWh
MD	1.30×10^{-1}	mg Sb/kWh	1.20×10^{-6}	kg Fe/kWh
FD	9.26	MJ oil/kWh	2.21×10^{-1}	kg oil/kWh

Table B4: Raw ILCD environmental impact values from Frischknecht (2017) natural gas power, and their conversion to ReCiPe units.

B3 Biomass

Stamford and Azapagic (2014) analysed a 500 MW power station in the UK using imported wood as fuel. Conversion factors from CML2001 to ReCiPe midpoint impacts are as given above in Section B1. Conversion was applied only to the operational impacts; total impacts were ignored but are given in Table B5 for completeness.

	Stamford and Azapagic (2014)			**Converted to ReCiPe units per kWh**	
	Operational	Total			
CC	1.04×10^{-1}	1.07×10^{-1}	kg CO_2/kWh	1.04×10^{-1}	kg CO_2/kWh
OD	9.48×10^{-9}	9.66×10^{-9}	kg CFC11/kWh	9.48×10^{-9}	kg CFC11/kWh
HT	6.09×10^{-2}	6.62×10^{-2}	kg DCB/kWh	6.09×10^{-2}	kg DCB/kWh

POF	2.28×10^{-4}	2.30×10^{-4}	kg C_2H_4/kWh	8.20×10^{-5}	kg NMVOC/kWh
PMF	-	-		-	
IR	4.33×10^{-10}	4.43×10^{-10}	DALY/kWh	4.02×10^{-2}	kg U235/kWh
TA	2.84×10^{-3}	2.86×10^{-3}	kg SO_2/kWh	2.84×10^{-3}	kg SO_2/kWh
FE	3.66×10^{-4}	3.75×10^{-4}	kg PO_4^{3-}/kWh	1.21×10^{-4}	kg P/kWh
ME	-	-		-	
FET	1.91×10^{-2}	2.16×10^{-2}	kg DCB/kWh	1.91×10^{-2}	kg DCB/kWh
LO	2.82×10^{-1}	2.82×10^{-1}	m^2·a/kWh	2.82×10^{-1}	m^2·a/kWh
WD	-	-		-	
MD	4.39×10^{-8}	7.09×10^{-8}	kg Sb/kWh	4.06×10^{-7}	kg Fe/kWh
FD	1.27	1.31	MJ/kWh	2.55×10^{-2}	kg oil/kWh

TABLE B5: Raw CML2001 enviromental impact values from Stamford and Azapagic (2014) for biomass power (imported wood), and their conversion to ReCiPe units.

Vázquez-Rowe et al. (2014) analysed scenarios for producing bio-methane in Luxembourg using a partial equilibrium model. The 'C' scenarios included the effects of a sudden 80 000 tonne increase in maize production, on both domestic agriculture (substitution of other crops) and imports/exports of crops abroad. The five 'C' scenarios were:

- AN = livestock modelling included,
- CR = only crops (no livestock) were modelled,
- MAR = minimal animal requirements,
- MP = meadows and pastures undergo unconstrained land use changes,
- RP = rapeseed plantations undergo unconstrained land use changes.

As they reported ReCiPe midpoint impacts per MJ bio-methane produced, these values were multiplied by 3.6 MJ/kWh and divided by 0.5 to give values per kWh electricity produced. These values are given in Table B6. Only their mean in each impact category i is used with other data sources to calculate the central estimate in that impact category. But for the uncertainty estimates, which are 1/4 the difference between the maximum and minimum values, all five values are included with other data sources.

		Vázquez-Rowe et al. (2014)				
		AN	CR	MAR	MP	RP
CC	kg CO_2/kWh	7.79×10^{-2}	6.87×10^{-2}	4.84×10^{-2}	9.49×10^{-2}	1.26×10^{-1}
OD	kg CFC11/kWh	4.47×10^{-9}	4.62×10^{-9}	4.29×10^{-9}	4.47×10^{-9}	4.29×10^{-9}
HT	kg DCB/kWh	1.13×10^{-2}	1.11×10^{-2}	1.00×10^{-2}	1.10×10^{-2}	1.00×10^{-2}
POF	kg NMVOC/kWh	2.44×10^{-4}	2.58×10^{-4}	2.40×10^{-4}	2.46×10^{-4}	2.40×10^{-4}
PMF	kg PM10/kWh	3.30×10^{-4}	3.63×10^{-4}	3.55×10^{-4}	3.38×10^{-4}	3.55×10^{-4}
IR	kg U235/kWh	4.25×10^{-3}	4.42×10^{-3}	4.06×10^{-3}	4.25×10^{-3}	4.06×10^{-3}
TA	kg SO_2/kWh	2.04×10^{-3}	2.27×10^{-3}	2.25×10^{-3}	2.10×10^{-3}	2.25×10^{-3}
FE	kg P/kWh	1.22×10^{-5}	1.34×10^{-5}	1.25×10^{-5}	1.24×10^{-5}	1.25×10^{-5}
ME	kg N/kWh	2.87×10^{-4}	3.14×10^{-4}	3.12×10^{-4}	2.94×10^{-4}	3.12×10^{-4}
FET	kg DCB/kWh	4.55×10^{-4}	5.04×10^{-4}	4.90×10^{-4}	4.67×10^{-4}	4.90×10^{-4}

LO	m^2·a/kWh	1.90×10^{-1}	1.76×10^{-1}	1.63×10^{-1}	1.81×10^{-1}	1.63×10^{-1}
WD	m^3/kWh	1.72×10^{-4}	1.88×10^{-4}	1.58×10^{-4}	1.72×10^{-4}	1.58×10^{-4}
MD	kg Fe/kWh	4.11×10^{-3}	4.31×10^{-3}	4.06×10^{-3}	4.14×10^{-3}	4.06×10^{-3}
FD	kg oil/kWh	1.02×10^{-2}	1.06×10^{-2}	9.82×10^{-3}	1.02×10^{-2}	9.82×10^{-3}

TABLE B6: ReCiPe midpoint impacts of bio-methane production in the five 'C' scenarios analysed by Vázquez-Rowe et al. (2014), converted to a functional unit of 1 kWh electricity generation.

Moretti et al. (2016) compared a biomass-fuelled heating and cooling system for a building, to a natural gas boiler with electric heat pumps. Their raw ReCiPe midpoint impact values are given in Table B7, along with their conversion to impacts per kWh of biomass-generated electricity. This was found by taking the ratio of biomass impacts to natural gas impacts, and multiplying them by the central estimates for CCGT (Table 3.6). As the CCGT impacts were found per kWh of electricity generation, and only the ratio of biomass to natural gas impacts was needed, it did not matter that the functional unit Moretti et al. (2016) used was one year of thermal comfort for the building they analysed.

	Moretti et al. (2016)			**Converted to impacts per kWh**	
	Natural gas	Biomass			
CC	9.80×10^3	3.10×10^3	kg CO_2	1.51×10^{-1}	kg CO_2/kWh
OD	6.10×10^{-3}	2.60×10^{-4}	kg CFC11	2.01×10^{-9}	kg CFC11/kWh
HT	1.27×10^3	3.62×10^3	kg DCB	1.17×10^{-1}	kg DCB/kWh
POF	1.41×10^1	4.05×10^1	kg NMVOC	1.42×10^{-3}	kg NMVOC/kWh
PMF	5.20	1.40×10^1	kg PM10	8.61×10^{-4}	kg PM10/kWh
IR	5.94×10^2	5.23×10^2	kg U235	1.08×10^{-2}	kg U235/kWh
TA	1.68×10^1	2.95×10^1	kg SO_2	2.05×10^{-3}	kg SO_2/kWh
FE	1.10	1.10	kg P	8.54×10^{-6}	kg P/kWh
ME	6.00×10^{-1}	1.70	kg N	3.38×10^{-4}	kg N/kWh
FET	1.91×10^1	3.05×10^1	kg DCB	9.22×10^{-4}	kg DCB/kWh
LO	3.48×10^1	1.44×10^4	m^2·a	6.66	m^2·a/kWh
WD	1.20×10^1	1.92×10^1	m^3	5.09×10^{-5}	m^3/kWh
MD	2.91×10^2	5.82×10^2	kg Fe	1.71×10^{-4}	kg Fe/kWh
FD	3.65×10^3	8.69×10^2	kg oil	4.00×10^{-2}	kg oil/kWh

TABLE B7: Raw enviromental impact values from Moretti et al. (2016) for a building using biomass compared to natural gas, and their conversion to impacts per kWh of biomass-generated electricity.

B4 Carbon Capture and Storage

Koornneef et al. (2008) conducted an LCA comparing supercritical coal combustion without and with CCS (cases 2 and 3 respectively, in their nomenclature). The raw CML2001 impacts they calculated are given in Table B8, along with their conversion to ReCiPe midpoint impacts per kWh of electricity generated by CCGT with CCS. This was achieved by taking the ratio of their results with CCS to without CCS, and multiplying by the central estimates for CCGT (Table 3.6). Since only the ratio was needed, it did not matter that they used CML2001 rather than ReCiPe, nor that they analysed supercritical

coal (although their case 1 was for subcritical coal without CCS, which would not have provided a fair comparison to supercritical coal with CCS).

	Koornneef et al. (2008)			**Converted to CCGT with CCS**	
	Without CCS	With CCS			
CC	8.37×10^{-1}	2.43×10^{-1}	kg CO_2/kWh	1.38×10^{-1}	kg CO_2/kWh
OD	6.41×10^{-9}	9.93×10^{-9}	kg CFC11/kWh	7.32×10^{-8}	kg CFC11/kWh
HT	5.84×10^{-2}	1.64×10^{-1}	kg DCB/kWh	1.15×10^{-1}	kg DCB/kWh
POF	5.13×10^{-5}	6.49×10^{-5}	kg C_2H_4/kWh	6.26×10^{-4}	kg NMVOC/kWh
PMF	-	-		-	
IR	-	-		-	
TA	1.44×10^{-3}	2.10×10^{-3}	kg SO_2/kWh	1.71×10^{-3}	kg SO_2/kWh
FE	1.61×10^{-4}	2.90×10^{-4}	kg PO_4^{3-}/kWh	1.54×10^{-5}	kg P/kWh
ME	-	-		-	
FET	9.17×10^{-3}	1.34×10^{-2}	kg DCB/kWh	8.44×10^{-4}	kg DCB/kWh
LO	-	-		-	
WD	-	-		-	
MD	6.32×10^{-3}	8.45×10^{-3}	kg Sb/kWh	1.15×10^{-4}	kg Fe/kWh
FD	-	-		-	

TABLE B8: Raw CML2001 enviromental impact values from Koornneef et al. (2008) for coal combustion without and with CCS, and their conversion to ReCiPe midpoint impacts per kWh of electricity generated by CCGT with CCS.

Schakel et al. (2014) conducted an LCA comparing electricity generation from combustion of pulverised coal with and without CCS. Their raw ReCiPe midpoint impacts given in Table B9 were multiplied by the central estimates for CCGT (Table 3.6). Note that they gave values for ALO and ULO separately, 6.58×10^{-3} and 7.62×10^{-3} m^2·a/kWh respectively, which were summed to give the single value for LO.

	Schakel et al. (2014)			**Converted to CCGT with CCS**	
	Without CCS	With CCS			
CC	9.03×10^{-1}	2.32×10^{-1}	kg CO_2/kWh	1.22×10^{-1}	kg CO_2/kWh
OD	6.88×10^{-9}	9.56×10^{-9}	kg CFC11/kWh	6.57×10^{-8}	kg CFC11/kWh
HT	2.41×10^{-1}	3.33×10^{-1}	kg DCB/kWh	5.68×10^{-2}	kg DCB/kWh
POF	1.45×10^{-3}	1.97×10^{-3}	kg NMVOC/kWh	6.72×10^{-4}	kg NMVOC/kWh
PMF	5.96×10^{-4}	7.42×10^{-4}	kg PM10/kWh	3.98×10^{-4}	kg PM10/kWh
IR	1.57×10^{-2}	2.18×10^{-2}	kg U235/kWh	1.71×10^{-2}	kg U235/kWh
TA	1.80×10^{-3}	2.35×10^{-3}	kg SO_2/kWh	1.53×10^{-3}	kg SO_2/kWh
FE	3.87×10^{-4}	5.36×10^{-4}	kg P/kWh	1.18×10^{-5}	kg P/kWh
ME	5.74×10^{-4}	8.05×10^{-4}	kg N/kWh	1.67×10^{-4}	kg N/kWh
FET	5.51×10^{-3}	7.62×10^{-3}	kg DCB/kWh	7.99×10^{-4}	kg DCB/kWh
LO	1.03×10^{-2}	1.42×10^{-2}	m^2·a/kWh	2.24×10^{-2}	m^2·a/kWh
WD	8.13×10^{-4}	1.13×10^{-3}	m^3/kWh	4.42×10^{-5}	m^3/kWh
MD	4.66×10^{-3}	6.67×10^{-3}	kg Fe/kWh	1.23×10^{-4}	kg Fe/kWh
FD	2.17×10^{-1}	3.00×10^{-1}	kg oil/kWh	2.32×10^{-1}	kg oil/kWh

TABLE B9: Raw enviromental impact values from Schakel et al. (2014) for coal combustion without and with CCS, and their conversion to impacts per kWh of electricity generated by CCGT with CCS.

B5 Nuclear

Stamford and Azapagic (2012) analysed a nuclear PWR power station with capacity factor 85 %. Conversion factors from CML2001 to ReCiPe midpoint impacts are as given above in Section B1. Conversion was applied only to the operational impacts; the ratio of operational to total impacts were used to adjust the results of Frischknecht (2017) below.

	Stamford and Azapagic (2012)				**Converted to ReCiPe units per kWh**	
	Operational	Total		%	Operational	
CC	4.38×10^{-3}	6.24×10^{-3}	kg CO_2/kWh	70.3	4.38×10^{-3}	kg CO_2/kWh
OD	4.66×10^{-10}	5.41×10^{-10}	kg CFC11/kWh	86.2	4.66×10^{-10}	kg CFC11/kWh
HT	1.08×10^{-1}	1.15×10^{-1}	kg DCB/kWh	94.2	1.08×10^{-1}	kg DCB/kWh
POF	4.23×10^{-6}	4.96×10^{-6}	kg C_2H_4/kWh	85.3	1.52×10^{-6}	kg NMVOC/kWh
PMF	-	-		(80.6)	-	
IR	2.02×10^{-8}	2.03×10^{-8}	DALY/kWh	99.9	1.88	kg U235/kWh
TA	3.63×10^{-5}	4.40×10^{-5}	kg SO_2/kWh	82.6	3.63×10^{-5}	kg SO_2/kWh
FE	9.85×10^{-6}	1.32×10^{-5}	kg PO_4^{3-}/kWh	74.4	3.25×10^{-6}	kg P/kWh
ME	-	-		(80.6)	-	
FET	1.95×10^{-2}	2.11×10^{-2}	kg DCB/kWh	92.8	1.95×10^{-2}	kg DCB/kWh
LO	2.55×10^{-4}	5.49×10^{-4}	m^2·a/kWh	46.5	2.55×10^{-4}	m^2·a/kWh
WD	-	-		(80.6)	-	
MD	5.36×10^{-8}	7.04×10^{-8}	kg Sb/kWh	76.2	4.96×10^{-7}	kg Fe/kWh
FD	5.94×10^{-2}	8.07×10^{-2}	MJ/kWh	73.6	1.19×10^{-3}	kg oil/kWh

TABLE B10: Raw CML2001 enviromental impact values from Stamford and Azapagic (2012) for nuclear power, and their conversion to ReCiPe units.

Frischknecht (2017) reported impacts under the ILCD framework for a nuclear PWR power station in Europe, with efficiency 33 % and capacity factor 80.4 %. The raw ILCD values were first adjusted to the percentages given in Table B10, to separate operational from total impacts. The operational impacts were then converted to ReCiPe units using conversion factors given by Owsianiak et al. (2014) - note that human toxicity cancer (0.60 $nCTU_h$) and non-cancer (1.56 $nCTU_h$) effects were summed for HT, ionising radiation (412.89 Bq) and ionising radiation accidents (4306.39 Bq) were summed for IR, and non-renewable CED was taken to be equal to FD.

	Frischknecht (2017)		**Converted to ReCiPe units per kWh**	
	Total		Operational	
CC	7.68	g CO_2/kWh	5.40×10^{-3}	kg CO_2/kWh
OD	1.87×10^{1}	μg CFC11/kWh	1.61×10^{-8}	kg CFC11/kWh
HT	2.10×10^{1}	$nCTU_h$/kWh	2.98×10^{-2}	kg DCB/kWh
POF	3.98×10^{1}	mg NMVOC/kWh	3.40×10^{-5}	kg NMVOC/kWh
PMF	5.45	mg PM2.5/kWh	4.39×10^{-6}	kg PM10/kWh
IR	4.72×10^{3}	Bq U235/kWh	4.72	kg U235/kWh
TA	7.00×10^{-2}	molc H^+/kWh	2.86×10^{-5}	kg SO_2/kWh
FE	5.20×10^{-1}	mg P/kWh	3.87×10^{-7}	kg P/kWh
ME	1.55×10^{1}	mg N/kWh	1.25×10^{-5}	kg N/kWh
FET	2.66×10^{1}	$mCTU_e$/kWh	2.52×10^{-5}	kg DCB/kWh

LO	3.42×10^{1}	g C deficit/kWh	1.64×10^{-3}	m^2·a/kWh
WD	1.22×10^{2}	cm^3/kWh	9.84×10^{-5}	m^3/kWh
MD	4.69	mg Sb/kWh	3.30×10^{-5}	kg Fe/kWh
FD	1.26×10^{1}	MJ oil/kWh	2.22×10^{-1}	kg oil/kWh

TABLE B11: Raw ILCD environmental impact values from Frischknecht (2017) for nuclear power, and their conversion to ReCiPe units (operational impacts only).

Appendix C

Second-Life Battery Pricing and Repurposing Environmental Impacts

C1 Capacities of BEVs and PHEVs

Sales data for the most common makes/models of BEV and PHEV from the EV Volumes website EV Volumes (2014, 2016a,b) and nominal battery capacity for each make/model from the websites of the EV manufacturers are tabulated in the spreadsheet BEV_PHEV_salesdata.xls which is available with the author's paper (Sun et al., 2018b). They are used along with unit sales data from the International Energy Agency (IEA, 2017b) to calculate total annual (kWh) first-time EV sales. These are summarized in Table C1 below.

Year	BEV sales (cumul.)	BEV sales (annual)	BEV average capacity (kWh)	PHEV sales (cumul.)	PHEV sales (annual)	PHEV average capacity (kWh)	Total annual sales (GWh)
2010	16 420	16 420	(26.0)	390	390	(9.0)	0.430
2011	55 160	38 470	(27.0)	9 420	9 030	(9.5)	1.132
2012	112 940	57 780	(28.0)	69 700	60 280	(10.0)	2.221
2013	226 780	113 840	30.8	161 290	91 590	10.5	4.468
2014	420 330	193 550	29.1	295 060	133 770	10.6	7.050
2015	745 610	325 280	31.7	517 000	221 940	12.0	12.97
2016	1 208 900	463 290	40.4	805 320	288 320	12.5	22.32

Table C1: Deriving total EV battery capacity annual sales from cumulative BEV and PHEV fleets (IEA, 2017b) and average battery capacities (EV Volumes, 2016a), values in 2010-2012 (in parentheses) extrapolated back from 2013-2016.

C2 EV Uptake Scenario Parameters

Tabulated below in Table C2 are parameters A, p, q to generate $f_{EV}(t)$ under Low, Medium and High scenarios in accordance with the Bass model solution, Equation (C.1).

$$r_0(t) = A\frac{(p+q)^2 \exp\left(-(p+q)t\right)}{p(1+\frac{q}{p}\exp\left(-(p+q)t\right))^2} \tag{C.1}$$

The EV penetration percentages are rough values derived from summing all the first-time sales $\sum r_0(y)$ and assuming average battery capacity 40 kWh and vehicle fleet of 2 billion.

	A (kWh)	p	q	EV penetration
Low	6.05×10^8	0.0112	0.6039	0.75 %
Medium	3.60×10^{10}	2.11×10^{-5}	0.5645	45 %
High	8.00×10^{10}	9.50×10^{-6}	0.5641	100 %

Table C2: Bass model parameters for various EV uptake scenarios, and corresponding eventual penetration of EVs into the vehicle fleet.

C3 Mathematical Formulation of Price-Supply Curve

The price-supply curve for second-life batteries is approximated as an exponential:

$$p_{sup}(E) = (c_{recyc} + c_{refurb}) + A_{sup}(e^{(\alpha_{sup}E)} - 1) \tag{C.2}$$

where the price p_{sup} (GBP/kWh) is a function of quantity E (kWh), and the dependence on year y is only implied above;
$A_{sup}(y) = \frac{1}{n_e}(c_{B,1,y} - (c_{recyc}(y) + c_{refurb}(y)))$,
where the elasticity coefficient n_e determines the shape of the price-supply curve (more elastic means a shallower gradient for more of the curve, that is, a smaller change in price leads to a greater change in quantity sold). $n_e = 10$ is used, though the author found negligible effect on equilibrium price when n_e was varied even up to 100 000 (Sun et al., 2018b).

The new battery per-kWh cost $c_{B,1,y}$ is taken to decrease exponentially from $c_{B,1,2019} = 390$ GBP/kWh in 2019 to a minimum eventual cost of $c_\infty = 50$ GBP/kWh, at a rate 18 % per year (see Chapter 2). Cost is extrapolated backwards at the same rate for previous years.

$$c_{B,1,y} = c_\infty + (c_{B,1,2019} - c_\infty)e^{(-0.18y)}, \tag{C.3}$$

Defining $A_{sup}(y)$ in this way ensures that $p_{sup}(E, y)$ remains between $(c_{recyc}(y) + c_{refurb}(y))$ and $c_{B,1,y}$ for all E and every year y.

$\alpha_{sup}(y)$ in Equation (C.2) is defined as $\frac{\ln(1+n_e)}{f_{EV}(y)}$. It is a factor used to ensure that $E \leq f_{EV}(y)$, that is, the quantity sold cannot exceed the supply of used EV batteries in year y.

C4 Mathematical Formulation of Price-Demand Curve

The niche-market and mass-market segments of the price-demand curve, Equations (C.4) and (C.5) respectively, are joined by a quadratic function to smooth the joint.

$$p_{dem(niche)}(E) = a_{d1}E + b_{d1} \qquad 0 \leq E < E^* \tag{C.4}$$

$$p_{dem(mass)}(E) = a_{d2}E + b_{d2} \qquad E^* < E \leq E_{max}. \tag{C.5}$$

The constraint that $p_{dem}(E, y)$ can never exceed $c_{B,1,y}$, leads to: $b_{d1}(y) = c_{B,1,y}$.

The other constraints are that $p_{dem(mass)}(E_{max}(y), y) = 0$, that is, the total possible demand $E_{max}(y)$ that year can only be reached when price goes to zero, and $p_{dem(niche)}(E)$ and $p_{dem(mass)}(E)$ join at the point (E^*, p^*_{dem}). This leads to:

$$a_{d1} = \begin{cases} -\left(\frac{c_{B,1,y} - p^*_{dem}(y)}{E^*(y)}\right) & c_{B,1,y} > p^*_{dem}(y) \\ 0 & c_{B,1,y} \leq p^*_{dem}(y) \end{cases},$$

$$a_{d2} = \begin{cases} -\left(\frac{p^*_{dem}(y)}{E_{max}(y) - E^*(y)}\right) & c_{B,1,y} > p^*_{dem}(y) \\ -\left(\frac{c_{B,1,y}}{E_{max}(y) - E^*(y)}\right) & c_{B,1,y} \leq p^*_{dem}(y) \end{cases},$$

$$b_{d2} = \begin{cases} \left(\frac{E_{max}(y)p^*_{dem}(y)}{E_{max}(y) - E^*(y)}\right) & c_{B,1,y} > p^*_{dem}(y) \\ \left(\frac{E_{max}(y)c_{B,1,y}}{E_{max}(y) - E^*(y)}\right) & c_{B,1,y} \leq p^*_{dem}(y) \end{cases}.$$

The quadratic function smoothing the joint around (E^*, p^*_{dem}), spans the domain $E \in [E_a, E_b]$, where:

$$E_a = \begin{cases} E^* - \frac{15}{100}f_{EV} & E^* > \frac{15}{100}f_{EV} \\ 0 & E^* \leq \frac{15}{100}f_{EV} \end{cases},$$

$$E_b = \begin{cases} E^* + \frac{15}{100}f_{EV} & E^* + \frac{15}{100}f_{EV} < f_{EV} \\ f_{EV} & E^* + \frac{15}{100}f_{EV} \geq f_{EV} \end{cases}.$$

The factor $\frac{15}{100}$ is chosen to ensure a joint that is smooth but the two linear segments are still distinct. To determine the coefficients a_{joint}, b_{joint}, c_{joint} of the quadratic polynomial

$$p_{joint}(E) = a_{joint}E^2 + b_{joint}E + c_{joint} \qquad E_a \leq E \leq E_b,$$

the following conditions are imposed:

- $p_{joint}(E_a) = p_{dem(niche)}(E_a)$
- $p_{joint}(E_b) = p_{dem(mass)}(E_b)$
- $\frac{dp_{joint}}{dE}|_{E_b} = a_{d2}$

In other words, the quadratic section joins continuously to each linear segment, at E_a and E_b, and the gradient is continuous at E_b. There are not enough degrees of freedom (only three coefficients determine a quadratic polynomial) to ensure continuous gradient at E_a as well. The option of a cubic function to smooth the joint was rejected because this can lead to inflection points, when the price-demand curve should be monotonically decreasing.

To evaluate the coefficients a_{joint}, b_{joint}, c_{joint}, a matrix equation is formed from the constraints, and solved:

$$\begin{bmatrix} y_a \\ y_b \\ a_{d2} \end{bmatrix} = \begin{bmatrix} E_a^2 & E_a & 1 \\ E_b^2 & E_b & 1 \\ 2E_b & 1 & 0 \end{bmatrix} \begin{bmatrix} a_{joint} \\ b_{joint} \\ c_{joint} \end{bmatrix}$$

where $y_a = p_{dem(niche)}(E_a)$, $y_b = p_{dem(mass)}(E_b)$, to find:
$a_{joint} = \left(\frac{y_a - y_b}{E_a^2 - 2*E_a*E_b + E_b^2}\right) - \left(\frac{a_{d2}}{E_a - E_b}\right)$
$b_{joint} = \left(\frac{2E_b(y_b - y_a)}{E_a^2 - 2*E_a*E_b + E_b^2}\right) + a_{d2}\left(\frac{E_a + E_b}{E_a - E_b}\right)$
$c_{joint} = \left(\frac{E_b^2 y_a + E_a y_b(E_a - 2E_b)}{E_a^2 - 2*E_a*E_b + E_b^2}\right) - a_{d2}\left(\frac{E_a E_b}{E_a - E_b}\right)$.

C5 Battery Repurposing environmental impacts

The repurposing of each usable kWh of used EV batteries is taken to include shipping across 1000 km in total, and 4 kWh of electricity for testing. The shipping is assumed to be done in a heavy fuel oil (HFO)-fuelled container ship, from EV dealership to repurposing facility, to second-life battery supplier. The testing involves four charge-discharge cycles, as Williams and Lipman (2012) specified, and the electricity used is assumed to be generated by a 2017 UK grid technology mix.

Øberg (2013) conducted an LCA of the operation of different types of shipping running on different fuels, including upstream extracting and processing of the fuels. They gave ReCiPe midpoint impacts per year of operation. The case of a container ship running on HFO was taken as a conservative representation of the sort of shipping that might be required in the battery repurposing process. Their figures for impacts per year of operation had to be divided by 1.07×10^9 to find impacts per MJ, as that is their figure for how many MJ of fuel the ship consumes in an average year of operation. Then the efficiency value of 1.81 MJ/tkm (Laugen, 2013) is used - that is, 1.81 MJ of HFO energy are required to transport each ton (1000 kg) of freight by 1 km. Finally, a density value is required for the batteries. Baczyńska et al.

(2018) reviewed an LFP and two NMC batteries designed for transport applications; the LFP pack had an energy density of 0.091 kWh/kg, while the NMC packs were 0.16 and 0.27 kWh/kg. The battery type considered in this thesis is NMC, but for a used EV battery, its energy density would be lower than for a new one, by 0.8 times on average if used packs are removed when they degrade to 80 % of their original capacity. A conservative estimate of 0.1 kWh/kg is taken. Table C3 shows how the calculation of shipping impacts per usable kWh are obtained from the impacts per year of operating the container ship: dividing by 1.07×10^9 MJ per year, multiplying by 1.81 MJ/tkm, by 1000 km, dividing by 1000 kg/ton, and again by 0.1 kWh/kg: in total, multiplying by 1.70×10^{-8} year/kWh.

	Øberg (2013)		**Converted to ReCiPe units per kWh**	
CC	9.96×10^7	kg CO_2/y	1.69	kg CO_2/kWh
OD	1.15×10^1	kg CFC11/y	1.95×10^{-7}	kg CFC11/kWh
HT	4.71×10^6	kg DCB/y	7.99×10^{-2}	kg DCB/kWh
POF	2.30×10^6	kg NMVOC/y	3.90×10^{-2}	kg NMVOC/kWh
PMF	1.28×10^6	kg PM10/y	2.17×10^{-2}	kg PM10/kWh
IR	1.81×10^6	kg U235/y	3.07×10^{-2}	kg U235/kWh
TA	3.02×10^6	kg SO_2/y	5.12×10^{-2}	kg SO_2/kWh
FE	2.46×10^3	kg P/y	4.17×10^{-5}	kg P/kWh
ME	2.63×10^5	kg N/y	4.46×10^{-3}	kg N/kWh
FET	8.03×10^4	kg DCB/y	1.36×10^{-3}	kg DCB/kWh
LO	1.86×10^5	m^2·a/y	3.16×10^{-3}	m^2·a/kWh
WD	3.95×10^4	m^3/y	6.70×10^{-4}	m^3/kWh
MD	3.14×10^5	kg Fe/y	5.33×10^{-3}	kg Fe/kWh
FD	3.18×10^7	kg oil/y	5.40×10^{-1}	kg oil/kWh

TABLE C3: ReCiPe midpoint impacts per year of operating a HFO-fuelled container ship (Øberg, 2013), and conversion to impacts per usable kWh of used EV battery transported 1000 km. Impacts were given separately for ALO and ULO (4.80×10^4 and 1.38×10^5 m^2·a/y respectively); these were summed to give a single value for LO.

The Gridwatch (2018) data for UK electricity generation in 2017 were multiplied element-wise by the T & D loss factor $\lambda(t)$, summed scross the year within each generator technology type (coal, CCGT, biomass, nuclear, hydroelectric, French import and Dutch import), multiplied by the environmental impacts per kWh of the corresponding generator type, as obtained in Chapter 3, summed across all generator types, and divided by the total generation in the year (289 TWh). This gave the average (rather than marginal) impact intensities per kWh consumed, in each ReCiPe midpoint impact category. These values are given in Table C4. Multiplying them by 4 gives the battery testing impacts per usable kWh of used EV batteries (for 4 charge-discharge cycles).

	Electricity consumption		**Battery testing**	
CC	3.20×10^{-1}	kg CO_2/kWh_e	1.28	kg CO_2/kWh
OD	2.52×10^{-8}	kg CFC11/kWh_e	1.01×10^{-7}	kg CFC11/kWh
HT	6.04×10^{-2}	kg DCB/kWh_e	2.42×10^{-1}	kg DCB/kWh
POF	3.47×10^{-4}	kg NMVOC/kWh_e	1.39×10^{-3}	kg NMVOC/kWh
PMF	2.15×10^{-4}	kg PM10/kWh_e	8.62×10^{-4}	kg PM10/kWh
IR	8.98×10^{-1}	kg U235/kWh_e	3.59	kg U235/kWh
TA	8.13×10^{-4}	kg SO_2/kWh_e	3.25×10^{-3}	kg SO_2/kWh

	Electricity consumption		**Battery testing**	
FE	2.89×10^{-5}	kg P/kWh$_e$	1.16×10^{-4}	kg P/kWh
ME	1.20×10^{-4}	kg N/kWh$_e$	4.81×10^{-4}	kg N/kWh
FET	3.90×10^{-3}	kg DCB/kWh$_e$	1.56×10^{-2}	kg DCB/kWh
LO	1.42×10^{-1}	m^2·a/kWh$_e$	5.67×10^{-1}	m^2·a/kWh
WD	9.90×10^{-5}	m^3/kWh$_e$	3.96×10^{-4}	m^3/kWh
MD	2.51×10^{-4}	kg Fe/kWh$_e$	1.00×10^{-3}	kg Fe/kWh
FD	1.35×10^{-1}	kg oil/kWh$_e$	5.40×10^{-1}	kg oil/kWh

TABLE C4: ReCiPe midpoint impacts per kWh$_e$ (electricity consumed), and per usable kWh of used EV battery tested.

The ReCiPe midpoint impact values in Tables C3 and C4 for shipping and testing each usable kWh of used EV batteries are summed together to give the total impacts for the battery repurposing process. These values are given in Table 4.3 of Chapter 4.

Appendix D

Non-normalised Life-Cycle Environmental Impact Results

D1 Non-normalised Environmental Impacts

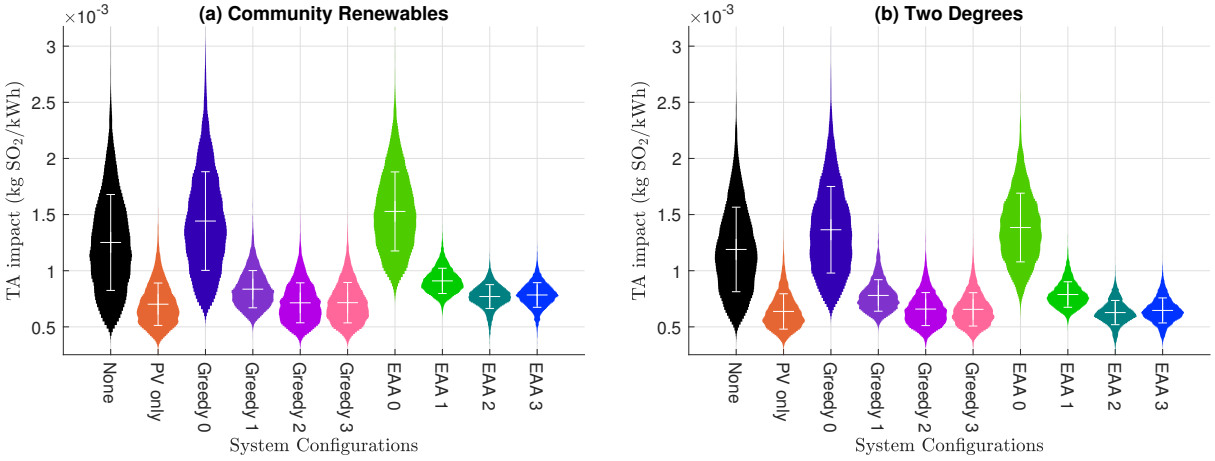

FIGURE D1: Distribution plots of Terrestrial Acidification impact in each configuration, in Community Renewables and Two Degrees future grid scenarios. Start year 2020.

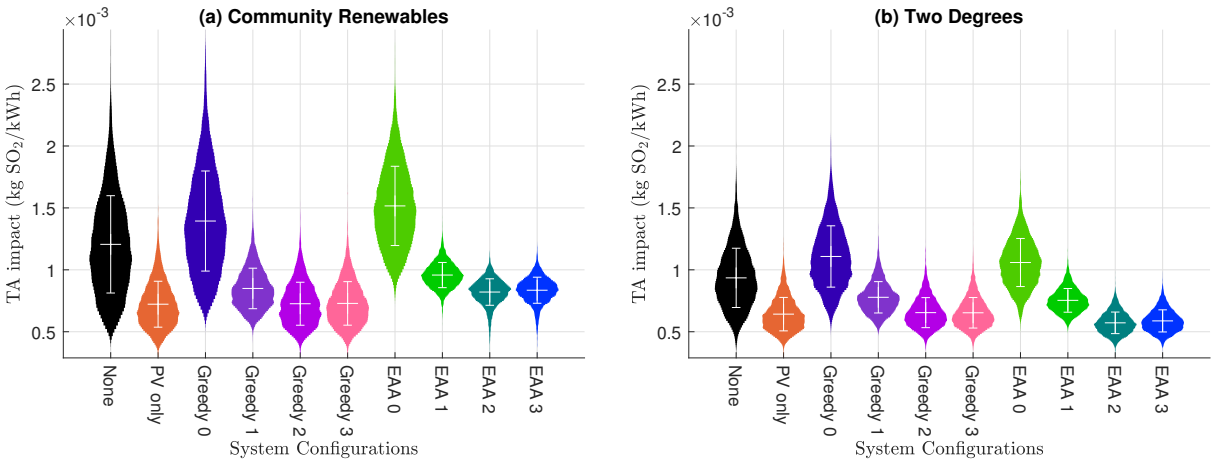

FIGURE D2: Distribution plots of Terrestrial Acidification impact in each configuration, in Community Renewables and Two Degrees future grid scenarios. Start year 2030.

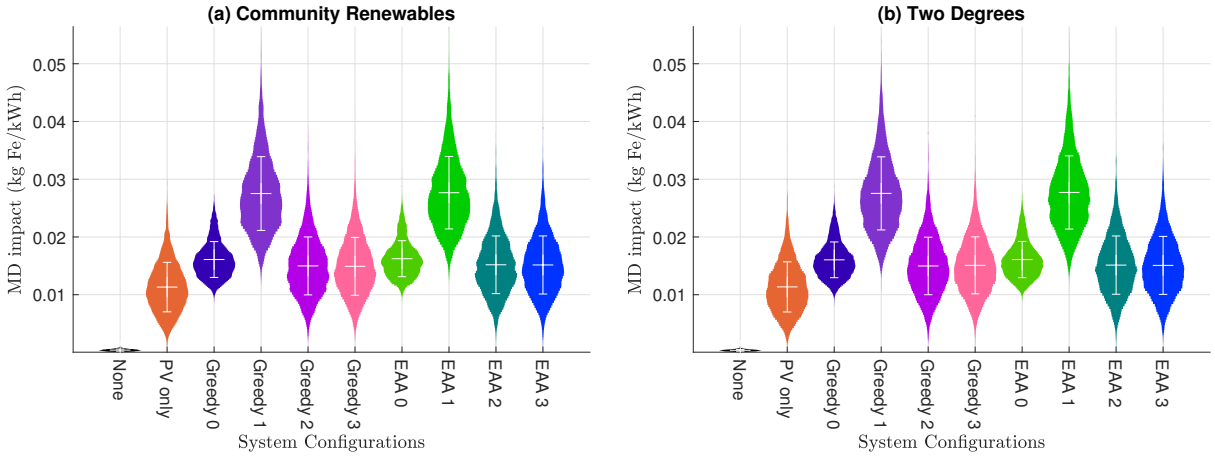

FIGURE D3: Distribution plots of Metals Depletion impact in each configuration, in Community Renewables and Two Degrees future grid scenarios. Start year 2020.

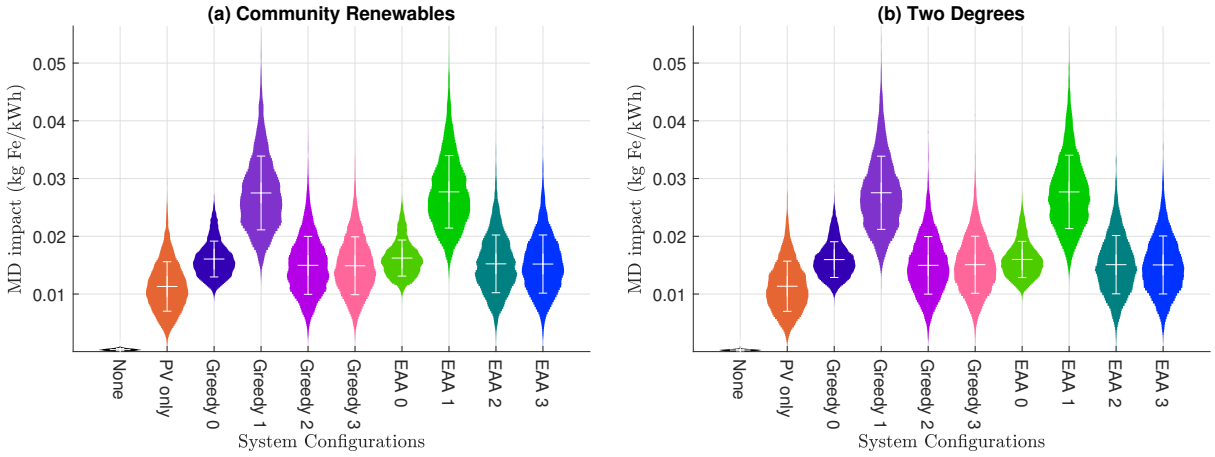

FIGURE D4: Distribution plots of Metals Depletion impact in each configuration, in Community Renewables and Two Degrees future grid scenarios. Start year 2030.

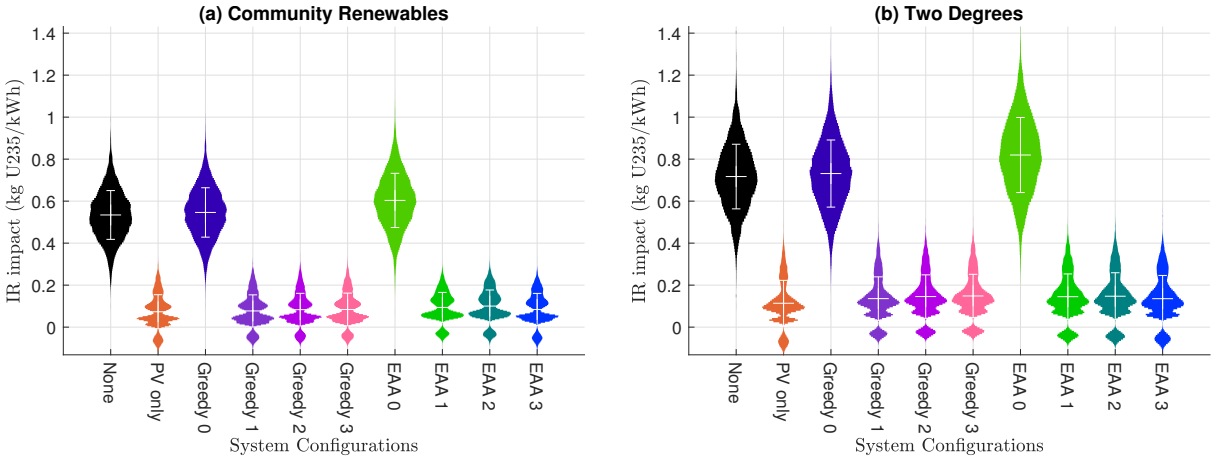

FIGURE D5: Distribution plots of Ionising Radiation impact in each configuration, in Community Renewables and Two Degrees future grid scenarios. Start year 2020.

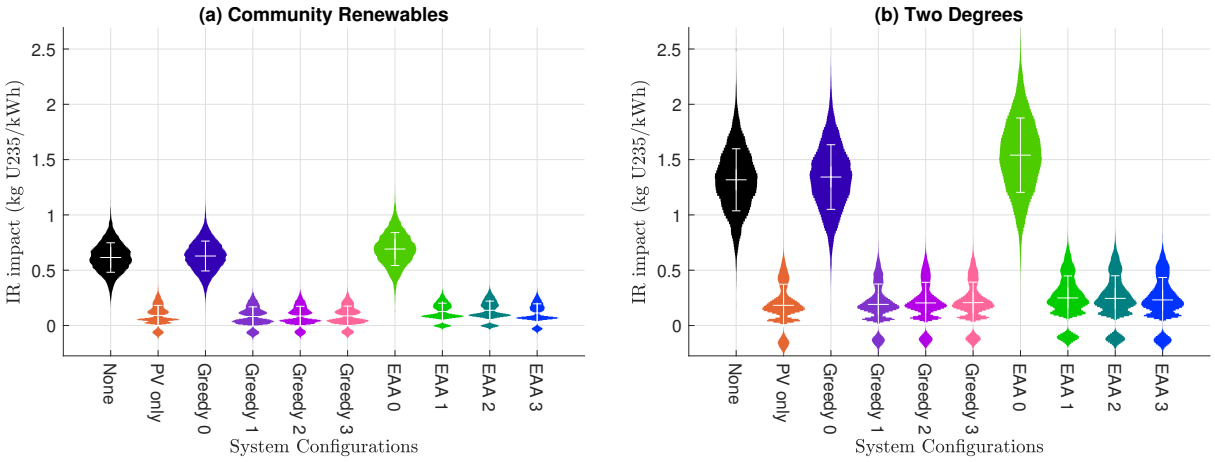

FIGURE D6: Distribution plots of Ionising Radiation impact in each configuration, in Community Renewables and Two Degrees future grid scenarios. Start year 2030.

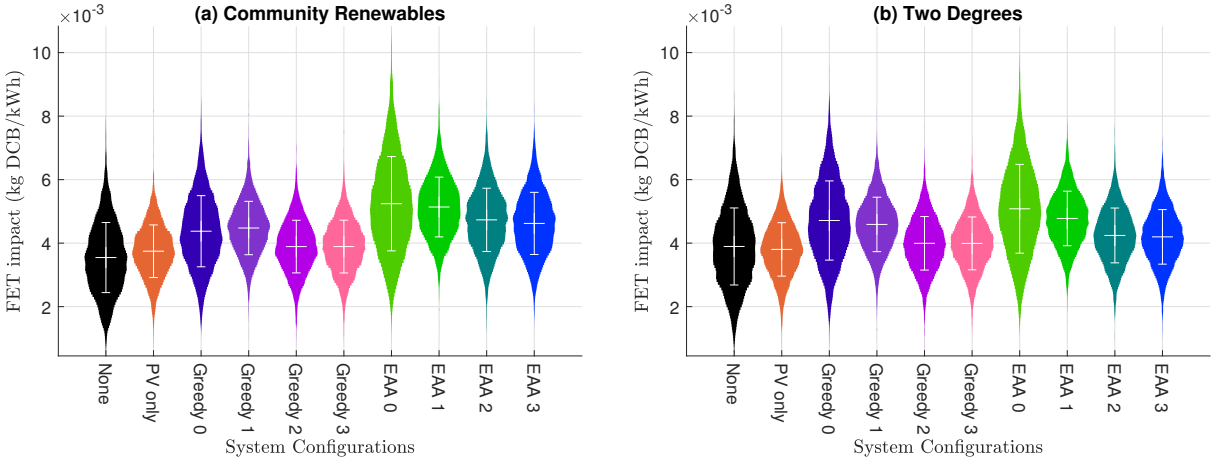

FIGURE D7: Distribution plots of Freshwater Ecotoxicity impact in each configuration, in Community Renewables and Two Degrees future grid scenarios. Start year 2020.

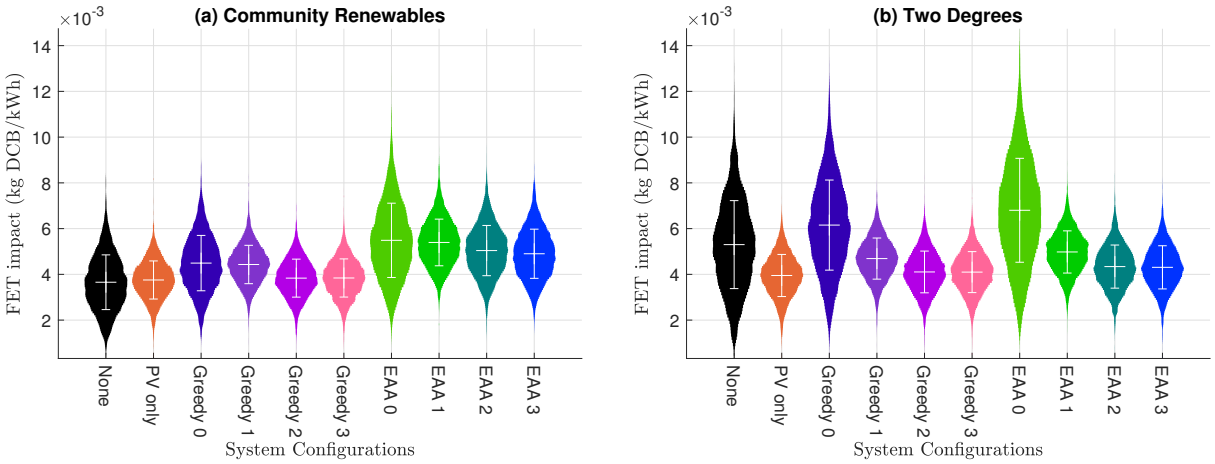

FIGURE D8: Distribution plots of Freshwater Ecotoxicity impact in each configuration, in Community Renewables and Two Degrees future grid scenarios. Start year 2030.

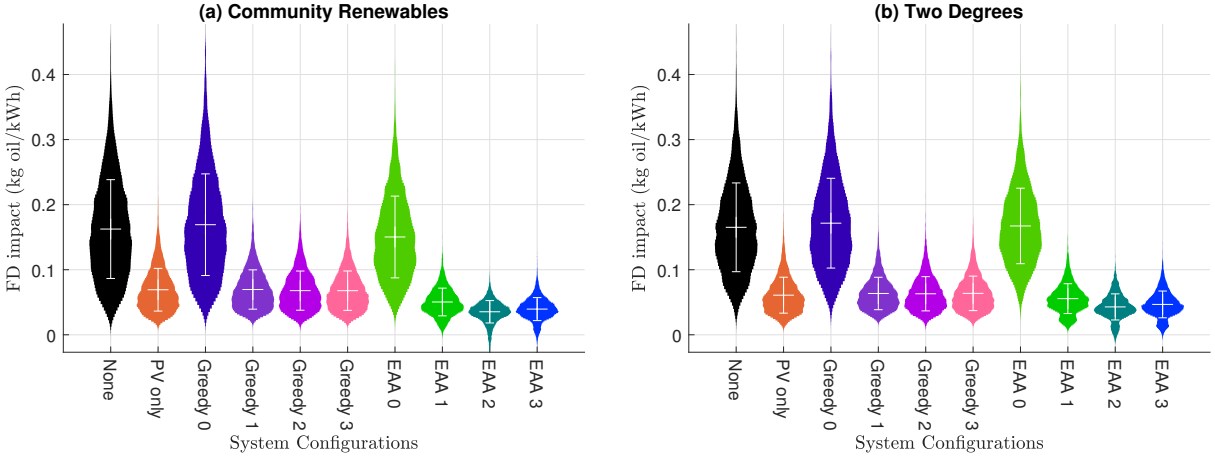

FIGURE D9: Distribution plots of Fossil fuel Depletion impact in each configuration, in Community Renewables and Two Degrees future grid scenarios. Start year 2020.

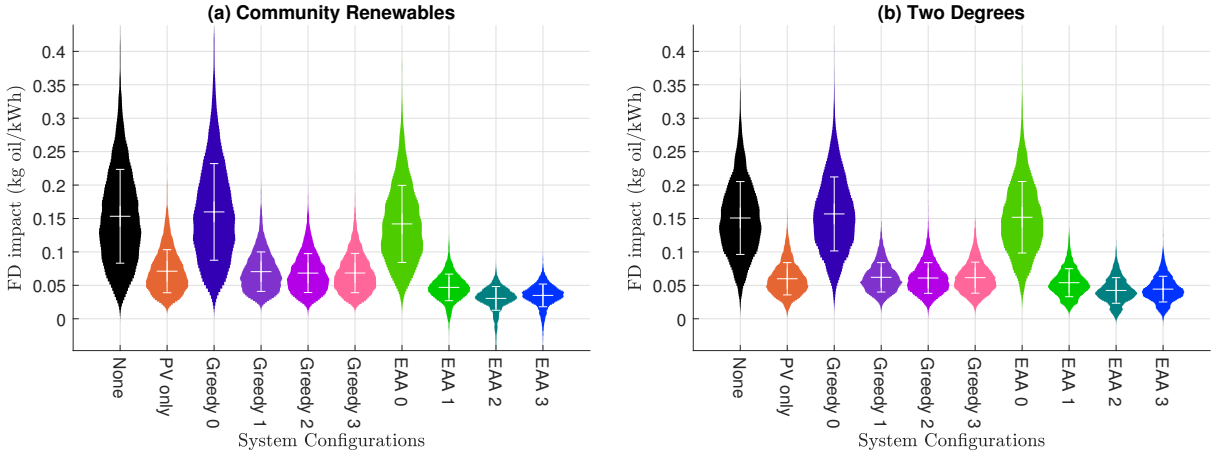

FIGURE D10: Distribution plots of Fossil fuel Depletion impact in each configuration, in Community Renewables and Two Degrees future grid scenarios. Start year 2030.

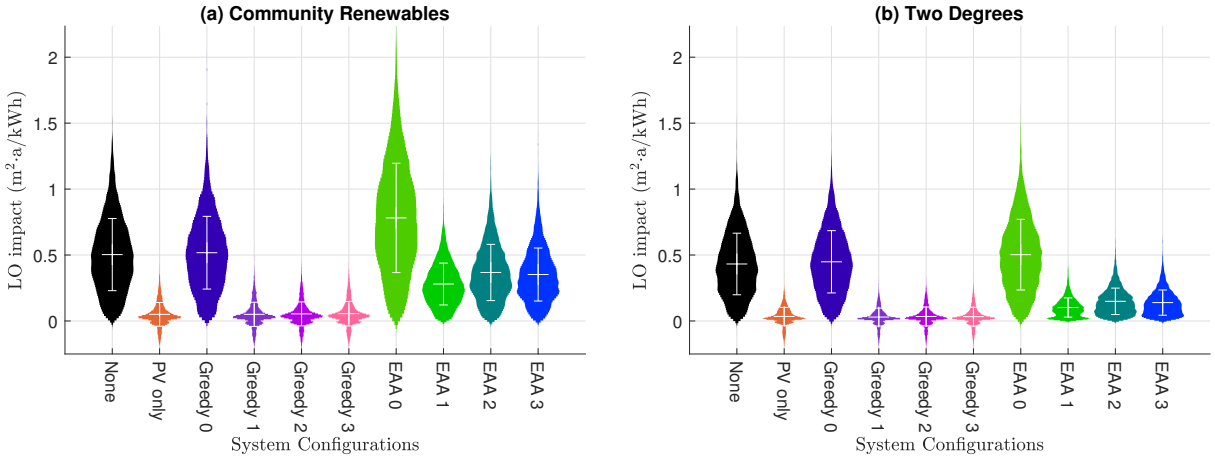

FIGURE D11: Distribution plots of Land Occupation impact in each configuration, in Community Renewables and Two Degrees future grid scenarios. Start year 2020.

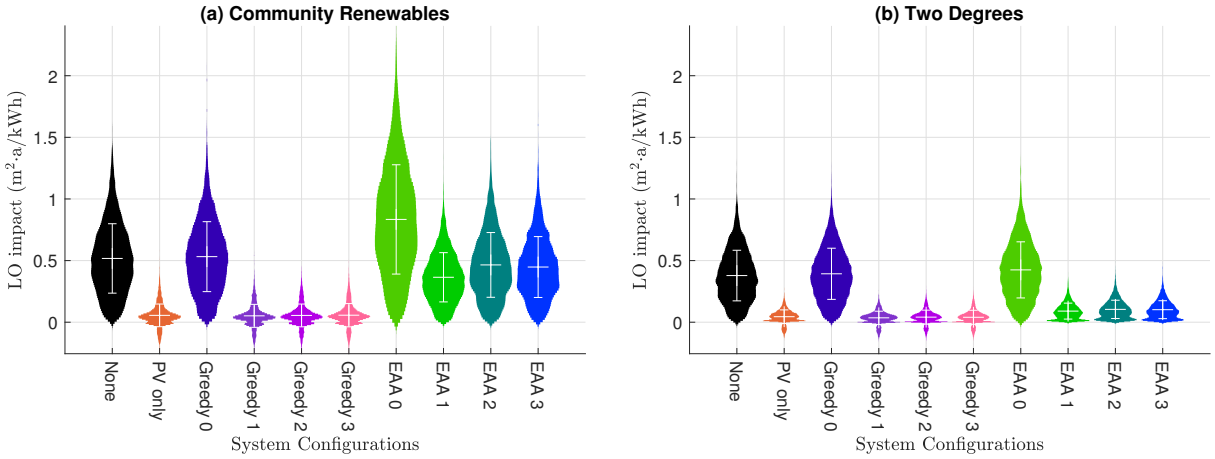

FIGURE D12: Distribution plots of Land Occupation impact in each configuration, in Community Renewables and Two Degrees future grid scenarios. Start year 2030.

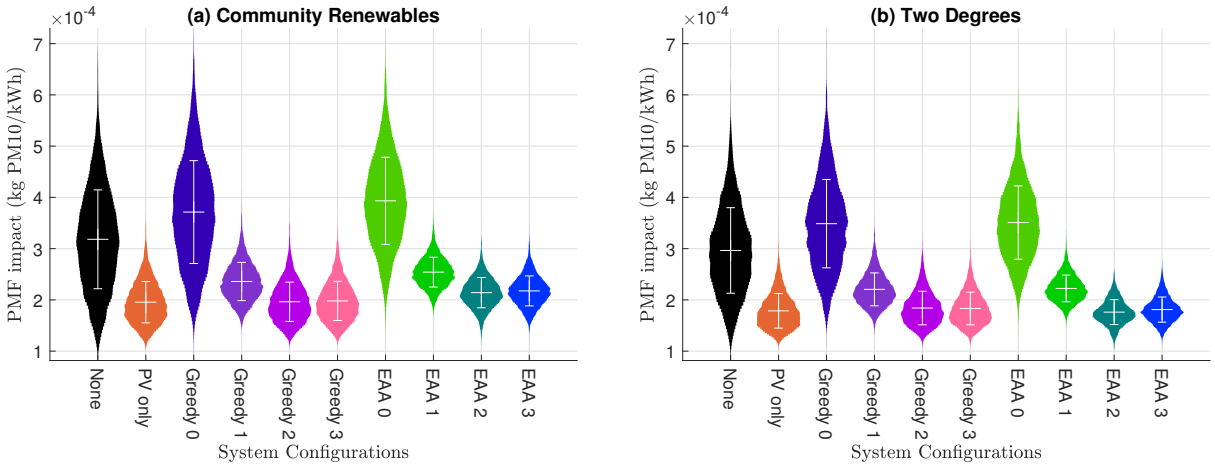

FIGURE D13: Distribution plots of Particulate Matter Formation impact in each configuration, in Community Renewables and Two Degrees future grid scenarios. Start year 2020.

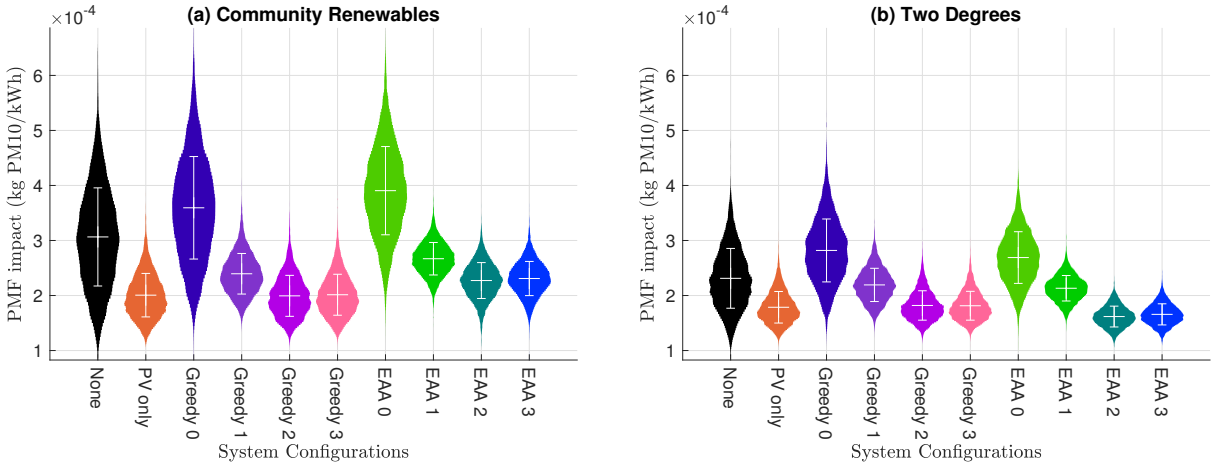

FIGURE D14: Distribution plots of Particulate Matter Formation impact in each configuration, in Community Renewables and Two Degrees future grid scenarios. Start year 2030.

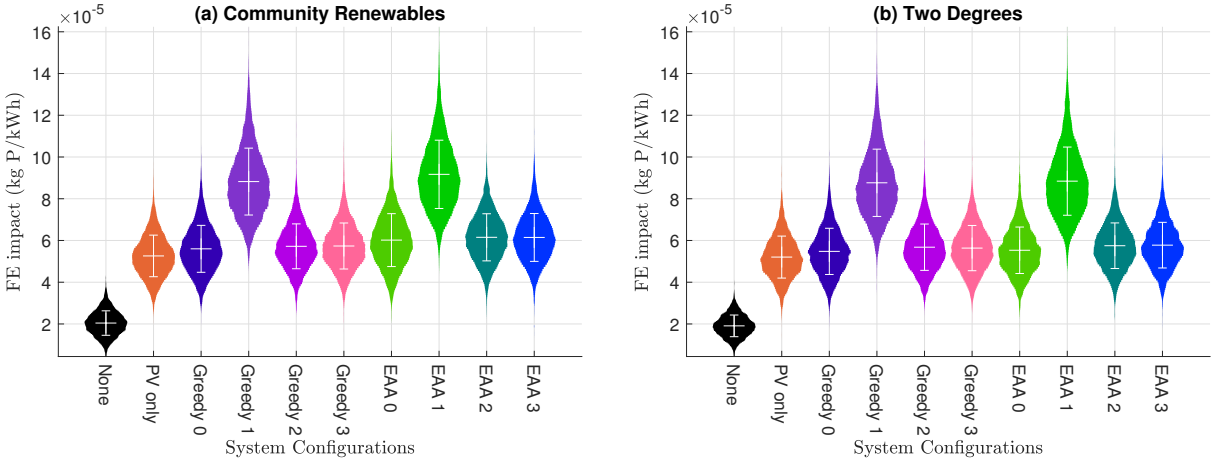

FIGURE D15: Distribution plots of Freshwater Eutrophication impact in each configuration, in Community Renewables and Two Degrees future grid scenarios. Start year 2020.

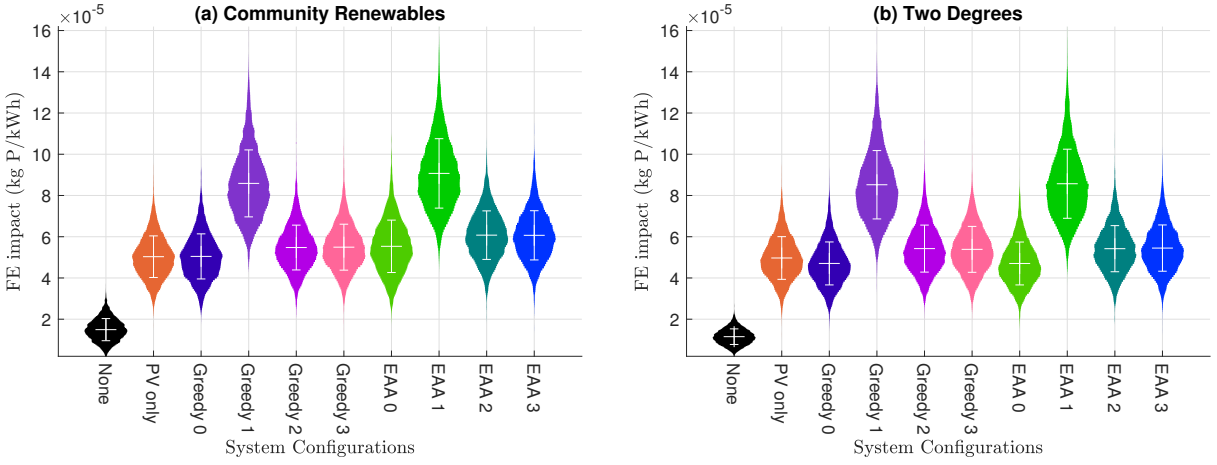

FIGURE D16: Distribution plots of Freshwater Eutrophication impact in each configuration, in Community Renewables and Two Degrees future grid scenarios. Start year 2030.

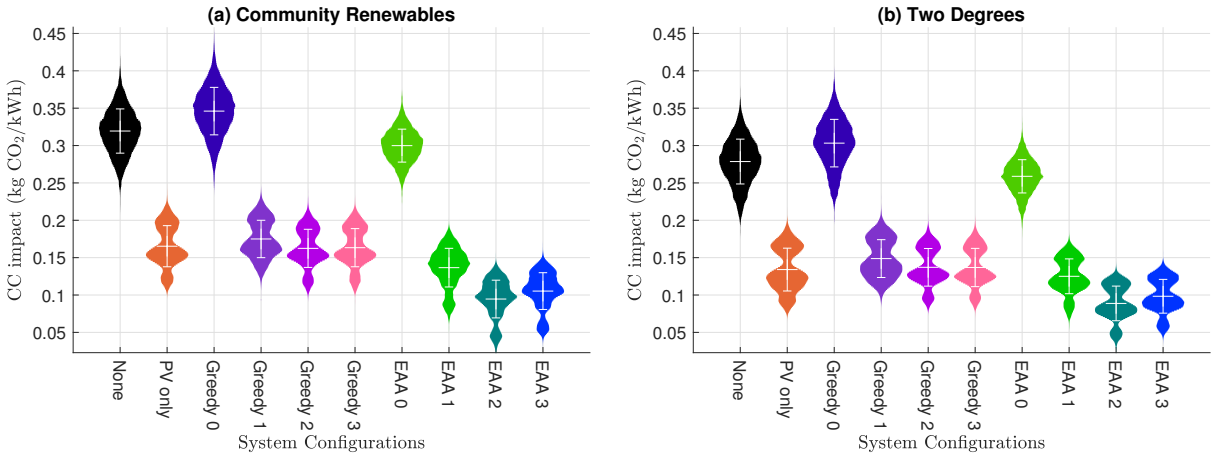

FIGURE D17: Distribution plots of Climate Change impact in each configuration, in Community Renewables and Two Degrees future grid scenarios. Start year 2020.

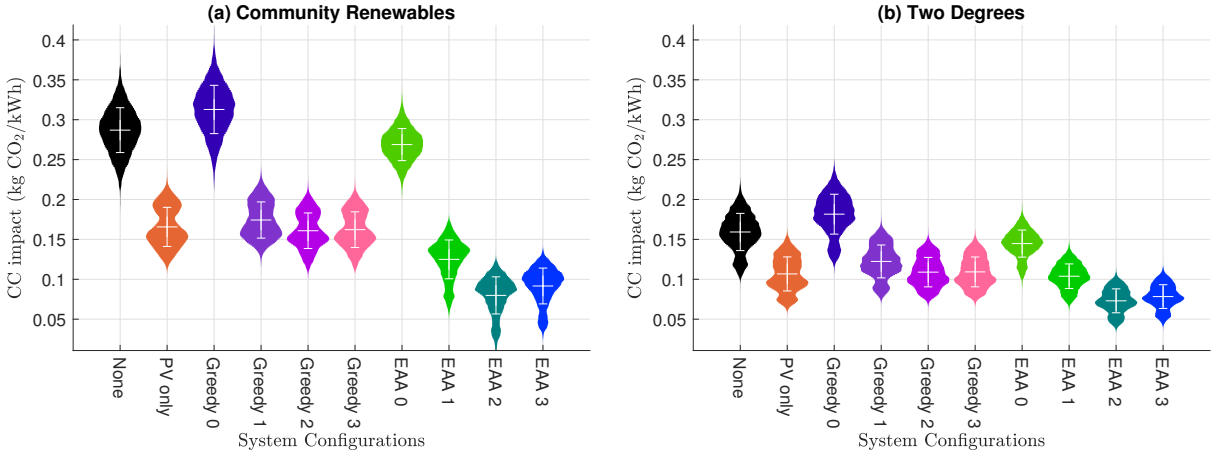

FIGURE D18: Distribution plots of Climate Change impact in each configuration, in Community Renewables and Two Degrees future grid scenarios. Start year 2030.

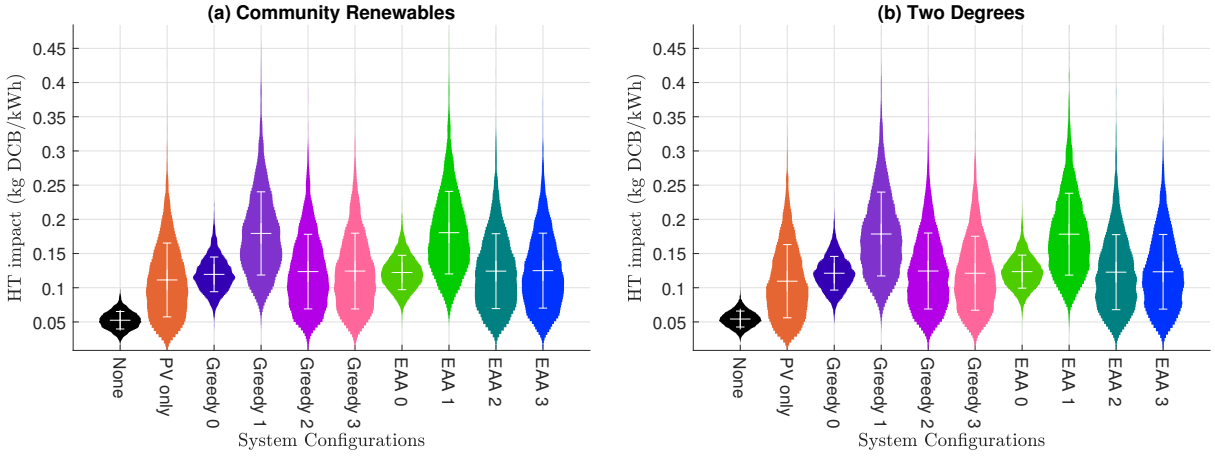

FIGURE D19: Distribution plots of Human Toxicity impact in each configuration, in Community Renewables and Two Degrees future grid scenarios. Start year 2020.

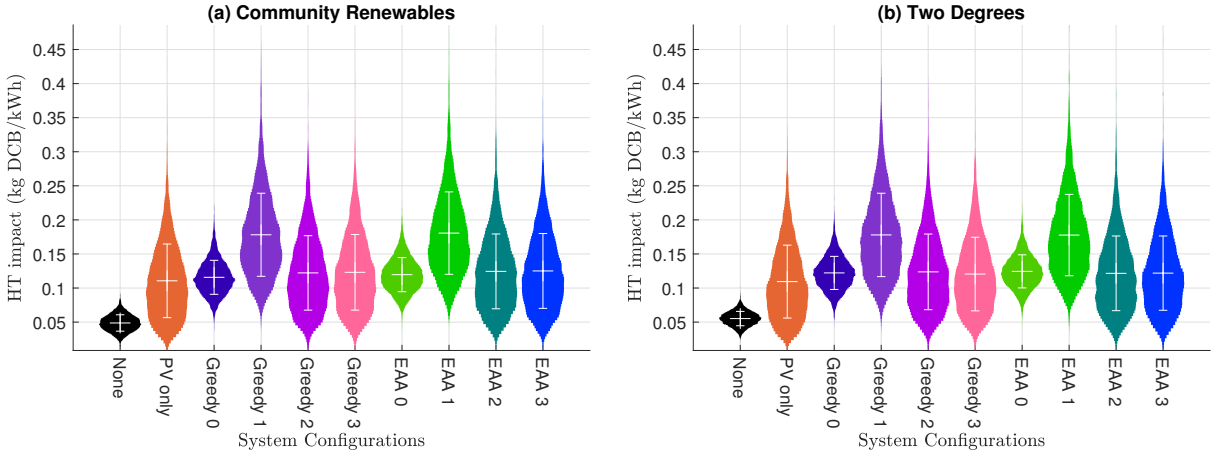

FIGURE D20: Distribution plots of Human Toxicity impact in each configuration, in Community Renewables and Two Degrees future grid scenarios. Start year 2030.

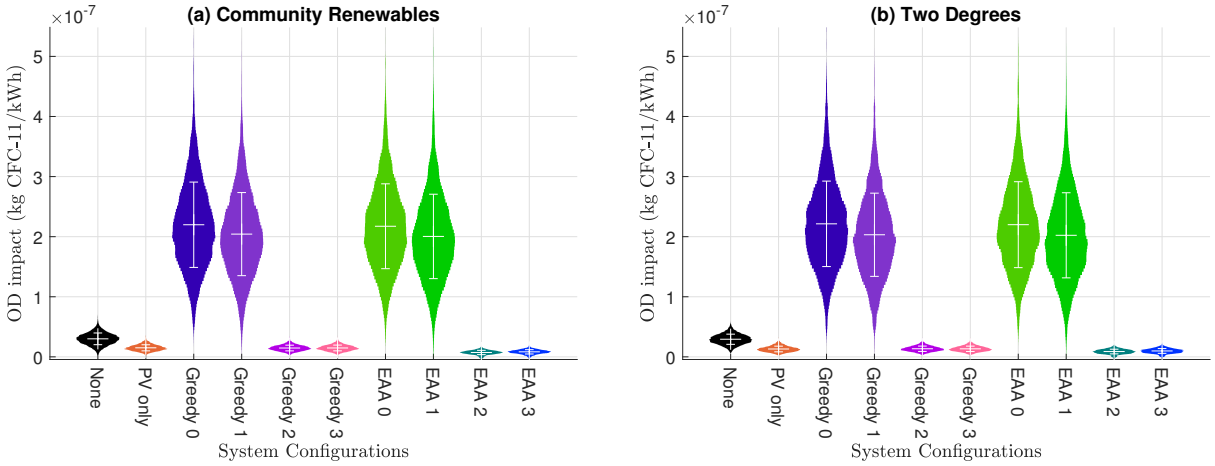

FIGURE D21: Distribution plots of Ozone Depletion impact in each configuration, in Community Renewables and Two Degrees future grid scenarios. Start year 2020.

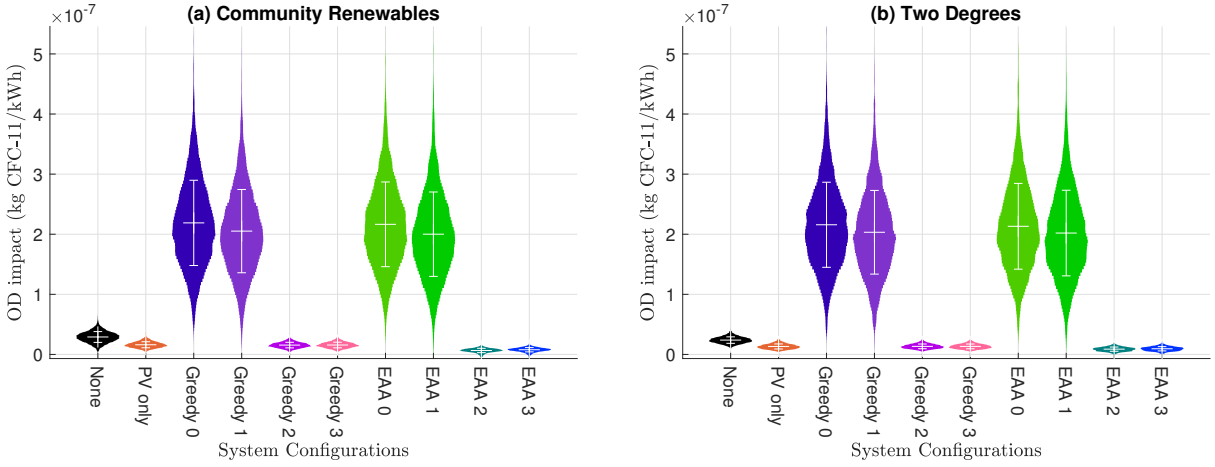

FIGURE D22: Distribution plots of Ozone Depletion impact in each configuration, in Community Renewables and Two Degrees future grid scenarios. Start year 2030.

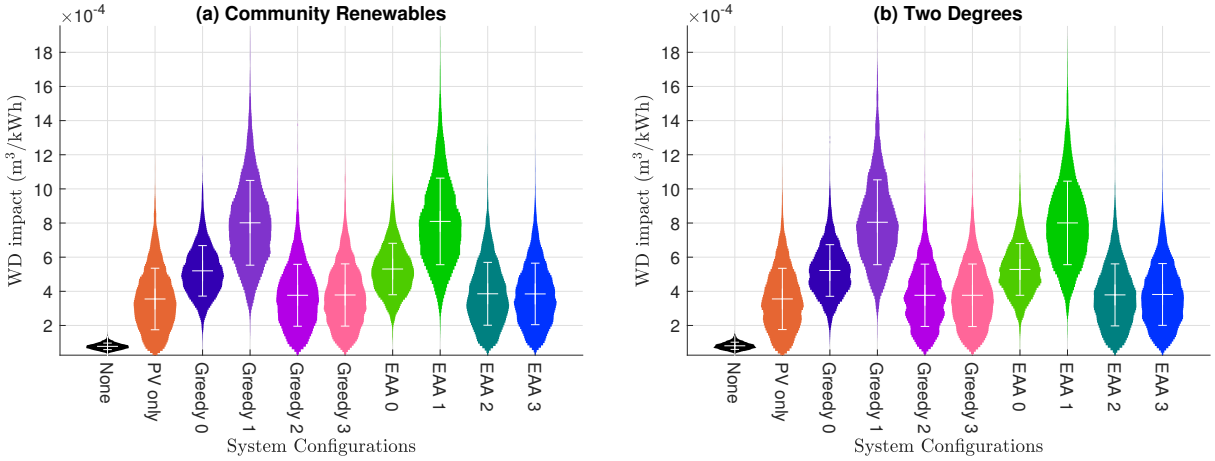

FIGURE D23: Distribution plots of Water Depletion impact in each configuration, in Community Renewables and Two Degrees future grid scenarios. Start year 2020.

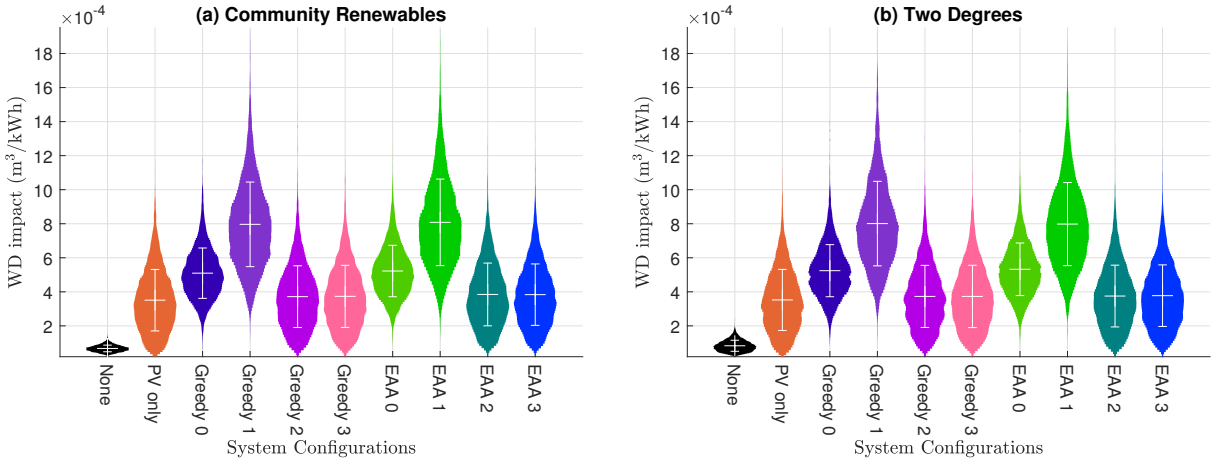

FIGURE D24: Distribution plots of Water Depletion impact in each configuration, in Community Renewables and Two Degrees future grid scenarios. Start year 2030.

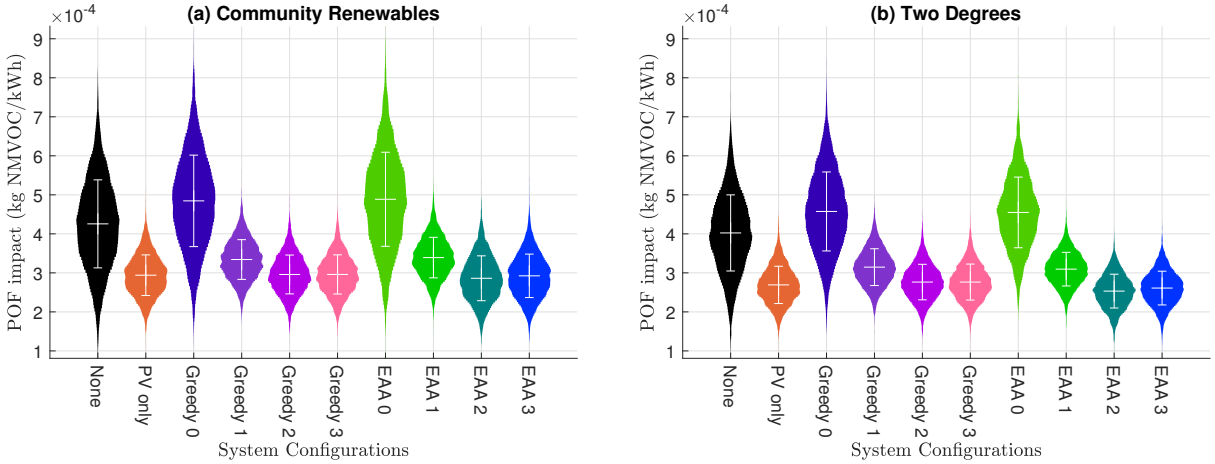

FIGURE D25: Distribution plots of Photochemical Oxidant Formation impact in each configuration, in Community Renewables and Two Degrees future grid scenarios. Start year 2020.

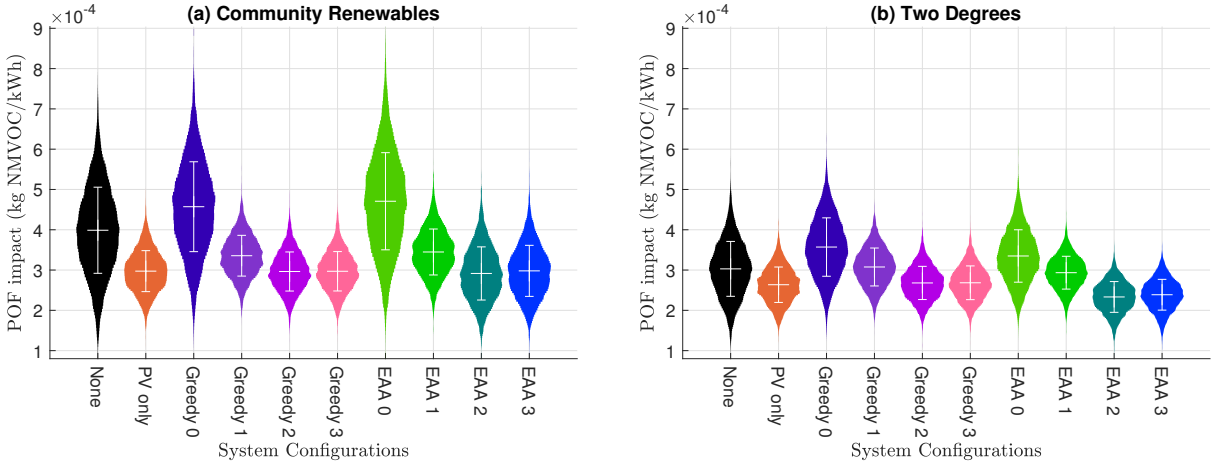

FIGURE D26: Distribution plots of Photochemical Oxidant Formation impact in each configuration, in Community Renewables and Two Degrees future grid scenarios. Start year 2030.

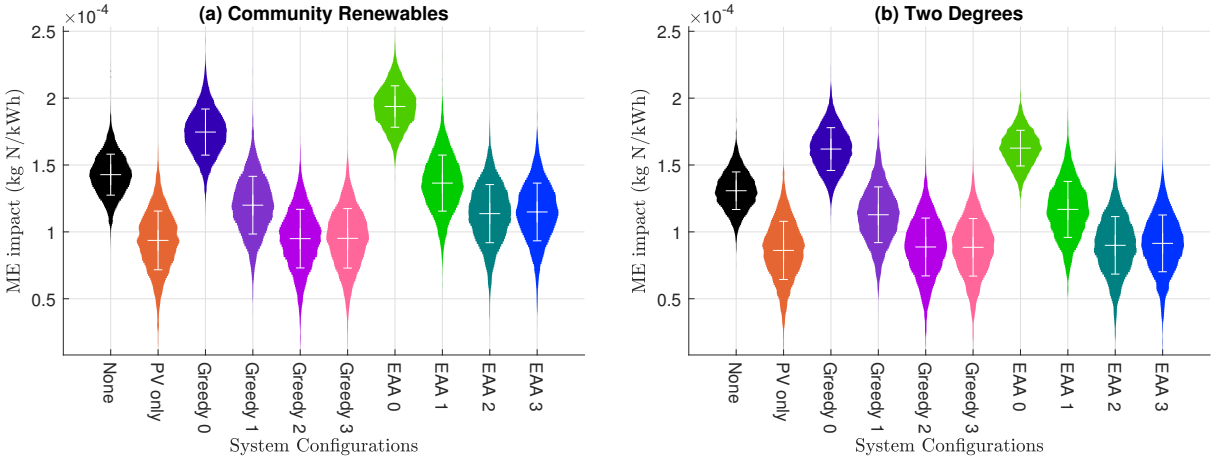

FIGURE D27: Distribution plots of Marine Eutrophication impact in each configuration, in Community Renewables and Two Degrees future grid scenarios. Start year 2020.

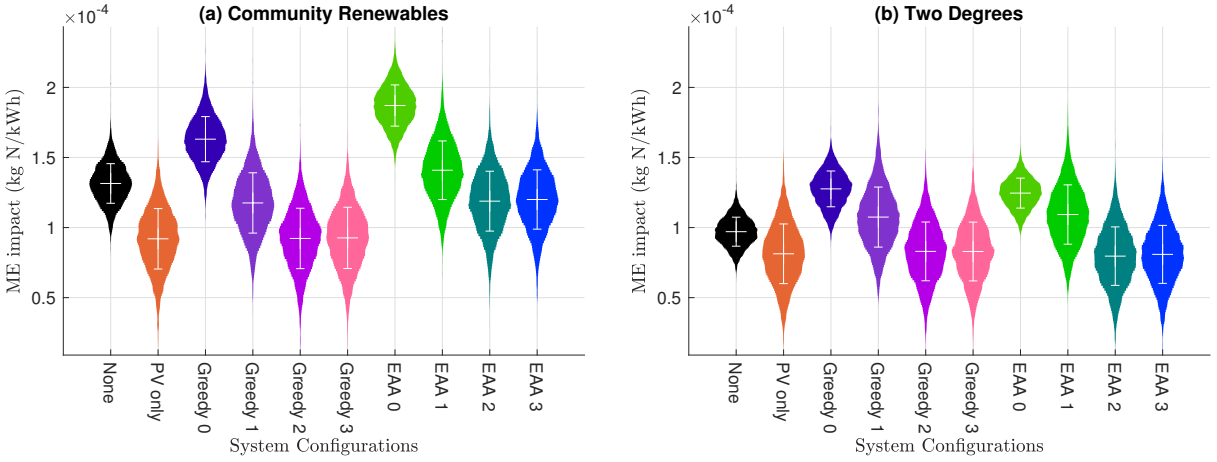

FIGURE D28: Distribution plots of Marine Eutrophication impact in each configuration, in Community Renewables and Two Degrees future grid scenarios. Start year 2030.

Appendix E

Guide to the Codebase

This appendix lists and explains the code and data files and their structure, modelling the PV-battery system described in this thesis. The code was developed in Matlab R2018a.

A note to those seeing this as a stand-alone user guide: there are references throughout to chapters and sections in a PhD thesis, yet to be published:
S. I. Sun (2020) "Financial and Environmental Life Cycle Assessment of Domestic PV-Battery Systems", University of Southampton, Faculty of Engineering and the Environment, PhD Thesis.

Please refer any feedback, corrections, and suggestions for improvement to the author. The reader is strongly encouraged to save a copy of the codebase and experiment with making improvements to it. Would any resulting publications please cite this work:
S. I. Sun (2020) "Code and Input Data for: Financial and Environmental Life Cycle Assessment of Domestic PV-Battery Systems in Great Britain, including Second-life Batteries".
URI `https://doi.org/10.5258/SOTON/D1269`.

E1 Listing of Code Files

E1.1 Input Data

- DickonPVdata15s.mat
  One year of 15-s resolution PV output data, cleaned from the raw data supplied by D. Hood. More details in Chapter 2 Section 2.2.2. Normalised to 1 kW_p capacity.
  Unit: kW.
- REFIT_Houses_15s_NEW.mat
  One year of 15-s resolution electrical consumption data, for Houses 5, 8, 7, 6, 2, 1, 12, 19, cleaned from the REFIT dataset (Murray et al., 2017). More details in Chapter 2 Section 2.2.1.
  Unit: kW.

- EV2ndlifeprices.mat
  Size-dependent portion of second-life battery price, per usable kWh capacity, for the years 2010-2050. More details in Chapter 4 Section 4.3.
  Unit: GBP/kWh.

- gridCarbonPaper.mat
  Arrays of size 1 × 17520 containing time series data of generation power from each generator type, and total national demand, for 2017, as read by the function `readGridWatch` from the CSV file downloaded from Gridwatch (2018).
  'b' = biomass
  'c' = coal
  'cc' = CCGT
  'du' = Dutch import (-ve = export)
  'ew' = East-West import (from Republic of Ireland to Wales - not used)
  'fr' = French import
  'hy' = hydroelectric
  'ir' = Irish import (from Northern Ireland to Scotland - not used)
  'n' = nuclear
  'nor' = North-South import (within England - not used)
  'Pd' = total national demand in GB
  'pu' = pumped hydroelectric
  'pv' = solar photovoltaic (estimated, all at distribution level)
  'sc' = Scottish import (not used)
  'w' = wind (transmission-connected only)
  Unit: MW.

- nationalMGRs.mat
  Contains the matrices `MGR30s`, `MGR50s`, `MGR30nats` and `MGR50nats`.

  `MGR30s` and `MGR50s` contain the marginal generator response time series $MGR_j(t)$ for years 2030 and 2050 respectively, calculated according to details in Chapter 3 Section 3.1.3, and used to calculate the marginal emissions factor $MEF(t)$. The matrices are each of size $11 \times 17520 \times 2 \times 2$:

  11 for each generator type j: coal, CCGT, biomass, nuclear, CCS, geothermal (unused), hydroelectric, French interconnector, Dutch interconnector, international imports, international exports, in that order;
  17520 for each half-hour (t) in one year;
  2 for either algorithm, Greedy or Emissions Arbitrage;
  2 for either future grid scenario, Community Renewables or Two Degrees;

  An 11×17520 array is selected from each 4-D matrix accordingly in order to calculate $MEF(t)$.
  Unit: MW/MW.

  `MGR30nats` and `MGR50nats` contain, for years 2030 and 2050, the difference between the scenarios with energy storage and with none in the whole country, of energy generated by each generator type j across the year (negative values mean that that type is generating more in the scenario with storage). The matrices are each of size $11 \times 2 \times 2$:

  11 for each generator type j;
  2 for either algorithm, Greedy or Emissions Arbitrage;
  2 for either future grid scenario, Community Renewables or Two Degrees;

An 11-element array is selected from each 3-D matrix accordingly. It is then used to find the difference in environmental impacts across the system lifetime, of the whole country having energy storage compared to not having any.
Unit: kWh.

E1.2 Workbooks

- Workbook_plottingfigures.m
  Generates the plots used as explanatory figures throughout the thesis (i.e. not results plots).
- Workbook_2019_10_02_initMGR.m
  Initialises marginal generator response (MGR) data, and saves it in the file nationalMGRs.mat. It is read in when running the code to calculate environmental impacts of added/displaced grid generation.
- Workbook_2019_10_07_EV2ndlife.m
  Applies the microeconomics-driven model to calculate second-life battery price, and saves it to EV2ndlifeprices.mat.
- Workbook_2019_08_09_timeres.m
  Runs the time resolution and time-slicing tests whose results are reported in Chapter 5 Section 5.1.2.
- Workbook_2019_09_05_sizing.m
  Runs the direct searches for system components sizing, as reported in Chapter 5 Section 5.2.
- Workbook_2019_10_12_results.m
  Runs the simulation in all 10 configurations to get financial and environmental results reported in Chapter 6.
- Workbook_2019_12_27_pricemap.m
  Runs analysis of MCoE sensitivity to Capex and electricity price increase.

E1.3 Classes

In the workbooks listed above, there are many references to class objects and their properties and methods. The class structure and their relationships are shown in Figure E1.

E1.4 Functions

In addition to the class methods listed above, there are some functions in their own files:

- readGridWatch.m
  Function auto-generated by Matlab to read in CSV file downloaded from Gridwatch (2018), and produce a Matlab table containing time series data of generation power (MW) from each generator type.

- coarsendata.m
  Reads in an array and coarsens its time resolution from δt to Δt, by averaging. This is used in Chapter 5 Section 5.1.2, for testing the effects of different time resolution.

- objfunc.m
  Reads in information on the PV-battery system configuration to be modelled, runs the model, and calculates and returns life-cycle CO_2 emissions (kg/kWh), mean cost of electricity (MCoE, in GBP/kWh), payback period (PP, years), and return on investment (RoI). This function is used extensively in Workbook_2019_09_05_sizing.m. See more on system components sizing in Chapter 5 Section 5.2.

FIGURE E1: Class structure of the code.